Eawag 05692

Diss. ETH No. 17934

Characterization of Ozone-Based Oxidative Treatment as a Means of Eliminating the Target-Specific Biological Activities of Municipal Wastewater-Borne Antibacterial Compounds

A Dissertation Submitted to
ETH ZURICH
for the degree of Doctor of Sciences

presented by
MICHAEL CAMERON DODD
Bachelor of Science, Civil Engineering - Georgia Institute of Technology, 2001
Master of Science, Environmental Engineering - Georgia Institute of Technology, 2003
born on May 14, 1978
citizen of the United States of America

accepted on the recommendation of
Prof. Dr. René P. Schwarzenbach, examiner
Prof. Dr. Urs von Gunten, co-examiner
Dr. Hans-Peter E. Kohler, co-examiner
Prof. Dr. Clemens von Sonntag, co-examiner

Zurich 2008

Acknowledgements

With the conclusion of nearly five years of extremely fruitful, enjoyable work and residence in the beautiful country of Switzerland, I now have a fitting opportunity to reflect back on the period leading up to my relocation from the United States to work on my doctoral thesis at Eawag and the period actively spent working here. With this reflection arises the need to recognize and express my deepest thanks to those people in my life who have played the greatest role in helping me to reach this point. So here goes:

First, and foremost, I would like to express my most heartfelt thanks to Urs von Gunten for providing the most incredible combination of advisor, colleague, mentor, and friend one could hope for in a Ph.D. supervisor. Words are truly inadequate to express how grateful I am to have had the opportunity to work with Urs over these years, or how much respect I have for him as a person and a researcher. Perhaps the best I can hope to do here is to say that he has provided the prototype for the type of advisor, teacher, and researcher I hope to become – a true model for leading a life in which one never forgets the importance of venturing outside of the laboratory into the sunshine (and on to the mountains); if for nothing else, than simply to enjoy the fresh air that we sometimes take for granted in our daily work. Thank you, Urs.

I would also like to thank my Ph.D. co-examiners, Hans-Peter Kohler, René Schwarzenbach, and Clemens von Sonntag, for their extensive time (even in the midst of the Summer vacation), much valued input, and support in completing this tremendous task. In particular, I would like to thank Hans-Peter for his instrumental role in developing the microbiological activity assay used so extensively during this work, and for his continuous guidance as I have ventured across the boundary between chemistry and microbiology. Without his support, this work would not have proven so rewarding or successful.

Next, I want to give deepest thanks to my girlfriend and constant companion My Quoc Meriaho, for many years of cherished partnership, exciting trips around Europe, the Caribbean, and the U.S.A., and huge quantities of never-ending support. You are always there when I need your help, and always ready with a hug whenever I need one. I love you very much, and cannot express how glad I am that I've been able to share my time in Switzerland with you. I'm looking forward to many more years with you on the other side of the Atlantic.

I also want to give a huge thank you to all of the close friends and colleagues in or affiliated with the von Gunten group with whom I have had the great pleasure (and great fortune) to work, chat, and hang out during my time at Eawag. In no particular order: Lisa Salhi, Marc-Olivier Buffle, Marc Huber, Marie Deborde, Andi Peter, Gretchen Onstad,

Yunho Lee, Bill Arnold, Manuel Sanchez-Polo, Holger Lutze, José Mendez-Diaz, Detlef Knappe, Jannis Wenk, Jessica Benner, Carolina Garcia, Sébastien Allard, Claire Wedema, Karl Linden, Dietmar Struebling, Ioannis Katsoyiannis, Maaike Ramseier, Saskia Zimmerman, Changha Lee, Erik Rosenfeldt, Brian Sinnet, Silvio Canonica, Anh Trung Kieu, Laurence Meunier, Jakob Helbing, Sébastien Meylan, Jörg Rüedi, Nadya Teutsch, Hans-Ueli Laubscher, Mathias Wittenwiller, Matthias Sturzenegger, Hana Mestankova, and Jacqueline Traber. Particularly big thanks to Marc, Marc-Olivier, and Claire for their key roles in helping me to decide to come to Eawag and settling in after moving over. Lisa – thank you so much for all of your technical support over the years. A very big acknowledgment to Yunho for so many interesting scientific discussions and many great trips to the Alps. Another very big thank you to Andi for so many thought-provoking (and sometimes intense) discussions about global politics and the state of the world, and for providing a constant sounding-board for improving my still no-so-perfect German skills. You guys are really the best!

A very big thank you to Dani Rentsch and Heinz Singer for their indispensable expertise and outstanding support in completing our analytical studies of β-lactam-O_3 transformation products.

Special thanks go to a number of collaborators on tremendously interesting (if often challenging, and sometimes very frustrating) projects outside of my thesis work: Steffen Zuleeg and Wouter Pronk for the extended, and ultimately extremely rewarding, work on urine ozonation; Ngoc Duy Vu, Van Chieu Le, Michael Berg, Reinhard Kissner, and Adi Ammann for the very successful collaborations on As(III) oxidation; Sonia Suarez for the great work and support in the investigation of triclosan oxidation and deactivation.

Thank you very, very much to Walter Giger, Anke Schaefer, and Marie-Jeanne Weyrich for their considerable support on my first publications, and for giving me the opportunity to review so many interesting manuscripts at such an early stage of my career. You have each played a central role in shaping my appreciation for the editorial process and scientific publishing in general.

I also want to acknowledge Olivier Leupin and Philipp Schneider for their critical roles in organizing so many of the annual W+T ski tours over these years. Without you guys, I might never have discovered how great it is to walk uphill on skis (even if with only one skin).

Lastly, a big thanks to all of my other friends and colleagues within and outside of W+T, as well as in the Schwaba GruFo, for making Eawag such an incredible place to work. Even during the most challenging periods of my thesis, I’ve never once taken for granted how fortunate I am to be here!

Table of Contents

Acknowledgements i
Table of Contents iii
List of Frequently Used Abbreviations and Symbols vii
Summary xi
Zusammenfassung xv

Chapter 1. Background and General Introduction 1

1.1 Overview 2
1.2. Detection of Antibiotic Resistant Bacteria in Municipal Wastewater Systems 5
1.3. Detection of Antibacterial Residues in Municipal Wastewaters 7
1.4. Selection for Antibacterial Resistance 8
1.5. Maintenance of Antibacterial Resistance Phenotypes 11
1.6. Implications for Risk Assessment 14
1.7. Transformation of Antibacterial Compounds during Ozonation 16
1.8. Thesis Scope 19
1.8.1. Model Antibacterial Compounds 20
1.8.1.1. Macrolides. 20
1.8.1.2. Sulfonamides. 22
1.8.1.3. Dihydrofolate Reductase (DHFR) Inhibitors. 23
1.8.1.4. Fluoroquinolones. 24
1.8.1.5. β-lactams. 26
1.8.1.6. Lincosamides. 27
1.8.1.7. Tetracyclines. 27
1.8.1.8. Glycopeptides. 29
1.8.1.9. Aminoglycosides. 30
1.8.1.10. Triclosan (Biocide). 31
1.9 . Thesis Layout 31

Chapter 2. Oxidation of Antibacterial Molecules by Aqueous Ozone: Moiety-Specific Reaction Kinetics and Application to Ozone-Based Wastewater Treatment 40

2.1 Introduction 42
2.2 Materials and Methods 45
2.2.1 Chemical Reactants and Reagents. 45
2.2.2 Measurement of Rate Constants. 45
2.2.3 Wastewater Matrix Experiments. 45
2.3 Results and Discussion 46

2.3.1 Moiety-specific Ozone Reaction Kinetics. 46
2.3.2 Studies in Wastewater Matrixes. 53

Supporting Information for Chapter 2. 61

Chapter 3. Kinetics of Triclosan Oxidation by Aqueous Ozone and Consequent Loss of Antibacterial Activity: Relevance to Municipal Wastewater Ozonation 87

3.1 Introduction 89
3.2 Materials and Methods 91
3.2.1 Standards and reagents 91
3.2.2 Analytical methods 91
3.2.3 Determination of the rate constants for reactions with ozone 92
3.2.4 Measurement of triclosan antibacterial activity after treatment with ozone 92
3.2.5 Municipal wastewater ozonation 95
3.3 Results and Discussion 96
3.3.1 Rate constants for reactions of triclosan with ozone 96
3.3.2 Site of initial reaction between triclosan and ozone 98
3.3.3 Elimination of triclosan antibacterial activity by reaction with ozone 99
3.3.4 Triclosan losses during ozonation of pilot-scale and full-scale wastewaters 101

Chapter 4. Oxidation of Antibacterial Compounds by Ozone and Hydroxyl Radical: Elimination of Biological Activity during Aqueous Ozonation Processes 107

4.1 Introduction 109
4.2 Materials and Methods 110
4.2.1 Chemical Reactants and Reagents. 110
4.2.2 Oxidation of antibacterial model compounds. 112
4.2.3 Measurement of antibacterial activities after treatment with ozone and hydroxyl radical. 114
4.3 Results and Discussion 117
4.3.1 Analysis and interpretation of microdilution assay data. 117
4.3.2 Deactivation of model clinical antibacterial compounds by ozone. 119
4.3.3 Deactivation of model clinical antibacterial compounds by hydroxyl radical. 124
4.3.4 Deactivation of triclosan by ozone and hydroxyl radical. 125
4.3.5 Implications for antibacterial deactivation during ozonation of municipal wastewater. 127

Supporting Information for Chapter 4. **135**

Chapter 5. Transformation of *β*-lactam Antibacterial Agents during Aqueous Ozonation: Reaction Pathways and Quantitative Bioassay of Biologically-Active Oxidation Products **142**

5.1. Introduction. **144**

5.2 Materials and Methods **146**

5.2.1 Chemical reactants and reagents. 146

5.2.2 Preparation of oxidant-treated antibacterial model compounds for product evolution and biological assay studies. 147

5.2.3 Preparation and purification of transformation products generated by reactions of ozone with PG and CP. 148

5.2.4 Chemical analyses of PG, CP, and purified transformation products. 149

5.2.5 Measurement of antibacterial activities via broth microdilution assay. 152

5.2.6 Measurement of apparent second-order rate constants for reactions of *β*-lactam-(*R*)-sulfoxides with O_3 and $^{\bullet}OH$. 153

5.3 Results and Discussion **153**

5.3.1. Identification of major products resulting from reactions of PG and CP with O_3. 153

5.3.2 Evolution of major products in O_3-treated PG and CP solutions with increasing transferred O_3 dose. 161

5.3.3 Antibacterial activities of transformation products resulting from reactions of PG and CP with O_3. 165

5.3.4. Modeling evolution of biological activities of O_3-treated PG and CP solutions with increasing transferred O_3 dose. 166

5.3.5 Deactivation of PG- and CP-(*R*)-sulfoxides by O_3 and $^{\bullet}OH$. 167

5.3.6 Implications for *β*-lactam deactivation during ozonation of municipal wastewaters. 168

Supporting Information for Chapter 5. **175**

Chapter 6. General Conclusions **200**

Appendix A. Ozonation of Source-separated Urine for Resource Recovery and Waste Minimization: Process Modeling, Reaction Chemistry, and Operational Considerations **A1**

A.1 Introduction **A3**

A.2 Experimental Section **A4**

A.2.1 Chemicals and urine matrixes. A4

A.2.2 Analytical Methods. A4

A.2.3 Experimental conditions and methods. A5

A.3 Results and Discussion A5

A.3.1 Oxidation of micropollutants in hydrolyzed urine. A5

A.3.2 Oxidation of micropollutants in ED effluents. A7

A.3.3 Quantitative modeling and system characterization. A9

A.3.4 Modeling homogeneous reaction chemistry and formation of secondary radicals. A14

A.3.5 Practical operational implications of experimental observations and model results. A17

Supporting Information for Appendix A. A23

Appendix B. Kinetics and Mechanistic Aspects of As(III) Oxidation by Aqueous Chlorine, Chloramines, and Ozone: Relevance to Drinking Water Treatment B1

B.1 Introduction B3

B.2 Materials and Methods B4

B.2.1 Chemical Reagents. B4

B.2.2 Analytical Methods. B4

B.2.3 Determination of Rate Constants. B4

B.2.4 Stoichiometric Measurements. B4

B.2.5 Real Water Experiments. B4

B.3 Results and Discussion B6

B.3.1 As(III) Oxidation Kinetics. B6

B.3.2 Mechanistic Considerations. B11

B.3.3 Oxidation of As(III) in Real Waters. B12

B.3.4 Implications for As(III) Oxidation during Full-Scale Drinking Water Treatment. B17

Supporting Information for Appendix B. B22

List of Frequently Used Abbreviations and Symbols

Abbreviation(s)	Dimensions	Item(s) or Parameter(s)
AM	-	Amikacin
APMS	-	4-aminophenyl methyl sulfone
ASMX	-	N4-acetyl-sulfamethoxazole
AZ	-	Azithromycin
CF	-	Ciprofloxacin
CFU	-	Colony forming unit
CH	-	Cyclohexylamine
CHM	-	Cyclohexanemethylamine
CFL		Continuous-flow
CK	-	Competition kinetics
CM	-	Carbamazepine
CP	-	Cephalexin
DAMP	-	2,4-diamino-5-methylpyrimidine
DC	-	Diclofenac
DMCH	-	*N,N*-dimethylcyclo-hexylamine
DMI	-	3,5-dimethylisoxazole
DOC	-	Dissolved organic carbon
DOM	-	Dissolved organic matter
DPD	-	*N*,*N*-diethyl-*p*-phenylenediamine
EC_{50}	mg/L, mol/L, or dimensionless	Concentration level of a sample at which 50% biological effect is observed relative to positive and negative controls – as obtained from fitted dose-response curves. EC_{50} can be expressed as a concentration or a dimensionless concentration factor or dilution factor.
EE2	-	17-α-ethinylestradiol
EF	-	Enrofloxacin
EPC	-	Ethyl *N*-piperazine-carboxylate
FAC	-	Free available chlorine
FLU	-	Flumequine
HMBC	-	Heteronuclear Multiple Bond Correlation
HMQC	-	Heteronuclear Multiple Quantum Correlation
HSQC	-	Heteronuclear Single Quantum Correlation
IP	-	Ibuprofen
LM	-	Lincomycin
LTQ	-	Linear Trap Quadrupole
LZ water	-	Lake Zurich water
LZ1 water	-	Lake Zurich water spiked with 1 mg N/L of ammonia

LZ20 water	-	Lake Zurich water spiked with 20 mg N/L of ammonia
MBDCH	-	2-(3-methylbutyryl)-5,5-dimethyl-1,3-cyclohexandione
MIC$_x$	mg/L, or mol/L	Minimal inhibitory concentration, or the minimal concentration of an antibacterial compound at which x% inhibition of bacterial growth is observed, relative to maximal (i.e., uninhibited) growth
MP	-	1-methylpyrrolidine
NOESY	-	Nuclear Overhauser Effect Spectroscopy
Ox	-	Oxidant
*p*CBA	-	*para*-Chlorobenzoic acid
PEQ	-	Potency equivalent, or the residual antibacterial potency of an oxidant-treated sample of an antibacterial compound compared to the potency of an untreated sample of the same compound, defined as EC$_{50,0}$/EC$_{50,x}$, where EC$_{50,0}$ and EC$_{50,x}$ correspond to the EC$_{50}$ values measured for the untreated and treated samples, respectively
PFO	-	Pseudo-first-order
PG	-	Penicillin G (or benzylpenicillin)
PP	-	Propranolol
PV water	-	Phap Van water
RX	-	Roxithromycin
SFL		Stopped-flow
t-BuOH	-	*tert*-Butanol (or 2-methyl-2-propanol)
TET	-	Tetracycline
TRI	-	Triclosan
TMP	-	Trimethoprim
TMT	-	3,4,5-trimethoxytoluene
TYL	-	Tylosin
VM	-	Vancomycin
WWTP	-	Wastewater treatment plant
YP water	-	Yen Phu water

Symbol(s)	**Dimensions**	**Parameter(s)**
α_i	-	Degree of dissociation, or proportion of a given model compound present as a specific acid-base species, i
A	Absorbance units	Sample absorbance at a given wavelength (by spectrophotometric measurement)
A$_{max}$, A$_{min}$	Absorbance units	Maximum and minimum measured sample absorbances at a given wavelength (by spectrophotometric measurement), corresponding to positive and negative growth controls in microbiological assays

A_s	m^2/m^3	Specific interfacial area relative to volume of the effective reactive zone (Figure SA.1)
$A_{s,f}$	m^2/m^3	Specific interfacial area relative to full reactor volume
A_{xs}	m^2	Average cross-sectional area of effective reactive zone
$A_{xs,f}$	m^2	Average cross-sectional area of full reactor
$C_{O3(g)}$	g/m^3, mg/L	Gas-phase O_3 concentration
δ	m	Film thickness
d_{bubble}	m	Average gas bubble diameter (Sauter mean (*2*), in urine)
$D_{l,O3}$	m^2/s	O_3 aqueous-phase diffusion coefficient
$D_{l,S}$	m^2/s	Micropollutant aqueous-phase diffusion coefficients
ε_g	-	Gas holdup fraction within the effective reactive zone
$\varepsilon_{g,f}$	-	Gas holdup fraction distributed over full reactor volume
E	-	Enhancement factor for O_3 consumption by RMCs
E_i	-	Enhancement factor for instantaneous O_3 consumption by RMCs
$f_{(\tau)}$	-	Cumulative fractional proportion of observed oxidative transformation of a given model compound by a given oxidant (e.g., O_3 or $^{\bullet}OH$), when more than one oxidant is present, after reaction time, τ
η	-	Stoichiometric factor for moles of O_3 consumed per mole of model compound (substrate) consumed
Ha	-	Hatta number
h_l	m	Height of liquid volume in effective reactive zone
$h_{l,f}$	m	Height of full liquid volume in reactor
H_{O3}, H_{O2}	-	Dimensionless O_3 and O_2 solubility ratios ($C_{liquid\ phase}/C_{gas\ phase}$)
%I, I	%, -	Percent, or fraction, of growth inhibition, respectively
$\%I_{max}$, $\%I_{min}$, I_{max}, I_{min}	%, %. -, -	Maximum and minimum growth inhibitions measured for positive and negative growth controls in microbiological assays. Expressed either as percentages or fractions.
J_{O3}	$mol/(m^2 \cdot s)$	O_3 flux into film
$J_{S,\delta}$	$mol/(m^2 \cdot s)$	Micropollutant flux into film
k', $k'_{obs.}$, $k_{obs.}$	s^{-1}	First-order or pseudo-first-order rate constant
k'', k	$M^{-1}s^{-1}$	Elementary, or species-specific second-order rate constant
$k''_{app.}$, $k_{app.}$	$M^{-1}s^{-1}$	Apparent (pH-dependent) second-order rate constant
k'''	$M^{-2}s^{-1}$	Third-order rate constant
K_a	-	Acid-base equilibrium constant
$k_{L,O2}$	m/s	O_2 liquid mass transfer coefficient (in hydrolyzed urine)

$k_{L,O3}$	m/s	O_3 liquid mass transfer coefficient (in hydrolyzed urine)
$k'_{O_3,\mathrm{RMC}}$	s^{-1}	Pseudo-first-order rate constant for O_3 consumption by RMCs
N_{O3}	mol/(L·s)	O_3 absorption into film
$N_{S,\delta}$	mol/(L·s)	Micropollutant absorption into film
$[O_3]_{l,x}$	mol/L, mol/m^3	Liquid-phase O_3 concentration at point, x, within the film
$[O_3]_{l,eq}$	mol/L, mol/m^3	Liquid-phase O_3 equilibrium concentration
$[O_3]_{bulk}$	mol/L, mol/m^3	O_3 concentration in the bulk solution
Q_g	m^3/s	Gas flow rate through reactor
$R_{ct(t)}$	-	Time-dependent ratio of $^{\bullet}OH$ exposure to O_3 exposure, equivalent to $[^{\bullet}OH]/[O_3]$ at a specific time, t
$R_{ct(\tau)}$	-	Cumulative time-dependent ratio of $^{\bullet}OH$ exposure to O_3 exposure after reaction time, τ, or $\int_0^{\tau}[\bullet\,\mathrm{OH}]dt \Big/ \int_0^{\tau}[O_3]dt$
σ_p^+, σ_m^+, σ_o^+		Brown-Okamoto LFER terms accounting for the effects of *para*-, *meta*-, and *ortho*-substituents, respectively, on kinetics of electrophilic reactions of aromatic systems
u	m/s	Superficial gas velocity through the effective reactive zone
[X]	mol/L	Aqueous-phase concentration, where X = C, S, M, or P (with C, S, M, and P variously representing different types of model compounds, depending on the nomenclature of the corresponding thesis chapter). Unless otherwise specified, [C] can generally be taken as the molar concentration of any model compound.

Summary

The reactions of ozone (O_3) and hydroxyl radical ($^{\bullet}OH$) with each of fourteen clinical-use antibacterial compounds (from nine different structural families) and one general-use, non-clinical antibacterial compound (i.e., the biocide triclosan, or TRI) that are frequently detected in municipal wastewaters were characterized by a wide array of chemical and microbiological analytical techniques, to determine: (a) the kinetics of model compound oxidation by O_3 and $^{\bullet}OH$ - via measurement of second-order rate constants for each reaction, at various pH conditions, (b) at which specific structural moieties within the antibacterial compounds direct reactions with O_3 take place, and how these reaction sites correlate with structural moieties known to play a role in each antibacterial class' target-specific modes of antibacterial activity, (c) whether reactions with each oxidant result in elimination of the parent antibacterial compounds' biological activities, (d) if not, the identities and relative potencies of transformation products generated during reaction with either O_3 or $^{\bullet}OH$ that retain appreciable antibacterial acivity, (e) the kinetics with which such biologically-active products are oxidized by O_3 and $^{\bullet}OH$, and (f) ultimately, whether application of O_3-based oxidative treatment to municipal wastewater matrixes will be likely to result in rapid, efficient elimination of the antibacterial activities of the model compounds investigated here, as well as of structurally-analogous compounds from the same antibacterial structural classes.

In the first portion of this work, kinetics investigations demonstrated that each of the model clinical-use antibacterial compounds are oxidized by O_3 with apparent second-order rate constants, $k''_{O_3,app} > 1 \times 10^3$ $M^{-1}s^{-1}$, at pH 7, with the exception of *N*(4)-acetyl-sulfamethoxazole, for which $k''_{O_3,app}$ is 2.5×10^2 $M^{-1}s^{-1}$. $k''_{O_3,app}$ (pH 7) for macrolides, sulfamethoxazole, trimethoprim, tetracycline, vancomycin, and amikacin appear to correspond directly to oxidation of biochemically essential moieties. Initial reactions of O_3 with N(4)-acetylsulfamethoxazole, fluoroquinolones, lincomycin, and β-lactams do not lead to appreciable oxidation of biochemically essential moieties, although O_3 does attack such moieties within the fluoroquinolones and lincomycin via slower secondary reactions. During ozonation of a sample of secondary municipal wastewater effluent, measured losses were dependent on $k''_{O_3,app}$, but independent of $k''_{^{\bullet}OH,app}$. O_3 doses ≥3 mg/L yielded ≥99% depletion of fast-reacting substrates ($k''_{O_3,app} > 5 \times 10^4$ $M^{-1}s^{-1}$). Ten substrates reacted predominantly

with O_3; only four were oxidized predominantly by $^{\bullet}OH$. These results indicate that many antibacterial compounds will be oxidized in wastewater via selective reactions with O_3.

In the second part of this work, oxidation of TRI by O_3 was investigated to determine reaction kinetics, reaction site(s), and consequent changes in TRI's antibacterial activity. TRI was found to react very rapidly with O_3 at circumneutral pH (i.e., $k''_{O_3,\mathrm{app}} = 3.8 \times 10^7$ $M^{-1}s^{-1}$ at pH 7). The observed positive dependence of $k''_{O_3,\mathrm{app}}$ on pH, comparison of TRI reactivity toward O_3 with that of other phenolic model compounds, and correlation of the elementary k_{O_3} values for neutral and anionic TRI to phenol ring substituent effects (via Brown-Okamoto correlation with other substituted phenols), are all consistent with electrophilic attack by O_3 at the TRI phenol ring. Biological assay of O_3-treated TRI solutions indicated that reaction with O_3 yields efficient elimination of TRI's antibacterial activity. TRI oxidation was also investigated during ozonation of effluent samples from two conventional wastewater treatment plants. Nearly 100% TRI depletion was achieved for a 4 mg/L (8.3×10^{-5} mol/L) O_3 dose applied to a wastewater containing 7.5 mg/L of DOC, and ~58% TRI depletion for dosage of 6 mg/L (1.3×10^{-4} mol/L) O_3 to a wastewater containing 12.4 mg/L of DOC. At O_3 doses greater than 1 mg/L (2.1×10^{-5} mol/L), $^{\bullet}OH$ reactions accounted for <35% of observed TRI losses in these wastewaters, indicating that TRI oxidation was due primarily to the direct TRI-O_3 reaction, which leads to deactivation of TRI.

In the third part of the investigation, microbiological assays were developed to quantify the resulting changes in antibacterial potencies during treatment of the model clinical-use antibacterial molecules investigated in the first portion of this work with increasing doses of O_3 and $^{\bullet}OH$, as well as during treatment of TRI with increasing $^{\bullet}OH$ exposures. Potency measurements were determined from dose-response relationships obtained by exposing *E. coli* or *B. subtilis* reference strains to treated samples of each antibacterial compound via broth micro- or macrodilution assays, and related to the measured residual concentrations of parent antibacterial in each sample. Data obtained from these experiments show that O_3 and $^{\bullet}OH$ reactions lead in nearly all cases to stoichiometric elimination of antibacterial activity (i.e., loss of one mole equivalent of potency per mole of parent compound consumed) for the clinical-use antibacterial compounds and for TRI. The β-lactams penicillin G (PG) and cephalexin (CP) represent the only two exceptions, as bioassay measurements indicate that the direct reaction of these two compounds with O_3 leads to formation of biologically active transformation products. Nevertheless, these data, coupled with knowledge of ozonation process data at the pilot- and full-scale, suggest that wastewater ozonation will generally yield sufficient structural modification of the investigated antibacterial molecules to eliminate their antibacterial activities, whether oxidation results from selective reactions with O_3 or from relatively non-selective reactions with incidentally-produced $^{\bullet}OH$.

In the fourth and final component of this work, O_3 reaction kinetics and pathways were evaluated in depth for the two β-lactam antibacterial compounds - PG and CP - found to yield biologically active products upon direct reaction with O_3. PG was found to yield two major products in nearly equal yields, together accounting for approximately 100% of the parent compound consumption. These two products were purified and isolated by C_2 reversed-phase silica gel chromatography, followed by freeze-drying, and identified by extensive chromatographic, MS/MS, multi-nuclear NMR, and FT-IR analyses as the stereoisomeric (*R*)- and (*S*)-sulfoxides of PG. The former of these was determined to retain roughly 15% of the potency of the parent PG molecule, whereas the latter was functionally inactive. Each of the PG sulfoxides was determined to be recalcitrant toward further oxidation by O_3. However, the (*R*)-sulfoxide was readily transformed by $^{\bullet}OH$ (with $k''_{\bullet\mathrm{OH,app}} = 7.4 \times 10^9\ \mathrm{M^{-1}s^{-1}}$, at pH 7), resulting in roughly quantitative elimination of its biological activity. CP was found to yield four major transformation products. These were identified after purification by C_{18} reversed-phase silica gel chromatography and isolation via freeze-drying as the (*R*)- and (*S*)-sulfoxides of CP (formed in ~34% and ~18% yields) and two C-2/C-3 double bond cleavage products (formed in ~5% and ≥28% yields); one a structural analogue of the penicilloic acid of CP - formed by intermolecular nucleophilic attack of H_2O on the electrophilic C-8 carbon of the CP β-lactam ring, and the other a 7-piperazine-8,12-dione containing rearrangement product - formed by intramolecular nucleophilic attack of the N-18 amino nitrogen on the same carbon. As in the case of PG, the (*R*)-sulfoxide of CP was found retain considerable biological activity (~85% that of the parent CP molecule), whereas each of the three other CP transformation products was determined to be functionally inactive. CP-(*R*)-sulfoxide was found to be susceptible to further oxidation by both O_3 and $^{\bullet}OH$ (with $k''_{\mathrm{O_3,app}} = 2.6 \times 10^4\ \mathrm{M^{-1}s^{-1}}$ and $k''_{\bullet\mathrm{OH,app}} = 7.6 \times 10^9\ \mathrm{M^{-1}s^{-1}}$, at pH 7), leading to approximately quantitative elimination of antibacterial activity in each case. These results, when evaluated in the context of the reaction kinetics measured for oxidation of PG, CP, and their O_3-derived transformation products, suggest that the antibacterial activities of these representative β-lactams, as well as the activities of many structurally-analogous penicillins and cephalosporins, should be effectively eliminated during ozonation of municipal wastewaters.

In summary, the results obtained from this investigation demonstrate that, not only are most antibacterial molecules rapidly oxidized during ozonation of municipal wastewater by selective reactions with O_3, but that these reactions generally occur at target sites for which structural modification by O_3 results in quantitative loss of the parent antibacterial molecules' mode-specific biological activities. Furthermore, oxidation of every antibacterial molecule included in this investigation by $^{\bullet}OH$ - which will be produced in high yield during any wastewater ozonation process - led to nearly quantitative elimination of the model antibacterials' biological activities. In the only cases for which biological activities were not eliminated via the initial reaction with O_3 – that is, for the two β-lactams PG and CP – the biologically active (*R*)-sulfoxide products formed in these reactions could be further oxidized by either O_3 (CP-(*R*)-sulfoxide only) or $^{\bullet}OH$ (both CP-(*R*)-sulfoxide and PG-(*R*)-sulfoxide) to inactive products. These findings, when taken into consideration with additional operational data obtained here and in other investigations of municipal wastewater ozonation, suggest that effectively complete deactivation of nearly every major antibacterial structural class will be achieved at the 5-10 mg/L O_3 doses typically required to achieve close to 100% depletion of such antibacterial molecules in such matrixes. This in turn leads to the more general conclusion that wastewater ozonation can now be expected to provide a robust, relatively efficient barrier to discharge of biologically-active antibacterial compounds - which are, outside of steroiod hormones, one of the most potent biologically-active sub-classes of micropollutants known to be present in wastewaters.

Zusammenfassung

Die Reaktionen von Ozon (O_3) und Hydroxylradikalen ($^{\bullet}OH$) mit vierzehn in klinischen Anwendungen eingesetzten Antibiotika aus neun verschiedenen Substanzklassen sowie einem breit verwendeten Biozid (Triclosan oder TRI), welche häufig in Kläranlagenabwässern nachgewiesen werden, wurden mit einer Vielzahl von chemischen und mikrobiologischen Methoden unter folgenden Aspekten untersucht: (a) Bestimmung der Kinetik von antibakteriellen Modellsubstanzen bei der Oxidation durch O_3 und $^{\bullet}OH$ mittels Messung der Zweitordnungs-Geschwindigkeitskonstanten unter verschiedenen pH-Bedingungen; (b) Bestimmung des spezifischen Angriffspunkts von O_3 bei den jeweiligen Modellsubstanzen und Vergleich dieser Stellen mit funktionellen Gruppen, welche für ihre antibakterielle Aktivität bekannt sind; (c) demzufolge Untersuchung, ob Reaktionen mit O_3 oder $^{\bullet}OH$ zur Eliminierung der antibakteriellen Aktivität der Modellsubstanzen führen, und (d) – falls dies nicht der Fall ist - Identifikation und Bestimmung der antibakteriellen Potenz von bioaktiven Umwandlungsprodukten, welche durch Reaktionen mit O_3 oder $^{\bullet}OH$ gebildet wurden, sowie (e) Bestimmung der Kinetik von solchen bioaktiven Produkten in Reaktionen mit O_3 und $^{\bullet}OH$ und (f) schliesslich Evaluation, ob die Verwendung von ozonbasierten Oxidationsverfahren in der Abwasserreinigung rasch und effizient zu einer Elimination der antibakteriellen Aktivität der untersuchten Modellsubstanzen sowie strukturähnlicher Stoffe derselben Substanzklassen führen kann.

Im ersten Teil dieser Arbeit konnte gezeigt werden, dass alle untersuchten antibakteriellen Modellsubstanzen aus klinischen Anwendungen bei pH 7 durch Ozon mit scheinbaren Zweitordnungs-Geschwindigkeitskonstanten $k''_{\mathrm{O_3,app}}$ grösser als 1×10^3 $M^{-1}s^{-1}$ oxidiert wurden, ausser *N*(4)-Acetylsulfamethoxazol, welches ein $k''_{\mathrm{O_3,app}}$ von 2.5×10^2 $M^{-1}s^{-1}$ aufwies. Die Geschwindigkeitskonstanten $k''_{\mathrm{O_3,app}}$ (pH 7) für Makrolide, Sulfonamide, Trimethoprim, Tetracycline, Vancomycin und Amikacin scheinen direkt mit der Oxidation der jeweiligen biochemisch aktiven Struktur im Molekül zu korrelieren. Bei N(4)-Acetylsulfamethoxazol, Fluoroquinolonen, Lincomycin und β-Lactamen hingegen führten die Initialreaktionen von O_3 nicht zu einer wesentlichen Oxidation solcher aktiven Strukturen, obwohl O_3 diese Stellen in langsameren Sekundärreaktionen angreifen kann. Die Elimination der untersuchten Substanzen während der Ozonung einer Probe aus dem sekundären Kläranlagenablauf hing von $k''_{\mathrm{O_3,app}}$ ab, war aber unabhängig von $k''_{\mathrm{^{\bullet}OH,app}}$. Ozondosen ≥3 mg/L führten zu einem ≥99-prozentigen Abbau von schnell reagierenden Modellsubstanzen

($k''_{O_3,app} > 5 \times 10^4$ M^{-1}s^{-1}). Zehn Modellsubstanzen wurden hauptsächlich durch O$_3$ oxidiert, während lediglich vier Substanzen vorwiegend mit $^{\bullet}$OH reagierten. Aufgrund dieser Ergebnisse kann davon ausgegangen werden, dass viele antibakterielle Substanzen im Abwasser durch selektive Reaktionen mit O$_3$ oxidiert werden.

Im zweiten Teil dieser Arbeit wurde die Oxidation von TRI durch O$_3$ erforscht, um die Reaktionskinetik, reaktive Stellen im Molekül und nachfolgende Veränderungen der Bioaktivität von TRI zu bestimmen. Es konnte gezeigt werden, dass TRI bei neutralen pH-Bedingungen sehr schnell mit O$_3$ reagiert ($k''_{O_3,app} = 3.8 \times 10^7$ M^{-1}s^{-1} bei pH 7). Die beobachtete pH-Abhängigkeit von $k''_{O_3,app}$, der Vergleich der O$_3$-Reaktivität von TRI mit anderen phenolischen Molekülen sowie die Korrelation der spezifischen k_{O_3}-Werte von neutralem und anionischem TRI mit Substitutionseffekten am Phenolring (via Brown-Okamoto-Korrelation mit anderen substituierten Phenolen) deuten alle auf einen elektrophilen Angriff von O$_3$ auf den TRI-Phenolring hin. Mikrobiologische Untersuchungen zeigten ferner, dass die Reaktion von TRI mit O$_3$ zu einer effizienten Elimination der Bioaktivität von TRI führt. Daneben wurde auch die Oxidation von TRI während der Ozonung von Abwasserproben, welche aus dem Ablauf von zwei verschiedenen Kläranlagen entnommen wurden, untersucht. Im einen Ablauf mit 7.5 mg/L DOC wurde bei einer O$_3$-Dosis von 4 mg/L (8.3×10^{-5} mol/L) ein beinahe 100-prozentiger TRI-Abbau beobachtet, während ungefähr 58% TRI-Abbau beim anderen Ablauf mit 12.4 mg/L DOC und einer O$_3$-Dosis von 6 mg/L (1.3×10^{-4} mol/L) erzielt wurden. Bei O$_3$-Dosen $\geq$ 1 mg/L (2.1×10^{-5} mol/L) trugen Reaktionen mit $^{\bullet}$OH weniger als 35% zum gemessenen TRI-Abbau in diesen Abwässern bei. Diese Ergebnisse deuten darauf hin, dass die Oxidation und entsprechend auch Deaktivierung von TRI hauptsächlich auf direkte Reaktionen mit O$_3$ zurückzuführen sind.

Im dritten Teil dieser Studie wurden mikrobiologische Methoden entwickelt, um Veränderungen der antibakteriellen Potenz der klinischen Modellsubstanzen aus dem ersten Teil dieser Arbeit in Abhängigkeit von O$_3$- und $^{\bullet}$OH-Exposition sowie Veränderungen der Bioaktivität von TRI mit steigenden $^{\bullet}$OH-Expositionen zu quantifizieren. Als Grundlage für die Potenzmessungen dienten Dosis-Wirkungsbeziehungen, welche durch Exposition von Referenzstämmen (*E. coli* oder *B. subtilis*) mit oxidierten Lösungen der jeweiligen Modellsubstanzen erstellt und mit der Restkonzentration des Wirkstoffes in der Probe korreliert wurden. Diese Versuche ergaben in nahezu allen Fällen eine stöchiometrische Elimination der antibakteriellen Aktivität (d.h. Verlust von einem Mol-Äquivalent Potenz beim gleichzeitigen Verlust von einem Mol Substanz) bei Reaktionen von O_3 und $^{\bullet}OH$ mit klinischen Antibiotika und TRI. Die *β*-Lactame Penicillin G (PG) und Cephalexin (CP) bildeten die einzigen Ausnahmen, da die direkte Reaktion von O_3 mit diesen zwei Molekülen zur Bildung von bioaktiven Umwandlungsprodukten führte. Dennoch lassen diese Daten – in Kombination mit dem Prozessverständnis von Ozonreaktoren in Pilot- und Grossanlagen – den Schluss zu, dass die Ozonung von Abwässern im allgemeinen genügend strukturelle Veränderungen an den untersuchten Modellsubstanzen hervorrufen wird, um deren antibakterielle Wirkung zu eliminieren. Dabei spielt es keine Rolle, ob die Oxidation hauptsächlich durch selektive Reaktionen mit O_3 oder vergleichbar unselektiven Reaktionen mit $^{\bullet}OH$ zustande kommt.

Im vierten und letzten Teil dieser Studie wurden die Kinetik sowie Reaktionspfade für die Reaktion von O_3 mit den zwei *β*-Lactamen PG und CP, welche zu teils bioaktiven Umwandlungsprodukten oxidiert werden, detailliert untersucht. Die Oxidation von PG ergab zwei Hauptprodukte, welche zu ungefähr gleichen Anteilen zusammen knapp 100% des beobachteten Abbaus der Muttersubstanz ausmachen. Diese zwei Produkte wurden per C_2 Reversed-phase-Chromatographie gefolgt von Gefriertrocknung gereinigt und isoliert. Mit Hilfe verschiedener analytischer Verfahren (chromatographische Analysen, MS/MS, ^{1}H-, ^{13}C-, und ^{15}N-NMR, sowie FT-IR Analysen) konnten die Produkte als die (*R*)- und (*S*)-Stereoisomere der PG-Sulfoxide identifiziert werden. Das PG-(*R*)-Sulfoxid behielt noch ~15% der Potenz der Muttersubstanz PG, während das PG-(*S*)-Sulfoxid als funktionell inaktiv befunden wurde. Die beiden PG-Sulfoxide reagierten nicht weiter mit O_3, jedoch konnte das PG-(R)-Sulfoxid rasch mit $^{\bullet}OH$ abgebaut ($k''_{\bullet\mathrm{OH,app}} = 7.4 \times 10^{9}\ \mathrm{M^{-1}s^{-1}}$, bei pH 7) und somit annähernd quantitativ deaktiviert werden. Im Falle von CP wurden vier verschiedene Oxidationsprodukte identifiziert. Diese wurden per C_{18} Reversed-phase-Chromatographie gefolgt von Gefriertrocknung gereinigt und isoliert. Die anschliessenden Analysen ergaben für die CP-Produkte zwei CP-(*R*)- und (*S*)-Sulfoxide (in ~34% and ~18% Ertrag) und zwei Spaltungsprodukte der C-2/C-3-Doppelbindung (in ~5% and ≥28% Ertrag). Von den letzteren beiden wurde das eine Spaltungsprodukt als ein Strukturanalog von CP-Penicilloinsäure identifiziert, welches durch einen intermolekularen nukleophilen Angriff von H_2O auf den elektrophilen C-8 Kohlenstoff des *β*-Lactamringes gebildet wurde, während das andere Spaltungsprodukt 7-Piperazine-8,12-dion enthielt, gebildet durch einen intramolekularen nukleophilen Angriff des N-18 Amino-Stickstoffes auf denselben Kohlenstoff. Wie im Fall von PG konnte gezeigt werden, dass das (*R*)-Sulfoxid von CP eine erhebliche antibakterielle

Aktivität behielt (~85% der CP-Muttersubstanz), während die drei anderen Produkte grundsätzlich inaktiv waren. Das CP-(*R*)-Sulfoxid konnte sowohl mit O_3 als auch ${}^{\bullet}OH$ weiter oxidiert werden (mit $k''_{O_3,app} = 2.6 \times 10^4\ M^{-1}s^{-1}$ und $k''_{\bullet OH,app} = 7.6 \times 10^9\ M^{-1}s^{-1}$, bei pH 7), was in beiden Fällen zu einer ungefähr quantitativen Eliminierung der antibakteriellen Aktivität führte. Diese Ergebnisse zeigen, dass die antibakterielle Aktivität von den repräsentativen *β*-Lactamen PG und CP sowie von vielen anderen strukturähnlichen Penicillinen und Cephalosporinen während der Ozonung von Abwässern weitgehend eliminiert werden sollte.

Zusammengefasst zeigen die Ergebnisse dieser Studie, dass die meisten antibakteriellen Stoffe während der Ozonung von Abwasser durch selektive Reaktionen mit O_3 nicht nur oxidiert, sondern auch soweit umgewandelt werden, dass sie schliesslich biologisch inaktiv sind. Darüber hinaus führte auch die Reaktion mit ${}^{\bullet}OH$ – welche bei der Ozonung von Abwasser mit hoher Ausbeute gebildet werden – zu einer nahezu quantitativen Deaktivierung der untersuchten Substanzen. In den beiden einzigen Fällen, bei welchen die antibakterielle Wirkung nicht direkt durch Initialreaktionen mit O_3 eliminiert wurde - nämlich bei den *β*-Lactamen PG und CP, sind die bioaktiven Produkte trotzdem per O_3 (im Falle des CP-(*R*)-Sulfoxids) oder ${}^{\bullet}OH$ (CP-(*R*)-Sulfoxid and PG-(*R*)-Sulfoxid) leicht deaktivierbar. Unter Berücksichtigung von zusätzlichen Prozessdaten aus dieser und anderen Studien über die Ozonung von Abwasser kann davon ausgegangen werden, dass bei O_3-Dosen von 5-10 mg/L, welche typischerweise für einen nahezu vollständigen Abbau der Muttersubstanzen gebraucht werden, eine komplette Deaktivierung von fast allen antibakteriellen Substanzklassen erreicht wird. Somit stellt die Ozonung eine zuverlässige und effiziente Barriere zur Elimination von bioaktiven antibakteriellen Substanzen aus Abwässern dar.

Chapter 1. Background and General Introduction

1.1 Overview

Dissemination of antibacterial resistance amongst pathogenic bacterial populations has contributed to gradually decreasing effectiveness of nearly all classes of medically-important antibacterial agents in treatment of bacterial illnesses since shortly after introduction of the first clinically-useful antibacterials (sulfonamides) during the first half of the 20th century *(1,2*). While some experts within the medical microbiology community suggest that diminished antibacterial efficacy is an unavoidable consequence of current medical doctrine *(3*), others are in agreement that certain steps can be taken to mitigate the diminishing susceptibility of many bacteria toward antibacterial agents *(1,2*). Thus far, discussion of strategies to slow the dissemination of antibacterial resistance has focused primarily on remedial efforts relevant to medical practice *(4,5*), drug design *(1,6*), or veterinary medicine *(7*). However, frequent detection of antibacterial compounds *(8-15*) and resistant bacterial strains *(16-27*) within many compartments of natural and engineered aquatic ecosystems indicates that the physical interconnection of clinical environments (e.g., hospitals, nursing homes) with aquatic systems (primarily via municipal wastewater collection systems) could also represent an important – yet potentially preventable – factor in promotion of antibacterial resistance within sensitive antibacterial populations. Notable aspects of the likely interactions amongst clinical and aquatic environments can be summarized as follows (see Scheme 1.1 for hypothesized spatial and temporal topologies):

1. Consumption of antibacterial agents by patients can lead to very high dissolved concentrations of antibacterial agents within their extravascular fluids *(28*) – particularly urine *(28,29*) – in turn creating environments in which evolution of resistant bacterial genotypes can occur via selection, chromosomal mutation, or a number of gene transfer mechanisms *(2,30-33*).
2. Many of the antibacterial classes currently in wide clinical use are excreted largely unmetabolized in both urine and feces *(29,34*). Furthermore, large quantities of resistant enteric bacteria can be excreted in the feces *(30*).
3. In the absence of pre-treatment measures, collection of wastewater from locations such as hospitals or nursing homes (where frequency of medicinal therapy is high) may result in significant point discharges (to municipal wastewater collection systems) of antibacterial residues *(12,35,36*) and antibiotic resistant bacteria (ARB) *(37-41*).
4. The presence of resistant bacterial genotypes in sewage, coupled with the presence of elevated antibacterial concentrations, could maintain environments similar to those

Scheme 1.1. Hypothetical environmental transport of antibiotic resistant bacteria, antibacterial agent residues, and resistance genes

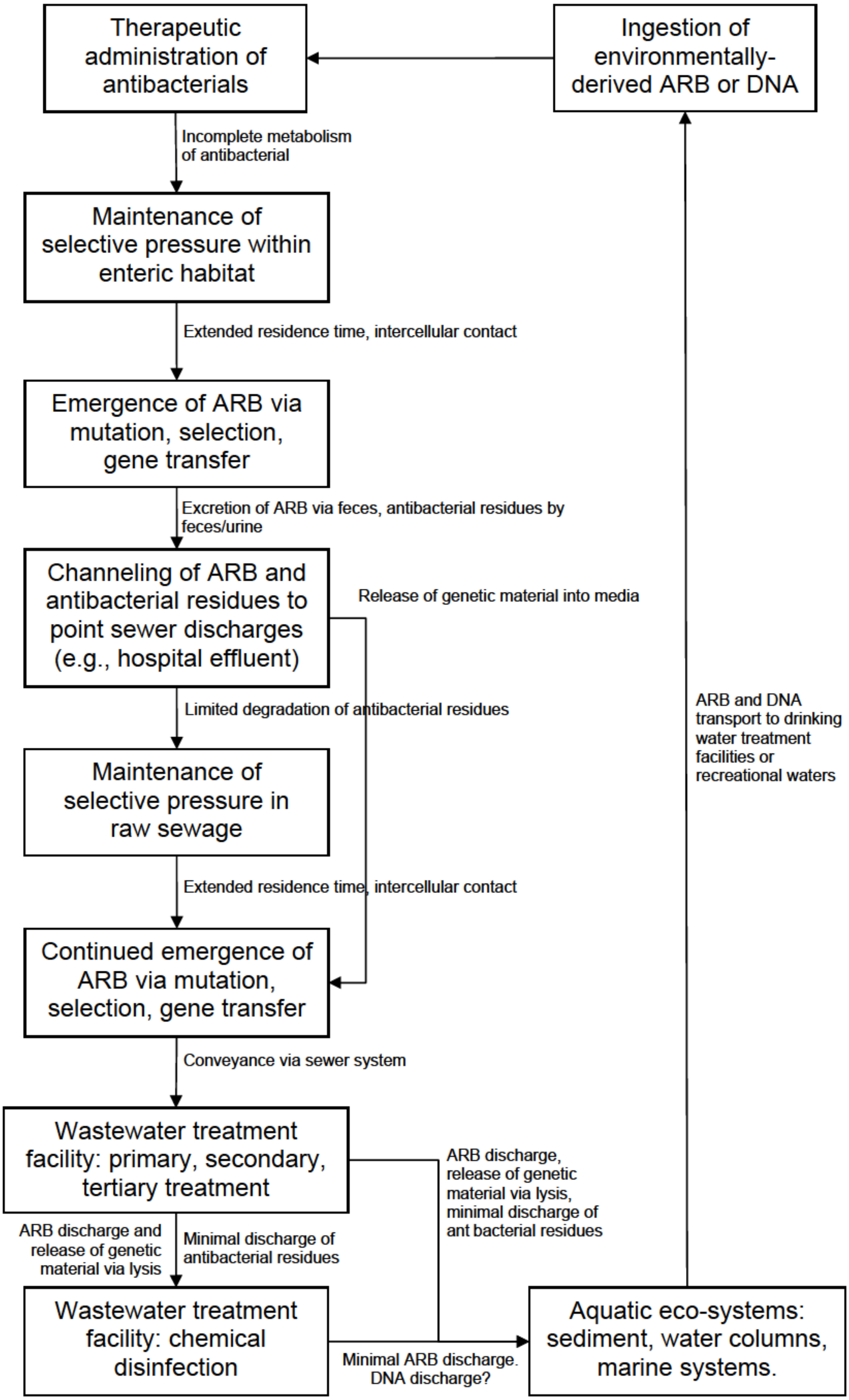
Therapeutic administration of antibacterials
Ingestion of environmentally-derived ARB or DNA
Incomplete metabolism of antibacterial
Maintenance of selective pressure within enteric habitat
Extended residence time, intercellular contact
Emergence of ARB via mutation, selection, gene transfer
Excretion of ARB via feces, antibacterial residues by feces/urine
Channeling of ARB and antibacterial residues to point sewer discharges (e.g., hospital effluent)
Release of genetic material into media
Limited degradation of antibacterial residues
Maintenance of selective pressure in raw sewage
Extended residence time, intercellular contact
Continued emergence of ARB via mutation, selection, gene transfer
Conveyance via sewer system
ARB and DNA transport to drinking water treatment facilities or recreational waters
Wastewater treatment facility: primary, secondary, tertiary treatment
ARB discharge, release of genetic material via lysis, minimal discharge of ant bacterial residues
ARB discharge and release of genetic material via lysis
Minimal discharge of antibacterial residues
Wastewater treatment facility: chemical disinfection
Minimal ARB discharge. DNA discharge?
Aquatic eco-systems: sediment, water columns, marine systems.

present *in vivo*, providing conditions that are potentially suitable for shifts of sensitive bacterial populations toward antibacterial resistance.

5. Cellular lysis or active DNA release processes could also lead to accumulation of extracellular resistance gene-containing DNA on surfaces or in biofilms within such systems *(42-44*).
6. Should accumulated DNA retain its transformational capacity, competent bacteria could potentially incorporate this material into their own genomes via natural transformation *(42*).
7. ARB – capable of maintaining antibacterial resistance phenotypes for many generations in the absence of selective pressure *(45-47*) – could be transported from point sources such as hospital sewage to downstream wastewater treatment facilities.
8. During passage through disinfection processes, absolute numbers of ARB would be significantly reduced, but the genetic heritage of the pre-disinfection population might survive via protection of DNA on surfaces, in biofilms, or within cellular material. Some of this genetic material might be discharged to the environment, where it could remain stable for periods of hours to weeks *(42*).
9. In the absence of disinfection processes, wastewater-derived ARB could be discharged into surface waters in high numbers.
10. Environmental bacteria strains could incorporate such DNA into their genomes *(42,48,49*), thereby inheriting resistance characteristics originally derived from clinically-relevant bacteria populations.
11. After disinfection, ARB surviving the wastewater treatment process might compete effectively enough with native environmental strains to recover to pre-treatment population sizes after discharge into receiving waters *(45,46*).
12. Either ARB, their genetic resistance determinants, or both might be transported downstream to locations from which they could re-enter the clinical environment (e.g., drinking water intakes or water recreation areas).

Antibacterial resistance gene pools could thereby be propagated via repeated passage through such a loop, resulting in gradually increasing incidences of resistance. This possibility clearly merits evaluation of options for minimizing the passage of ARB, their associated resistance genes, and the chemical stressors contributing to the emergence and dissemination of antibacterial resistance, into the aquatic environment.

The present work addresses the application of ozonation as a barrier to passage of chemical antibacterial resistance determinants (i.e., antibacterial agents) from municipal wastewaters to downstream aquatic environments. Specifically, this project addresses two primary issues critical to evaluating the utility of wastewater ozonation in this context: (1) Reaction kinetics and efficiency of ozone oxidation processes in removing selective pressure (i.e., antibacterial residues) from environmental systems and (2) Effects of ozone-mediated structural transformations on the residual biochemical potency of oxidized antibacterial molecules. Relevant background and important details of the investigations conducted during this work are provided in the following sections.

1.2. Detection of Antibiotic Resistant Bacteria in Municipal Wastewater Systems

Antibiotic resistant bacteria (ARB) have been detected within numerous samples of raw sewage (*16-19*) and treated municipal wastewater (*20,21*). Alcaide and Garay (1984) found that – of 865 *Salmonella* isolates (mixed samples obtained from a wastewater treatment plant and nearby eutrophic coastal lagoon) tested for resistance to tetracycline, ampicillin, chloramphenicol, streptomycin, kanamycin, and amoxicillin (all at broth concentrations of 25 μg/L) – 12.7% were resistant to one or more compounds (*20*). 63.4% of these were multiply antibacterial resistant (MAR). Furthermore, the investigators demonstrated that all resistance phenotypes except for streptomycin were transferable to a recipient *Escherichia coli* strain. Heier and Tschäpe (1984) discovered that 70.2% and 86.7% of a subset of ARB isolates taken from municipal wastewaters and hospital sewages, respectively, were MAR (*17*). Tschäpe et al. (1986) found correlations amongst initiation of gentamicin, trimethoprim, and streptomycin usage in human medicine, veterinary medicine, and animal husbandry and increase of plasmid-encoded resistance to these agents in municipal wastewaters surveyed between 1979 and 1982 (*18*). Guardabassi et al. (1999) noted a measurable increase in the incidence of ARB bacteria from upstream to downstream of a pharmaceutical manufacturing plant discharge point in raw sewage (*19*). In subsequent studies, Guardabassi et al. (2002) observed small increases in ampicillin resistant presumptive coliform isolates from influent to effluent of two wastewater treatment facilities (51.4% to 60.3% and 47.7% to 50.5%), while decreases or no significant changes were observed in incidence of resistance to gentamicin and tetracycline (*21*). In addition, these researchers found small increases in prevalence of *Acinetobacter spp.* resistance to tetracycline and aztreonam, while data for other antibacterials tested showed either conflicting results, decreases, or no significant changes. Absolute prevalence of coliform and *Acinetobacter spp.* resistance to ampicillin centered around 50% and between 20% to 40%, respectively. Resistance to tetracycline and gentamicin ranged from 5% to app. 15%, and 0% to app. 5%, respectively, for both types of isolates. Prevalences up to 45%, 12%, 22%, 18%, 6%, and 10% were noted for resistances of *Acinetobacter spp.* isolates to aztreonam, cefotaxime, cefoxitin, ciprofloxacin, chloramphenicol, nalidixic acid, respectively, in wastewaters effluents. Wastewater underwent solids screening, grit removal, primary clarification, nutrient removal (via activated sludge), and secondary clarification at either plant before discharge.

Schwartz et al. (2002) isolated colonies of bacteria exhibiting resistance to various antibacterials from biofilms obtained from a hospital sewage system. Results of their study indicated that 7%, 45%, 58%, 71%, and 8% of such isolates were resistant to vancomycin, ceftazidime, ceftazolin, pencillin G, and imipenem, respectively. Furthermore, they found that 15%, 27%, 39%, and 20% isolates from biofilms obtained at the outlet of a wastewater treatment plant were resistant to vancomycin, ceftazidime, ceftazolin, and penicillin G, respectively. Reinthaler et al. (2003) studied the antibacterial resistance profiles of 767 *E. coli* isolates from sewage and wastewater sludge samples in southern Austria, with respect to a battery of 16 different antibacterials. These investigators found that a number of bacteria in various wastewater compartments (e.g., influent, sludge, effluent) were resistant to the penicillins (up to 18% for resistance to ampicillin), cephalosporins (up to 35% for cefolathin), quinolones (up to 15% for nalidixic acid), tetracyclines (up to 57% for tetracycline), and co-trimoxazole (up to 13%), in wastewaters derived from three different activated sludge facilities. No increase in resistance levels was found in correlation to wastewater passage through various treatment processes. The highest proportions of ARB relative to 14 of the 16 antibacterial compounds studied were observed in samples from a plant which processes hospital and nursery home waste in addition to municipal sewage (*22,50*). Rhodes et al. (2000) recently identified a link between plasmids rRAS1 (originally isolated from aquacultural operations in Scotland and Norway) and PIE420 (isolated from an E. coli strain obtained from a German hospital), noting that all fragments hybridized together, and that the two plasmids (which contain tetracycline resistance determinants) exhibited identical restriction fragment length polymorphism (RFLP) profiles, a finding that lends strong support to the hypothesized interconnectivity of even geographically distant clinical and aquatic environments. A contradictory result was obtained from a study conducted by Guardabassi et al. (2000), in which in vitro conjugative transfer of various tetracycline determinants from clinical to aquatic *Acinetobacter* spp. could not be achieved, although transfer of tetracycline resistance determinants between ecologically dissimilar aquatic *Acinetobacter* strains was observed (*23*).

1.3. Detection of Antibacterial Residues in Municipal Wastewaters

One of the earliest comprehensive surveys of antibacterials in aquatic environmental compartments was produced by Hirsch et al. (1999), in a study assessing the occurrence of antibacterial compounds in German wastewaters, surface waters, and groundwaters (*9*). The investigators found that roxithromycin, sulfamethoxazole, and trimethoprim were detectable at mean concentrations of 1.0, 2.0, and 0.66 μg/L in wastewater treatment facility effluents. Clarithromycin and chloramphenicol were also detected, at maximum concentrations of 0.24 and 0.56 μg/L. The inability to detect any of the tetracyclines and β-lactams included in the analytical methods of this study was attributed to the instability of β-lactams toward water (as they hydrolyze relatively quickly in aqueous solution), or the facile complexation or adsorption of tetracyclines to metal cations and sediments (respectively). An additional study conducted in the same year verified these results with regard to sulfonamide concentrations, yielding measured concentrations of up to 2.46 and 1.5 μg/L for sulfamethoxazole in primary and secondary wastewater effluent samples, respectively (*51*).

Fluoroquinolone antibacterial agents have recently been detected at relatively high concentrations within various wastewaters (*8,52,53*). Hospital wastewaters apparently (though not surprisingly) represent a significant source of these compounds, according to results obtained by Hartmann et al. (1998), as concentrations of ciprofloxacin ranging from 3 to 87 μg/L were found in sewage derived from hospital wastewater discharges (*8*) (MICs as low as 0.002 mg/L have been reported for ciprofloxacin (*54*)). Subsequent studies have indicated that the fluoroquinolones are relatively persistent with respect to removal from wastewater. Observed concentrations of ciprofloxacin in raw sewage (obtained from sewer systems in various Swiss locales) span the range between 0.313 and 0.568 μg/L (norfloxacin was detected in quantities ranging from 0.255 to 0.553 μg/L) (*53*). Golet et al. (2001, 2002, 2003) reported similar ciprofloxacin concentrations between 0.249 and 0.405 μg/L for samples of primary wastewater effluent, and between 0.045 and 0.108 μg/L for secondary wastewater effluent (concentrations of norfloxacin obtained during the same study paralleled those of ciprofloxacin) (*11,52,53*). The results of these and a number of more recent investigations focusing on antibacterial compound concentrations and fate during wastewater treatment are summarized in Figure 1.1, which also compares the reported concentrations with available measurements of effect levels for various reference bacterial strains.

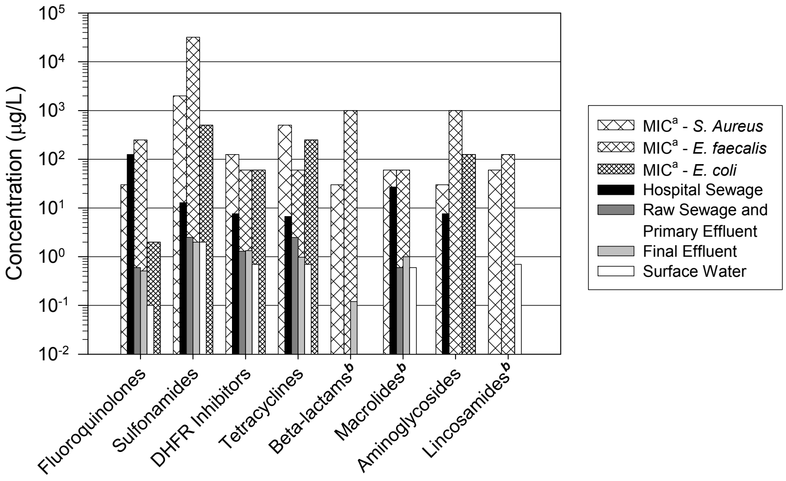

Figure 1.1. Maximum single-compound* concentrations of various antibacterial classes detected in municipal wastewater systems and surface waters, in the context of minimum reported clinical MIC values for sensitive bacterial reference strains. Data for fluoroquinolones (*10,11,13,14,35,36,55*), sulfonamides (*9,10,13,14,36,51,55,56*), DHFR (dihydrofolate reductase) inhibitors (*9,10,14,36,55,57,58*), tetracyclines (*10,36,58*), *β*-lactams (*15*), macrolides (*10,13,55,56,59,60*), aminoglycosides (*12*), and lincosamides (*10*) was obtained from various environmental analytical studies. [a]MIC – minimal inhibitory concentration, or minimal concentration resulting in a measurable reduction in bacterial growth relative to an antibacterial blank. MICs listed for each class correspond (in order from left to right) to reported values for ciprofloxacin, sulfamethoxazole, trimethoprim, tetracycline, penicillin, erythromycin, gentamicin, and clindamycin, respectively (*61*), [b]MIC values not reported for *E. coli*. *More than one compound from a given antibacterial class may be present in the same municipal wastewater.

1.4. Selection for Antibacterial Resistance

Pre-existing bacterial genotypes may contain information that imparts intrinsic resistance to various antibacterial compounds. Such modes of antibacterial resistance likely evolved during the course of many bacterial generations from some chance mutation in the past. Accordingly, these resistance genotypes – whether induced by the antibacterials to which they impart resistance or not – likely result from the same mechanism as that which yields new modes of resistance. However, as such intrinsic resistance traits are pre-existing, drugs can be tailored to the treatment of organisms based on the organisms' intrinsic susceptibilities. For example, enterocci are intrinsically resistant to all clinically available cephalosporins (*62*), and so this particular class of antibacterials is not used in treatment of associated infections. Thus, intrinsic resistance is not a problem with regard to the issue of antibacterial resistance dissemination; it simply serves to dictate the choice(s) of antibacterial for a given treatment.

On the other hand, occurrence of genetic mutations in direct response to administration of antibacterial agents (including both antibacterials and chemical disinfectants) is of significant concern. Several modes of mutation may contribute to the development of antibacterial resistance in susceptible bacterial strains: 1. Structural mutations in pre-existing genetic determinants, 2. Regulatory mutations in pre-existing genetic determinants, and 3. Structural mutations in acquired resistance genes. The first – which results from point mutations (e.g., addition, deletion, or substitution of nucleotides or nucleotide sequences) – can be induced by addition of a large number of bacteria on to an agar plate (or into liquid medium) containing a particular antibacterial, or by gradually exposing bacterial population to increasing concentrations of that antibacterial over an extended timeframe. This one-step mutation mechanism, as it is also called, is typical of streptomycin, rifampin, and fluoroquinolone resistance. The second mechanism – which also results from point mutations (but in regulatory sequences, as opposed to structural gene features) – can be activated in a similar manner as the first. However, it results from the expression of a gene that is otherwise inactive. For example, Gram-negative bacterial strains such as *Bacteroides fragilis* already possess a β-lactamase gene which encodes production of the enzyme β-lactamase (capable of degrading β-lactam antibacterials). However, unless a promoter supplied by insertion sequence IS1186 (located upstream of the bacterium's structural gene) is present, the β-lactamase gene will not be expressed, and thus will not lead to production of β-lactamase (*62*). Presumably, exposure of such a bacterial strain to β-lactam antibacterials would result in induction of the genetic sequence that in other cases remains silent. The third mechanism proceeds by a combination of genetic transfer and mutation, where a genetic element (e.g., a plasmid) is received by a particular bacterium and incorporated into that organism's genome. This new genetic information – perhaps the same as that imparting β-lactam resistance in *Bacteroides fragilis* – might simply remain dormant in the absence of activating stressors, but could be induced in the same manner as for the second mechanism described above. Thus, though mutations can result in increased incidence of antibacterial resistance in bacterial communities, they do not contribute to the horizontal transfer of genetic information, which can result in rapid dissemination of resistance traits across species.

An additional matter which factors into the issue of waterborne ARB is the level of environmental stress required to either induce chromosomal mutations or enhance transfer of genetic determinants from resistant to sensitive strains in the first place. More specifically, antibacterial resistant populations of bacteria – even if they persist in the environment independently of antibacterial stimulus – were most likely induced by the presence of stressors at some time. Past investigators have focused on the minimal inhibitory concentration (MIC) (i.e., the concentration level of an antibacterial agent at which bacterial growth is inhibited to a particular degree relative to uninhibited growth), as a threshold concentration associated with increased levels of antibiotic resistant bacteria. However, quite a substantial body of research now points toward the existence of biological responses to sub-inhibitory levels of antibacterial compounds in culture. In some cases, antibacterial resistance can be induced in a population of bacteria (through mutations or gene transfer) by the application of sub-MIC levels of antibacterials (*63-66*). However, in some cases, alternative biological effects have been noted in the presence of low levels of antibacterial compounds (*67,68*), as the mode of antibacterial action is different for lower concentrations than for higher concentrations. Thus, the type of effect that antibacterial compounds impart on a susceptible organism at sub-inhibitory concentrations may be quite unexpected. In some cases, expression of bacterial virulence may be enhanced by the presence of sub-MIC antibacterial concentrations, while in others it may be depressed. Often, a low concentration of antibacterial can result in morphological changes to an organism (e.g., development of filaments, appearance of dwarf or giant forms of bacterial cells) (*68*). The potential importance of unintended biological responses to trace-level concentrations of antibacterial residues should not be overlooked, and may represent an unheeded and unexplored avenue of risk associated with discharge of these agents into environmental systems. The findings of several recent studies addressing effects of low-level concentrations of antibacterial compounds on aquatic microorganisms add an additional dimension to the difficult task of assessing risks associated with spread of antibacterial resistance or impact of antibacterial residues on environmental systems (*69-72*).

The observation that sub-inhibitory concentrations of antibacterial compounds can affect bacterial growth and biological activity has led to creation of an additional descriptor for low-concentration effects; that being the minimum effect concentration (MEC), which is also sometimes referred to as the minimum selection concentration (MSC) in the context of antibacterial resistance (*73*). This additional term is intended to provide an estimate of the particular concentration at which an antibacterial begins to exert any measurable effect on a particular bacterial strain. O'Reilly and Smith demonstrated that the MEC and MSC were numerically equivalent for growth dependent development of resistance to oxytetracycline in two strains of *E. coli*, and found that the MSC (and MEC) for an oxytetracycline resistant strain of *E. coli* was 0.625 mg/L, relative to measured MICs of 4 mg/L (oxytetracycline-sensitive strain) and 128 mg/L (oxytetracycline-sensitive strain) (*73*). Thus, the MSC was determined to be 5/32 of the MIC for this particular bacterial population. Jones et al. (2002) reported that a levofloxacin concentration of 0.03 mg/L functioned as a threshold concentration (essentially the same as MSC) in selecting for populations of levofloxacin-resistant *E. coli* (25 mg/L levofloxacin < MIC < 100 mg/L levofloxacin) in liquid culture, although the MIC of sensitive *E. coli* strains was approximately 1.6 mg/L (in liquid culture) (*47*). Erythromycin has been shown to induce increasing resistance to macrolide antibacterials in populations of *Micrococcus luteus* strain MAW843 when applied in P or LB media at concentrations ranging from 0.02 to 0.05 mg/L (relative to a measured MIC of 0.5 mg/L for an antibacterial sensitive strain of *M. luteus*). *M. luteus* strains sensitive to tylosin also developed increasing resistance to this antibacterial in the presence of such sub-MIC levels of erythromycin (*65*). In addition, erythromycin was shown to induce phenotypic resistance (i.e., substantially reduced susceptibility to lysis in presence of vancomycin) to vancomycin in Staphylococcus pneumoniae strains within C+Y medium even at concentrations of 0.004 mg/L (where MIC has been determined to be within the range 0.015 mg/L to 4 mg/L).

In a number of cases – e.g., for exceptionally potent antibacterial compounds (e.g., various fluoroquinolones and *β*-lactams), or with respect to organisms which are particularly susceptible to a certain type of antibacterial – environmental levels of antibacterial residues may approach MIC values (see Figure 1.1). In such cases, the risk of selection for strains of ARB is clear.

1.5. Maintenance of Antibacterial Resistance Phenotypes

Once a resistance trait is acquired – either by horizontal gene transfer or by point mutations, it may become a stable part of the host's genotype (whether it be actively expressed or not), or it may eventually be discarded. The question of how antibacterial resistance phenotypes proliferate and are maintained in various environments is an extremely important one, and is open to quite a bit of debate – characterized primarily by perspectives originating from two opposing doctrines of thought. The "reservoir hypothesis" holds that, in order for antibacterial resistance genes to remain stable within their host cells, selective pressure must be applied to the hosts by presence of the antibacterials to which resistance is expressed. Accordingly, in order for antibacterial resistance hot-spots to occur and spread, sustainable reservoirs of antibacterial resistant microorganisms must exist and remain available to respond to transient conditions which favor their selective growth, or perhaps the spread of their genetic material.

The foundation of this hypothesis relates to an inherent assumption that antibacterial resistance plasmids or chromosomal elements impart a metabolic cost on the recipient to which they are transferred, and thus will result in out-competition of that recipient by metabolically-superior, resistance-free variants in a culture lacking the requisite antibacterial stressor. As a result, the “handicapped” bacterial strain (that exhibiting the resistance determinant) would soon be overtaken by the unburdened (and faster multiplying) strain via process of selection. By this line of reasoning, if strictly applied, the presence of antibacterial-resistant bacteria should be limited to only those environments which reward the otherwise metabolically-burdened strain with a competitive advantage over its antibacterial-sensitive brethren, namely those in which conditions are such that selection for the antibacterial resistant phenotype occurs, i.e., for which antibacterial concentrations equal or exceed the minimum inhibitory concentration (MIC) for a particular compound or class of compounds. In such an environment, the resistant phenotype could be expected to overtake the sensitive bacterium and thrive. This is perhaps the case in situations for which high concentrations of antibacterial compounds are the norm, such as in the intestinal tracts of animals or humans undergoing antibacterial therapy, or in animal feed which has been supplemented with high concentrations of antibacterial growth-promoters.

However, this line of reasoning does not address the regular and increasingly frequent detection of large proportions of antibiotic resistant bacterial strains in environmental systems such as wastewater, surface water, and drinking water for which antibacterial concentrations – though often detectable – are generally hundreds or even thousands of times lower than corresponding MIC values. According to the doctrine discussed above, resistant bacteria should not exist in such systems (except perhaps as rare genetic mutants), let alone in significant proportion to relevant populations. Such examples as these have provided ample reason to question tenets of the reservoir hypothesis.

Several studies conducted within the past twenty years have generated results which indicate that antibacterial resistance determinants can indeed persist in populations of bacteria even in the absence of selective pressure. Bouma and Lenski (1988) - focusing on the association between bacteria and plasmid elements – demonstrated quite clearly that, after an initial metabolic deficit (resulting from acquisition of chloramphenicol and tetracycline resistance plasmid pACYC184), *E. coli* B grown in chloramphenicol-spiked growth medium for 500 generations (75 days in culture) adapted via chromosomal genetic change to the plasmid's presence (*74*). After this adaptation period, the evolved bacterium was able to compete effectively with plasmid-free chloramphenicol-sensitive strains and actually exhibited enhanced fitness in cultures for which the selective stressor (chloramphenicol) was absent. Similar results were obtained for a strain of *E. coli* which evolved to a competitive tetracycline-resistant mutant (*45*). Schrag and Perrot (1996) provided additional evidence for such phenomena when they showed that spontaneous streptomycin-resistant mutants of *E. coli* strain CAB281 could adapt across multiple generations to overcome initial Darwinian fitness costs associated with possession of the antibacterial resistance phenotype, even in the absence of antibacterial stimulus. The two initial mutants – which originally exhibited 14% and 19% fitness disadvantages relative to sensitive strains – were able to evolve over 135 generations to 6.97% and 9.55% fitness costs. After 45 additional generations, these fitness costs were further reduced to 4.63% and 6.68%, respectively. In addition, the adaptation of the two mutants occurred without any clinically significant reduction in level of streptomycin resistance, indicating that the bacteria were able to fully maintain their phenotypical resistance while at the same time competing effectively against sensitive strains, in the absence of selective pressure (*75*).

A subsequent study indicated not only that streptomycin-resistant *E. coli* strains were able to adapt to improved levels of fitness in the absence of antibacterials, but also that streptomycin sensitive wild-type bacteria (i.e., those which retained the original phenotype from which the antibacterial-resistant, adapted bacteria were derived) exhibited reduced fitness levels relative to the adapted strains in antibacterial-free environments. More importantly, this study showed that a single mutation leading either to loss of the antibacterial resistance trait or loss of the adaptive allele would result in significant decrease of fitness relative to the adapted ARB. Thus, at least two mutations would be required for such an adapted ARB to return to its parental phenotype, i.e., the high-fitness, streptomycin-sensitive strain, making a return to the original phenotype quite unlikely. Accordingly, the investigators demonstrated that, even after 10,000 generations, the evolved *E. coli* strain retained identical rpsL sequence to its evolved parent (*46*).

Björkman et al. (1999) utilized an in vivo mouse model to study the ability of an antibacterial-resistant, virulence-deficient *Salmonella typhimurium* strain to compete against fully-virulent, antibacterial sensitive strains in antibacterial-free clinical environments. Results of this investigation showed that the avirulent ARB were able to adapt to in vivo conditions in the absence of antibacterial and recover virulence. The adapted strains exhibited a competitive advantage over sensitive strains, without loss of resistance (to streptomycin, rifampicin, and nalidixic acid). Generational studies indicated that compensatory evolution resulted in reversion to parental phenotypes in only 4 of 26 mutations, and that the other 22 mutants exhibited second-site compensatory mutations that did not result in decreased resistance. Furthermore, reversion required substitution of a single target base, while compensatory mutations were thought to be achievable via substitutions at various sites. Thus, the likelihood of reversion to antibacterial sensitive phenotypes appeared lower than that for compensatory adaptation (*76*). Jones et al. (2000) reported on the apparent permanence of induced resistance to the fluoroquinolone antibacterial agent ciprofloxacin. Fluoroquinolone resistance – which is generally thought to be achieved only through point mutations – was induced in two strains of *Staphylococcus aureus* by incubating cultures in media containing sub-MIC concentrations of ciprofloxacin. The antibacterial resistance phenotype was fully retained in antibacterial free cultures, even after 500 subsequent generations, and continued culture at the original MIC level (1 mg/L) of ciprofloxacin actually led to an increased level of resistance via an additional point mutation in the host bacterium's genome (*47*). A thorough discussion of antibacterial resistance maintenance in the absence of antibacterials and by mechanisms other than selection is presented by Heinemann et al. (2000) (*77*).

1.6. Implications for Risk Assessment

Typically, antibacterial concentrations in aquatic systems only approach MIC values within such environments as raw hospital sewage or municipal wastewater influent, where input levels of both bacteria and antibacterial compounds are high enough to provide a critical combination of stressor and target (Figure 1.1). However, the potential dangers associated with their release into the environment may ultimately have more to do with their initial, or primary input concentrations (i.e., from ultimate source, such as hospital sewage to municipal wastewater), rather than their discharge concentrations (i.e., from municipal wastewater effluent to surface water), particularly in light of the possible stability of antibacterial resistance genotypes within a bacterial lineage once resistance has been induced (irrespective of environmental stressor influence). Wastewater treatment facilities are not completely biocidal, even those including disinfection steps, and thus do not represent an absolute barrier to dissemination of ARB into natural water systems. Should conditions in a particular environment – such as at the point discharge of untreated excrement and urine from hospital patients undergoing antibacterial therapy into municipal wastewater systems – favor the evolution of antibacterial-resistant phenotypes, those phenotypes might be induced in a relatively irreversible manner, and so could potentially travel over great distances and through many generations into locations from which they might be re-introduced into clinical situations (e.g., recreational surface waters, drinking water).

With regard to the present topic, the role of disinfection/oxidation in reducing the overall risk associated with spread of antibacterial resistance genes is important with primary regard to two interconnected factors: 1. Oxidation of residual antibacterial compounds, leading (hopefully) to subsequent elimination of bioactivity and action as selective agents, which in turn should result in elimination of selective pressure, and 2. Inactivation of organisms carrying antibacterial resistance genotypes, accompanied by oxidation of genetic material contained within or released during structural modification of the organisms.

A number of oxidation/disinfection techniques – the most notable of which include chlorination, ozonation, and ultraviolet light irradiation – are commonly employed in modern water treatment facilities. Chlorine disinfection – through still widely practiced – is decreasing in frequency of application within wastewater treatment (due primarily to issues associated with disinfection by-product formation), and may gradually lose importance as a primary disinfection mechanism over time. UV irradiation – which is quickly proving to be a very effective tool for inactivation of problematic microorganisms (e.g., Cryptosporidium parvum, Giardia lamblia) – seemingly avoids the issue of by-product formation, and will likely become one of the favored means of disinfecting municipal water supplies in future years. Ozone disinfection also represents an effective means of inactivating persistent pathogens, and if the issue of bromate formation – which has represented a significant hindrance to wider application – can be overcome, will likely join UV disinfection as a preferred method of water purification. One advantage of ozonation, in comparison to UV irradiation, is that – due to ozone's strong oxidizing potential and selectivity – this process provides a means of oxidizing and degrading specific functional moieties of chemical pollutants (*78,79*), in addition to inactivating pathogenic microbial communities. Although UV disinfection can be modified to provide oxidative capacity (e.g., through addition of H_2O_2 to irradiated waters) the resulting radical-mediated reactions with pollutants are often non-specific, and can result in extremely complex mixtures of unpredictable by-products. On the other hand, ozonation presents a potential means of oxidizing antibacterials to eliminate their biological activity through predictable reaction mechanisms. Thus , as discussed in more detail below, ozone may provide an effective means of achieving targeted elimination of any selective pressure associated with the presence of these compounds in municipal wastewater.

1.7. Transformation of Antibacterial Compounds during Ozonation

The effect of ozonation processes on antibacterial residues in aquatic systems appears to be quite significant, i.e., most antibacterial compounds evaluated in ozone oxidation studies to this point are rapidly degraded. Adams et al. (2002) found that a number of antibacterials, including trimethoprim, carbadox, and several sulfonamides, were degraded to below method detection limits within 90 seconds of ozone addition (for 50 μg/L and 0.3 mg/L starting analyte and oxidant concentrations, respectively) in deionized/distilled and Missouri River waters (*80*). However, kinetic data were not reported, and no information was available regarding structures or quantities of products formed during the oxidation reactions. Huber et al. (2003) provided more extensive information on degradation of the antibacterials sulfamethoxazole and roxithromycin in the presence of ozone and hydroxyl radicals; reporting ozone oxidation rate constants of app. 2.5×10^6 $M^{-1}s^{-1}$ and 4.5×10^6 $M^{-1}s^{-1}$, respectively, in addition to a hydroxyl radical oxidation rate constant of 5.5×10^9 $M^{-1}s^{-1}$ for sulfamethoxazole. Experiments conducted in natural waters collected from several European locations indicated that the reported rate constants (obtained from reactions in reagent water systems) were equally applicable to environmental samples. The results from this investigation also illustrate the importance of pH-dependent speciation with respect to oxidation reactions involving ozone, as roxithromycin exhibited a significant decline in reactivity for decreasing pH (corresponding to increasing protonation of its tertiary amino group). Although attention was given to discussion of potential products and toxicological significance, no attempt was made to identify products or evaluate transformation pathways for the compounds included in this study (*81*). Qiang et al. (2003) have recently formulated a pH-dependent kinetic model for reaction of the antibacterials spectinomycin and lincomycin which highlights the effect of acid-base speciation on substrate reactivities toward ozone (*82*).

To evaluate probable reaction pathways with various classes of antibacterials, it is important to consider likely sites and modes of oxidative attack on the compounds' structures. Prior studies with representative model compounds can provide some indication as to what results might be expected to occur for reaction of ozone or hydroxyl radicals with certain antibacterial compounds. A number of representative structures of the major classes of antibacterials relevant to environmental samples are shown with probable sites of direct attack by O_3 in Table 1.1. Ozone is a highly selective electrophile, and as such, will exhibit preferential reactivity toward specific functional groups associated with such chemical structures. Olefinic double bonds, activated aromatic rings, amino groups, and sulfide groups

Table 1.1. Model antibacterial compounds[a]

Macrolides

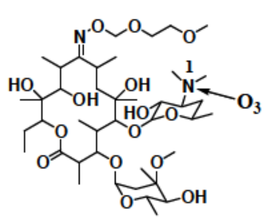

Roxithromycin (RX)
pKa = 9.2

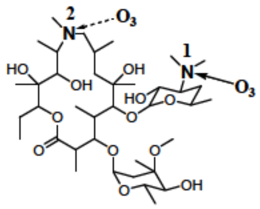

Azithromycin (AZ)
p$K_{a1,2}$ = 8.7, 9.5

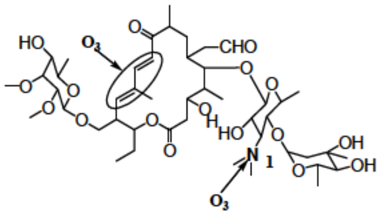

Tylosin (TYL)
pK_a = 7.7

Sulfonamides

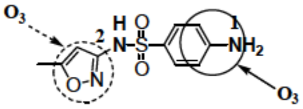

Sulfamethoxazole (SMX)
p$K_{a1,2}$ = 1.7, 5.6

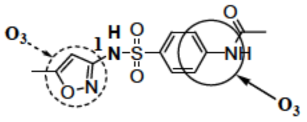

N(4)-acetyl-sulfamethoxazole (ASMX)
pK_a = 5.5

DHFR Inhibitor[e]

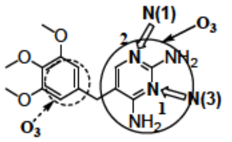
N(1)
O3
2
1
N(3)
O3

Trimethoprim (TMP)
p$K_{a1,2}$ = 3.2, 7.1

Fluoroquinolones

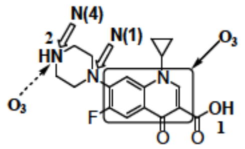
N(4)
2
N(1)
O3
O3
1

Ciprofloxacin (CF)
p$K_{a1,2}$ = 6.1, 8.8

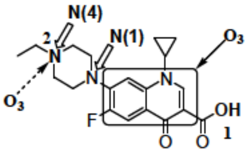
N(4)
2
N(1)
O3
O3
1

Enrofloxacin (EF)
p$K_{a1,2}$ = 6.1, 7.7

Lincosamide

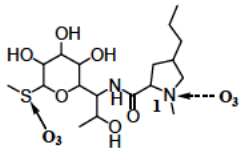

Lincomycin (LM)
pK_a = 7.8

β-lactams

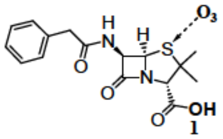

Penicillin G (PG)
pK_a = 2.7

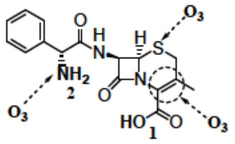

Cephalexin (CP)
p$K_{a1,2}$ = 2.5, 7.1

Tetracycline

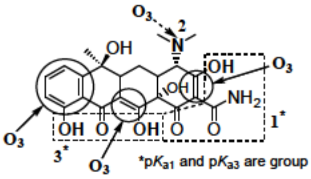
O3
2
O3
1*
O3
3*
O3

*pK_{a1} and pK_{a3} are group values

Tetracycline (TET)
p$K_{a1,2,3}$ = 3.3, 7.7, 9.7

Glycopeptide

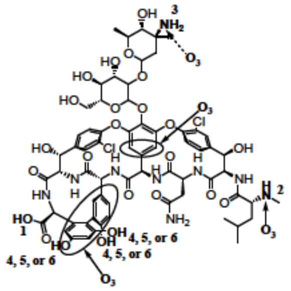
3
O3
O3
2
O3
1
4, 5, or 6
4, 5, or 6
4, 5, or 6
O3

Vancomycin (VM)
p$K_{a1,2,3,4,5,6}$ =
2.9, 7.2, 8.6, 9.6, 10.5, 11.7

Aminoglycoside

Amikacin (AM)
p$K_{a1,2,3,4}$ = 6.7, 8.4, 8.4, 9.7

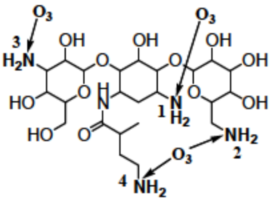
O3
3
O3
1
2
O3
4

---

[a]Structural families are listed in bold. [b]Likely O_3 target sites are indicated by arrows. [c]References from which pK_a values were obtained are summarized in Chapter 2, Table S2.1. [d]Sites of ionization are numbered according to order of deprotonation. For compounds possessing a single pK_a, the ionizable site is labeled 1. [e]DHFR – dihydrofolate reductase.

represent attractive nucleophilic targets for ozone (*79*). Amino groups (primary, secondary, and tertiary) happen to be quite common amongst various classes of antibacterials – including the tetracyclines, fluoroquinolones, sulfonamides, dihydrofolate reductase inhibitors, macrolides, and aminoglycosides. Activated aromatic rings are present in the sulfonamides, dihydrofolate reductase inhibitors, and tetracyclines. Hydroxyl radicals are much less selective as oxidants, and are thus not quite as constrained in their modes of action on organic substrates. As a first step in assessment of antibacterial susceptibility to ozone/•OH reactions, the expected reactivities of functional groups can be gauged through comparison to published kinetic data for various reactions.

Depending on substitution patterns, olefinic groups may yield rate constants ranging from $< 0.1\ M^{-1}s^{-1}$ (e.g., tetrachloroethene) to $\sim 2 \times 10^5\ M^{-1}s^{-1}$ (e.g., ethene), for oxidation by ozone, where substitution of electrophiles or nucleophiles on adjacent carbons can be expected to either decrease or increase the rate of reaction, respectively (*79*). Measured rate constants for reaction of amines range from $20\ M^{-1}s^{-1}$ for NH_3 to $> 10^6\ M^{-1}s^{-1}$ for triethylamine (*79*), where increasing degree of alkyl substitution typically correlates to increasing degree of reactivity. Protonation of amino groups greatly reduces their reactivity toward ozone (rendering them essentially non-reactive in most cases). Thus, speciation patterns of compounds containing amino groups can be expected to be quite important in determination of rate constants. Activated aromatic rings, such as phenols, anilines, or methoxybenzenes exhibit reactivities exhibit grossly elevated reactivities toward ozone, relative to benzene (which exhibits a $k_{O3} = 2\ M^{-1}s^{-1}$ (*83*)), where phenolate's k_{O3} is equal to $1.4 \times 10^9\ M^{-1}s^{-1}$ (*84*). Rate constants for oxidation of organic compounds by hydroxyl radicals are generally close to diffusion-controlled, with the exception of some highly deactivated aliphatic hydrocarbons such as chloroform ($k_{\bullet OH} = 5 \times 10^7\ M^{-1}s^{-1}$).

Consideration of the available kinetic data for such reactive groups allows preliminary estimation of reactivities for oxidation of the antibacterials presented in Table 1.1 by ozone or hydroxyl radicals. Huber et al. (2003) provided estimates for reactions of ozone with several classes of antibacterials: fluoroquinolones, sulfonamides, macrolides, and tetracyclines (*81*). These are provided with additional estimates for each of the antibacterial compounds or classes included in Table 1.1.

Evaluation of product formation and reaction pathways associated with reaction of complex molecules presents an additional challenge in monitoring degradation of antibacterial compounds by ozone or hydroxyl radicals. Thus far, evaluation of reaction products generated by ozonation reactions or hydroxyl radical oxidation has been limited primarily to relatively simple molecules, although less generally applicable studies associated with specific structures are distributed throughout the available literature. Fortunately, findings from mechanistic studies can be utilized to assess the likelihood of various structural modifications in the context of more complex molecules. In addition, the use of relatively simple model compounds can be used to develop most probable degradation pathways for similar moieties included within larger molecules. Selection of appropriate model compounds can greatly facilitate identification of reaction products as well as elucidation of reaction pathways, as illustrated by recent work conducted on ozonation of the synthetic hormone 17α-ethinylestradiol (*85*).

Evaluation of product formation is quite critical in the case of parent compounds exhibiting high biological activity, such as antibacterials, hormones (or hormone mimics), and microtoxins (e.g., aflatoxins, cyanotoxins). Retention of biological potency after oxidation could be possible in cases for which structural modification either fails to inactivate bio-active functional groups or where structures are modified to configurations which possess additional or alternative modes of toxicity. Data regarding the toxicological significance of oxidation products generated during ozonation of antibacterial compounds is not currently available, and will be an important component in development of risk assessment protocols for release of antibacterials into environmental systems. Application of MIC screening procedures (*86-88*) (via liquid cultures or plating techniques) according to methods similar to those utilized by Huber et al. (2003) (*85*) – for evaluation of hormone degradation products – could provide one useful tool in determining the antibacterial properties of such oxidation products.

1.8. Thesis Scope

Ozone-based oxidation/disinfection processes (involving both O_3 and the hydroxyl radical, •OH (*79,89*)) are known to result in considerable degradation of several different antibacterial classes (*81,90*). Thus far, however, accurate O_3 reaction rate constants have only been reported for compounds from a few antibacterial classes (*81,91,92*), and •OH rate constants for members of only three classes (sulfonamides and macrolides (*81*) and *β*-lactams (*93*)). Furthermore, very little is known with regards to how these reactions alter the biochemical potency of the parent antibacterial substrates, outside of recent work on the macrolide clarithromoycin (*92*). This knowledge is absolutely critical in attempting to accurately evaluate the potential effectiveness of such oxidative treatment strategies in reducing or eliminating biochemical activities of targeted antibacterial substrates.

A primary objective of this work was to quantitatively assess the ability of ozone to eliminate the biochemical activity of model antibacterial substrates from a wide variety of different structural classes. Model antibacterial substrates have been selected from the nine antibacterial structural classes most important within human medicine (Table 1.1). Individual model substrates were selected on the basis of their occurrence in environmental systems, frequency of application, or utility as generic structural surrogates of members within their structural family as a whole. These compounds include members of the macrolide, fluoroquinolone, sulfonamide, dihydrofolate-reductase inhibitor, glycopeptide, β-lactam, aminoglycoside, tetracycline, and lincosamide structural classes.

Rate constants for both ozone and hydroxyl radical reactions were investigated using methods appropriate to each model substrate. pH-dependent variations in measured second-order ozone rate constants were utilized to determine O_3 rate constants for specific neutral or ionic species of dissociable antibacterial molecules. In addition, O_3 reaction kinetics were measured for various model compounds representing reactive or non-reactive substructures of the parent antibacterial molecules. Modeling of apparent rate constant pH-dependencies (*94*) was used in conjunction with substructure reaction kinetics to isolate the site-specific O_3 reaction kinetics for each antibacterial substrate. Additional experiments were conducted in real wastewater matrixes to verify applicability of laboratory results in such waters.

An antibacterial potency assay was used to measure the residual antimicrobial activity of oxidation product mixtures resulting from exposure of antibacterial compounds to O_3, •OH, or various ratios of simultaneous exposure to both oxidants. Standard protocols for measurement of antibacterial potencies were adapted to this purpose (*87*). Reference bacterial strains appropriate to each class of antibacterials were used to measure the antibacterial potency of bulk oxidation product mixtures via benchmarking against reference MIC values for each parent antibacterial substrate. Limited attention was dedicated to elucidating specific reaction mechanisms or reaction products, except in cases for which oxidation reactions appear to yield transformation products which retain substantial antibacterial potency relative to the parent substrate. A toxicity identification and evaluation (TIE) approach was used to identify of oxidation product mixture components responsible for any measured antibacterial activity remaining after treatment with O_3.

1.8.1. Model Antibacterial Compounds

1.8.1.1. Macrolides. Azithromycin (AZ), roxithromycin (RX), and tylosin (TYL) were selected to represent the macrolide antibacterials (Table 1.1). AZ – commonly used in treatment of respiratory and urinary tract infections – represents one of the most commonly prescribed drugs in the United States at the current time (*95*). Most environmental occurrence studies – with respect to macrolides – have focused on the measurement of erythromycin and other macrolides, so little data is available with respect to the frequency of azithromycin occurrence in environmental system. However, detection of various macrolide antibacterials in raw and treated wastewater (*96*), coupled with the similar structural character of most macrolide antibacterials, merits concern over the potential presence of azithromycin in aquatic systems. RX – which has been detected in wastewater effluents (*9,96*) – has previously been studied in the context of ozonation reactions, and kinetic data is available for this particular compound (k_{O3} = 4.5 x 10^6 $M^{-1}s^{-1}$ for the neutral RX species) (*81*), making it a convenient choice for the current study. TYL has been detected in surface waters samples obtained from the United States (*10*), but is utilized primarily in veterinary applications, as opposed to human medicine. Thus, TYL does not necessarily represent a target for oxidation processes in municipal wastewater treatment. Rather, it has been selected here to provide additional information as to the reactivities of double bonds incorporated into the macrocyclic rings of similar human-use macrolides, such as spiramycin.

In general, the structures of AZ, RX, and TYL are quite typical of other macrolide antibacterials. As in the case of all macrolides, AZ, RX, and TYL each possess a single tertiary amino group as a substituent on their side-chain sugars. This particular group could be expected to represent a primary site of oxidative attack in reactions with ozone. However, AZ is also characterized by a second tertiary amine which is integrated into the compound’s lactone ring. This likely represents an additional reactive site. TYL, which possesses the tertiary amino group typical of other macrolides, also contains two double bonds within its macrocyclic ring. These groups likely also represent attractive targets for ozone, and could be expected to react with rate constants (k_{O3}) in the vicinity of 10^5 $M^{-1}s^{-1}$. RX and TYL should be representative compounds for use in evaluation of macrolide reactivity toward ozone in general. Additionally, evaluation of AZ oxidation should yield useful information about the reactivity of this uniquely-constructed erythromycin derivative.

The antibacterial activity of the macrolide family is related to their ability to form hydrogen bonds (up to seven, in the case of narrow- and expanded-spectrum macrolides) with various nucleobases and phosphodiester linkages in bacterial 23S rRNA (*1*). Most of the hydrogen bonding sites are hydroxyl groups located on the macrolactone ring or desosamine sugar side chain. Of the three relevant functional group types (see above) that could be expected to react with ozone, only the amine group of the desosamine sugar (Table 1.1) appears to be directly involved in these intermolecular interactions. However, since this particular group is present in all macrolides, it is of interest to understand how its reaction with ozone alters the ability of the overall macrolide structure to bind bacterial rRNA. In addition, oxidation of the heterocyclic nitrogen atom in AZ, or the diene system in TYL may still contribute to the inactivation of macrolide molecules, simply by disrupting the macrolactone ring structure characteristic of these compounds. Such severe alteration (i.e., rupture of the macrocyclic ring) could certainly be expected to contribute to decreased or lost ability to maintain the hydrogen-bonding configurations necessary to form complexes with bacterial 23S rRNA. The antimicrobial activity of macrolide antibacterials could also possibly be reduced via alteration of their solubility and intracellular mobility (e.g., via oxidation of amino groups imparting polarity, or by loss of structural attributes imparting trans-membrane permeability).

1.8.1.2. Sulfonamides. Sulfamethoxazole (SMX) – a human-use antibacterial, frequently prescribed in combination with trimethoprim (see below) as the antimicrobial agent "co-trimoxazole" – was selected to represent the sulfonamide antibacterials for several reasons. First, SMX has been frequently detected in sewage, treated wastewater, and surface water samples. Second, kinetic data has already been obtained for reaction of SMX with ozone ($k_{O3} \approx 2.5 \times 10^6$ $M^{-1}s^{-1}$ for the dissociated SMX species) (*81*), thus simplifying the overall evaluation of its fate in drinking water treatment. In addition, the structure of SMX is representative of most other sulfonamides, with variations only in the interchangeable heterocyclic moieties attached to the sulfonamide group (see Table 1.1). Thus, SMX appears to present a reasonable compound with which to assess the general character of sulfonamide antibacterials in oxidative treatment processes involving ozone.

Sulfonamide structures are all derivatives of *p*-aminobenzenesulfonamide – a structural analog of *p*-aminobenzoic acid – and are differentiated only by the particular side chain attached to the sulfonamide nitrogen (see Figure 1.2). These compounds derive their antibacterial activity from antagonistic competition with *p*-aminobenzoic acid for dihydropteroate synthase enzyme during bacterial synthesis of dihydropteroic acid (the precursor to folic acid) (*97*). In consideration of this mode of action, one could suppose that

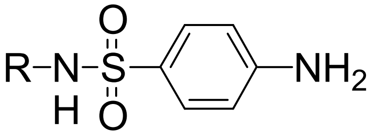

Figure 1.2 Sulfonamide core structure

any disruption of the *p*-aminobenzenesulfonamide group in a sulfonamide antibacterial would lead to a loss of the parent substrate's antimicrobial activity. Similarly, it would seem that attack of the heterocyclic side chains differentiating the various sulfonamide compounds might not be sufficient to eliminate their antibacterial potential (though it might result in reduction of antibacterial activity).

The aniline moiety of the *p*-aminobenzenesulfonamide group would seem to represent an attractive target for O_3 (whether at the amino nitrogen, or at one of the ortho-positions of the aromatic ring). Oxidative attack of this moiety would be expected to lead to elimination of the parent substrate's antibacterial activity, as it would most likely result in disruption of the structure responsible for imparting antibacterial potential to the sulfonamide parent. However, although a rate constant has been measured previously for oxidation of SMX by ozone, the reactive site and mode of oxidation for this reaction has not been verified. One objective of this study was to verify the position of oxidative attack by ozone, as a prerequisite to formulating likely degradation pathways for the sulfonamide antibacterials, and to determining potential mechanisms by which these antibacterial structures can be inactivated. Alterations to the heterocyclic side chain group (methylisoxazole) attached to the sulfonamide nitrogen are not expected to significantly affect the antimicrobial activity of sulfamethoxazole, as even the most fundamental sulfa drug structure (e.g., sulfanilamide – which lacks any side chain functional group) exhibits appreciable antibacterial activity. This tenet should similarly apply to any sulfonamide antibacterial.

1.8.1.3. Dihydrofolate Reductase (DHFR) Inhibitors. Trimethoprim (TMP) is frequently prescribed with SMX for use in treatment of respiratory infections, particularly with respect to chemotherapy of AIDS patients (*98,99*). As in the case of SMX, TMP is also frequently detected in various environmental water systems (*10,100*), which might be expected (at least partially) as a result of the concurrent usage of these two compounds. Trimethoprim possesses two functional moieties which might be expected to react with an electrophilic oxidant such as ozone: the 2,4-diaminopyrimidinyl moiety (typified by two heterocyclic amino groups and two exocyclic amino groups) and the 3,4,5-trimethoxybenzyl moiety.

Although no specific evaluation of diaminopyrimidine reactivity with O_3 exists to date, several prior studies have evaluated oxidation of structural analogues by ozone. Reactivities of the pyrimidine bases uracil, cytosine, and thymine toward ozone have been studied previously (*101-104*). Each was found to react readily with ozone, though uracil appeared to exhibit somewhat slower rates than the other bases (*102*). The trimethoxybenzyl moiety could also be expected to exhibit relatively facile oxidation by ozone, as illustrated by the measured rate constant for 1,3,5 trimethoxybenzene ($k_{O3} = 9.4 \times 10^5$ $M^{-1}s^{-1}$) (*105*). Thus, TMP would appear to be quite susceptible to oxidative degradation by ozone. Estimated rate constant ranges are provided for TMP and other model compounds in Table 1.1. As for the sulfonamides, other DHFR inhibitors (such as pyrimethamine) differ significantly from TMP only in the form of their secondary structural group (opposite the diaminopyrimidine moeity, which is common to all DHFR inhibitors). Thus, TMP is also expected to provide useful insight into the reactions between other DHFR inhibitors and ozone.

The TMP structure was synthesized from 2,4-diaminopyrimidine specifically for the purpose of inhibiting the activity of DHFR during cellular synthesis of folate (*97*). The diaminopyrimidine structure represents the active portion of the antibacterial molecule, where the protonated nitrogen atom, N-1, of the heterocyclic ring (Figure 1.3) participates in charge interactions with DHFR (*106*). Therefore, oxidative attack of the diaminopyrimidine moiety by ozone should presumably result in elimination of the TMP structure's antimicrobial activity. On the other hand, alteration of the side-chain substituent (a 3,4,5-trimethoxybenzyl group in this case) might also result in reduction of activity, but via affectation of the TMP molecule's physico-chemical characteristics (e.g., solubility, polarity, hydrophilicity, etc.) rather than direct loss of its ability to interact with the intended target. Accordingly, the affinity of O_3 for each potential reactive site is a matter of some importance, and was evaluated in conjunction with measurement of reaction kinetics.

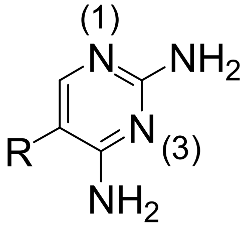

Figure 1.3. Dihydrofolate reductase inhibitor core structure

1.8.1.4. Fluoroquinolones. Ciprofloxacin (CF) – a commonly-prescribed human-use antibacterial agent, and enrofloxacin (EF) – more commonly used in veterinary applications – were selected to represent the synthetic fluoroquinolone family. CF is characterized by a secondary N-4 nitrogen, while EF exhibits tertiary substitution of this amine (Table 1.1). The typical fluoroquinolone structure presents two primary targets for oxidative attack by ozone. First is the N-4 amino group, which on the basis of oxidation-reduction potential considerations and expected electron density, would appear to represent an attractive target for the electrophilic ozone molecule. Second is the double bond located adjacent to the carboxylic group of the quinolone structure. Both sites could represent reactive sites for oxidation by ozone, though the more likely site of attack is unclear at this time, and represents one of the intended findings of this study. It is also possible that ozone could attack the aromatic ring located adjacent to the fluroquinolones' piperazine moiety, though the presence of the strongly electron-withdrawing flourine atom on this ring would likely make the aromatic ring a relatively poor target (as a result of negative inductive effects). Reactivities of these two model substrates were compared to assess the affect of varying degrees of N-4 substitution on reaction kinetics.

The core 4-quinolone structure which is characteristic of all quinolone antibacterials is shown in Figure 1.4. The R-1 to R-8 positions can be filled by a number of different substituent groups (R-7 is filled by various piperazine moiety configurations for fluoroquinolones), while X and Y can represent either C or N atoms. Nalidixic acid – the first quinolone antibacterial – exemplifies one of the simplest structures for this class, in which X = N, Y = C, R-1 = C_2H_5, R_5=H , R-6 = H, R-7 = CH_3, and R-8 = H. Seemingly, destruction of the piperazine ring – as observed for reactions of CF with free chlorine and chloramines (*107*) – might not result in complete elimination of antibacterial activity. Accordingly, degradation of the fluoroquinolone structure with ozone may or may not result in reduction or elimination of antimicrobial activity.

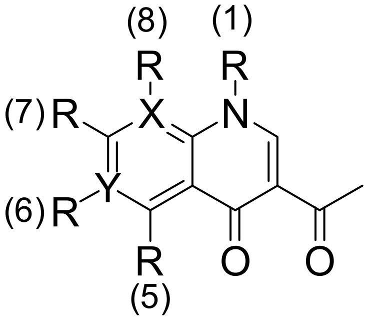

Figure 1.4. Quinolone core structure

Current models of fluoroquinolone binding to DNA gyrase enzymes indicate that the quinolone structure (inclusive of the aromatic and heterocyclic rings) participates in "stacking," or co-planar alignment with purine bases contained in the subunits of gyrase enzyme intermediates produced during DNA strand cleavage. Although alteration or loss of the fluoroquinolone structure's piperazine moiety might reduce these compounds' antimicrobial potency, such changes would not be expected to eliminate their biochemical activity. As mentioned above, even quinolone structures which lack the piperazine ring (e.g., simple quinolones such as nalidixic and oxolinic acids) exhibit considerable antibacterial activity. Thus, of the likely sites of oxidative attack for O_3 (which would appear to be at the basic N of the piperazine ring and at the olefinic bond adjacent to the quinolone carboxyl group), disruption of the heterocyclic ring shown in Figure 1.4 – via attack at the olefinic bond – would seem most likely to lead to an accompanying elimination of antimicrobial activity.

1.8.1.5. β-lactams. Penicillin G (PG, Table 1.1) is perhaps the most fundamental of the *β*-lactams, and cephalexin (CP, Table 1.1) the most fundamental of the cephalosporins. The fundamental structure of these compounds have been modified substantially over time via incorporation of various functional groups and structural modifications to yield hundreds of analogues possessing features such as improved acid stability, resistance to β-lactamases, and improved solubility (*1,108*). However, the β-lactam ring system (Figure 1.5) remains the primary source of these compounds' antibacterial activities, due to its interaction with peptidoglycan transpeptidase (and subsequent disruption of cell wall synthesis) in bacterial cells. With the exception of the less commonly used carbapenems, monobactams, and clavams (which contain significantly different configurations of the β-lactam system's fused five- or six-membered ring), the β-lactams are well represented by the core structures contained within PG and CP (Figure 1.5). Thus, evaluation of PG's and CP's susceptibilities to oxidation by ozone should permit a broadly applicable determination of β-lactam susceptibility toward ozone.

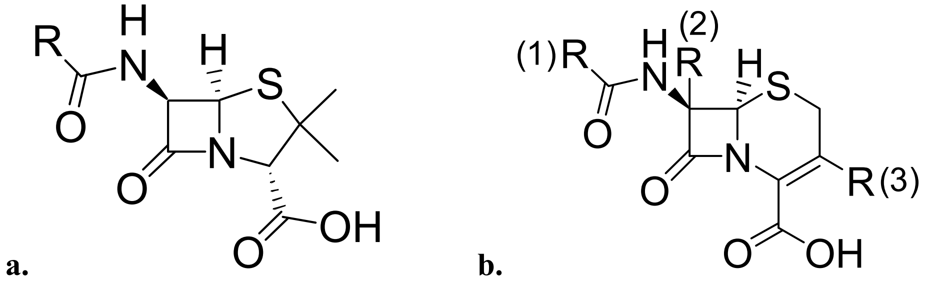

Figure 1.5. β-lactam core structures. (a) penicillins, (b) cephalosporins

With respect to the PG and CP structures, the thioethers contained within the fused five- and six-membered β-lactam ring systems present probable reactive targets for ozone molecules. Ideally, oxidation of the thioether group would result in deactivation of the β-lactam ring system and a corresponding loss of antibacterial activity. The double bond of CP likely also represents a significant target for attack by O_3.

1.8.1.6. Lincosamides. Lincomycin (LM) was chosen to represent the lincosamide class of antibacterials (which also includes clindamycin – a frequently prescribed antibacterial compound in the United States (*95*)). Lincomycin (LM) has been detected in surface water samples obtained from the U.S. (*10*), and recent work has addressed its reaction kinetics in oxidation processes involving ozone ($k_{O3} = 2.9 \times 10^6$ $M^{-1}s^{-1}$ for the neutral LM species (*109*)). Thus, selection of lincomycin (LM) for this study allows focus to be directed more rapidly from evaluation of reaction rates to reaction mechanisms. Clindamycin differs from lincomycin (LM) only in the substitution of a chlorine atom (clindamycin) for a hydroxyl group on the side-chain adjacent to the LM amide nitrogen. Use of lincomycin in the proposed study should therefore also yield results applicable to clindamycin. As noted by Zhimin et al. (2003), attack of the LM structure with ozone could occur at the compound's tertiary cyclic nitrogen (*109*). However, the LM structure also possesses a highly reactive thioether group, which could explain the relative minor effect of pH on reaction rate observed in that study. One objective of this study was to clarify which (if either) site represents the primary target for ozone.

Lincosamides act on bacterial cells by inhibiting their ability to synthesize proteins, primarily through hydrogen-bonding of hydroxyl groups on their sugar side chain to an amino nitrogen in the bacterial 50S rRNA subunit (the same target of macrolide antibacterials) (*1,97*). Accordingly, the effect of ozone oxidation on the lincosamide structure (through expected attack of the thioether and pyrrolidine functional moieties) may not be direct degradation of the antibacterial's ability to bind the ribosomal RNA, but rather a reduction in its ability to reach the rRNA via loss of solubility or membrane permeability.

1.8.1.7. Tetracyclines. Tetracycline (TET) was selected as a model compound for study of reactions involving ozone and tetracycline antibacterials. Even though prescription of tetracyclines has become less effective in ensuing years (primarily due to increasing incidences of bacterial resistance to this class of drugs) (*32*), tetracycline itself is still amongst the two-hundred most commonly prescribed pharmaceutical products in the United States (*95*). Although not as common in aquatic environmental compartments as the compounds described thus far, tetracyclines (TET, in particular) have been detected at ppt concentrations in surface water samples taken within the United States (*10*). TET is believed to interact strongly with metal ions in aquatic systems (*110*), in turn leading to relatively high levels of complexation with mineral surfaces – one explanation for the comparatively low concentrations of tetracycline antibacterials found in environmental occurrence studies. However, in situations for which metal concentrations are comparatively low, substantially higher concentrations of tetracycline antibacterials may yet be available for interaction with bacteria, and should thus still be a concern in the context of antibacterial resistance induction. Accordingly, the fate of this antibacterial class after exposure to oxidants such as ozone is certainly still of interest.

First- and second-generation natural tetracyclines are typified by the presence of a phenol moiety, two double bonds, and a tertiary amine group (Figure 1.6), and structures of such compounds as chlortetracycline, oxytetracycline, methacycline, and doxycycline do not differ markedly from that of TET (*32*). Reaction with ozone is expected to take place primarily at these sites (Table 1.1). Third-generation tetracycline antibacterials (i.e., the glycylcyclines) exhibit additional substition on the phenol moiety, and may be expected to exhibit different reactivity toward ozone than the first- and second-generation tetracyclines. However, most of these third-generation drugs are still in clinical evaluation, and are not yet in widespread use (*32*). Accordingly, the use of TET should provide a means to evaluate the general reactivity of ozone with the most commonly employed tetracycline antibacterials.

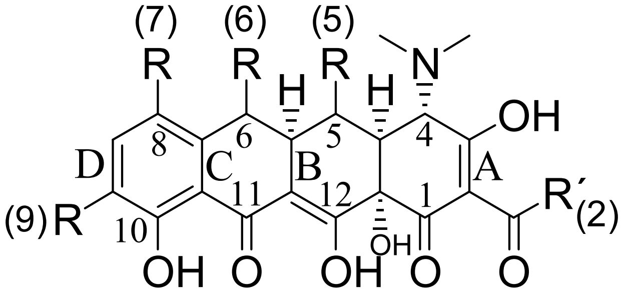

Figure 1.6. Tetracycline core structure

The simplest tetracycline structure exhibiting antibacterial activity is portrayed in Figure 1.6. This core tetracycline structure - 6-deoxy-6-demethyltetracycline – is characterized invariably by the amino group, olefinic bonds, and phenolic moiety described above. Various substitution patterns can be utilized to improve antibacterial activity (e.g., through improved solubility or improved mobility through cellular membranes). However, the fundamental structure shown in Figure 1.6 must remain intact for maintenance of antimicrobial effect. Only in one example has alteration of this core structure not diminished or eliminated antibacterial activity, and that is with regard to the thiatetrayclines (e.g., 6-thiatetracycline), in which the 6-position of the C ring is substituted with a sulfur atom (although the mode of antibacterial activity is completely different in this case, as compared to the conventional tetracyclines) (*32*).

The antibacterial activity of the tetracycline ring system appears to be derived primarily from direct or indirect (through metal cations) electrostatic charge interactions between the keto- and hydroxyl oxygens on the underside of the tetracycline molecule (Figure 1.6) and the oxygens of various internucleotide phosphodiester linkages on the 16S rRNA helix contained within the 30S subunit of the bacterial ribosome (*1*). Thus, oxidation of the tetracycline molecule with ozone would appear to present a promising means of eliminating the antibacterial properties of the parent structure, as O_3 will presumably attack both the phenol moiety and olefinic bonds affiliated with the tetracycline's active polyketide structure, likely leading to disruption of the conjugated tetracycline system, in turn leading to a decrease or loss of antibacterial activity (*32*). Additional reactions involving the TET structure's characteristic tertiary amine might not necessarily lead to elimination of TET's rRNA binding capability, but might result in significant enough structural alteration (perhaps via loss of the amine functional group) that the antibacterial molecule is unable to access the interior of the cell, and thus not able to reach the intended RNA target structure.

1.8.1.8. Glycopeptides. VM (Table 1.1) represents the more commercially available and more thoroughly studied compound of the two glycopeptides in frequent clinical use today (teicoplanin is the other). As seen in Table 1.1, the vancomycin structure is characterized by a number of functional groups that could be expected to react readily with ozone, namely activated aromatic structures and amine groups. Teicoplanin differs in several ways, but maintains the same types of reactive functional groups (same trimethoxybenzyl moiety, four phenols to VM's two, and one primary amine to VM's primary and secondary amines). However, consideration of the model for glycopeptides' sequestration of peptidoglycan (the means by which these antibacterials disrupt cell wall biosynthesis) (*1*), points toward the trimethoxybenzyl moiety as the functional group likely to be most important in reactions with ozone. Oxidation of the phenolic groups or amine groups could certainly alter the physico-chemical properties of the glycopeptide structure (and perhaps result in reduced ability of VM to access its intended cell targets), but some change to the six-amide chain (the nitrogen atoms of which are involved in hydrogen bonding with the peptidoglycan terminus) on the underside of the glycopeptide molecule would likely be necessary to eliminate these antibacterials' peptidoglycan complexation capability, and so remove their biochemical activity. Such an alteration to the glycopeptide structure could presumably be implemented by ozone attack on either meta position of the trimethoxybenzyl moiety, which could foreseeably lead either to a complete disruption of the glycopeptide core, or at least to an alteration of the glycopeptide molecule's stereochemistry that could prevent effective hydrogen bonding to peptidoglycan.

1.8.1.9. Aminoglycosides. Amikacin is a semi-synthetic antibacterial derived from the natural antibacterial kanamycin (actually a mixture produced by Streptomyces kanamyceticus – containing structural analogues kanamycin A, B, and C). Aminoglycoside antibacterials vary in the number of amino groups present in each structure, but in most cases, these amines are the only functional groups expected to exhibit appreciable reactivity toward ozone. Amikacin can be taken as approximately representative of most other aminoglycosides, including streptomycin, gentamicin, tobramycin, and the kanamycins. Though amikacin has not been detected explicitly in wastewater systems, the aminoglycoside gentamicin has been recently quantified in German hospital wastewaters (*12*).

Aminoglycosides are inhibitors of bacterial protein synthesis, and derive much of their antimicrobial activity from mechanisms similar to macrolides and tetracyclines; that is, through charge interactions with nucleobase and phosphodiester functional groups in the bacterial rRNA. Several of the primary and secondary amine groups characteristic of aminoglycoside antibacterials are involved in these interactions, but much of their RNA binding capability is derived from hydroxyl groups located on their sugar moieties (*1*). Additionally, aminoglycosides are thought to contribute to disruption of bacterial cell membranes (and subsequent cell death) via competitive displacement of Mg^{2+} and Ca^{2+} cations linking adjacent lipopolysaccharides in the cell membrane structure – an attribute derived from their unique polycationic character (*97*).

The presence of so many electron-rich amino groups in the aminoglycosides' structures is likely to result in their rapid oxidation by such disinfectants as ozone. Accordingly, a detailed examination of ozone-aminoglycoside reactivity and product yields should verify their susceptibility to O_3, though the complexity of reaction processes (e.g., with respect to sites of attack, and product distributions) is likely to be quite high, due to the high number of potential reactive sites for each substrate molecule.

Ozonation of the aminoglycosides could foreseeably lead to reduction or elimination of their antimicrobial activity, via oxidation of the amine groups involved in bacterial rRNA binding and cell membrane disruption. The extent to which such oxidation reactions actually effect the rRNA binding activity of these compounds may not be complete, as a number of hydroxyl groups would most likely remain unaltered after ozonation, and even the amine oxidation reactions might not lead to anything more than loss of the amine groups via aminoxide/aminyl radical-induced decarboxylation (*111*). In fact, the bulk of the aminoglycoside structure might be expected to remain intact during ozone oxidation, due to the presence of so many saturated aliphatic systems. Thus, any major reduction in rRNA binding might be derived more from reduction in the ability of these compounds to reach their target (e.g., by loss of the amines from which their polycationic character and resulting intracellular transport characteristics are due) (*1*), or by a decrease in their ability to displace metal cations in the cell membrane superstructure.

1.8.1.10. Triclosan (Biocide). Triclosan, 5-chloro-2-(2,4-dichlorophenoxy)phenol (Figure 1.7), is used as a generic antimicrobial agent, or biocide, in a large number of medical and personal-hygiene products (e.g., soaps, deodorants, toothpaste). To a lesser extent, triclosan is used in textiles and plastics (sportswear, bed clothes, shoes, carpets) to control the growth of disease or odor-causing bacteria. In Europe, ~ 350 tons of triclosan are sold per year as the active ingredient of Irgasan DP 300 or Irgacare MP (*112*).

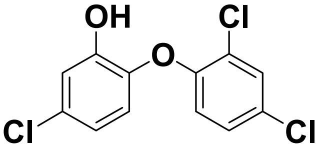

Figure 1.7. Triclosan, shown with site of protonation and probable sites of initial O_3 attack

O_3 is expected to react primarily with TRI's phenol ring (*113*), which mediates TRI's target-specific inhibition of bacterial fatty acid synthesis via van der Waals and hydrogen-bonding interactions with the enoyl-acyl carrier protein reductase (ENR) enzyme (*114,115*). Furthermore, $^{\bullet}$OH – on account of its low selectivity – would be expected to react not only with the phenolic ring, but also with TRI's dichlorophenoxyl ring, which also plays an important role in mediating TRI's interactions with the ENR enzyme, mainly via additional van der Waals interactions with the target enzyme (*114,115*). Each of the possible oxidation pathways is thus expected to result in attenuation of TRI's target-specific antibacterial activity.

1.9 . Thesis Layout

The work reported in this dissertation is based upon the compilation of peer-review research articles published, submitted, or prepared from experimental work conducted prior to the official Ph.D. defense in the context of or while pursuing the objectives described above. The content of these articles is briefly summarized as follows:

Chapter 1. Introduction – An overview of the motivations for conducting this investigation, as well as relevant background, a brief discussion of the scope of work conducted, as well as the characteristics of the model compounds chosen for use in this work.

Chapter 2. Oxidation of Antibacterial Molecules by Aqueous Ozone: Moiety-Specific Reaction Kinetics and Application to Ozone-Based Wastewater Treatment – A detailed investigation of the second-order rate constants (apparent and elementary) for oxidation of each of the model compounds shown in Table 1.1 by O_3 and $^{\bullet}OH$, with additional experiments conducted in a sample of secondary wastewater effluent to facilitate interpretation of the role of these rate constants in governing antibacterial oxidation during wastewater ozonation

Chapter 3. Kinetics of Triclosan Oxidation by Aqueous Ozone and Consequent Loss of Antibacterial Activity: Relevance to Municipal Wastewater Ozonation – A study of the kinetics of triclosan oxidation by O_3, with investigation of probable reaction site(s), consequent changes in antibacterial activity, and the role of reaction kinetics in governing triclosan oxidation during ozonation of two municipal wastewater effluent samples

Chapter 4. Oxidation of Antibacterial Compounds by Ozone and Hydroxyl Radical: Elimination of Biological Activity during Aqueous Ozonation Processes – A combined chemical and microbiological investigation focusing on changes in antibacterial compound activities upon oxidation by O_3 and $^{\bullet}OH$, which were quantified by a broth microdilution assay using references strains of *E. coli* or *B. subtilis*.

Chapter 5. Transformation of *β*-lactam Antibacterial Agents during Aqueous Ozonation: Reaction Pathways and Quantitative Bioassay of Biologically-Active Oxidation Products – A comprehensive study in which biologically-active transformation products (as well as all other major products) generated in the reactions of O_3 with penicillin G and cephalexin were isolated and characterized by a combination of chemical and microbiological techniques.

Chapter 6. General Conclusions – A summary overview of the major findings of this investigation and their importance in the context of municipal wastewater ozonation.

Appendix A. Ozonation of Source-separated Urine for Resource Recovery and Waste Minimization: Process Modeling, Reaction Chemistry, and Operational Considerations – A collaborative study on the use of ozone to degrade organic micropollutants present in source-separated human urine prior to discharge to municipal sewerage or reuse in agriculture;

conducted in parallel to the core work performed in the context of this thesis. A number of the core findings from this study are directly relevant to the topics explored in the thesis.

Appendix B. Kinetics and Mechanistic Aspects of As(III) Oxidation by Aqueous Chlorine, Chloramines, and Ozone: Relevance to Drinking Water Treatment – An additional collaborative investigation conducted to elucidate the kinetics and mechanisms of arsenite (As(III)) oxidation to arsenate (As(V)) by oxidant species commonly applied for As(III) pre-oxidation in drinking water treatment; also conducted in parallel to the core work performed in the context of this thesis. Several of the methods developed within this study were also applied to experiments conducted as part of the thesis.

Literature Cited

(1) Walsh, C. *Antibiotics: Actions, Origins, Resistance*; ASM Press: Washington, D.C., 2003.
(2) Levy, S. B.; Marshall, B. Antibacterial resistance worldwide: causes, challenges and responses. *Nature Medicine* **2004**, *10*, S122-S129.
(3) Heinemann, J. A. How antibiotics cause antibiotic resistance. *Drug. Disc. Today* **1999**, *4*, 72-79.
(4) APUA Home Page. Available at http://www.tufts.edu/med/apua/. Alliance for the Prudent Use of Antibiotics: Boston, Massachussetts (U.S.A.).
(5) Schlaes, D. M.; Gerding, D. N.; John, J. F., Jr.; Craig, W. A.; Bornstein, D. L.; Duncan, R. A.; Eckman, M. R.; Farrer, W. E.; Greene, W. H.; Lorian, V.; Levy, S.; McGowan, J. E., Jr.; Paul, S. M.; Ruskin, J.; Tenover, F. C.; Watanakunakorn, C. Society for Healthcare Epidemiology of America and Infectious Diseases Society of America Joint Committee on the Prevention of Antimicrobial Resistance:Guidelines for the prevention of antimicrobial resistance in hospitals. *Clinical Infectious Diseases* **1997**, *25*, 584-599.
(6) Walsh, C. Molecular mechanisms that confer antibacterial drug resistance. *Nature* **2000**, *406*, 775-781.
(7) National Academy Press. *The Use of Drugs in Food Animals*; Washington, D.C., 1999.
(8) Hartmann, A.; Alder, A. C.; Koller, T.; Widmer, R. M. Identification of fluoroquinolone antibiotics as the main source of umuC genotoxicity in native hospital wastewater. *Environ. Toxicol. Chem.* **1998**, *17*, 377-382.
(9) Hirsch, R.; Ternes, T. A.; Haberer, K.; Kratz, K.-L. Occurrence of antibiotics in the environment. *Sci. Total Environ.* **1999**, *225*, 109-118.
(10) Kolpin, D. W.; Furlong, E. T.; Meyer, M. T.; Thurman, E. M.; Zaugg, S. D.; Barber, L. B.; Buxton, H. T. Pharmaceuticals, hormones, and other organic wastewater contaminants in U.S. Streams, 1999-2000: A national reconnaissance. *Environ. Sci. Technol.* **2002**, *36*, 1202-1211.
(11) Golet, E. M.; Xifra, I.; Siegrist, H.; Alder, A. C.; Giger, W. Environmental exposure assessment of fluoroquinolone antibacterial agents from sewage to soil. *Environ. Sci. Technol.* **2003**, *37*, 3243-3249.

(12) Löffler, D.; Ternes, T. A. Analytical method for the determination of the aminoglycoside gentamicin in hospital wastewater via liquid chromatography–electrospray-tandem mass spectrometry. *J. Chromatogr., A* **2003**, *1000*, 583-588.

(13) Miao, X.-S.; Bishay, F.; Chen, M.; Metcalfe, C. D. Occurrence of antimicrobials in the final effluents of wastewater treatment plants in Canada. *Environ. Sci. Technol.* **2004**, *38*, 3542-3550.

(14) Renew, J. E.; Huang, C.-H. Simultaneous determination of fluoroquinolone, sulfonamide, and trimethoprim antibiotics in wastewater using tandem solid phase extraction and liquid chromatography–electrospray mass spectrometry. *J. Chromatogr., A* **2004**, *1042*, 113-121.

(15) Andreozzi, R.; Caprio, V.; Ciniglia, C.; de Champdoré, M.; lo Giudice, R.; Marotta, R.; Zuccato, E. Antibiotics in the environment: occurrence in Italian STPs, fate, and preliminary assessment on algal toxicity of amoxicillin. *Environ. Sci. Technol.* **2004**, *38*, 6832-6838.

(16) Filali, B. K.; Taoufik, J.; Zeroual, Y.; Dzairi, F. Z.; Talbi, M.; Blaghen, M. Waste Water Bacterial Isolates Resistant to Heavy Metals and Antibiotics. *Curr. Microbiol* **2000**, *41*, 151-156.

(17) Heier, H.; Tschape, H. Über das Vorkommen von R-Plasmiden in Escherichia coli und koliformen Keimen aus Wasser und Abwasser. Teil 2: Methoden der Isolierung von R^+ - Bakterien aus Oberflächen - und Abwasser, des Transfers ihrer R-Plasmide sowie die Bestimmung der Resistenzbilder. *Acta Hydrochim. Hydrobiol.* **1984**, *12*, 47-54.

(18) Tschäpe, H.; Tietze, E.; Prager, R.; Heier, H. Occurrence in Water and Waste Water of E. coli and Coliform Bacteria Carrying R-Plasmids. Part 3. Plasmids Encoding Gentamicin, Trimethoprim, or Streptothricin Resistance. *Acta Hydrochim. Hydrobiol.* **1986**, *14*, 167-174.

(19) Guardabassi, L.; Dalsgaard, A.; Olsen, J. E. Phenotypic characterization and antibiotic resistance of Acinetobacter spp. isolated from aquatic sources. *J. Appl. Microbiol.* **1999**, *87*, 659-667.

(20) Alcaide, E.; Garay, E. R-Plasmid Transfer in Salmonella spp. Isolated from Wastewater and Sewage-Contaminated Surface Waters. *Appl. Environ. Microbiol.* **1984**, *48*, 435-438.

(21) Guardabassi, L.; Lo Fo Wong, D. M. A.; Dalsgaard, A. The Effects of Tertiary Wastewater Treatment on the Prevalence of Antimicrobial Resistant Bacteria. *Water Res.* **2002**, *36*, 1955-1964.

(22) Rhodes, G.; Huys, G.; Swings, J.; McGann, P.; Hiney, M.; Smith, P.; Pickup, R. W. Distribution of Oxytetracycline Resistance Plasmids between Aeromonads in Hospital and Aquaculture Environments: Implication of Tn1721 in Dissemination of the Tetracycline Resistance Determinant Tet A. *Appl. Environ. Microbiol.* **2000**, *66*, 3883-3890.

(23) Guardabassi, L.; Dijkshoorn, L.; Collard, J.-M.; Olsen, J. E.; Dalsgaard, A. Distribution and in-vitro transfer of tetracycline resistance determinants in clinical and aquatic Acinetobacter strains. *J. Med. Microbiol.* **2000**, *49*, 929-936.

(24) Umaran, A.; J., G.; Cisterna, R. Antibiotic Resistance and Transferable R Plasmids in Coliforms from a Polluted Estuary. *Acta Hydrochim. Hydrobiol.* **1989**, *17*, 543-551.

(25) Goni-Urriza, M.; Capdepuy, M.; Arpin, C.; Raymond, N.; Caumette, P.; Quentin, C. Impact of an Urban Effluent on Antibiotic Resistance of Riverine *Enterobacteriaceae* and *Aeromonas* spp. *Appl. Environ. Microbiol.* **2000**, *66*, 125-132.

(26) Guardabassi, L.; Dalsgaard, A.; Raffatellu, M.; Olsen, J. E. Increase in the Prevalence of Oxolinic Acid Resistant *Acinetobacter* spp. Observed in a Stream Receiving the

Effluent from a Freshwater Trout Farm Following the Treatment with Oxolinic Acid-Medicated Feed. *Aquaculture* **2000**, *188*, 205-218.

(27) Arvanitidou, M.; Tsakkris, A.; Constantinidis, T. C.; Katsouyannopoulos, V. C. Transferable Antibiotic Resistance among Salmonella Strains Isolated from Surface Waters. *Water Res.* **1997**, *31*, 1112-1116.

(28) Gerding, D. N.; Hughes, C. e.; Bamberger, D. M.; Foxworth, J.; Larson, T. A. In *Antibiotics in Laboratory Medicine*; 4 ed.; Lorian, V., Ed.; Waverly and Wilkins: Baltimore, MD, 1996, pp 835-899.

(29) Nicolle, L. E. In *Antibiotics in Laboratory Medicine*; 4 ed.; Lorian, V., Ed.; Waverly and Wilkins: Baltimore, MD, 1996, pp 793-812.

(30) Levy, S. B.; Marshall, B.; Schluederberg, S.; Rowse, D.; Davis, J. High frequency of antimicrobial resistance in human fecal flora. *Antimicrob. Agents Chemother.* **1988**, *32*, 1801-1806.

(31) Drlica, K.; Zhao, X. L. DNA gyrase, topoisomerase IV, and the 4-quinolones. *Microbiol. Mol. Biol. Rev.* **1997**, *61*, 377-&.

(32) Chopra, I.; Roberts, M. Tetracycline antibiotics: Mode of action, applications, molecular biology, and epidemiology of bacterial resistance. *Microbiol. Mol. Biol. Rev.* **2001**, *65*, 232-260.

(33) Courvalin, P.; Trieu-Cuot, P. Minimizing potential resistance: The molecular view. *Clinical Infectious Diseases* **2001**, *33*, S138-S146.

(34) RxList, The Internet Drug Index. Available at http://www.rxlist.com/top200.htm. NDC Health. 2003

(35) Hartmann, A.; Golet, E. M.; Gartiser, S.; Alder, A. C.; Koller, T.; Widmer, R. M. Primary DNA damage but not mutagenicity correlates with ciprofloxacin concentrations in German hospital wastewaters. *Arch. Environ. Contam. Toxicol.* **1999**, *36*, 115-119.

(36) Lindberg, R.; Jarnheimer, P.-Å.; Olsen, B.; Johansson, M.; Tysklind, M. Determination of antibiotic substances in hospital sewage water using solid phase extraction and liquid chromatography/mass spectrometry and group analogue internal standards. *Chemosphere* **2004**, *57*, 1479-1488.

(37) Walter, M. V.; Vennes, J. W. Occurrence of Multiple-Antibiotic-Resistant Enteric Bacteria in Domestic Sewage and Oxidation Lagoons. *Appl. Environ. Microbiol.* **1985**, *50*, 930-933.

(38) Guardabassi, L.; Petersen, A.; Olsen, J. E.; Dalsgaard, A. Antibiotic resistance in *Acinetobacter* spp. isolated from sewers receiving waste effluent from a hospital and a pharmaceutical plant. *Appl. Environ. Microbiol.* **1998**, *64*, 3499-3502.

(39) Harwood, V. J.; Brownwell, M.; Perusek, W.; Whitlock, J. E. Vancomycin-Resistant *Enterococcus* spp. Isolated from Wastewater and Chicken Feces in the United States. *Appl. Environ. Microbiol.* **2001**, *67*, 4930-4933.

(40) Schwartz, T.; Kohnen, W.; Jansen, B.; Obst, U. Detection of antibiotic-resistant bacteria and their resistance genes in wastewater, surface water, and drinking water biofilms. *FEMS Microbiol. Ecol.* **2003**, *43*, 325-335.

(41) Iversen, A.; Kuhn, I.; Rahman, M.; Franklin, A.; Burman, L. G.; Olsson-Liljequist, B.; Torell, E.; Mollby, R. Evidence for transmission between humans and the environment of a nosocomial strain of Enterococcus faecium. *Environ. Microbiol.* **2004**, *6*, 55-59.

(42) Lorenz, M. G.; Wackernagel, W. Bacterial Gene Transfer by Natural Genetic Transformation in the Environment. *Microbiol. Reviews* **1994**, *58*, 563-602.

(43) Frolund, B.; Palmgren, R.; Keiding, K.; Nielsen, P. H. Extraction of Extracellular Polymers from Activated Sludge using a Cation Exchange Resin. *Water Res.* **1996**, *30*, 1749-1758.

(44) Nielsen, P. H.; Frolund, B.; Keiding, K. Changes in the composition of extracellular polymeric substances in activated sludge during anaerobic storage. *Appl. Microbiol. Biotechnol.* **1996**, *44*, 823-830.
(45) Lenski, R. E.; Simpson, S. C.; Nguyen, T. T. Genetic analysis of a plasmid-encoded, host genotype-specific enhancement of bacterial fitness. *J. Bacteriol.* **1994**, *176*, 3140-3147.
(46) Schrag, S. J.; Perrot, V.; Levin, B. R. Adaptation to the fitness costs of antibiotic resistance in *Escherichia coli*. *Proc.: Biol. Sci.* **1997**, *264*, 1287.
(47) Jones, M. E.; Boenink, N. M.; Verhoef, J.; Köhrer, K.; Schmitz, F.-J. Multiple mutations conferring ciprofloxacin resistance in *Staphylococcus aureus* demonstrate long-term stability in an antibiotic-free environment. *J. Antimicrob. Chemother.* **2000**, *45*, 353-356.
(48) Paget, E.; Simonet, P. On the track of natural transformation in soil. *FEMS Microbiol. Ecol.* **1994**, *15*, 109-118.
(49) Baur, B.; Hanselmann, K.; Schlimme, W.; Jenni, B. Genetic Transformation in Freshwater: Escherichia coli Is Able To Develop Natural Competence. *Appl. Environ. Microbiol.* **1996**, *62*, 3673-3678.
(50) Reinthaler, F. F.; Posch, J.; Feierl, G.; Wüst, G.; Haas, D.; Ruckenbauer, G.; Mascher, F.; Marth, E. Antibiotic resistance of E. coli in sewage and sludge. *Water Res.* **2003**, *37*, 1685-1690.
(51) Hartig, C.; Storm, T.; Jekel, M. Detection and identification of sulphonamide drugs in municipal waste water by liquid chromatography coupled with electrospray ionisation tandem mass spectrometry. *J. Chromatogr., A* **1999**, *854*, 163-173.
(52) Golet, E. M.; Alder, A. C.; Hartmann, A.; Ternes, T. A.; Giger, W. Trace determination of fluoroquinolone antibacterial agents in urban wastewater by solid-phase extraction and liquid chromatography with fluorescence detection. *Anal. Chem.* **2001**, *73*, 3632-3638.
(53) Golet, E. M.; Alder, A. C.; Giger, W. Environmental exposure and risk assessment of fluoroquinolone antibacterial agents in wastewater and river water of the Glatt Valley watershed, Switzerland. *Environ. Sci. Technol.* **2002**, *36*, 3645-3651.
(54) Wiedmann, B.; Grimm, H. In *Antibiotics in Laboratory Medicine*; Lorian, V., Ed.; Williams and Wilkins: Baltimore, MD, 1996, pp 900-1168.
(55) Ohlsen, K.; Ternes, T. A.; Werner, G.; Wallner, U.; Löffler, D.; Wilma, Z.; Witte, W.; Hacker, J. Impact of antibiotics on conjugational resistance gene transfer in Staphylococcus aureus in sewage. *Environ. Microbiol.* **2003**, *5*, 711-716.
(56) Göbel, A.; Thomsen, A.; McArdell, C. S.; Joss, A.; Giger, W. Occurrence and sorption behavior of sulfonamides, macrolides, and trimethoprim in activated sludge treatment. *Environ. Sci. Technol.* **2005**, *39*, 3981-3989.
(57) Metcalfe, C. D.; Miao, X.-S.; Koenig, B. G.; Struger, J. Distribution of acidic and neutral drugs in surface waters near sewage treatment plants in the lower Great Lakes, Canada. *Environ. Toxicol. Chem.* **2003**, *22*, 2881-2889.
(58) Lindberg, R. H.; Wennberg, P.; Johansson, M. I.; Tysklind, M.; Andersson, B. A. V. Screening of human antibiotic substances and determination of weekly mass flows in five sewage treatment plants in Sweden. *Environ. Sci. Technol.* **2005**, *39*, 3421-3429.
(59) McArdell, C. S.; Molnar, E.; Suter, M. J. F.; Giger, W. Occurrence and fate of macrolide antibiotics in wastewater treatment plants and in the Glatt Valley Watershed, Switzerland. *Environ. Sci. Technol.* **2003**, *37*, 5479-5486.
(60) Göbel, A.; McArdell, C. S.; Suter, M. J.-F.; Giger, W. Trace determination of macrolide and sulfonamide antimicrobials, a human sulfonamide metabolite, and trimethoprim in

wastewater using liquid chromatography coupled to electrospray tandem mass spectrometry. *Anal. Chem.* **2004**, *76*, 4756-4764.

(61) Wiedemann, B.; Grimm, H. In *Antibiotics in Laboratory Medicine*; Lorian, V., Ed.; Williams and Wilkins: Baltimore, MD, 1996, pp 900-1168.

(62) Rice, L. B.; Bonomo, R. A. In *Antibiotics in Laboratory Medicine*; Lorian, V., Ed.; Williams and Wilkins: Baltimore, MD, 1996, pp 453-501.

(63) Fleming, G. T.; McCarthy, D. M.; Colombet, N.; Patching, J. W. The effect of levofloxacin concentration on the development and maintenance of antibiotic-resitant clones of Escherichia coli in chemostat culture. *J. Ind. Microbiol. Biotech.* **2002**, *29*, 155-162.

(64) Joynson, J. a.; Forbes, B.; Lambert, R. J. W. Adaptive resistance to benzalkonium chloride, amikacin and tobramycin: the effect on susceptibility to other antimicrobials. *J. Appl. Microbiol.* **2002**, *93*, 96-107.

(65) Liebl, W.; Kloss, W. E.; Ludwig, W. Plasmid-borne macrolide resistance in Micrococcus luteus. *Microbiol.* **2002**, *148*, 2479-2487.

(66) Robertson, G. T.; Zhao, J.; Desai, B. V.; Coleman, W. H.; Nicas, T. I.; Gilmour, R.; Grinius, L.; Morrison, D. A.; Winkler, M. E. Vancomycin Tolerance Induced by Erythromycin but Not by Loss of vncRS, vex3, or pep27 Function in Streptococcus pneumoniae. *J. Bacteriol.* **2002**, *184*, 6987-7000.

(67) Goh, E.-B.; Yim, G.; Tsui, W.; McClure, J.; Surette, M. G.; Davies, J. Transcriptional modulation of bacterial gene expression by subinhibitory concentrations of antibiotics. *Proc. Natl. Acad. Sci. U.S.A.* **2002**, *99*, 17025-17030.

(68) Gemmell, C. G.; Lorian, V. In *Antibiotics in Laboratory Medicine*; Lorian, V., Ed.; Williams and Wilkins: Baltimore, MD, 1996, pp 453-501.

(69) Wilson, B. A.; Smith, V. H.; Denoyelles, F.; Larive, C. K. Effects of three pharmaceutical and personal care products on natural freshwater algal assemblages. *Environ. Sci. Technol.* **2003**, *37*, 1713-1719.

(70) Yang, L. H.; Ying, G. G.; Su, H. C.; Stauber, J. L.; Adams, M. S.; Binet, M. T. Growth-inhibiting effects of 12 antibacterial agents and their mixtures on the freshwater microalga Pseudokirchneriella subcapitata. *Environ. Toxicol. Chem.* **2008**, *27*, 1201-1208.

(71) Knapp, C. W.; Engemann, C. A.; Hanson, M. L.; Keen, P. L.; Hall, K. J.; Graham, D. W. Indirect evidence of transposon-mediated selection of antibiotic resistance genes in aquatic systems at low-level oxytetracycline exposures. *Environ. Sci. Technol.* **2008**, *42*, 5348-5353.

(72) Cordova-Kreylos, A. L.; Scow, K. M. Effects of ciprofloxacin on salt marsh sediment microbial communities. *Isme Journal* **2007**, *1*, 585-595.

(73) O'Reilly, A.; Smith, P. Development of methods for predicting the minimum concentrations of oxytetracycline capable of exerting a selection for resistance to this agent. *Aquaculture* **1999**, *180*, 1-11.

(74) Bouma, J. E.; Lenski, R. E. Evolution of a bacteria/plasmid association. *Nature* **1988**, *335*.

(75) Schrag, S. J.; Perrot, V. Reducing antibiotic resistance. *Nature* **1996**, *381*, 120-121.

(76) Björkman, J.; Hughes, D.; Andersson, D. I. Virulence of antibiotic-resistant *Salmonella typhimurium*. *Proc. Natl. Acad. Sci. U.S.A.* **1998**, *95*, 3949-3953.

(77) Heinemann, J. A.; Ankenbauer, R. G.; Amabile-Cuevas, C. F. Do Antibiotics Maintain Antibiotic Resistance? *Drug. Disc. Today* **2000**, *5*, 195-204.

(78) Hoigné, J. In *The Handbook of Environmental Chemistry*; Hrubec, J., Ed.; Springer Verlag: Berlin, Germany, 1998, pp 83-141.

(79) von Gunten, U. Ozonation of drinking water: Part I. Oxidation kinetics and product formation. *Water Res.* **2003**, *37*, 1443-1467.

(80) Adams, C. A.; Austin, B.; Meaden, P. G.; McIntosh, D. Molecular Characterization of Plasmid-Mediated Oxytetracycline Resistance in Aeromonas salmonicida. *Appl. Environ. Microbiol.* **1998**, *64*, 4194-4201.

(81) Huber, M. M.; Canonica, S.; Park, G.-Y.; von Gunten, U. Oxidation of Pharmaceuticals during Ozonation and Advanced Oxidation Processes. *Environmental Science and Technology* **2003**, *37*, 1016-1024.

(82) Huang, W.; Peng, P.; Yu, Z.; Fu, J. Effects of organic matter heterogeneity on sorption and desorption of organic contaminants by soils and sediments*1. *Applied Geochemistry* **2003**, *18*, 955-972.

(83) Hoigné, J.; Bader, H. Rate constants of reactions of ozone with organic and inorganic compounds in water – I : Non-dissociating organic compounds. *Water Res.* **1983**, *17*, 173-183.

(84) Hoigné, J.; Bader, H. Rate constants of reactions of ozone with organic and inorganic compounds in water – II : Dissociating organic compounds. *Water Res.* **1983**, *17*, 185-194.

(85) Huber, M. M.; McDowell, D.; Ternes, T. A.; von Gunten, U. Oxidation of Pharmaceuticals during Ozonation: Kinetics and Product Formation. Extended abstracts of the *Internation Ozone Association, 16th World Congress*, Las Vegas, NV, 2003; International Ozone Association.

(86) NCCLS, Performance Standards for Antimicrobial Disk Susceptibility Tests-Sixth Edition; Approved Standard. Available at. NCCLS.

(87) NCCLS, Methods for Dilution Antimicrobial Susceptibility Tests for Bacteria that Grow Aerobically-Fourth Edition; Approved Standard. Available at. NCCLS.

(88) *Antibiotics in Laboratory Medicine*; 4 ed.; Williams and Wilkins: Baltimore, MD, 1996.

(89) von Gunten, U. Ozonation of drinking water: Part II. Disinfection and by-product formation in presence of bromide, iodide, or chloride. *Water Res.* **2003**, *37*, 1469-1487.

(90) Adams, C.; Wang, Y.; Loftin, K.; Meyer, M. Removal of antibiotics from surface and distilled water in conventional water treatment processes. *J. Environ. Eng.* **2002**, *128*, 253-260.

(91) Qiang, Z.; Adams, C.; Surampalli, R. Determination of ozonation rate constants for lincomycin and spectinomycin. *Ozone: Sci. Eng.* **2004**, *26*, 525-537.

(92) Lange, F.; Cornelissen, S.; Kubac, D.; Sein, M. M.; von Sonntag, J.; Hannich, C. B.; Golloch, A.; Heipieper, H. J.; Moder, M.; von Sonntag, C. Degradation of macrolide antibiotics by ozone: A mechanistic case study with clarithromycin. *Chemosphere* **2006**, *65*, 17-23.

(93) Phillips, G. O.; Power, D. M.; Robinson, C. Chemical changes following γ-irradiation of benzylpenicillin in aqueous solution. *J. Chem. Soc., Perkin Trans. 2* **1973**, 575-582.

(94) Dodd, M. C.; Huang, C.-H. Transformation of the antibacterial agent sulfamethoxazole in reactions with chlorine: kinetics, mechanisms, and pathways. *Environ. Sci. Technol.* **2004**, *38*, 5607-5615.

(95) RxList, The Internet Drug Index. Available at http://www.rxlist.com/top200.htm. NDC Health. 2002

(96) McArdell, C. S.; Molnar, E.; Suter, M. J.-F.; Giger, W. Occurrence and Fate of Macrolide Antibiotics in Wastewater Treatment Plants and in the Glatt Valley Watershed, Switzerland. *Environmental Science and Technology* **2003**.

(97) Stratton, C. W. In *Antibiotics in Laboratory Medicine*; Lorian, V., Ed.; Williams and Wilkins: Baltimore, MD, 1996, pp 579-603.

(98) Uetrecht, J. P.; Shear, N. H.; Zahid, N. N-Chlorination of Sulfamethoxazole and Dapsone by the Myeloperoxidase System. *Drug Metab. Dispos.* **1993**, *21*, 830-834.

(99) Lai, W. G.; Zahid, N.; Uetrecht, J. P. Metabolism of trimethoprim to a reactive iminoquinone methide by activated human neutrophils and hepatic microsomes. *J. Pharmacol. Exp. Ther.* **1999**, *291*, 292-299.

(100) Ternes, T. A. Analytical methods for the determination of pharmaceuticals in aqueous environmental samples. *Trends Anal. Chem.* **2001**, *20*, 419-434.

(101) Matsui, M.; Kamiya, K.; Shibata, K.; Muramatsu, H.; Nakazumi, H. Ozonolysis of Substituted Uracils. *J. Org. Chem.* **1990**, *55*, 1396-1399.

(102) Theruvathu, J. A.; Flyunt, R.; Aravindakumar, C. T.; von Sonntag, C. Rate constants of ozone reactions with DNA, its constituents, and related compounds. *J. Chem. Soc., Perkin Trans. 2* **2001**, 269-274.

(103) Flyunt, R.; Theruvathu, J. A.; Leitzke, A.; von Sonntag, C. The reactions of thymine and thymidine with ozone. *J. Chem. Soc., Perkin Trans. 2* **2002**, 1572-1582.

(104) Matsui, M.; Shibata, K.; Muramatsu, H.; Nakazumi, H. Ozonolyses of cytosines and guanine. *J. Org. Chem.* **1991**, *56*, 4987-4990.

(105) Muñoz, F.; von Sonntag, C. Determination of fast ozone reactions in aqueous solution by competition kinetics. *J. Chem. Soc., Perkin Trans. 2* **2000**, *2*, 661-664.

(106) Cocco, L.; Roth, B.; Temple, C., Jr.; Montgomery, J. A.; London, R. E.; Blakley, R. L. Protonated state of methotrexate, trimethoprim, and pyrimethamine bound to dihydrofolate reductase. *Arch. Biochem. Biophys.* **1983**, *226*, 567-577.

(107) Dodd, M. C., *Chemical oxidation of aquatic antibiotic microcontaminants by free and combined chlorine*. M.S. Thesis, School of Civil and Environmental Engineering, Georgia Institute of Technology: Atlanta, GA, 2003.

(108) Livermore, D. M.; Williams, J. D. In *Antibiotics in Laboratory Medicine*; 4 ed.; Lorian, V., Ed.; Williams and Wilkins: Baltimore, MD, 1996, pp 502-578.

(109) Qiang, Z.; Adams, C.; Surampalli, R. Determination of Ozonation Rate Constants for Lincomycin and Spectinomycin. Extended abstracts of the *International Ozone Association, 16th World Congress*, Las Vegas, NV, 2003; International Ozone Association.

(110) Tolls, J. Sorption of Veterinary Pharmaceuticals in Soils: A Review. *Environ. Sci. Technol.* **2001**, *35*, 3397-3406.

(111) Muñoz, F.; von Sonntag, C. The reactions of ozone with tertiary amines including the complexing agents nitrilotriacetic acid (NTA) and ethylenediaminetetraacetic acid (EDTA) in aqueous solution. *J. Chem. Soc., Perkin Trans. 2* **2000**, 2029-2033.

(112) Singer, H.; Muller, S.; Tixier, C.; Pillonel, L. Triclosan: Occurrence and fate of a widely used biocide in the aquatic environment: Field measurements in wastewater treatment plants, surface waters, and lake sediments. *Environ. Sci. Technol.* **2002**, *36*, 4998-5004.

(113) Suarez, S.; Dodd, M. C.; Omil, F.; von Gunten, U. Kinetics of triclosan oxidation by aqueous ozone and consequent loss of antibacterial activity: Relevance to municipal wastewater ozonation. *Water Res.* **2007**, *41*, 2481-2490.

(114) Heath, R. J.; Rubin, J. R.; Holland, D. R.; Zhang, E. L.; Snow, M. E.; Rock, C. O. Mechanism of triclosan inhibition of bacterial fatty acid synthesis. *J. Biol. Chem.* **1999**, *274*, 11110-11114.

(115) Levy, C. W.; Roujeinikova, A.; Sedelnikova, S.; Baker, P. J.; Stuitje, A. R.; Slabas, A. R.; Rice, D. W.; Rafferty, J. B. Molecular basis of triclosan activity. *Nature* **1999**, *398*, 383-384.

Chapter 2. Oxidation of Antibacterial Molecules by Aqueous Ozone: Moiety-Specific Reaction Kinetics and Application to Ozone-Based Wastewater Treatment

Dodd, M. C.; Buffle, M.-O.; von Gunten, U. *Environmental Science and Technology* **2006,** 40(6), 1969-1977

Abstract

Ozone and hydroxyl radical (•OH) reaction kinetics were measured for 14 antibacterial compounds from nine structural families, to determine whether municipal wastewater ozonation is likely to result in selective oxidation of these compounds' biochemically essential moieties. These compounds are oxidized by ozone with apparent second-order rate constants, $k''_{O_3,app}$ > 1 × 10^3 $M^{-1}s^{-1}$, at pH 7, with the exception of *N*(4)-acetylsulfamethoxazole ($k''_{O_3,app}$ is 2.5 × 10^2 $M^{-1}s^{-1}$). $k''_{O_3,app}$ (pH 7) for macrolides, sulfamethoxazole, trimethoprim, tetracycline, vancomycin, and amikacin appear to correspond directly to oxidation of biochemically essential moieties. Initial reactions of ozone with N(4)-acetylsulfamethoxazole, fluoroquinolones, lincomycin, and *β*-lactams do not lead to appreciable oxidation of biochemically essential moieties. However, ozone oxidizes these moieties within fluoroquinolone and lincomycin via slower reactions. Measured $k''_{O_3,app}$ values and second-order •OH rate constants, $k''_{\bullet OH,app}$, were utilized to characterize pollutant losses during ozonation of secondary municipal wastewater effluent. Measured losses were dependent on $k''_{O_3,app}$, but independent of $k''_{\bullet OH,app}$. Ozone doses ≥3 mg/L yielded ≥99% depletion of fast-reacting substrates ($k''_{O_3,app}$ > 5 × 10^4 $M^{-1}s^{-1}$) at pH 7.7. Ten substrates reacted predominantly with ozone; only four were oxidized predominantly by •OH. These results indicate that many antibacterial compounds will be oxidized in wastewater via moiety-specific reactions with ozone.

2.1 Introduction

Clinically-important antibacterial agents are virtually ubiquitous contaminants of municipal wastewaters (Supporting Information for Chapter 2, Figure S2.1) (*1-5*). Raw and primary wastewaters typically contain compounds from various antibacterial classes at individual concentrations ranging from 0.5-3 μg/L (Figure S2.1). These concentrations can often be reduced by 60-90% during conventional activated sludge treatment combined with tertiary filtration (*2,4,6*). This is generally sufficient to achieve effluent concentrations below levels known to be detrimental to bacteria (Figure S2.1) and other aquatic life (*7,8*). However, effluent concentrations of certain antibacterials (e.g., fluoroquinolones (*2,3*)) may still be harmful to organisms present in effluent-dominated receiving waters (*9*). In addition, because activated sludge processes typically operate at solids retention times of several days, conventional wastewater treatment results in prolonged exposure of wastewater-borne bacteria to significantly higher antibacterial concentrations than are present in treated effluents (*2,4-6*). In the case of fluoroquinolones, these concentrations can approach minimal growth inhibitory concentrations (MICs) for *E. coli* (Figure S2.1) and other bacterial strains (*10*) - a condition which may favor evolution of low-level antibacterial resistance in affected bacterial communities (*11,12*).

In the interest of precaution, unnecessary exposure of wastewater-borne and environmental microbiota to biochemical stress originating from antibacterial compounds should be minimized when possible. Supplemental wastewater treatment technologies capable of yielding rapid biochemical deactivation of such compounds could aid in achieving this objective. Ozonation, which is utilized in advanced treatment of secondary wastewater effluent (*13*), and has shown potential as a means of pre-oxidizing and disinfecting primary wastewater effluents (*14,15*), appears promising in this regard (*16-18*). Recent studies have shown that relatively low ozone (O_3) doses ($\leq$ 5 mg/L) can yield > 90% depletion of many antibacterial compounds in wastewaters containing up to 23 mg-C/L of DOC (*18,19*). Although mineralization of antibacterial molecules will be infeasible during municipal wastewater ozonation, partial oxidation may be sufficient to achieve their biochemical deactivation, provided that O_3 reacts with the parent molecules in a manner leading to rapid, selective oxidation of functional moieties related to their antibacterial activities. Such an outcome has been demonstrated for the steroid hormone 17α-ethinylestradiol, in which case ozone selectively oxidizes the phenol moiety responsible for the parent molecule's estrogenic activity (*20*). Similar results appear likely for many antibacterial molecules (Table 2.1, Text S2.1). However, some antibacterial compounds' biochemically-essential moieties may be O_3-

---

Table 2.1. Antibacterial substrates and expected sites of O_3 attack[a,b,c,d]

Macrolides

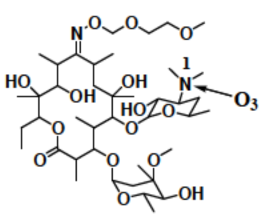

Roxithromycin (RX)
p*K*a = 9.2

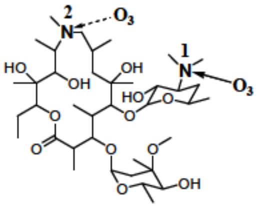

Azithromycin (AZ)
$pK_{a1,2}$ = 8.7, 9.5

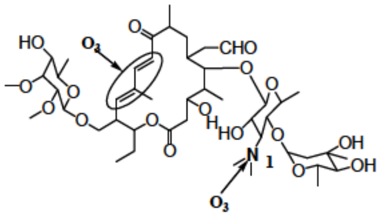

Tylosin (TYL)
pK_a = 7.7

Sulfonamides

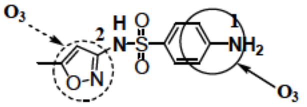

Sulfamethoxazole (SMX)
$pK_{a1,2}$ = 1.7, 5.6

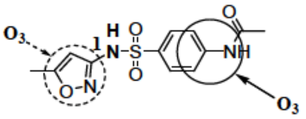

N(4)-acetyl-sulfamethoxazole (ASMX)
pK_a = 5.5

DHFR Inhibitor[e]

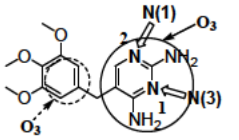
N(1)
O3
2
1
N(3)
O3

Trimethoprim (TMP)
$pK_{a1,2}$ = 3.2, 7.1

Fluoroquinolones

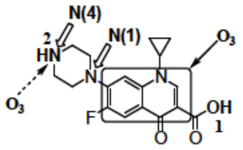
N(4)
2
N(1)
O3
O3
1

Ciprofloxacin (CF)
$pK_{a1,2}$ = 6.2, 8.8

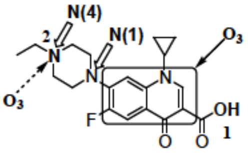
N(4)
2
N(1)
O3
O3
1

Enrofloxacin (EF)
$pK_{a1,2}$ = 6.1, 7.7

Lincosamide

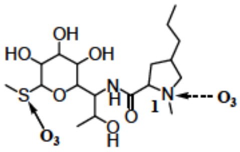

Lincomycin (LM)
pK_a = 7.8

β-lactams

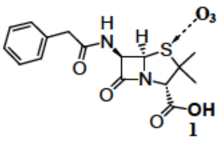

Penicillin G (PG)
pK_a = 2.7

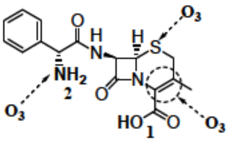

Cephalexin (CP)
$pK_{a1,2}$ = 2.5, 7.1

Tetracycline

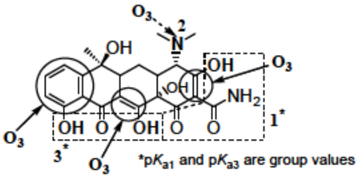
O3
2
O3
1*
O3
3*
O3

*pK_{a1} and pK_{a3} are group values

Tetracycline (TET)
$pK_{a1,2,3}$ = 3.3, 7.7, 9.7

Glycopeptide

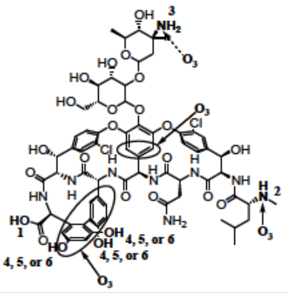
3
O3
O3
2
O3
1
4, 5, or 6
4, 5, or 6
4, 5, or 6
O3

Vancomycin (VM)
$pK_{a1,2,3,4,5,6}$ =
2.9, 7.2, 8.6, 9.6, 10.5, 11.7

Aminoglycoside

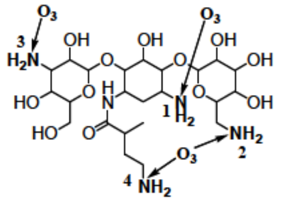
O3
3
O3
1
2
O3
4

Amikacin (AM)
$pK_{a1,2,3,4}$ = 6.7, 8.4, 8.4, 9.7

---

[a] Structural families are listed in bold. [b] O_3 target sites are classified as: "essential" (i.e., these moieties are directly responsible for the parent molecules' antibacterial activities – Text S2.1) – indicated by solid arrows, and "nonessential" (i.e.,these moieties are not directly responsible for the parent molecules' antibacterial activities) – indicated by dotted arrows. [c] References from which pK_a values were obtained are summarized in Table S2.1. [d] Sites of ionization are numbered according to order of deprotonation. For compounds possessing a single pK_a, the ionizable site is labeled 1. [e] DHFR – dihydrofolate reductase.

Table 2.2. Substructure model substrates and expected sites of O_3 attack[a,b]

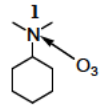	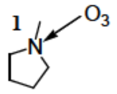	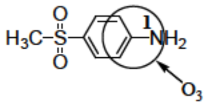	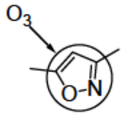
N,N-dimethylcyclohexylamine (DMCH)	1-methylpyrrolidine (MP)	4-aminophenyl methyl sulfone (APMS)	3,5-dimethylisoxazole (DMI)
$pK_a = 10.7$	$pK_a = 10.2$	$pK_a = 1.5$	
Model for: RX, AZ, TYL, TET	Model for: AZ, LM	Model for: SMX	Model for: SMX, ASMX
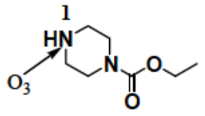	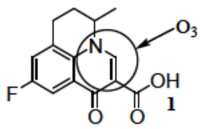	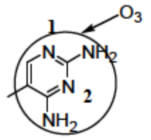	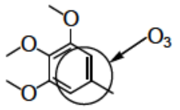
Ethyl *N*-piperazinecarboxylate (EPC)	Flumequine (FLU)	2,4-diamino-5-methylpyrimidine (DAMP)	3,4,5-trimethoxytoluene (TMT)
$pK_a = 8.3$	$pK_a = 6.5$	$pK_{a1,2} = 3.2, 7.1$	
Model for: CF, EF	Model for: CF, EF	Model for. TMP	Model for: TMP, VM
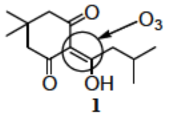	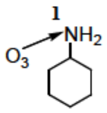	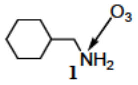	
2-(3-methylbutyryl)-5,5-dimethyl-1,3-cyclohexandione (MBDCH)	Cyclohexylamine (CH)	Cyclohexanemethylamine (CHM)	
$pK_a = 3.5$	$pK_a = 10.6$	$pK_a = 10.3$	
Model for: TET	Model for: AM	Model for: AM	

[a]References from which pK_a values were obtained are summarized in Table S2.2. [b]In the case of DAMP, which has two pK_as, sites of ionization are numbered according to order of deprotonation. Sites of ionization are labeled 1 for all other ionizable compounds.

refractory, or O_3 may react preferentially with moieties nonessential to the parent molecules' biochemical activities (Table 2.1). In such cases, relative reactivities of "essential" and "nonessential" functional moieties will influence the likelihood that antibacterial compounds can be biochemically deactivated during wastewater ozonation.

pH-dependent variations in measured "apparent" rate constants can be used to determine "specific" rate constants for reactions of O_3 with each individual acid-base species of an ionizable substrate (*21-23*). This approach was applied in the present study to evaluate O_3 reaction kinetics measured for fourteen antibacterial molecules representing nine of the most widely-used antibacterial structural families (Table 2.1). O_3 reaction kinetics for substructure model substrates (Table 2.2) representing the theorized reactive moieties within each antibacterial molecule were measured to facilitate assignment of calculated species-specific reactivities to individual functional moieties.

Pollutant transformation during wastewater ozonation is also influenced by hydroxyl radicals (•OH) generated through reactions of O_3 with specific functional moieties in dissolved organic matter (*24,25*) or from auto-catalytic O_3 decomposition (*26*). Because •OH reacts rapidly with a wider variety of functional moieties than O_3, the oxidative specificity of an ozonation process may be diminished if dominated by •OH reactions. The importance of •OH and O_3 in the context of antibacterial compound oxidation was investigated by using rate constants determined here to characterize observed antibacterial compound losses during ozonation of a secondary wastewater effluent.

2.2 Materials and Methods

2.2.1 Chemical Reactants and Reagents. All reagents and reactants were of 95% purity or greater, with the exception of ASMX, which was ~70% pure. Descriptions of chemical sources and stock solutions are given in Text S2.2.

2.2.2 Measurement of Rate Constants. O_3 and •OH rate constant measurements were conducted according to seven experimental protocols (designated I to VII), which are summarized in Table 2.3 and described in detail within Text S2.3. Solution pH was maintained in all kinetic experiments with phosphate buffers of approximately 10-mM concentration. Ten-mM *t*-BuOH was added as a •OH scavenger to solutions used for measurement of O_3 rate constants. O_3 and •OH rate constants were measured at 20(±0.5) °C (in accordance with previously determined O_3 reaction kinetics (*17,21,27,28*)) and 25(±0.5) °C, respectively.

2.2.3 Wastewater Matrix Experiments. Wastewater experiments were conducted in batch, by monitoring loss of each substrate in a sample of Kloten-Opfikon secondary wastewater effluent for various O_3 doses, at 20(±0.5) °C (see Text S2.4 for experimental details). Sample pH, alkalinity, and DOC were 7.7, 3.5 mM as HCO_3^- and 5.3 mg-C/L, respectively.

Table 2.3. Experimental methods used for rate constant measurements (details in Text S2.3)

Method	**Oxidant**	**Experimental Procedure**[a]	**Measurement Endpoint**
I	O_3	SFL	O_3 loss (measured at $\lambda = 258$ nm)
II	O_3	Batch	Substrate loss (measured by HPLC)
III	O_3	CK	Reaction product yields (measured by various techniques[b])
IV	O_3	CK	Losses of each competitor (measured by HPLC)
V	•OH	CK (H_2O_2-photolysis)	Losses of each competitor (measured by HPLC)
VI	•OH	CK (γ-radiolysis)	Losses of each competitor (measured by HPLC)
VII	•OH	CK (H_2O_2-photolysis, amine derivatization)	Losses of each competitor (measured by HPLC)

[a]SFL - stopped-flow spectrophotometry, CK – competition kinetics, [b]Reaction products were measured either spectrophotometrically or by HPLC, depending on the analyte

2.3 Results and Discussion

2.3.1 Moiety-specific Ozone Reaction Kinetics. pH-dependent, apparent second-order rate constants, $k''_{\mathrm{O_3,app}}$, were determined for each substrate at pH values ranging from 3 to 8, according to the methods described within Text S2.3. pH-dependencies of measured $k''_{\mathrm{O_3,app}}$ values were modeled according to a modified second-order rate expression (eq 1) that incorporates acid-base speciation of substrate, M,

$$\frac{\mathrm{d[M]_T}}{\mathrm{dt}} = \frac{1}{\eta}\frac{\mathrm{d[O_3]}}{\mathrm{dt}} = -k''_{O_3,app,M}[\mathrm{O_3}][\mathrm{M}]_\mathrm{T} = -\sum_{i=1}^{n} k''_i[\mathrm{O_3}]\ \alpha_i[\mathrm{M}]_\mathrm{T} \qquad (1)$$

where $[\mathrm{M}]_\mathrm{T}$ represents the total concentration of M (including all n acid-base species), η represents an apparent stoichiometric factor accounting for moles of O_3 consumed per mole of substrate consumed, k''_i is the specific rate constant corresponding to reaction of O_3 with substrate acid-base species i, and α_i represents the equilibrium distribution coefficients for species i. k''_i values – summarized in Tables 2.4 and S2.3 – were calculated by nonlinear regression of experimental data according to eq 2,

$$k''_{O_3,app,M} = \sum_{i=1}^{n} k''_i \alpha_i \qquad (2)$$

via a Marquardt-Levenberg curve-fitting routine (SigmaPlot 2002, SPSS software).

Table 2.4. Second-order rate constants ($M^{-1}s^{-1}$) for reactions of antibacterial substrates with O_3 and $\bullet OH$[a]

Substrate[b] (Rate constant measurement methods[c])	k''_{O_3} [d]			$k''_{O_3,app}$ [d] **(pH 7)**	$k''_{O_3,app}$ [d] **(pH 7.7)**	$k''_{\bullet OH,app}$ [e] **(pH 7)**
	diprotonated species	**monoprotonated species**	**deprotonated species**			
RX (I, V)	NA[f]	< 1 (*17*)[g]	$1.0 (\pm 0.1) \times 10^7$ (*17*)[k]	6.3×10^4	3.1×10^5	$5.4 (\pm 0.3) \times 10^9$
AZ (I, V)	< 1[g]	$6.0 (\pm 1.1) \times 10^6$	$6.0 (\pm 21.9) \times 10^6$ [l]	1.1×10^5	5.2×10^5	$2.9 (\pm 0.6) \times 10^9$
TYL (IV, VI)	NA[f]	$7.7 (\pm 1.4) \times 10^4$	$2.7 (\pm 0.5) \times 10^6$	5.1×10^5	1.4×10^6	$8.2 (\pm 0.1) \times 10^9$
SMX (IV)	ND[f]	$4.7 (\pm 0.9) \times 10^4$	$5.7 (\pm 1.0) \times 10^5$	5.5×10^5	5.7×10^5	$5.5 (\pm 0.7) \times 10^9$ (*17*)
ASMX (II, V)	NA[f]	$2.0 (\pm 0.2) \times 10^1$	$2.6 (\pm 0.1) \times 10^2$	2.5×10^2	2.6×10^2	$6.8 (\pm 0.1) \times 10^9$
CF (II, IV,VI)	$4.0 (\pm 1.2) \times 10^2$	$7.5 (\pm 2.8) \times 10^3$ [i]	$9.0 (\pm 3.1) \times 10^5$	1.9×10^4	7.1×10^4	$4.1 (\pm 0.3) \times 10^9$
EF (II, IV, VI)	$3.3 (\pm 1.3) \times 10^2$	$4.6 (\pm 1.2) \times 10^4$ [i]	$7.8 (\pm 1.9) \times 10^5$	1.5×10^5	4.1×10^5	$4.5 (\pm 0.4) \times 10^9$
TMP (IV, V)	$3.3 (\pm 3.0) \times 10^4$	$7.4 (\pm 1.8) \times 10^4$	$5.2 (\pm 1.0) \times 10^5$	2.7×10^5	4.3×10^5	$6.9 (\pm 0.2) \times 10^9$
LM (V)	NA[f]	$3.3 (\pm 0.1) \times 10^5$ (*23*)	$2.8 (\pm 0.1) \times 10^6$ (*23*)	6.7×10^5	1.4×10^6	$8.5 (\pm 0.2) \times 10^9$
PG (II, V)	NA[f]	$4.8 (\pm 0.1) \times 10^3$ [j]	$4.8 (\pm 0.1) \times 10^3$ [j]	4.8×10^3	4.8×10^3	$7.3 (\pm 0.3) \times 10^9$ [m]
CP (III, V)	ND[f]	$8.2 (\pm 2.9) \times 10^4$	$9.3 (\pm 2.2) \times 10^4$	8.7×10^4	9.1×10^4	$8.5 (\pm 0.7) \times 10^9$
TET (III, VI)	$9.4 (\pm 0.6) \times 10^4 – 4.7 (\pm 0.3) \times 10^6$ (pH 3 to 9, see Figure 2.2)[h]			1.9×10^6	3.2×10^6	$7.7 (\pm 1.2) \times 10^9$
VM (IV, V)	$1.1 (\pm 0.1) \times 10^4$ - $9.1 (\pm 1.1) \times 10^5$ (pH 3 to 8, see Figure 2.2)[h]			6.1×10^5	8.1×10^5	$8.1 (\pm 0.3) \times 10^9$
AM (I, VII)	$1.3 (\pm 0.7) \times 10^1 – 1.1 (\pm 0.2) \times 10^4$ (pH 4 to 9) see Figure 2.2)[h]			1.8×10^3	4.9×10^3	$7.2 (\pm 0.3) \times 10^9$

[a] Values obtained from the current investigation, unless indicated otherwise. [b] For full names, see Table 2.1. [c] Described in Table 2.3. For CF, II was used from pH 3-6, and IV from pH 6.5-8. For EF, II was used from pH 3-5.5, and IV from pH 6-8. [d] 20(±0.5) °C. [e] 25(±0.5) °C. [f] NA – Not applicable, ND – Not determined. [g] Protonated amine reactivity assumed to be negligible, on the basis of prior observations (*21,22*). [h] Only ranges of $k''_{O_3,app}$ are listed for these compounds. [i] k''_{O_3} for the "monoprotonated" fluoroquinolone species represents an "effective" rate constant for the combination of zwitterionic and neutral species. [j] PG reactivity assumed to be independent of acid-base speciation, because its dissociable functional groups are not conjugated with its thioether (Table 2.1). [k] Rate constant recalculated with $pK_{a,RX} = 9.2$, using data reported by Huber et al. (*17*). [l] The small difference between AZ's pK_{a1} and pK_{a2} – combined with lack of data at pH > 6.8 – prevented accurate determination of k''_{O_3} for neutral AZ. [m] This value agrees well with that reported by Phillips et al. (*29*) - corrected according to Neta and Dorfman (1968) (*30*) ($k''_{\bullet OH,app,PG} = 7.1 \times 10^9\ M^{-1}s^{-1}$).

Macrolides. Roxithromycin (RX). The strong pH-dependency of $k''_{O_3,\mathrm{app,RX}}$ (Figure 2.1a)

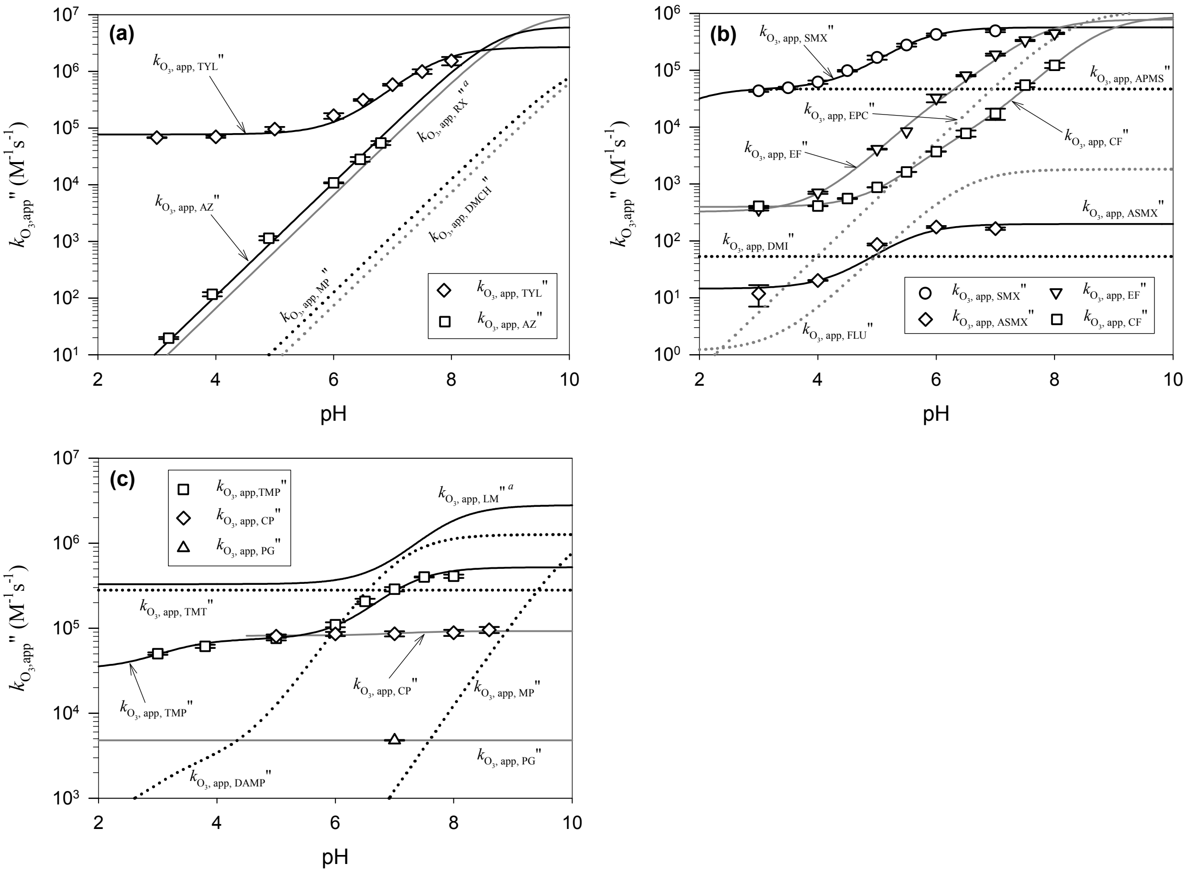

Figure 2.1. Apparent second-order rate constants for reactions of parent substrates and associated substructure model substrates with O_3 at 20(±0.5) °C (symbols = measurements, lines = model predictions): (a) macrolides (RX, AZ, and TYL) with associated substructure models, (b) sulfonamides (SMX and ASMX) and fluoroquinolones (CF and EF) with associated substructure models, (c) TMP, LM, and β-lactams (PG and CP) with associated substructure models. $^{a}k''_{O_3,\mathrm{app,RX}}$ and $k''_{O_3,\mathrm{app,LM}}$ calculated from data reported by Huber et al. (*17*) and Qiang et al. (*23*), respectively.

indicates that O_3 reacts initially at the RX structure's neutral tertiary amine moiety (Table 2.1). The continuous decrease in $k''_{O_3,\mathrm{app,RX}}$ with decreasing pH – due to protonation of RX's tertiary amine (*17,21,22*) – suggests that O_3 reactivity with the remainder of the RX structure is very low, and that oxidation at circumneutral pH will occur exclusively at the deprotonated tertiary amine. This conclusion is supported by the pH-dependency and magnitudes of $k''_{O_3,\mathrm{app}}$ measured for *N,N*-dimethylcyclohexylamine (DMCH, Table 2.2) (Figure 2.1a), as well as data reported for reaction of O_3 with the structurally analogous macrolide clarithromycin (*31*).

Azithromycin (AZ). $k''_{\mathrm{O_3,app,AZ}}$ exhibits nearly the same pH-dependency as $k''_{\mathrm{O_3,app,RX}}$ (Figure 2.1a). However, the close proximity of pK_{a1} and pK_{a2} values for AZ prevents one from determining whether $k''_{\mathrm{O_3,app,AZ}}$ is due primarily to reaction of O_3 with the parent molecule's exocyclic tertiary amine or with its heterocyclic tertiary amine (Table 2.1). Comparison of the rate constant for reaction of neutral 1-methylpyrrolidine (MP in Table 2.2) with O_3 to that for neutral DMCH shows that the two values are quite similar (Figure 2.1a). This suggests that the corresponding moieties in the AZ structure (Table 2.1) react with O_3 at roughly equivalent rates.

Tylosin (TYL). TYL reacts with O_3 significantly faster than RX and AZ at acidic pH (Figure 2.1a). This can be attributed primarily to the conjugated diene moiety within TYL's macrolactone ring (Table 2.1). Olefins typically react with O_3 at rates that are independent of pH, within the range 10^5-10^6 $M^{-1}s^{-1}$, unless substituted with strong electron-withdrawing groups (*27,32*). The rate constant reported for the neutral form of the model diene sorbic acid ($k''_{\mathrm{O_3}}$ = 3.2×10^5 $M^{-1}s^{-1}$ (*33*)) is within a factor of ~4 of that for the TYL cation (Figure 2.1a). This provides additional evidence that the diene moiety is responsible for TYL's high reactivity toward O_3 under acidic conditions. At pH > 6, the proportion of neutral TYL (i.e., deprotonated tertiary amine) becomes high enough to influence the magnitude of $k''_{\mathrm{O_3,app,TYL}}$, and dominates measured reactivities for more alkaline pH ranges (Figure 2.1a).

Sulfonamides. Sulfamethoxazole (SMX). The apparent rate constants measured for reaction of SMX with O_3 range from ~5×10^4 to ~5×10^5 $M^{-1}s^{-1}$ between pH 3 and 7 (Figure 2.1b). The specific rate constant calculated for the SMX anion (Table 2.4) agrees within a factor of 2.2 with that previously determined by Huber et al. (*17*), after correction for the different O_3 consumption stoichiometries of the reference competitor substrates – cinnamic acid (*28*) and phenol (*24,34*) – used in the current and former studies. Neutral 4-aminophenyl methyl sulfone (APMS in Table 2.2) – which approximates SMX's aniline moiety – reacts with O_3 with the same rate constant calculated for the neutral SMX species (Table 2.4, Figure 2.1b). In contrast, 3,5-dimethylisoxazole (DMI in Table 2.2) – a model for SMX's isoxazole group – reacts very slowly with O_3 (Figure 2.1b). These results indicate that reaction of O_3 with the SMX structure takes place primarily at the biochemically-active *p*-sulfonyl aniline moiety. The pH-dependency of $k''_{\mathrm{O_3,app,SMX}}$ (Figure 2.1b) appears to correlate with deprotonation of SMX's sulfonamide-nitrogen (Table 2.1). However, rapid reaction between O_3 and the sulfonamide-nitrogen can be ruled out (*21,22*). Therefore, this effect seems to be due to activation of the SMX molecule's aniline moiety (Table 2.1) toward electrophilic attack by O_3, via deprotonation of the sulfonamide-nitrogen.

N(4)-acetyl-sulfamethoxazole (ASMX). A high percentage of SMX enters wastewater treatment facilities as the metabolite ASMX (Table 2.1) – which can be retransformed to SMX during biological treatment (*4*). The rate constants determined for reaction of ozone with ASMX's neutral and anionic species are 2.0×10^1 and 2.6×10^2 $M^{-1}s^{-1}$, respectively; more than three orders of magnitude lower than for SMX (Figure 2.1b). These results agree with prior observations that ASMX is poorly degraded during ozonation of secondary wastewater effluent (*18*). The decrease in reactivity from anionic ASMX to neutral ASMX (Table 2.4, Figure 2.1b) likely reflects enhancement of the sulfonamide moiety's electron-withdrawing strength upon sulfonamide-nitrogen protonation. Because this effect should reduce the O_3-reactivities of both the ASMX isoxazole ring and the *p*-sulfonyl aniline ring, it is unclear which moiety dominates observed reaction kinetics (Figure 2.1b).

Fluoroquinolones. Ciprofloxacin (CF). CF's reactivity toward O_3 is strongly dependent on pH, where $k''_{O_3,\mathrm{app,CF}}$ ranges from ~2×10^2 to more than 10^5 $M^{-1}s^{-1}$ between pH 3 and 8 (Figure 2.1b). The pH-dependency of $k''_{O_3,\mathrm{app,CF}}$ indicates that this trend is governed by deprotonation of CF's *N*(4) amine (Table 2.1). This hypothesis is supported by the reactivity of O_3 with ethyl *N*-piperazinecarboxylate (EPC in Table 2.2). $k''_{O_3,\mathrm{app,EPC}}$ exhibits nearly the same pH-dependency and magnitudes as $k''_{O_3,\mathrm{app,CF}}$ between pH 5 and 8 (Figure 2.1b). Flumequine (FLU in Table 2.2) – a surrogate for the biochemically-active quinolone moiety (Table 2.1) – also exhibits pH-dependent reaction kinetics. However, values of $k''_{O_3,\mathrm{app,FLU}}$ are several orders of magnitude lower than those observed for CF's N(4) amine (Figure 2.1b). The baseline reactivity observed for the CF molecule at pH < 4 (Figure 2.1b) cannot be attributed to reactions with the N(4) atom or the quinolone heterocyclic ring (Figure 2.1b). This reactivity must therefore be due either to reactions taking place at the piperazine N(1) atom or at the unsubstituted *ortho*-position of the adjacent aromatic ring.

Enrofloxacin (EF). EF reacts with O_3 at higher rates than CF in the pH region between 3 and 8 (Figure 2.1b). This effect is due primarily to the difference in CF's and EF's pK_{a2} values (Table 2.1). At pH 7, for example, the molar fraction of anionic CF (in which the N(4) amine is deprotonated) is 0.01, compared to 0.15 for EF. However, the apparent rate constants for CF and EF converge at higher pH (Figure 2.1b), indicating a close similarity in the absolute reactivities of their N(4) atoms.

Trimethoprim (TMP). Measured magnitudes of $k''_{O_3,\text{app,TMP}}$ range from high-10^4 to mid-10^5 $M^{-1}s^{-1}$ (Figure 2.1c). The observed variation in $k''_{O_3,\text{app,TMP}}$ (Figure 2.1c) can most likely be attributed to speciation of its diaminopyrimidine moiety (Table 2.1). Protonation at the heterocyclic N(1) and N(3) nitrogens (Table 2.1) should reduce this moiety's O_3 reactivity via coordination of the resonant lone-pair electrons associated with each of TMP's two exocyclic amines. 2,4-diamino-5-methylpyrimidine (DAMP in Table 2.2) also exhibits pH-dependent variation in its apparent O_3 reaction rate constant (Figure 2.1c). However, the specific rate constants calculated for mono- and diprotonated DAMP (Table S2.3) are substantially lower than those calculated for the corresponding TMP species (Table 2.4, Figure 2.1c). The high O_3 reactivity of 3,4,5-trimethoxytoluene (TMT in Table 2.2) – a surrogate for TMP's trimethoxytolyl moiety (Table 2.1) – suggests that the trimethoxytolyl moiety accounts for the high reactivity of the protonated TMP species (Figure 2.1c). The difference in reactivities of TMT and TMP's protonated species could be a consequence of the TMP diaminopyrimidine moiety's bulk, which may hinder attack by O_3 at the 2- and 6-positions of the TMP structure's trimethoxytolyl moiety (Table 2.1).

Lincomycin (LM). $k''_{O_3,\text{app,LM}}$ is constant below pH 5, and increases above pH 5 to a calculated maximum of 2.8 x 10^6 $M^{-1}s^{-1}$ (Figure 2.1c). LM's baseline reactivity can be attributed to pH-independent kinetics of the reaction between its thioether and O_3, since its heterocyclic amine is protonated – and essentially unreactive toward O_3 – under these conditions (*23*). Likewise, the variation in $k''_{O_3,\text{app,LM}}$ above pH 5 can be attributed to reaction of O_3 with the neutral heterocyclic amine (*23*). $k''_{O_3,\text{app}}$ values measured for MP – a model for LM's heterocyclic tertiary amine (Table 2.1) – are consistent with these conclusions (Figure 2.1c).

β-lactams. Penicillin G (PG). PG possesses only one functional moiety - a thioether (Table 2.1) - that can be expected to account for its observed reactivity toward O_3 (Figure 2.1c). Reaction kinetics for this moiety are expected to be independent of pH (*22,23*).

Cephalexin (CP). $k''_{O_3,\text{app,CP}}$ is a little more than one order of magnitude higher than $k''_{O_3,\text{app,PG}}$ on average (Figure 2.1c). The relatively high magnitude of $k''_{O_3,\text{app,CP}}$ at pH < 7 suggests that reactivity of CP at acidic pH is attributable either to oxidation of its double bond or thioether (Table 2.1), each of which is expected exhibit pH-independent O_3 reaction kinetics. However, the slight increase in $k''_{O_3,\text{app,CP}}$ above pH 7 (Figure 2.1c) suggests that the primary amine (pK_a = 7.1, Table 2.1) may govern CP reactivity at circumneutral and higher pH values.

Substrates with more than two pK_a *values.* The complexity of TET's, VM's, and AM's speciation patterns precluded accurate modeling of O_3 reaction kinetics by the approaches utilized above. However, $k''_{O_3,\text{app,TET}}$, $k''_{O_3,\text{app,VM}}$, and $k''_{O_3,\text{app,AM}}$ were compared to substructure model substrate data (Figure 2.2) to facilitate preliminary assignment of moiety-specific O_3 reaction kinetics.

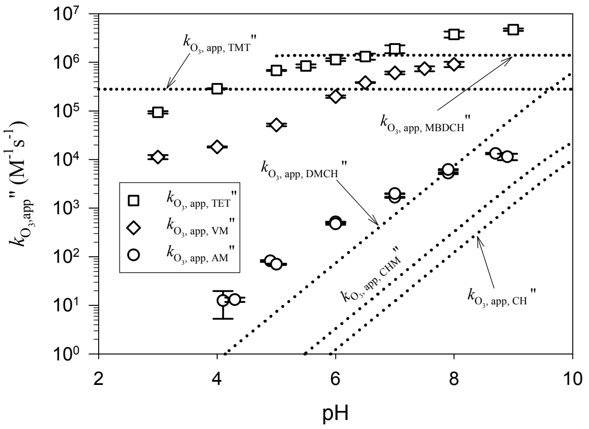

Figure 2.2. Apparent second-order rate constants for reactions of TET, VM, AM, and associated substructure models with O_3 at 20(±0.5) °C (symbols = measurements, lines = model predictions)

TET reacts rapidly with O_3 over a wide range of pH (Figure 2.2). Because the rate of reaction with the tertiary amine (pK_a = 7.7, Table 2.1) is not likely to be appreciable relative to the remainder of the TET molecule below pH 5 (Figure 2.2), the TET structure's observed reactivity toward O_3 at acidic pH is likely due to oxidation of the tetracycline ring system. Although tertiary amine reactivity could be important above pH 7, the high reactivity of various phenolic structures (*21,24*) and 2-(3-methylbutyryl)-5,5-dimethyl-1,3-cyclohexandione (MBDCH in Table 2.2) – a surrogate for the olefinic bonds within TET's tetracyclic ring system (Table 2.1) – indicate that O_3 reacts primarily with the ring system at circumneutral pH, as well.

VM is also highly reactive toward O_3 between pH 3 and 8 (Figure 2.2). The high measured reactivity of TMT (Table 2.2, Figure 2.2) – a surrogate for VM's trimethoxybenzyl moiety, in addition to the high known reactivity of phenols and resorcinols toward O_3 at all pH conditions (*21,24*), suggests that $k''_{O_3,\text{app,VM}}$ at pH < 7 corresponds to oxidation of the biochemically-essential aromatic target sites shown in Table 2.1, since oxidation of VM's amine moieties should not be important at acidic pH. However, the secondary *N*-methylleucine moiety may react rapidly enough with O_3 to influence observed reaction kinetics at pH > 7, on the basis of known secondary amine reaction kinetics (*21,22*).

$k''_{O_3,app,AM}$ varies from roughly 10^1 to just over 10^4 $M^{-1}s^{-1}$ between pH 2 and 8.6 (Figure 2.2). The measured pH-dependency of $k''_{O_3,app,AM}$ is consistent with oxidation of AM's primary amine moieties (with pK_a values ranging from 6.7 to 9.7, Table 2.1). In addition, $k''_{O_3,app,AM}$ near pH 9 (at which all but one of AM's amines are predominantly deprotonated) is of the same order of magnitude as k''_{O_3} for neutral butylamine (1.2×10^5 (*22*)), cyclohexanemethylamine (CHM in Table 2.2, with 7.1×10^4, from Table S2.3), and cyclohexylamine (CH in Table 2.2, with 4.9×10^4 $M^{-1}s^{-1}$, from Table S2.3) – which can be taken as structural approximations of AM's primary amine groups (Table 2.1).

Moiety-specific Oxidation vs. Parent Molecule Disappearance. The preceding discussion indicates that initial reactions of O_3 with many parent antibacterial substrates occur at the substrates' essential target moieties (Table 2.1). Consequently, $t_{1/2}$ values for observed transformations of many parent molecules correspond to $t_{1/2}$ for their essential target moieties (Figure S2.11). However, $t_{1/2}$ for reaction of O_3 with FLU – which approximates CF's and EF's biochemically-essential quinolone moieties – is 14 times longer at pH 7 than $t_{1/2,CF}$ (which corresponds to oxidation of the nonessential piperazine moiety) and 109 times longer than $t_{1/2,EF}$ (Figure S2.11), indicating that observed losses of parent fluoroquinolones during ozonation may not necessarily correspond directly to elimination of their antibacterial activities. In addition, O_3 does not appear to oxidize essential targets in the ASMX, PG, or CP molecules at appreciable rates. However, the O_3-recalcitrance of these three compounds' essential target moieties may be of relatively minor importance, since prior findings indicate that ASMX and β-lactams in general are unlikely to be discharged to surface waters at significant concentrations (*1,4*).

2.3.2 Studies in Wastewater Matrixes. *Depletion of Parent Substrates.* Oxidation of 1 μM ASMX – the substrate reacting slowest with O_3 (Table 2.4) – was monitored in batch experiments with Kloten-Opfikon wastewater at an O_3 dose of 63 μM (3 mg/L) (Figure S2.12). Approximately 35% of $[ASMX]_0$ remained after nearly complete depletion of O_3. The observed recalcitrance of ASMX is consistent with observations for pilot-scale ozonation of Kloten-Opfikon secondary effluent (*18*).

Measured losses of fast-reacting (i.e., $k''_{O_3,app,M} > 10^3\ M^{-1}s^{-1}$) antibacterial substrates during ozonation of Kloten-Opfikon wastewater were > 99% at O_3 doses ≥ 3 mg/L (63 µM) (Figure 2.3a). TET was > 99% transformed at an O_3 dose of 1.5 mg/L (31 µM) (Figure 2.3a), consistent with the high magnitude of $k''_{O_3,app,TET}$ at pH 7.7 (Table 2.4). However, significant residuals of PG remained even at an O_3 dose of 3 mg/L (63 µM) (Figure 2.3a), consistent with the low magnitude of $k''_{O_3,app,PG}$. Ninety-nine % PG loss was only achieved at an O_3 dose of 5 mg/L (104 µM). Observed losses of SMX (Figure 2.3a) agree well with results reported for pilot-scale ozonation of Kloten-Opfikon wastewater at an O_3 dose of 1 mg/L (*18*). RX, AZ, AM, and LM were not included in these experiments because of analytical difficulties. Predicted losses for these four substrates were calculated for an applied O_3 dose of 1 mg/L (Figure 2.3a), as described in Text S2.5. The values calculated for RX and AZ (Figure 2.3a) agree very well with pilot-scale measurements under similar conditions (*18*).

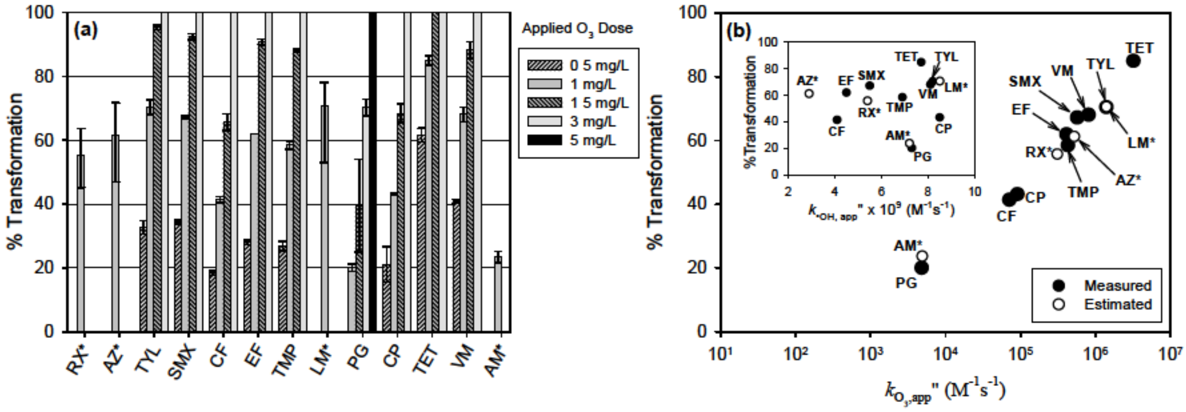

Figure 2.3. Antibacterial substrate transformation during ozonation of Kloten-Opfikon wastewater at 20(±0.5) °C, pH 7.7, and $[\text{substrate}]_0 = 1$ µM: (a) Measured transformation efficiencies at varying O_3 dosages, for substrates with $k''_{O_3,app} > 10^3\ M^{-1}s^{-1}$. (b) Dependence of transformation efficiencies on $k''_{O_3,app}$, at an O_3 dose of 1 mg/L (21 µM). Inset shows independence of transformation efficiency from $k''_{\bullet OH,app}$. *% transformation for RX, AZ, LM, and AM estimated via procedures described in Text S2.5.

Role of O_3 and •OH in Oxidation of Parent Substrates. Substrate transformation during a real water ozonation process can be characterized by eq 3 (*35*),

$$\ln\left(\frac{[M]_\tau}{[M]_0}\right) = -k''_{O_3,app,M}\int_0^\tau [O_3]dt - k''_{\bullet OH,app,M}\int_0^\tau [\bullet OH]dt \tag{3}$$

where the two integral terms in eq 3 represent the O_3 and •OH exposures *(26,35)* governing transformation of substrate, M, over reaction time, τ, where $[\bullet\text{OH}] = f(t)$ and $[O_3] = g(t)$. $k''_{\bullet\text{OH,app,M}}$ values measured for each antibacterial compound range from 2.9 to $8.5 \times 10^9\ \text{M}^{-1}\text{s}^{-1}$ at pH 7 (Table 2.4).

As illustrated in Figure 2.3b, the transformation efficiencies determined for each substrate in Kloten-Opfikon wastewater correlate well with magnitude of $k''_{O_3,\text{app,M}}$. In contrast, there is no clear relation between transformation efficiency and $k''_{\bullet\text{OH,app,M}}$ for these conditions (inset to Figure 2.3b). This indicates that $[M]/[M]_0$ is governed primarily by the O_3 oxidation term in eq 3. The •OH oxidation term becomes important only if the magnitude of the O_3 oxidation term is relatively small, either as a consequence of low $k''_{O_3,\text{app,M}}$, low $\int_0^\tau [O_3]dt$, or high $\int_0^\tau [\bullet\,\text{OH}]dt$.

Contributions of O_3 and •OH to oxidation of ASMX were evaluated according to eq 4,

$$\text{f}_{\bullet\text{OH,M}(\tau)} = \frac{k''_{\bullet\text{OH,app,M}}\int_0^\tau [\bullet\,\text{OH}]dt}{k''_{O_3,\text{app,M}}\int_0^\tau [O_3]dt + k''_{\bullet\text{OH,app,M}}\int_0^\tau [\bullet\,\text{OH}]dt} = \left(1 + \frac{k''_{O_3,\text{app,M}}}{k''_{\bullet\text{OH,app,M}}}\left(\frac{1}{\int_0^\tau [\bullet\,\text{OH}]dt \Big/ \int_0^\tau [O_3]dt}\right)\right)^{-1} \tag{4}$$

where $\text{f}_{\bullet\text{OH,M}(\tau)}$ represents the fraction of substrate oxidation due to •OH after reaction time, τ. $\int_0^\tau [O_3]dt$ was obtained by direct measurement of O_3 (via the indigo method (*36*)), and $\int_0^\tau [\bullet\,\text{OH}]dt$ was determined from measured loss of the •OH probe *p*CBA, which reacts rapidly with •OH and very slowly with O_3, according to eq 5 (*35*).

$$\ln\left(\frac{[p\text{CBA}]_\tau}{[p\text{CBA}]_0}\right) = -k''_{\bullet\text{OH,app},p\text{CBA}}\int_0^\tau [\bullet\,\text{OH}]dt \tag{5}$$

These calculations indicated that ASMX was transformed exclusively by •OH (Figure S2.12).

Transformations of fast-reacting substrates were also characterized according to the relationships shown in eq 4. However, because $\int_0^\tau [O_3]dt$ could not be measured during the course of each substrate's transformation in Kloten-Opfikon wastewater, $\text{f}_{\bullet\text{OH,M}(\tau)}$ was actually calculated from eq 6 (*18*), which is obtained by substitution of eqs 3 and 5 into eq 4.

$$\mathrm{f}_{\bullet\mathrm{OH,M}} = \frac{\dfrac{k''_{\bullet\mathrm{OH,app,M}}}{k''_{\bullet\mathrm{OH,app},p\mathrm{CBA}}} \ln\left(\dfrac{[p\mathrm{CBA}]_\tau}{[p\mathrm{CBA}]_0}\right)}{\ln\left(\dfrac{[\mathrm{M}]_\tau}{[\mathrm{M}]_0}\right)} \qquad (6)$$

Although values obtained via eq 6 provide no information as to temporal variation of $\int_0^\tau [\mathrm{O}_3]dt$ during ozonation, this expression can still provide reliable estimates of the absolute contributions of •OH and O_3 to bulk substrate oxidation. For example, $\mathrm{f}_{\bullet\mathrm{OH,M}(\tau)}$ values calculated by eq 6 for the antiepileptic drug carbamazepine (with $k''_{\mathrm{O}_3,\mathrm{app}} \sim 3 \times 10^5$ $\mathrm{M}^{-1}\mathrm{s}^{-1}$, $k''_{\bullet\mathrm{OH}} = 8.8$ (± 1.2) × 10^9 $\mathrm{M}^{-1}\mathrm{s}^{-1}$ at pH 7 (*17*)) typically exhibit deviations of less than 10% from values determined by eq 4, using measurements of O_3 and •OH exposure actually taken within the first few hundred milliseconds after application of O_3 to various municipal wastewaters (Figure S2.14). $\mathrm{f}_{\bullet\mathrm{OH,M}(\tau)}$ values calculated by eq 6 are summarized in Figure 2.4a.

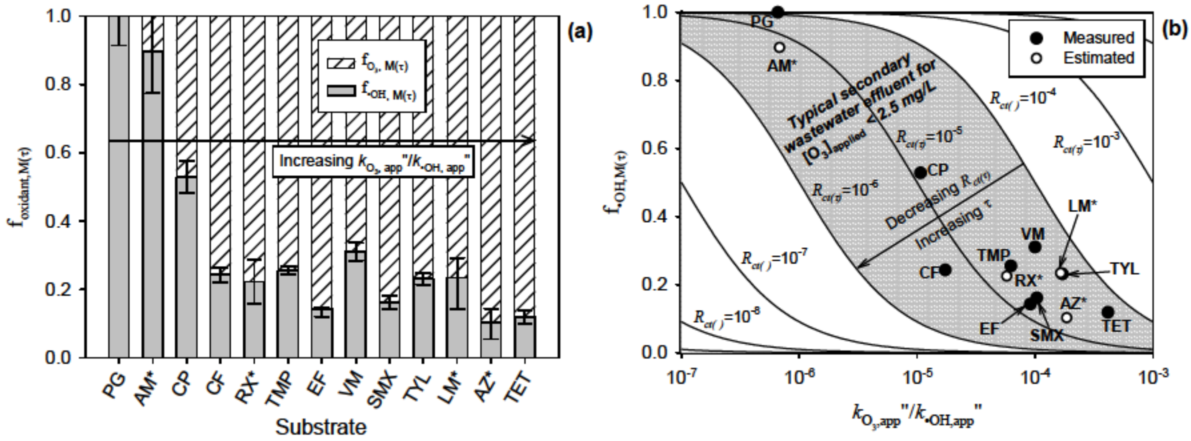

Figure 2.4. Importance of O_3 and •OH in transformation of fast-reacting substrates ($k''_{\mathrm{O}_3,\mathrm{app.}} > 10^3$ $\mathrm{M}^{-1}\mathrm{s}^{-1}$) during ozonation of Kloten-Opfikon secondary effluent at 20(±0.5) °C, pH 7.7, $[\text{substrate}]_0 = 1$ μM, and $[\mathrm{O}_3]_0 = 21$ μM (1 mg/L): (a) Calculated fractions of observed substrate transformation due to O_3 and •OH. (b) Correlation of measured values of $\mathrm{f}_{\bullet\mathrm{OH,M}(\tau)}$ (obtained via eq 6) with values calculated via eq 4 for the range of $R_{ct(\tau)}$ values (*25*) expected for Kloten-Opfikon wastewater at these conditions. τ corresponds to reaction time after O_3 dosage. $R_{ct(\tau)}$ represents the cumulative ratio of •OH exposure to O_3 exposure for a pollutant molecule after reaction time, τ. *Estimates of % transformation and $\mathrm{f}_{\bullet\mathrm{OH,M}(\tau)}$ for RX, AZ, LM, and AM were calculated via procedures described in Text S2.5.

According to eq 4 (from which eq 6 is derived), $f_{\bullet\mathrm{OH,M}(\tau)}$ should be inversely related to the ratio $k''_{\mathrm{O_3,app,M}}/k''_{\bullet\mathrm{OH,app,M}}$, consistent with the general trend shown in Figure 2.4a.

Effects of Matrix Characteristics on Relative Importance of O₃ and •OH in Observed Substrate Transformation. As evident from eq 4, $f_{\bullet\mathrm{OH,M}(\tau)}$ for a given substrate will also depend on the time-dependent ratio of $\int_0^\tau [\bullet\,\mathrm{OH}]dt \Big/ \int_0^\tau [\mathrm{O_3}]dt$, or $R_{ct(\tau)}$ (*25,34,35,37*) during wastewater ozonation. $R_{ct(\tau)}$ is particularly sensitive to wastewater DOC concentrations, where higher DOC typically translates to higher $R_{ct(\tau)}$ values (*25,37*). The solid lines shown in Figure 2.4b illustrate expected $f_{\bullet\mathrm{OH,M}(\tau)}$ values (calculated from eq 4) as a function of $k''_{\mathrm{O_3,app,M}}/k''_{\bullet\mathrm{OH,app,M}}$, for a number of $R_{ct(\tau)}$ values. The shaded region shown in Figure 2.4b represents the apparent range of $R_{ct(\tau)}$ values previously observed (at O_3 doses varying from 1 to 2.5 mg/L) for various municipal wastewaters during the time-scales (< 10 s) within which the bulk of fast-reacting substrate loss (i.e., > 90%) is expected to occur. In accordance with these expectations, the $f_{\bullet\mathrm{OH,M}(\tau)}$ values obtained by eq 6 (for an applied O_3 dose of 1 mg/L) for each fast-reacting substrate included in the present investigation fall within this shaded region (Figure 2.4b). The relationships presented in Figure 2.4b suggest that $f_{\bullet\mathrm{OH,M}(\tau)}$ for substrates with values of $k''_{\mathrm{O_3,app,M}}/k''_{\bullet\mathrm{OH,app,M}} < 10^{-6}$ will range from about 0.5 to 1 during ozonation of a typical wastewater. However, $f_{\bullet\mathrm{OH,M}(\tau)}$ can be expected to fall anywhere between 0.1 and 0.9 for substrates with $k''_{\mathrm{O_3,app,M}}/k''_{\bullet\mathrm{OH,app,M}}$ ranging from 10^{-6} to 10^{-4}. In contrast, $f_{\bullet\mathrm{OH,M}(\tau)}$ will generally be relatively small (< 0.5) for substrates with $k''_{\mathrm{O_3,app,M}}/k''_{\bullet\mathrm{OH,app,M}} > 10^{-4}$.

Implications for Selective Oxidation during Wastewater Ozonation. The majority of antibacterial substrates included in this study are expected to be transformed predominantly via direct oxidation by O_3 during wastewater ozonation (Figure 2.4b). However, PG, CP, AM, and ASMX (each with $k''_{\mathrm{O_3,app,M}}/k''_{\bullet\mathrm{OH,app,M}} < 10^{-4}$) will generally be transformed to a large extent by •OH during wastewater ozonation. This may be undesirable in the case of AM, since •OH will likely react indiscriminately with many sites not associated with the AM molecule's antibacterial activity (Table 2.1 and Text S2.1). With respect to ASMX, however, •OH may be no less desirable as an oxidant than O_3, because O_3 appears to react only very slowly (if at all) with the essential *p*-sulfonyl aniline target (Table 2.1, Table 2.4). Oxidation of PG and CP by •OH may actually be more desirable than oxidation by O_3, since •OH reactions lead primarily to production of biochemically-inactive (*38*) benzylpenilloic and benzylpenicilloic acids (*29*). In the case of CF and EF, the relatively low ratios of $k''_{O_3,app,target}$ (i.e., $k''_{O_3,app,FLU}$) to $k''_{\bullet OH,app,M}$ (i.e., < 10^{-6}, according to Figure 2.1b and Table 2.4) suggest that nonessential locations within each fluoroquinolone's structure may be oxidized to a significant extent by •OH and O_3 prior to reaction of O_3 with their essential target moieties. On the assumption that pre-oxidation of other locations within the parent structures (by O_3 or •OH) does not significantly reduce the reactivity of their target moieties toward O_3, full oxidation of the target moieties can likely still be achieved by selecting applied O_3 dose to maintain a sufficiently high $\int [O_3]dt$, which should be chosen on the basis of moiety-specific oxidation kinetics, as opposed to observed parent substrate transformation kinetics.

Acknowledgements

Michael Dodd gratefully acknowledges financial support from a U.S. National Science Foundation Graduate Research Fellowship. The authors thank Marc Huber, Gretchen Onstad, Andreas Peter, Silvio Canonica, and Yunho Lee for helpful discussions, and Elisabeth Salhi for technical assistance. Two anonymous reviewers are thankfully acknowledged for their constructive comments.

Literature Cited

(1) Hirsch, R.; Ternes, T. A.; Haberer, K.; Kratz, K.-L. Occurrence of antibiotics in the environment. *Sci. Total Environ.* **1999**, *225*, 109-118.

(2) Golet, E. M.; Xifra, I.; Siegrist, H.; Alder, A. C.; Giger, W. Environmental exposure assessment of fluoroquinolone antibacterial agents from sewage to soil. *Environ. Sci. Technol.* **2003**, *37*, 3243-3249.

(3) Miao, X.-S.; Bishay, F.; Chen, M.; Metcalfe, C. D. Occurrence of antimicrobials in the final effluents of wastewater treatment plants in Canada. *Environ. Sci. Technol.* **2004**, *38*, 3542-3550.

(4) Göbel, A.; Thomsen, A.; McArdell, C. S.; Joss, A.; Giger, W. Occurrence and sorption behavior of sulfonamides, macrolides, and trimethoprim in activated sludge treatment. *Environ. Sci. Technol.* **2005**, *39*, 3981-3989.

(5) Lindberg, R. H.; Wennberg, P.; Johansson, M. I.; Tysklind, M.; Andersson, B. A. V. Screening of human antibiotic substances and determination of weekly mass flows in five sewage treatment plants in Sweden. *Environ. Sci. Technol.* **2005**, *39*, 3421-3429.

(6) Kim, S.; Eichorn, P.; Jensen, J. N.; Weber, A. S.; Aga, D. S. Removal of antibiotics in wastewater: effect of hydraulic and solid retention times on the fate of tetracycline in the activated sludge process. *Environ. Sci. Technol.* **2005**, *39*, 5816-5823.

(7) Brain, R. A.; Johnson, D. J.; Richards, S. M.; Hanson, M. L.; Sanderson, H.; Lam, M. W.; Young, C.; Mabury, S. A.; Sibley, P. K.; Solomon, K. R. Microcosm evaluation of

the effects of an eight pharmaceutical mixture to the aquatic macrophytes *Lemna gibba* and *Myriophyllum sibiricum*. *Aquat. Toxicol.* **2004**, *70*, 23-40.

(8) Wilson, C. J.; Brain, R. A.; Sanderson, H.; Johnson, D. J.; Bestari, K. T.; Sibley, P. K.; Solomon, K. R. Structural and functional responses of plankton to a mixture of four tetracyclines in aquatic microcosms. *Environ. Sci. Technol.* **2004**, *38*, 6430-6439.

(9) Wilson, B. A.; Smith, V. H.; Denoyelles, F.; Larive, C. K. Effects of three pharmaceutical and personal care products on natural freshwater algal assemblages. *Environ. Sci. Technol.* **2003**, *37*, 1713-1719.

(10) Lorian, V., Ed.^Eds. *Antibiotics in Laboratory Medicine*; 4th ed.; Williams and Wilkins: Baltimore, MD, 1996.

(11) Baquero, F. Low-level antibacterial resistance: a gateway to clinical resistance. *Drug Resistance Updates* **2001**, *4*, 93-105.

(12) Drlica, K. The mutant selection window and antimicrobial resistance. *J. Antimicrob. Chemother.* **2003**, *52*, 11-17.

(13) Paraskeva, P.; Graham, N. J. D. Ozonation of municipal wastewater effluents. *Water Environ. Res.* **2002**, *74*, 569-581.

(14) Beltran, F. J.; Garcia-Araya, J. F.; Alvarez, P. M. Integration of continuous biological and chemical (ozone) treatment of domestic wastewater: 2. Ozonation followed by biological oxidation. *J. Chem. Technol. Biotechnol.* **1999**, *74*, 884-890.

(15) Gehr, R.; Wagner, M.; Veerasubramanian, P.; Payment, P. Disinfection efficiency of peracetic acid, UV and ozone after enhanced primary treatment of municipal wastewater. *Water Res.* **2003**, *37*, 4573-4586.

(16) Adams, C.; Wang, Y.; Loftin, K.; Meyer, M. Removal of antibiotics from surface and distilled water in conventional water treatment processes. *J. Environ. Eng.* **2002**, *128*, 253-260.

(17) Huber, M. M.; Canonica, S.; Park, G.-Y.; von Gunten, U. Oxidation of pharmaceuticals during ozonation and advanced oxidation processes. *Environmental Science and Technology* **2003**, *37*, 1016-1024.

(18) Huber, M. M.; Göbel, A.; Joss, A.; Hermann, N.; Löffler, D.; McArdell, C. S.; Ried, A.; Siegrist, H.; Ternes, T. A.; von Gunten, U. Oxidation of pharmaceuticals during ozonation of municipal wastewater effluents: a pilot study. *Environmental Science and Technology* **2005**, *39*, 4290-4299.

(19) Ternes, T. A.; Stüber, J.; Herrmann, N.; McDowell, D.; Ried, A.; Kampmann, M.; Teiser, B. Ozonation: a tool for removal of pharmaceuticals, contrast media and musk fragrances from wastewater? *Water Research* **2003**, *37*, 1976-1982.

(20) Huber, M. M.; Ternes, T.; von Gunten, U. Removal of estrogenic activity and formation of oxidation products during ozonation of 17α-ethinylestradiol. *Environmental Science and Technology* **2004**, *38*, 5177-5186.

(21) Hoigné, J.; Bader, H. Rate constants of reactions of ozone with organic and inorganic compounds in water – II : Dissociating organic compounds. *Water Res.* **1983**, *17*, 185-194.

(22) Pryor, W. A.; Giamalva, D. H.; Church, D. F. Kinetics of ozonation. 2. Amino acids and model compounds in water and comparisons to rates in nonpolar solvents. *J. Am. Chem. Soc.* **1984**, *106*, 7094-7100.

(23) Qiang, Z.; Adams, C.; Surampalli, R. Determination of ozonation rate constants for lincomycin and spectinomycin. *Ozone: Sci. Eng.* **2004**, *26*, 525-537.

(24) Mvula, E.; von Sonntag, C. Ozonolysis of phenols in aqueous solution. *Org. Biomol. Chem.* **2003**, *1*, 1749-1756.

(25) Buffle, M.-O.; Schumacher, J.; von Gunten, U. Ozonation and advanced oxidation of wastewater: Effect of O_3 dose, pH, DOC and HO•-scavengers on ozone decomposition and HO• generation. *Ozone Science and Engineering* **2005**, *Accepted for publication*.

(26) von Gunten, U. Ozonation of drinking water: Part I. Oxidation kinetics and product formation. *Water Res.* **2003**, *37*, 1443-1467.

(27) Hoigné, J.; Bader, H. Rate constants of reactions of ozone with organic and inorganic compounds in water – I : Non-dissociating organic compounds. *Water Res.* **1983**, *17*, 173-183.

(28) Leitzke, A.; Reisz, E.; Flyunt, R.; von Sonntag, C. The reactions of ozone with cinnamic acids: formation and decay of 2-hydroperoxy-2-hydroxyacetic acid. *J. Chem. Soc., Perkin Trans. 2* **2001**, 793-797.

(29) Phillips, G. O.; Power, D. M.; Robinson, C. Chemical changes following γ-irradiation of benzylpenicillin in aqueous solution. *J. Chem. Soc., Perkin Trans. 2* **1973**, 575-582.

(30) Neta, P.; Dorfman, L. M. Pulse radiolysis studies. XIII. Rate constants for the reaction of hydroxyl radicals with aromatic compounds in aqueous solutions. *Adv. in Chem.* **1968**, *81*, 222-230.

(31) Lange, F.; Cornelissen, S.; Kubac, D.; Sein, M. M.; von Sonntag, J.; Hannich, C. B.; Golloch, A.; Heipieper, H. J.; Moder, M.; von Sonntag, C. Degradation of macrolide antibiotics by ozone: A mechanistic case study with clarithromycin. *Chemosphere* **2006**, *65*, 17-23.

(32) Dowideit, P.; von Sonntag, C. Reaction of ozone with ethene and its methyl- and chlorine-substituted derivatives in aqueous solution. *Environ. Sci. Technol.* **1998**, *32*, 1112-1119.

(33) Onstad, G. D.; Strauch, S.; Meriluoto, J.; Codd, G.; von Gunten, U. Selective oxidation of key functional groups in cyanotoxins during drinking water ozonation. *Environ. Sci. Technol.* **2005**, *Submitted.*

(34) Buffle, M.-O.; Schumacher, J.; Salhi, E.; von Gunten, U. Measurement of the initial phase of ozone decomposition in water and wastewater by means of a continuous quench flow system: Application to disinfection and pharmaceutical oxidation. *Water Research* **2005**, *Accepted for publication*.

(35) Elovitz, M. S.; von Gunten, U. Hydroxyl radical/ozone ratios during ozonation processes. I. The R_{ct} concept. *Ozone Science and Engineering* **1999**, *21*, 239-260.

(36) Bader, H.; Hoigné, J. Determination of ozone in water by the indigo method. *Water Res.* **1981**, *15*, 449-456.

(37) Elovitz, M. S.; von Gunten, U.; Kaiser, H. P. Hydroxyl radical/ozone ratios during ozonation processes. II. The effect of temperature, pH, alkalinity, and DOM properties. *Ozone: Sci. Eng.* **2000**, *22*, 123-150.

(38) Walsh, C. *Antibiotics: Actions, Origins, Resistance*; ASM Press: Washington, D.C., 2003.

Supporting Information for Chapter 2.

Oxidation of Antibacterial Molecules by Aqueous Ozone: Moiety-Specific Reaction Kinetics and Application to Ozone-Based Wastewater Treatment

26 pages, including 5 narratives, 3 tables, and 14 figures

Text S2.1 Mechanisms of antibacterial compounds' biochemical activities and relevance to target sites at which O_3 is expected to react with parent antibacterial molecules.

Macrolides. Macrolide antibacterials are believed to derive their biochemical activity from specific hydrogen bonding with various nucleobases and phosphodiester linkages in the peptidyl transferase cavity of bacterial 23S rRNA (Figure S2.2) *(1)*. The bonding interaction most likely to be interrupted by direct reaction with O_3 is that involving each macrolide's characteristic tertiary amine (Figure S2.2), which is expected to be highly reactive toward O_3 *(2,3)*. Oxidation of the tertiary amine via formation of an aminoxide or via demethylation *(3)* should prevent its hydrogen bonding with 23S rRNA, leading to reduction or elimination of each parent macrolide's antibacterial activity. Macrolides with fifteen- and sixteen-membered macrolactone rings generally possess additional moieties that can be expected to react rapidly with O_3. For example azithromycin (AZ – a fifteen-membered macrolide – shown in Table 2.1 within the main text) and tylosin (TYL – a sixteen-membered macrolide – shown in Table 2.1) contain an additional tertiary amine and a conjugated diene, respectively. Oxidation of azithromycin's (AZ) heterocyclic nitrogen would likely be sufficient to impair the parent structure's antibacterial activity if such a reaction resulted in rupture of its macrolactone ring (e.g., via dealkylation of the nitrogen atom *(3)*). This would presumably result in interruption of the specific stereochemistry necessary for appropriate hydrogen bonding between the AZ structure and bacterial rRNA (Figure S2.2), consistent with the observed deactivation of the macrolide clarithromycin upon reaction with O_3 (*4*). Similarly, reaction of O_3 with tylosin's (TYL) diene moiety should lead to impairment of TYL's antibacterial activity, where ozonolysis of either olefinic bond would result in rupture of TYL's macrolactone ring (*5*).

Sulfonamides. All sulfonamide antibacterial structures are derivatives of *p*-aminobenzenesulfonamide – a structural analog of *p*-aminobenzoic acid (*p*ABA) – and are differentiated only by the particular R-substituent attached to the sulfonamide nitrogen (Figure S2.3). These compounds derive their antibacterial activity from antagonistic competition with *p*ABA for dihydropteroate synthase enzyme during bacterial synthesis of dihydropteroic acid (the precursor to folic acid) (Figure S2.3) (*6*). The *p*-sulfonyl aniline moiety, in particular, is responsible for each sulfonamide's interference with bacterial folate synthesis (Figure S2.3). This moiety should present a very favorable target for O_3, since aromatic amines are generally very reactive toward O_3 (*2,7,8*). Sulfonamides' R-substituent moieties (e.g., isoxazole in the case of sulfamethoxazole, SMX – shown in Table 2.1 within the main text), can also be expected to react with O_3. These latter reactions will not lead to oxidation of the functional moiety responsible for the parent structures' antibacterial potency.

However they may indirectly influence the parent molecules' antibacterial activity either positively or negatively, by altering the parent molecule's bioavailability.

Fluoroquinolones. Fluoroquinolones are believed to derive their biochemical activity from several specific hydrogen-bonding and charge interactions with relaxed bacterial DNA in the presence of DNA gyrase enzyme (Figure S2.4) (*9*). According to the accepted model for fluoroquinolone-DNA binding, the characteristic quinolone moiety is responsible for these interactions (Figure S2.4). Oxidation of this moiety by O_3 (as expected on the basis of relatively fast reaction kinetics measured for the structurally-similar substrate uracil-6-carboxylic, or isoorotic, acid (*10*)) should therefore lead to a reduction or elimination of fluoroquinolones' antibacterial potencies. However, the heterocyclic substituent groups (typically piperazine derivatives, as for CF and EF – shown in Table 2.1 within the main text) attached to many fluoroquinolones' quinolone moieties do not appear to be essential to fluoroquinolone antibacterial activity. For example, first-generation quinolones such as nalidixic acid lack the heterocycle, but still exhibit considerable antibacterial potency (*11*). Thus, oxidation of the N(4) amine – expected on the basis of secondary and tertiary amines' generally high reactivities toward O_3 *(2,3)* – may not contribute to a significant reduction in CF's antibacterial activity.

Dihydrofolate Reductase (DHFR) Inhibitors. DHFR inhibitors (e.g., trimethoprim, TMP – shown in Table 2.1 within the main text) inhibit bacterial folate synthesis via competition with dihydrofolate for DHFR enzyme (hence TMP's common role as a synergist to the sulfonamide, SMX) (Figure S2.5) (*6*). The diaminopyrimidine structure represents the active portion of these antibacterial molecules, where the protonated nitrogen atom, N(1), of the heterocyclic ring (Figure S2.5) participates in charge interactions with DHFR (*12*). Oxidation of the 2,4-diaminopyrimidine structure – anticipated on the basis of pyrimidine structures' generally high reactivity toward O_3 (*10*) – is therefore likely to yield a reduction in the parent structure's antibacterial potency. TMP's 3,4,5-trimethoxytolyl moiety will also likely react relatively rapidly with O_3 (*13*). As in the case of sulfonamide R-substituent oxidation, this latter reaction may indirectly influence the parent molecule's antibacterial activity by altering its bioavailability.

Lincosamides. Lincosamides interact with bacteria via hydrogen-bonding to specific nucleotides in bacterial 23S rRNA, leading to inhibition of the bacteria cells' ability to synthesize proteins (Figure S2.6) *(1)*. None of the functional moieties directly responsible for lincosamide antibacterial activity are expected to react appreciably with O_3. However, O_3 is likely to oxidize the lincosamide thioether moiety to its sulfoxide derivative (*14,15*). In the case of lincomycin (LM – shown in Table 2.1 within the main text), this reaction should lead to LM-sulfoxide, which is known to possess significantly lower antibacterial potency than the parent structure (*16*) – presumably due to interruption of requisite intermolecular hydrogen bonding patterns at adjacent hydroxyl and methyl groups by thioether oxidation (Figure S2.6). It is unclear whether oxidation of LM's pyrrolidine moiety would produce such an effect, since the pyrrolidine moiety is spatially and electronically isolated from most of LM's biochemically-relevant functional moieties (Figure S2.6).

β-lactams. *β*-lactams (including the major penicillin and cephalosporin sub-classes) derive their antibacterial activities from the fused *β*-lactam ring system, which operates via sequestration of bacterial peptidoglycan transpeptidase enzyme, leading to disruption of bacterial cell wall synthesis (Figure S2.7) (*6,17*). The *β*-lactam ring itself is unlikely to be reactive toward O_3. However, O_3 can be expected to react with *β*-lactams' characteristic thioether moieties (see PG and CP – Table 2.1 in the main text). Oxidation of the thioether by O_3 is known to lead to high yields (>95%) of many *β*-lactams' *R*- and *S*-sulfoxide enantiomers (in *R*:*S* ratios ranging from 1:4 to 24:1) (*14*). Although *S*-sulfoxide analogues of *β*-lactams exhibit negligible antibacterial activities, their *R*-sulfoxide analogues are still quite potent (*18,19*), suggesting that oxidation of the thioether by O_3 may not be sufficient to eliminate the parent *β*-lactam compounds' antibacterial activities. Oxidation of the double bond present in cephalosporin structures (e.g., cephalexin, CP – shown in Table 2.1 within the main text) – most likely leading either to ozonolytic cleavage or epoxidation (*5,20*) – may also be insufficient to eliminate the parent structure's antibacterial properties, since the *β*-lactam ring would not likely be disrupted by such a reaction. Similarly, oxidation of CP's primary amine (Table 2.1) is not expected to lead to significant reduction of the parent structure's antibacterial activity.

Tetracyclines. The antibacterial activities of tetracycline antibacterials appear to be derived primarily from direct or indirect (metal cation-mediated) electrostatic charge interactions between the keto and hydroxyl oxygens on the underside of the tetracycline molecule and the oxygens of various internucleotide phosphodiester linkages on the 16S rRNA helix contained within the 30S subunit of the bacterial ribosome (Figure S2.8) (*21*). Oxidation of the tetracyclic system by O_3 – expected on the basis of its activated unsaturated and aromatic character (*2,5,22,23*) – should lead to reduction of the parent molecules' antibacterial properties, since such reactions would likely lead to extensive modification of the relevant aromatic and olefinic moieties (*5,23*). However, oxidation of a the tertiary amine moiety appears less likely to yield a significant reduction in antibacterial potency of the parent molecule, since this trialkylamine moiety is spatially isolated from most biochemically-relevant tetracycline functional moieties and not essential to the tetracyclines' modes of action (Figure S2.8).

Glycopeptides. Glycopeptides (e.g., vancomycin, VM – shown in Table 2.1 within the main text) are believed to derive their antibacterial activity from sequestration of specific subunits of the peptidoglycan used in cell wall synthesis (Figure S2.9) (*24*). Although none of the amide moieties directly involved in the hydrogen-bonding responsible for these interactions should be appreciably reactive toward O_3 (*25*), several of the adjacent aromatic moieties (Table 2.1) should be highly reactive (*2,13*). One would expect that ozonation of VM's phenol or trimethoxybenzyl moieties by O_3 should lead to ring cleavage, oxidation to quinone structures, or formation of oxyl radicals (the latter of which could foreseeably cross-link with proximal components of the VM structure) (*23,26*). Each of these structural modifications would likely lead at least to impairment, if not elimination of VM's antibacterial activity, via interruption of the specific VM stereochemistry necessary for binding of bacterial peptidoglycan (Figure S2.9). Oxidation of the secondary *N*-methylleucine moiety by O_3 (presumably leading to hydroxylation or dealkylation of the amine (*27*)) may also lead to disruption of hydrogen bonding at the adjacent amide (Figure S2.9). However, oxidation of the primary vancosamine will not likely lead to sufficient disruption of stereochemistry to substantially diminish VM's antibacterial potency, as a consequence of the vancosamine moiety's isolation from VM's biochemically-relevant amide moieties (Figure S2.9).

Aminoglycosides. Aminoglycosides – which are inhibitors of bacterial protein synthesis – derive much of their antimicrobial activity from charge interactions with nucleobase and phosphodiester functional groups in bacterial rRNA (*28*). One proposed binding scheme – developed with streptomycin as a model – suggests that these interactions involve various hydroxyl and amine groups within the typical aminoglycoside structure (Figure S2.10). Aminoglycosides also contribute to disruption of cell walls; an attribute apparently derived in large part from their ability to displace Mg^{2+} and Ca^{2+} from outer membrane-associated lipopolysaccharide bridges (*29*). Oxidation of an aminoglycoside's primary amine moieties by O_3 (e.g., to nitro groups, aminoxides, or via deamination (*15*)) would presumably prevent the bacterial rRNA hydrogen bonding and cationic charge-interactions from which aminoglycoside antibacterial activity is largely derived (Figure S2.10), in turn leading to reduction or elimination of the parent compounds' antibacterial potencies.

Text S2.2 Chemical reagents

Commercially-available antibacterial substrates and substructure model substrates were purchased from Sigma-Aldrich, with the exception of cephalexin (CP) hydrate – which was purchased from MP Biomedicals. Azithromycin (AZ) dihydrate was a gift from Pfizer, Inc. 2,4-diamino-5-methyl pyrimidine (DAMP) – produced by Daniels Fine Chemicals, Ltd., and 4-aminophenyl methyl sulfone – produced by Sigma-Aldrich, were gifts from Professor Ching-Hua Huang, Georgia Institute of Technology, Atlanta, GA. *N*(4)-acetyl-sulfamethoxazole (ASMX) was synthesized as described by Göbel et al. (*30*). All substrates were of 95% purity or higher, with the exception of ASMX – which was ~ 70% pure. Other chemicals (e.g., buffers, H_2O_2, reducing agents, etc.) were of reagent grade quality or better. O_3 stock solutions were produced as described previously (*31*), and standardized according to direct O_3 absorbance at $\lambda = 258$ nm (using $\varepsilon \cong 3000$ $M^{-1}cm^{-1}$). Stock solutions of antibacterials and substructure models were prepared in Nanopure or Milli-Q water. Acetone and acetonitrile – •OH scavengers which should not accelerate radical-chain O_3 decay in the aqueous systems typical of this study (*32-34*) – were used to facilitate preparation of several poorly soluble reactant stock solutions for O_3 rate constant determinations. Acetone and acetonitrile concentrations never exceeded 1 % by volume, so co-solvent effects should have been negligible (*35*). Solutions used for determination of •OH rate constants and for municipal wastewater experiments contained no co-solvents.

Text S2.3 Measurement of apparent second-order rate constants for O_3 and •OH reactions

Method I (O_3 kinetics): Used for RX, AZ, AM, CH, CHM, DMCH, EPC, and MP (Tables 2.1 and 2.2 within the main text). Rate constants for model substrates which react relatively slowly with O_3, but do not absorb UV radiation appreciably at $\lambda = 258$ nm were measured by directly following the consumption of O_3 at this wavelength. These experiments were conducted under conditions of excess substrate, where $[\text{substrate}]_0:[O_3]_0$ was at least 10:1 (typically 20:1 or greater) in all cases. Pseudo-first-order rate constants determined from plots of $\ln([O_3]/[O_3]_0)$ vs. time were linear ($r^2 \geq 0.98$) in all cases. A stopped-flow spectrophotometry system was constructed in house to permit measurement of pseudo-first-order rate constants $k'_{O_3,\text{obs,M}}$ up to approximately 2.3 s^{-1}. Solutions of substrate and O_3 were prepared at 100 to 200 μM and 10 to 20 μM (to yield 50 to 100 μM and 5 to 10 μM after 1:1 mixing), respectively, in reagent water buffered to the desired pH with approximately 0.01 M phosphate. These solutions were injected at flow rates ranging from 25-35 mL/min from two self-contained Dosimat syringe pumps (Metrohm, Switzerland), through 1.5 mm I.D. PEEK tubing, and into the inlet ports of a 60° inner angle PEEK mixing tee. The outlet of the mixing tee was connected with a ~7 cm length of 0.5 mm I.D. FEP tubing to a 5 cm flow-through UV-spectrophotometry cell with a cylindrical 3 mm I.D. optical path. The effluent line of the stopped-flow system was connected via PEEK tubing to a 25-mL luer-lock gas-tight syringe clamped on to a lab-stand with the needle-side facing down, and the outside end of the piston several centimeters below a fixed metal plate. Effluent from the spectrophotometer cell flowed into the needle-end of the syringe until the piston contacted the metal plate – resulting in abrupt stoppage of system flow. Reactions were monitored after stoppage by following decay of O_3 at $\lambda = 258$ nm. The effective dead-time for this system was calculated to be $0.08 + 0.21 = 0.29 \sim 0.3$ s (minimum instrument resolution of the spectrophotometer was 0.1 s). On the basis of this dead-time, the limit of accurate measurement was estimated to be that for a reaction with $t_{1/2}$ of approximately 0.3 s, or $k'_{O_3,obs} \sim 2.3$ s^{-1}. This translated to a practical quantification limit of $k''_{O_3,app.} \sim 4.6 \times 10^4$ M^{-1}s^{-1}, for [substrate]$_0$ = 50 µM. The stopped-flow apparatus was calibrated by comparison of the second-order rate constant determined for the neutral species of RX ($k''_{O_3,\text{neutral RX}} = 1.2\ (\pm\ 0.1) \times 10^7$ M^{-1}s^{-1}) with that reported previously ($k''_{O_3,\text{neutral RX}} = 1.0\ (\pm\ 0.1) \times 10^7$ M^{-1}s^{-1} (*36*)), after calculation of the latter value for pK_a = 9.2 (*37*) (a pK_a of 8.8 was used in the prior study).

Method II (O_3 kinetics): Used for ASMX, CF (pH 3-6), EF (pH 3-5.5), PG, DMI, and FLU (Tables 2.1 and 2.2 within the main text). Rate constants for slowly-reacting substrates which absorb strongly at wavelengths close to 258 nm could not be determined by direct measurement of O_3 decay. These rate constants were instead determined under pseudo-first-order conditions of excess O_3 ($[O_3]_0$:[substrate]$_0$ ≥ 20) by following loss of substrate via HPLC with UV or fluorescence detection. All HPLC analyses were performed on either a Hewlett-Packard 1050 HPLC system equipped with a Supelco Discovery RP Amide C16 column (3 mm × 250 mm, 5 µM), fluorescence detector (FLD), and single-wavelength UV detector, or an Agilent 1100 HPLC system equipped with the same column and a variable wavelength UV diode-array detector. Separations were performed with acetonitrile and 0.05 M H_3PO_4 (adjusted to pH 2.2 with NaOH) as mobile phases, using isocratic or gradient methods as required for the analyte(s) of interest. UV detection was performed at wavelengths from 205 to 280 nm, depending on the analyte (limits of quantification ≅ 0.05 µM). Fluorescence detection was performed at $\lambda_{ex.} = 278$ nm and $\lambda_{em.} = 445$ nm for [CF]$_0$ and [EF]$_0$

< 1 μM, and at $\lambda_{ex.} = 278$ nm and $\lambda_{em.} = 360$ nm for $[\mathrm{FLU}]_0 < 1$ μM (limits of quantification ≅ 0.01 μM). Standard deviations for each measurement varied from ±1-5%.

Reactions were initiated by injecting – under constant stirring – 10-20-fold excess concentration of O_3 into 1-5 μM solutions of substrate contained within 100-mL amber, borosilicate bottles fitted with screw-cap piston-type dispensers (*38*), and thermostatted by a recirculating water bath. 1-mL samples were subsequently dispensed at pre-determined time intervals into amber, borosilicate HPLC vials containing 25 μL of 10 mM cinnamic acid to quench residual O_3, and subsequently transferred to HPLC for analysis of residual substrate, O_3 (as benzaldehyde (*39*)), and *p*-chlorobenzoic acid (*p*CBA – used as an internal standard used to correct for sample dispensation inaccuracies). Pseudo-first-order rate constants determined from plots of $\ln([\mathrm{M}]:[\mathrm{M}]_0)$ (where M represents the model substrate) vs. time were linear ($r^2 \geq 0.98$) in all cases. All experiments were conducted in duplicate.

Method III (O_3 kinetics): Used for CP, TET, DAMP, and MBDCH (Tables 2.1 and 2.2 within the main text). A number of model substrates included in this study do not significantly absorb UV radiation at wavelengths above 200 nm, are unstable in aqueous solution of extended periods of time, or are difficult to analyze, but react too rapidly with O_3 to follow by available manual methods. In each of these cases O_3 reaction rate constants were determined by application of a competition kinetics method requiring the measurement of only a single endpoint P, which is typically the formation of a product resulting from oxidation of either the model substrate, M, or competitor substrate, C (*13*). Experiments were conducted by adding a fixed dosage of O_3 to rapidly-stirred, 20-mL volumes of ten different buffered solutions containing various ratios of $[\mathrm{M}]_0:[\mathrm{C}]_0$ (both in at least 10-fold molar excess of O_3). Cinnamic acid ($k''_{\mathrm{O_3,neutral}} = 5 \times 10^4$ $\mathrm{M^{-1}s^{-1}}$ and $k''_{\mathrm{O_3,anion}} = 3.8 \times 10^5$ $\mathrm{M^{-1}s^{-1}}$ (*39*), pK_a = 4.4 (*40*)) or buten-3-ol ($k''_{\mathrm{O_3}} = 7.9 \times 10^4$ $\mathrm{M^{-1}s^{-1}}$ (*5*)) were used as competitor substrates in these experiments. Yields of benzaldehyde – measured by HPLC-UV – or formaldehyde – determined spectrophotometrically at λ = 412 nm as diacetyldihydrolutidine (*41*) – were selected as respective measurement endpoints, P. Model substrate rate constants were evaluated using eq S1,

$$\frac{[\mathrm{P}]_{\mathrm{absence}}}{[\mathrm{P}]_{\mathrm{presence}}} = 1 + \frac{k''_{O_3,app,C}[\mathrm{C}]_0}{k''_{O_3,app,M}[\mathrm{M}]_0} \tag{S1}$$

where $[\mathrm{P}]_{\mathrm{absence}}$ represents the measured endpoint yield in the absence of competitor substrate (obtained from duplicate C controls), and $[\mathrm{P}]_{\mathrm{presence}}$ represents endpoint yield in the presence of varying doses of competitor substrate. $k''_{\mathrm{O_3,app,C}}$ was determined from the slopes of plots of $\frac{[\mathrm{P}]_{\mathrm{absence}}}{[\mathrm{P}]_{\mathrm{presence}}} - 1$ vs. $\frac{[\mathrm{C}]_0}{[\mathrm{M}]_0}$.

Method IV (O₃ kinetics): Used for TYL, SMX, TMP, CF (pH 6.5-8), EF (pH 6-8), VM, APMS, and TMT (Tables 2.1 and 2.2 within the main text). A competition kinetics method requiring the measurement of two-endpoints was used to determine $k''_{\mathrm{O_3,app}}$ for substrates with $k''_{\mathrm{O_3,app}} > 5 \times 10^3\ \mathrm{M^{-1}s^{-1}}$ that absorb UV radiation strongly at wavelengths above 200 nm (*36*). In this approach, a different O_3 dose was added to each of ten rapidly-stirred, 20-mL volumes of a buffered solution containing a fixed ratio of $[\mathrm{M}]_0$:$[\mathrm{C}]_0$. The two endpoints – residual reference substrate (cinnamic acid) and competitor substrate concentrations remaining after O_3 addition – were measured by HPLC-UV. Model substrate rate constants were evaluated according to eq S2,

$$\ln\left(\frac{[C]}{[C]_0}\right) = \ln\left(\frac{[M]}{[M]_0}\right)\frac{k''_{O_3,app,C}}{k''_{O_3,app,M}} \tag{S2}$$

where $k''_{\mathrm{O_3,app,C}}$ could be determined from the slope of a plot of $\ln\left(\frac{[C]}{[C]_0}\right)$ vs. $\ln\left(\frac{[M]}{[M]_0}\right)$. $[\mathrm{M}]_0$ and $[\mathrm{C}]_0$ were taken from analyses of duplicate O_3 controls included in each experiment.

Method V (•OH kinetics): Used for RX, AZ, ASMX, TMP, LM, PG, CP, and VM. •OH rate constants were determined for photo-stable model substrates via application of the same competition kinetics approach as utilized for Method IV, except that eq S2 was modified to eq S3.

$$\ln\left(\frac{[C]}{[C]_0}\right) = \ln\left(\frac{[pCBA]}{[pCBA]_0}\right)\frac{k''_{\bullet OH,app,C}}{k''_{\bullet OH,app,pCBA}} \tag{S3}$$

Hydroxyl radicals were generated by in situ UV-photolysis of H_2O_2 in solutions containing the reference substrate *p*-chlorobenzoic acid (*p*CBA, with $k''_{\bullet OH,app,pCBA} = 5.0 \times 10^9\ \mathrm{M^{-1}s^{-1}}$ (*42*)), and competitor substrate, C, according to a previously described procedure (*36*). Briefly, reaction solutions buffered at pH 7 with approximately 0.01 M phosphate were dosed with 2 mM H_2O_2, and fixed $[\mathrm{C}]_0$:$[\mathrm{pCBA}]_0$. These solutions were irradiated with a 500-W medium pressure lamp ($\lambda < 308$ nm screened by a UV-cutoff filter) for repeated ten-minute intervals up to two-hour total irradiation periods. Samples were withdrawn from these solutions between each irradiation period for residual substrate analysis by HPLC-UV. RX, AZ, and LM were detected at λ = 205 nm. Experiments included a minimum of 10 different irradiation times. H_2O_2 controls were included in all experiments.

Method VI (•OH kinetics): Used for TET, TYL, CF, and EF. These substrates were moderately to highly photo-labile in the presence of UV radiation passing the 308 nm cutoff filter used in Method V. •OH rate constants were determined for these substrates according to the same competition kinetics procedure used in Method V (i.e., via eq S3), except that •OH was generated by γ-radiolysis (via a lead-shielded ^{60}Co γ-source) of aqueous solutions purged with a 4:1 N_2O:O_2 mixture, according to (*43*). Each such experiment included at least eight different irradiation times (•OH exposures).

Method VII (•OH kinetics): Used for AM. The •OH rate constant for AM was determined according to Method V, except that AM was derivatized with 9-fluoroenylmethyl chloroformate (FMOC) (*44*), to permit detection by UV. One-mL samples (containing starting concentrations of 5 μM AM, 5 μM *p*CBA, and 2 mM H_2O_2) taken from the photo-reaction system described above were dosed into amber, borosilicate HPLC vials containing 25 mM of sodium pyruvate to quench residual H_2O_2 (*45*) – which appeared to interfere with the derivatization process – and 25 mM of NaOH (to prevent losses of AM to adsorption onto glass surfaces prior to derivatization (*46*) and to accelerate the reaction between pyruvate and H_2O_2 (*45,47*)). 500 μL of these samples were subsequently transferred to separate HPLC vials containing 500 μL of 2.5 mM FMOC in acetonitrile and 200 μL of 0.8 M boric acid (to maintain a solution pH of ~ 9) for derivatization (*44*). The remainder of the underivatized samples were used for analysis of residual *p*CBA by HPLC-UV (λ = 205 nm). Derivatized AM was measured by HPLC-UV (λ = 200 nm) a minimum of one hour after initiation of the derivatization reaction (15 minute reaction times are reported to be sufficient for derivatization of gentamicin, another aminoglycoside (*44*)). AM concentrations in dark controls containing H_2O_2 were stable over the 135-minute experimental period, indicating that adsorption of AM to reactor tube surfaces was negligible during each experiment.

Text S2.4 Wastewater matrix experiments.

A 10-L grab sample of secondary wastewater effluent was obtained from the Kloten-Opfikon wastewater treatment facility near Zurich, Switzerland. This sample was transported to the laboratory in a polypropylene carboy within several hours of sampling and vacuum-filtered with a 0.45 μm cellulose-nitrate membrane prior to storage at 4 °C. Sample alkalinity and DOC were 3.5 mM as HCO_3^- and 5.3 mg C/L, respectively. Native sample pH was 7.7. Kloten-Opfikon secondary wastewater effluent is known to contain - on average - less than 1 μg/L of RX, AZ, SMX, ASMX, and TMP (*48,49*). The concentration of CF in the influent to this plant has been reported as < 1 μg/L on average, and should be significantly lower after secondary treatment. These levels are negligible relative to the concentrations spiked to Kloten-Opfikon sample for wastewater ozonation experiments, which were 1 μM for each substrate (translating to a minimum concentration of 253 μg/L, for - SMX - the substrate with the lowest molecular weight).

Only the reaction between O_3 and ASMX was slow enough to permit direct monitoring of ASMX loss during ozonation of the wastewater sample. 63 mM (3 mg/L) of O_3 was added under constant, rapid stirring to a 20-mL volume of Kloten-Opfikon wastewater containing 1 μM of ASMX and 1 μM of pCBA. Samples were taken every 10 s until O_3 was completely depleted, for subsequent analysis of residual ASMX and pCBA by HPLC-UV.

For all other substrates, various doses of O_3 (ranging from 5 μM (0.25 mg/L) to 104 μM (5 mg/L)) were added under constant, rapid stirring to 20-mL volumes of Kloten-Opfikon wastewater – each containing 1 μM of the model substrate of interest and 1 μM of *p*CBA. Reactions were allowed to proceed until complete O_3 depletion (except in the case of solutions dosed with 104 μM O_3 doses, which were quenched with buten-3-ol after ~ 90 s of reaction to remove O_3 residual). One-mL samples were then taken from each reaction solution and transferred to amber, borosilicate HPLC vials for direct HPLC-UV analysis of residual model substrate and *p*CBA concentrations.

Each experiment was conducted in duplicate. In addition, duplicate O_3 controls were included with each set of samples to verify substrate stability in the wastewater matrix. Analyte recoveries were calculated from measurements obtained for control samples of distilled water dosed with 1 μM concentrations of each substrate, and found to be 100 ± 10% for all analytes except TET, for which a recovery of 117% was recorded. All experiments were conducted at T = 20 ± 0.5 °C.

Text S2.5 Estimation of transformation efficiencies and $f_{\bullet OH,M}$ for RX, AZ, AM, and LM

Transformation of a substrate (M) is governed by eq S4 (*50*) during ozonation of a real water, where the two integral terms on the right hand-side represent the O_3 and •OH exposures governing its conversion (M/M_0) for a reaction time, τ, where $[\bullet OH] = f(t)$ and $[O_3] = g(t)$.

$$\ln\left(\frac{[M]_\tau}{[M]_0}\right) = -k''_{O_3,app,M}\int_0^\tau [O_3]dt - k''_{\bullet OH,app,M}\int_0^\tau [\bullet OH]dt \qquad (S4)$$

The •OH exposure term, $\int_0^\tau [\bullet\,\mathrm{OH}]dt$, can be calculated by using an O_3-recalcitrant compound such as *p*CBA as a probe to measure *in situ* •OH exposures, according to eq S5 (*50,51*). Theoretically, such an

$$\int_0^\tau [\bullet\,\mathrm{OH}]dt = -\frac{1}{k''_{\bullet\mathrm{OH,app},p\mathrm{CBA}}}\ln\left(\frac{[p\mathrm{CBA}]_\tau}{[p\mathrm{CBA}]_0}\right) \tag{S5}$$

approach should also be applicable to determining relative O_3 exposures for substrates with $k''_{\mathrm{O_3,app}} > 10^3\ \mathrm{M^{-1}s^{-1}}$ during ozonation processes; i.e., one should be able to determine $\int_0^\tau [\mathrm{O_3}]dt$ for a certain probe compound and use this value to estimate $\ln\left(\frac{[\mathrm{M}]_\tau}{[\mathrm{M}]_0}\right)$ for other substrates exposed to the same reaction conditions. However, unlike •OH exposure, O_3 exposure can only be calculated indirectly from eqs S4 and S5 (via eq S6), since no •OH-refractory, O_3-susceptible probe compound is available to provide an *in situ* measurement of this value.

$$\int_0^\tau [\mathrm{O_3}]dt = \left(\frac{k''_{\bullet\mathrm{OH,app,M}}}{k''_{\bullet\mathrm{OH,app},p\mathrm{CBA}}}\ln\left(\frac{[p\mathrm{CBA}]_\tau}{[p\mathrm{CBA}]_0}\right) - \ln\left(\frac{[\mathrm{M}]_\tau}{[\mathrm{M}]_0}\right)\right)\Bigg/ k''_{\mathrm{O_3,app,M}} \tag{S6}$$

The applicability of this approach was evaluated by calculating $\ln\left(\frac{[\mathrm{M}]_\tau}{[\mathrm{M}]_0}\right)$ (at O_3 dosages of 1 and 1.5 mg/L) for each of the nine substrates TYL, SMX, TMP, CF, EF, CP, PG, TET, and VM, by using each of the $\int_0^\tau [\mathrm{O_3}]dt$ terms determined with eq S6 for the other eight substrates. $\int_0^\tau [\bullet\,\mathrm{OH}]dt$ was calculated for each substrate according to eq S5. As shown in Figure S2.13, this procedure yielded good estimates of transformation efficiencies, $\ln\left(\frac{[\mathrm{M}]_\tau}{[\mathrm{M}]_0}\right)$, as long as $\int_0^\tau [\mathrm{O_3}]dt$ terms were selected from the $\int_0^\tau [\mathrm{O_3}]dt$ value measured for the substrate with the *most* similar $k''_{\mathrm{O_3,app}}$ at the wastewater pH of 7.7 (e.g., PG transformation was estimated on the basis of CF transformation, EF transformation from TMP transformation, and TET transformation from TYL transformation). In contrast, significant discrepancies were observed when estimates were based on $\int_0^\tau [O_3]dt$ obtained from substrates with markedly different magnitudes of $k''_{O_3,\text{app}}$ (i.e., differing by more than one order of magnitude from each other). Estimates of $\ln\left(\frac{[M]_\tau}{[M]_0}\right)$ for RX, AZ, AM, and LM were obtained by using the $\int_0^\tau [O_3]dt$ terms for TMP, SMX, CF, and TYL, respectively. These estimates were in turn used to calculate $f_{\bullet OH,M}$ by eq 6 in the main text (see Figure 2.4 in the main text).

The discrepancies noted above – for $\ln\left(\frac{[M]_\tau}{[M]_0}\right)$ estimates based on comparison of substrate pairs with dissimilar $k''_{O_3,\text{app}}$ values – may have been a consequence of incomplete mixing on the time-scales of initial O_3 consumption in each reaction system. Since initial consumption of O_3 by wastewater matrixes such as that utilized here is typically extremely rapid ($t_{1/2}$ on the order of 0.01 to 0.05 s) (*52*), such a mixing effect may have resulted in disproportionate O_3 consumption by locally abundant sample matrix constituents (relative to very small local concentrations of the given antibacterial substrate) within the vicinity of O_3 injection. This could have resulted in lower observed transformation of substrates than predicted on the basis of their O_3 rate constants alone. Estimation errors would be more pronounced for substrate pairs exhibiting large differences in $k''_{O_3,\text{app}}$ (i.e., > two orders of magnitude), as indicated above.

Table S2.1. pK_a values and corresponding source references for each antibacterial substrate

Structural Class	**Substrate***	**pK_{a1}**	**pK_{a2}**	**pK_{a3}**	**pK_{a4}**	**pK_{a5}**	**pK_{a6}**
Macrolide	RX	9.2 (*37*)					
	AZ	8.7 (*53*)	9.5 (*53*)				
	TYL	7.7 (*53*)					
Sulfonamide	SMX	1.7 (*54*)	5.6 (*54*)				
	ASMX	5.5 (*55*)					
Fluoroquinolone	CF	6.2 (*56*)	8.8 (*56*)				
	EF	6.1 (*57*)	7.7 (*57*)				
DHFR Inhibitor	TMP	3.2 (*37,58,59*)	7.1 (*59*)				
Lincosamide	LM	7.8 (*37*)					
β-lactam	PG	2.7 (*60*)					
	CP	2.5 (*61*)	7.1 (*61*)				
Tetracycline	TET	3.3 (*62*)	7.7 (*62*)	9.7 (*62*)			
Glycopeptide	VM	2.9 (*63,64*)	7.2 (*63,64*)	8.6 (*63,64*)	9.6 (*63*)	10.5 (*63*)	11.7 (*63*)
Aminoglycoside	AM	6.7 (*65*)	8.4 (*65*)	8.4 (*65*)	9.7 (*65*)		

*For full names, see Table 2.1 in the main text

Table S2.2. pK_a values and corresponding source references for each substructure model substrate

Substrate[a]	**pK_{a1}**	**pK_{a2}**
DMCH	10.7 (*66*)	
MP	10.2 (*67*)	
APMS	1.5 (*68*)	
DMI	NA	
EPC	8.3 (*69*)	
FLU	6.5 (*70*)	
DAMP	3.2[b]	7.1[b]
TMT	NA	
MBDCH	3.5 (*67*)	
CH	10.6 (*66*)	
CHM	10.3 (*67*)	

NA – Not applicable. [a]For full names, see Table 2.2 in the main text. [b]pK_a values assumed to approximate those for TMP, since DAMP is identical to TMP's 2,4-diamino-5-methylpyrimdine moiety.

Table S2.3. Second-order rate constants ($M^{-1}s^{-1}$) for reactions of O_3 with substructure model substrates

Substrate[a] **(Rate constant measurement methods**[b]**)**	k''_{O_3} [c]		
		Species	
	Diprotonated	**Monoprotonated**	**Deprotonated**
DMCH (I)	NA	< 1[d]	3.7 (± 0.1) × 10^6
MP (I)	NA	< 1[d]	2.0 (± 0.1) × 10^6
APMS (IV)	NA	ND	4.7 (± 0.1) × 10^4
DMI (II)	NA	NA	5.4 (± 0.3) × 10^1
EPC (I)	NA	< 1[d]	1.1 (± 0.1) × 10^6
FLU (II)	NA	1.2 (± 0.7)	1.8 (± 0.1) × 10^3
DAMP (III)	5.0 (± 12) × 10^2	2.9 (± 1.3) × 10^3	1.3 (± 0.2) × 10^6
TMT (IV)	NA	NA	2.8 (± 0.1) × 10^5
MBDCH (III)	NA	ND	1.4 (± 0.4) × 10^6
CH (I)	NA	< 1[d]	4.9 (± 0.2) × 10^4
CHM (I)	NA	< 1[d]	7.1 (± 0.2) × 10^4

NA – Not applicable, ND – Not determined. [a]For full names, see Table 2.2 in the main text. [b]Described in Text S2.3. [c]O_3 reaction rate constants were measured at T = 20 ± 0.5° C. [d]These rate constants were assumed to be negligible, on the basis of prior observations for protonated amine reaction centers (*2,25*).

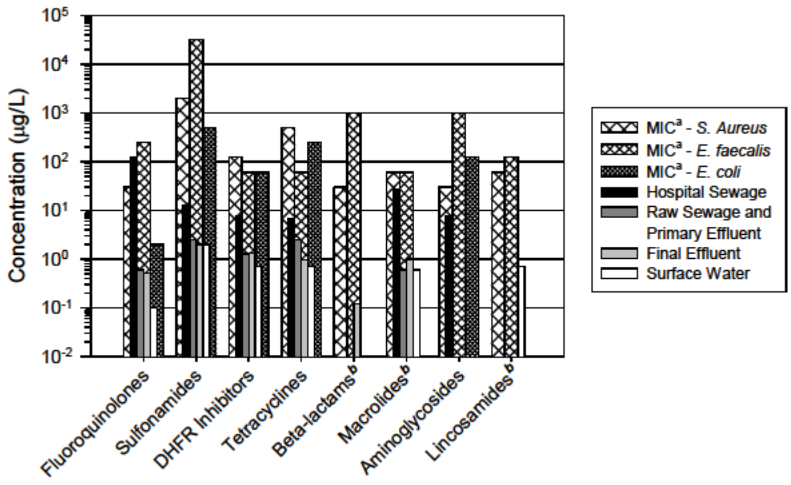

Figure S2.1. Maximum single-compound* concentrations of various antibacterial classes detected in municipal wastewater systems and surface waters, in the context of minimum reported clinical MIC values for sensitive bacterial reference strains. Data for fluoroquinolones (*71-77*), sulfonamides (*49,73-79*), DHFR (dihydrofolate reductase) inhibitors (*73,74,76-78,80,81*), tetracyclines (*73,74,81*), *β*-lactams (*82*), macrolides (*30,49,74,75,77,83*), aminoglycosides (*84*), and lincosamides (*74*) was obtained from various environmental analytical studies. [a]MIC – minimal inhibitory concentration, or minimal concentration resulting in a measurable reduction in bacterial growth relative to an antibacterial blank. MICs listed for each class correspond (in order from left to right) to reported values for ciprofloxacin, sulfamethoxazole, trimethoprim, tetracycline, penicillin, erythromycin, gentamicin, and clindamycin, respectively (*11*), [b]MIC values not reported for *E. coli*. *More than one compound from a given antibacterial class may be present in the same municipal wastewater.

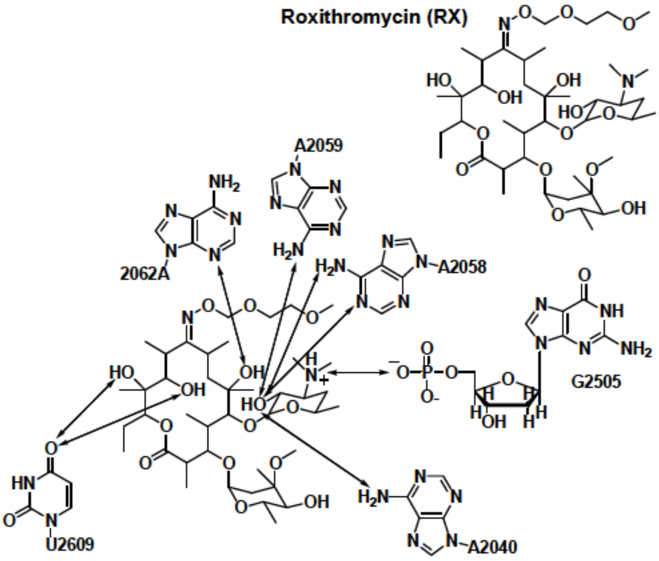

Figure S2.2. Biochemical model for mechanism of macrolide antibacterial activity (adapted with permission from Schlünzen et al. *(1)*).

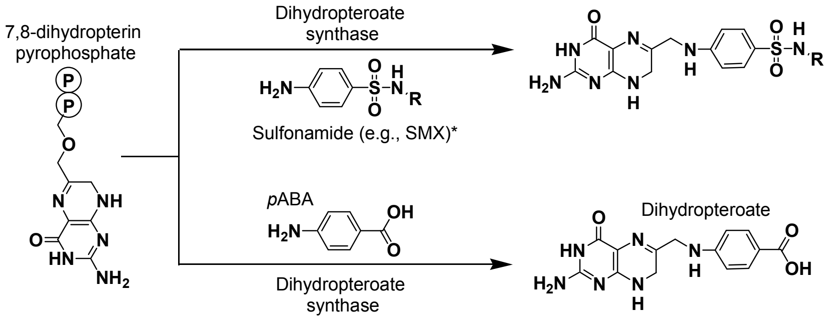
7,8-dihydropterin pyrophosphate
Dihydropteroate synthase
Sulfonamide (e.g., SMX)*
pABA
Dihydropteroate
Dihydropteroate synthase

Figure S2.3. Biochemical mechanism of sulfonamide antibacterial activity (*6*). *R represents an aromatic substituent that varies, depending on the particular sulfonamide compound.

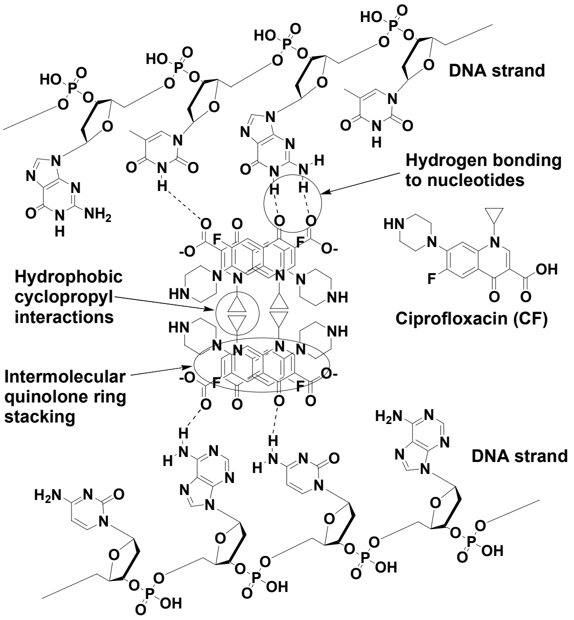
DNA strand
Hydrogen bonding to nucleotides
Hydrophobic cyclopropyl interactions
Intermolecular quinolone ring stacking
Ciprofloxacin (CF)
DNA strand

Figure S2.4. Biochemical model for mechanism of fluoroquinolone antibacterial activity (adapted with permission from Shen et al. (*9*)).

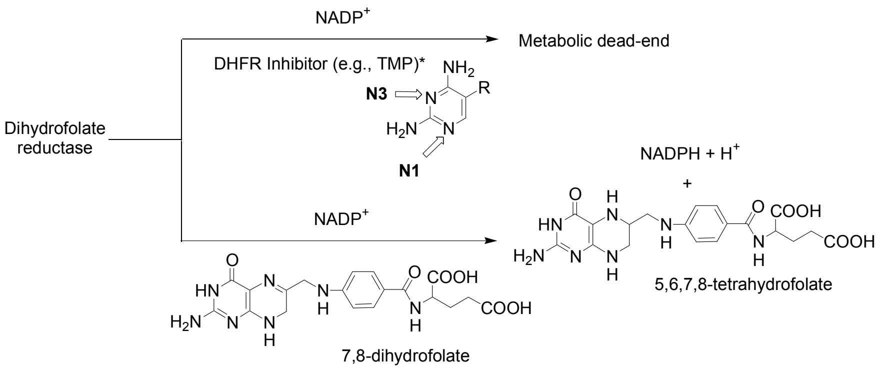
NADP+
Metabolic dead-end
DHFR Inhibitor (e.g., TMP)*
N3
N1
Dihydrofolate reductase
NADPH + H+
+
NADP+
5,6,7,8-tetrahydrofolate
7,8-dihydrofolate

Figure S2.5. Biochemical mechanism of dihydrofolate reductase (DHFR) inhibitor antibacterial activity (*6*). *R represents an aromatic substituent that varies, depending on the particular DHFR inhibitor.

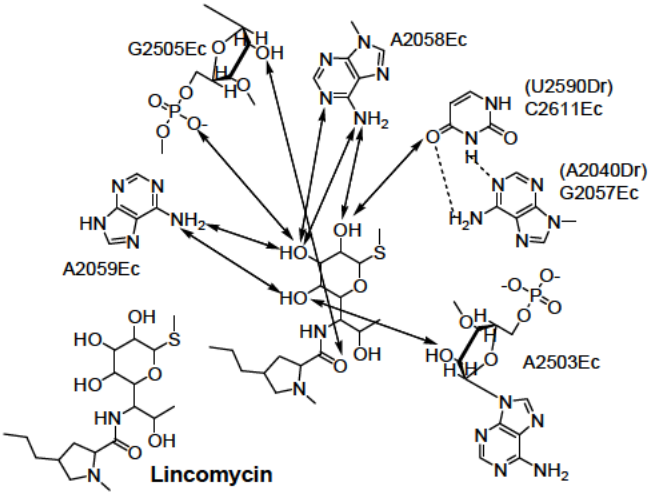
G2505Ec
A2058Ec
(U2590Dr)
C2611Ec
(A2040Dr)
G2057Ec
A2059Ec
A2503Ec
Lincomycin

Figure S2.6. Biochemical model for mechanism of lincosamide antibacterial activity (adapted with permission from Schlünzen et al. *(1)*).

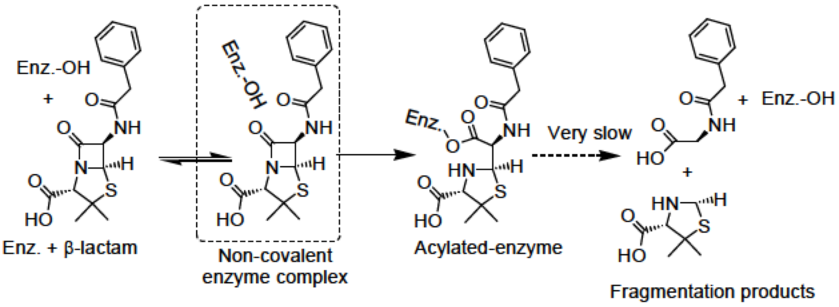
Enz.-OH
Enz. + β-lactam
Non-covalent enzyme complex
Acylated-enzyme
Very slow
Enz.-OH
Fragmentation products

Figure S2.7. Biochemical mechanism of *β*-lactam antibacterial activity (depicted for penicillin G) (*6,17*).

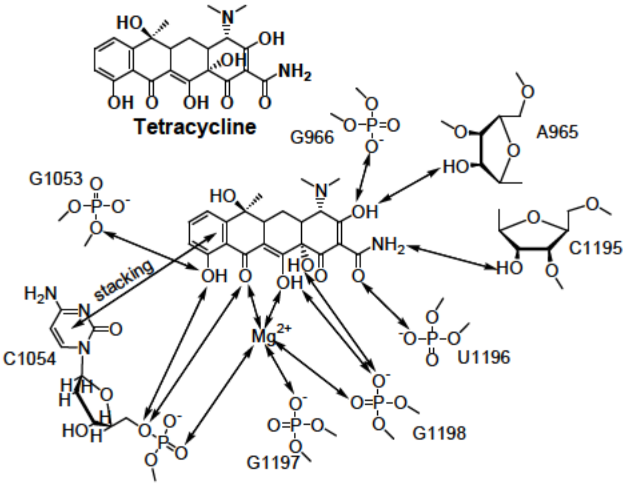
Tetracycline
G966
A965
G1053
C1195
stacking
C1054
Mg2+
U1196
G1197
G1198

Figure S2.8. Biochemical model for primary* mechanism of tetracycline antibacterial activity (adapted with permission from Broderson et al. (*21*)). *Tetracycline binding at a secondary site within the bacterial ribosome is believed to involve many of the same functional moieties as binding at the primary site (*21*).

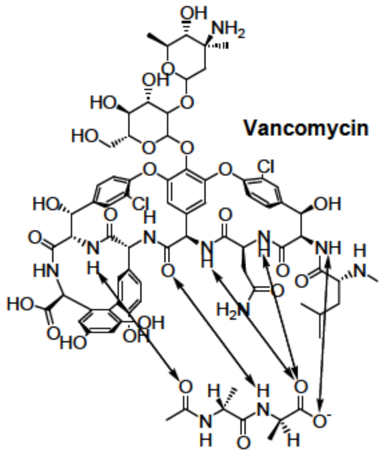
Vancomycin

Figure S2.9. Biochemical model for mechanism of glycopeptide antibacterial activity (adapted with permission from Williams and Bardsley (1999) (*24*)).

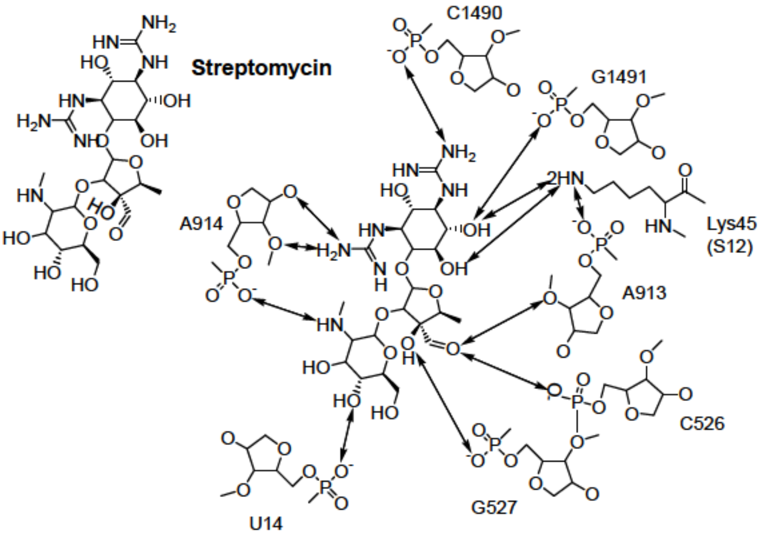
Streptomycin
C1490
G1491
A914
Lys45
(S12)
A913
C526
G527
U14

Figure S2.10. Biochemical model for mechanism of aminoglycoside antibacterial activity (adapted with permission from Carter et al. (*28*)).

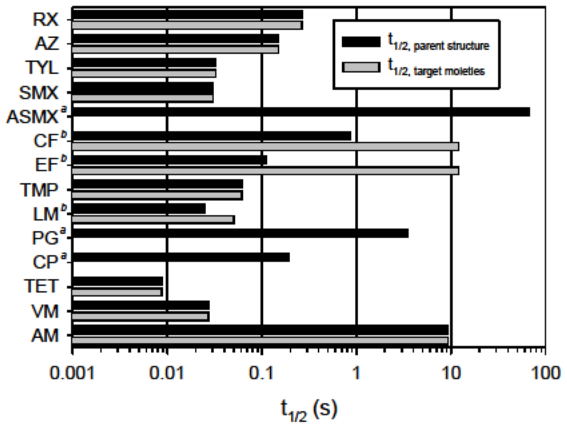

Figure S2.11. Calculated $t_{1/2}$ values for the apparent transformation of model antibacterial substrates by O_3, in comparison to corresponding estimated half-lives for reaction of O_3 with the targeted functional moieties (Table 2.1 in the main text) associated with each substrate's biochemical activity at 20(±0.5) °C, pH 7, and $[O_3]$ = 42 μM (2 mg/L). [a]Either O_3 does not appear to react directly with biochemically-active target moieties (PG, CP), or $t_{1/2}$ for this reaction could not be determined (ASMX). [b]$t_{1/2,target}$ estimates for CF and EF are based on the $t_{1/2}$ value determined for FLU and $t_{1/2,target}$ for LM based on $t_{1/2}$ determined for cationic LM, as discussed in the main text.

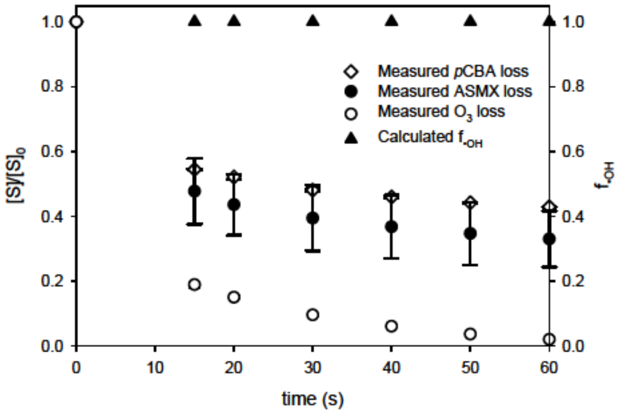

Figure S2.12. Transformation of ASMX during ozonation of Kloten-Opfikon wastewater at 20(±0.5) °C, pH 7.7, $[O_3]_0$ = 63 μM (3 mg/L), and $[substrate]_0$ = 1 μM. S represents each monitored substance – O_3, *p*CBA, and ASMX.

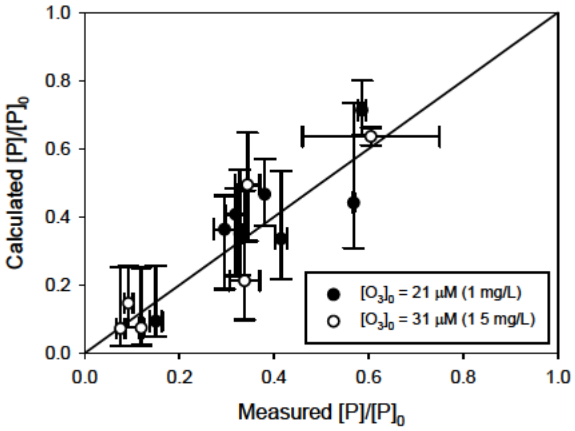

Figure S2.13. Correlations of predicted substrate transformation with measured values, for data sets obtained at T = 20° C, pH 7.7, and $[O_3]_0$ = 1 and 1.5 mg/L (21 and 31 μM, respectively).

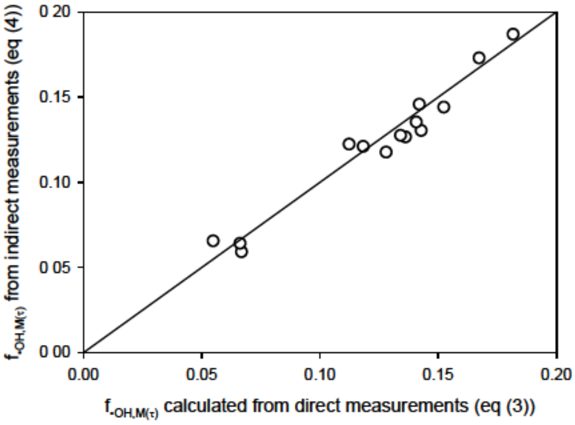

Figure S2.14. Comparison of $f_{\bullet OH,M(\tau)}$ values calculated from indirect determinations of O_3 exposure (by eq 6 in the main text) with those calculated from direct measurements of O_3 exposure (by eq 4 in the main text). Calculations were performed with data reported elsewhere (*52*) for $[\text{carbamazepine}]_0$ = 1-2 μM, $[O_3]$ = 25-50 μM (1.2-2.4 mg/L), in various municipal wastewater samples.

Literature Cited

(1) Schlünzen, F.; Zarivach, R.; Harms, J.; Bashan, A.; Tocilj, A.; Albrecht, R.; Yonath, A.; Franceschi, F. Structural basis for the interaction of antibiotics with the peptidyl transferase centre in eubacteria. *Nature* **2001**, *413*, 814-821.

(2) Hoigné, J.; Bader, H. Rate constants of reactions of ozone with organic and inorganic compounds in water – II : Dissociating organic compounds. *Water Res.* **1983**, *17*, 185-194.

(3) Muñoz, F.; von Sonntag, C. The reactions of ozone with tertiary amines including the complexing agents nitrilotriacetic acid (NTA) and ethylenediaminetetraacetic acid (EDTA) in aqueous solution. *J. Chem. Soc., Perkin Trans. 2* **2000**, 2029-2033.

(4) Lange, F.; Cornelissen, S.; Kubac, D.; Sein, M. M.; von Sonntag, J.; Hannich, C. B.; Golloch, A.; Heipieper, H. J.; Moder, M.; von Sonntag, C. Degradation of macrolide antibiotics by ozone: A mechanistic case study with clarithromycin. *Chemosphere* **2006**, *65*, 17-23.

(5) Dowideit, P.; von Sonntag, C. Reaction of ozone with ethene and its methyl- and chlorine-substituted derivatives in aqueous solution. *Environ. Sci. Technol.* **1998**, *32*, 1112-1119.

(6) Walsh, C. *Antibiotics: Actions, Origins, Resistance*; ASM Press: Washington, D.C., 2003.

(7) Spanggord, R. J.; Yao, D.; Mill, T. Kinetics of aminodinitrotoluene oxidations with ozone and hydroxyl radical. *Environ. Sci. Technol.* **2000**, *34*, 450-454.

(8) Pierpoint, A. C.; Hapeman, C. J.; Torrents, A. Linear free energy study of ring-substituted aniline ozonation for developing treatment of aniline-based pesticide wastes. *J. Agric. Food Chem.* **2001**, *49*, 3827-3832.

(9) Shen, L. L.; Mitscher, L. A.; Sharma, P. N.; O'Donnell, T. J.; Chu, D. W. T.; Cooper, C. S.; Rosen, T.; Pernet, A. G. Mechanism of inhibition of DNA gyrase by quinolone antibacterials: a cooperative drug-DNA binding model. *Biochemistry* **1989**, *28*, 3886-3894.

(10) Theruvathu, J. A.; Flyunt, R.; Aravindakumar, C. T.; von Sonntag, C. Rate constants of ozone reactions with DNA, its constituents, and related compounds. *J. Chem. Soc., Perkin Trans. 2* **2001**, 269-274.

(11) Wiedemann, B.; Grimm, H. In *Antibiotics in Laboratory Medicine*; Lorian, V., Ed.; Williams and Wilkins: Baltimore, MD, 1996, pp 900-1168.

(12) Cocco, L.; Roth, B.; Temple, C., Jr.; Montgomery, J. A.; London, R. E.; Blakley, R. L. Protonated state of methotrexate, trimethoprim, and pyrimethamine bound to dihydrofolate reductase. *Arch. Biochem. Biophys.* **1983**, *226*, 567-577.

(13) Muñoz, F.; von Sonntag, C. Determination of fast ozone reactions in aqueous solution by competition kinetics. *J. Chem. Soc., Perkin Trans. 2* **2000**, *2*, 661-664.

(14) Spry, D. O. Oxidation of penicillin and dihydrocephalosporin derivatives with ozone. *J. Org. Chem.* **1972**, *37*, 793-795.

(15) Bailey, P. S. *Ozonation in organic chemistry. II. Non-olefinic compounds*; Academic Press: New York, NY, 1982.

(16) Sztaricskai, F.; Dinya, Z.; Batta, G.; Mocsári, A. Chemical synthesis and structural study of lincomycin sulfoxides and a sulfone. *The Journal of Antibiotics* **1997**, *50*, 866-873.

(17) Livermore, D. M.; Williams, J. D. In *Antibiotics in Laboratory Medicine*; 4 ed.; Lorian, V., Ed.; Williams and Wilkins: Baltimore, MD, 1996, pp 502-578.

(18) de Koning, J. J.; Marx, A. F.; Poot, M. M.; Smid, P. M.; Verweij, J. In *Recent Advances in the Chemistry of β-Lactam Antibiotics*; Elks, J., Ed.; The Chemical Society: Burlington House, London (England), 1977; Vol. 28, pp 161-166.

(19) Torii, H.; Asano, T.; Matsumoto, N.; Kato, K.; Tsushima, S.; Kakinuma, A. Microbial oxidation of cephalosporins to cephalosporin sulfoxides. *Agricultural and Biological Chemistry* **1980**, *44*, 1431-1433.

(20) Bailey, P. S. *Ozonation in organic chemistry. I. Olefinic compounds*; Academic Press: New York, NY, 1978.

(21) Brodersen, D. E.; Clemons, W. M., Jr.; Carter, A. P.; Morgan-Warren, R. J.; Wimberly, B. T.; Ramakrishnan, V. The structural basis for the action of the antibiotics tetracycline, pactamycin, and hygromycin B on the 30S ribosomal subunit. *Cell* **2000**, *103*.

(22) Hoigné, J.; Bader, H. Rate constants of reactions of ozone with organic and inorganic compounds in water – I : Non-dissociating organic compounds. *Water Res.* **1983**, *17*, 173-183.

(23) Mvula, E.; von Sonntag, C. Ozonolysis of phenols in aqueous solution. *Org. Biomol. Chem.* **2003**, *1*, 1749-1756.

(24) Williams, D. H.; Bardsley, B. The vancomycin group of antibiotics and the fight against resistant bacteria. *Angewandte Chemie-International Edition* **1999**, *38*, 1173-1193.

(25) Pryor, W. A.; Giamalva, D. H.; Church, D. F. Kinetics of ozonation. 2. Amino acids and model compounds in water and comparisons to rates in nonpolar solvents. *J. Am. Chem. Soc.* **1984**, *106*, 7094-7100.

(26) Ragnar, M.; Eriksson, T.; Reitberger, T.; Brandt, P. A new mechanism in the ozone reaction with lignin like structures. *Holzforschung* **1999**, *53*, 423-428.

(27) von Gunten, U. Ozonation of drinking water: Part I. Oxidation kinetics and product formation. *Water Res.* **2003**, *37*, 1443-1467.

(28) Carter, A. P.; Clemons, W. M., Jr.; Brodersen, D. E.; Morgan-Warren, R. J.; Wimberly, B. T.; Ramakrishnan, V. Functional insights from the structure of the 30S ribosomal subunit and its interactions with antibiotics. *Nature* **2000**, *407*, 340-348.

(29) Kadurugamuwa, J. L.; Lam, J. S.; Beveridge, T. J. Interaction of gentamicin with the A band and B band lipopolysaccharides of *Pseudomonas aeruginosa* and its possible lethal effect. *Antimicrob. Agents Chemother.* **1993**, *37*, 715-721.

(30) Göbel, A.; McArdell, C. S.; Suter, M. J.-F.; Giger, W. Trace determination of macrolide and sulfonamide antimicrobials, a human sulfonamide metabolite, and trimethoprim in wastewater using liquid chromatography coupled to electrospray tandem mass spectrometry. *Anal. Chem.* **2004**, *76*, 4756-4764.

(31) Bader, H.; Hoigné, J. Determination of ozone in water by the indigo method. *Water Res.* **1981**, *15*, 449-456.

(32) Hoigné, J.; Bader, H. The role of hydroxyl radical reactions in ozonation processes in aqueous solutions. *Water Res.* **1976**, *10*, 377-386.

(33) Staehelin, J.; Hoigné, J. Decomposition of ozone in water in the presence of organic solutes acting as promoters and inhibitors of radical chain reactions. *Environ. Sci. Technol.* **1985**, *19*, 1206-1213.

(34) Mosseri, S.; Neta, P.; Meisel, D. The mechanism of cyanide release in the radiolysis of acetonitrile. Formation and decay of the cyanomethylperoxyl radical. *Radiat. Phys. Chem.* **1990**, *36*, 683-687.

(35) Schwarzenbach, R. P.; Gschwend, P. M.; Imboden, D. M. *Environmental Organic Chemistry*; 2nd ed.; John Wiley & Sons, Inc.: Hoboken, NJ, 2003.

(36) Huber, M. M.; Canonica, S.; Park, G.-Y.; von Gunten, U. Oxidation of pharmaceuticals during ozonation and advanced oxidation processes. *Environmental Science and Technology* **2003**, *37*, 1016-1024.

(37) Qiang, Z. M.; Adams, C. Potentiometric determination of acid dissociation constants (pK(a)) for human and veterinary antibiotics. *Water Res.* **2004**, *38*, 2874-2890.

(38) Hoigné, J.; Bader, H. Characterization of water-quality criteria for ozonation processes. 2. Lifetime of added ozone. *Ozone: Sci. Eng.* **1994**, *16*, 121-134.

(39) Leitzke, A.; Reisz, E.; Flyunt, R.; von Sonntag, C. The reactions of ozone with cinnamic acids: formation and decay of 2-hydroperoxy-2-hydroxyacetic acid. *J. Chem. Soc., Perkin Trans. 2* **2001**, 793-797.

(40) Lide, D. R., Ed.^Eds. *CRC Handbook of Chemistry and Physics*; 82 ed.; CRC Press: Boca Raton, FL, 2001.

(41) Nash, T. The colorimetric estimation of formaldehyde by means of the Hantzsch reaction. *Biochem. J.* **1953**, *55*, 416-421.

(42) Buxton, G. V.; Greenstock, W. P.; Helman, W. P.; Ross, A. B. Critical review of rate constants for reactions of hydrated electrons, hydrogen atoms, and hydroxyl radicals ($^{\bullet}OH/O^{\bullet -}$) in aqueous solution. *J. Phys. Chem. Ref. Data* **1988**, *17*, 513-886.

(43) von Gunten, U.; Oliveras, Y. Advanced oxidation of bromide-containing waters: Bromate formation mechanisms. *Environ. Sci. Technol.* **1998**, *32*, 63-70.

(44) Stead, D. A.; Richards, R. M. E. Sensitive fluorimetric detection of gentamicin sulfate in biological matrices using solid-phase extraction, pre-column derivatization with 9-fluoroenylmethyl chloroformate and reversed phase high-performance liquid chromatography. *Journal of Chromatography B* **1996**, *675*, 295-302.

(45) Bunton, C. A. Oxidation of α-diketones and α-keto acids by hydrogen peroxide. *Nature* **1949**, *163*, 444.

(46) Josephson, L.; Houle, P.; Haggerty, M. Stability of dilute aqueous solutions of gentamicin and tobramycin. *Clinical Chemistry* **1979**, *25*, 298-300.

(47) Siegel, B.; Lanphear, J. Kinetics and mechanisms for the acid-catalyzed oxidative decarboxylation of benzylformic acid. *J. Org. Chem.* **1979**, *44*, 942-946.

(48) Golet, E. M.; Alder, A. C.; Giger, W. Environmental exposure and risk assessment of fluoroquinolone antibacterial agents in wastewater and river water of the Glatt Valley watershed, Switzerland. *Environ. Sci. Technol.* **2002**, *36*, 3645-3651.

(49) Göbel, A.; Thomsen, A.; McArdell, C. S.; Joss, A.; Giger, W. Occurrence and sorption behavior of sulfonamides, macrolides, and trimethoprim in activated sludge treatment. *Environ. Sci. Technol.* **2005**, *39*, 3981-3989.

(50) Elovitz, M. S.; von Gunten, U. Hydroxyl radical/ozone ratios during ozonation processes. I. The R_{ct} concept. *Ozone Science and Engineering* **1999**, *21*, 239-260.

(51) Huber, M. M.; Göbel, A.; Joss, A.; Hermann, N.; Löffler, D.; McArdell, C. S.; Ried, A.; Siegrist, H.; Ternes, T. A.; von Gunten, U. Oxidation of pharmaceuticals during ozonation of municipal wastewater effluents: a pilot study. *Environmental Science and Technology* **2005**, *39*, 4290-4299.

(52) Buffle, M.-O.; Schumacher, J.; Salhi, E.; von Gunten, U. Measurement of the initial phase of ozone decomposition in water and wastewater by means of a continuous quench flow system: Application to disinfection and pharmaceutical oxidation. *Water Research* **2005**, *Accepted for publication*.

(53) McFarland, J. W.; Berger, C. M.; Froshauer, S. A.; Hayashi, S. F.; Hecker, S. J.; Jaynes, B. H.; Jefson, M. R.; Kamicker, B. J.; Lipinski, C. A.; Lundy, K. M.; Reese, C. P.; Vu, C. B. Quantitative structure-activity relationships among macrolide antibacterial agents: In Vitro and in Vivo potency against *Pasteurella multocida*. *J. Med. Chem.* **1997**, *40*, 1340-1346.

(54) Lucida, H.; Parkin, J. E.; Sunderland, V. B. Kinetic study of the reaction of sulfamethoxazole and glucose under acidic conditions I. Effect of pH and temperature. *Int. J. Pharm.* **2000**, *202*, 47-61.

(55) Rieder, J. Physikalisch-chemische und biologische Untersuchungen an Sulfonamiden. 1. Mitteilung: Pharmakologisch interessante physikalisch-chemische Merkmale von 21 Sulfonamiden und 6 Sulfonamid-Metaboliten. *Arzneim.-Forsch.* **1963**, *13*, 81-88.

(56) Vázquez, J. L.; Berlanga, M.; Merino, S.; Domènech, Ò.; Viñas, M.; Montero, M. T.; Hernández-Borrell, J. Determination by fluorimetric titration of the ionization constants of ciprofloxacin in solution and in the presence of liposomes. *Photochem. Photobiol.* **2001**, *73*, 14-19.

(57) Barbosa, J.; Barrón, D.; Jiménez-Lozano, E.; Sanz-Nebot, V. Comparison between capillary electrophoresis, liquid chromatography, potentiometric, and spectrophotometric techniques for evaluation of $\mathrm{pK_a}$ values of zwitterionic drugs in acetonitrile-water mixtures. *Analytica Chimica Acta* **2001**, *437*, 309-321.

(58) Riand, J.; Chenon, M. T.; Lumbrosobader, N. Proton and C-13 Nuclear Magnetic-Resonance Studies of Substituted Pyrimidines .2. Monoprotonation of Methylpyrimidines and Aminopyrimidines. *J. Am. Chem. Soc.* **1977**, *99*, 6838-6845.

(59) Roth, B.; Strelitz, J. Z. The protonation of 2,4-diaminopyrimidines. I. Dissociation constants and substituent effects. *J. Org. Chem.* **1969**, *34*, 821-836.

(60) Rapson, H. D. C.; Bird, A. E. Ionisation constants of some penicillins and of their alkaline and penicillinase hydrolysis products. *J. Pharm. Pharmacol.* **1963**, *15*, T222-T231.

(61) Takács-Novák, K.; Box, K. J.; Avdeef, A. Potentiometric $\mathrm{p}K_\mathrm{a}$ determination of water-insoluble compounds: validation study in methanol/water mixtures. *Int. J. Pharm.* **1997**, *151*, 235-248.

(62) Stephens, C. R.; Murai, K.; Brunings, K. J.; Woodward, R. B. Acidity constants of tetracycline antibiotics. *J. Am. Chem. Soc.* **1956**, *78*, 4155-4158.

(63) Nieto, M.; Perkins, H. R. Physicochemical properties of vancomycin and iodovancomycin and their complexes with diacetyl-L-lysyl-D-alanyl-D-alanine. *Biochem. J.* **1971**, *123*, 773-&.

(64) Antipas, A. S.; Vandervelde, D.; Stella, V. J. Factors affecting the deamidation of vancomycin in aqueous-solutions. *Int. J. Pharm.* **1994**, *109*, 261-269.

(65) Kane, R. S.; Glink, P. T.; Chapman, R. G.; McDonald, J. C.; Jensen, P. K.; Gao, H.; Pasa-Tolic, L.; Smith, R. D.; Whitesides, G. M. Basicity of the amino groups of the aminoglycoside amikacin using capillary electrophoresis and coupled CE-MS-MS techniques. *Anal. Chem.* **2001**, *73*, 4028-4036.

(66) Christensen, J. J.; Izatt, R. M.; Wrathall, D. P.; Hansen, L. D. Thermodynamics of proton ionization in dilute aqueous solution. Part XI. $\mathrm{p}K$, $\Delta H°$, and $\Delta S°$ values for proton ionization from protonated amines at 25°. *Journal of the Chemical Society A: Inorganic, Physical, Theoretical* **1969**, 1212-1223.

(67) Weber, E. J.; Kenneke, J. F., SPARC. Available at http://www.epa.gov/athens/research/projects/sparc. US EPA, National Exposure Research Laboratory: Athens, GA.

(68) Pankratov, A. N.; Uchaeva, I. M.; Doronin, S. Y.; Chernova, R. K. Correlations between the basicity and proton affinity of substituted anilines. *J. Struct. Chem.* **2001**, *42*, 739-746.

(69) Hall, H. K., Jr. Potentiometric determination of the base strengths of amines in non-protolytic solvents. *J. Phys. Chem.* **1956**, *60*, 63-70.

(70) Barbosa, J.; Barrón, D.; Cano, J.; Jiménez-Lozano, E.; Sanz-Nebot, V.; Toro, I. Evaluation of electrophoretic method versus chromatographic, potentiometric, and absorptiometric methodologies for determining $\mathrm{p}K_\mathrm{a}$ values of quinolones in hydroorganic mixtures. *J. Pharm. Biomed. Anal.* **2001**, *24*, 1087-1098.

(71) Hartmann, A.; Golet, E. M.; Gartiser, S.; Alder, A. C.; Koller, T.; Widmer, R. M. Primary DNA damage but not mutagenicity correlates with ciprofloxacin concentrations in German hospital wastewaters. *Arch. Environ. Contam. Toxicol.* **1999**, *36*, 115-119.

(72) Golet, E. M.; Xifra, I.; Siegrist, H.; Alder, A. C.; Giger, W. Environmental exposure assessment of fluoroquinolone antibacterial agents from sewage to soil. *Environ. Sci. Technol.* **2003**, *37*, 3243-3249.

(73) Lindberg, R.; Jarnheimer, P.-Å.; Olsen, B.; Johansson, M.; Tysklind, M. Determination of antibiotic substances in hospital sewage water using solid phase extraction and liquid chromatography/mass spectrometry and group analogue internal standards. *Chemosphere* **2004**, *57*, 1479-1488.

(74) Kolpin, D. W.; Furlong, E. T.; Meyer, M. T.; Thurman, E. M.; Zaugg, S. D.; Barber, L. B.; Buxton, H. T. Pharmaceuticals, hormones, and other organic wastewater contaminants in U.S. Streams, 1999-2000: A national reconnaissance. *Environ. Sci. Technol.* **2002**, *36*, 1202-1211.

(75) Miao, X.-S.; Bishay, F.; Chen, M.; Metcalfe, C. D. Occurrence of antimicrobials in the final effluents of wastewater treatment plants in Canada. *Environ. Sci. Technol.* **2004**, *38*, 3542-3550.

(76) Renew, J. E.; Huang, C.-H. Simultaneous determination of fluoroquinolone, sulfonamide, and trimethoprim antibiotics in wastewater using tandem solid phase extraction and liquid chromatography–electrospray mass spectrometry. *J. Chromatogr., A* **2004**, *1042*, 113-121.

(77) Ohlsen, K.; Ternes, T. A.; Werner, G.; Wallner, U.; Löffler, D.; Wilma, Z.; Witte, W.; Hacker, J. Impact of antibiotics on conjugational resistance gene transfer in Staphylococcus aureus in sewage. *Environ. Microbiol.* **2003**, *5*, 711-716.

(78) Hirsch, R.; Ternes, T. A.; Haberer, K.; Kratz, K.-L. Occurrence of antibiotics in the environment. *Sci. Total Environ.* **1999**, *225*, 109-118.

(79) Hartig, C.; Storm, T.; Jekel, M. Detection and identification of sulphonamide drugs in municipal waste water by liquid chromatography coupled with electrospray ionisation tandem mass spectrometry. *J. Chromatogr., A* **1999**, *854*, 163-173.

(80) Metcalfe, C. D.; Miao, X.-S.; Koenig, B. G.; Struger, J. Distribution of acidic and neutral drugs in surface waters near sewage treatment plants in the lower Great Lakes, Canada. *Environ. Toxicol. Chem.* **2003**, *22*, 2881-2889.

(81) Lindberg, R. H.; Wennberg, P.; Johansson, M. I.; Tysklind, M.; Andersson, B. A. V. Screening of human antibiotic substances and determination of weekly mass flows in five sewage treatment plants in Sweden. *Environ. Sci. Technol.* **2005**, *39*, 3421-3429.

(82) Andreozzi, R.; Caprio, V.; Ciniglia, C.; de Champdoré, M.; lo Giudice, R.; Marotta, R.; Zuccato, E. Antibiotics in the environment: occurrence in Italian STPs, fate, and preliminary assessment on algal toxicity of amoxicillin. *Environ. Sci. Technol.* **2004**, *38*, 6832-6838.

(83) McArdell, C. S.; Molnar, E.; Suter, M. J. F.; Giger, W. Occurrence and fate of macrolide antibiotics in wastewater treatment plants and in the Glatt Valley Watershed, Switzerland. *Environ. Sci. Technol.* **2003**, *37*, 5479-5486.

(84) Löffler, D.; Ternes, T. A. Analytical method for the determination of the aminoglycoside gentamicin in hospital wastewater via liquid chromatography–electrospray-tandem mass spectrometry. *J. Chromatogr., A* **2003**, *1000*, 583-588.

Chapter 3. Kinetics of Triclosan Oxidation by Aqueous Ozone and Consequent Loss of Antibacterial Activity: Relevance to Municipal Wastewater Ozonation

Suarez, S.;* Dodd, M. C.;* Omil, F.; von Gunten, U. *Water Research*, **2007**, 41(12), 2481-2490.
*Co-primary authors contributed equally to this work

Abstract

Oxidation of the antimicrobial agent triclosan by aqueous ozone (O_3) was investigated to determine associated reaction kinetics, reaction site(s), and consequent changes in antibacterial activity of triclosan. Specific second-order rate constants, k_{O_3}, were determined for reaction of O_3 with each of triclosan's acid-base species. The value of k_{O_3} determined for neutral triclosan was 1.3 (± 0.1) × 10^3 $M^{-1}s^{-1}$, while that measured for anionic triclosan was 5.1 (± 0.1) × 10^8 $M^{-1}s^{-1}$. Consequently, triclosan reacts very rapidly with O_3 at circumneutral pH (the pH-dependent, apparent second-order rate constant, k_{app,O_3}, is 3.8 × 10^7 $M^{-1}s^{-1}$ at pH 7). The pH-dependence of k_{app,O_3} and comparison of triclosan reactivity toward O_3 with that of other phenolic compounds indicates that O_3 reacts initially with triclosan at the latter's phenol moiety. k_{O_3} values for neutral and anionic triclosan were successfully related to phenol ring substituent effects via Brown-Okamoto correlation with other substituted phenols, consistent with electrophilic attack of the triclosan phenol ring. Biological assay of O_3-treated triclosan solutions indicates that reaction with O_3 yields efficient elimination of triclosan's antibacterial activity. In order to evaluate the applicability of these observations to actual wastewaters, triclosan oxidation was also investigated during ozonation of effluent samples from two conventional wastewater treatment plants. Nearly 100% triclosan depletion was achieved for a 4 mg/L (8.3 x 10^{-5} mol/L) O_3 dose applied to a wastewater containing 7.5 mg/L of DOC, and ~58% triclosan depletion for dosage of 6 mg/L (1.3 x 10^{-4} mol/L) O_3 to a wastewater containing 12.4 mg/L of DOC. At O_3 doses greater than 1 mg/L (2.1 x 10^{-5} mol/L), hydroxyl radical reactions accounted for <35% of observed triclosan losses in these wastewaters, indicating that triclosan oxidation was due primarily to the direct triclosan-O_3 reaction. Thus, ozonation appears to present an effective means of eliminating triclosan's antibacterial activity during wastewater treatment.

3.1 Introduction

Triclosan, 5-chloro-2-(2,4-dichlorophenoxy)phenol (Figure 3.1), is used as an antimicrobial agent (i.e., a biocide) in a large number of medical and personal-hygiene products (e.g., soaps, deodorants, toothpaste). To a lesser extent, triclosan is used in textiles and plastics (sportswear, bed clothes, shoes, carpets) to control the growth of disease or odor-causing bacteria. In Europe, ~ 350 tons of triclosan are sold per year as the active ingredient of Irgasan DP 300 or Irgacare MP (*1*).

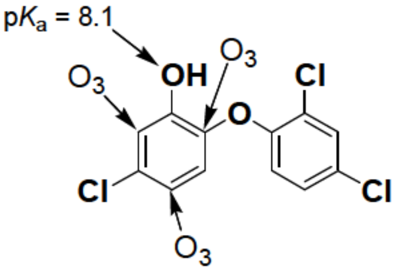

Figure 3.1. Triclosan structure, shown with site of protonation and probable sites of initial O_3 attack

Residues of triclosan are expected to reach municipal wastewaters after application and disposal. In fact, prior investigators have detected this compound in numerous wastewater samples, at concentrations in the range of 0.6-1.3 μg/L (2.1-4.5 × 10^{-9} mol/L) (*2*). Triclosan is quite hydrophobic (log K_{OW} ~ 4.2 (*3*)), suggesting that it should be removed with relatively high efficiency during wastewater treatment (as a consequence of partitioning into biomass). Accordingly, removal rates achieved for triclosan in wastewater treatment plants (WWTPs) can be quite high for modern, well-designed plants. For example, Singer et al. (2002) reported a total removal (biodegradation plus sorption onto sludge) of 94%. This efficiency could be even higher if free-chlorine is used to disinfect final effluent, as the free chlorine-TRI reaction is quite fast (*4*).

However, despite the generally high performance of modern WWTPs, residual triclosan concentrations of ~ 40-200 ng/L (1.4-6.9 × 10^{-10} mol/L) are common in secondary wastewater effluents (*1,5*), leading to triclosan discharge into many receiving surface waters. In fact, triclosan was detected in 57% of 139 surface water samples tested during a study in the United States (at a median concentration of 140 ng/L (4.8 × 10^{-10} mol/L)), with a maximum reported concentration of 2.3 μg/L (7.9 × 10^{-9} mol/L) (*6*), and at concentrations ranging from ~ 20-100 ng/L (0.7-3.5 × 10^{-10} mol/L) in representative surface waters within Switzerland (*1*).

Discharges of triclosan residuals to surface water are undesirable for a number of reasons. For example, the predicted no-effect concentration determined for the algal species *S. subspicatus* was reported as 500 ng/L (1.7 × 10^{-9} mol/L) (*7*), which is near the range of reported surface water and wastewater effluent concentrations. Continuous exposure of such aquatic microbiota to triclosan concentrations in the ranges listed above may in turn result in unanticipated alterations in microbial community structure (*8*). Furthermore, triclosan's target-specific mode of antibacterial activity (i.e., disruption of lipid biosynthesis, by inhibition of the enoyl-acyl carrier protein reductase enzyme (*9,10*)) is understood to facilitate the evolution of triclosan resistance at sub-lethal triclosan concentrations (*11,12*). Although the relevance of environmental triclosan concentrations to development of bacterial triclosan resistance remains unclear, particular caution is warranted in light of numerous *in vitro* studies illustrating that triclosan can select for triclosan-resistant mutants that overexpress multi-drug efflux pumps conferring cross-resistance to various clinical antibacterials (*13*). Another point of concern is the formation of 2,8-dichlorodibenzo-*p*-dioxin during triclosan photolysis (*14*), which is a major process by which triclosan is depleted from surface waters (*1,15*).

Additional transformation of triclosan (via photochemical pathways (*14,15*) and/or metal-oxide-mediated oxidation (*16*)) can be expected to occur in natural environments. However, in light of possible negative interactions with aquatic biota, it may be prudent to achieve higher triclosan removal and/or elimination of triclosan's antibacterial activity during wastewater treatment, thus avoiding the discharge of the biologically active parent compound into surface waters.

Ozonation, which has proven to be an effective post-treatment technique for other pharmaceutical and personal care products (*17,18*), presents one possible option for achieving these ends. Ozone (O_3) typically exhibits very rapid reaction kinetics with phenolic compounds (*19*). Thus, triclosan, which contains a phenol moiety (Figure 3.1), is also expected to react rapidly with O_3; presumably at the 2, 4, and 6 positions of the phenol ring, on the basis of known phenol-O_3 reaction mechanisms (*20*). Furthermore, according to prior investigations, the antibacterial activity of the triclosan molecule is derived primarily from its phenol ring, via van der Waals and hydrogen-bonding interactions with the bacterial enoyl-acyl carrier protein reductase enzyme (*10*). Thus, direct oxidation of the triclosan molecule by O_3 - yielding oxygen addition to the phenol ring or phenol ring opening (*20*) - is expected to reduce or eliminate its target-specific biochemical activity. Similarly, treatment of the steroid hormone 17-α-ethinylestradiol with O_3 has been demonstrated to yield nearly complete, stoichiometric elimination of the latter's estrogenic activity, via oxidation of its phenol ring (*21*).

The present investigation was conducted to determine the rate constants and reactive site(s) for the reaction of O_3 with triclosan, as well as to evaluate the effect of ozonation on the antibacterial activity of the triclosan molecule. Kinetic measurements and microbiological assay results were also utilized to characterize triclosan oxidation during ozonation of effluent samples taken from two municipal wastewater treatment facilities, for the purpose of assessing the potential of ozonation as a means of eliminating triclosan antibacterial activity in full-scale wastewater treatment.

3.2 Materials and Methods

3.2.1 Standards and reagents Triclosan, cinnamic acid, benzaldehyde, and *para*-chlorobenzoic acid (*p*CBA) were obtained from Sigma-Aldrich or Fluka with purities higher than 97%. All other reagents were commercially available, and were of reagent grade quality or higher. All reagent solutions were prepared using water obtained from NANOpure (Barnstead) or Milli-Q (Millipore) water purification systems. Triclosan stock solutions for kinetic experiments were prepared at a concentration of 100 µM, by dissolution of the solid compound in water adjusted to pH 11 with NaOH. Subsequently, H_2SO_4 was used to readjust pH to 7. Triclosan stock solutions for microbiological assay experiments were prepared by dissolving 100 µM triclosan in 0.001 M NaOH, buffering with 1-mM phosphate, and readjusting pH to 9 with H_2SO_4. *E. coli* K12 wild-type cultures (ATCC 23716) were obtained from LGC-Promochem. Stock solutions of O_3 (~ 1.5 mM) were prepared by sparging an O_3-containing gas stream through Milli-Q water that was cooled in an ice bath. The O_3-containing gas stream was produced by passing pure O_2 through an Innovatec CMG 3-4 pulsed corona-discharge O_3 generator. Working O_3 stock solutions (~0.1-0.5 mM) were prepared by diluting the O_3 stock in Milli-Q water and acidifying to pH ~ 4 with H_2SO_4. *E. coli* K12 cultures were maintained at 37 °C on #3 nutrient agar. Broth cultures were prepared under sterile conditions by suspending cells sampled from an agar plate (taken from a minimum of five separate colonies) in 5-6 mL of Mueller-Hinton broth within polypropylene test tubes, and incubating overnight at 37 °C on a shaker plate rotating at 200 rpm.

3.2.2 Analytical methods Organic analytes were measured by HPLC-UV, via isocratic elutions with a 150 × 4.6-mm (5-µm) Nucleosil-100 C18 column (Macherey-Nagel). Mobile-phases were 80% acetonitrile/20% pH 5, 2-mM acetate buffer or 80% acetonitrile/20% pH

2.2, 10-mM phosphate buffer for triclosan, and 30% acetonitrile/70% pH 2.2, 50-mM phosphate buffer for cinnamic acid, *p*CBA, and benzaldehyde. Triclosan was detected at 280, 270, or 205 nm, whereas cinnamic acid, *p*CBA, and benzaldehyde were detected at 250 nm.

3.2.3 Determination of the rate constants for reactions with ozone Experiments for the determination of O_3 rate constants were performed at 23 (±2) °C with a continuous-flow, quenched-reaction monitoring (CFL) system, which has been described in detail previously (*22*). Briefly, a multi-position syringe pump was used to simultaneously inject triclosan and O_3 solutions at equal flow rates, from separate, 25-mL Hamilton gas-tight syringes, into a 60° mixing tee. The mixed reaction solution subsequently continued through one of seven reaction loops with varying size, until entering a second mixing tee, in which it contacted a solution of quenching reagent (injected from a third syringe, using the same syringe pump) to stop the reaction. Samples were collected from the effluent of the second mixing tee for measurement of residual reactant concentrations. Reaction times were varied by switching the reaction loop (i.e., by switching reaction volume, and hence, residence time) or by adjusting system flow-rate, to obtain measurements of reactant depletion at various reaction times.

All kinetic experiments were conducted under pseudo-first-order conditions of excess O_3, to permit measurement of pseudo-first-order rate constants, $k_{\mathrm{obs,O_3}}$ (in s^{-1}), by monitoring triclosan loss after varying reaction times up to approximately two half-lives. Triclosan was dissolved at 0.5-1 μM concentrations in a 10-mM phosphate buffer for the experiments conducted at pH 2 to 4, and in a 20-mM acetate buffer for those carried out at pH 4.5 to 5.5. Ten-mM *tert*-butyl alcohol (*t*-BuOH) was added to working triclosan solutions as a hydroxyl radical (•OH) scavenger. Working O_3 solutions were prepared in Milli-Q water acidified to pH ~ 4 with sulfuric acid, at $[O_3] \geq 20 \times$ [triclosan]. Cinnamic acid (1 mM) - which yields benzaldehyde in 1:1 stoichiometry upon reaction with a mole of O_3 (*23*) - was used as a quenching agent. Benzaldehyde formation was used to quantify residual O_3 concentrations. Experiments were performed at least in duplicate. $k_{\mathrm{obs,O_3}}$ values were determined by linear regression of plots of $\ln([\mathrm{triclosan}]/[\mathrm{triclosan}]_0)$ vs time. Calculated r^2 values for the regressions were generally greater than 0.99, and not lower than 0.97.

3.2.4 Measurement of triclosan antibacterial activity after treatment with ozone Twenty-μM solutions of triclosan were prepared at pH 8 using 1-mM phosphate buffer, dosed with 2 mM of *t*-BuOH (used as a •OH scavenger), and distributed in 25-mL volumes amongst 15 amber, screw-top, borosilicate glass vials. The vials were then placed in a 20 (±0.5) °C water bath placed on top of a magnetic stir plate. Under constant, rapid stirring, the 25-mL triclosan solutions were dosed with a range of O_3 concentrations from 4 to 80 µM, by directly injecting various volumes of ~ 1.5-mM O_3 stock via gas-tight, glass syringe (Step A1 in Scheme 3.1a). These ozonated solutions were then capped and allowed to sit for at least 24 hrs prior to sampling (to ensure complete decomposition of O_3 residual). No quenching agent was added to consume residual O_3. One-mL samples of each solution were collected for analysis of residual triclosan by HPLC-UV.

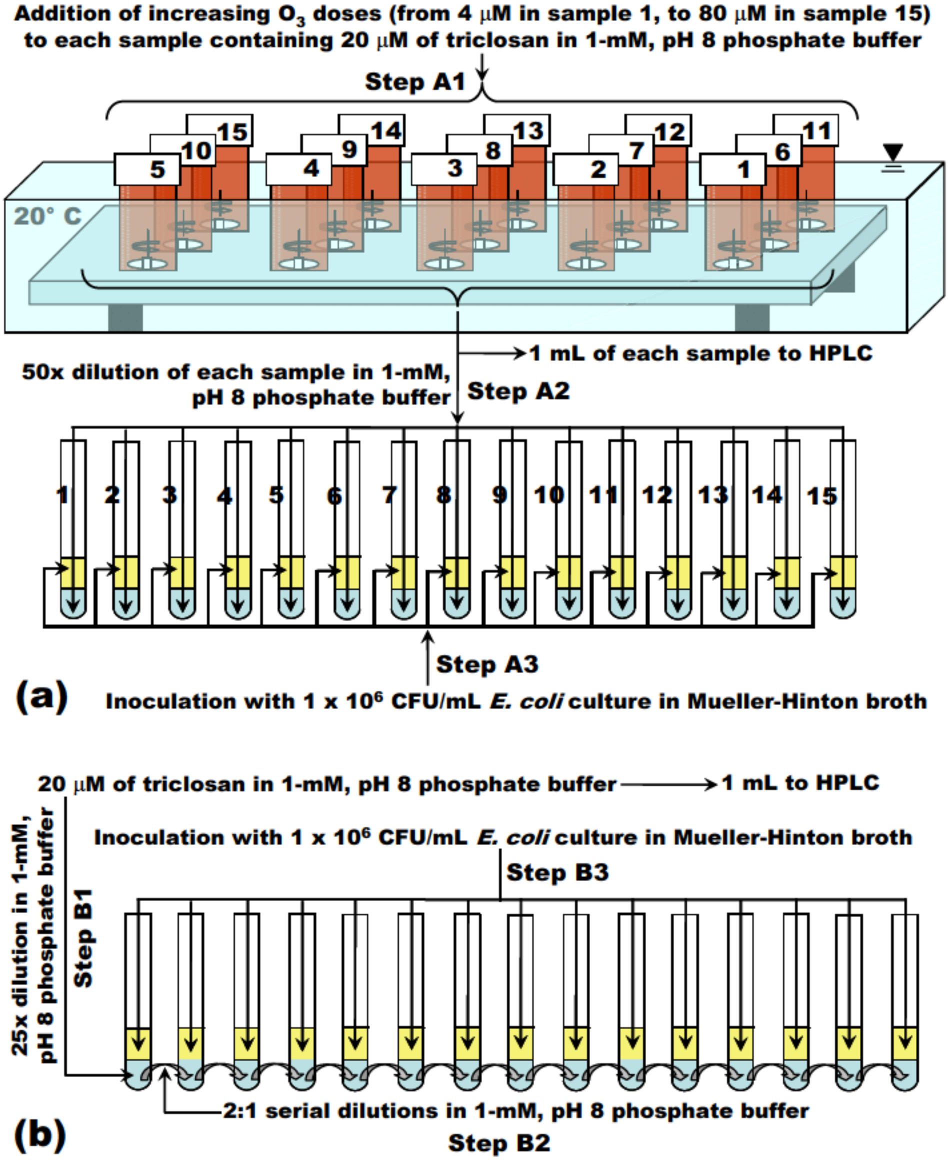
Addition of increasing O3 doses (from 4 µM in sample 1, to 80 µM in sample 15)
to each sample containing 20 µM of triclosan in 1-mM, pH 8 phosphate buffer
Step A1
15
14
13
12
11
10
9
8
7
6
5
4
3
2
1
20° C
1 mL of each sample to HPLC
50x dilution of each sample in 1-mM, pH 8 phosphate buffer
Step A2
1
2
3
4
5
6
7
8
9
10
11
12
13
14
15
Step A3
(a)
Inoculation with 1 x 10⁶ CFU/mL E. coli culture in Mueller-Hinton broth
20 µM of triclosan in 1-mM, pH 8 phosphate buffer
1 mL to HPLC
25x dilution in 1-mM, pH 8 phosphate buffer
Step B1
Inoculation with 1 x 10⁶ CFU/mL E. coli culture in Mueller-Hinton broth
Step B3
2:1 serial dilutions in 1-mM, pH 8 phosphate buffer
(b)
Step B2

Scheme 3.1. Procedure used in preparation of (a) ozone-treated triclosan samples, and (b) triclosan standard dilution series for antibacterial activity assays, up to the step immediately prior to incubation for 8 hours at 37 °C

Changes in the antibacterial potencies of O_3-treated triclosan solutions were measured according to a protocol based on procedures reported for monitoring the loss of triclosan potency during UV irradiation (*24*). Briefly, 30-μL aliquots of each of the O_3-treated samples described above were added to 15 separate glass culture tubes containing 1.47 mL of 1-mM, pH 8 phosphate buffer amended with 2-mM *t*-BuOH (to yield 50-fold dilution of the original samples) (Step A2 in Scheme 3.1a). In addition, 180 μL of the untreated 20-μM triclosan solution was dosed to a glass culture tube containing 4.32 mL of 1-mM phosphate buffer amended with 2-mM t-BuOH (to yield a 25-fold dilution of the original sample) (Step B1 in Scheme 3.1b). A set of fourteen 2:1 serially-diluted standards was then prepared by transferring 3 mL of the 25x-diluted triclosan sample to a culture tube containing 1.5 mL of 1-mM phosphate buffer amended with 2-mM t-BuOH, mixing, then transferring 3-mL of the resulting solution to another 1.5-mL buffer volume, and so on, to yield a series of triclosan standards with [triclosan] ranging from 2.0 x 10^{-5} M to 6.7 x 10^{-8} M (Step B2 in Scheme 3.1b).

Each of the culture tubes contained within the 15-member sample and standard sets was subsequently inoculated with 1.5 mL of a broth *E. coli* K12 culture containing approximately 1 x 10^{6} CFU/mL (prepared by 100-fold dilution of a 0.5 McFarland standard broth culture in Mueller-Hinton broth (*25*)) (Steps A3 and B3 in Schemes 3.1a and 3.1b, respectively). The resulting *in vitro* triclosan concentrations ranged from 1.8 x 10^{-7} M to 2.9 x 10^{-9} M for the O_3-treated sample series, and from 3.9 x 10^{-7} M to 1.3 x 10^{-9} for the standard dilution series. In addition, positive and negative growth control tubes were prepared by dosing 1.5 mL of the 1 x 10^{6} CFU/mL inoculum or 1.5 mL of sterile Mueller-Hinton broth, respectively, to culture tubes containing 1.5 mL of 1-mM, pH 8 phosphate buffer spiked with 2-mM *t*-BuOH. After inoculation, each culture tube was capped and incubated for 8 hours at 37 °C on a shaker plate rotating at 200 rpm.

After completion of the incubation periods, the culture tubes were collected as rapidly as possible and transferred to plastic tubs for storage on ice. Each sample was agitated with a vortex mixer to resuspend any precipitated cells before a ~ 1.5-mL aliquot was transferred by glass Pasteur pipette to a plastic cuvette for measurement of cell density, as sample absorbance at 625 nm. Absorbance measurements were then converted to growth inhibition, I, according to eq 1,

$$I = \frac{A_{\max} - A}{A_{\max}} \qquad (1)$$

where A_{max} represents the maximum absorbance recorded for each sample set (i.e., the absorbance corresponding to uninhibited culture growth), and I varies from 0 to 1 (with a value of 1 indicating complete inhibition). Sample and standard activity assays were each performed in triplicate.

Dose-response curves were obtained for the serially-diluted triclosan standards by plotting inhibition vs the *in vitro* assay concentration of triclosan and fitting the data to a four-parameter, logistic regression (eq 2) , using SigmaPlot 2002 (SPSS Software),

$$I = I_{min} + \frac{I_{max} - I_{min}}{1 + 10^{(\log(EC_{50}/[\text{triclosan}]) \times H)}} = I_{min} + \frac{I_{max} - I_{min}}{1 + (EC_{50}/[\text{triclosan}])^{H}} \qquad (2)$$

where EC_{50} represents the *in vitro* concentration of triclosan yielding 50% growth inhibition relative to a sample in which growth is uninhibited, I_{min} and I_{max} represent the apparent minimum and maximum values of growth inhibition, respectively, and H represents the dimensionless Hill slope.

3.2.5 Municipal wastewater ozonation Additional experiments were conducted with effluent samples obtained from two municipal WWTPs (one at pilot-scale and the other at full-scale). The pilot-scale plant - located in Duebendorf, Switzerland - incorporates solids removal, primary sedimentation, secondary activated sludge clarification, and tertiary nitrification, whereas the full-scale plant - located in Santiago de Compostela, Spain - incorporates solids removal, primary sedimentation, and secondary activated sludge clarification. Pilot-scale samples were collected in glass bottles and transported to the laboratory as rapidly as possible (10-20 minutes transport time), at which point they were vacuum-filtered through 0.45-µm cellulose nitrate membranes prior to storage at 4 °C. Full-scale samples were collected in aluminum bottles, filtered, and shipped to the laboratory as rapidly as possible (1-2 days transport time), whereupon they were placed in storage at 4 °C. Important water quality parameters are shown in Table 3.1.

Table 3.1. Water quality parameters of pilot-scale and full-scale effluents

Effluent	**pH**	**DOC (mg/L)**	**Alkalinity (mM as HCO_3^-)**	**Calculated •OH scavenging rate (s^{-1})^a**
Pilot-scale	7.9	7.5	8.1	2.5×10^5
Full-scale	7.5	12.4	0.9	3.2×10^5

[a] •OH scavenging rate calculated at pH 8 and 23°C (Elovitz and von Gunten, 1999b)

These experiments were conducted in 30-ml amber, borosilicate glass vials containing the respective wastewaters, which were spiked before each experiment with triclosan (0.5 μM) and *p*CBA (0.5 μM) - the latter compound being used as a •OH probe (*26*). Reactions were started by injecting defined volumes of O_3 stock solution to each reactor, to achieve an O_3 dose range of 0.1 to 6 mg/L (2.1×10^{-6} to 1.3×10^{-4} mol/L). After 60 s of reaction time, each solution was dosed with 200 μM of cinnamic acid to quench any residual O_3, and samples were transferred to HPLC for analysis of residual triclosan and *p*CBA concentrations. Reactions were conducted at least in duplicate at 20ºC by thermostating the reactors in a constant-temperature bath.

Additional experiments were conducted to assess O_3 demand within each of the municipal wastewater matrixes. These experiments were conducted with the CFL apparatus described above, according to the same procedures used for reaction kinetics measurements, except that triclosan solutions were replaced with the wastewater matrix of interest. Neither *t*-BuOH nor buffer were added to the wastewater matrixes. Working O_3 solutions were prepared at 10 mg/L (2.1×10^{-4} mol/L), to yield initial concentrations of 5 mg/L upon 1:1 mixing with the wastewater matrixes.

3.3 Results and Discussion

3.3.1 Rate constants for reactions of triclosan with ozone The direct reactions of O_3 with organic compounds have been demonstrated to follow bimolecular, second-order kinetics (*27*). Therefore, the kinetics of the reaction between triclosan and ozone can be described by eq 3,

$$\frac{d[\text{triclosan}]_T}{dt} = -k_{\text{app,O}_3}[\text{triclosan}]_T[\text{O}_3] \tag{3}$$

where $k_{\text{app,O}_3}$ is the apparent second-order rate constant for the reaction at a given pH, and $[\text{triclosan}]_T$ the total triclosan concentration (including neutral and anionic species). Under pseudo-first-order conditions, with a large excess of O_3, eq 3 becomes eq 4.

$$\frac{d[\text{triclosan}]_T}{dt} = -k_{\text{obs,O}_3}[\text{triclosan}]_T \tag{4}$$

Apparent second-order rate constants, $k_{\text{app,O}_3}$, for the triclosan-O_3 reaction were determined from the magnitudes of $k_{\text{obs,O}_3}$ measured at various pH values (where $k_{\text{app,O}_3}$ is equal to $k_{\text{obs}}/[O_3]$, with O_3 in large excess). The averages of the corresponding measurements are presented in Figure 3.2. These data show that $k_{\mathrm{app,O_3}}$ values for the triclosan-O_3 reaction increase significantly with increasing pH.

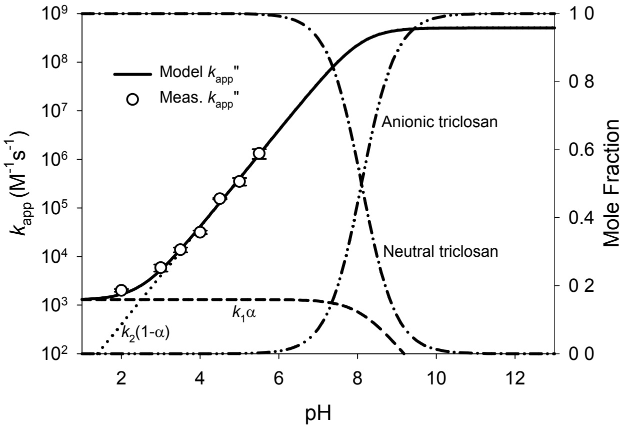

Figure 3.2. Apparent second-order rate constants for the triclosan- O_3 reaction as a function of pH

The pH-dependence of $k_{\mathrm{app,O_3}}$ can be quantitatively evaluated by incorporating terms accounting for the specific reactions of O_3 with neutral and anionic triclosan into eq 3, to yield eq 5,

$$\frac{d[\mathrm{triclosan}]_{\mathrm{T}}}{dt} = -(k_1\alpha + k_2(1-\alpha))[\mathrm{triclosan}]_{\mathrm{T}}[\mathrm{O_3}] \tag{5}$$

where α which can be calculated from eq 6,

$$\alpha = \frac{1}{1+\dfrac{10^{-\mathrm{p}K_{\mathrm{a}}}}{10^{-\mathrm{pH}}}} \tag{6}$$

where pK_a = 8.1 (*28*), and k_1 and k_2 represent the species-specific rate constants for reaction of O_3 with neutral and anionic triclosan, respectively. $k_{\mathrm{app,O_3}}$ can in turn be described by eq 7.

$$k_{\mathrm{app,O_3}} = k_1\alpha + k_2(1-\alpha) \tag{7}$$

The specific second-order rate constants, k_1 and k_2 were calculated by non-linear regression (using SigmaPlot 2002, SPSS Software) of the experimentally determined $k_{\mathrm{app,O_3}}$ values (Figure 3.2), according to eq 7. Values of 1.3 (± 0.1) × 10^3 $M^{-1}s^{-1}$ and 5.1 (± 0.1) × 10^8 $M^{-1}s^{-1}$ were determined for k_1 and k_2, respectively. These constants were then used to model $k_{\mathrm{app,O_3}}$ by substitution into eq 7. Model results are presented as a solid line in Figure 3.2 for comparison with measured data. As shown in Figure 3.2, the predicted value of $k_{\mathrm{app,O_3}}$ at pH

7 is 3.8 × 10^7 $M^{-1}s^{-1}$ (corresponding to a triclosan half-life of 0.9 ms for an excess O_3 concentration of 1 mg/L, or 2.1 × 10^{-5} M), indicating that triclosan will be rapidly oxidized during ozonation at circumneutral pH.

3.3.2 Site of initial reaction between triclosan and ozone The enhancement of triclosan's reactivity toward O_3 upon deprotonation is presumably due to activation of its phenol ring toward electrophilic attack as a result of the enhanced electron-donating character of O^- relative to OH (*29*). Neutral phenols generally react with O_3 with rate constants between 10^2 and 10^3 $M^{-1}s^{-1}$, whereas their anionic forms exhibit rate constants between 10^7 and 10^9 $M^{-1}s^{-1}$ (Hoigné and Bader, 1983). Rate constants for both neutral and anionic phenol species are strongly influenced by the number and type of aromatic ring substituents. In order to probe the mechanism and site of triclosan attack by O_3, $k_{1,\text{triclosan}}$ and $k_{2,\text{triclosan}}$ were quantitatively correlated with k_{O_3} values reported for numerous other substituted phenols via linear-free energy relation. Brown-Okamoto $\Sigma\sigma_{o,m,p}^+$ terms (*30*), which account for inductive and resonance interactions between the aromatic center and ring substituent(s) of such target compounds as phenols, were selected as free-energy descriptors on account of their suitability for characterizing electrophilic reactions (*4,31*).

The $\Sigma\sigma_{o,m,p}^+$ terms for triclosan and the other substituted phenols were obtained by summing σ_o^+, σ_m^+, and σ_p^+ (i.e., *ortho*-, *meta*-, and *para*-) values for each relevant substituent, where σ_o^+ and σ_p^+ values were obtained from the literature (*29,32*) and σ_p^+ values from the relationship $\sigma_o^+ = 0.66\sigma_p^+$ (*33*). Log-magnitudes of the rate constants for reactions of O_3 with the neutral and anionic forms of each target compound were then plotted against the corresponding $\Sigma\sigma_{o,m,p}^+$ values, as shown in Figure 3.3, and fitted according to the relationship $\log(k_{O_3}) = \rho\sum\sigma_{o,m,p}^{\;\;+} + y_0$.

The negative sign of the calculated sensitivity factors, *p* (Figure 3.3), for neutral and anionic phenol species indicate that electron-donating substituents activate the phenolic structures toward attack by O_3, whereas electron-withdrawing substituents result in deactivation, as expected for an electrophilic reaction mechanism. Thus, the success of the Brown-Okamoto relationship in predicting k_1 and k_2 for the triclosan-O_3 reaction verifies the dependence of triclosan-O_3 reaction kinetics on phenol substituent effects and supports the hypothesis that O_3 reacts initially with triclosan by electrophilic attack at the latter's phenol moiety.

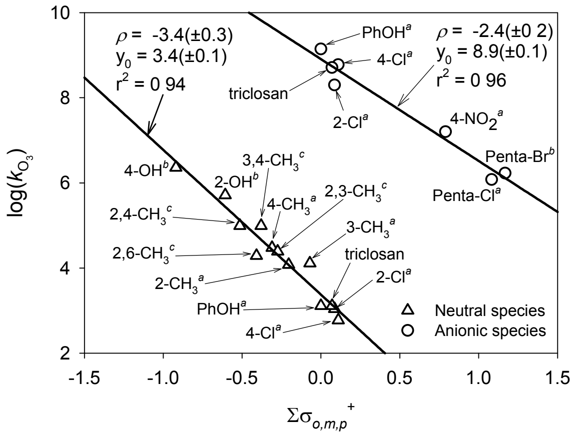

Figure 3.3. Brown-Okamoto correlations of $k_{\mathrm{O_3}}$ values measured for neutral and anionic triclosan, in relation to $k_{\mathrm{O_3}}$ values previously reported for the neutral and anionic species of other substituted phenols (^{a}(*19*); ^{b}(*20*); ^{c}(*34*)). σ_p^+ values were obtained from (*29*), σ_m^+ values from (*32*), and σ_o^+ values from the relationship $\sigma_o^+ = 0.66\ \sigma_p^+$ (*33*).

3.3.3 Elimination of triclosan antibacterial activity by reaction with ozone

Residual antibacterial activities, I, of O_3-treated triclosan solutions were evaluated by comparing their ability to inhibit growth of *E. coli* K12 to the inhibitory activities measured for a set of fifteen standards obtained by 2:1 serial dilution of an untreated triclosan sample. Prior to inoculation with working *E. coli* K12 broth cultures, the O_3-treated samples and standard series were diluted 50-fold and 25-fold, respectively (Scheme 3.1), to yield *in vitro* triclosan concentrations ranging from 1.8×10^{-7} M to 2.9×10^{-9} M for the O_3-treated series and 3.9×10^{-7} M to 1.3×10^{-9} for the standard series.

The dose-response relationships observed for O_3-treated samples and the standard series (in terms of % *E. coli* K12 growth inhibition vs *in vitro* triclosan concentration) are depicted in Figure 3.4a. As demonstrated here, when plotted vs *in vitro* triclosan concentration, the I values measured for O_3-treated samples coincide nearly completely with the dose-response curve obtained from the 15-member standard series, indicating that the inhibitory activities of the O_3-treated samples are essentially the same as would be expected on the basis of their residual triclosan concentrations. More importantly, the very close agreement between dose-response curves for O_3-treated samples and triclosan standards indicates (Figure 3.4a) that oxidation-products generated by ozonation of these triclosan-containing solutions do not exhibit an appreciable degree of inhibitory activity relative to triclosan itself. The inset to Figure 3.4a illustrates the approximately 1:1 correspondence between inhibitory activities measured for O_3-treated triclosan samples and inhibitory activities predicted for these samples on the basis of their *in vitro* triclosan concentrations, according to the dose-response relationship shown in Figure 3.4a, which was obtained from serially-diluted triclosan standards.

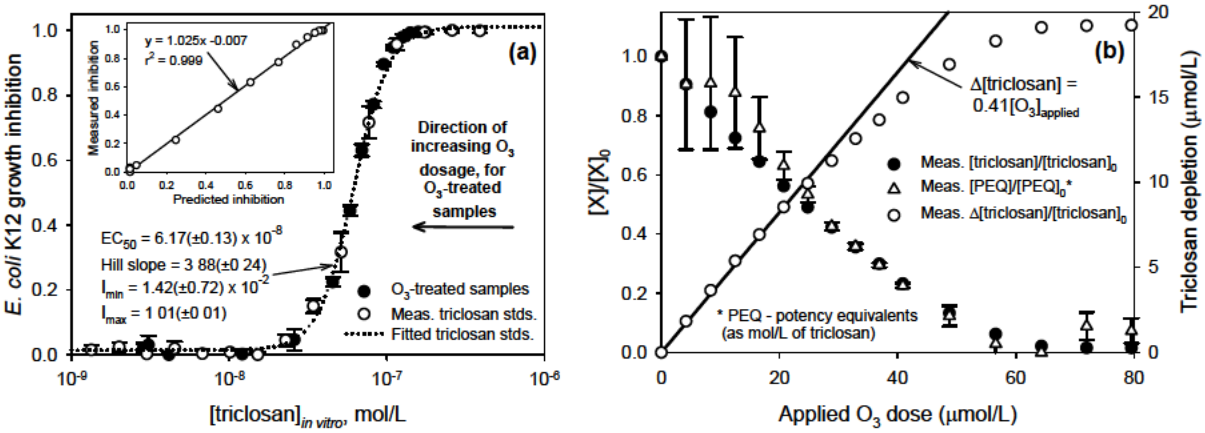

Figure 3.4. Correlations between extent of triclosan depletion and measured losses of antibacterial activity in samples of triclosan treated with increasing doses of O_3. (a) Dose-response relationships for triclosan samples treated with increasing O_3 doses (filled circles) at pH 8 and 20 (±0.5) °C, in the presence of 2-mM *t*-BuOH, compared with a standard series of 2:1 serial dilutions (unfilled circles) derived from a control containing untreated triclosan. Each point in the O_3-treated sample series corresponds to an individual triclosan sample treated with a specific O_3 dose. The inset to Figure 3.4a depicts the correlation between values of growth inhibition measured for the O_3-treated sample series, and values of growth inhibition predicted for these same samples on the basis of the dose-response curve derived from triclosan standards (eq 2). (b) Reaction stoichiometry and the relationship between consumed triclosan and measured loss of antibacterial potency equivalents (PEQs) for 20-µM triclosan samples treated with increasing O_3 doses, at pH 8 and 20 (±0.5) °C, in the presence of 2-mM *t*-BuOH.

The change in inhibitory activities, or "potencies", of O_3-treated triclosan solutions can be related to the activity of the untreated triclosan solution by means of potency equivalents (PEQs), which represent the *in vitro* concentrations of untreated triclosan necessary to yield the growth inhibition values observed in each O_3-treated sample. PEQs can be calculated for O_3-treated samples from eq 8, which is obtained by re-arrangement of eq 2,

$$\text{PEQ (in mol/L)} = [\text{triclosan}]_{\text{equivalent}} = \text{EC}_{50}\left(\frac{\text{I}_{\text{max}} - \text{I}}{\text{I} - \text{I}_{\text{min}}}\right)^{\left(-\frac{1}{\text{H}}\right)} \tag{8}$$

where values of I_{max}, I_{min}, EC_{50}, and Hill slope, H, are obtained from the standard dose-response curve, and I corresponds to the growth inhibition observed for the sample of interest. Figure 3.4b depicts the relationship between O_3 dose, triclosan depletion, and residual PEQs in O_3-treated samples.

Approximately 0.4 moles of triclosan were consumed per mole of O_3 at pH 8, up to O_3 doses of 20-30 μM. Triclosan consumption per mole of O_3 decreased above this dose - presumably due to increasing yields of reaction products, as previously observed for phenol (*20*). O_3 doses above 20 μM (i.e., at greater than 40% triclosan depletion) yielded stoichiometric elimination of triclosan's antibacterial activity (i.e., one mole of PEQs was eliminated for each mole of triclosan lost), whereas several PEQ values calculated for samples treated with less than 20 μM of O_3 were higher than expected on the basis of corresponding *in vitro* triclosan concentrations.

The latter observation may be attributable to incomplete deactivation of triclosan upon reaction with O_3. However, it should be noted that PEQ values calculated by eq 8 are very sensitive to small measurement errors at very low or very high measured growth inhibition, I, on account of the asymptotic nature of the sigmoidal dose-response model (eq 2) from which eq 8 is derived. That is, at low and high values of growth inhibition (i.e., within the lower and upper shoulders of the dose-response curve shown in Figure 3.4a), large changes in triclosan concentration elicit relatively small changes in measured growth inhibition. Accordingly, relatively small changes (or small errors) in measured growth inhibition, I, correspond to large changes in the equivalent triclosan concentrations (i.e., PEQs) calculated by eq 8. This sensitivity is evident in the large model error limits determined (by propagation of the errors attributable to each model parameter through eq 8) at lower and higher O_3 doses (Figure 3.4b). In this light, the discrepancies in PEQs and residual triclosan concentrations at low O_3 doses may only be artifactual. In fact, the PEQ values and residual triclosan concentrations depicted in Figure 3.4b are in relatively strong agreement within model error limits over the entire range of O_3 doses. However, more detailed investigation of triclosan deactivation at low O_3 doses would be necessary to provide a definitive answer. Regardless, at higher O_3 doses (i.e., higher triclosan turnovers), each mole of triclosan lost clearly corresponds to elimination of approximately one mole of PEQ.

3.3.4 Triclosan losses during ozonation of pilot-scale and full-scale wastewaters The feasibility of wastewater ozonation as a means of oxidizing and deactivating triclosan was qualitatively evaluated by monitoring depletion of 0.5 μM triclosan from samples of pilot-scale and full-scale wastewaters dosed with various O_3 concentrations. Triclosan transformation reactions occurred too rapidly ($t_{1/2} < 3$ ms) during ozonation of pilot-scale and full-scale wastewaters to permit direct, time-resolved reaction monitoring by the CFL system used for rate constant measurements. Consequently, triclosan removal efficiencies were evaluated by applying varying O_3 doses to each wastewater matrix in batch (Figure 3.5).

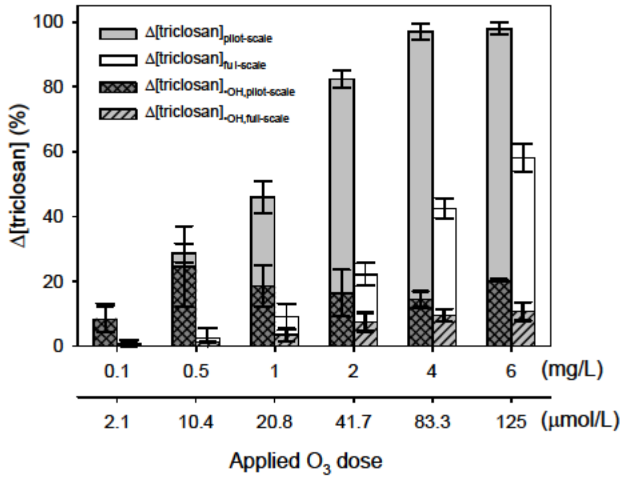

Figure 3.5. Total measured losses (Δ[triclosan]) of 0.5 μM $[\text{triclosan}]_0$, compared with calculated contributions of •OH to total observed triclosan losses ($\Delta[\text{triclosan}]_{\bullet\text{OH}}$) during application of various O_3 doses to pilot-scale and full-scale effluents at 20(±0.5) °C. •OH exposures were determined by utilizing *p*CBA as a •OH probe, as described in the main text

For the pilot-scale effluent, application of O_3 doses higher than 4 mg/L (8.3×10^{-5} mol/L) ensured complete depletion of triclosan (Figure 3.5). However, for the full-scale effluent, there was still a considerable residual triclosan concentration even after dosing 6 mg/L (1.3×10^{-4} mol/L) of O_3 (Figure 3.5). This is most likely due to the latter water's substantially higher concentration of DOC, which can compete with the target compound for O_3, as well as for •OH generated by O_3 decomposition and reactions with matrix constituents (*35,36*). The greater O_3 demand of the full-scale matrix was verified by comparing decomposition of a 5 mg/L (1.0×10^{-4} mol/L) O_3 dose in each matrix, as described above. These experiments showed that after 33 ms (the first time-point at which a measurement could be obtained), 82% (4.1 mg/L) of the initial O_3 dose remained in the pilot-scale wastewater, whereas only 14% (0.7 mg/L) remained in the full-scale wastewater. After ~ 0.5 s, 66% (3.3 mg/L) of the initial dose remained in the pilot-scale wastewater, whereas none remained in the full-scale wastewater.

The individual contributions of O_3 and •OH to triclosan oxidation during ozonation of these wastewaters can be accounted for according to eq 9 (*26*),

$$\ln\left(\frac{[\text{triclosan}]}{[\text{triclosan}]_0}\right) = -k_{\text{app},O_3,\text{triclosan}}\int_0^t [O_3]dt - k_{\text{app},\bullet\text{OH},\text{triclosan}}\int_0^t [\bullet\,\text{OH}]dt \tag{9}$$

where $k_{app,\bullet OH}$ is the apparent second-order rate constant for the reaction of •OH with triclosan. O_3 and •OH exposures must be known to permit the direct application of eq 9 in modeling pollutant oxidation in wastewater ozonation processes. Under appropriate conditions, O_3 exposures can be measured directly (e.g., by use of the indigo method (*37*)), and •OH exposures can be indirectly determined by monitoring the depletion of an O_3-resistant •OH probe compound (e.g., *p*CBA (*38*)) during ozonation of a water sample, according to eq 10 (*26*).

$$\ln\left(\frac{[\mathrm{pCBA}]}{[\mathrm{pCBA}]_0}\right) = -k_{\mathrm{app},\cdot\mathrm{OH,pCBA}}\int_0^t [\bullet\ \mathrm{OH}]dt \tag{10}$$

However, neither O_3 exposures, nor •OH exposures could be measured over the extremely low time-scales of the triclosan-O_3 reaction. These difficulties were circumvented by using eq 11 to obtain an indirect estimate of the fraction, $f_{\bullet OH}$, of total triclosan oxidation attributable to •OH at various O_3 doses in pilot-scale and full-scale wastewaters,

$$f_{\bullet\mathrm{OH}} = \frac{k_{\mathrm{app},\cdot\mathrm{OH,triclosan}}\int_0^t [\bullet\ \mathrm{OH}]dt}{k_{\mathrm{app},\mathrm{O_3},\mathrm{triclosan}}\int_0^t [\mathrm{O_3}]\mathrm{dt} + k_{\mathrm{app},\cdot\mathrm{OH,triclosan}}\int_0^t [\bullet\ \mathrm{OH}]\mathrm{dt}} = \frac{\frac{k_{\mathrm{app},\cdot\mathrm{OH,triclosan}}}{k_{\mathrm{app},\cdot\mathrm{OH,pCBA}}}\ln\left(\frac{[\mathrm{pCBA}]}{[\mathrm{pCBA}]_0}\right)}{\ln\left(\frac{[\mathrm{triclosan}]}{[\mathrm{triclosan}]_0}\right)} \tag{11}$$

where $k_{\mathrm{app},\cdot\mathrm{OH,triclosan}} = 5.4 \times 10^9\ \mathrm{M^{-1}s^{-1}}$ (*14*) and $k_{\mathrm{app},\cdot\mathrm{OH,pCBA}} = 5.0 \times 10^9\ \mathrm{M^{-1}s^{-1}}$ (*39*).

As shown in Figure 3.5, the apparent contributions of •OH to the overall oxidation of triclosan in these wastewaters, calculated according to eq 11, decreased as the O_3 dose applied to each water was increased. Presumably, higher O_3 doses led to higher cumulative O_3 exposures, and - as a consequence of the temporally-decreasing yields of •OH during wastewater ozonation (*40*) - to lower apparent, cumulative ratios of $\int_0^t [\bullet\ \mathrm{OH}]dt$ to $\int_0^t [\mathrm{O_3}]\mathrm{dt}$, as estimated from eq 11. Consequently, direct oxidation of triclosan by O_3 appeared to be enhanced at higher O_3 doses.

In general, the contributions of •OH to triclosan oxidation were relatively low for O_3 doses representative of those likely to be applied in wastewater treatment (i.e., > 1 mg/L, or 2.1×10^{-5} mol/L) (Figure 3.5), due primarily to the high values of $k_{\mathrm{app,O_3}}$ for the O_3-TRI reaction at the pH of each wastewater. Thus, the high rate constant and selectivity of the direct triclosan-O_3 reaction, which results in oxidation of triclosan's phenol ring and consequent elimination of the parent compound's antibacterial activity, appears to be maintained even during ozonation of wastewaters containing relatively high DOC concentrations. This suggests that municipal wastewater ozonation can provide an efficient means of eliminating the antibacterial activity of dissolved triclosan molecules.

Acknowledgements

S.S. and M.C.D. contributed equally to this work. Financial support for S.S. was provided by the Galician Government (Project PGIDIT03TAM02E) and Spanish Ministry of Education and Science (Project CTM2004-04475 and Research Fellowship). M.C.D. gratefully acknowledges financial support from a U.S. National Science Foundation Graduate Research Fellowship. The authors thank Hans-Peter Kohler for guidance in developing the antibacterial activity assay and for reviewing the manuscript. Yunho Lee, Silvio Canonica, and Beate Escher are gratefully acknowledged for their helpful comments. The authors also acknowledge Lisa Salhi for technical assistance, and Jacqueline Traber, Monica Dosil, and Marta Carballa for support in obtaining wastewater samples. Two anonymous reviewers are thanked for their helpful comments.

Literature Cited

(1) Singer, H.; Muller, S.; Tixier, C.; Pillonel, L. Triclosan: Occurrence and fate of a widely used biocide in the aquatic environment: Field measurements in wastewater treatment plants, surface waters, and lake sediments. *Environ. Sci. Technol.* **2002**, *36*, 4998-5004.

(2) Lindström, A.; Buerge, I. J.; Poiger, T.; Bergqvist, P. A.; Muller, M. D.; Buser, H. R. Occurrence and environmental behavior of the bactericide triclosan and its methyl derivative in surface waters and in wastewater. *Environ. Sci. Technol.* **2002**, *36*, 2322-2329.

(3) Lopez-Avila, V.; Hites, R. A. Organic compounds in an industrial wastewater. Their transport into sediments. *Environ. Sci. Technol.* **1980**, *14*, 1382-1390.

(4) Rule, K. L.; Ebbett, V. R.; Vikesland, P. J. Formation of chloroform and chlorinated organics by free-chlorine-mediated oxidation of triclosan. *Environ. Sci. Technol.* **2005**, *39*, 3176-3185.

(5) Glassmeyer, S. T.; Furlong, E. T.; Kolpin, D. W.; Cahill, J. D.; Zaugg, S. D.; Werner, S. L.; Meyer, M. T.; Kryak, D. D. Transport of chemical and microbial compounds from known wastewater discharges: Potential for use as indicators of human fecal contamination. *Environ. Sci. Technol.* **2005**, *39*, 5157-5169.

(6) Kolpin, D. W.; Furlong, E. T.; Meyer, M. T.; Thurman, E. M.; Zaugg, S. D.; Barber, L. B.; Buxton, H. T. Pharmaceuticals, hormones, and other organic wastewater contaminants in U.S. Streams, 1999-2000: A national reconnaissance. *Environ. Sci. Technol.* **2002**, *36*, 1202-1211.

(7) Orvos, D. R.; Versteeg, D. J.; Inauen, J.; Capdevielle, M.; Rothenstein, A.; Cunningham, V. Aquatic toxicity of triclosan. *Environ. Toxicol. Chem.* **2002**, *21*, 1338-1349.

(8) Wilson, B. A.; Smith, V. H.; Denoyelles, F.; Larive, C. K. Effects of three pharmaceutical and personal care products on natural freshwater algal assemblages. *Environ. Sci. Technol.* **2003**, *37*, 1713-1719.

(9) McMurry, L. M.; Oethinger, M.; Levy, S. B. Triclosan targets lipid synthesis. *Nature* **1998**, *394*, 531-532.

(10) Levy, C. W.; Roujeinikova, A.; Sedelnikova, S.; Baker, P. J.; Stuitje, A. R.; Slabas, A. R.; Rice, D. W.; Rafferty, J. B. Molecular basis of triclosan activity. *Nature* **1999**, *398*, 383-384.

(11) McMurry, L. M.; Oethinger, M.; Levy, S. B. Overexpression of marA, soxS, or acrAB produces resistance to triclosan in laboratory and clinical strains of Escherichia coli. *FEMS Microbiol. Lett.* **1998**, *166*, 305-309.

(12) Heath, R. J.; Rubin, J. R.; Holland, D. R.; Zhang, E. L.; Snow, M. E.; Rock, C. O. Mechanism of triclosan inhibition of bacterial fatty acid synthesis. *J. Biol. Chem.* **1999**, *274*, 11110-11114.

(13) Poole, K. Efflux-mediated antimicrobial resistance. *J. Antimicrob. Chemother.* **2005**, *56*, 20-51.

(14) Latch, D. E.; Packer, J. L.; Stender, B. L.; VanOverbeke, J.; Arnold, W. A.; McNeill, K. Aqueous photochemistry of triclosan: Formation of 2,4-dichlorophenol, 2,8-dichlorodibenzo-p-dioxin, and oligomerization products. *Environ. Toxicol. Chem.* **2005**, *24*, 517-525.

(15) Tixier, C.; Singer, H. P.; Canonica, S.; Muller, S. R. Phototransformation of triclosan in surface waters: A relevant elimination process for this widely used biocide - Laboratory studies, field measurements, and modeling. *Environ. Sci. Technol.* **2002**, *36*, 3482-3489.

(16) Zhang, H.; Huang, C.-H. Oxidative Transformation of Triclosan and Chlorophene by Manganese Oxides. *Environ. Sci. Technol.* **2003**, *37*, 2421-2430.

(17) Huber, M. M.; Canonica, S.; Park, G.-Y.; von Gunten, U. Oxidation of pharmaceuticals during ozonation and advanced oxidation processes. *Environmental Science and Technology* **2003**, *37*, 1016-1024.

(18) Huber, M. M.; Göbel, A.; Joss, A.; Hermann, N.; Löffler, D.; McArdell, C. S.; Ried, A.; Siegrist, H.; Ternes, T. A.; von Gunten, U. Oxidation of pharmaceuticals during ozonation of municipal wastewater effluents: a pilot study. *Environmental Science and Technology* **2005**, *39*, 4290-4299.

(19) Hoigné, J.; Bader, H. Rate constants of reactions of ozone with organic and inorganic compounds in water – II : Dissociating organic compounds. *Water Res.* **1983**, *17*, 185-194.

(20) Mvula, E.; von Sonntag, C. Ozonolysis of phenols in aqueous solution. *Org. Biomol. Chem.* **2003**, *1*, 1749-1756.

(21) Huber, M. M.; Ternes, T.; von Gunten, U. Removal of estrogenic activity and formation of oxidation products during ozonation of 17α-ethinylestradiol. *Environmental Science and Technology* **2004**, *38*, 5177-5186.

(22) Dodd, M.; Shah, A. D.; von Gunten, U.; Huang, C.-H. Interactions of fluoroquinolone antibacterial agents with aqueous chlorine: Reaction kinetics, mechanisms, and transformation pathways. *Environ. Sci. Technol.* **2005**, *39*, 7065-7076.

(23) Leitzke, A.; Reisz, E.; Flyunt, R.; von Sonntag, C. The reactions of ozone with cinnamic acids: formation and decay of 2-hydroperoxy-2-hydroxyacetic acid. *J. Chem. Soc., Perkin Trans. 2* **2001**, 793-797.

(24) Wammer, K. H.; Lapara, T. M.; McNeill, K.; Arnold, W. A.; Swackhamer, D. L. Changes in antibacterial activity of triclosan and sulfa drugs due to photochemical transformations. *Environ. Toxicol. Chem.* **2006**, *25*, 1480-1486.

(25) NCCLS, Methods for Dilution Antimicrobial Susceptibility Tests for Bacteria that Grow Aerobically-Fourth Edition; Approved Standard. Available at. NCCLS.
(26) Elovitz, M. S.; von Gunten, U. Hydroxyl radical/ozone ratios during ozonation processes. I. The R_{ct} concept. *Ozone Science and Engineering* **1999**, *21*, 239-260.
(27) Hoigné, J. In *The Handbook of Environmental Chemistry*; Hrubec, J., Ed.; Springer Verlag: Berlin, Germany, 1998, pp 83-141.
(28) Pillonel, L. Diploma Thesis, Swiss Federal Institute of Technology, Zurich, 1999.
(29) Hansch, C.; Leo, A.; Taft, R. W. A Survey of Hammett Substituent Constants and Resonance and Field Parameters. *Chem. Rev.* **1991**, *91*, 165-195.
(30) Okamoto, Y.; Brown, H. C. A Quantitative Treatment for Electrophilic Reactions of Aromatic Derivatives. *J. Org. Chem.* **1957**, *22*, 485-494.
(31) Li, C.; Hoffman, M. Z. One-electron redox potentials of phenols in aqueous solution. *Journal of Physical Chemistry B* **1999**, *103*, 6653-6656.
(32) Hansch, C.; Leo, A. *Substituent Constants for Correlation Analysis in Chemistry and Biology*; John Wiley & Sons, Inc.: New York, 1979.
(33) Jonsson, M.; Lind, J.; Eriksen, T. E.; Merenyi, G. O-H Bond Strengths and One-Electron Reduction Potentials of Multisubstituted Phenols and Phenoxyl Radicals - Predictions Using Free-Energy Relationships. *Journal of the Chemical Society-Perkin Transactions 2* **1993**, 1567-1568.
(34) Gurol, M. D.; Nekouinaini, S. Kinetic Behavior of Ozone in Aqueous-Solutions of Substituted Phenols. *Industrial & Engineering Chemistry Fundamentals* **1984**, *23*, 54-60.
(35) Elovitz, M. S.; von Gunten, U.; Kaiser, H. P. Hydroxyl radical/ozone ratios during ozonation processes. II. The effect of temperature, pH, alkalinity, and DOM properties. *Ozone: Sci. Eng.* **2000**, *22*, 123-150.
(36) Buffle, M. O.; von Gunten, U. Phenols and amine induced HO• generation during the initial phase of natural water ozonation. *Environ. Sci. Technol.* **2006**, *40*, 3057-3063.
(37) Bader, H.; Hoigné, J. Determination of ozone in water by the indigo method. *Water Res.* **1981**, *15*, 449-456.
(38) Yao, C. C. D.; Haag, W. R. Rate constants for direct reactions of ozone with several drinking water contaminants. *Water Res.* **1991**, *25*, 761-773.
(39) Neta, P.; Dorfman, L. M. Pulse radiolysis studies. XIII. Rate constants for the reaction of hydroxyl radicals with aromatic compounds in aqueous solutions. *Adv. in Chem.* **1968**, *81*, 222-230.
(40) Buffle, M. O.; Schumacher, J.; Salhi, E.; Jekel, M.; von Gunten, U. Measurement of the initial phase of ozone decomposition in water and wastewater by means of a continuous quench-flow system: Application to disinfection and pharmaceutical oxidation. *Water Res.* **2006**, *40*, 1884-1894.

Chapter 4. Oxidation of Antibacterial Compounds by Ozone and Hydroxyl Radical: Elimination of Biological Activity during Aqueous Ozonation Processes

Dodd, M. C.; Kohler, H.-P. E..; and von Gunten, Urs
Submitted for publication in *Environmental Science and Technology*

Abstract

A wide variety of antibacterial compounds are rapidly oxidized by O_3 and hydroxyl radical ($^{\bullet}OH$) during aqueous ozonation. Microbiological assays have been developed to quantify the resulting changes in antibacterial potencies during treatment of 13 antibacterial molecules (roxithromycin, azithromycin, tylosin; sulfamethoxazole; trimethoprim; ciprofloxacin, enrofloxacin; penicillin G, cephalexin; lincomycin; tetracycline; vancomycin; and amikacin) from 9 structural classes (macrolides; sulfonamides; dihydrofolate reductase inhibitors; fluoroquinolones; β-lactams; lincosamides; tetracyclines; glycopeptides; and aminoglycosides), as well as the biocide triclosan. Potency measurements were determined from dose-response relationships obtained by exposing *E. coli* or *B. subtilis* reference strains to treated samples of each antibacterial compound via broth micro- or macrodilution assays, and related to the measured residual concentrations of parent antibacterial in each sample. Data obtained from these experiments show that O_3 and $^{\bullet}OH$ reactions lead in nearly all cases to stoichiometric elimination of antibacterial activity (i.e., loss of one mole equivalent of potency per mole of parent compound consumed). The *β*-lactams penicillin G and cephalexin represent the only two exceptions, as bioassay measurements indicate that the direct reaction of these two compounds with O_3 generates transformation products that retain at least 10% of the parent compounds' antibacterial activities. Nevertheless, on the basis of the data reported in this investigation, it can be expected that wastewater ozonation will generally yield sufficient structural modification of antibacterial molecules to eliminate their antibacterial activities, whether oxidation results from selective reactions with O_3 or from relatively non-selective reactions with incidentally-produced $^{\bullet}OH$.

4.1 Introduction

Antibacterial agents (including clinical-use antibiotics and general-purpose biocides such as triclosan) are ubiquitous contaminants of municipal wastewaters (*1-6*). Typical aqueous-phase concentrations of individual antibacterial compounds have been reported to range from ~0.5-5 μg/L in raw and primary wastewaters (*2-4,6*). However, the frequent co-occurence of multiple members of a given antibacterial structural class suggests that the actual biologically-effective levels of these compounds – when interpreted in terms of their structural classes as a whole – are likely appreciably higher (*2-4,7*). Passage through conventional biological treatment processes may significantly lower aqueous-phase concentrations of certain antibacterial compounds (e.g., fluoroquinolones, triclosan), though removal is generally incomplete (*2,6*), and such processes are of limited effectiveness in attenuating concentrations of many other structural classes (*3,4,7*). Consequently, effluent concentrations of certain antibacterials (e.g., fluoroquinolones (*2*) or triclosan (*6*)) may still be harmful to organisms present in effluent-dominated receiving waters (*8*). In addition, because activated sludge processes typically operate at solids retention times of several days, conventional wastewater treatment actually results in prolonged exposure of wastewater-borne bacteria to significantly higher antibacterial concentrations than are present in treated effluents (*2-4,7*). With regard to fluoroquinolones and β-lactams, secondary influent levels can approach minimal growth inhibitory concentrations (MICs) for various bacterial strains (*9*) - a condition which may favor evolution of low-level antibacterial resistance in affected bacterial communities (*10,11*). Furthermore, recent work focusing on the exposure of environmental microbial consortia to oxytetracycline indicates that even sub-inhibitory levels of antibacterials may elicit measurable changes in the production of resistance genes per bacterial cell (*12*).

Taken together, these considerations indicate that unnecessary exposure of wastewater-borne and environmental microbiota to biologically-active antibacterial compounds should be minimized when possible. Supplemental wastewater treatment technologies capable of yielding rapid deactivation of such compounds represent one means of achieving this objective. Ozonation, which may be utilized in advanced treatment of secondary wastewater effluent (*13*), as well as pre-oxidation of primary wastewater effluents (*14-16*), appears highly promising in this regard (*17*).

Recent studies have shown that relatively low ozone (O_3) doses ($\leq$ 5 mg/L) can yield > 90% depletion of many antibacterial compounds in wastewaters containing up to 23 mg-C/L of DOC (*18-20*), yet mineralization of such compounds will generally be infeasible under such conditions (*21*). Thus, for ozonation to prove truly effective in this context, partial oxidation should be sufficient to achieve deactivation of the parent antibacterial molecules. Prior work has demonstrated that the initial reactions between O_3 and representative members of numerous antibacterial structural classes take place preferentially at structural moieties that are responsible for or related to the parent compounds' biological activities, suggesting that biological deactivation is a likely consequence (*20*). Such outcomes have been semi-quantitatively verified for the lincosamide lincomycin (with respect to several algal strains) (*22*), macrolide clarithromycin (with respect to *P. putida*) (*23*) and the biocide triclosan (with respect to *E. coli*) (*24*). However, little additional data is available on the subject. Furthermore, pollutant transformation during wastewater ozonation will also be influenced to varying degrees by hydroxyl radicals ($^{\bullet}OH$), which are continuously generated through reactions of O_3 with specific functional moieties in dissolved organic matter (*25,26*) or from auto-catalytic O_3 decomposition (*21*). Because $^{\bullet}OH$ reacts rapidly with a wider variety of functional moieties than O_3 (*21*), it is less clear whether oxidation of antibacterial molecules by $^{\bullet}OH$ will result in structural modifications leading to biological deactivation.

In response to the present dearth of quantitative data on this topic, microbiological assays have been developed and applied to quantify the changes in antibacterial potencies of 14 antibacterial molecules from 10 structural classes (Table 4.1) following transformation by O_3 and $^{\bullet}OH$. Briefly, dose-response relationships were obtained for exposure of *E. coli* or *B. subtilis* reference strains to O_3- or $^{\bullet}OH$-treated samples of each antibacterial compound via broth microdilution or macrodilution assay and compared to the measured residual concentrations of parent antibacterial in each sample to obtain quantitative relationships between residual activity and residual concentration. The data obtained in this manner were then evaluated in the context of previously reported pilot- and full-scale wastewater ozonation data to determine probable implications for wastewater treatment.

4.2 Materials and Methods

4.2.1 Chemical Reactants and Reagents. Antibacterial compounds were purchased from Sigma-Aldrich, with the exception of cephalexin (CP) hydrate – which was purchased from MP Biomedicals – and azithromycin (AZ) dehydrate, which was a gift from Pfizer, Inc. All reagents and reactants were of 95% purity or greater. O_3 stock solutions were produced as described previously (*27*), and standardized according to direct O_3 absorbance at $\lambda = 258$ nm (using $\varepsilon \cong 3000\ M^{-1}cm^{-1}$). Stock solutions of antibacterials were prepared in Nanopure or

Table 4.1. Model antibacterial compounds (shown with applied activity assay, $k_{O3,app}$ [a], O_3 target sites [b], and $k_{\bullet OH,app}$ [a] at pH 7)

Roxithromycin (RX) 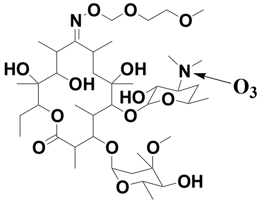 **Assay:** Microdil. **Bacterium:** *B. subtilis* $k_{O3,app,RX}$” = 6.3 x 10^4 $M^{-1}s^{-1}$ $k_{\bullet OH,app,RX}$” = 5.4 x 10^9 $M^{-1}s^{-1}$	**Azithromycin (AZ)** 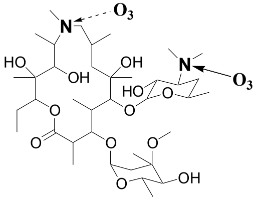 **Assay:** Microdil. **Bacterium:** *B. subtilis* $k_{O3,app,AZ}$” = 1.1 x 10^5 $M^{-1}s^{-1}$ $k_{\bullet OH,app,AZ}$” = 2.9 x 10^9 $M^{-1}s^{-1}$	**Tylosin (TYL)** 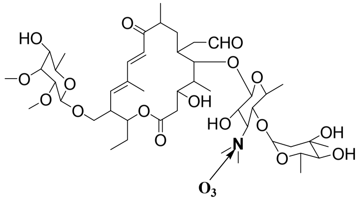 **Assay:** Microdil. **Bacterium:** *B. subtilis* $k_{O3,app,TYL}$” = 5.1 x 10^5 $M^{-1}s^{-1}$ $k_{\bullet OH,app,TYL}$” = 8.2 x 10^9 $M^{-1}s^{-1}$	**Vancomycin (VM)** 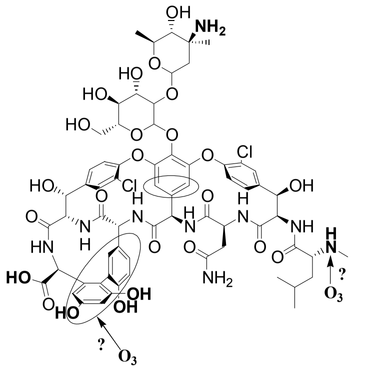 **Assay:** Microdilution **Bacterium:** *B. subtilis* $k_{O3,app,VM}$” = 6.1 x 10^5 $M^{-1}s^{-1}$ $k_{\bullet OH,app,VM}$” = 8.1 x 10^9 $M^{-1}s^{-1}$
Sulfamethoxazole (SMX) 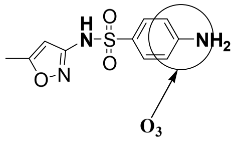 **Assay:** Microdil. **Bacterium:** *E. coli* $k_{O3,app,SMX}$” = 5.5 x 10^5 $M^{-1}s^{-1}$ $k_{\bullet OH,app,SMX}$” = 5.5 x 10^9 $M^{-1}s^{-1}$	**Ciprofloxacin (CF)** 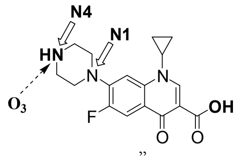 **Assay:** Microdil. **Bacterium:** *E. coli* $k_{O3,app,CF}$” = 1.9 x 10^4 $M^{-1}s^{-1}$ $k_{\bullet OH,app,CF}$” = 4.1 x 10^9 $M^{-1}s^{-1}$	**Enrofloxacin (EF)** 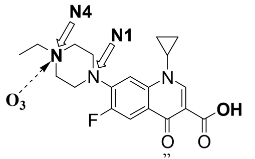 **Assay:** Microdil. **Bacterium:** *E. coli* $k_{O3,app,EF}$” = 1.5 x 10^5 $M^{-1}s^{-1}$ $k_{\bullet OH,app,EF}$” = 4.5 x 10^9 $M^{-1}s^{-1}$	
Trimethoprim (TMP) 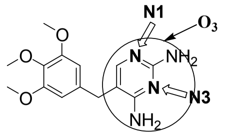 **Assay:** Microdil. **Bacterium:** *E. coli* $k_{O3,app,TMP}$” = 2.7 x 10^5 $M^{-1}s^{-1}$ $k_{\bullet OH,app,TMP}$” = 6.9 x 10^9 $M^{-1}s^{-1}$	**Penicillin G (PG)** 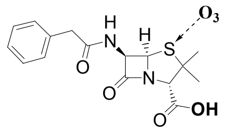 **Assay:** Microdil. **Bacterium:** *B. subtilis* $k_{O3,app,PG}$” = 4.8 x 10^3 $M^{-1}s^{-1}$ $k_{\bullet OH,app,PG}$” = 7.3 x 10^9 $M^{-1}s^{-1}$	**Cephalexin (CP)** 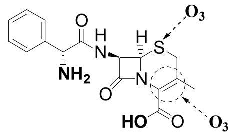 **Assay:** Microdil. **Bacterium:** *B. subtilis* $k_{O3,app,CP}$” = 8.7 x 10^4 $M^{-1}s^{-1}$ $k_{\bullet OH,app,CP}$” = 8.5 x 10^9 $M^{-1}s^{-1}$	**Triclosan (TRI)** 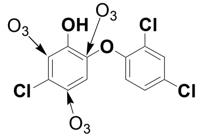 **Assay:** Macrodilution **Bacterium:** *E. coli* $k_{O3,app,TRI}$” = 3.8 x 10^7 $M^{-1}s^{-1}$ $k_{\bullet OH,app,TRI}$” = 5.4 x 10^9 $M^{-1}s^{-1}$
Lincomycin (LM) 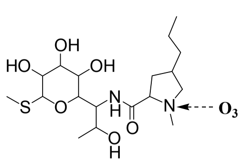 **Assay:** Microdil. **Bacterium:** *B. subtilis* $k_{O3,app,LM}$” = 6.7 x 10^5 $M^{-1}s^{-1}$ $k_{\bullet OH,app,LM}$” = 8.5 x 10^9 $M^{-1}s^{-1}$	**Tetracycline (TET)** 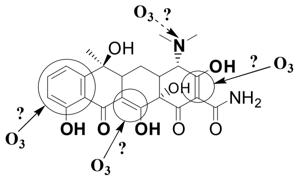 **Assay:** Microdil. **Bacterium:** *E. coli* $k_{O3,app,TET}$” = 1.9 x 10^6 $M^{-1}s^{-1}$ $k_{\bullet OH,app,TET}$” = 7.7 x 10^9 $M^{-1}s^{-1}$	**Amikacin (AM)** 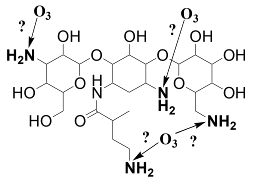 **Assay:** Microdil. **Bacterium:** *E. coli* $k_{O3,app,AM}$” = 1.8 x 10^3 $M^{-1}s^{-1}$ $k_{\bullet OH,app,AM}$” = 7.2 x 10^9 $M^{-1}s^{-1}$	[a] k_{app}” at pH 7 from (*20,28,29*) [b] O_3 targets at pH 7 shown according to (*20,30*). Targets responsible for model compounds’ antibacterial activities indicated by solid arrows; targets not responsible for activities indicated by dotted arrows.

Milli-Q water. Freeze-dried *E. coli* K12 wild-type (ATCC 23716) and *B. subtilis* Marburg (ATCC 6051) seed cultures were obtained from LGC-Promochem. Working *E. coli* and *B. subtilis* stock cultures were maintained at 37 °C and 30° C, respectively, on #3 nutrient agar. Broth cultures were prepared under sterile conditions by suspending *E. coli* and *B. subtilis cells* sampled from the working cultures (from a minimum of five separate colonies) in 5-6 mL of Mueller-Hinton broth within polypropylene test tubes, and incubating overnight at 37 °C and 30°C, respectively on a shaker plate rotating at 200 rpm.

4.2.2 Oxidation of antibacterial model compounds. *Ozone.* Solutions of each of the antibacterial compounds listed in Table 4.1 (aside from triclosan, for which O_3 data were previously obtained as described in (*24*)) were prepared in 1-mM, pH 7 phosphate buffer at initial concentrations of 10 μM, with the exceptions of SMX, LM, and AZ, which were prepared at 50, 50, and 200 μM, respectively. These solutions were dosed with 5 mM of *t*-BuOH (used as a $^{\bullet}$OH scavenger) and distributed in 25-mL volumes amongst eleven 30-mL, amber, borosilicate glass vials (Scheme 4.1). The vials were then placed in a 20 (±0.5) °C water bath placed on top of a magnetic stir plate. After thermal equilibration, and under constant, rapid stirring, 10 of the vials were dosed with O_3 over a range of concentrations sufficient to cover from between approximately 0.1- to 2-log depletion of the respective parent compound, by directly injecting various volumes of ~ 1.5-mM O_3 stock via gas-tight, glass syringe. The eleventh vial was left untreated, as a negative O_3 control. All vials were then capped and allowed to sit for at least 12 hrs prior to sampling to ensure complete decomposition of O_3 residual in the treated solutions. Prior to biological assay, all oxidized solutions were treated with catalase to quench H_2O_2 produced during O_3 treatment. Aliquots of catalase-treated samples were then transferred to HPLC vials for analysis of residual parent compound concentrations by HPLC-UV according to (*20*). One-mL samples of each solution were then collected for analysis of residual parent antibacterial compounds by HPLC-UV, prior to transferring appropriate volumes of each sample to microtiter plates for assay of residual antibacterial activity according to the microdilution method described below. Amikacin (AM) was derivatized with 9-fluoroenylmethyl chloroformate (FMOC) (*31*) immediately prior to HPLC analysis, in order to permit detection by UV.

Hydroxyl radical ($^{\bullet}$OH). For the majority of compounds investigated, $^{\bullet}$OH was generated in situ by γ-radiolysis (via a lead-shielded ^{60}Co source) of aqueous solutions, according to (*32*). Briefly, 100-mL solutions of each model compound were prepared in 1-mM, pH 7 phosphate buffer at initial concentrations of 10 μM for tylosin (TYL), ciprofloxacin (CF), enrofloxacin (EF), trimethoprim (TMP), tetracycline (TET), vancomycin

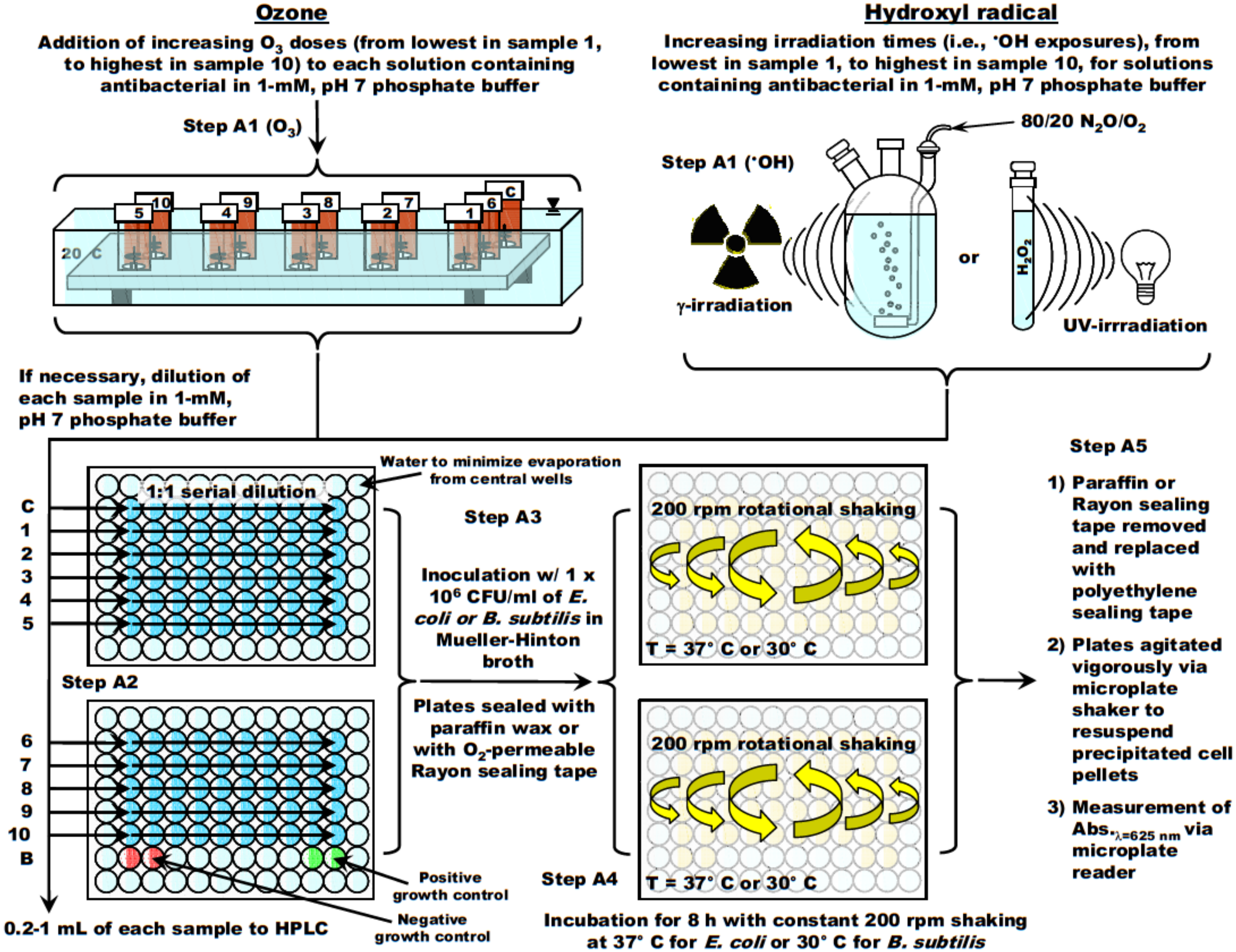
Ozone
Addition of increasing O_3 doses (from lowest in sample 1, to highest in sample 10) to each solution containing antibacterial in 1-mM, pH 7 phosphate buffer
Step A1 (O_3)
5 10 4 9 3 8 2 7 1 6 C
20 °C
Hydroxyl radical
Increasing irradiation times (i.e., •OH exposures), from lowest in sample 1, to highest in sample 10, for solutions containing antibacterial in 1-mM, pH 7 phosphate buffer
80/20 N_2O/O_2
Step A1 (•OH)
γ-irradiation
or
H_2O_2
UV-irradiation
If necessary, dilution of each sample in 1-mM, pH 7 phosphate buffer
Water to minimize evaporation from central wells
1:1 serial dilution
C
1
2
3
4
5
Step A2
6
7
8
9
10
B
Positive growth control
Negative growth control
0.2-1 mL of each sample to HPLC
Step A3
Inoculation w/ 1 x 10^6 CFU/ml of *E. coli or B. subtilis* in Mueller-Hinton broth
Plates sealed with paraffin wax or with O_2-permeable Rayon sealing tape
200 rpm rotational shaking
T = 37° C or 30° C
200 rpm rotational shaking
T = 37° C or 30° C
Step A4
Incubation for 8 h with constant 200 rpm shaking at 37° C for *E. coli* or 30° C for *B. subtilis*
Step A5
1) Paraffin or Rayon sealing tape removed and replaced with polyethylene sealing tape
2) Plates agitated vigorously via microplate shaker to resuspend precipitated cell pellets
3) Measurement of Abs.$_{\lambda=625\ nm}$ via microplate reader

Scheme 4.1. Procedures used in analysis of O_3- and •OH-treated antibacterial samples via microdilution activity assays

(VM), and AM, or 50 μM for sulfamethoxazole (SMX) and AZ, then dosed to borosilicate glass bombs (Scheme 4.1), and purged with a 4:1 mixture of $N_2O:O_2$. Prior to irradiation, a sample was taken from each solution as a control. Each solution was then irradiated for repeated pre-defined time intervals up to total irradiation periods sufficient to achieve ~90% or greater depletion of the parent compound. After each irradiation interval, samples were withdrawn from these solutions for residual substrate analysis and subsequent microbiological assay and transferred to amber, borosilicate vials for storage prior to HPLC analysis (according to (*20*)) and microbiological activity assay (as described below), with the exception of irradiated CF and EF solutions, which were stored in capped polystyrene culture tubes. AM was derivatized prior to HPLC analysis, as for O_3 experiments.

CP was treated with $^{\bullet}OH$ generated via UV-photolysis of H_2O_2 using a 500-W medium pressure lamp with emission wavelengths < 308 nm screened by a UV-cutoff filter to minimize direct CP photolysis. 1-mM, pH 7 phosphate solutions were dosed with 10 μM of CP and 10 mM of H_2O_2, sampled to obtain an untreated control, and then irradiated in 30-mL quartz test tubes (Scheme 4.1) for pre-defined time intervals up to total irradiation periods sufficient to achieve at least 90% depletion of the parent compound. Samples were withdrawn from these solutions between each irradiation period for residual substrate analysis and subsequent microbiological assay. Experiments included a minimum of 10 different irradiation times. Direct photolytic losses of CP were demonstrated via negative H_2O_2 control to be less than 5% during the full irradiation period.

Roxithromycin (RX), penicillin G (PG), and lincomycin (LM) samples were prepared in the same manner as CP, except that $^{\bullet}OH$ was generated via UV-photolysis of H_2O_2 using a 15-W low pressure lamp ($\lambda_{max,emission} \sim 254$ nm) without a cutoff filter. Solutions were prepared at initial model compound concentrations of 10 μM for RX and PG, and 200 μM for LM, and dosed with an initial H_2O_2 concentration of 5-10 mM. Direct photolytic losses of PG were demonstrated via negative H_2O_2 control to be less than 5% during the full irradiation period, whereas RX and LM are each UV-transparent.

4.2.3 Measurement of antibacterial activities after treatment with ozone and hydroxyl radical. *Broth microdilution assay.* With the exception of $^{\bullet}OH$-treated triclosan solutions, the activities of antibacterial solutions prepared according to the procedures described above were quantified in triplicate by means of a microdilution assay based on the NCCLS clinical microdilution standard (*33*) (Scheme 4.1). Prior to biological assay, all oxidized solutions were treated with catalase to quench any residuals of H_2O_2 generated in situ or remaining from H_2O_2 photolysis experiments. Ten-member dilution series were prepared from each sample via 1:1 serial dilution of the sample in 1-mM phosphate buffer (also containing 5-mM of *t*-BuOH in the case of O_3-treated samples), across an individual row of the corresponding 96-well microtiter plate. Matching standard dilution series were prepared from the untreated samples of each parent antibacterial compound for assay with the oxidant-treated samples. Each sample and standard solution volume was then inoculated with an equal volume of Mueller-Hinton broth containing a 1 x 10^6 CFU/mL cell density of the reference *E. coli* or *B. subtilis* strains, sealed with either paraffin or breathable Rayon sealing tape to minimize evaporative water loss, and allowed to incubate under 200 rpm agitation, at 37 °C (for *E. coli* cultures) or 30°C (for *B. subtilis* cultures), for 8 h. After incubation, the paraffin or sealing tape was removed, the plates were temporarily re-sealed with impermeable polyester sealing tape, and each plate was agitated vigorously using a Vortex microtiter plate shaker attachment to re-suspend any pelleted cell material from the bottoms of the microtiter wells. Subsequently, the polyester tape was removed and the absorbances of the sample and standard solutions in each microtiter well were measured at 625 nm (as a surrogate for cell density (*33*)), using a Spectra Rainbow microplate reader (Tecan, Switzerland).

Absorbance measurements were then converted to % growth inhibition (%I) by scaling to the absorbance measurements A_{min} (i.e., 100% growth inhibition, corresponding to negative growth controls) and A_{max} (i.e., 0% growth inhibition, corresponding to positive growth controls), according to eq 1.

$$\%\mathrm{I} = \frac{\left(\mathrm{A}_{\max} - \mathrm{A}\right)}{\left(\mathrm{A}_{\max} - \mathrm{A}_{\min}\right)} \times 100 \tag{1}$$

The resulting data for each sample dilution series were plotted against the log of the corresponding sample dilution, $1/m^n$ - where m represents the serial dilution factor used in preparing dilution series (i.e., 2 in the present case) and n represents the number of the dilution step for an individual member of the dilution series derived from a given sample (e.g., 5 for the 5th serial dilution in a dilution series), to yield dose-response relationships from which quantitative measures of potency could be extracted. The relationships between sample dilution and %I were then quantitatively evaluated by simultaneous non-linear regression of the 11 replicate data-sets corresponding to the untreated standard and 10 samples collected for each treatment process, according to eq 2,

$$\%\,\text{Growth Inhibition} = \%\mathrm{I}_{\min} + \frac{\%\mathrm{I}_{\max} - \%\mathrm{I}_{\min}}{1 + 10^{\left(\log\left(\mathrm{EC}_{50}/\left(1/m^{n}\right)\right)\times \mathrm{H}\right)}} = \%\mathrm{I}_{\min} + \frac{\%\mathrm{I}_{\max} - \%\mathrm{I}_{\min}}{1 + \left(\mathrm{EC}_{50}/\left(1/m^{n}\right)\right)^{\mathrm{H}}} \tag{2}$$

using GraphPad Prism (GraphPad Software), where EC_{50} represents the effective antibacterial concentration (or in this case, sample dilution) at which 50% growth inhibition is observed, m

represents the dilution factor for each serial dilution step (i.e., 2 in the present case), *n* is the number of times a given member of the dilution series has been diluted relative to the parent sample, H represents the Hill slope inherent to the dose-response relationships for each combination of antibacterial compound and reference bacterial strain, and $\%\mathrm{I}_{\mathrm{max}}$ and $\%\mathrm{I}_{\mathrm{min}}$ represent the maximum and minimum growth inhibition values for a given data set, respectively. To maximize the accuracy of these model fits, Prism was constrained to solve for the shared, best-fit values of H, $\%\mathrm{I}_{\mathrm{max,t}}$, and $\%\mathrm{I}_{\mathrm{min,t}}$ characterizing dose-responses for each sample set as a whole, while $\log\mathrm{EC}_{50}$ was allowed to vary across samples.

Dose-response relationships for CF, EF, and AM were evaluated by fitting sample data to the five-parameter modified Hill model (i.e., the Richard's equation (*34*)) represented by eq 3 (also using GraphPad Prism),

$$\%\,\text{Growth inhibition} = \%\mathrm{I}_{\mathrm{min}} + \frac{\%\mathrm{I}_{\mathrm{max}} - \%\mathrm{I}_{\mathrm{min}}}{\left(1 + 10^{\left(\log\mathrm{EC}_{50} - \log\left(1/m^{n}\right)\right)\times \mathrm{H}}\right)^{\mathrm{S}}} = \%\mathrm{I}_{\mathrm{min}} + \frac{\%\mathrm{I}_{\mathrm{max}} - \%\mathrm{I}_{\mathrm{min}}}{\left(1 + \left(\mathrm{EC}_{50}/\left(1/m^{n}\right)\right)^{\mathrm{H}}\right)^{\mathrm{S}}} \qquad (3)$$

where EC_{50}, *m*, *n*, H, $\%\mathrm{I}_{\mathrm{max}}$, and $\%\mathrm{I}_{\mathrm{min}}$ are the same as in eq 2, and S is a parameter quantifying the asymmetry of the dose-response curve's slope, and all other parameters are as defined in eq 1. Uncertainties (as 95% confidence limits) for each of the microdilution measurements described here were determined according to Text S4.1 in the Supporting Information for Chapter 4.

Broth macrodilution assay. The macrodilution methodology utilized for measurement of residual activity in •OH-treated solutions of triclosan (TRI) was essentially the same as that described in (*24*), with several minor exceptions. Briefly, 120-μL aliquots of •OH-treated TRI solutions ($[\mathrm{TRI}]_0$ = 5 μM) prepared as described above were added to glass culture tubes containing 1.38 mL of 1-mM, pH 7 phosphate buffer (to yield 12.5-fold dilution of the original samples). In addition, 360 μL of the untreated 5-μM TRI solution was dosed to a glass culture tube containing 4.14 mL of 1-mM phosphate buffer (to yield 25-fold dilution of the original sample). A set of eleven 2:1 serially-diluted standards was then prepared by transferring 3 mL of the 12.5×-diluted TRI standard to a culture tube containing 1.5 mL of 1-mM, pH 7 phosphate buffer, mixing, then transferring 3-mL of the resulting solution to another 1.5-mL buffer volume, and so on, to yield a series of TRI standards with [TRI] ranging from 5.0×10^{-6} M to 8.5×10^{-8} M. Each of the culture tubes contained within the 11-member sample and standard sets was subsequently inoculated with 1.5 mL of a broth *E. coli* K12 culture containing approximately 1×10^{6} CFU/mL, capped, and incubated at 37° C under constant agitation (200 rpm on a rotating shaker plate), and processed for analysis as described previously (*24*). As before, absorbance measurements were obtained for each sample at 625 nm after appropriate incubation periods. These absorbance values were then converted to growth inhibition, I, according to eq 1. A dose-response curve was obtained for the serially-diluted triclosan standards by plotting inhibition vs. the in vitro assay concentration of triclosan and fitting the data to eq 2 (using GraphPad Prism),

$$\%\mathrm{I} = \%\mathrm{I}_{\mathrm{min}} + \frac{\%\mathrm{I}_{\mathrm{max}} - \%\mathrm{I}_{\mathrm{min}}}{1 + 10^{\left(\log\left(\mathrm{EC}_{50}/[\mathrm{TRI}]_{\mathrm{in\ vitro}}\right)\times \mathrm{H}\right)}} = \%\mathrm{I}_{\mathrm{min}} + \frac{\%\mathrm{I}_{\mathrm{max}} - \%\mathrm{I}_{\mathrm{min}}}{1 + \left(\mathrm{EC}_{50}/[\mathrm{TRI}]_{\mathrm{in\ vitro}}\right)^{\mathrm{H}}} \tag{4}$$

where $[\mathrm{TRI}]_{\mathrm{in\ vitro}}$ is the in vitro concentration of TRI present in a given culture tube after any preceding dilution steps, and all other variables are as in eq 2. The $\%\mathrm{I}_{\mathrm{min}}$, $\%\mathrm{I}_{\mathrm{max}}$, EC_{50}, and H terms obtained by fitting eq 4 to the standard data set were then used to calculate theoretical %I values for the residual $[\mathrm{TRI}]_{\mathrm{in\ vitro}}$ values present in each oxidant-treated TRI sample for comparison with the corresponding measured %I values. All sample and standard activity assays processed by this method were performed in triplicate. Uncertainties (as 95% confidence limits) were calculated for each of the macrodilution measurements described here according to Text S4.1.

4.3 Results and Discussion

4.3.1 Analysis and interpretation of microdilution assay data. Examples of the dose-response relationships obtained via microbiological assay of untreated standards of the macrolide antibacterial agent roxithromycin (RX) and O_3-treated RX samples by the broth microdilution approach are illustrated in Figure 4.1a. Treatment of RX with increasing O_3 doses results in a shift of the corresponding dose-response curves toward the right of the graph, relative to the curve corresponding to untreated RX, which is at the far left of the graph. This indicates that (a) ozonation lowers RX's antibacterial activity, and (b) the potencies of oxidation products resulting from treatment of RX with O_3 are significantly lower than that of the parent compound. The changes in dose-response relationships for RX samples during treatment with increasing O_3 exposures can be quantitatively correlated to the measured decrease in [RX] by calculation of a "potency-equivalent" (PEQ) value for each O_3-treated sample via eq 5,

$$\mathrm{PEQ\ (in\ mol/L)} = \mathrm{EC}_{50,0}/\mathrm{EC}_{50,\mathrm{x}} \tag{5}$$

where $\mathrm{EC}_{50,0}$ is the EC_{50} value calculated from the measured dose-response relationship for the untreated RX standard (Figure 4.1a), and $\mathrm{EC}_{50,\mathrm{x}}$ represents the EC_{50} value calculated from the measured dose-response relationship obtained for each treated sample (as illustrated in

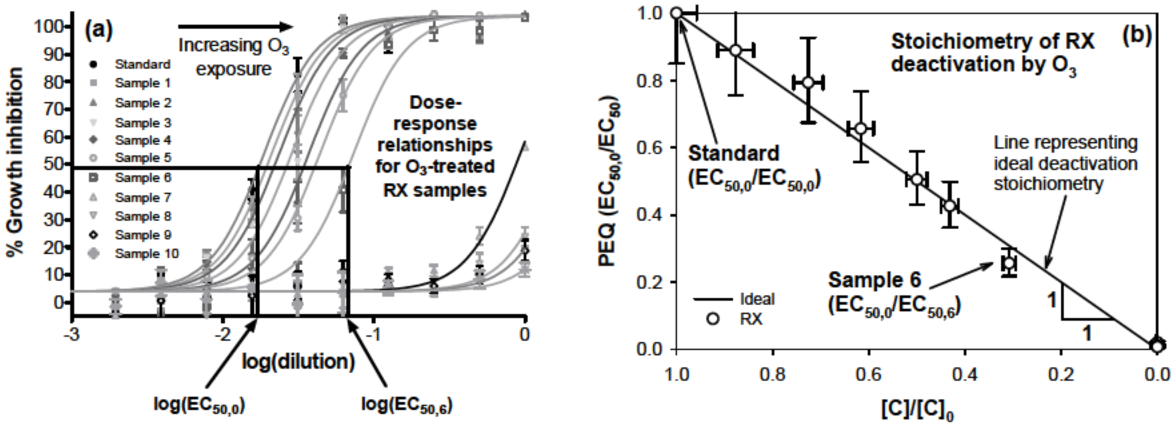

Figure 4.1. Example plot of (a) dose-response relationships for RX samples treated with increasing O_3 exposures, and (b) corresponding plot of the stoichiometry with which RX is deactivated by O_3. Measurements shown in Figure 4.1a are depicted with 95% confidence intervals calculated for the corresponding triplicate data sets by GraphPad Prism, using eq 1. Measurements shown in Figure 4.1b are depicted with 95% confidence limits calculated as described in Text S4.1. The independent variable "dilution" is equal to $1/2^n$, where "2" is the serial dilution factor used in preparing dose-response series (i.e., for 2-fold, or 1:1 dilution), and "n" the number of times a given sample has been serially diluted relative to the corresponding parent sample (i.e., $1/2^0$ corresponds to the dilution of each parent sample).

Figure 4.1a, using Sample 6 as an example). The PEQ calculated for each sample can then be plotted vs. $[C]/[C]_0$ for the parent compound (RX in this case) to evaluate the quantitative relationship between loss of parent compound and corresponding changes in biological activity. For the ideal case, in which consumption of one mole fraction of parent antibacterial compound results in a loss of one PEQ, measured PEQ values plotted in this manner should trace a hypothetical line with the form $y = x$, as depicted for the RX data in Figure 4.1b (where the apparent slope of the line is only negative because the x-axis is reversed).

In the event that oxidation of the parent compound does not yield a complete loss of antibacterial activity (i.e., that transformation products retain biological activity), measured values would be expected to deviate positively and systematically (within statistical significance) from the solid line beyond the range of calculated uncertainty limits. In contrast, systematic, statistically significant, negative deviations from the line of ideal stoichiometry would suggest inhibition of a given parent compound's activity by transformation products. Although every effort was undertaken to control for possible sources of error, random (as opposed to systematic), statistically significant, positive or negative deviations from the ideal case were still observed in several cases (as will be discussed below); most likely as a consequence of unquantified, non-systematic methodological uncertainties associated with such factors as evaporative water loss in the microdilution assay or variable derivatization yields in the case of amikacin (AM) analyses.

4.3.2 Deactivation of model clinical antibacterial compounds by ozone. *Macrolides.* Measured antibacterial activities of the three macrolide antibacterial compounds, RX, AZ, and TYL, following treatment with O_3, are depicted in Figure 4.2a. As shown here, RX exhibits an apparent deactivation stoichiometry of approximately one PEQ lost per mole fraction equivalent of RX consumed by direct reaction with O_3. This value is consistent with findings previously reported for deactivation of the structurally-analogous macrolide clarithromycin by O_3 (*23*), and agrees with the mechanism by which macrolide antibacterials are believed to derive their biochemical activity; that is, from specific hydrogen bonding with various nucleobases and phosphodiester linkages in the peptidyl transferase cavity of bacterial 23S rRNA (*35*). The bonding interaction most likely to be interrupted by direct reaction with O_3 is that involving RX's tertiary amine (Table 4.1), which is the primary site of attack by O_3 (*20,23,28*). Modification of the tertiary amine via oxidation to the corresponding *N*-oxide or

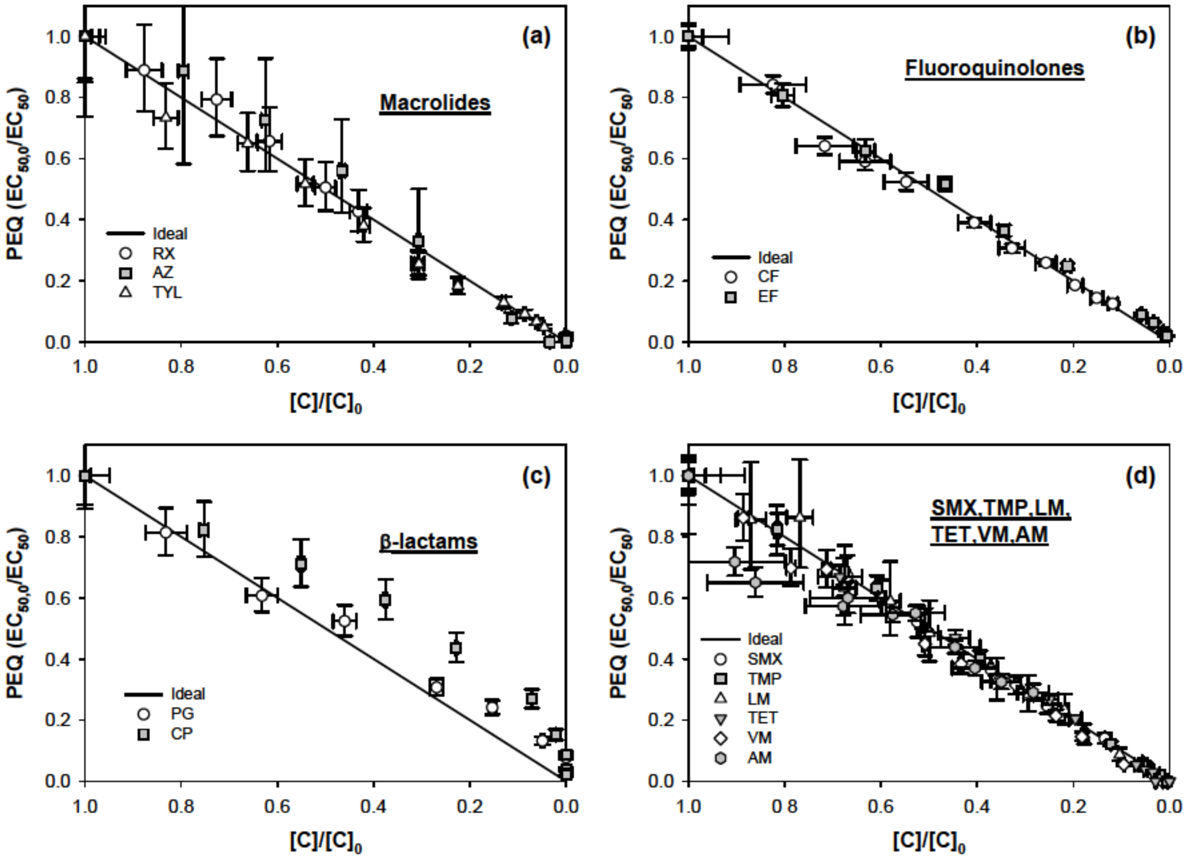

Figure 4.2. Deactivation stoichiometries for oxidation of (a) macrolides, (b) fluoroquinolones, (c) *β*-lactams, and (d) SMX, TMP, LM, TET, VM, and AM by O_3 at pH 7. All data points are shown with 95% confidence limits calculated as described in Text S4.1. Averages of the raw dose-response data (obtained in triplicate) from which PEQ measurements were derived are provided in Figures S4.1a-S4.13a.

via demethylation (*23,36*) should prevent its hydrogen bonding with 23S rRNA, leading to reduction or elimination of each parent macrolide's antibacterial activity. As shown in Figure 4.2a, AZ (a fifteen-membered macrolide) and TYL (a sixteen-membered macrolide) are also deactivated with apparently ideal stoichiometry upon reaction with O_3, in agreement with the previously reported observation that their tertiary desosamine moieties (Table 4.1) are also the primary sites of attack by O_3 at circumneutral pH (*20*). As nearly all macrolides contain the characteristic desosamine sugar moiety, these findings can presumably be generalized across most of the macrolide antibacterial structural class; permitting one to conclude that O_3 can effectively deactivate not only macrolides possessing the 14-member macrolactone ring template, but also those possessing 15- and 16-membered rings.

Fluoroquinolones. According to the data presented in Figure 4.2b, CF and EF - which are differentiated only by the degree of their N4 atoms' alkyl substitution (Table 4.1), each exhibit stoichiometric deactivation upon direct reaction with O_3. Fluoroquinolones derive their biochemical activity from blockage of DNA replication, via several highly specific hydrogen-bonding and charge interactions with relaxed bacterial DNA in the presence of DNA topoisomerase enzymes (*37,38*). According to a widely accepted model for fluoroquinolone-DNA binding (*37*), the characteristic quinolone moiety is responsible for these interactions. Consequently, one would expect that oxidation of this moiety by O_3 would generally be required to achieve substantial reduction or elimination of fluoroquinolones' antibacterial potencies. However, the heterocyclic piperazine moieties present in the CF and EF parent molecules (Table 4.1) - which are apparently not essential to fluoroquinolone antibacterial activity (i.e., first-generation quinolones such as nalidixic acid lack the heterocycle, but still exhibit considerable antibacterial potency (*39*)) - represent the primary sites at which CF and EF react with O_3, whereas reactions at the model compounds' quinolone moieties are actually quite slow (*20*). Thus, even modification of the N4 tertiary amine (via oxidation to the corresponding *N*-oxide or partial dealkylation (*23,36*)) appears to modify the fluoroquinolone structures to a degree sufficient to diminish either fluoroquinolone access to the bacterial cell target or the binding interactions necessary for their interruption of DNA replication once inside the cell. These observations are expected to be broadly applicable amongst members of the fluoroquinolone structural class containing the piperazine moiety.

β-lactams. As shown in Figure 4.2c, apparent deactivation stoichiometries for the penicillin PG and the cephalosporin CP both exhibit systematic, statistically significant positive deviation from the ideal case, pointing toward the formation of products retaining an appreciable degree of antibacterial activity. These trends are more evident when PEQ measurements are plotted against O_3 dose, as in Figure 4.3. As illustrated for PG in Figure 4.3a, as O_3 does is increased (and PG is progressively depleted), measured activity of O_3-treated solutions decreases with approximately ideal stoichiometry until roughly 10% of the control solution's activity remains, after which measured activity remains constant with further O_3 addition. In contrast, the data depicted in Figure 4.3b show that the activity of O_3-treated CP solutions decreases initially to ~80% of the control's, after which the activity of O_3-treated samples deviates substantially from the ideal and only decreases toward zero following addition of ~1.6× excess O_3 beyond that needed to yield >99% CP depletion.

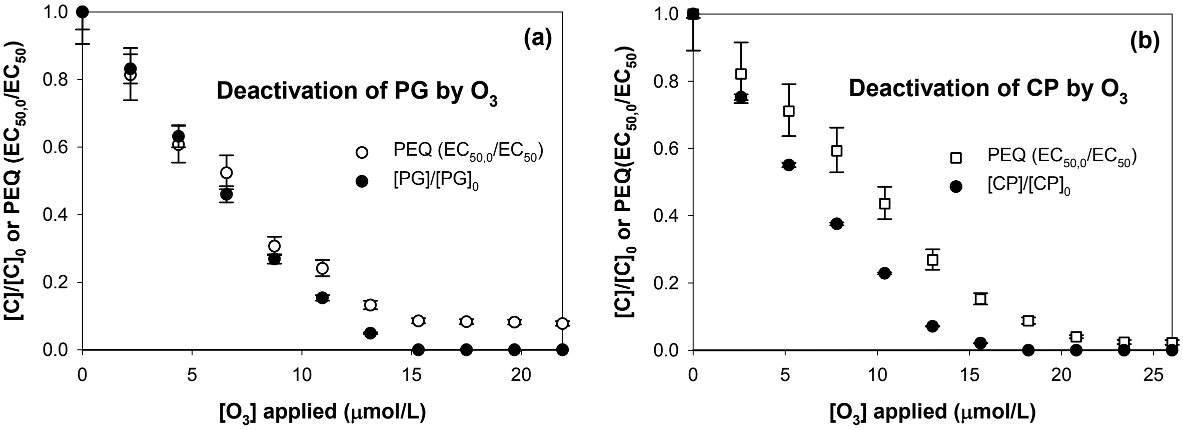

Figure 4.3. Deactivation of (a) PG and (b) CP with increasing O_3 dose at pH 7. All data points are shown with 95% confidence limits calculated as described in Text S4.1. Averages of the raw dose-response data (obtained in triplicate) from which PEQ measurements were derived are provided in Figures S4.6a and S4.7a.

Direct O_3 reactions are known to occur predominantly at the thioether in PG, whereas O_3 may attack either the thioether or the C-2/C-3 double bond in CP at pH 7 (*20,30*). Reaction of O_3 with the thioether group of many penicillin structures is known to lead to high yields (>95%) of enantiomeric *R*- and *S*-sulfoxides (in *R*:*S* ratios ranging from 1:4 to 24:1) (*40*). Ozone attack at the cephalosporin C-2/C-3 bond leads to heterolytic cleavage via Criegee ozonolysis (*30*). However, the fused *β*-lactam ring - from which all *β*-lactams ultimately derive their antibacterial activities (via sequestration of bacterial peptidoglycan transpeptidase enzyme and consequent disruption of bacterial cell wall synthesis (*38,41*)) is quite recalcitrant to O_3 in each case. Although *S*-sulfoxide analogues of *β*-lactams are generally reported to exhibit negligible antibacterial activities, their *R*-sulfoxide analogues can be quite potent (*42,43*), indicating that oxidation of the thioether alone will be insufficient to eliminate the parent *β*-lactam compounds' antibacterial activities. In contrast, ozonolytic cleavage of the cephalosporins' characteristic C-2/C-3 double bond (shown for CP in Table 4.1) may eliminate the parent structure's antibacterial properties – even though the *β*-lactam ring may not be directly modified via such a reaction – by sufficiently disrupting the requisite conformational alignment of the *β*-lactam ring and its peptidoglycan transpeptidase target to prevent enzyme sequestration or by hindering transport to the target through the cell wall (*41*). The mechanisms and consequences of these reactions, as well as their general implications for the fate of structurally analogous *β*-lactams during O_3-based wastewater treatment, are the focus of a detailed investigation (*30*).

Sulfonamides. Deactivation stoichiometries for SMX, are depicted in Figure 4.2d. As illustrated by these data, SMX also exhibits stoichiometric deactivation upon reaction with O_3. This is consistent with prior identification of the *p*-sulfonylaniline moiety (Table 4.1) as the primary site at which the SMX molecule is attacked by O_3 (*20*), as this characteristic moiety is directly responsible for every sulfonamide antibacterial compound's interference with bacterial folate synthesis (*38*). Namely, modification of this moiety - via oxidation of the aromatic amine (*44*), or by ring opening pathways characteristic of reactions between O_3 and activated aromatics (*25*) - would be expected to preclude SMX's function as a competitive analogue of *p*ABA (*38*). Although certain sulfonamides possess alternative heterocyclic substituents (in place of the dimethylisoxazole moiety shown for SMX - Table 4.1) that may also be rapidly oxidized by $O_{3,}$ reactivity of the *p*-sulfonylaniline moiety should generally be sufficiently high (*20,28*) to ensure that all sulfonamide antibacterial agents will be efficiently deactivated by direct reaction with O_3.

Dihydrofolate Reductase (DHFR) Inhibitor. As shown in Figure 4.2d, TMP is also stoichiometrically deactivated upon reaction with O_3. This is consistent with identification of the 2,4-diaminopyrimidine structure (Table 4.1) as the primary target of direct attack by O_3 at circumneutral pH (*20*), as the intact 2,4-diaminopyrimidinyl structure plays a critical role in enabling TMP's ability to inhibit bacterial folate synthesis (*38*). That is, modification of this moiety - via oxidation of an aromatic amine (*44*), or by the ring opening/contraction pathways characteristic of reactions between O_3 and various pyrimidine nucleobases (*45,46*) - would be expected to eliminate TMP's ability to compete with the structural analogue 7,8-dihydrofolate for available DHFR by disrupting the specific modes of binding between the N1, 2-amino, and 4-amino nitrogens of the 2,4-diaminopyrimidine ring and target sites within the bacterial DHFR enzyme structure (*47*). It is also worth noting that the secondary site of O_3 attack at pH 7 - the 3,4,5-trimethoxybenzyl ring - is also believed to play an important role in mediating TMP binding to bacterial DHFR (*47*).

Lincosamide. The deactivation data shown in Figure 4.2d illustrate that direct reaction with O_3 also yields stoichiometric elimination of LM's biological activity. Previous kinetics measurements indicate that the initial reaction of O_3 with LM takes place at its tertiary pyrrolidine nitrogen (Table 4.1) at circumneutral pH, whereas secondary attack likely occurs at the LM thioether (*29*). Oxidation of the former by O_3 should proceed via *N*-oxide formation or dealkylation (*23,36*), and oxidation of the latter should lead to LM-sulfoxide (*40,48*), which is already known to possess significantly lower antibacterial potency than the parent structure (*49*). However, in neither case do these reactions occur at sites responsible for the specific hydrogen-bonding interactions between lincosamides and target nucleotides in bacterial 23S rRNA (*35*) that actually lead to inhibition of bacterial protein synthesis. These observations suggest that minor structural changes - even at spatially and electronically isolated regions of the LM structure - are sufficient to either hinder LM access to bacterial target sites or to disrupt the H-bonding patterns ultimately responsible for LM's and other lincosamides' antibacterial activities. Analogous reaction mechanisms and outcomes are expected to apply to the clinical-use lincosamide, clindamycin, on account of its nearly identical structure.

Tetracycline. The data shown in Figure 4.2d illustrate that oxidation of TET by O_3 results in rapid, stoichiometric elimination of the former's antibacterial activity. This is consistent with evidence that reactions of O_3 with TET proceed by attack of the latter's fused tetracyclic system at circumneutral pH (*20*). As the tetracycline structure is likely extensively modified upon direct reaction with O_3 via O-addition to or ozonolysis of its aromatic and olefinic structural moieties (*25,50*), the requisite charge interactions (direct or metal-mediated) of the tetracycline molecule's keto and hydroxy oxygens (Table 4.1) with specific internucleotide phosphodiester linkages of the bacterial ribosome would likely be disrupted, leading to elimination of the antibacterial molecule's biological activity (*51*). These observations can be expected with a high degree of confidence to apply to all tetracycline antibacterials, due to the nearly universal commonality of the template tetracycline system (*52*).

Glycopeptide. The data shown in Figure 4.2d indicate that the reaction of O_3 with VM also yields an apparent loss of one PEQ per fractional mole equivalent of VM consumed. These data indicate that chemical modifications by O_3 disrupt the glycopeptide structure's interactions with cellular targets to a degree sufficient to substantially diminish VM's antibacterial potency. More specifically, although the hydroxyphenol, trimethylbenzyl, and *N*-methylleucine moieties identified as the most probable sites at which VM is attacked O_3 at circumneutral pH (*20*) are not directly involved in the hydrogen-bonding interactions responsible for bacterial peptidoglycan sequestration (the explicit means by which glyocopeptides inhibit cell wall synthesis (*53*)), their oxidation by O_3 should lead to disruption of the VM stereochemistry necessary for such specific H-bonding to occur (*25,54*). This should in turn result in elimination of VM's antibacterial activity, as observed in Figure 4.2d.

Aminoglycoside. Although the data shown in Figure 4.2d for the AM-O_3 reaction deviate substantially from the plot of ideally stoichiometric deactivation at low AM turnovers, it is nevertheless clear from these and the data shown for higher O_3 doses that AM is efficiently deactivated by direct reaction with O_3. This finding is consistent with identification of AM's primary amines as the primary sites of attack by O_3 at circumneutral pH (*20*), as these functional groups are believed to play an important role in both of the modes from which the aminoglycosides' antibacterial activities are derived; namely, bacterial rRNA hydrogen bonding and charge-interactions and competitive displacement of the divalent cations, Mg^{2+} and Ca^{2+}, from the bacterial cell wall (*55,56*).

4.3.3 Deactivation of model clinical antibacterial compounds by hydroxyl radical. As illustrated in Figure 4.4, nearly all of the clinical antibacterial model compounds included in this investigation are also deactivated by $^{\bullet}OH$ with a stoichiometry of approximately one PEQ lost for each mole fraction equivalent consumed by reaction with $^{\bullet}OH$. However, the EC_{50} values measured for the β-lactams during treatment with $^{\bullet}OH$ appear to deviate marginally (relative to error limits) from the line of ideal stoichiometry at low to moderate degrees of depletion; possibly due to formation of biologically-active oxidation products via reaction of PG and CP with $^{\bullet}OH$. According to prior studies, *o*-, *m*-, and *p*-hydroxybenzylpenicillin are formed with respective $G_{formation}$ values (in units of molecules formed/100 eV applied) of ~0.39, ~0.19, and ~0.18 (i.e., in ~9%, ~5%, and ~4% yield) during γ-irradiation of 100 μM PG (for which $G_{depletion} \sim 4.2$) in N_2O-saturated aqueous solutions (*57*). The last of these - also referred to as penicillin X - has been reported to exhibit in vitro potencies equivalent to or greater than PG toward various *Bacillus* spp. (*58,59*). Similar characteristics might therefore be expected of the *o*- and *m*- hydroxy PG isomers, as well as the anticipated *p*-, *o*-, or *m*-hydroxylated analogues of CP. Assuming ~20% yields of total hydroxylated PG or CP products with antibacterial potencies approximately equivalent to those of PG and CP, respectively, a corresponding maximum of ~20% deviation from ideal deactivation stoichiometries would be expected to result during treatment with $^{\bullet}OH$; consistent with the data shown in Figure 4.4c. In any case, as illustrated in Figure 4.4c, the

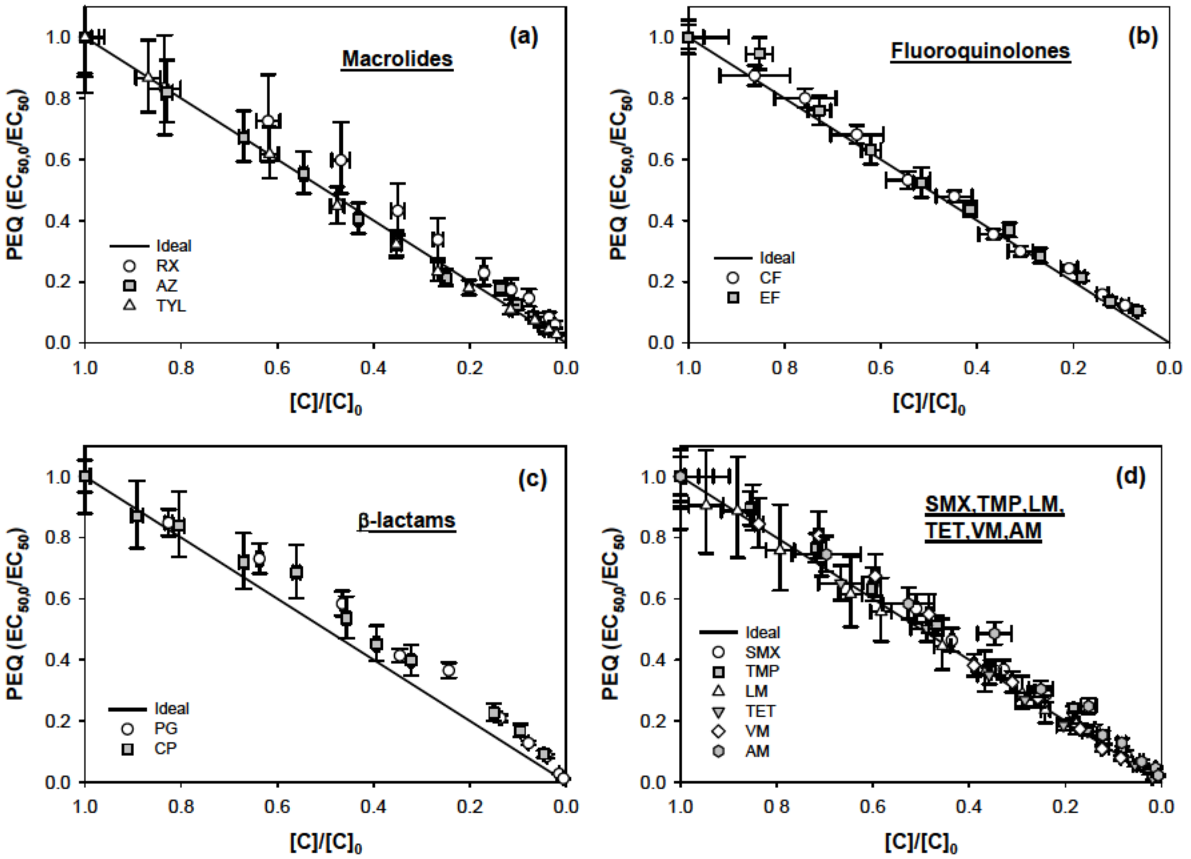

Figure 4.4. Deactivation stoichiometries for oxidation of (a) macrolides, (b) fluoroquinolones, (c) *β*-lactams, and (d) SMX, TMP, LM, TET, VM, and AM by $^{\bullet}$OH at pH 7. All data points are shown with 95% confidence limits calculated as described in Text S4.1. Averages of the triplicate dose-response curves from which these data were derived are provided in Figures S4.1b-S4.13b.

activities of PG and CP solutions continue to decrease toward zero at higher $^{\bullet}$OH exposure (i.e., more extensive parent compound depletion), indicating that any active products such as penicillin X are ultimately deactivated by $^{\bullet}$OH, as well.

Summarily, these findings indicate that, despite the fact that only certain functional groups within each antibacterial molecule are involved in direct binding interactions with biochemical targets in a given bacterial cell, even relatively non-selective $^{\bullet}$OH-mediated modifications to other regions of the model compounds' molecular structures are sufficient to interrupt the conformational or ionic properties required for effective growth inhibition or bactericidal effects.

4.3.4 Deactivation of triclosan by ozone and hydroxyl radical. Oxidation of TRI by O_3 is already known to result in elimination of the former's target-specific antibacterial activity (*24*). However, for purposes of comparison, the previously reported data – for which uncertainties have been re-examined according to the methods described in Text S4.1 – are shown here with accompanying 95% confidence limits in Figure 4.5a, which has been adapted from (*24*). The corresponding results for treatment of TRI with $^{\bullet}$OH are depicted in Figure 4.5b. As is clear from both figures, the activities measured for each oxidant-treated TRI sample dataset very closely overlay the regions bounded by the 95% confidence limits of the dose-response relationships fitted to the corresponding TRI control series. Although a robust, fully quantitative comparison of the sample and standard activities could not be performed solely on the basis of the single activity measurements obtained via the macrodilution activity assay, the close agreement of the %I values obtained for the sample data sets with the corresponding control data for each oxidant suggest that TRI deactivation occurs with close to ideal stoichiometries in both cases.

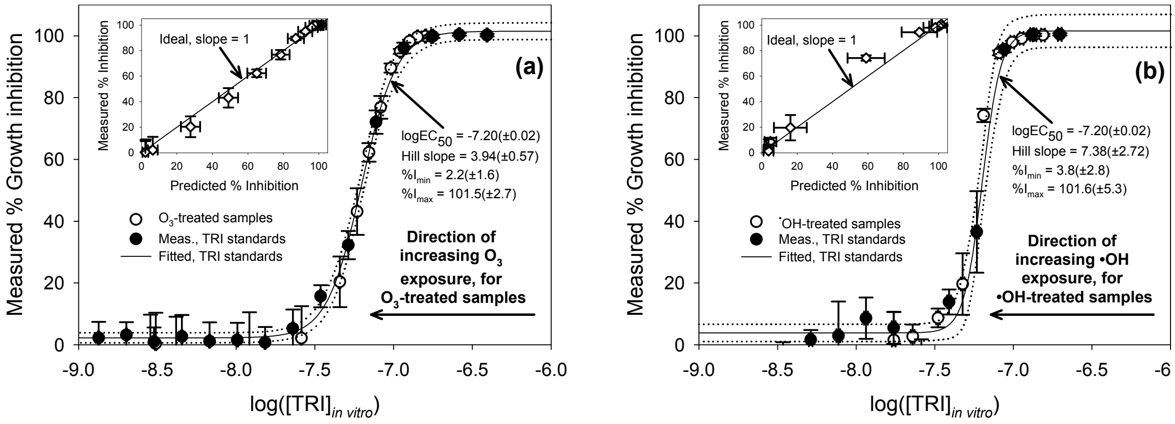

Figure 4.5. TRI deactivation plots for oxidation by (a) O_3 (at pH 8) (adapted from (*24*)) and (b) $^{\bullet}$OH (from the present investigation, at pH 7). All data points are shown with 95% confidence limits calculated as described in Text S4.1. Lines (solid) fitted to the four-parameter logistic model are shown with corresponding upper and lower 95% confidence limits (dotted lines) – also calculated according to Text S4.1. The insets to each figure depict the correlations of measured %I values with %I values predicted from eq 4 (using the fitted $\%I_{min}$, $\%I_{max}$, EC_{50}, and Hill slope parameters for each data set) on the basis of measured TRI residuals in the corresponding O_3- or $^{\bullet}$OH-treated solutions.

This conclusion is also supported by comparison of activities measured for the oxidant-treated samples with activities predicted for the same samples on the basis of the fit parameters included in Figures 4.5a and 4.5b (see insets to each figure). Although the correlation of measured and predicted sample activities for $^{\bullet}$OH treatment is not as strong as for the O_3-treated data set, these data nevertheless suggest that – within uncertainty limits – TRI is deactivated with nearly ideal stoichiometry by both O_3 and $^{\bullet}$OH.

These observations are all consistent with the known modes of TRI antibacterial activity and the sites at which O_3 and $^{\bullet}OH$ are expected to attack the TRI molecule. That is, O_3 reacts primarily with TRI's phenol ring (*24*), which mediates TRI's target-specific inhibition of bacterial fatty acid synthesis via van der Waals and hydrogen-bonding interactions with the enoyl-acyl carrier protein reductase (ENR) enzyme (*60,61*). Furthermore, $^{\bullet}OH$ – on account of its low selectivity – would be expected to react not only with the phenolic ring, but also with TRI's dichlorophenoxyl ring, which also plays an important role in mediating TRI's interactions with the ENR enzyme, mainly via additional van der Waals interactions with the target enzyme (*60,61*).

4.3.5 Implications for antibacterial deactivation during ozonation of municipal wastewater. The data provided in Figures 4.2-4.5 illustrate that nearly all of the model antibacterial compounds included in this investigation are quantitatively deactivated by both O_3 and $^{\bullet}OH$. This in turn implies that, for each mole of a given antibacterial compound oxidized during ozonation of a wastewater matrix, a corresponding loss of one PEQ will result, whether the observed oxidation is due to direct reactions with O_3 or to reactions with $^{\bullet}OH$. Thus, observations of parent compound elimination during ozonation (as monitored by, for example, LC/MS/MS) should correlate directly with a corresponding loss of antibacterial activity. The only exceptions noted here are the β-lactams PG and CP, which are not completely deactivated by direct reactions with O_3 (due to their transformation to biologically-active transformation products (*30*)), but *are* effectively deactivated by $^{\bullet}OH$ (Figures 4.2c and 4.4c). In these latter two cases, deactivation efficiency during wastewater ozonation will therefore depend on the degree to which oxidative transformations are driven by reactions with O_3 vs. $^{\bullet}OH$.

The likely importance of O_3 and $^{\bullet}OH$ reactions in governing PG and CP oxidation during wastewater ozonation may be examined by calculating the theoretical fractions of model compound transformation attributable to reactions with $^{\bullet}OH$ ($f_{\bullet OH,M(\tau)}$, or $1 - f_{O3,M(\tau)}$) for various values of $R_{ct(\tau)}$ (i.e., the cumulative in situ ratio of $^{\bullet}OH$ and O_3 exposures, or $\int_0^{\tau}[\bullet OH]dt \Big/ \int_0^{\tau}[O_3]dt$, after an arbitrary reaction time, τ), according to eq 5 (*62*),

$$f_{\bullet OH,M(\tau)} = \left(1+\frac{k''_{O_3,app,M}}{k''_{\bullet OH,app,M}}\left(\int_0^{\tau}[\bullet OH]dt \Big/ \int_0^{\tau}[O_3]dt\right)^{-1}\right)^{-1} = \left(1+\frac{k''_{O_3,app,M}}{k''_{\bullet OH,app,M}}\left(\frac{1}{R_{ct(\tau)}}\right)\right)^{-1} \qquad (5)$$

where M represents the model compound of interest (i.e., PG or CP), and the rate constants for PG and CP may be obtained from (*20*). Plots of such theoretical $f_{\bullet OH,M(\tau)}$ values are depicted for PG and CP in Figure 4.6 (solid lines) at $R_{ct(\tau)}$ between 10^{-8} and 10^{-3}, where the

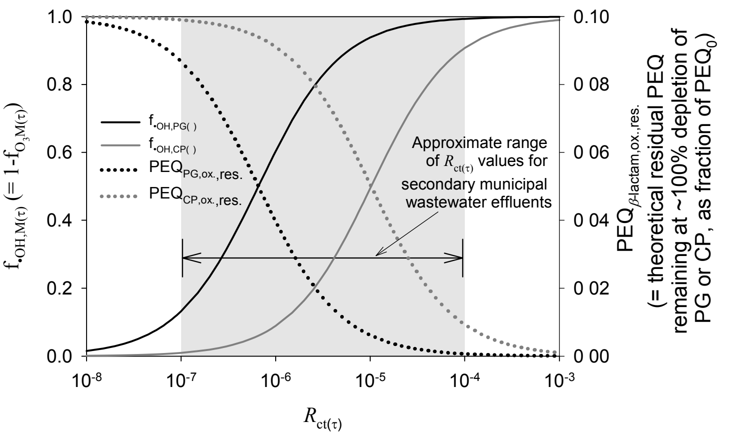

Figure 4.6. Theoretical variations in PG and CP deactivation efficiencies with changing $R_{ct(\tau)}$ (i.e., the cumulative in situ ratio of $^\bullet$OH and O_3 exposures up to an arbitrary reaction time, τ), during ozonation at pH 7. Theoretical fractions, $f_{\bullet OH,M(\tau)}$, of PG and CP oxidation attributable to reactions with $^\bullet$OH are depicted with the corresponding residual antibacterial potencies, $PEQ_{\beta\text{-lactam,ox,res.}}$, expected to result from formation of O_3-derived PG and CP transformation products at oxidant exposures sufficient to yield ~100% depletion of PG and CP. O_3-derived PG and CP products were assumed to contribute activities of ~0.1 PEQ (relative to untreated PG and CP, respectively) to O_3-treated solutions at ~100% depletion of the respective parent molecules (on the basis of the data shown in Figure 4.3), whereas $^\bullet$OH reactions were assumed to lead to roughly stoichiometric elimination of activity (according to the data shown in Figure 4.4c). The approximate range of $R_{ct(\tau)}$ values shown here (shaded in gray) for municipal wastewaters is based on data reported in (*63*).

range of $R_{ct(\tau)}$ values likely to be encountered during ozonation of a typical secondary municipal wastewater (i.e., ~10^{-7}-10^{-4}, based on extrapolation of data reported in (*63,64*) to τ = 0) is shaded gray.

The expected degree of PG and CP deactivation at varying $R_{ct(\tau)}$ values can then be examined by estimating the residual antibacterial activities likely to remain in O_3-treated PG and CP solutions at oxidant doses sufficient to yield complete elimination of each parent *β*-lactam under each $R_{ct(\tau)}$ condition. According to the data presented in Figure 4.3, PG and CP solutions treated with just enough O_3 to completely consume the parent compounds still exhibit ~10% of the corresponding activities of untreated PG and CP solutions, respectively. That is, the levels of biologically-active *β*-lactam oxidation products generated under such conditions are such that their measured activities are equivalent to 0.1 × $PEQ_{\beta\text{-lactam},0}$. On the basis of these data, if one assumes that only O_3 reactions lead to biologically-active products, and that $^{\bullet}$OH reactions lead to nearly quantitative deactivation of PG and CP (consistent with the data shown in Figure 4.4c), the theoretical residual activities, $PEQ_{\beta\text{-lactam,ox.,res.}}$, of O_3-treated PG and CP solutions at oxidant doses sufficient to achieve ~100% PG and CP transformation can be estimated for various hypothetical $R_{ct(\tau)}$ values via eq 6,

$$PEQ_{\beta\text{-lactam,ox.,res.}} = 0.1 \times PEQ_{\beta\text{-lactam,0}} \times f_{O3,M(\tau)} = 0.1 \times (1 - f_{^{\bullet}OH,M(\tau)}) \qquad (6)$$

where $f_{^{\bullet}OH,M(\tau)}$ can be calculated from eq 5, and $PEQ_{\beta\text{-lactam,0}}$ is taken as 1. Plots of the resulting $PEQ_{\beta\text{-lactam,ox.,res.}}$ values for PG and CP are depicted as dotted lines within Figure 4.6.

From these data, one may conclude that the magnitudes of antibacterial activities attributable to formation of biologically-active products during the direct reactions of O_3 with PG or CP will decrease toward zero as the oxidative transformation of each β-lactam is increasingly dominated by $^{\bullet}$OH (i.e., as $R_{ct(\tau)}$ increases). Accordingly, residual activity associated with biologically-active β-lactam products is likely to be appreciable only at the low end of the $R_{ct(\tau)}$ range observed during secondary effluent ozonation, for which O_3 exposure would be sufficient to yield relatively high proportions of O_3-derived oxidation products. Such conditions – which will be found at the left side of the shaded gray region in Figure 4.6 – are most likely to occur only in effluents containing relatively low DOC concentrations (e.g., < 5 mg/L) or high $^{\bullet}$OH scavenger concentrations (e.g., $[\text{carbonate}]_{total}$ > 10 mM), or at high transferred O_3 doses (e.g., > 10 mg/L) (*63,64*). At higher $R_{ct(\tau)}$ values, the proportion of O_3-derived products will be relatively small, and the corresponding antibacterial activity attributable to such products negligible. Furthermore, one should note that the values of $PEQ_{\beta\text{-lactam,ox.,res.}}$ depicted in Figure 4.6 may be interpreted as maximal values, as they do not take into account possible deactivation of biologically-active oxidation products by further reaction with either O_3 or $^{\bullet}$OH. The importance of such secondary reactions, as well as their implications for wastewater ozonation, are discussed in detail within (*30*).

In light of the above discussion, one can infer that the vast majority of the model antibacterial compounds investigated here (including the β-lactams under certain conditions of high $^{\bullet}$OH exposure), in addition to many analogous molecules belonging to the same structural classes, are likely to be ≥99% deactivated at transferred ozone doses sufficient to lower their aqueous concentrations to ≤1% of initial concentrations during ozonation of typical secondary wastewater effluents. According to results reported for various laboratory and pilot-scale investigations of antibacterial compound transformation during wastewater ozonation, this degree of parent compound elimination can typically be achieved at transferred O_3 doses ranging from ~5-10 mg/L during treatment of wastewater effluents containing DOC concentrations of ~5-23 mg/L (*19,20,65*). In the context of total effluent quality considerations, it bears noting here that this level of treatment can also be expected to yield elimination of estrogenic activity derived from phenolic steroid estrogens such as 17-α-ethinylestradiol and 17-β-estradiol (*66*). Thus, municipal wastewater ozonation appears to present an effective, generally-applicable means of rapidly eliminating undesirable biological effects derived from two of the most prevalent biologically-active wastewater-borne micropollutant classes.

Acknowledgements

M.C.D. gratefully acknowledges financial support from a U.S. National Science Foundation Graduate Research Fellowship and the project RECLAIM WATER (Contract-No. 018309) - funded through the Sixth Framework Programme of the European Commission. The authors thank Silvio Canonica, Bill Arnold, Kris Wammer, and Yunho Lee for helpful discussions. Elisabeth Salhi, Thomas Fleischmann, Christoph Werlen, Hans-Ueli Weilenmann, and Vishakha Raina are gratefully acknowledged for technical assistance.

Literature Cited

(1) Hirsch, R.; Ternes, T. A.; Haberer, K.; Kratz, K.-L. Occurrence of antibiotics in the environment. *Sci. Total Environ.* **1999**, *225*, 109-118.
(2) Golet, E. M.; Xifra, I.; Siegrist, H.; Alder, A. C.; Giger, W. Environmental exposure assessment of fluoroquinolone antibacterial agents from sewage to soil. *Environ. Sci. Technol.* **2003**, *37*, 3243-3249.
(3) Göbel, A.; Thomsen, A.; McArdell, C. S.; Joss, A.; Giger, W. Occurrence and sorption behavior of sulfonamides, macrolides, and trimethoprim in activated sludge treatment. *Environ. Sci. Technol.* **2005**, *39*, 3981-3989.
(4) Lindberg, R. H.; Wennberg, P.; Johansson, M. I.; Tysklind, M.; Andersson, B. A. V. Screening of human antibiotic substances and determination of weekly mass flows in five sewage treatment plants in Sweden. *Environ. Sci. Technol.* **2005**, *39*, 3421-3429.
(5) Singer, H.; Muller, S.; Tixier, C.; Pillonel, L. Triclosan: Occurrence and fate of a widely used biocide in the aquatic environment: Field measurements in wastewater treatment plants, surface waters, and lake sediments. *Environ. Sci. Technol.* **2002**, *36*, 4998-5004.
(6) Halden, R. U.; Paull, D. H. Co-occurrence of triclocarban and triclosan in US water resources. *Environ. Sci. Technol.* **2005**, *39*, 1420-1426.
(7) Watkinson, A. J.; Murby, E. J.; Costanzo, S. D. Removal of antibiotics in conventional and advanced wastewater treatment: Implications for environmental discharge and wastewater recycling. *Water Res.* **2007**, *41*, 4164-4176.
(8) Wilson, B. A.; Smith, V. H.; Denoyelles, F.; Larive, C. K. Effects of three pharmaceutical and personal care products on natural freshwater algal assemblages. *Environ. Sci. Technol.* **2003**, *37*, 1713-1719.
(9) Lorian, V., Ed.^Eds. *Antibiotics in Laboratory Medicine*; 4th ed.; Williams and Wilkins: Baltimore, MD, 1996.

(10) Baquero, F. Low-level antibacterial resistance: a gateway to clinical resistance. *Drug Resistance Updates* **2001**, *4*, 93-105.

(11) Drlica, K. The mutant selection window and antimicrobial resistance. *J. Antimicrob. Chemother.* **2003**, *52*, 11-17.

(12) Knapp, C. W.; Engemann, C. A.; Hanson, M. L.; Keen, P. L.; Hall, K. J.; Graham, D. W. Indirect evidence of transposon-mediated selection of antibiotic resistance genes in aquatic systems at low-level oxytetracycline exposures. *Environ. Sci. Technol.* **2008**, *42*, 5348-5353.

(13) Paraskeva, P.; Graham, N. J. D. Ozonation of municipal wastewater effluents. *Water Environ. Res.* **2002**, *74*, 569-581.

(14) Beltran, F. J.; Garcia-Araya, J. F.; Alvarez, P. M. Integration of continuous biological and chemical (ozone) treatment of domestic wastewater: 2. Ozonation followed by biological oxidation. *J. Chem. Technol. Biotechnol.* **1999**, *74*, 884-890.

(15) Boehler, M.; Siegrist, H. Potential of activated sludge disintegration. *Water Sci. Technol.* **2006**, *53*, 207-216.

(16) Dytczak, M. A.; Londry, K. L.; Siegrist, H.; Oleszkiewicz, J. A. Ozonation reduces sludge production and improves denitrification. *Water Res.* **2007**, *41*, 543-550.

(17) Joss, A.; Siegrist, H.; Ternes, T. A. Are we about to upgrade wastewater treatment for removing organic micropollutants? *Water Sci. Technol.* **2008**, *57*, 251-255.

(18) Ternes, T. A.; Stüber, J.; Herrmann, N.; McDowell, D.; Ried, A.; Kampmann, M.; Teiser, B. Ozonation: a tool for removal of pharmaceuticals, contrast media and musk fragrances from wastewater? *Water Research* **2003**, *37*, 1976-1982.

(19) Huber, M. M.; Gobel, A.; Joss, A.; Hermann, N.; Loffler, D.; McArdell, C. S.; Ried, A.; Siegrist, H.; Ternes, T. A.; von Gunten, U. Oxidation of pharmaceuticals during ozonation of municipal wastewater effluents: A pilot study. *Environ. Sci. Technol.* **2005**, *39*, 4290-4299.

(20) Dodd, M. C.; Buffle, M.-O.; von Gunten, U. Oxidation of antibacterial molecules by aqueous ozone: Moiety-specific reaction kinetics and application to ozone-based wastewater treatment. *Environ. Sci. Technol.* **2006**, *40*, 1969-1977.

(21) von Gunten, U. Ozonation of drinking water: Part I. Oxidation kinetics and product formation. *Water Res.* **2003**, *37*, 1443-1467.

(22) Andreozzi, R.; Canterino, M.; Lo Giudice, R.; Marotta, R.; Pinto, G.; Pollio, A. Lincomycin solar photodegradation, algal toxicity and removal from wastewaters by means of ozonation. *Water Res.* **2006**, *40*, 630-638.

(23) Lange, F.; Cornelissen, S.; Kubac, D.; Sein, M. M.; von Sonntag, J.; Hannich, C. B.; Golloch, A.; Heipieper, H. J.; Moder, M.; von Sonntag, C. Degradation of macrolide antibiotics by ozone: A mechanistic case study with clarithromycin. *Chemosphere* **2006**, *65*, 17-23.

(24) Suarez, S.; Dodd, M. C.; Omil, F.; von Gunten, U. Kinetics of triclosan oxidation by aqueous ozone and consequent loss of antibacterial activity: Relevance to municipal wastewater ozonation. *Water Res.* **2007**, *41*, 2481-2490.

(25) Mvula, E.; von Sonntag, C. Ozonolysis of phenols in aqueous solution. *Org. Biomol. Chem.* **2003**, *1*, 1749-1756.

(26) Buffle, M.-O.; Schumacher, J.; von Gunten, U. Ozonation and advanced oxidation of wastewater: Effect of O_3 dose, pH, DOC and HO•-scavengers on ozone decomposition and HO• generation. *Ozone Science and Engineering* **2005**, *Accepted for publication*.

(27) Bader, H.; Hoigné, J. Determination of ozone in water by the indigo method. *Water Res.* **1981**, *15*, 449-456.

(28) Huber, M. M.; Canonica, S.; Park, G. Y.; von Gunten, U. Oxidation of pharmaceuticals during ozonation and advanced oxidation processes. *Environ. Sci. Technol.* **2003**, *37*, 1016-1024.

(29) Qiang, Z.; Adams, C.; Surampalli, R. Determination of ozonation rate constants for lincomycin and spectinomycin. *Ozone: Sci. Eng.* **2004**, *26*, 525-537.

(30) Dodd, M. C.; Rentsch, D.; Singer, H. P.; Kohler, H.-P. E.; von Gunten, U. Transformation of *β*-lactam antibacterials during aqueous ozonation: Reaction mechanisms and quantitative bioassay-directed characterization of biologically-active oxidation products. *In preparation*.

(31) Stead, D. A.; Richards, R. M. E. Sensitive fluorimetric detection of gentamicin sulfate in biological matrices using solid-phase extraction, pre-column derivatization with 9-fluoroenylmethyl chloroformate and reversed phase high-performance liquid chromatography. *Journal of Chromatography B* **1996**, *675*, 295-302.

(32) von Gunten, U.; Oliveras, Y. Advanced oxidation of bromide-containing waters: Bromate formation mechanisms. *Environ. Sci. Technol.* **1998**, *32*, 63-70.

(33) NCCLS, Methods for Dilution Antimicrobial Susceptibility Tests for Bacteria that Grow Aerobically-Fourth Edition; Approved Standard. Available at. NCCLS.

(34) Van der Graaf, P. H.; Schoemaker, R. C. Analysis of asymmetry of agonist concentration-effect curves. *Journal of Pharmacological and Toxicological Methods* **1999**, *41*, 107-115.

(35) Schlünzen, F.; Zarivach, R.; Harms, J.; Bashan, A.; Tocilj, A.; Albrecht, R.; Yonath, A.; Franceschi, F. Structural basis for the interaction of antibiotics with the peptidyl transferase centre in eubacteria. *Nature* **2001**, *413*, 814-821.

(36) Muñoz, F.; von Sonntag, C. The reactions of ozone with tertiary amines including the complexing agents nitrilotriacetic acid (NTA) and ethylenediaminetetraacetic acid (EDTA) in aqueous solution. *J. Chem. Soc., Perkin Trans. 2* **2000**, 2029-2033.

(37) Shen, L. L.; Mitscher, L. A.; Sharma, P. N.; O'Donnell, T. J.; Chu, D. W. T.; Cooper, C. S.; Rosen, T.; Pernet, A. G. Mechanism of inhibition of DNA gyrase by quinolone antibacterials: a cooperative drug-DNA binding model. *Biochemistry* **1989**, *28*, 3886-3894.

(38) Walsh, C. *Antibiotics: Actions, Origins, Resistance*; ASM Press: Washington, D.C., 2003.

(39) Wiedemann, B.; Grimm, H. In *Antibiotics in Laboratory Medicine*; Lorian, V., Ed.; Williams and Wilkins: Baltimore, MD, 1996, pp 900-1168.

(40) Spry, D. O. Oxidation of penicillin and dihydrocephalosporin derivatives with ozone. *J. Org. Chem.* **1972**, *37*, 793-795.

(41) Livermore, D. M.; Williams, J. D. In *Antibiotics in Laboratory Medicine*; 4 ed.; Lorian, V., Ed.; Williams and Wilkins: Baltimore, MD, 1996, pp 502-578.

(42) de Koning, J. J.; Marx, A. F.; Poot, M. M.; Smid, P. M.; Verweij, J. In *Recent Advances in the Chemistry of β-Lactam Antibiotics*; Elks, J., Ed.; The Chemical Society: Burlington House, London (England), 1977; Vol. 28, pp 161-166.

(43) Torii, H.; Asano, T.; Matsumoto, N.; Kato, K.; Tsushima, S.; Kakinuma, A. Microbial oxidation of cephalosporins to cephalosporin sulfoxides. *Agricultural and Biological Chemistry* **1980**, *44*, 1431-1433.

(44) Chan, W. F.; Larson, R. A. Formation of Mutagens from the Aqueous Reactions of Ozone and Anilines. *Water Res.* **1991**, *25*, 1529-1538.

(45) Matsui, M.; Shibata, K.; Muramatsu, H.; Nakazumi, H. Ozonolyses of cytosines and guanine. *J. Org. Chem.* **1991**, *56*, 4987-4990.

(46) Flyunt, R.; Theruvathu, J. A.; Leitzke, A.; von Sonntag, C. The reactions of thymine and thymidine with ozone. *J. Chem. Soc., Perkin Trans. 2* **2002**, 1572-1582.

(47) Matthews, D. A.; Bolin, J. T.; Burridge, J. M.; Filman, D. J.; Volz, K. W.; Kaufman, B. T.; Beddell, C. R.; Champness, J. N.; Stammers, D. K.; Kraut, J. Refined crystal structures of *Escherichia coli* and chicken liver dihydrofolate reductase containing bound trimethoprim. *J. Biol. Chem.* **1985**, *260*, 381-391.

(48) Bailey, P. S. *Ozonation in organic chemistry. II. Non-olefinic compounds*; Academic Press: New York, NY, 1982.

(49) Sztaricskai, F.; Dinya, Z.; Batta, G.; Mocsári, A. Chemical synthesis and structural study of lincomycin sulfoxides and a sulfone. *The Journal of Antibiotics* **1997**, *50*, 866-873.

(50) Dowideit, P.; von Sonntag, C. Reaction of ozone with ethene and its methyl- and chlorine-substituted derivatives in aqueous solution. *Environ. Sci. Technol.* **1998**, *32*, 1112-1119.

(51) Brodersen, D. E.; Clemons, W. M., Jr.; Carter, A. P.; Morgan-Warren, R. J.; Wimberly, B. T.; Ramakrishnan, V. The structural basis for the action of the antibiotics tetracycline, pactamycin, and hygromycin B on the 30S ribosomal subunit. *Cell* **2000**, *103*.

(52) Chopra, I.; Roberts, M. Tetracycline antibiotics: Mode of action, applications, molecular biology, and epidemiology of bacterial resistance. *Microbiol. Mol. Biol. Rev.* **2001**, *65*, 232-260.

(53) Williams, D. H.; Bardsley, B. The vancomycin group of antibiotics and the fight against resistant bacteria. *Angewandte Chemie-International Edition* **1999**, *38*, 1173-1193.

(54) Ragnar, M.; Eriksson, T.; Reitberger, T.; Brandt, P. A new mechanism in the ozone reaction with lignin like structures. *Holzforschung* **1999**, *53*, 423-428.

(55) Carter, A. P.; Clemons, W. M., Jr.; Brodersen, D. E.; Morgan-Warren, R. J.; Wimberly, B. T.; Ramakrishnan, V. Functional insights from the structure of the 30S ribosomal subunit and its interactions with antibiotics. *Nature* **2000**, *407*, 340-348.

(56) Kadurugamuwa, J. L.; Lam, J. S.; Beveridge, T. J. Interaction of gentamicin with the A band and B band lipopolysaccharides of *Pseudomonas aeruginosa* and its possible lethal effect. *Antimicrob. Agents Chemother.* **1993**, *37*, 715-721.

(57) Phillips, G. O.; Power, D. M.; Robinson, C. Chemical changes following γ-irradiation of benzylpenicillin in aqueous solution. *J. Chem. Soc., Perkin Trans. 2* **1973**, 575-582.

(58) Housewright, R. D.; Berkman, S.; Henry, R. J. The relative effectiveness of pure penicillins against Bacillus anthracis in vitro and in vivo. *J. Immunol.* **1947**, *57*, 343-349.

(59) Kavanagh, F. Activities of twenty-two antibacterial substances against nine species of bacteria. *J. Bacteriol.* **1947**, *54*, 761-766.

(60) Heath, R. J.; Rubin, J. R.; Holland, D. R.; Zhang, E. L.; Snow, M. E.; Rock, C. O. Mechanism of triclosan inhibition of bacterial fatty acid synthesis. *J. Biol. Chem.* **1999**, *274*, 11110-11114.

(61) Levy, C. W.; Roujeinikova, A.; Sedelnikova, S.; Baker, P. J.; Stuitje, A. R.; Slabas, A. R.; Rice, D. W.; Rafferty, J. B. Molecular basis of triclosan activity. *Nature* **1999**, *398*, 383-384.

(62) Elovitz, M. S.; von Gunten, U. Hydroxyl radical/ozone ratios during ozonation processes. I. The R_{ct} concept. *Ozone: Sci. Eng.* **1999**, *21*, 239-260.

(63) Buffle, M. O.; Schumacher, J.; Meylan, S.; Jekel, M.; von Gunten, U. Ozonation and advanced oxidation of wastewater: Effect of O_3 dose, pH, DOM and HO•-scavengers on ozone decomposition and HO• generation. *Ozone: Sci. Eng.* **2006**, *28*, 247-259.

(64) Buffle, M. O.; Schumacher, J.; Salhi, E.; Jekel, M.; von Gunten, U. Measurement of the initial phase of ozone decomposition in water and wastewater by means of a continuous quench-flow system: Application to disinfection and pharmaceutical oxidation. *Water Res.* **2006**, *40*, 1884-1894.

(65) Ternes, T. A.; Stuber, J.; Herrmann, N.; McDowell, D.; Ried, A.; Kampmann, M.; Teiser, B. Ozonation: a tool for removal of pharmaceuticals, contrast media and musk fragrances from wastewater? *Water Res.* **2003**, *37*, 1976-1982.

(66) Lee, Y.; Escher, B. I.; von Gunten, U. Efficient removal of the estrogenic activity during oxidative treatment of waters containing steroid estrogens. *Environ. Sci. Technol.* **2008**, *Research ASAPs - DOI: 10.1021/es7023302*

Supporting Information for Chapter 4.

Oxidation of Antibacterial Compounds by Ozone and Hydroxyl Radical: Elimination of Biological Activity during Aqueous Ozonation Processes

7 pages, including 1 narrative and 13 figures

Text S4.1 Error calculations for microdilution and macrodilution assay data

Microdilution assay error calculations. Standard errors of the calibration curves used in HPLC analyses of each model compound were multiplied by the appropriate t-distribution constants to obtain 95% confidence intervals of individual concentration measurements, [C]. Overall confidence intervals for each $[C]/[C]_0$ value were then calculated by propagating the confidence limits of each [C] measurement through the error function obtained via partial differentiation of the expression, $[C]/[C]_0$, with respect to [C] and $[C]_0$. Ninety-five percent confidence intervals were calculated for each EC_{50} value by first multiplying the anti-log of the logarithmic standard errors generated by Prism for each $\log EC_{50}$ value by a t-distribution constant of 1.967 or 1.968, calculated from: (a) d.f. = 3 replicates x 11 samples x 10 serial dilutions/sample - 14 variables = 316, or (b) d.f. = 3 replicates x 11 samples x 10 serial dilutions/sample - 15 variables = 315, where the variables are the 11 sample-specific values of EC_{50} and either (a) the 3 shared values of H, $\%I_{max,t}$, and $\%I_{min,t}$ for eq 2, or (b) the 4 shared values of H, $\%I_{max,t}$, $\%I_{min,t}$, and S for eq 3) to obtain linearized error coefficients. The resulting error coefficients were next multiplied or divided by the appropriate EC_{50} values to obtain the corresponding positive or negative confidence interval, respectively, for each individual EC_{50} value. Ninety-five percent confidence intervals were then calculated for each PEQ (= $EC_{50,0}/EC_{50}$) value in the same manner as for $[C]/[C]_0$.

Macrodiluation assay error calculations. Ninety-five percent confidence intervals for each $[TRI]_{in\ vitro}$ value were calculated according to the same procedure used for concentration measurements obtained via microdilution assay. However, as no serial dilutions of TRI samples other than the control were performed (precluding measurement of EC_{50} values for all but the control), uncertainties were instead calculated for individual %I measurements as follows. First, 95% confidence intervals of triplicate %I, values were calculated from the standard deviations of raw absorbance measurements, A, for each sample replicate and for the respective A_{min} and A_{max} values obtained from replicate negative and positive growth controls. The resulting confidence interval calculations were then propagated through the error function obtained via partial differentiation of eq 1 with respect to A, A_{min}, and A_{max} to obtain overall 95% confidence limits for each %I value. Uncertainties of %I values predicted for the $[TRI]_{in\ vitro}$ values of each oxidant-treated TRI sample were determined by propagating the 95% confidence limits corresponding to $\%I_{min}$, $\%I_{max}$, EC_{50}, and H values obtained via GraphPad Prism for the control data set, in addition to those for the $[TRI]_{in\ vitro}$ values of each oxidant-treated sample (calculated as described above), through the error function obtained via partial differentiation of eq 4 with respect to each of these variables.

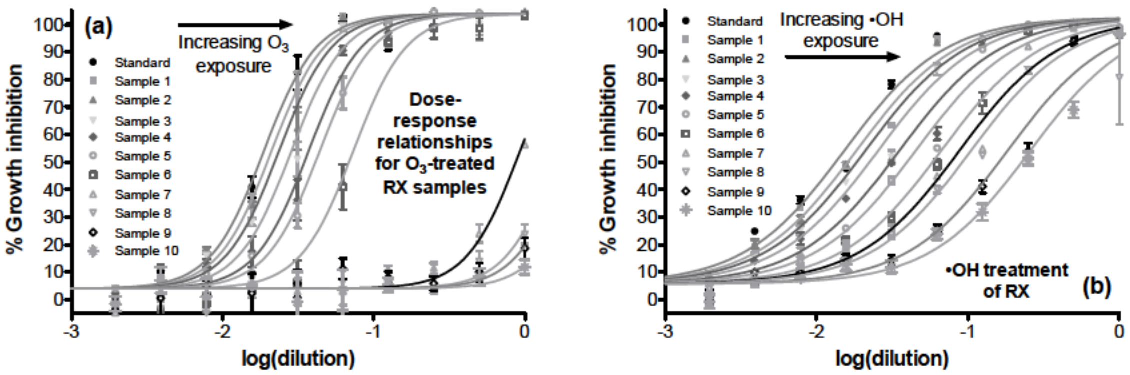

Figure S4.1. Dose-response relationships for oxidation of RX by (a) O_3 and (b) •OH. %I measurements (symbols) depicted with 95% confidence intervals determined for triplicate data sets. Fits (lines) obtained using eq 2 in the main text. The independent variable "dilution" is determined as described in the caption to Figure 4.1 in the main text.

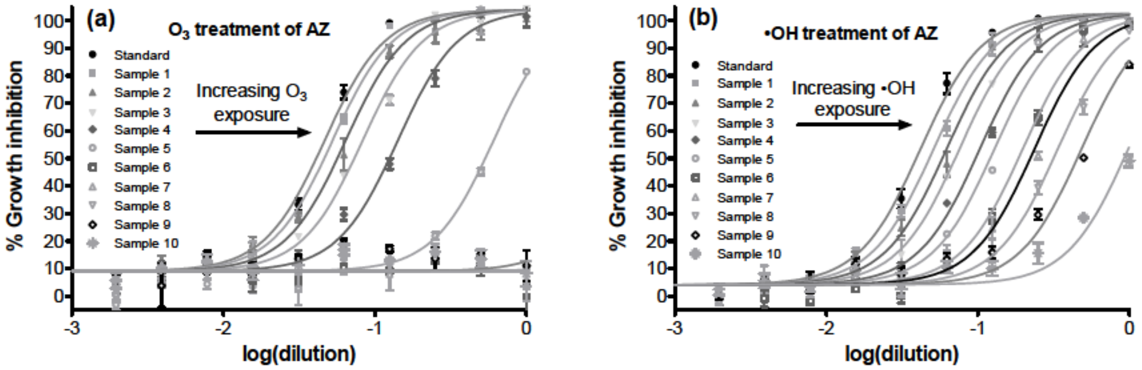

Figure S4.2. Dose-response relationships for oxidation of AZ by (a) O_3 and (b) •OH. %I measurements (symbols) depicted with 95% confidence intervals determined for triplicate data sets. Fits (lines) obtained using eq 2 in the main text. The independent variable "dilution" is determined as described in the caption to Figure 4.1 in the main text.

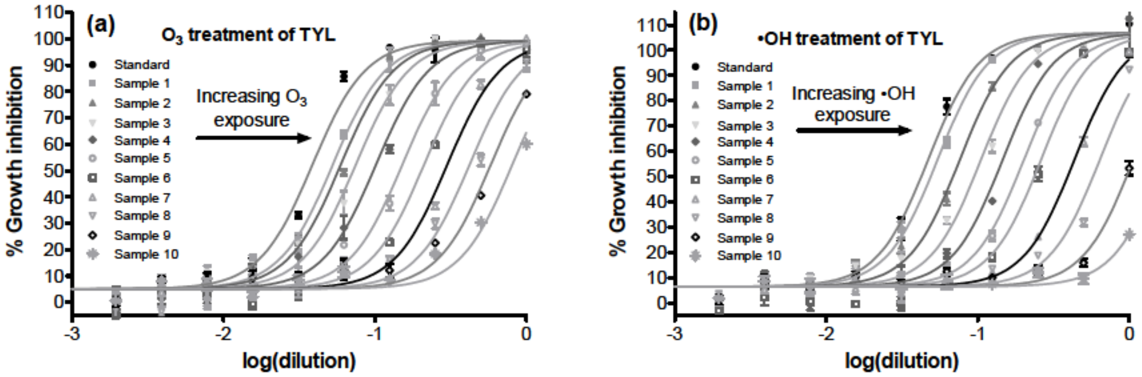

Figure S4.3. Dose-response relationships for oxidation of TYL by (a) O_3 and (b) •OH. %I measurements (symbols) depicted with 95% confidence intervals determined for triplicate data sets. Fits (lines) obtained using eq 2 in the main text. The independent variable "dilution" is determined as described in the caption to Figure 4.1 in the main text.

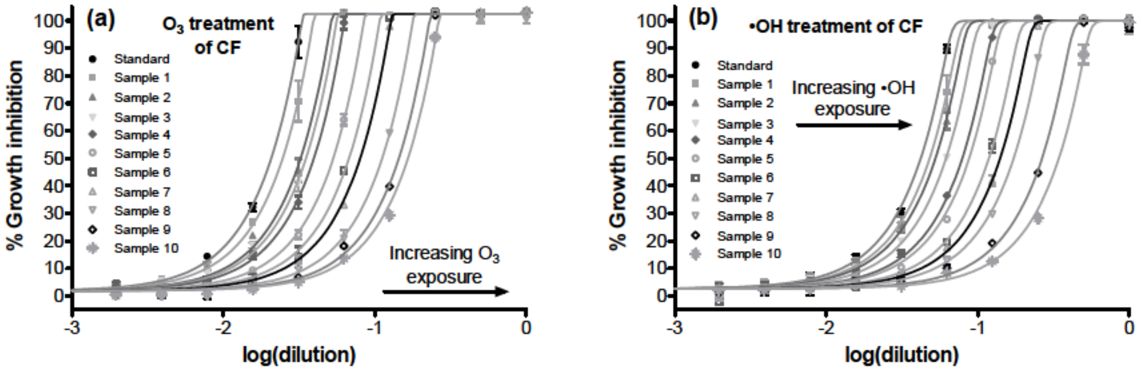

Figure S4.4. Dose-response relationships for oxidation of CF by (a) O_3 and (b) •OH. %I measurements (symbols) depicted with 95% confidence intervals determined for triplicate data sets. Fits (lines) obtained using eq 3 in the main text. The independent variable "dilution" is determined as described in the caption to Figure 4.1 in the main text.

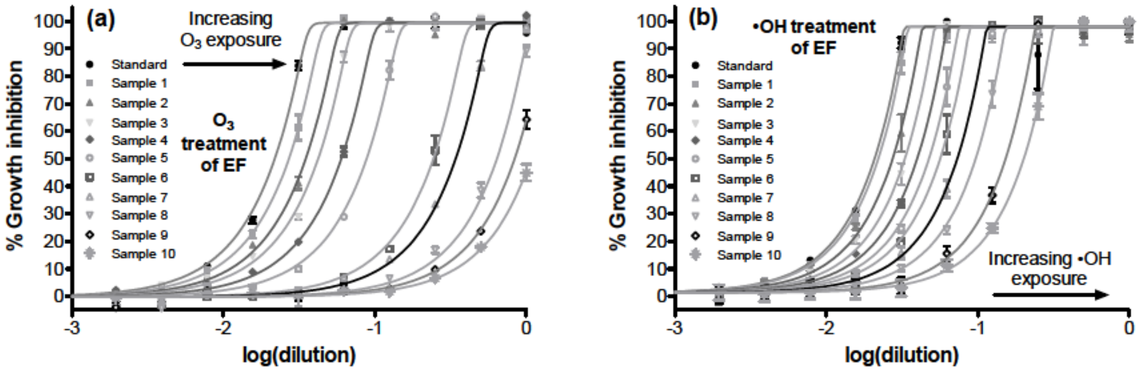

Figure S4.5. Dose-response relationships for oxidation of EF by (a) O_3 and (b) •OH. %I measurements (symbols) depicted with 95% confidence intervals determined for triplicate data sets. Fits (lines) obtained using eq 3 in the main text. The independent variable "dilution" is determined as described in the caption to Figure 4.1 in the main text.

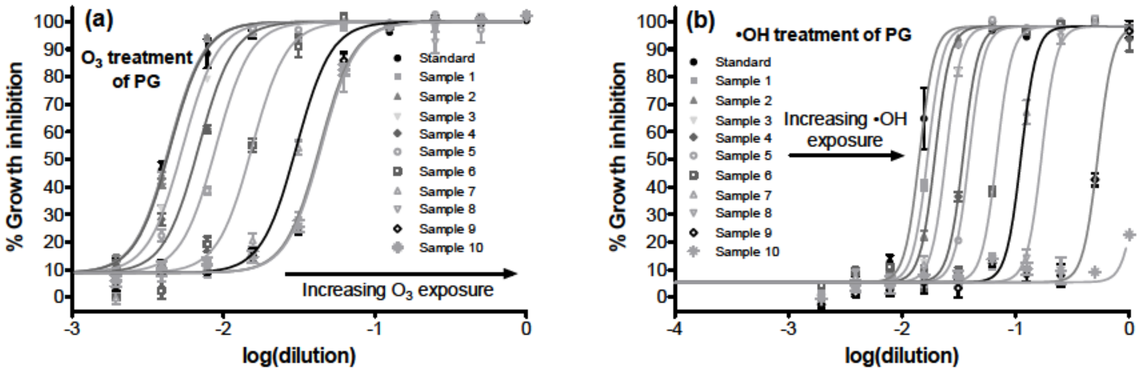

Figure S4.6. Dose-response relationships for oxidation of PG by (a) O_3 and (b) •OH. %I measurements (symbols) depicted with 95% confidence intervals determined for triplicate data sets. Fits (lines) obtained using eq 2 in the main text. The independent variable "dilution" is determined as described in the caption to Figure 4.1 in the main text.

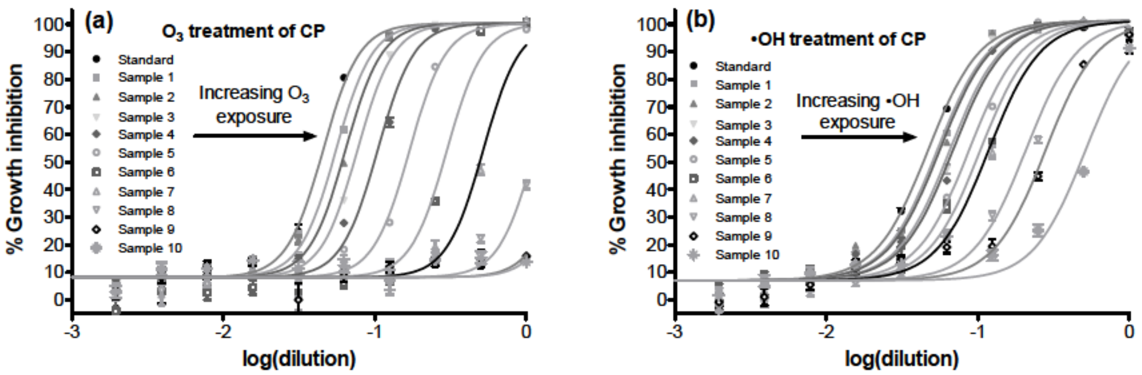

Figure S4.7. Dose-response relationships for oxidation of CP by (a) O_3 and (b) •OH. %I measurements (symbols) depicted with 95% confidence intervals determined for triplicate data sets. Fits (lines) obtained using eq 2 in the main text. The independent variable “dilution” is determined as described in the caption to Figure 4.1 in the main text.

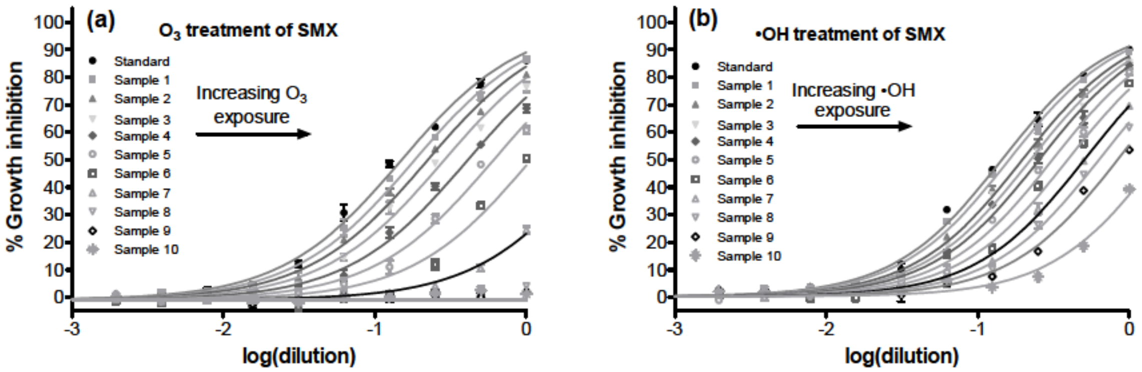

Figure S4.8. Dose-response relationships for oxidation of SMX by (a) O_3 and (b) •OH. %I measurements (symbols) depicted with 95% confidence intervals determined for triplicate data sets. Fits (lines) obtained using eq 2 in the main text. The independent variable “dilution” is determined as described in the caption to Figure 4.1 in the main text.

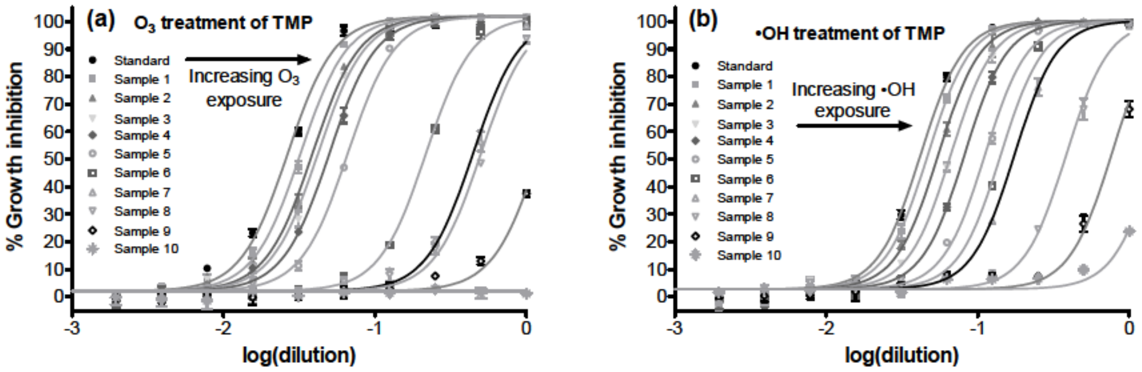

Figure S4.9. Dose-response relationships for oxidation of TMP by (a) O_3 and (b) •OH. %I measurements (symbols) depicted with 95% confidence intervals determined for triplicate data sets. Fits (lines) obtained using eq 2 in the main text. The independent variable “dilution” is determined as described in the caption to Figure 4.1 in the main text.

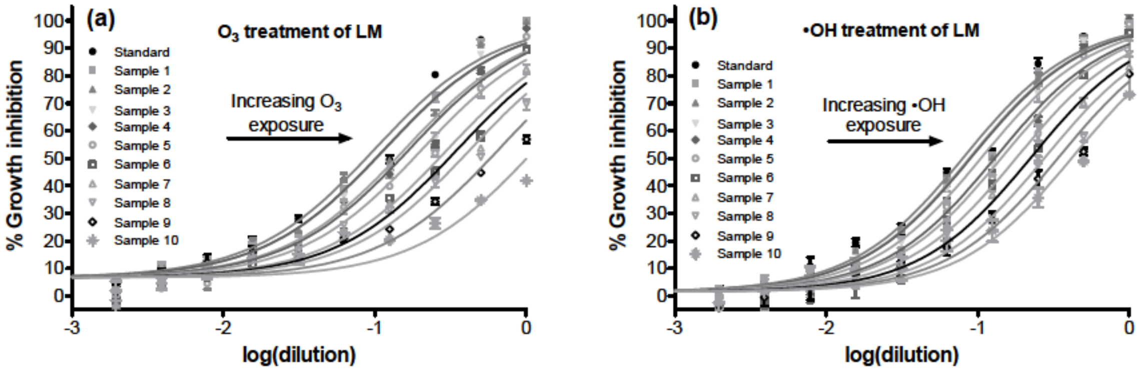

Figure S4.10. Dose-response relationships for oxidation of LM by (a) O_3 and (b) •OH. %I measurements (symbols) depicted with 95% confidence intervals determined for triplicate data sets. Fits (lines) obtained using eq 2 in the main text. The independent variable “dilution” is determined as described in the caption to Figure 4.1 in the main text.

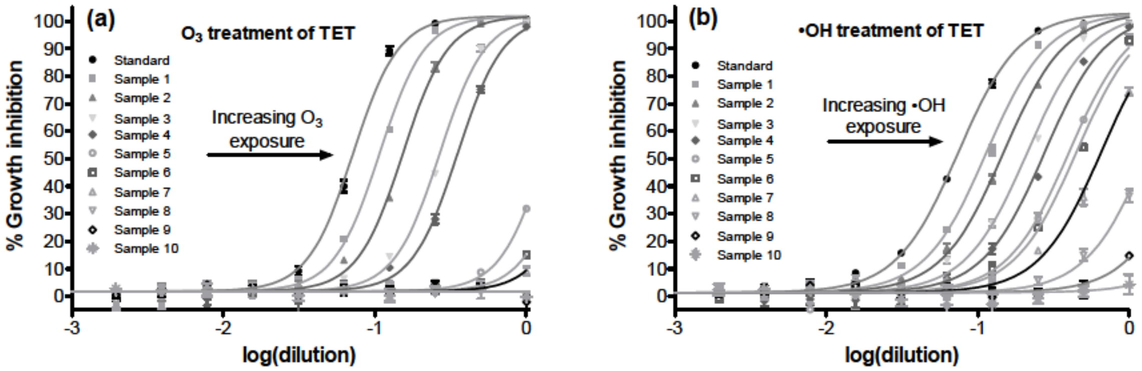

Figure S4.11. Dose-response relationships for oxidation of TET by (a) O_3 and (b) •OH. %I measurements (symbols) depicted with 95% confidence intervals determined for triplicate data sets. Fits (lines) obtained using eq 2 in the main text. The independent variable “dilution” is determined as described in the caption to Figure 4.1 in the main text.

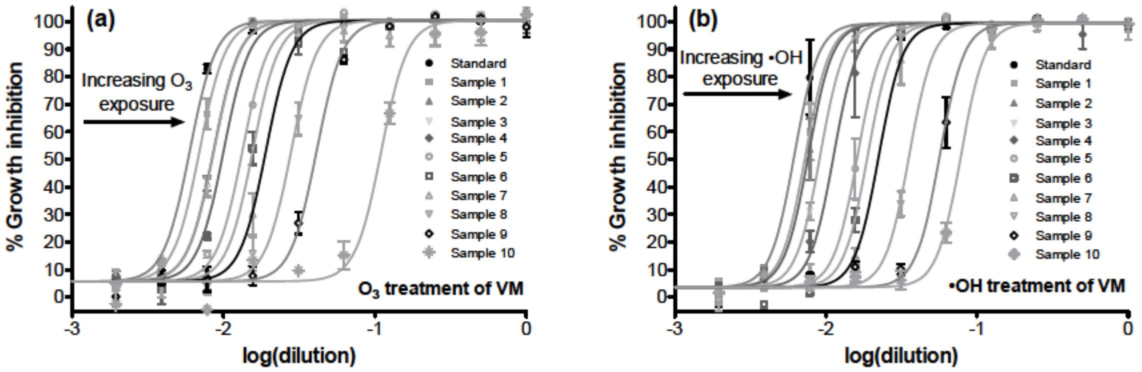

Figure S4.12. Dose-response relationships for oxidation of VM by (a) O_3 and (b) •OH. %I measurements (symbols) depicted with 95% confidence intervals determined for triplicate data sets. Fits (lines) obtained using eq 2 in the main text. The independent variable “dilution” is determined as described in the caption to Figure 4.1 in the main text.

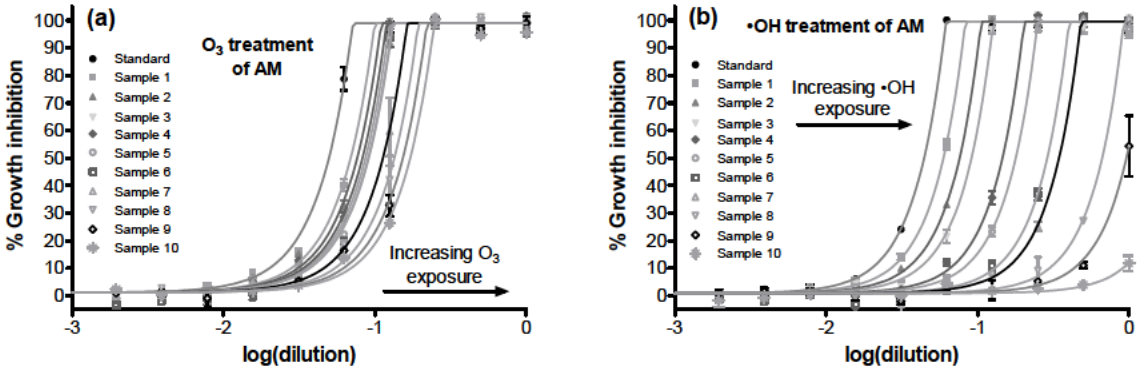

Figure S4.13. Dose-response relationships for oxidation of AM by (a) O$_3$ and (b) •OH. %I measurements (symbols) depicted with 95% confidence intervals determined for triplicate data sets. Fits (lines) obtained using eq 3 in the main text. The independent variable “dilution” is determined as described in the caption to Figure 4.1 in the main text.

Chapter 5. Transformation of *β*-lactam Antibacterial Agents during Aqueous Ozonation: Reaction Pathways and Quantitative Bioassay of Biologically-Active Oxidation Products

Dodd, M. C.; Rentsch, D.; Singer, H. P.; Kohler, H.-P. E.; von Gunten, U.
In preparation for submission to *Environmental Science and Technology*

Abstract

Ozone (O_3) reaction kinetics and pathways were evaluated in depth for the two *β*-lactam antibacterial compounds - penicillin G (PG) and cephalexin (CP) - found to yield biologically active products upon direct reaction with O_3. PG was found to yield two stereoisomeric (*R*)- and (*S*)-sulfoxides, accounting for approximately 100% of the parent compound consumption, in ~55% and ~45% yields, respectively. The former of these was determined to retain ~15% of the potency of the parent PG molecule, whereas the latter was functionally inactive. Each of the PG sulfoxides was determined to be recalcitrant toward further oxidation by O_3. However, the (*R*)-sulfoxide was readily transformed by $^\bullet$OH (with $k''_{\bullet\mathrm{OH,app}} = 7.4 \times 10^9\ \mathrm{M^{-1}s^{-1}}$, at pH 7), resulting in roughly quantitative elimination of its biological activity. CP was found to yield four major transformation products identified as the (*R*)- and (*S*)-sulfoxides of CP (formed in ~34% and ~18% yields) and two C-2/C-3 double bond cleavage products; one a structural analogue of the penicilloic acid of CP - formed in ~5% yield by intermolecular nucleophilic attack of H_2O on the electrophilic C-8 carbon of the CP *β*-lactam ring, the other a 7-piperazine-8,12-dione containing CP derivative - formed in ≥28% yield by intramolecular nucleophilic attack of the N-18 amino nitrogen on the same carbon. The CP-(*R*)-sulfoxide was found to retain ~83% of the parent CP molecule's antibacterial activity, whereas each of the three other CP transformation products was determined to functionally inactive. CP-(*R*)-sulfoxide was found to be susceptible to further oxidation by both O_3 and $^\bullet$OH (with $k''_{\mathrm{O_3,app}} = 2.6 \times 10^4\ \mathrm{M^{-1}s^{-1}}$ and $k''_{\bullet\mathrm{OH,app}} = 7.6 \times 10^9\ \mathrm{M^{-1}s^{-1}}$, at pH 7), leading to approximately quantitative elimination of antibacterial activity in each case. These results indicate that the antibacterial activities of PG, CP, and many structurally-analogous penicillins and cephalosporins should be effectively eliminated during ozonation of municipal wastewaters.

5.1. Introduction.

The *β*-lactams are the largest, most frequently utilized family of organic, clinical-use antibacterial agents (*1-3*). They comprise five primary structural classes – penicillins, cephalosporings, carbapenems, monobactams, and clavans, all of which are naturally- or semi-synthetically constructed around the four-membered *β*-lactam ring (*2*). The most prominent of these classes in North America, according to annual prescriptions are the penicillins and cephalosporins (*3*). The former are characterized by a five-membered 3,3-dimethyl-4-thiaheptane-2-carboxylic acid system fused to the *β*-lactam ring, whereas the latter - which can be semi-synthetically prepared from the former (*1*) - are characterized by a likewise-fused six-membered 3-methyl-5-thiahex-2-ene-2-carboxylic acid system. Two prominent examples of these classes are depicted in Table 5.1, where penicillin G (PG) and cephalexin (CP) provide representative examples of the penicillins and cepalosporins, respectively.

Table 5.1. *β*-lactam model compounds, shown with sites of attack by O_3 at pH 7

Model Compound	Penicillin G (PG)	Cephalexin (CP)
Structure	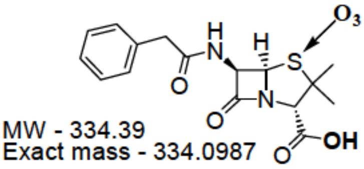 MW - 334.39 Exact mass - 334.0987	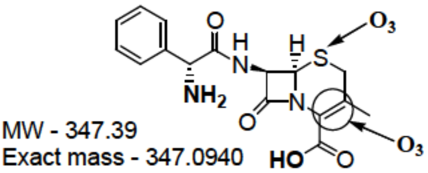 O H N H S O3 NH2 O N O3 HO O MW - 347.39 Exact mass - 347.0940
Structural class	Penicillin	Cephalosporin
$k''_{O_3,app}$ ($M^{-1}s^{-1}$), pH 7	4.8 x 10^{3} [a]	8.7 x 10^{4} [a]
$k''_{\bullet OH,app}$ ($M^{-1}s^{-1}$), pH 7	7.3 x 10^{9} [a]	8.5 x 10^{9} [a]

[a]Apparent rate constants, k''_{app} , obtained from ref. (*4*)

As the annual consumption of penicillin and cephalosporin antibacterials is generally quite large (*3,5,6*), and human metabolism of these compounds relatively minor (*1,7*), they are expected to be excreted in large part intact and discharged in substantial quantities to municipal sewerage systems. Despite this, prior investigators focusing on the fate of penicillins in municipal sewerage and wastewater treatment have concluded that - as a class - these compounds will be generally be easily eliminated during conventional wastewater treatment (*5*), on account of the early-generation penicillins' high susceptibility to acid and/or *β*-lactamase catalyzed hydrolysis of the *β*-lactam ring. However, the penicillins and cephalosporins have each been produced in a multitude of structural variations, many of which were designed to be acid-stable and/or *β*-lactamase resistant (*1,2*). Thus, the widely assumed inconsequentiality of *β*-lactams in municipal wastewater may warrant a second look. This sentiment would seem to be supported by several recent reports in which cephalexin was detected at substantial concentrations in the influents (1-5 μg/L) (*6,8*) and the effluents (0.1-0.3 μg/L) (*8*) of conventional secondary activated sludge clarifiers in Hong Kong and Australia, and even in wastewater-influenced coastal surface water in Hong Kong at levels ranging from 0.01-0.2 μg/L (*9*). The penicillins amoxicillin and penicillin V have also been reported in wastewater effluents at concentrations ranging from 0.01-0.1 μg/L in Italy and Australia, respectively (*6,10*).

Considering the tremendous variety of β-lactams in clinical use (*1,2*), and the knowledge that numerous structural analogues of PG and CP may inhibit the growth of various Gram-negative and -positive bacterial strains at levels within an order of the magnitude of β-lactam levels reported in secondary wastewater influent (*1,11*) (a condition that may favor selection for resistant sub-populations (*12,13*)), the behaviors of these compounds during wastewater treatment take on particular significance. Furthermore, a recent investigation focusing on the exposure of environmental microbial consortia to oxytetracycline indicates that even sub-inhibitory levels of antibacterials may elicit measurable changes in the production of antibiotic resistance genes per bacterial cell in aquatic microbial communities (*14*).

In this context, investigation of wastewater treatment technologies capable of minimizing the exposure of wastewater-borne and environmental bacterial to biologically-active levels of β-lactams and other antibacterial compounds is clearly desirable. Ozonation appears highly promising in this regard, as recent work illustrates that reactions with both O_3 and $^{\bullet}OH$ lead to rapid, quantitative elimination of biological activity (i.e., loss of one mole equivalent of potency per mole of parent compound consumed) for most major classes of antibacterial agents during aqueous ozonation (*4,15*). However, the direct reactions of O_3 with penicillin G and cephalexin – selected as representative models for the penicillin and cephalosporin structural groups, respectively – were found to lead to formation of biologically active transformation products. That is, the measured losses of antibacterial activity during treatment of PG and CP with ozone were observed to lag behind corresponding measured losses of the parent molecules, indicating that one or more of the transformation products generated in these reactions maintain appreciable biological activity (*15*).

O_3 reactions occur primarily at the thioether S atom in PG, and at potentially at either the thioether S, the primary amine, or the C-C double bond in CP (*4,16*). However, the fused *β*-

lactam ring - from which all *β*-lactams ultimately derive their antibacterial activities (via sequestration of bacterial peptidoglycan transpeptidase enzyme and consequent disruption of bacterial cell wall synthesis (*1,2*)), appears to be quite recalcitrant to O_3 in each case (*16*). Reaction of O_3 with the thioether group of many penicillin structures is known to lead to high yields (>95%) of enantiomeric *R*- and *S*-sulfoxides (in *R*:*S* ratios ranging from 1:4 to 24:1) (*16*). Although *S*-sulfoxide analogues of *β*-lactams are generally reported to exhibit negligible antibacterial activities, their *R*-sulfoxide analogues can be quite potent (*17,18*), suggesting that these latter products may be the source of the lags in biological deactivation observed during treatment of PG and CP with O_3. However, the C-2/C-3 double bond or primary amine characteristic of cephalosporins such as CP present potential alternative targets for attack by O_3, for which chemical and biological consequences of resulting structural modifications are unknown.

The present study was undertaken with the objective of identifying the transformation products responsible for the residual antibacterial activities measured in O_3-treated PG and CP solutions. With this goal in mind, the major products generated upon treatment of PG and CP with O_3 were isolated via silica gel chromatography and characterized by a combination of (a) chemical analysis methods including ^{1}H,^{13}C, and ^{15}N-NMR, HPLC-MS/MS, and FT-IR, and (b) microbiological analytical techniques recently developed for measurement of antibacterial activities in oxidant treated solutions of antibacterial compounds. Through this approach, biologically active products were identified, structurally characterized, and quantified, enabling material balances for PG and CP transformation products, as well as quantitative prediction of residual antibacterial activities expected for O_3-treated solutions of PG and CP. Finally, the kinetics and biological outcomes of further reactions of the identified biologically-active products with O_3 and $^{\bullet}$OH were investigated to facilitate assessment of the likelihood that PG and CP will be fully deactivated during municipal wastewater ozonation, in which organic micropollutant oxidation is driven to varying degrees by both O_3 and $^{\bullet}$OH (*4,19,20*).

5.2 Materials and Methods

5.2.1 Chemical reactants and reagents. Penicillin G (PG) sodium salt was purchased from Sigma-Aldrich, whereas cephalexin (CP) hydrate was purchased from both Sigma-Aldrich and MP Biomedicals. These and all other commercially available reagent stocks were of at least 95% purity. O_3 stock solutions were produced as described previously (*21*), and standardized according to direct O_3 absorbance at $\lambda = 258$ nm (using $\varepsilon \cong 3000\ M^{-1}cm^{-1}$).

Stock solutions of antibacterials were prepared in Nanopure or Milli-Q water. Freeze-dried *B. subtilis* Marburg (ATCC 6051) seed cultures were obtained from LGC-Promochem. Working *B. subtilis* stock cultures were maintained at 30° C on #3 nutrient agar. Broth cultures were prepared under sterile conditions by suspending *B. subtilis cells* sampled from the working cultures (from a minimum of five separate colonies) in 5-6 mL of Mueller-Hinton broth within polypropylene test tubes, and incubating overnight at 30°C on a shaker plate rotating at 200 rpm.

5.2.2 Preparation of oxidant-treated model compound solutions for product evolution and biological assay studies. *Ozone.* Solutions of PG, CP, and CP-(*R*)-sulfoxide were prepared at initial concentrations of ~10 μM in 1-mM, pH 7 phosphate buffer, dosed with 5 mM of *t*-BuOH (used as a •OH scavenger), and distributed in 25-mL volumes amongst 11 amber, screw-top, borosilicate glass vials. The vials were then placed in a 20 (±0.5) °C water bath placed on top of a magnetic stir plate. After thermal equilibration, and under constant, rapid stirring, 10 of the vials were dosed with O_3 over a range of concentrations sufficient to cover from between approximately 0.1- to 2-log depletion of the respective parent compound, by directly injecting various volumes of ~ 1.5-mM O_3 stock via gas-tight, glass syringe. The eleventh vial was left untreated, as a negative O_3 control. All vials were then capped and allowed to sit for at least 12 hrs prior to sampling to ensure complete decomposition of O_3 residual in the treated solutions. One-mL aliquots of each O_3-treated sample were then transferred to HPLC vials for analysis of parent compound and/or transformation product concentrations by HPLC-UV (as described below). Prior to biological assay of O_3-treated CP-(*R*)-sulfoxide solutions (according to the broth microdilution assay described below), each solution was treated with catalase to quench any H_2O_2 produced during O_3 treatment.

Hydroxyl radical (•OH). PG-(*R*)-sulfoxide and CP-(*R*)-sulfoxide were treated by $^{\bullet}$OH generated via UV-photolysis of H_2O_2 using a 500-W medium pressure lamp with emission wavelengths < 308 nm screened by a UV-cutoff filter to minimize direct sulfoxide photolysis. One-millimolar, pH 7 phosphate solutions were dosed with initial ~10 μM concentrations of each sulfoxides and 10 mM of H_2O_2, sampled prior to irradiation to obtain an untreated control, and then irradiated in 30-mL quartz test tubes for pre-defined time intervals up to total irradiation periods sufficient to achieve at least 90% depletion of the parent compound. Samples were withdrawn from these solutions between each irradiation period for residual substrate analysis and subsequent microbiological assay. Experiments included a minimum of 10 different irradiation times. Direct photolytic losses of each sulfoxide were demonstrated via negative H_2O_2 control to be < 7% (and typically < 5%) during the full extent of the corresponding irradiation periods. Each •OH-treated sulfoxide solution was analyzed via the HPLC-UV methods listed below for the corresponding parent compound, and assayed for residual antibacterial activity according to the broth microdilution method described below.

5.2.3 Preparation and purification of transformation products generated by reactions of ozone with PG and CP. PG and CP were each dissolved in separate 100 mL volumes of unbuffered deionized water to achieve starting *β*-lactam concentrations of 10 mM. O_3-containing oxygen gas (produced as described in (*21*)) was subsequently bubbled through these solutions for a time sufficient to reach >50% depletion of the parent molecule while still achieving substantial transformation product yields. Each solution was then lyophilized to remove water.

Individual PG transformation products were purified by adding 10-25 mg of freeze-dried solids (per separation) to a 30 x 1.0 cm glass column packed with ~10 g of reversed-phase, silanized (C_2) silica-gel column, eluting isocratically with 25% CH_3CN/75% 0.2% (v/v) CHOOH at a flow rate of ~0.5 mL/min, recovering the eluted fractions (in volumes of ~4 mL) via automated fraction collector for purity determination by HPLC-UV, recombining fractions containing only the same individual product, and lyophilizing to recover the pure (hydrated) solids. Each of the PG sulfoxides was recovered as a fluffy white solid.

Individual CP transformation products were purified by gradient elution of 50-300 mg of freeze-dried solids applied to a 43-g, reversed-phase, RediSep C_{18} silica-gel flash chromatography column, using a Teledyne-ISCO RediSep flash chromatography system operated at 30 mL/min with a gradient method in which conditions were initially held at 100% 10-mM aqueous trifluoroacetic acid (TFA) for 5 minutes, ramped to 5% CH_3CN/95% 10-mM TFA over 10 minutes, held at 5% CH_3CN/95% 10-mM TFA for 25 minutes, ramped to 20% CH_3CN/80% 10-mM TFA over 30 minutes, and finally ramped to 100% CH_3CN over 5 minutes. Eluted 15-mL fractions were collected in glass culture tubes via automated fraction collector, analyzed by HPLC-UV for purity determination, recombined with any other fractions containing – when possible – only the same individual product, and lyophilized to recover the pure (hydrated) solids. Under the chromatographic conditions used, CP-(*R*)-sulfoxide, CP-(*S*)-sulfoxide, and CP-P33 could be isolated in relatively high purity, though CP-P24 and CP-P28 could only be recovered as a mixture with CP-(*S*)-sulfoxide. Each of these CP transformation products (and mixtures thereof) was recovered as a compact, white to yellowish-white solid.

Standards of each product were then prepared by dissolving the isolated, purified solids in solvents appropriate for structural characterization by MS/MS, ^{1}H-NMR, and FT-IR spectroscopy as described below, as well as for biological characterization by the antibacterial activity assay described in detail within (*15*) and summarized below. Purities of each PG and CP sulfoxide were determined via HPLC-UV, by comparing the relative peak heights of the parent molecule with its sulfoxide products at 205 nm (for PG and products) or 254 nm (for CP and products), assuming negligible differences amongst the spectra and/or molar absorptivities of each species (on account of the effectively identical structures of their chromophoric functional groups). The purities of CP-P24, CP-P28, and CP-P33 were estimated via ^{1}H-NMR as described below. The purity values of the solids used for quantification were in turn determined as ~66%, ~99%, ~65%, ~36%, ~36, ~4%, and ≥51% for PG-(*R*)-sulfoxide, PG-(*S*)-sulfoxide, CP-(*R*)-sulfoxide, CP-(*S*)-sulfoxide (mixture), CP-P24 (mixture), CP-P28 (mixture), and CP-P33, respectively.

5.2.4 Chemical analyses of PG, CP, and purified transformation products. *HPLC-UV analyses.* PG and PG transformation products were analyzed at 205 nm via gradient elution with a flow rate of 0.5 mL/min, using a 250 mm × 3.0 mm, 5-µM particle size Supelco Discovery RP Amide C_{16} column on either an Agilent 1100 or Dionex UltiMate 3000 HPLC system, each equipped with thermostatted autosampler chambers (cooled to 5 °C), photodiode array detectors, and column thermostats (heated to 30 °C), where the mobile phase was pre-equilibrated at 25% CH_3CN/75% 10-mM H_3PO_4 for 5 minutes prior to sample injection, ramped to 45% CH_3CN/55% 10-mM H_3PO_4 over 15 minutes following injection, and finally ramped to 95% CH_3CN/5% 10-mM H_3PO_4 over 5 minutes. CP and CP transformation products were analyzed at 205 and 254 nm via gradient elution with a flow rate of 0.25 mL/min, using a 250 mm × 2.0 mm, 5-µM particle size Macherey-Nagel Nucleosil RP C_{18} HD column on either of the previously described HPLC systems, where the mobile phase was pre-equilibrated at 100% 0.2% (v/v) CHOOH for 10 minutes prior to sample injection, held at 100% 0.2% (v/v) CHOOH for 10 minutes following injection, ramped to 10% CH_3CN/90% 0.2% (v/v) CHOOH over 20 minutes, ramped to 20% CH_3CN/80% 0.2% (v/v) CHOOH over 10 minutes, and finally ramped to 95% CH_3CN/5% 0.2% (v/v) CHOOH over 5 minutes. All other HPLC analyses of the *β*-lactams and their transformation products were conducted according to these procedures unless stated otherwise.

NMR analyses. Stereochemical information for each purified *β*-lactam transformation product was obtained from ^{1}H, ^{13}C and ^{15}N NMR spectra recorded at 400.13 (100.61 and 40.56) MHz on a Bruker Avance-400 NMR spectrometer (Bruker Bio-spin AG, Fällanden, Switzerland) operated at 297 K, using samples of 1-2 mg solids dissolved in appropriate deuterated solvents, where chemical shifts of each PG product were acquired for DMSO-d_6 and $CDCl_3$, and shifts of each CP product were acquired for D_2O and DMSO-d_6.

The ^1H and 1D-NOESY spectra, the 1D-^{13}C NMR spectra and the ^1H,^{13}C HSQC, ^1H,^{13}C HMBC and ^1H,^{15}N HMQC correlation experiments were performed at 298 K using a 5-mm broadband inverse probe with z-gradient (100% gradient strength of 53.5 G/cm) and 90° pulse lengths of 6.8 μs (^1H), 14.9 μs (^{13}C) and 20.7 μs (^{15}N). All spectra were recorded with the Bruker standard pulse programs and parameter sets with selection of coupling constants of 145Hz (HSQC), 10 Hz (HMBC), 3 or 90 Hz (HMQC) and mixing times of 1s (1D-NOESY, 50 ms selective 180º inversion pulses). The ^1H/^{13}C chemical shifts were referenced internally using the resonance signals of DMSO-d_6 at 2.49/39.5 ppm, $CDCl_3$ at 7.26/77.0 ppm and D_2O at 4.70 ppm (^{13}C chemical shifts in water were referenced to an external sample of 3-trimethylsilyl tetradeutero sodium propionate in D_2O at -0.2 ppm). The ^{15}N chemical shifts were externally referenced to a sample containing nitromethane (2M in DMSO-d_6) at 0 ppm.

Estimation of transformation product isolate purities by ^1H-NMR. The relative purities of CP-(*S*)-sulfoxide, CP-P24, and CP-P28 within the mixture of these three components were estimated on the basis of relative component-specific ^1H peak areas observed in ^1H-NMR spectra of the mixture. The relative magnitudes of these per-proton peak areas were found to be roughly 1.05:0.95:0.05. The mass proportions of the CP-P24 and CP-P28 solids in the solids mixture were calculated on the basis of the known purity of CP-(*S*)-sulfoxide (determined as described above), the per-proton peak areas, and the molecular weights of each product. The molecular weight of CP-P28 was estimated as ~397 (within the range of molecular weights observed for all identified CP transformation products), in the absence of definitive mass spectral data.

The minimum purity of isolated CP-P33 solids was estimated by analysis of the approximate water content of the solids via H^1-NMR. Pure samples of the DMSO-d_6 used in this investigation were analyzed via ^1H-NMR to determine their approximate H_2O content. The H_2O peaks in these samples were found to have areas equal to no less than ~6% of the corresponding DMSO-d_6 peaks. On the basis of this value, the areas of water peaks observed in the ^1H spectra of a sample of CP-P33 were corrected by subtracting a peak area equal to 6% of the DMSO-d_6 peak area measured for this sample. The resulting value was further adjusted by subtracting the areas of any overlapping peaks attributable to protons within the CP-P33 molecule(s). The residual water peak area was then divided by two (the number of protons in H_2O), to obtain the approximate signal area per water proton. Subsequently, the signal areas obtained for all protons belonging to CP-P33 were summed and divided by the total expected number of CP-P33 protons to obtain the approximate per proton signal area for CP-P33. Finally, the water content of CP-P33 was estimated from the ratio of the calculated per proton signal areas for water and CP-P33. Assuming that the only significant impurity present in the isolated solids of the isolated CP-P33 solids was H_2O (consistent with NMR and HPLC-UV_{205nm} analyses of each sample), the minimum purity of CP-P33 was calculated directly from its measured water content (where purity = 100% – %H_2O).

LC-MS/MS analyses. Samples of each purified β-lactam transformation product were prepared at concentrations ranging from 100 μM to 1 mM and transferred to amber, borosilicate glass HPLC vials for analysis by HPLC-MS/MS using a HPLC system comprising the same Macherey-Nagel column as above, a Rheos 2200 quaternary pump (Flux Instruments; Reinach, Switzerland), and a PAL autosampler (CTC Analytics; Zwinger, Switzerland), interfaced with a LTQ-Orbitrap hybrid MS^n system consisting of a LTQ linear-ion trap and Orbitrap Fourier-transform (FT) mass spectrometer (Thermo Scientific; Waltham, MA, U.S.A.).

PG and PG transformation products were eluted by HPLC using a gradient method in which mobile phase composition was held at 10% CH_3CN/90% 0.2% (v/v) CHOOH for 5 minutes prior to sample injection and ramped to 80% CH_3CN/20% 0.2% (v/v) CHOOH over 20 minutes following injection, whereas CP and CP transformation product elutions were performed according to the same gradient conditions described above. LTQ and Orbitrap analyses were generally conducted using positive mode electrospray ionization (ESI^+) with collisional induced dissociation (CID) over a typical mass scan range of 50 to 600 m/z, with normalized collisional energy set to between 35 and 50%, source voltage to 3.5 kV, tube lens voltage to 80 V, capillary voltage to 20 V, and capillary temperature to 350º C. Sheath and auxiliary gas flow rates (using N_2) were set to 0.6 and 1.5 L/min. High-resolution MS and MS^2 analyses conducted for acquisition of exact analyte masses (to four-decimal accuracy) were performed using the Orbitrap as detector. Several negative mode (ESI^-) analyses were performed of CP-P33, with the source voltage, tube lens voltage, capillary voltage, and capillary temperature set to 4 kV, -78 V, -19 V, and 325º C, respectively, and the sheath and auxiliary gas flow rates (also using N_2) set to 0.4 and 6 L/min.

FT-IR analyses. Solid-state FTIR spectra for purified samples of each β-lactam transformation product were recorded on a Biorad FTS 575C instrument equipped with a mercury cadmium telluride (MCT) detector and a nine-reflection diamond ATR unit with KRS-5 optics (SensIR Technologies, Danbury, CT). The diameter of the round probing area of the diamond was 4 mm. Scans were acquired at 0.5 cm^{-1} resolution, from 400 to 4000 cm^{-1}, with subtraction of the appropriate background spectrum.

5.2.5 Measurement of antibacterial activities via broth microdilution assay. *Assay of purified transformation products resulting from treatment of PG and CP with O_3.* The biological activities of each major β-lactam transformation product relative to its parent molecule were determined according to the broth microdilution assay described in detail within (*15*). Briefly, ~1-10 μM solutions (prior to dilution) of each transformation product in 1-mM, pH 7 phosphate buffer were used to prepare 10-member 1:1 serial dilution series across each row of a standard 96-well microtiter plate. Standard dilution series were prepared from a corresponding untreated sample of each parent molecule for assay with the treated samples. Each sample and standard solution volume was then inoculated with an equal volume of Mueller-Hinton broth containing a 1 x 10^6 CFU/mL cell density of the *B. subtilis* reference strain, and allowed to incubate under 200 rpm agitation, at 30 °C, for 8 h. After incubation, the absorbance of each sample and standard solution was taken at 625 nm, as a surrogate for cell density (*22*). Absorbance measurements were then analyzed according to the procedures described for PG and CP in (*15*) to obtain fitted dose-response relationships and corresponding uncertainties.

Measured activities of the transformation products were then evaluated relative to the corresponding parent molecule in terms of "potency-equivalent" (PEQ) values, via eq 1,

$$\text{PEQ (in mol/L)} = \text{EC}_{50,\beta\text{-lactam}} / \text{EC}_{50,\text{x}} \quad (1)$$

where $\text{EC}_{50,\beta\text{-lactam}}$ is the EC_{50} value (the effective antibacterial concentration, or sample dilution in this case, at which 50% growth inhibition is observed) calculated from the measured dose-response relationship for the parent molecule, and $\text{EC}_{50,\text{x}}$ represents the EC_{50} value calculated from the measured dose-response relationship obtained for a given transformation product or transformation product mixture.

Assay of β-lactam sulfoxide solutions following treatment with O_3 and $^{\bullet}OH$. The biological activities of each β-lactam-(*R*)-sulfoxide following treatment with O_3 or $^{\bullet}OH$ were also determined according to the broth microdilution assay described in (*15*). Briefly, oxidant-treated, catalase-amended solutions of each sulfoxide were used to prepare 10-member 1:1 serial dilution series across each row of a standard 96-well microtiter plate. Standard dilution series were prepared from a corresponding untreated sample of each sulfoxide for assay with the treated samples. Each sample and standard solution volume was then processed as described above to obtain the corresponding $\text{EC}_{50,\text{x}}$ values. PEQ values were then calculated from eq 1 and correlated with normalized residual concentrations, $[C]/[C]_0$, of the corresponding parent molecule (measured by HPLC-UV) to evaluate the stoichiometry of *β*-lactam sulfoxide activity elimination.

5.2.6 Measurement of apparent second-order rate constants for reactions of β-lactam-(*R*)-sulfoxides with O_3 and $^\bullet$OH. The apparent second-order rate constants, $k''_{\mathrm{O_3,app}}$, for CP-(*R*)-sulfoxide, and, $k''_{^\bullet\mathrm{OH,app}}$, for PG-(*R*)-sulfoxide and CP-(*R*)-sulfoxide, at pH 7 were determined using a two-endpoint measurement competition kinetics method as described in (*4*). Briefly, 10 uM solutions of each sulfoxide in 1-mM, pH 7 phosphate buffer (also amended with 5-mM of *t*-BuOH for O_3 kinetics experiments) were dosed with 10 μM of a reference competitor for which the corresponding rate constant was already known (i.e., PG for the O_3 experiment, where $k''_{\mathrm{O_3,app,PG}} = 4.8 \times 10^3\ \mathrm{M^{-1}s^{-1}}$ (*4*), and *para*-chlorobenzoic acid (*p*CBA) for $^\bullet$OH experiments, where $k''_{^\bullet\mathrm{OH,app},p\mathrm{CBA}} = 5 \times 10^9\ \mathrm{M^{-1}s^{-1}}$ (*23*)). Following treatment with varying oxidant exposures (via the same methods described above for evaluation of PG and CP product evolution), two endpoints – residual model compound and reference competitor concentrations remaining after oxidant treatment – were measured for each experimental solution by HPLC-UV (using adaptations of the HPLC methods described above). Rate constants were then obtained via eq 2,

$$\ln\left(\frac{[\mathrm{M}]}{[\mathrm{M}]_0}\right) = \ln\left(\frac{[\mathrm{C}]}{[\mathrm{C}]_0}\right)\frac{k''_{\mathrm{O_3,app,M}}}{k''_{\mathrm{O_3,app,C}}} \qquad (2)$$

where M represents the sulfoxide, C the reference competitor, $k''_{\mathrm{O_3,app,M}}$ could be determined from the slope of a plot of $\ln\left(\frac{[\mathrm{M}]}{[\mathrm{M}]_0}\right)$ vs. $\ln\left(\frac{[\mathrm{C}]}{[\mathrm{C}]_0}\right)$, $k''_{\mathrm{O_3,app,C}}$ was known, and $[M]_0$ and $[C]_0$ were obtained from HPLC-UV analyses of oxidant controls included in each experiment. $k''_{\mathrm{O_3,app,CP\text{-}(\mathit{R})\text{-}sulfoxide}}$ was obtained from a series of 10 individual solutions treated with distinct O_3 doses, whereas $k''_{^\bullet\mathrm{OH,app,PG\text{-}(\mathit{R})\text{-}sulfoxide}}$ and $k''_{^\bullet\mathrm{OH,app,CP\text{-}(\mathit{R})\text{-}sulfoxide}}$ were each determined via exposure of duplicate solutions of each sulfoxide to increasing $^\bullet$OH exposures.

5.3 Results and Discussion

5.3.1. Identification of major products resulting from reactions of PG and CP with O_3. *Products of the PG-O_3 reaction.* Only two major transformation products were detected in

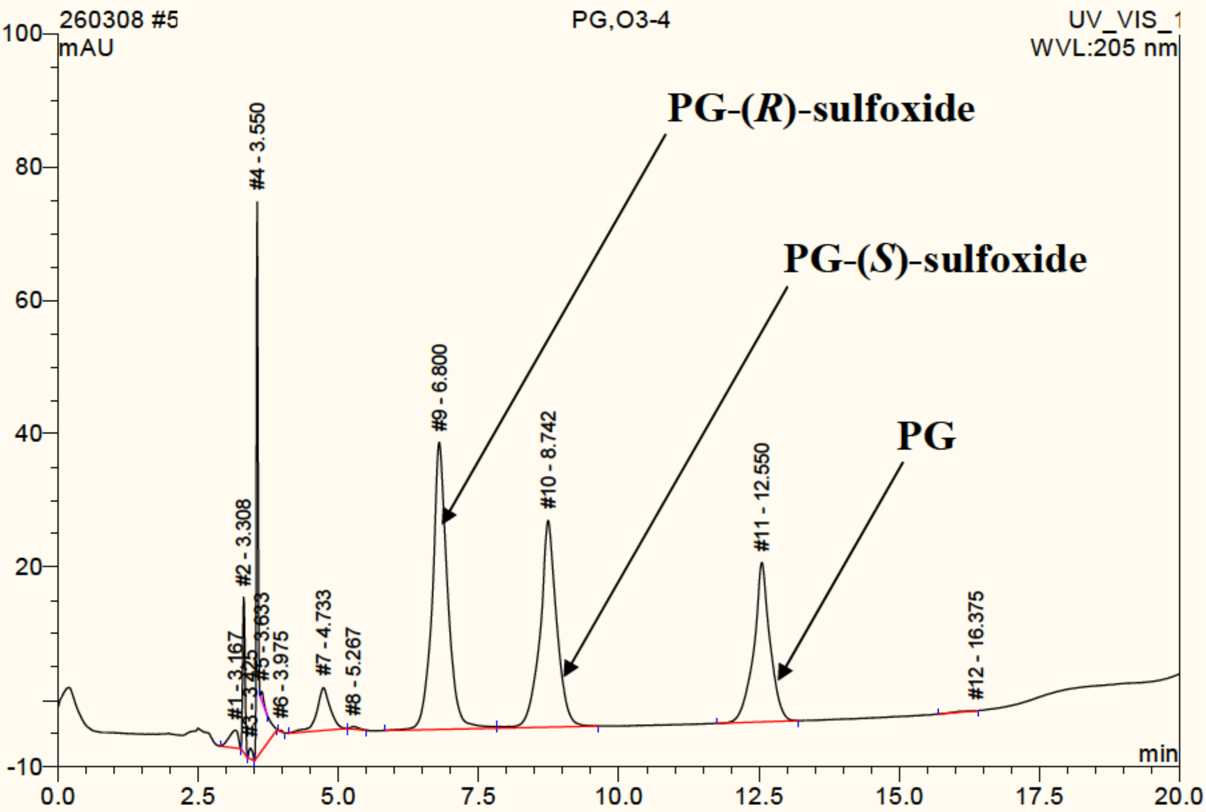

Figure 5.1. Chromatogram of 10 µM PG treated with ~8 µM of O_3 at pH 7, in 1-mM phosphate buffer amended with 5-mM *t*-BuOH, acquired at $\lambda = 205$ nm with the HPLC-UV method described for PG analyses in the Materials and Methods section

the O_3-PG reaction, as shown in a representative UV chromatogram obtained for a sample of an O_3-treated PG solution at $\lambda = 205$ nm (Figure 5.1). The UV spectra of the two products (acquired via HPLC-UV) were effectively identical to that of PG (Figure S5.1). Each of the products was substantially more polar (i.e., earlier eluting) than PG, permitting their isolation from the parent molecule via C_2 reversed-phase silica gel chromatography. Following lyophilisation of the recovered chromatographic fractions, purified solids were subjected to structural analysis by LC-MS/MS, ^{1}H-, ^{13}C-, and ^{15}N-NMR, and FT-IR.

High-resolution mass spectrometry of PG and the two isolated products yielded the mass spectra shown in the Supporting Information, Figures S5.3-S5.5, from which exact masses could be determined for each analyte. The exact mass of the two products were found to be identical (i.e., 350.0933). Comparison of the exact product masses with that of PG (334.0984) illustrates that both products contain an additional oxygen atom (M + 15.9949). Furthermore, isolation and fragmentation of each product's molecular ion via MS^2 yields the spectra depicted in Figures S5.4b and S5.5b, which are also effectively identical. FT-IR spectra demonstrating a strong absorbance band between 1000 and 1100 cm^{-1} suggest the presence of a sulfoxide group in each product molecule (Figure S5.12b and c) (*24*), which is consistent with the available mass spectral data. Taken together with the previous observation that O_3 reacts directly with the PG thioether (*4*), as well as prior identification of typical products of the reaction between penicillins and O_3 (*16*), these data allow one to tentatively conclude that the two PG transformation products are stereoisomeric sulfoxides of PG (Figure 5.2), but do not permit distinction between their individual stereochemistries.

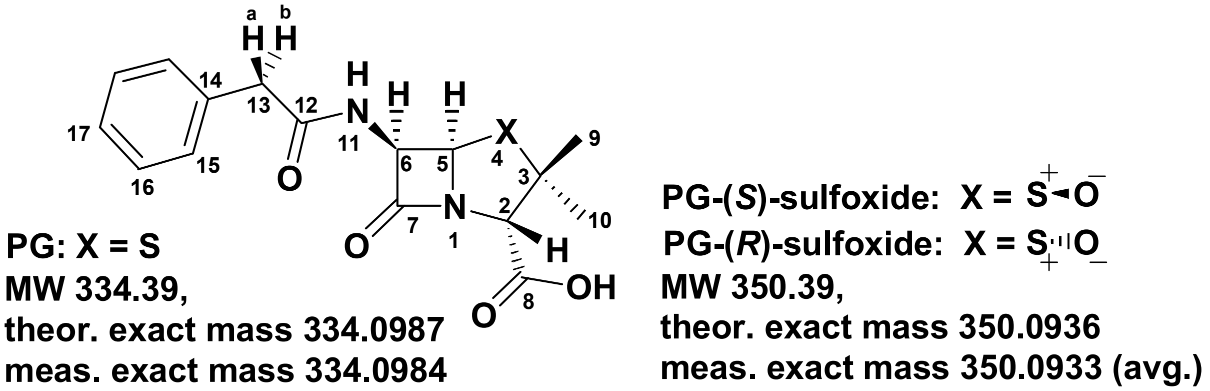

PG: X = S
MW 334.39,
theor. exact mass 334.0987
meas. exact mass 334.0984

PG-(*S*)-sulfoxide: X = $S^{+}\rightarrow O^{-}$
PG-(*R*)-sulfoxide: X = $S^{+}\cdots O^{-}$
MW 350.39,
theor. exact mass 350.0936
meas. exact mass 350.0933 (avg.)

Figure 5.2. Atom numbering and postulated stereochemistries of PG and PG sulfoxides

Multi-nuclear NMR of the isolated solids for each sulfoxide in DMSO-d_6 and $CDCl_3$ was conducted to acquire more detailed information as to the sulfoxide stereochemistries. The spectra and corresponding tabular data obtained from these analyses are summarized in Figures S5.14-S5.15 and Tables S5.1, S5.2, and S5.7. Examination of the orientations of the sulfoxide oxygen atoms for the two PG sulfoxide configurations depicted in Figure 5.2 indicates that the O-5 atom of PG-(*S*)-sulfoxide may form an intramolecular H-bond with its H-11 (NH) atom, whereas a corresponding *intra*molecular H-bond cannot form for PG or PG-(*R*)-sulfoxide. This characteristic of the penicillin and cephalosporin sulfoxides has previously been demonstrated to provide a reliable means of identifying (*R*)- and (*S*)-sulfoxides via ^{1}H-NMR studies of hydrogen-bonding behavior in polar, H-bonding and non-H-bonding solvents (*25,26*). In $CDCl_3$ (which can form no H-bonds with H-11), a $\delta(^1H)$ value of 6.02 was observed for the more polar (i.e., earler eluting, Figure 5.1) of the two sulfoxides, and a value of 7.08 ppm was observed for the less polar (i.e., later eluting, Figure 5.1) sulfoxide (Figure S5.14). However, in DMSO-d_6 (which can form a stable *inter*molecular H-bond with the H-11 proton), a $\Delta\delta(^1H)$ of ~3.2 ppm was found for H-11 of the more polar sulfoxide (Figure S5.15), whereas a comparably small $\Delta\delta(^1H)$ of 0.9 ppm was observed for H-11 of the less polar sulfoxide. With regards to the less polar sulfoxide, the observation of moderate deshielding for H-11 in $CDCl_3$, combined with the observation of relative shielding of this H-11 in DMSO-d_6, are indicative of the presence of an *intra*molecular H-bond. When taken with the very large deshielding effect observed for the more polar sulfoxide in switching from $CDCl_3$ to DMSO-d_6 (indicative of strong *inter*molecular H-bonding in the latter solvent), these data strongly suggest the (*R*)- and (*S*)-configurations for the more polar and less polar sulfoxide isomers, respectively.

The resonances of the H-10 methyl trio for all three compounds were assigned from the 1D-NOESY spectra with magnetization transfers from H-5 to H-10. The introduction of the sulfoxide groups in position 4 appeared to induce downfield shifts of 10-12 ppm for C-5 via deshielding effects, whereas the ^{13}C chemical shifts of C-2 exhibited upfield shifts of 8-10 ppm. The effects on C-3 were less pronounced. Strong HMBC cross signals were found for H-2 to C-10 but only weak correlation signals were found from H-2 to C-9 for the two PG-sulfoxides. On account of the apparently small H-2/C-9 coupling constants and H-2/C-2/C-3/C-9 bond angles (near 90º), C-9 atoms are suspected to sit in pseudo equatorial and C-10 atoms in pseudo axial positions. These and all other available spectra data are consistent with identification of the two PG transformation products as the *R*- and *S*-sulfoxide molecules depicted in Figure 5.2, in agreement with prior investigations of the reactions between O_3 and various penicillins (not including penicillin G) (*16*).

Products of the CP-O_3 reaction. Five major products were observed upon treatment of CP with O_3, as shown in a representative UV chromatogram for a sample obtained for an O_3-treated solution of CP at $\lambda = 254$ nm (Figure 5.3). The UV spectra of the two most polar products (acquired via HPLC-UV) were effectively identical to that of CP, whereas the spectra for the three other products lacked the 254 nm absorbance band characteristic of CP's conjugated alkene-carboxylic acid system (Figure S5.2). All five products were substantially more polar (i.e., earlier eluting) than CP, permitting their isolation from the parent molecule via reversed-phase silica gel chromatography. On account of their highly similar polarities and poor retention on C_2 reversed-phase silica gel, chromatography on C_{18} reversed-phase silica gel with a strong ion-pairing reagent (i.e., TFA) was necessary to improve resolution each of the products. Ultimately, however, even using a C_{18} stationary-phase with TFA was insufficient to resolve several of the products. Consequently, only the two most polar and the least polar of the five transformation products (Figure 5.3) could be isolated as relatively pure solids, whereas the third and fourth most polar (Figure 5.3) could only be isolated in a mixture with the second most polar. As for PG, following chromatographic purification, the recovered fractions of each product or product mixture were freeze-dried to facilitate recovery of solids for subsequent structural analysis by LC-MS/MS, multi-nuclear NMR, and FT-IR.

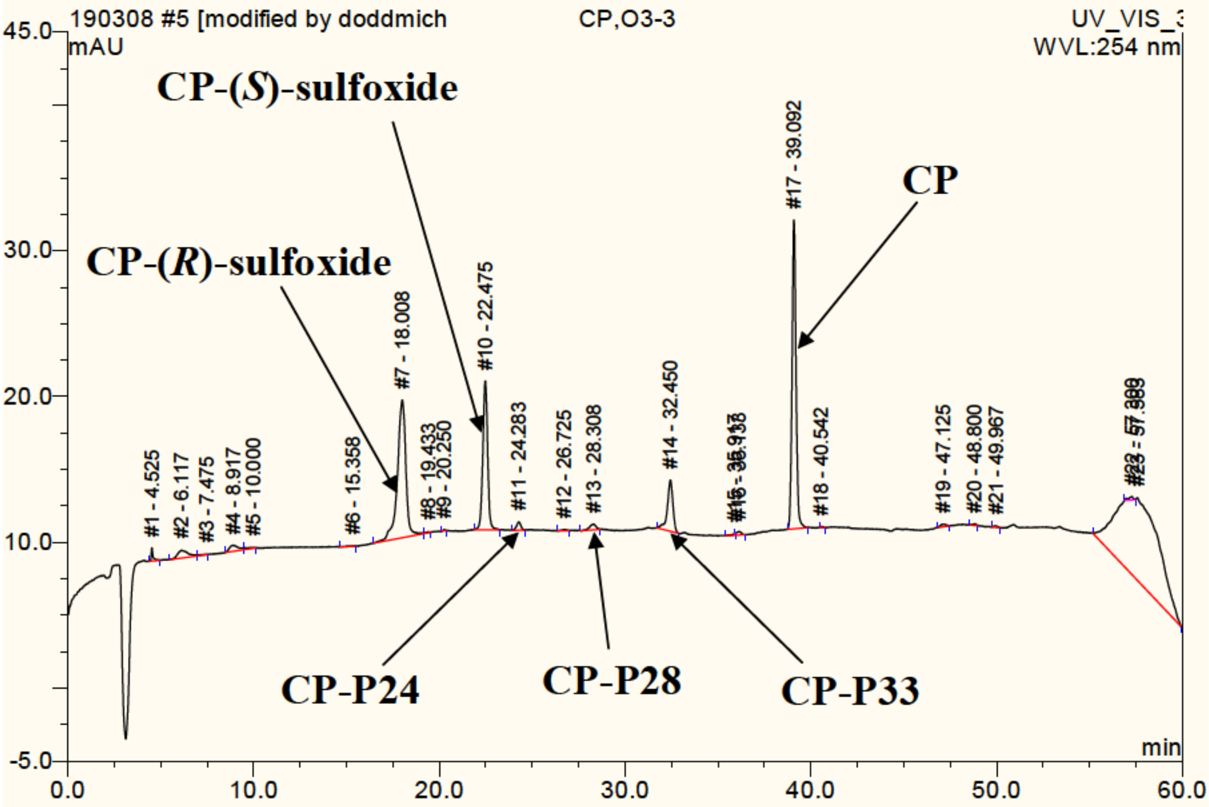

Figure 5.3. Chromatogram of 10 µM CP treated with ~9 µM of O_3 at pH 7, in 1-mM phosphate buffer amended with 5-mM *t*-BuOH, acquired at λ = 254 nm with the HPLC-UV method described for CP analyses in the Materials and Methods section

Analysis of CP and the two most polar CP transformation products by high-resolution mass spectrometry yielded the mass spectra shown in Figures S5.6-S5.8. In analogy to the results obtained for the PG sulfoxides, the MS data for these two CP products provide identical exact masses (363.0891), each offset by the mass of one oxygen atom from the mass of the parent CP molecule (347.0941). In addition, the MS^2 spectra for each of these CP products exhibit the same major fragment peak (at m/z 346.06, corresponding to a loss of H_2O). Furthermore, the FT-IR spectra for these two analytes also exhibit significant absorbance bands in the range of 1000-1100 cm^{-1}, consistent with the presence of sulfoxide moieties within each product's molecular structure (Figure S5.13). On the basis of these data, analogy with the results observed for PG, and previous observations for reactions of O_3 with various dihydrocephalosporin analogues of CP (*16*), the two most polar CP products were initially hypothesized to be stereoisomeric sulfoxides of CP, as depicted in Figure 5.4.

^{1}H-NMR was again utilized in a manner similar to that applied for analysis of the two PG sulfoxides to distinguish between the two postulated CP sulfoxide stereoisomers. However, as neither of the two CP sulfoxides were soluble in $CDCl_3$, the importance of intra-

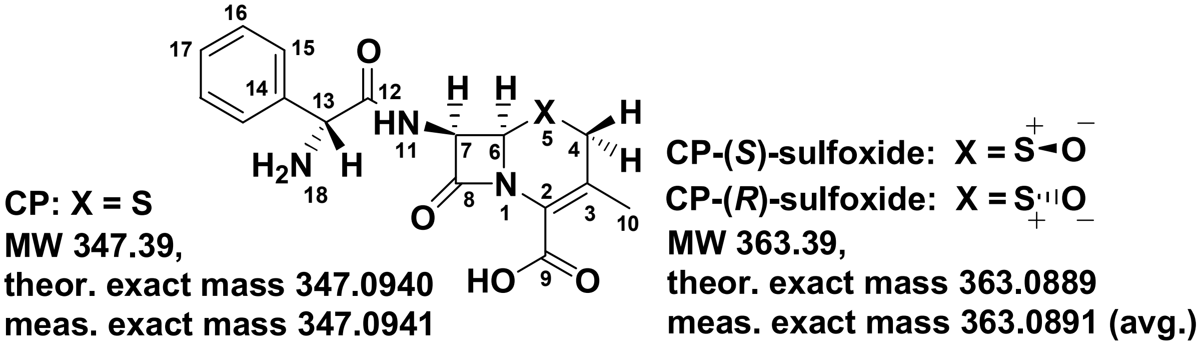
16
17
15
O
14
13
12
H H
HN
X
H
5
4
H
H₂N H
11
7 6
N
2
18
O
8
1
3
10
HO 9 O
CP: X = S
MW 347.39,
theor. exact mass 347.0940
meas. exact mass 347.0941
CP-(S)-sulfoxide: X = S⁺→O⁻
CP-(R)-sulfoxide: X = S⁺···O⁻
MW 363.39,
theor. exact mass 363.0889
meas. exact mass 363.0891 (avg.)

Figure 5.4. Atom numbering and postulated stereochemistries of CP and CP sulfoxides

vs. intermolecular H-bonding was only investigated in DMSO-d_6. The results of these analyses demonstrate that H-11 (NH) of the less polar sulfoxide is shielded by ~0.8 ppm with respect to H-11 of the more polar sulfoxide in DMSO-d_6 solution (Figure S5.16 and Table S5.3), consistent with formation of an *intra*molecular NH--O bond in the former molecule and an *inter*molecular NH--O bond with DMSO-d_6 for the latter, when comparing to the $\Delta\delta(^1H)$ value of 1.3 ppm measured for the two PG-sulfoxides. The (*R*) and (*S*) configurations were therefore assigned to the more polar and less polar CP sulfoxides, respectively.

The resonances of H-4b for CP and the two CP sulfoxides were assigned from the NOE effect observed from H-6 onto H-4b in the 1D-NOESY spectra. Further, small $^1H,^1H$ coupling constants were found for the pairs H-6/H-4b, typical values for a so called “w” coupling. This again, is a positive proof for the relative configuration assigned for H-4a and H-4b. For all CP derivatives pronounced HMBC correlation signals were observed from H-4a to C-10, whereas from H-4b to C-10 no or remarkably less pronounced correlation were found owing a bond angles H-4b/C-4/C-3/C-10 near 90º. One may therefore conclude that H-4b must be in a pseudo-axial position, whereas H-4a is attached in a pseudo equatorial position. For CP-(*S*)-sulfoxide with the oxide group “looking up”, absolutely no HMBC correlation form H-4b to C-10 was observed, whereas for CP-(*R*)-sulfoxide a weak cross signal was found. Owing to the 5-oxide group “looking down” (see Figure 5.4), the geometry at C-4 must be distorted in such a way that the angle H-4b/C-4/C-3/C-10 deviates distinctly from 90º as a result. The spectral data discussed to this point are all consistent with assignment of the molecular topologies and stereochemistries depicted in Figure 5.4 to CP and its two CP sulfoxides.

The two CP transformation products corresponding to the third and fifth peaks depicted in Figure 5.3 (henceforth labeled CP-P24 and CP-P33, respectively, based on their average HPLC retention times) were also analyzed by high-resolution mass spectrometry, yielding the mass spectra shown in Figures S5.9-S5.11. The exact mass of CP-P24 (397.0944) was obtained from the distinct molecular $M+H^+$ peak shown in Figure S5.9a at 398.1019.

However, that of CP-P33 was not at first clear on the basis of positive-mode ESI spectra alone, as several peaks were present at m/z values within the range reasonable for CP transformation products. Therefore, in order to identify the true molecular CP-P33 peak, its MS and MS^2 spectra were examined on the basis of exact mass differences and fragmentation patterns for each of the three candidate ions. Upon examination of the mass spectrum depicted in Figure S5.10a, it is evident that the peak detected at m/z 362.0807 differs by the mass of one H_2O molecule (18.0106) from that at m/z 380.0913, which in turn differs from those at m/z 397.1178 and 402.0730 by exactly (within measurement error) the masses of a NH_4^+ molecule and a Na^+ molecule minus one proton (i.e., 18.0344-1.0078 = 17.0265 and 22.9898-1.0078 = 21.9820), respectively. This suggests that the two higher mass peaks are likely due to NH_4^+ and Na^+ adducts formed in the ESI source from the ion at 380.0913 (where the NH_4^+ is likely derived from ammonium acetate buffers utilized by other users on the same instrument and the Na^+ from occasional processing of sodium-containing standard materials), whereas the ion at 362.0807 is generated via loss of H_2O from that at 380.0913. This hypothesis is supported by the MS^2 fragmentation patterns shown in Figures S5.10b-d, which illustrate that the 362.0807 ion arises from fragmentation of the isolated 380.0913 ion, that both of these ions are produced via fragmentation of the presumably labile NH_4^+ adduct at 397.1178, and that none of these ions are generated via fragmentation of the presumably more stable Na^+ adduct at 402.0730. Furthermore, a separate high-resolution analysis of CP-P33 via negative-mode ESI yielded a base (and presumably also molecular) peak at 378.0744, which corresponds to the peak in positive-mode minus two protons), without any corresponding peaks at higher masses - as would be expected in negative-mode if the higher mass observed in positive-mode were indeed attributable to cation adducts. Taken together, these analyses permit confident assignment of an exact mass of 379.0838 to CP-P33.

The molecular topologies and stereochemistries of CP-P24 and CP-P33 were then fully characterized via analysis of $^1H,^{13}C$-correlated NMR spectra, with the exception of the configurations of C-2 and C-9 (which were deduced from MS/MS data and mechanistic considerations). NMR analyses were run with a relatively pure fraction of CP-P33, whereas CP-P24 was always present as a mixture together with CP-(*S*)-sulfoxide. However, the signals originating from CP-P24 were easily distinguishable from those of CP-(*S*)-sulfoxide, as reference spectra for the latter were obtained via analysis of purified single-component solids in separate NMR analyses.

Characteristic carbonyl signals observed at ~208 ppm in the ^{13}C NMR spectra for both CP-P24 and CP-P33 are strongly suggestive of C-2/C-3 ozonolysis - leading to oxidation of

C-3 to the corresponding ketone. This conclusion is also fully consistent with the disappearance of the secondary absorbance maximum corresponding to the conjugated C-2/C-3 π–bond system from the UV spectra obtained for CP-P24 and CP-P33 (Figure S5.2). No HMBC correlations were observed from H-10 to either C-2 or C-9 in the spectra of these two molecules. Furthermore, the ^{13}C chemical shifts of 41 and 57 ppm obtained for the C-4 and C-6 atoms of both CP-P24 and CP-P33 strongly indicate that the S atom must still be present in the -2 oxidation state (by comparison with the significantly greater deshielding of these resonances for the two CP-sulfoxides, as shown in Table S5.5). The lack of a well-defined absorbance band between 1000 and 1100 cm^{-1} in the FT-IR spectrum for CP-P33 is consistent with this conclusion (Figure S5.13d).

The magnitude of $J_{6,7}$ = 6.4 Hz obtained for H-6 and H-7 of CP-P24 points to a marked change in the H-6/C-6/C-7/H-7 bond angle relative to CP and the CP sulfoxides (Tables S5.4 and Table S5.6), which would also be consistent with the assigned stereochemistry. Furthermore, the presence of the NH_2 group at N-18 is reflected by the corresponding ^{15}N chemical shift of -340 ppm observed for CP-P24. On the basis of these observations and additional details obtained from its HSQC and HMBC spectra, the constitution of the CP-P24 skeleton - with the exception of C-2 and C-9 - was assigned as depicted in Figure 5.5a.

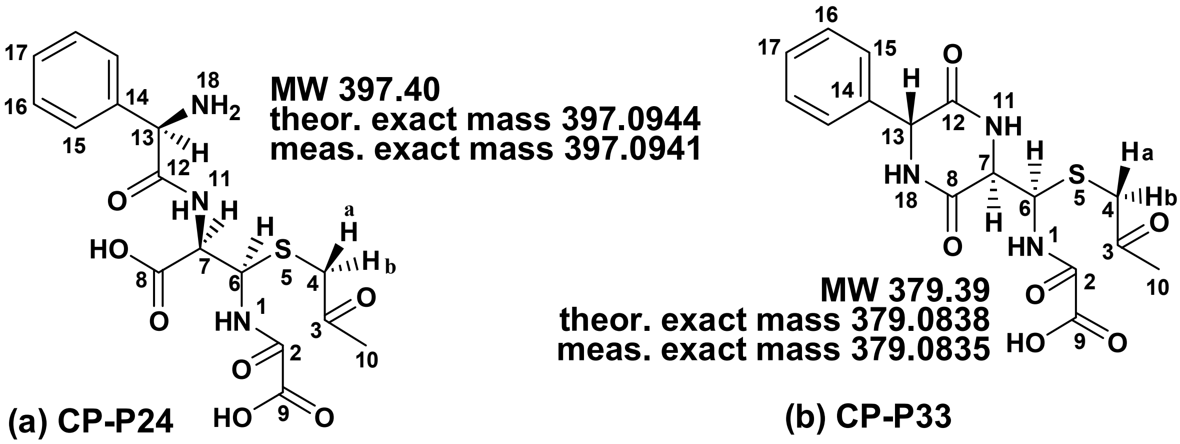
MW 397.40
theor. exact mass 397.0944
meas. exact mass 397.0941
MW 379.39
theor. exact mass 379.0838
meas. exact mass 379.0835

(a) CP-P24

(b) CP-P33

Figure 5.5. Atom numbering and postulated stereochemistries of CP-P24 and CP-P33

Additional compound-specific spectral details were obtained for CP-P33 from its HMBC, NOE, 1D ^{1}H, and ^{15}N spectra. A unique correlation observed from H-13 at 5.25 ppm to two carbonyl resonances at 169.5 and 166.0 ppm (C-12 and C-8) in the HMBC spectrum of CP-P33 is a strong indicator of a cyclization reaction involving formation of a N-18, C-8 bond in this molecule. No such cross-correlation peaks were observed for H-13 and C-8 in the spectra obtained for CP or any of the other four transformation products discussed here.

Furthermore, a ^{15}N chemical shift of -256.6 ppm in the corresponding CP-P33 spectrum (Figure S5.20, Table S5.7) is strong evidence that the N-18 atom is present as an amide. In addition, NOE effects observed from H-7 to H-15 and from H-15 to H-7 for CP-P33 samples were only observed for this particular molecule. The magnitude of $J_{6,7}$ = 3.3 Hz observed for the H-6 and H-7 atoms of CP-P33 is in the same order as for CP and the CP sulfoxide isomers (Tables S5.4 and S5.6), which may be indicative of hindered rotation around the C-6,C-7 bond, owing to bulky substituents present in the CP-P33 molecule. Roughly 100-Hz resonances were detected at 162 and 163 ppm in the 1D ^{1}H-NMR spectra - presumably attributable to two carbonyl or carboxyl groups at the C-2 and C-9 positions, although no correlations were observed from C-2 or C-9 to any other components of the HMBC spectra (DMSO-d_6 and D_2O solutions). Finally, three unique ^{1}H and ^{15}N signals were detected for N-1, N-11, and N-18, at 9.13, 8.39, and 9.04 ppm (^{1}H) and -257.5, -266.8, and -256.6 ppm (^{15}N), demonstrating that all three of the N atoms in CP-P33 are present as primary amides. Taken together, these data permit assignment of the structure and stereochemistries shown in Figure 5.5b to CP-P33.

Apart from the signals attributable to CP-(*S*)-sulfoxide and CP-P24, a third set of weak signals with similar chemical shifts was observed in spectra obtained for the mixture of these products (data not shown), presumably due to the fifth product peak (CP-P28) depicted in Figure 5.3, as HPLC-UV analyses also indicated the presence of this component in the isolated mixture solids. Due to the low concentration of this third constituent in the mixture, and the overlap of its signals with resonances of CP-(*S*)-sulfoxide and CP-P24, no detailed structural assignments could be made. However, the presence of a weak ^{13}C signal at ~208.3 ppm (the diagnostic shift for a C-3 carbonyl) does permit the conclusion that the C-2/C-3 double bond was also ozonolytically cleaved in the CP-P28 molecule (data not shown). This conclusion is also supported by the lack of the secondary absorbance maximum corresponding the C-2/C-3 π–bond system in the UV spectra obtained for CP-P28 (Figure S5.2e).

5.3.2 Evolution of major products in O_3-treated PG and CP solutions with increasing transferred O_3 dose. Evolution of the transformation products generated in reactions of O_3 with PG and CP was quantitatively monitored by HPLC-UV, using the purified solids of each product for quantification of observed product yields. The measured concentrations of each transformation product are shown with the corresponding parent molecule concentrations at increasing O_3 doses in Figure 5.6. From these data, it is clear that PG-(*R*)-sulfoxide and PG-(*S*)-sulfoxide are generated in parallel at nearly equal yield (1.2:1

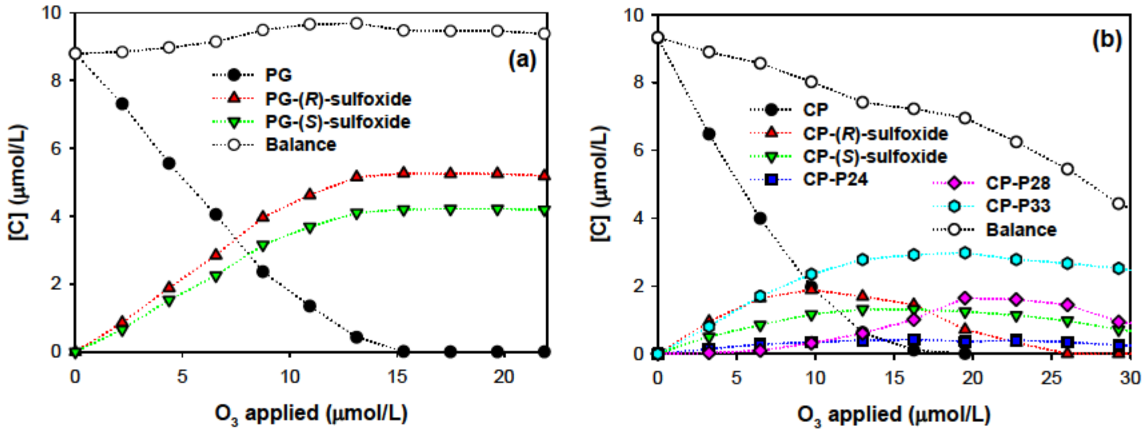

Figure 5.6. Transformation product formation during O_3-treatment of (a) PG and (b) CP as a function of O_3 dose, in 1-mM, pH 7 phosphate buffer amended with 5-mM *t*-BuOH.

(*R*):(*S*) to be more precise) (Figure 5.6a). Furthermore, a mass balance on the measured concentrations of two sulfoxides accounts for ~100% of the PG concentrations consumed at increasing transferred O_3 doses up to at least 1.5× the amount of O_3 necessary to yield 100% PG depletion. This illustrates that the two PG sulfoxides are effectively non-reactive toward O_3 (i.e., the rate constants for their direct reaction are negligible) and represent a reaction terminus when O_3 is the only oxidant present. In addition, when taken into consideration with the measured biological activity of PG-(*R*)-sulfoxide, this is consistent with prior observations that stable levels of residual antibacterial activity persist in O_3-treated PG solutions even at O_3 doses in excess of those needed for complete depletion of PG (*15*). These observations can be summarized via the pathways depicted in Scheme 5.1.

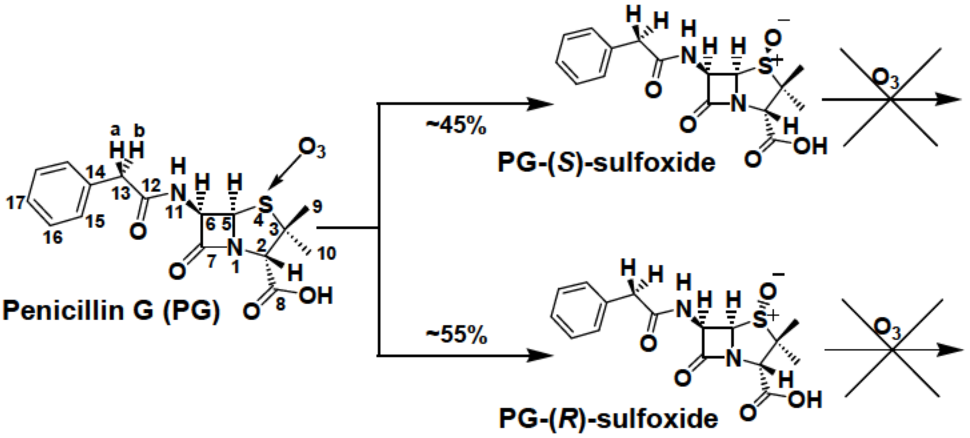

Scheme 5.1. Postulated reaction pathways and initial yields of transformation products resulting from attack of O_3 at the thioether of PG, on the basis of UV, MS/MS, ^{1}H-NMR, and FT-IR data obtained for purified isolates

The data in Figure 5.6b illustrate that all four major products identified for the reaction of O_3 with CP are generated approximately in parallel. This indicates that the kinetics of O_3 attack at the CP thioether and the CP C-2/C-3 double bond are quite similar (k''_{O_3} for both target sites must be on the order of 8.7×10^4 $M^{-1}s^{-1}$, according to previous measurements of $k''_{O_3,app,CP}$ (*15*)). These data also show that CP-(*R*)-sulfoxide, CP-(*S*)-sulfoxide, CP-P24, and CP-P33 are generated in ~34%, ~18%, ~5%, and ≥28% initial yield (where the yield given for CP-P33 can only be interpreted as a minimum value, on account of the uncertainty as to the exact purity of the CP-P33 solids used for calibration), with a maximum of 15% of total initial CP consumption resulting in the formation of unidentified products. At turnovers up to ~100% CP depletion, these four major products still account for - at a minimum - 75% of the total CP consumption, leaving no more than 25% unaccounted for. At higher relative O_3 doses, the proportion of unidentified products increases relatively steeply

CP-(*R*)-sulfoxide itself is clearly also consumed relatively rapidly by O_3 (in comparison to CP and the other transformation products), apparently resulting in formation of CP-P28. This was confirmed in separate experiments, in which O_3 was applied directly to pure CP-(*R*)-sulfoxide, where CP-P28 accounted for roughly 30% of the initial CP-(*R*)-sulfoxide consumption (leaving ~70% of the total reacted CP-(*R*)-sulfoxide concentrations unaccounted for) (data not shown). These observations also indicate that CP-(*R*)-sulfoxide is more reactive toward O_3 than any of the other major products formed via the CP-O_3 reaction, as each of the other three major products persists at relatively stable levels even at O_3 doses high enough to yield ~100% depletion of CP-(*R*)-sulfoxide. Taking into account the measured antibacterial potency of CP-(*R*)-sulfoxide, its susceptibility toward further modification by O_3 is also consistent with prior indications that a biologically-active transformation product is formed upon treatment of CP with O_3, reaches peak yield at moderate CP turnover, and is then progressively depleted at higher O_3 doses (*15*). Each of the above observations can be summarized via Scheme 5.2, in which the CP sulfoxides are shown to result from O_3 attack at the CP thioether, CP-P24 and CP-P33 are formed upon ozonolytic cleavage of CP's C-2/C-3 double bond, and CP-P28 is produced upon ozonolysis of CP-(*R*)-sulfoxide's double bond.

The formation of CP-P24 and CP-P33 must proceed in each case via C-2/C-3 ozonolysis. However, the competing reaction mechanisms leading to cleavage of the β-lactam and formation of either (a) the penicilloic acid group of CP-P24 or (b) the 7-piperazine-8,12-dione ring of CP-P33 require additional explanation. In analogy to pathways reported in a previous investigation for ozonolysis of the double bond of the nucleobase thymine (*27*), the

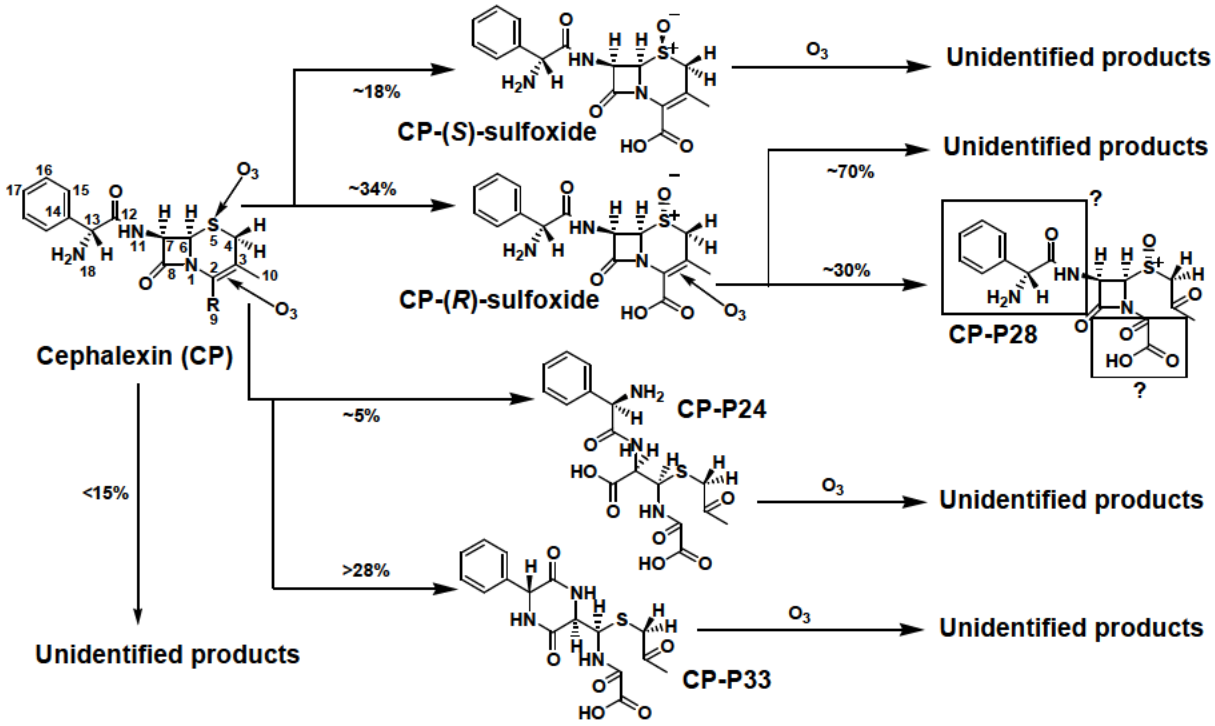
~18%
CP-(S)-sulfoxide
O_3
Unidentified products
~34%
CP-(R)-sulfoxide
~70%
Unidentified products
~30%
CP-P28
?
?
Cephalexin (CP)
~5%
CP-P24
O_3
Unidentified products
<15%
>28%
CP-P33
O_3
Unidentified products
Unidentified products

Scheme 5.2. Postulated reaction pathways and initial yields of transformation products resulting from attack of O_3 at the C-2/C-3 double bond of CP, on the basis of UV, MS/MS, ^{1}H-NMR, and FT-IR data obtained for purified isolates

ozonolytic cleavage of CP's C-2/C-3 double bond is believed to proceed initially via formation of a Criegee (or primary) ozonide intermediate, which may decompose to either of the C-2 or C-3 hydroperoxide intermediates depicted in Scheme 5.3.

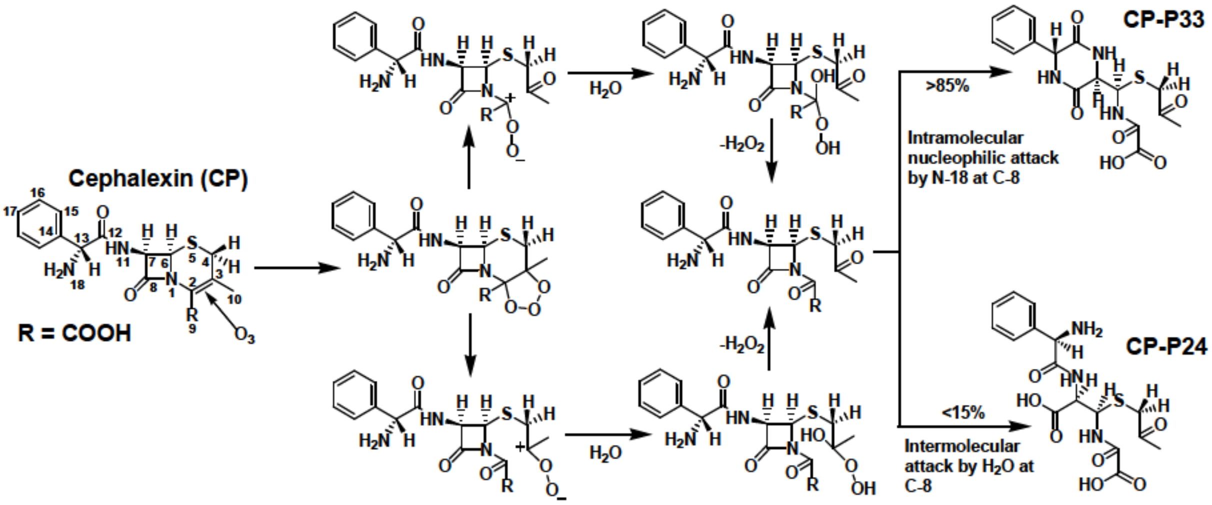
Cephalexin (CP)
R = COOH
H_2O
$-H_2O_2$
$-H_2O_2$
H_2O
>85%
Intramolecular nucleophilic attack by N-18 at C-8
CP-P33
<15%
Intermolecular attack by H_2O at C-8
CP-P24

Scheme 5.3. Postulated pathways leading to formation of CP-P24 and CP-P33 in the reaction of O_3 with CP

Each of these hydroperoxides may then decay via heterolytic H_2O_2 loss to the same intermediate 3-keto,2-keto-9-carboxylic acid *β*-lactam structure, which is expected to be highly susceptible to nucleophilic attack at the already labile C-8/N-1 bond of the *β*-lactam ring, on account of the added electron-withdrawing strength of the adjacent C-2 carbonyl. Subsequently, in aqueous solution, it is expected that C-8 will be attacked by H_2O (or OH^-), resulting in cleavage of the C-8/N-1 bond, formation of the primary amide at N-1 and carboxyl group at C-8, and production of CP-P24 (Scheme 5.3). Alternatively, C-8 may be attacked intramolecularly by the proximal N-18 amine group, yielding cleavage of the C-8/N-1 bond, formation of the N-1 primary amide and cyclicization of the C-8/C-7/N-11/C-12/C-13/N-18 chain to the piperazinedione ring characteristic of CP-P33 (Scheme 5.3). This reaction has been demonstrated to take place in a number of studies focusing on intramolecular nucleophilic cleavage of various cephalosporins' *β*-lactam rings, in each case yielding the characteristic piperazinedione structure (for which reported spectral data is also consistent with the results described here) (*28-30*). As is clear from the relative CP-P24 and CP-P33 yields shown in Figure 5.6b and Scheme 5.2, the intramolecular pathway appears to take place approximately 2× faster than the competing intermolecular pathway under the conditions studied here (i.e., pH 7, ~20° C).

5.3.3 Antibacterial activities of transformation products resulting from reactions of PG and CP with O_3. Biological activities of each transformation product generated in the treatment of PG and CP with O_3 were quantified for comparison with the corresponding activities of the parent molecules via broth microdilution assay. The resulting dose-response relationships obtained for each parent molecule and its products are depicted in Figure 5.7. The EC_{50} values determined for each dose-response relationship are reported here in terms of the sample dilution, $1/2^n$, where n corresponds to the number of times a given sample on the microtiter plate was serially diluted. Thus, one can simply calculate the relative potencies of each product (or product mixture) by dividing the EC_{50} of the parent molecule by the measured EC_{50} value of the product of interest and multiplying this ratio by the ratio of the in vitro parent concentration to the in vitro product concentration (where in vitro concentrations are given in the caption to Figure 5.7). This calculation indicates that PG-(*R*)-sulfoxide and PG-(*S*)-sulfoxide are approximately 15% and 0.7% as active as PG relative to *B. subtilis* ATCC 6051. Similarly, CP-(*R*)-sulfoxide is roughly 83% as active as CP for *B. subtilis* ATCC 6051, while the mixture of CP-(*S*)-sulfoxide, CP-P24, and CP-P28, as well as the sample of CP-P33, elicited effectively zero response in the microdilution assay. These values are consistent with prior reports that the antibacterial activities of the penicillin and cephalosporin

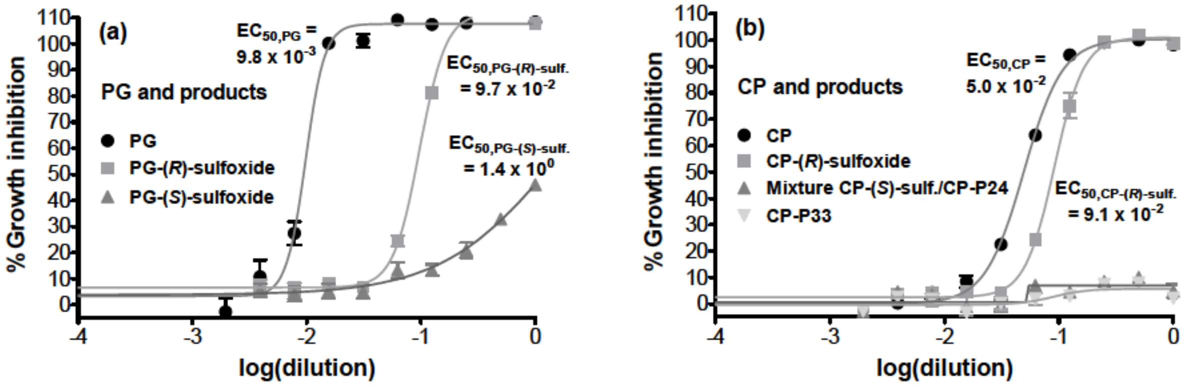

Figure 5.7. Averages of measured replicate (6-fold) dose-response relationships (using *B. subtilis* ATCC 6051 as reference bacterium) for transformation products resulting from the reaction of O_3 with (a) PG, and (b) CP, where undiluted in vitro concentrations of PG, PG-(*R*)-sulfoxide, PG-(*S*)-sulfoxide were 2.5, 1.7, and 2.5 μM, respectively, and those of CP, CP-(*R*)-sulfoxide, CP-(*S*)-sulfoxide, CP-P24, CP-P28, and CP-P33 were 5, 3.3, 1.4, 1.4, ~0.2, and 2.6 μM, respectively. The independent variable "dilution" is equal to $1/2^n$, where "2" is the serial dilution factor used in preparing dose-response series (i.e., for 2-fold, or 1:1 dilution), and "n" the number of times a given sample has been serially diluted relative to the corresponding parent sample (i.e., $1/2^0$ corresponds to the dilution of each parent sample).

(*R*)-sulfoxides may be appreciable in comparison to the parent *β*-lactams, whereas the corresponding (*S*)-isomers are typically much less potent (*17,18,31*).

5.3.4. Modeling evolution of biological activities of O_3-treated PG and CP solutions with increasing transferred O_3 dose. On the basis of the product concentration measurements depicted in Figure 5.6, the biological activity measurements shown in Figure 5.7, and the reaction pathways proposed in Schemes 5.1 and 5.2, one can attempt to quantitatively account for the observed trends in bulk biological activities measured for solutions of PG and CP treated with O_3. By assuming that the only active components of the O_3-treated *β*-lactam solutions are the parent molecules themselves and the (*R*)-sulfoxide transformation products, and applying the relative per potency values obtained via microdilution assay of each sulfoxide on a per mole basis to the measured concentrations of PG, PG-(*R*)-sulfoxide, CP, and CP-(*R*)-sulfoxide, one can calculate the expected activities due to (a) the parent molecules, (b) their (*R*)-sulfoxides, and (c) the sum of the parent molecules and their (*R*)-sulfoxides for each O_3-treated PG or CP sample, to obtain plots of predicted vs. measured activities, as shown in Figures 5.8a and 5.8b, for PG and CP, respectively. As apparent from each of these figures, the predicted bulk activities (i.e., the sums of the parent molecule and (*R*)-sulfoxide activities) agree very well with the measured bulk activities for the O_3-treated solutions of PG and CP.

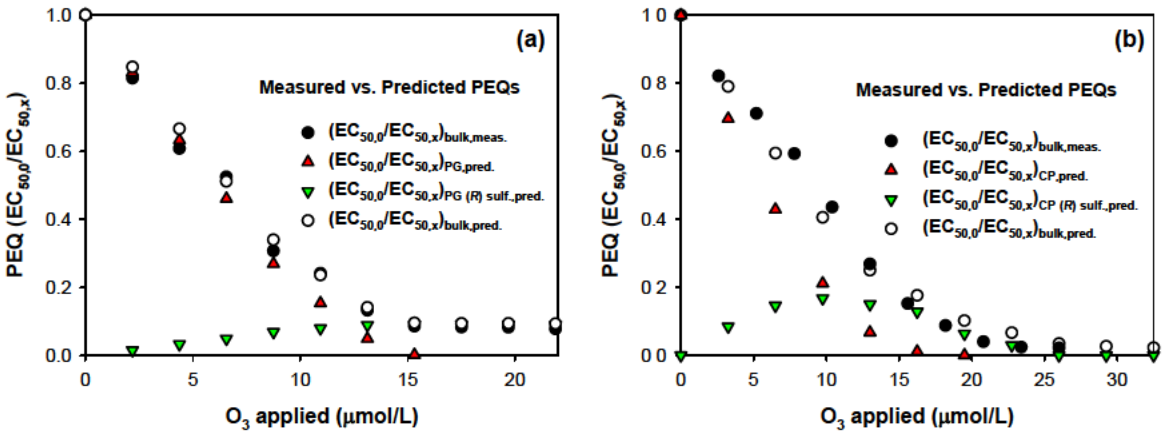

Figure 5.8. Correlations of measured and predicated antibacterial activities of O_3-treated (a) PG and (b) CP solutions with approximate transferred O_3 dose, in 1-mM, pH 7 phosphate buffer amended with 5-mM *t*-BuOH, assuming that any residual activity not attributable to the parent molecules can be attributed solely to their (*R*)-sulfoxide transformation products

5.3.5 Deactivation of PG- and CP-(*R*)-sulfoxides by O_3 and $^{\bullet}OH$. As shown in Figure 5.6a, PG-(*R*)-sulfoxide is recalcitrant toward further reaction with O_3. This suggests that, if the only oxidant present during oxidative treatment of PG is O_3, no further loss of biological activity will be achievable once all PG has been depleted and PG-(*R*)-sulfoxide has been formed in full yield. However, hydroxyl radical ($^{\bullet}OH$) will always be present during ozonation of wastewaters, on account of its production in the autocatalytic decomposition of O_3 and the direct reactions of O_3 with various functional groups present in dissolved organic matter (*20,32-34*). Thus, it is of substantial interest to determine the reactivity of PG-(*R*)-sulfoxide toward $^{\bullet}OH$, as well as to investigate the consequences of this reaction for the sulfoxide's biological activity.

Via competition kinetics experiments (using *p*CBA as a competitor), the apparent second-order rate constant for oxidation of PG-(*R*)-sulfoxide by $^{\bullet}OH$, $k''_{\bullet\mathrm{OH,app,PG\text{-}}(R)\mathrm{\text{-}sulfoxide}}$, was determined as 7.4 (±0.1) × 10^9 $M^{-1}s^{-1}$ at pH 7 (see Figure S5.21 for a detailed plot of the corresponding experimental data). Accompanying changes in the antibacterial activity of a $^{\bullet}OH$-treated PG-(*R*)-sulfoxide solution were monitored via microdilution assay. The results of the biological assay are shown in Figure 5.9, plotted in terms of residual potency equivalents (PEQs) (calculated from eq 1) vs. the normalized residual concentration of parent molecule, $[C]/[C]_0$. These data illustrate that slightly less than 1 PEQ appears to be depleted per mole equivalent of the parent molecule oxidized. This may be indicative of the formation of moderately active oxidation products such as *p*-hydroxy benzylpenicillin-(*R*)-sulfoxide, in analogy to the potent antibacterial molecule *p*-hydroxybenzylpenicillin (penicillin X) (*35,36*),

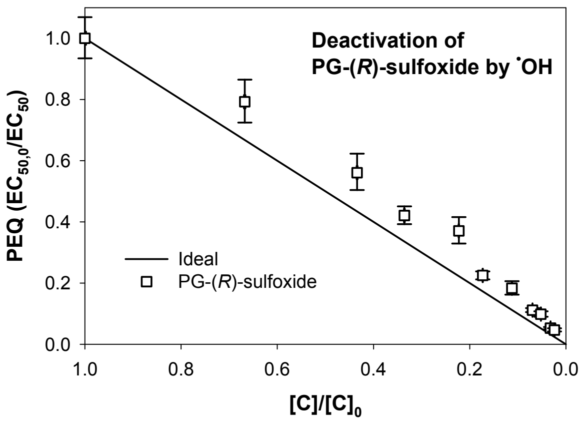

Figure 5.9. Deactivation of PG-(*R*)-sulfoxide samples treated with increasing •OH exposures in 1-mM, pH 7 phosphate buffer. The raw dose-response relationships from which these data were obtained are shown in Figure S5.23.

which is reportedly formed during •OH treatment of PG (*37*). Nevertheless, the measured deviation from ideal deactivation stoichiometry is relatively minor (generally < 20%), and PG-(*R*)-sulfoxide is clearly deactivated quite effectively by •OH.

In contrast to PG-(*R*)-sulfoxide, CP-(*R*)-sulfoxide is susceptible to further transformation by O_3 (as illustrated in Figure 5.6b and Scheme 5.2), and presumably also to •OH. The $k''_{O_3,\text{app,CP-}(R)\text{-sulfoxide}}$ and $k''_{\bullet OH,\text{app,CP-}(R)\text{-sulfoxide}}$ values corresponding to these reactions were determined to be 2.6 (±0.3) × 10^4 $M^{-1}s^{-1}$ and 7.6 (±0.2) × 10^9 $M^{-1}s^{-1}$, respectively, at pH 7 (see Figure S5.22 for detailed plots of the corresponding experimental data). The good agreement between measured and predicted activities in CP solutions treated with O_3 (Figure 5.8b) provides a preliminary indication that the former reaction results in loss of CP-(*R*)-sulfoxide's antibacterial activity, as formation of any appreciably active product from CP-(*R*)-sulfoxide would have resulted in a marked positive deviation of measured activities from predicted values. As shown in Figure 5.10a, which depicts the results obtained from microdilution assay of O_3-treated CP-(*R*)-sulfoxide samples, this is indeed the case. In addition, corresponding results for •OH-treatment (Figure 5.10b) illustrate that CP-(*R*)-sulfoxide is also deactivated with effectively ideal stoichiometry by •OH.

5.3.6 Implications for *β*-lactam deactivation during ozonation of municipal wastewaters. The results of this investigation, when evaluated in the context of the reaction kinetics measured for oxidation of PG, CP, and their corresponding (*R*)-sulfoxides by O_3 and •OH, suggest that the antibacterial activities of these representative *β*-lactams, as well as the activities of many other structurally-analogous penicillins and cephalosporins, should be

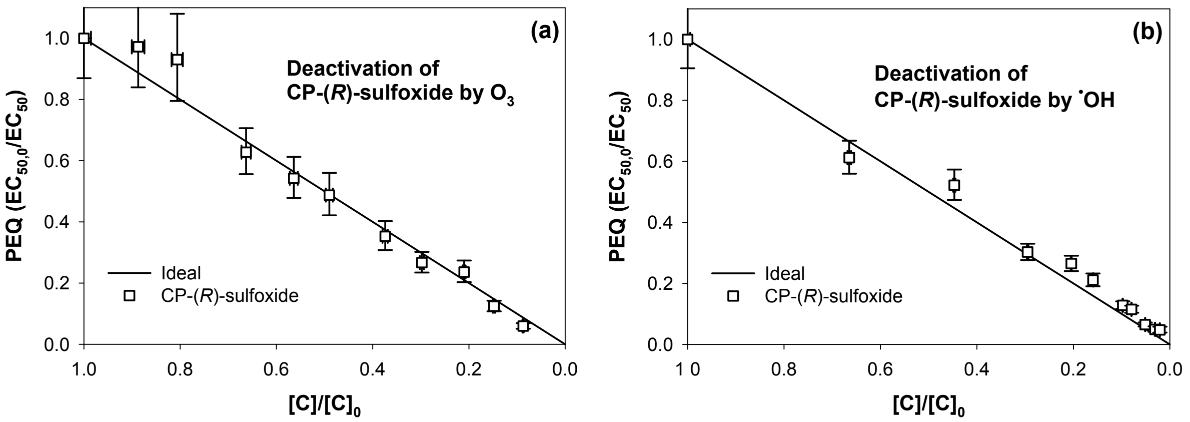

Figure 5.10. Deactivation of CP-(*R*)-sulfoxide samples treated with increasing (a) O_3 and (b) $^{\bullet}OH$ exposures in 1-mM, pH 7 phosphate buffer (which also contained 5-mM *t*-BuOH for the O_3 experiments). The raw dose-response relationships from which these data were obtained are shown in Figure S5.24.

effectively eliminated during ozonation of aqueous matrixes as long as the parent β-lactam is itself analytically verified (e.g., by LC/MS/MS) to be depleted from solution, and as long as $^{\bullet}OH$ plays a significant role in the oxidation process (as the biologically-active (*R*)-sulfoxides are apparently formed only via direct reactions of PG and CP with O_3).

Accordingly, a semi-quantitative estimate of the relative degree to which O_3 and $^{\bullet}OH$ influence PG and CP oxidation during ozonation of a hypothetical wastewater can aid substantially in evaluating the likely significance of (*R*)-sulfoxide formation under varying conditions. This can be achieved by first calculating the parameter $f_{\bullet OH,M(\tau)}$ (i.e., the fraction of model compound, M, oxidation attributable to $^{\bullet}OH$) for varying ratios of cumulative $^{\bullet}OH$ exposure to cumulative O_3 exposure after an arbitrary exposure time, τ, according to eq 3 (*4,19,38*),

$$f_{\bullet OH,M(\tau)} = \left(1 + \frac{k''_{O_3,app,M}}{k''_{\bullet OH,app,M}} \left(\int_0^\tau [\bullet OH]dt \Big/ \int_0^\tau [O_3]dt \right)^{-1} \right)^{-1} = \left(1 + \frac{k''_{O_3,app,M}}{k''_{\bullet OH,app,M}} \left(\frac{1}{R_{ct(\tau)}} \right) \right)^{-1} \tag{3}$$

where $R_{ct(\tau)}$ represents the cumulative ratio of $^{\bullet}OH$ exposure, $\int_0^\tau [\bullet OH]dt$, to O_3 exposure, $\int_0^\tau [O_3]dt$, after time, τ, and the rate constants for PG and CP can be obtained from (*4*). The results of these calculations are depicted in Figure 5.11, for which the range of $R_{ct(\tau)}$ values likely to be encountered during ozonation of municipal wastewaters (estimated on the basis of data reported in (*20,39*)) is shaded in gray.

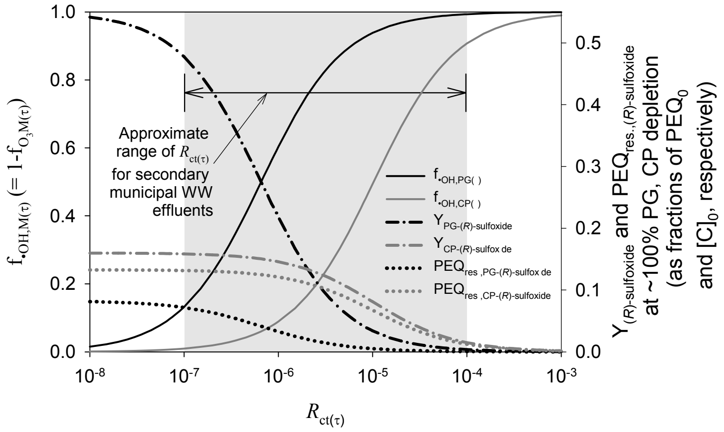

Figure 5.11. Theoretical variations in PG and CP deactivation efficiencies with changing $R_{ct(\tau)}$ (i.e., the cumulative in situ ratio of $^{\bullet}OH$ and O_3 exposures up to an arbitrary reaction time, τ), during ozonation at pH 7. Theoretical fractions, $f_{\bullet OH(\tau)}$, of PG and CP oxidation attributable to reactions with $^{\bullet}OH$ are depicted with theoretical (*R*)-sulfoxide yields ($Y_{(R)\text{-sulfoxide}}$) in mole product/mole parent compound reacted at oxidant doses sufficient to yield ~100% depletion of PG and CP, as well as the corresponding residual antibacterial activities, $PEQ_{res.,(R)\text{-sulfoxide}}$, attributable to the resulting (*R*)-sulfoxide concentrations. The data shown in this figure were obtained by assuming ~55% and ~16% (*R*)-sulfoxide yields for ~100% PG and CP consumption by O_3, respectively (according to Figure 5.6), 15% and 83% potencies for PG- and CP-(*R*)-sulfoxide (relative to PG and CP, respectively, according to Figure 5.7), and roughly quantitative elimination of PG and CP activity via $^{\bullet}OH$ reactions (according to the data reported in (*15*)). The approximate range of $R_{ct(\tau)}$ values shown here (shaded in gray) for municipal wastewaters is based on data reported in (*20*).

Assuming that the *β*-lactam-(*R*)-sulfoxides are formed only by direct reaction of O_3 with each *β*-lactam, one may then evaluate the variation in theoretical yields of PG- and CP-(*R*)-sulfoxide ($Y_{(R)\text{-sulfoxide}}$) with changing $R_{ct(\tau)}$ values for a particular degree of PG or CP depletion. This can be achieved by multiplying the $f_{O3,M(\tau)}$ (i.e., $1 - f_{\bullet OH,M(\tau)}$) values calculated for PG and CP at each $R_{ct(\tau)}$ value (via eq 3) by the (*R*)-sulfoxide yields, $y_{(R)\text{-sulfoxide}}$, measured for the selected degree of parent compound consumption in O_3-treated, phosphate-buffered solutions of PG and CP (Figure 5.6). As an example, theoretical $Y_{(R)\text{-sulfoxide}}$ values calculated for oxidant doses sufficient to achieve ~100% consumption of PG and CP are depicted as dash-dot-dashed lines in Figure 5.11, where the $y_{(R)\text{-sulfoxide}}$ values measured for PG-(*R*)-sulfoxide and CP-(*R*)-sulfoxide formation at ~100% PG and CP consumption were ~0.55 and ~0.16 mole/mole of parent compound consumed by O_3, respectively (Figure 5.6).

Theoretical residual antibacterial activities, $PEQ_{res.,(R)\text{-sulfoxide}}$, attributable to the (*R*)-sulfoxide yields at each $R_{ct(\tau)}$ value can likewise be calculated by multiplying each $Y_{(R)\text{-sulfoxide}}$ value by the measured potency of the corresponding purified (*R*)-sulfoxide relative to its parent *β*-lactam (where each yield and potency is expressed as a fractional value). Values of $\mathrm{PEQ}_{\mathrm{res.},(R)\text{-sulfoxide}}$ calculated for complete consumption of PG and CP at each $R_{\mathrm{ct}(\tau)}$ are depicted as dotted lines in Figure 5.11 (taking the measured potencies of PG- and CP-(*R*)-sulfoxide to be ~0.15× and ~0.83× those of PG and CP, respectively, according to the dose-response relationships presented in Figure 5.7).

The data shown in Figure 5.11 indicate that the magnitude of $\mathrm{PEQ}_{\mathrm{res.},(R)\text{-sulfoxide}}$ is likely to be appreciable only at the low end of the $R_{\mathrm{ct}(\tau)}$ range likely to be observed during secondary effluent ozonation, for which O_3 exposure will be sufficiently high to result in appreciable formation of O_3-derived oxidation products. Such conditions - which will be found at the left side of the shaded gray region in Figure 5.11 - are most likely to occur only in effluents containing relatively low DOC concentrations (e.g., < 5 mg/L) or high $^{\bullet}$OH scavenger concentrations (e.g., $[\text{carbonate}]_{\text{total}} > 10$ mM), or at high transferred O_3 doses (e.g., > 10 mg/L) (*34,39*). Thus, it may be concluded that PG and CP (*R*)-sulfoxides will generally be formed in relatively minor yields during wastewater ozonation. Furthermore, the data presented in Figure 5.11 are inherently conservative, as they do not account for further oxidation of the biologically-active (*R*)-sulfoxides by O_3 or $^{\bullet}$OH. That is, even if these (*R*)-sulfoxides are formed in appreciable yields, they will ultimately be deactivated by reactions with either O_3 (CP-(*R*)-sulfoxide only) or $^{\bullet}$OH, even at the relatively low transferred O_3 doses likely to be applied to municipal wastewater effluents (i.e., ~5-10 mg/L (*19,40*)), according to Figures 5.9 and 5.10. The same conclusions should apply generally to any *β*-lactam antibacterial compound for which the main targets of direct attack by O_3 are the characteristic thioether or cephalosporin C-2/C-3 double bond, during ozonation of aqueous matrixes for which $R_{\mathrm{ct}(\tau)}$ values consistently exceed ~10^{-7}.

Acknowledgements

Michael Dodd gratefully acknowledges financial support from a U.S. National Science Foundation Graduate Research Fellowship and the project RECLAIM WATER (Contract-No. 018309) - funded through the Sixth Framework Programme of the European Commission. The authors thank Silvio Canonica and Yunho Lee for helpful discussions. Elisabeth Salhi, Thomas Fleischmann, Christoph Werlen, and Hans-Ueli Weilenmann, and Vishakha Raina are gratefully acknowledged for technical assistance. Andrea Härer is thanked for substantial assistance with flash chromatography, and Roland Hany for use of the RediSep instrument. Stephan Hug is gratefully acknowledged for assistance in performing FT-IR measurements and access to the FT-IR spectrometer.

Literature Cited

(1) Livermore, D. M.; Williams, J. D. In *Antibiotics in Laboratory Medicine*; 4 ed.; Lorian, V., Ed.; Williams and Wilkins: Baltimore, MD, 1996, pp 502-578.

(2) Walsh, C. *Antibiotics: Actions, Origins, Resistance*; ASM Press: Washington, D.C., 2003.

(3) RxList, RxList, The Internet Drug Index. Available at http://www.rxlist.com/script/main/art.asp?articlekey=79509. NDC Health. 2005

(4) Dodd, M. C.; Buffle, M.-O.; von Gunten, U. Oxidation of antibacterial molecules by aqueous ozone: Moiety-specific reaction kinetics and application to ozone-based wastewater treatment. *Environ. Sci. Technol.* **2006**, *40*, 1969-1977.

(5) Hirsch, R.; Ternes, T. A.; Haberer, K.; Kratz, K.-L. Occurrence of antibiotics in the environment. *Sci. Total Environ.* **1999**, *225*, 109-118.

(6) Watkinson, A. J.; Murby, E. J.; Costanzo, S. D. Removal of antibiotics in conventional and advanced wastewater treatment: Implications for environmental discharge and wastewater recycling. *Water Res.* **2007**, *41*, 4164-4176.

(7) Gerding, D. N.; Hughes, C. e.; Bamberger, D. M.; Foxworth, J.; Larson, T. A. In *Antibiotics in Laboratory Medicine*; 4 ed.; Lorian, V., Ed.; Waverly and Wilkins: Baltimore, MD, 1996, pp 835-899.

(8) Gulkowska, A.; Leung, H. W.; So, M. K.; Taniyasu, S.; Yamashita, N.; Yeunq, L. W. Y.; Richardson, B. J.; Lei, A. P.; Giesy, J. P.; Lam, P. K. S. Removal of antibiotics from wastewater by sewage treatment facilities in Hong Kong and Shenzhen, China. *Water Res.* **2008**, *42*, 395-403.

(9) Gulkowska, A.; He, Y. H.; So, M. K.; Yeung, L. W. Y.; Leung, H. W.; Giesy, J. P.; Lam, P. K. S.; Martin, M.; Richardson, B. J. The occurrence of selected antibiotics in Hong Kong coastal waters. *Mar. Pollut. Bull.* **2007**, *54*, 1287-1293.

(10) Andreozzi, R.; Caprio, V.; Ciniglia, C.; de Champdoré, M.; lo Giudice, R.; Marotta, R.; Zuccato, E. Antibiotics in the environment: occurrence in Italian STPs, fate, and preliminary assessment on algal toxicity of amoxicillin. *Environ. Sci. Technol.* **2004**, *38*, 6832-6838.

(11) Wiedemann, B.; Grimm, H. In *Antibiotics in Laboratory Medicine*; Lorian, V., Ed.; Williams and Wilkins: Baltimore, MD, 1996, pp 900-1168.

(12) Baquero, F. Low-level antibacterial resistance: a gateway to clinical resistance. *Drug Resistance Updates* **2001**, *4*, 93-105.

(13) Drlica, K. The mutant selection window and antimicrobial resistance. *J. Antimicrob. Chemother.* **2003**, *52*, 11-17.

(14) Knapp, C. W.; Engemann, C. A.; Hanson, M. L.; Keen, P. L.; Hall, K. J.; Graham, D. W. Indirect evidence of transposon-mediated selection of antibiotic resistance genes in aquatic systems at low-level oxytetracycline exposures. *Environ. Sci. Technol.* **2008**, *42*, 5348-5353.

(15) Dodd, M. C.; Kohler, H.-P. E.; von Gunten, U. Oxidation of antibacterial compounds by ozone and hydroxyl radical: Elimination of biological activity during aqueous ozonation processes. *Environ. Sci. Technol.*, *Submitted.*

(16) Spry, D. O. Oxidation of penicillin and dihydrocephalosporin derivatives with ozone. *J. Org. Chem.* **1972**, *37*, 793-795.

(17) de Koning, J. J.; Marx, A. F.; Poot, M. M.; Smid, P. M.; Verweij, J. In *Recent Advances in the Chemistry of β-Lactam Antibiotics*; Elks, J., Ed.; The Chemical Society: Burlington House, London (England), 1977; Vol. 28, pp 161-166.

(18) Torii, H.; Asano, T.; Matsumoto, N.; Kato, K.; Tsushima, S.; Kakinuma, A. Microbial oxidation of cephalosporins to cephalosporin sulfoxides. *Agricultural and Biological Chemistry* **1980**, *44*, 1431-1433.

(19) Huber, M. M.; Gobel, A.; Joss, A.; Hermann, N.; Loffler, D.; McArdell, C. S.; Ried, A.; Siegrist, H.; Ternes, T. A.; von Gunten, U. Oxidation of pharmaceuticals during ozonation of municipal wastewater effluents: A pilot study. *Environ. Sci. Technol.* **2005**, *39*, 4290-4299.

(20) Buffle, M. O.; Schumacher, J.; Meylan, S.; Jekel, M.; von Gunten, U. Ozonation and advanced oxidation of wastewater: Effect of O_3 dose, pH, DOM and HO•-scavengers on ozone decomposition and HO• generation. *Ozone: Sci. Eng.* **2006**, *28*, 247-259.

(21) Bader, H.; Hoigné, J. Determination of ozone in water by the indigo method. *Water Res.* **1981**, *15*, 449-456.

(22) NCCLS, Methods for Dilution Antimicrobial Susceptibility Tests for Bacteria that Grow Aerobically-Fourth Edition; Approved Standard. Available at. NCCLS.

(23) Neta, P.; Dorfman, L. M. Pulse radiolysis studies. XIII. Rate constants for the reaction of hydroxyl radicals with aromatic compounds in aqueous solutions. *Adv. in Chem.* **1968**, *81*, 222-230.

(24) Bellamy, L. J. *The Infra-red Spectra of Complex Molecules*; 3rd edition ed.; Chapman and Hall Ltd.: London, England, 1975.

(25) Cooper, R. D. G.; Demarco, P. V.; Cheng, J. C.; Jones, N. D. Structural studies on penicillin derivatives. I. Configuration of phenoxymethyl penicillin sulfoxide. *J. Am. Chem. Soc.* **1969**, *91*, 1408-&.

(26) Cooper, R. D. G.; Demarco, P. V.; Murphy, C. F.; Spangle, L. A. Chemistry of cephalosporin antibiotics. Part XVI. Configurational and conformational analysis of deacetoxy-Δ^2-cephalosporins and deacetoxy-Δ^3-cephalosporins and their corresponding sulphoxide isomers by nuclear magnetic resonance. *Journal of the Chemical Society C-Organic* **1970**, 340-344.

(27) Flyunt, R.; Theruvathu, J. A.; Leitzke, A.; von Sonntag, C. The reactions of thymine and thymidine with ozone. *J. Chem. Soc., Perkin Trans. 2* **2002**, 1572-1582.

(28) Indelicato, J. M.; Norvilas, T. T.; Pfeiffer, R. R.; Wheeler, W. J.; Wilham, W. L. Substituent effects upon base hydrolysis of penicillins and cephalosporins. Competitive intramolecular nucleophilic amino attack in cephalosporins. *J. Med. Chem.* **1974**, *17*, 523-527.

(29) Cohen, A. I.; Funke, P. T.; Puar, M. S. Alkaline degradation product of cephradine. *J. Pharm. Sci.* **1973**, *62*, 1559-1561.

(30) Indelicato, J. M.; Dinner, A.; Peters, L. R.; Wilham, W. L. Hydrolysis of 3-chloro-3-cephems. Intramolecular nucleophilic attack in cefaclor. *J. Med. Chem.* **1977**, *20*, 961-963.

(31) Gottstein, W. J.; Kim, C. U.; Shih, K. M.; McGregor, D. N. Hetacillin (*R*)-sulfoxides and (*S*)-sulfoxides. Synthesis and structure-activity relationships. *J. Med. Chem.* **1978**, *21*, 240-242.

(32) von Gunten, U. Ozonation of drinking water: Part I. Oxidation kinetics and product formation. *Water Res.* **2003**, *37*, 1443-1467.

(33) Mvula, E.; von Sonntag, C. Ozonolysis of phenols in aqueous solution. *Org. Biomol. Chem.* **2003**, *1*, 1749-1756.

(34) Buffle, M. O.; von Gunten, U. Phenols and amine induced HO• generation during the initial phase of natural water ozonation. *Environ. Sci. Technol.* **2006**, *40*, 3057-3063.

(35) Housewright, R. D.; Berkman, S.; Henry, R. J. The relative effectiveness of pure penicillins against Bacillus anthracis in vitro and in vivo. *J. Immunol.* **1947**, *57*, 343-349.

(36) Kavanagh, F. Activities of twenty-two antibacterial substances against nine species of bacteria. *J. Bacteriol.* **1947**, *54*, 761-766.
(37) Phillips, G. O.; Power, D. M.; Robinson, C. Chemical changes following γ-irradiation of benzylpenicillin in aqueous solution. *J. Chem. Soc., Perkin Trans. 2* **1973**, 575-582.
(38) Elovitz, M. S.; von Gunten, U. Hydroxyl radical/ozone ratios during ozonation processes. I. The R_{ct} concept. *Ozone: Sci. Eng.* **1999**, *21*, 239-260.
(39) Buffle, M. O.; Schumacher, J.; Salhi, E.; Jekel, M.; von Gunten, U. Measurement of the initial phase of ozone decomposition in water and wastewater by means of a continuous quench-flow system: Application to disinfection and pharmaceutical oxidation. *Water Res.* **2006**, *40*, 1884-1894.
(40) Ternes, T. A.; Stuber, J.; Herrmann, N.; McDowell, D.; Ried, A.; Kampmann, M.; Teiser, B. Ozonation: a tool for removal of pharmaceuticals, contrast media and musk fragrances from wastewater? *Water Res.* **2003**, *37*, 1976-1982.

Supporting Information for Chapter 5.

Transformation of *β*-lactam Antibacterial Agents during Aqueous Ozonation: Reaction Pathways and Quantitative Bioassay of Biologically-Active Oxidation Products

24 pages, including 7 tables and 23 figures

Table S5.1. ^{1}H and ^{13}C chemical shifts of PG, PG-(*S*)- sulfoxide and PG-(*R*)- sulfoxide

Position[a]	**δ(^{1}H) / ppm (br = broad)**					**δ (^{13}C) / ppm**		
Compound	**PG**	**PG-(*S*)-sulfoxide**	**PG-(*S*)-sulfoxide**	**PG-(*R*)-sulfoxide**	**PG-(*R*)-sulfoxide**	**PG**	**PG-(*S*)-sulfoxide**	**PG-(*R*)-sulfoxide**
solvent	DMSO-d_6	DMSO-d_6	$CDCl_3$	DMSO-d_6	$CDCl_3$	DMSO-d_6	DMSO-d_6	DMSO-d_6
2	3.83	4.29	4.66	4.28	4.43	73.9	65.4	63.7
3						64.1	74.1	67.6
5	5.30	5.39	5.00	4.73	4.74	66.5	75.4	77.8
6	5.30	5.74	6.05	5.43	5.36	57.3	54.9	56.7
7						172.7	173.5	170.4
8						168.9	168.8	168.5
9	1.56	1.56	1.72	1.54	1.64	31.0	18.9	23.6
10	1.43	1.18	1.28	1.20	1.39	27.3	17.7	15.2
12						170.0	170.1	170.5
13	3.55+3.49	3.62+3.54	3.60	3.54	3.68	41.2	41.5	41.1
14						135.8	135.1	135.1
15	7.24	7.25	7.2-7.4[b]	7.26	7.2-7.4[b]	128.8	128.9	128.6
16	7.27	7.28	7.2-7.4[b]	7.28	7.2-7.4[b]	127.9	128.1	128.0
17	7.19	7.22	7.2-7.4[b]	7.22	7.2-7.4[b]	126.1	126.4	126.3
11(NH)	8.69 br	7.92	7.08	9.23	6.02			

[a] For atom numbering, see Figure 5.2 in the main text

[b] ^{1}H resonances of aromatic protons not assigned (no 2D correlations performed).

Table S5.2. Resolved ^{1}H,^{1}H coupling constants, observed correlations in 1D-NOESY spectra and ^{1}H,^{13}C-HMBC correlations used for NMR shift assignments of PG, PG-(*S*)-sulfoxide and PG-(*R*)-sulfoxide (measured in DMSO-d_6).

Compound	J(^{1}H, ^{1}H) / Hz	1D-NOESY	Observed HMBC correlations (w = weak)
PG	$J_{13a,13b}$ = 14.1	H-5, 6 → H-2, 10, 11 (NH); H-10 → H-2, 5	H-2 → C-3, 5, 7, 8, 9, 10; H-5, 6 → C-5, 6, 7, 12; H-9 → C-2, 3, 10; H-10 → C-2, 3, 9; H-13 → C-12, 14, 15; H-15 → C-13, 15, 17; H-16 → C-14, 16; H-17 → C-15; H-11 (NH) → C-6, 7w, 12
PG-(*S*)-sulfoxide	$J_{5,6}$ = 4.6 $J_{6,11(NH)}$ = 9.1 $J_{13a,13b}$ = 14.5	H-2 → H-9; H-5 → H-6; 10; H-6 → H-5, 11 (NH)	H-2 → C-3, 7, 8, 9w, 10; H-5 → C-7; H-6 → C-5w, 7, 12; H-9 → C-2, 3, 10; H-10 → C-2, 3, 9; H-13 → C-12, 14, 15; H-15 → C-13, 15, 17; H-16 → C-14, 16; H-17 → C-15; H-11 (NH) → C-12
PG-(*R*)-sulfoxide	$J_{5,6}$ = 4.1 $J_{6,11(NH)}$ = 7.5	H-2 → H-9; H-5 → H-6; 10; H-6 → H-5, 11 (NH)	H-2 → C-3, 7, 8, 9w, 10; H-5 → C-7; H-6 → C-7, 12; H-9 → C-2, 3, 10; H-10 → C-2, 3, 9; H-13 → C-12, 14, 15; H-15 → C-15, 17; H-16 → C-14, 16; H-17 → C-15; H-11 (NH) → C-12

Table S5.3. ^{1}H and ^{13}C chemical shifts of CP, CP-(*S*)-sulfoxide and CP-(*R*)-sulfoxide

Position[a]	**δ(^{1}H) / ppm (br = broad)**						**δ (^{13}C) / ppm**		
Compound	**CP**	**CP**	**CP-(*S*)-sulfoxide**	**CP-(*S*)-sulfoxide**	**CP-(*R*)-sulfoxide**	**CP-(*R*)-sulfoxide**	**CP**	**CP-(*S*)-sulfoxide**	**CP-(*R*)-sulfoxide**
solvent	DMSO-d_6	D_2O	DMSO-d_6	D_2O	DMSO-d_6	D_2O	D_2O	D_2O	D_2O
2							121.7	123.0	123.3
3							126.2	123.5	125.4
4a	3.22	2.96	3.65	3.56	4.03	3.98	28.0	48.1	51.6
4b	3.45	3.38	3.47	3.46	3.56	3.48	28.0	48.1	51.6
6	4.93	4.95	4.77	4.79	4.76	4.80	56.7	66.2	72.4
7	5.58	5.55	5.84	5.85	5.70	5.61	58.3	57.7	59.1
8							163.3	164.1	161.7
9							169.7	165.5	166.9
10	1.94	1.76	1.98	1.95	1.99	1.87	18.2	19.0	18.2
12							169.7	168.8	169.0
13	4.61	5.08	5.30	5.18	5.08	5.21	56.5	56.3	56.5
14							132.0	131.4	130.9
15	7.2-7.45[b]	7.43	7.3-7.6[b]	7.45	7.25-7.55[b]	7.43	128.0	127.9	128.2
16	7.2-7.45[b]	7.43	7.3-7.6[b]	7.42	7.25-7.55[b]	7.46	129.5	129.5	129.5
17	7.2-7.45[b]	7.44	7.3-7.6[b]	7.42	7.25-7.55[b]	7.47	130.2	130.3	130.5
11 (NH)	9.0 br		8.80		9.61				
18 (NH_2)			8.65 br		8.65 br				

[a] For atom numbering, see Figure 5.4 in the main text

[b] ^{1}H resonances of aromatic protons not assigned (no 2D correlations performed).

Table S5.4. **Resolved $^1H,^1H$ coupling constants, observed correlations in 1D-NOESY spectra and $^1H,^{13}C$-HMBC correlations used for NMR shift assignments of CP, CP-(*S*)-sulfoxide and CP-(*R*)-sulfoxide (measured in D_2O).**

Compound	J(^{1}H, ^{1}H) / Hz	1D-NOESY	Observed HMBC correlations (w = weak)
CP	$J_{4a,4b} = 18.0$ $J_{4b,6} = 0.7$ $J_{6,7} = 4.4$	H-6 → H-4b, 7; H-7 → H-6	H-4a → C-2, 3, 6, 8w, 9w, 10; H-4b → C-2, 3, 6w, 8w, 9w, 10w; H-6 → C-4, 8; H-7 → C-8, 12, 13; H-10 → C-2, 3, 4, 8w, 9w; H-13 → C-12, 14, 15; H-15, 16, 17 → C-13, 14, 15, 16, 17
CP-(*S*)-sulfoxide	$J_{4a,4b} = 19.1$ $J_{4b,6} = 0.9$ $J_{6,7} = 4.4$	H-4b → H-6; H-6 → H-4b, 7; H-7 → H-6; H-13 → H-15	H-4a → C-2, 3, 6, 10; H-4b → C-2, 3; H-6 → C-8; H-7 → C-6, 8, 12; H-10 → C-2, 3, 4, 8w, 9; H-13 → C-12, 14, 15; H-15/16/17 → C-13, 14, 15, 16, 17
CP-(*R*)-sulfoxide	$J_{4a,4b} = 16.6$ $J_{4b,6} = 0.9$ $J_{6,7} = 4.2$	H-6 → H-4b, 7; H-7 → H-6	H-4a → C-2, 3, 6, 10; H-4b → C-2, 3, 6w, 10w; H-6 → C-4, 8; H-7 → C-6, 8, 12; H-10 → C-2, 3, 4, 8w, 9w; H-13 → C-12, 14, 15; H-15, 16, 17 → C-13, 14, 15, 16, 17

Table S5.5. ^{1}H and ^{13}C chemical shifts of CP-P24 and CP-P33

Position[a]	**δ(^{1}H) / ppm (br = broad)**			**δ (^{13}C) / ppm (br = broad)**		
Compound	**CP-P24**	**CP-P33**	**CP-P33**	**CP-P24**	**CP-P33**	**CP-P33**
solvent	D_2O	DMSO-d_6	D_2O	D_2O	DMSO-d_6	D_2O
2				162.5 br[b]		163 br[b]
3				208.4	203.6	208.3
4	3.45+3.38	3.64	3.71+3.66	41.1	41.9	41.2
6	5.17	5.27	5.35	55.3 br	57.4	57.3
7	4.80	4.49	4.55	56.1 br	56.5	57.7
8				171.4		166.0
9				161.4 br[b]		162 br[b]
10	2.09	2.17	2.22	27.7	28.4	27.9
12				168.3		169.5
13	5.11	4.96	5.25	56.5	58.4	58.5
14				131.2	138.7	136.1
15	7.42	7.34	7.33	127.8	127.4	127.7
16	7.47	7.36	7.39	129.6	128.4	129.1
17	7.48	7.33	7.46	130.5	128.0	129.6
1 (NH)		9.13				
11 (NH)		8.39 br				
18 (NH)		9.04				

[a] For atom numbering, see Figure 5.5 in the main text

[b] Assignment of C-2/C-9 arbitrarily.

Table S5.6. Resolved ^{1}H,^{1}H coupling constants, observed correlations in 1D-NOESY spectra and ^{1}H,^{13}C-HMBC correlations used for NMR shift assignments of CP-P24 and CP-P33 (measured in D_2O).

Compound	**J(^{1}H, ^{1}H) / Hz**	**1D-NOESY**	**Observed HMBC correlations (w = weak)**
CP-P24	$J_{4a,4b}$ = 17.0 $J_{6,7}$ = 6.4	H-7 → H-6	H-4a, 4b → C-3, 6; H-6 → C-4, 7; H-7 → C-6, 8, 12; H10 → C-3, 4; H-13 → C-12, 14, 15; H-15, 16, 17 → C-13, 14, 15, 16, 17
CP-P33	$J_{4a,4b}$ = 17.1 $J_{6,7}$ = 3.3	H-6 → H-7; H-7 → H-6, 15; H-10 → H-4a, 4b; H-13 → H- 15; H-15 → H-7, 13	H-4a, 4b → C-3, 6; H-6 → C-4, 7, 8; H-7 → C-6, 8, 12; H-10 → C-3, 4; H-13 → C-6w, 8, 12, 14, 15; H-15, 16, 17 → C-13, 14, 15, 16, 17

Table S5.7. **^{15}N chemical shifts obtained from ^{1}H,^{15}N HMQC of all PG and CP isomers discussed.**

Position[a]	**δ(^{15}N) / ppm**							
Compound	**PG**	**PG-(*S*)-sulfoxide**	**PG-(*R*)-sulfoxide**	**CP**	**CP-(*S*)-sulfoxide**	**CP-(*R*)-sulfoxide**	**CP-P24**	**CP-P33**[b]
solvent	DMSO-d_6	DMSO-d_6	DMSO-d_6	D_2O	D_2O	D_2O	D_2O	DMSO-d_6
N-1	-212.3	-238.7	-240.7	-227.7	-252.0	-234.6	-256.8	-257.5
N-11	-268.1	-271.7	-269.1	-273.4	-273.3	-274.8	-264.5	-266.8
N-18				-339.7	-340.1	-339.3	-340.0	-256.6

[a] For atom numbering, see Figures 5.3, 5.5, and 5.6 in the main text

[b] Correlations obtained over $^{1}J(NH)$ coupling, no signals obtained in D_2O solution.

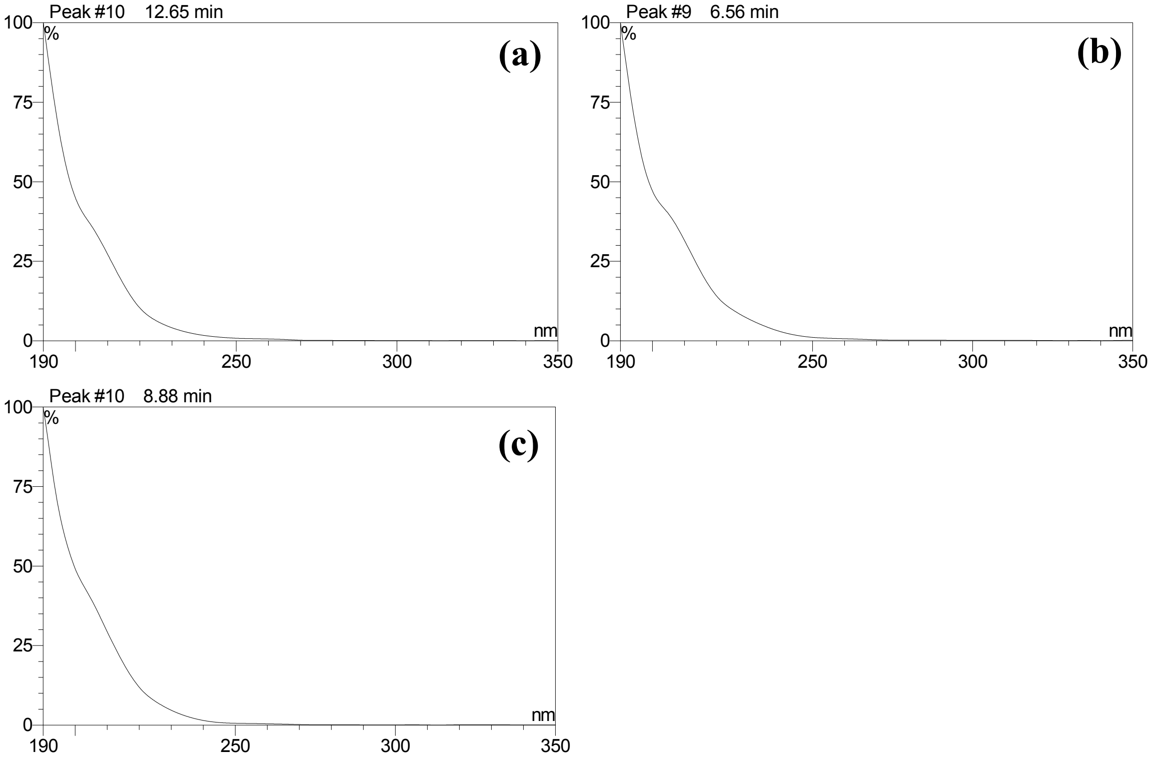

Figure S5.1. Ultraviolet spectra of (a) PG, (b) PG-(*R*)-sulfoxide, (c) and PG-(*S*)-sulfoxide, acquired via the HPLC-UV analytical method described for PG in the Materials and Methods section of the main text

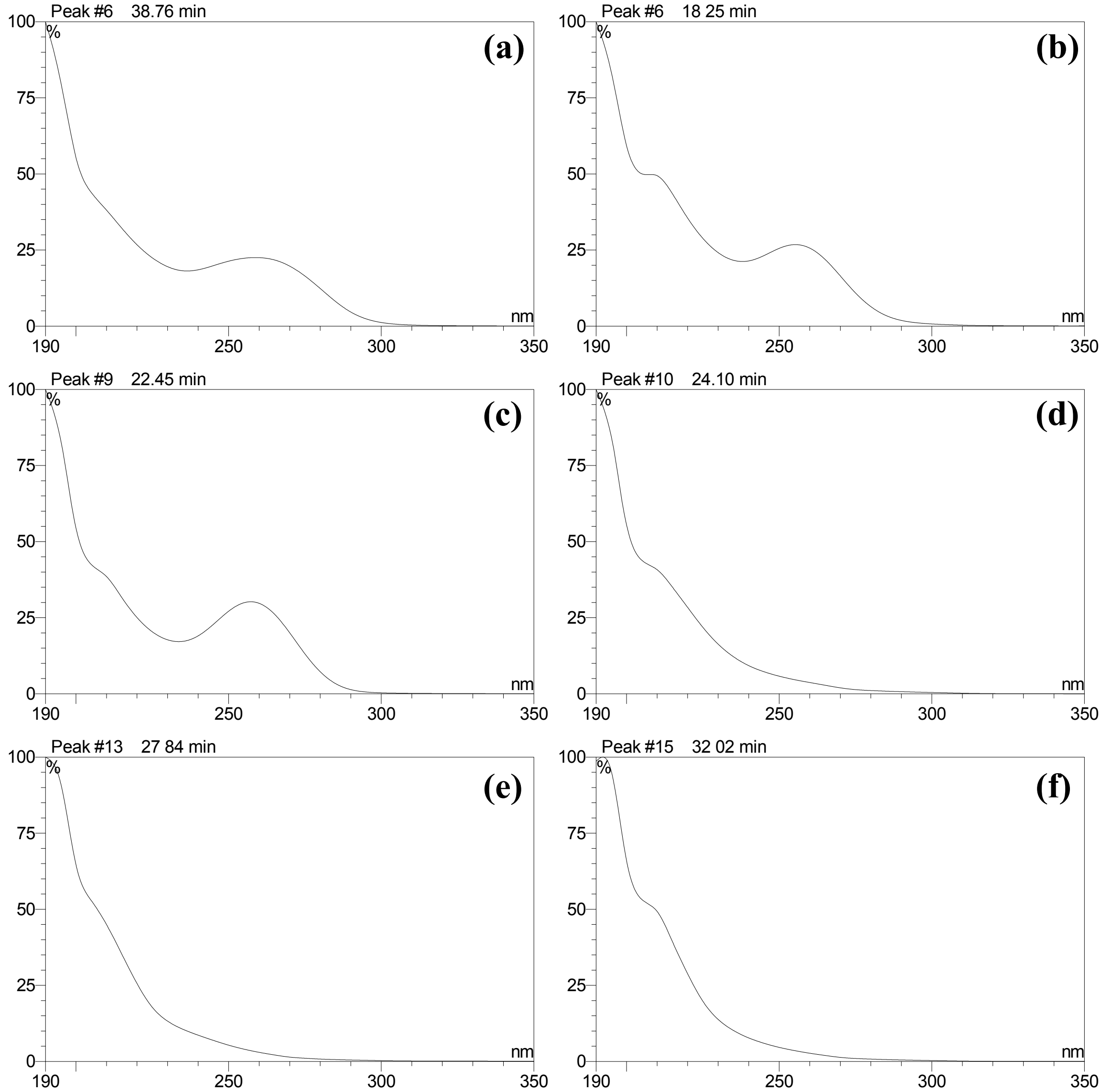

Figure S5.2. Ultraviolet spectra of (a) CP, (b) CP-(*R*)-sulfoxide, (c) CP-(*S*)-sulfoxide, (d) CP-P24, (e) CP-P28, and (f) CP-P33, acquired via the HPLC-UV analytical method described in the Materials and Methods section of the main text

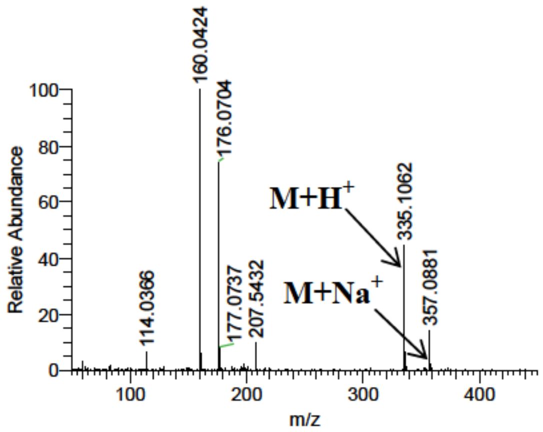

Figure S5.3. High-resolution, full-scan, positive-mode ESI mass spectrum acquired for PG, using the Orbitrap FT-MS as detector

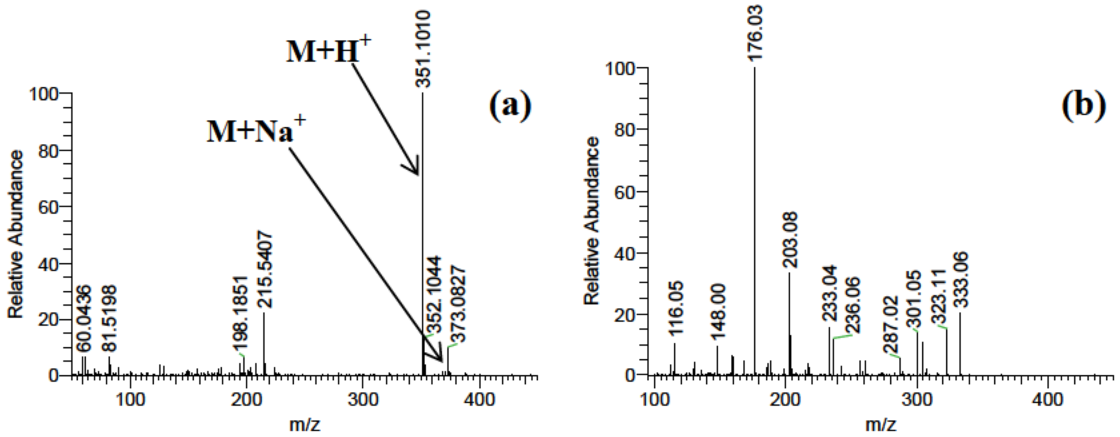

Figure S5.4. (a) High-resolution, full-scan, positive-mode ESI mass spectrum acquired for PG-(*R*)-sulfoxide, using the Orbitrap FT-MS as detector, and (b) Normal-resolution, positive-mode ESI MS^2 spectrum acquired for PG-(*R*)-sulfoxide, using the LTQ linear-ion trap for target ion fragmentation and product detection

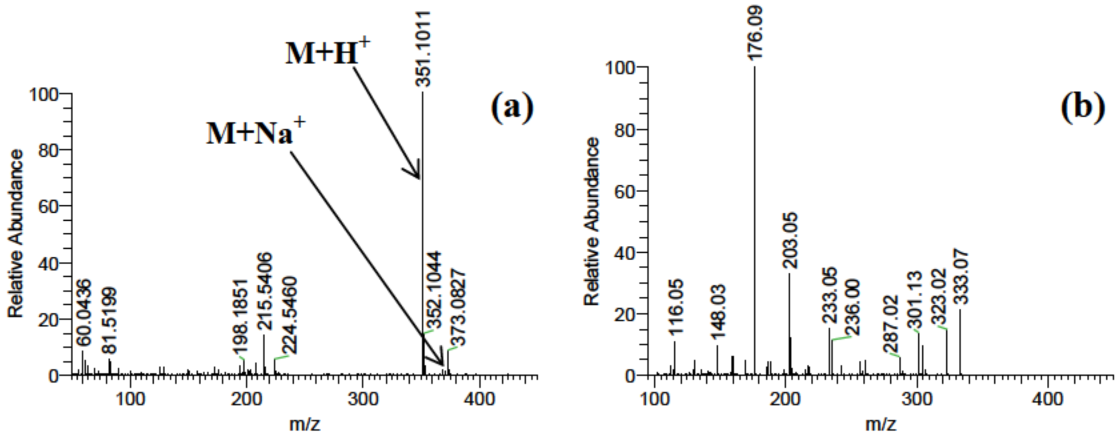

Figure S5.5. (a) High-resolution, full-scan, positive-mode ESI mass spectrum acquired for PG-(*S*)-sulfoxide, using the Orbitrap FT-MS as detector, and (b) Normal-resolution, positive-mode ESI MS^2 spectrum acquired for PG-(*S*)-sulfoxide, using the LTQ linear-ion trap for target ion fragmentation and product detection

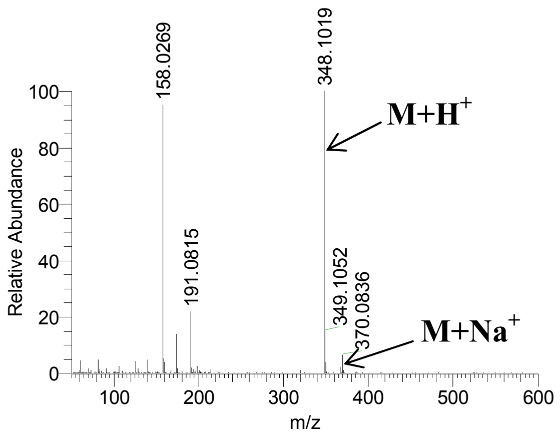

Figure S5.6. High-resolution, full-scan, positive-mode ESI mass spectrum acquired for CP, using the Orbitrap FT-MS as detector

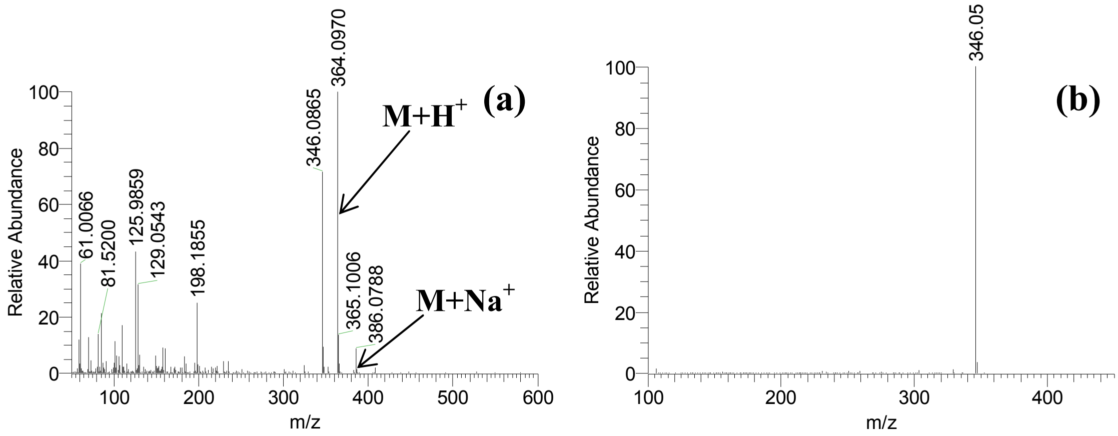

Figure S5.7. (a) High-resolution, full-scan, positive-mode ESI mass spectrum acquired for CP-(*R*)-sulfoxide, using the Orbitrap FT-MS as detector, and (b) Normal-resolution, positive-mode ESI MS^2 spectrum acquired for CP-(*R*)-sulfoxide, using the LTQ linear-ion trap for target ion fragmentation and product detection

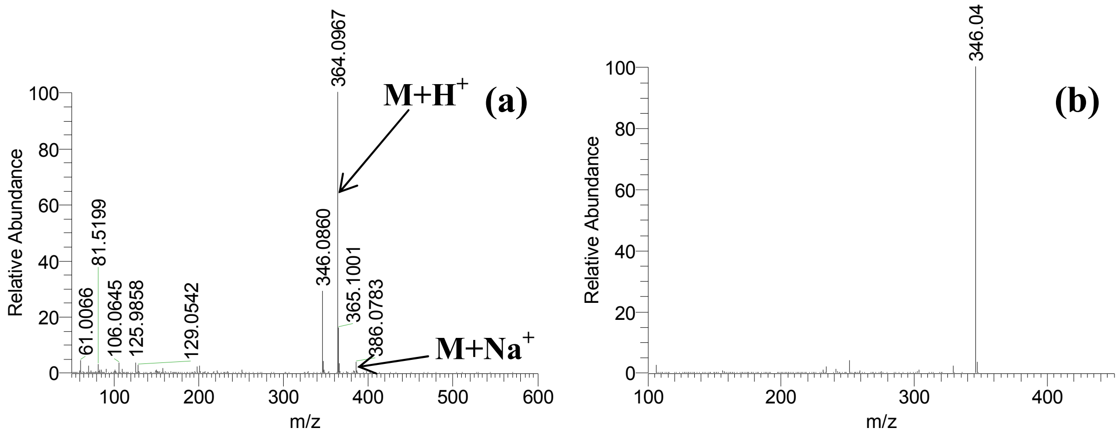

Figure S5.8. (a) High-resolution, full-scan, positive-mode ESI mass spectrum acquired for CP-(*S*)-sulfoxide, using the Orbitrap FT-MS as detector, and (b) Normal-resolution, positive-mode ESI MS^2 spectrum acquired for CP-(*S*)-sulfoxide, using the LTQ linear-ion trap for target ion fragmentation and product detection

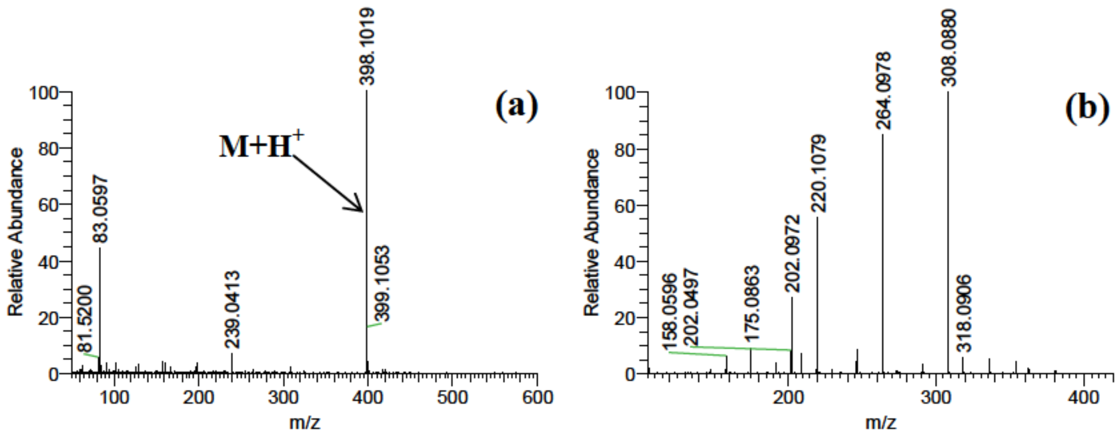

Figure S5.9. (a) High-resolution, full-scan, positive-mode ESI mass spectrum acquired for CP-P24, using the Orbitrap FT-MS as detector, and (b) High-resolution, positive-mode ESI MS^2 spectrum acquired for CP-P24, using the Orbitrap for target ion fragmentation and product detection

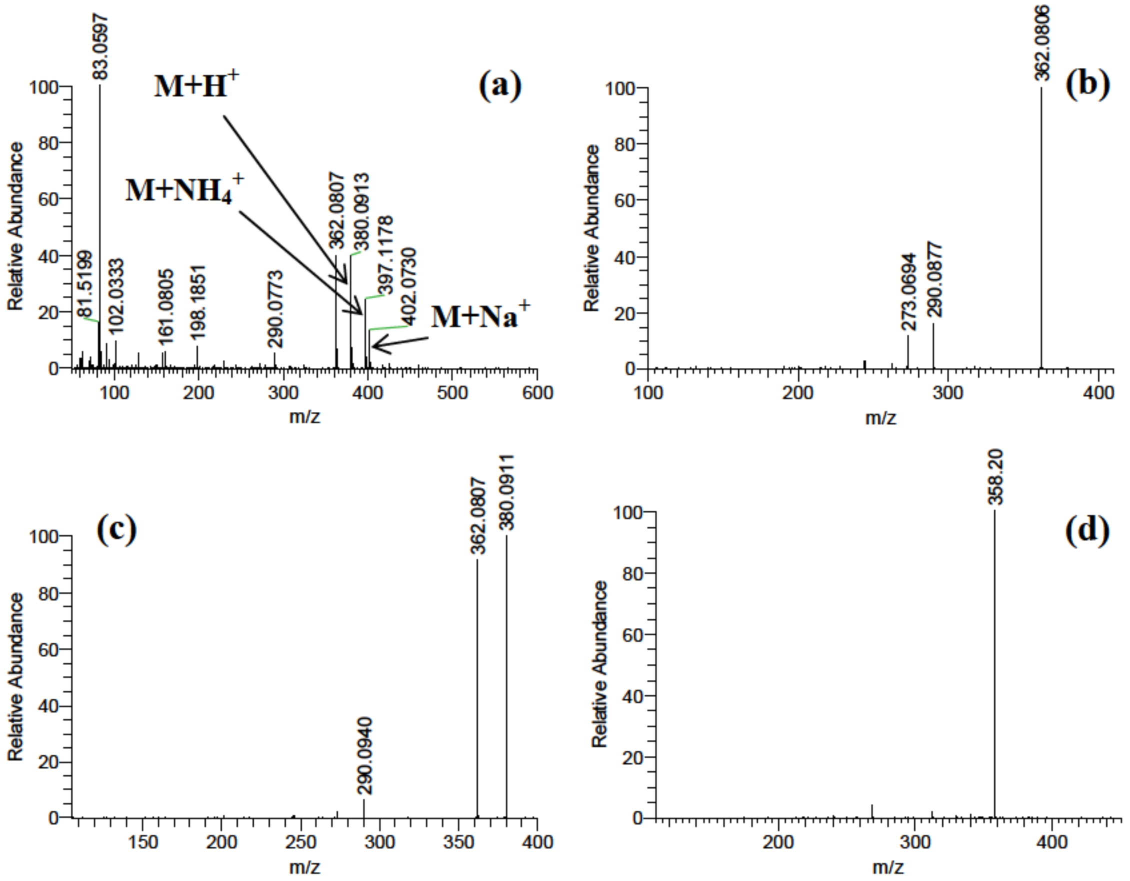

Figure S5.10. (a) High-resolution, full-scan, positive-mode ESI mass spectrum acquired for CP-P33, using the Orbitrap FT-MS as detector, (b) High-resolution, positive-mode ESI MS^2 spectrum acquired for CP-P33, using the Orbitrap for target ion fragmentation and product detection, (c) High-resolution, positive-mode ESI MS^2 spectrum acquired for the CP-P33 + NH$_4^+$ adduct (m/z 397.1178), using the Orbitrap for target ion fragmentation and product detection, and (d) Normal-resolution, positive-mode ESI MS^2 spectrum acquired for CP-P33 + Na$^+$ adduct (m/z 402.0730), using the LTQ linear-ion trap for target ion fragmentation and product detection

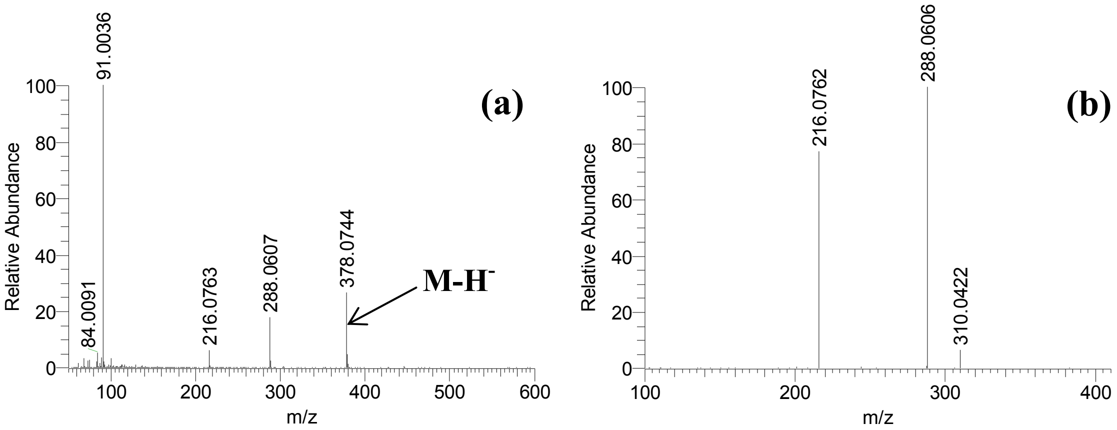

Figure S5.11. (a) High-resolution, full-scan, negative-mode ESI mass spectrum acquired for CP-P33, using the Orbitrap FT-MS as detector, and (b) High-resolution, negative-mode ESI MS^2 spectrum acquired for CP-P33, using the Orbitrap for target ion fragmentation and product detection

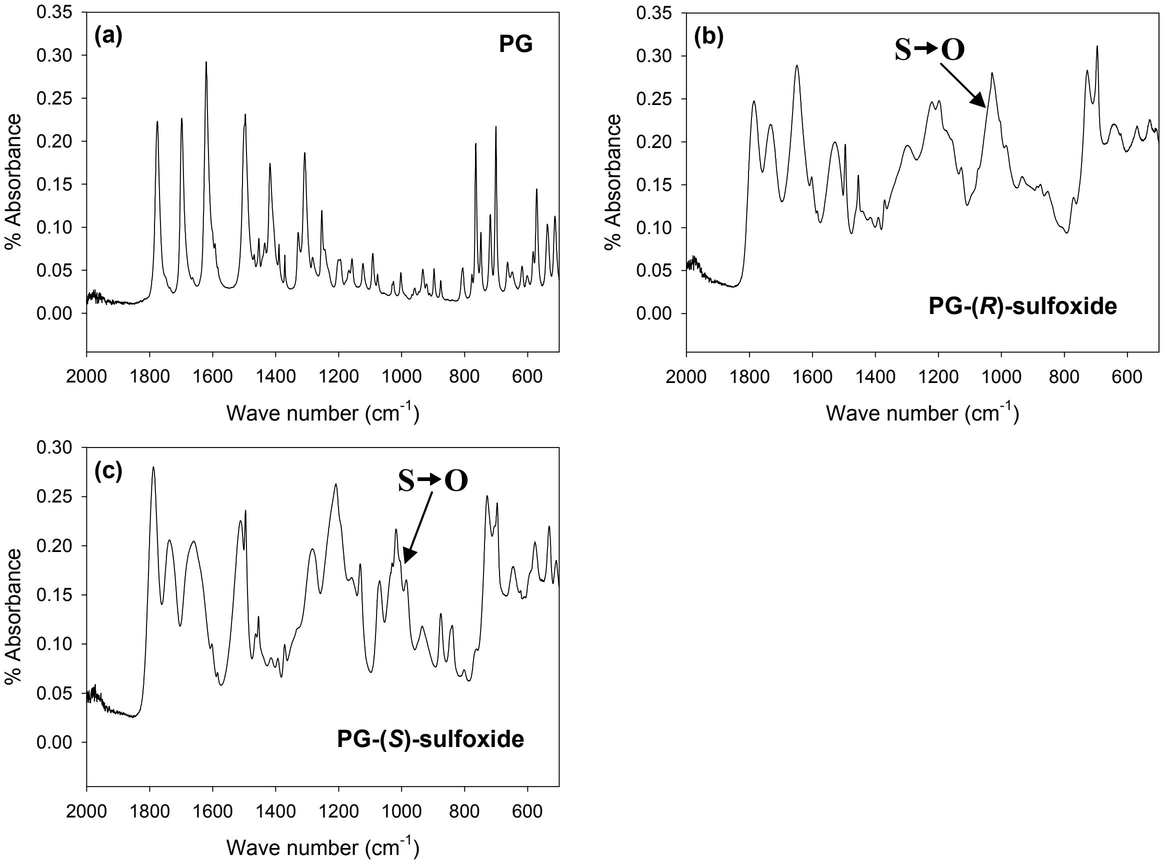

Figure S5.12. Solid-state FT-IR spectra acquired for (a) PG, (b) PG-(*R*)-sulfoxide, (c) PG-(*S*)-sulfoxide

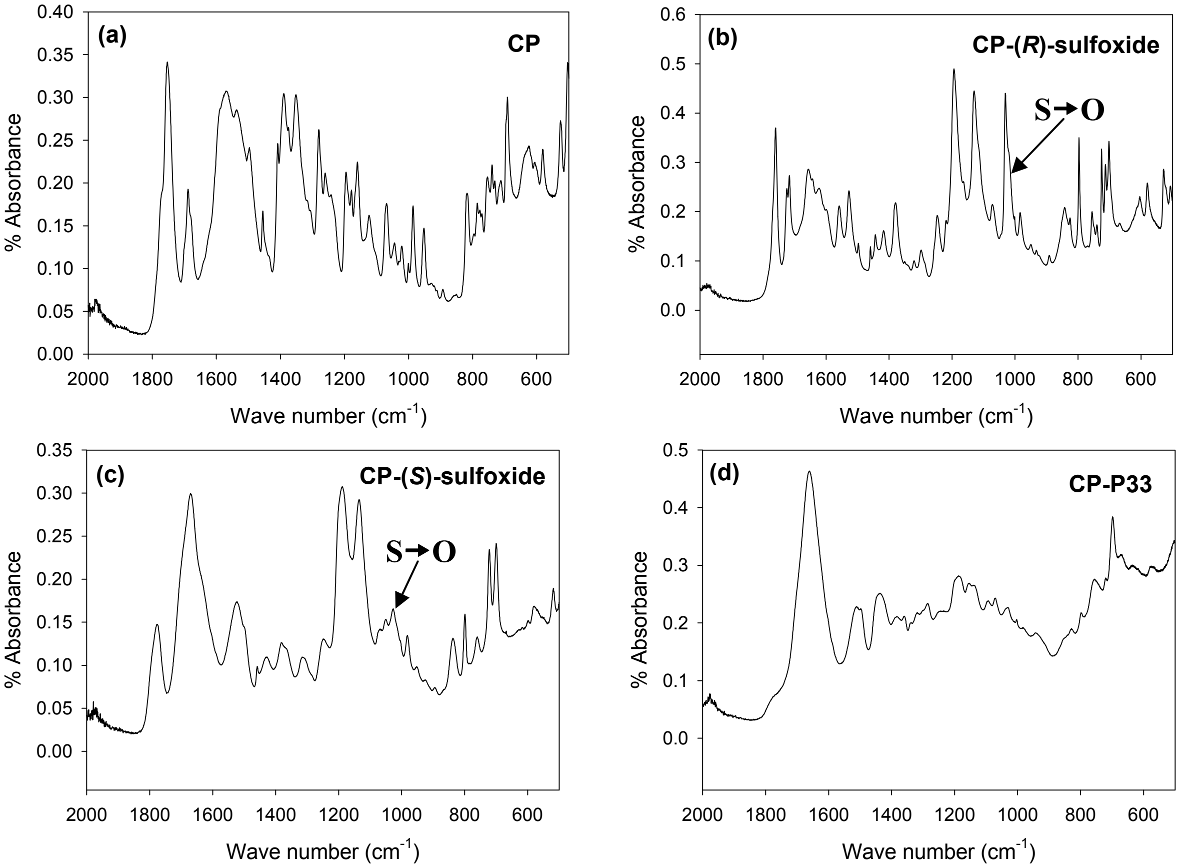

Figure S5.13. Solid-state FT-IR spectra acquired for (a) CP, (b) CP-(*R*)-sulfoxide, (c) CP-(*S*)-sulfoxide, and (d) CP-P33

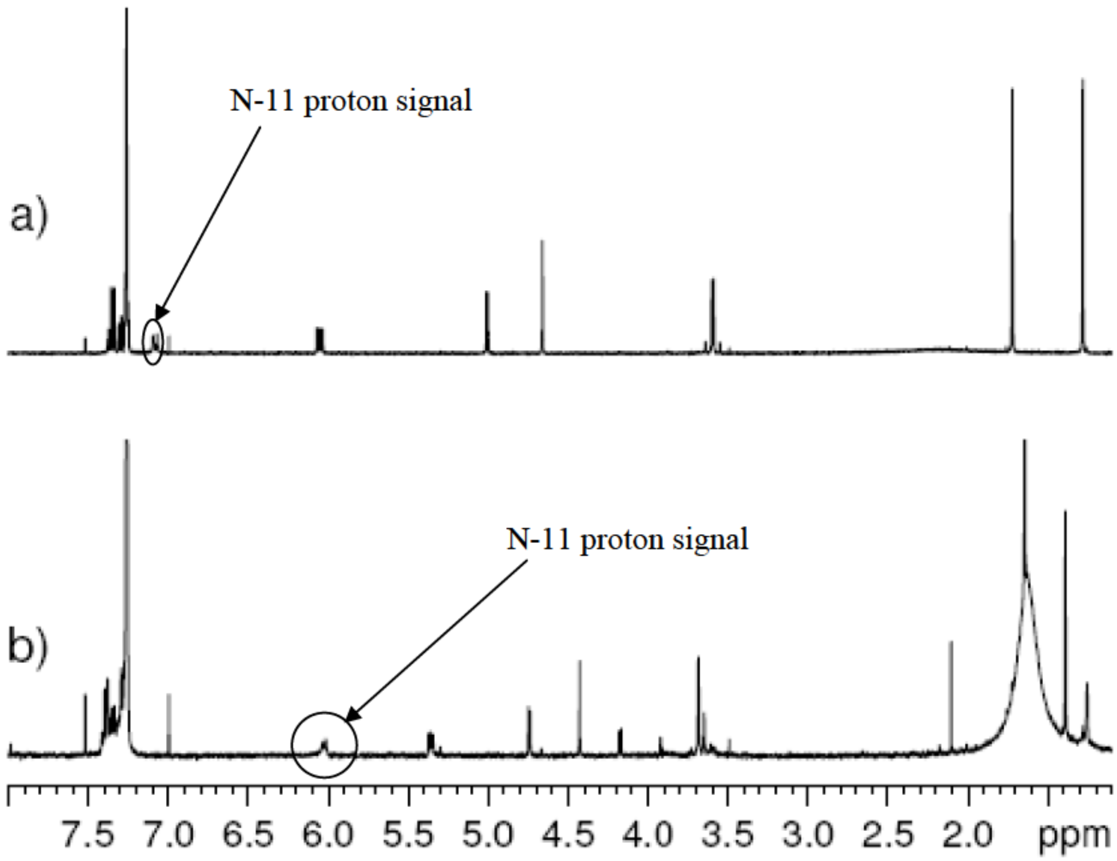

Figure S5.14. **^{1}H NMR spectra acquired for $CDCl_3$ solutions of (a) PG-(*S*)-sulfoxide and (b) PG-(*R*)-sulfoxide**

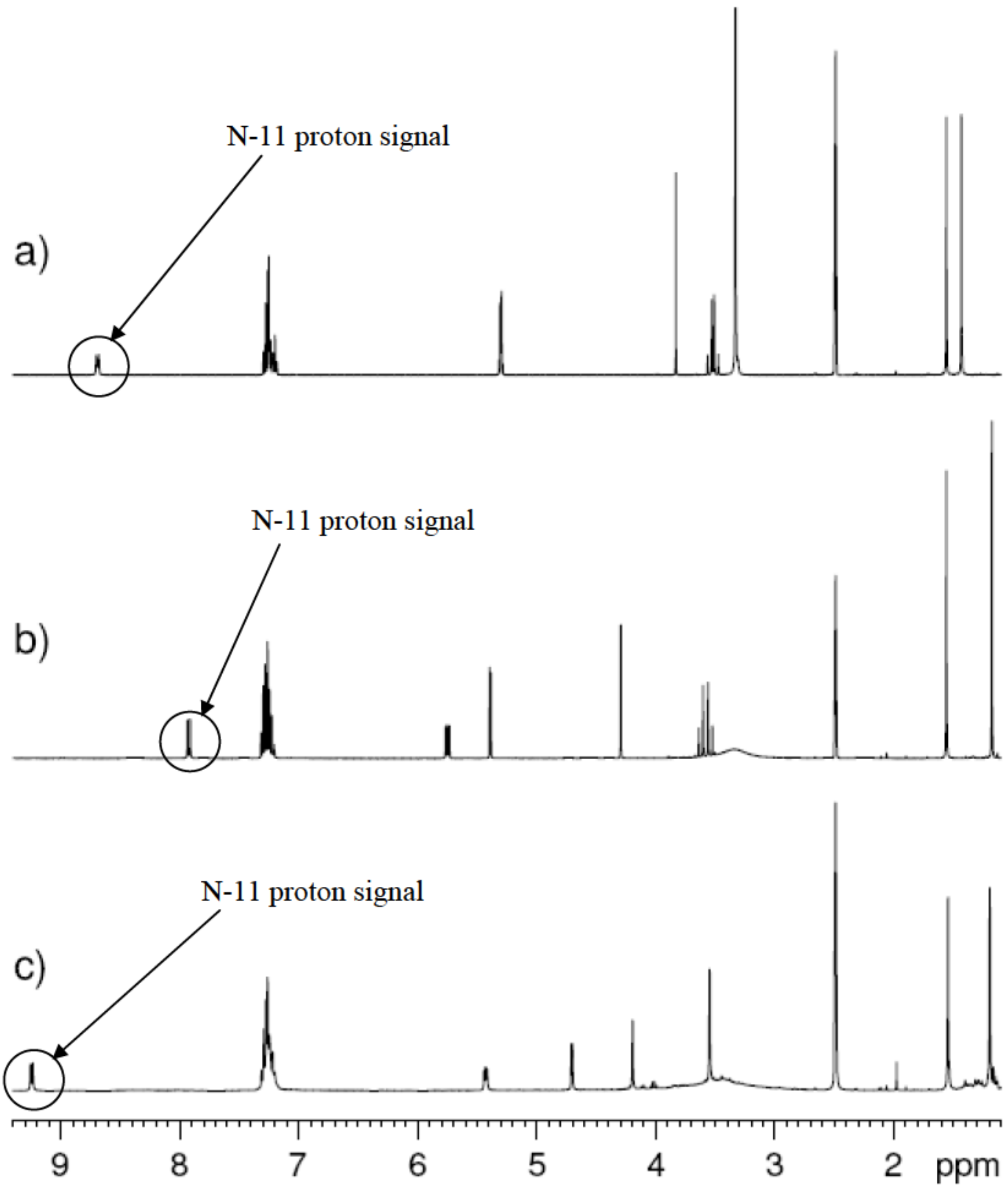

Figure S5.15. **^{1}H NMR spectra acquired for DMSO-d$_6$ solutions of (a) PG, (b) PG-(*S*)-sulfoxide, and (c) PG-(*R*)-sulfoxide**

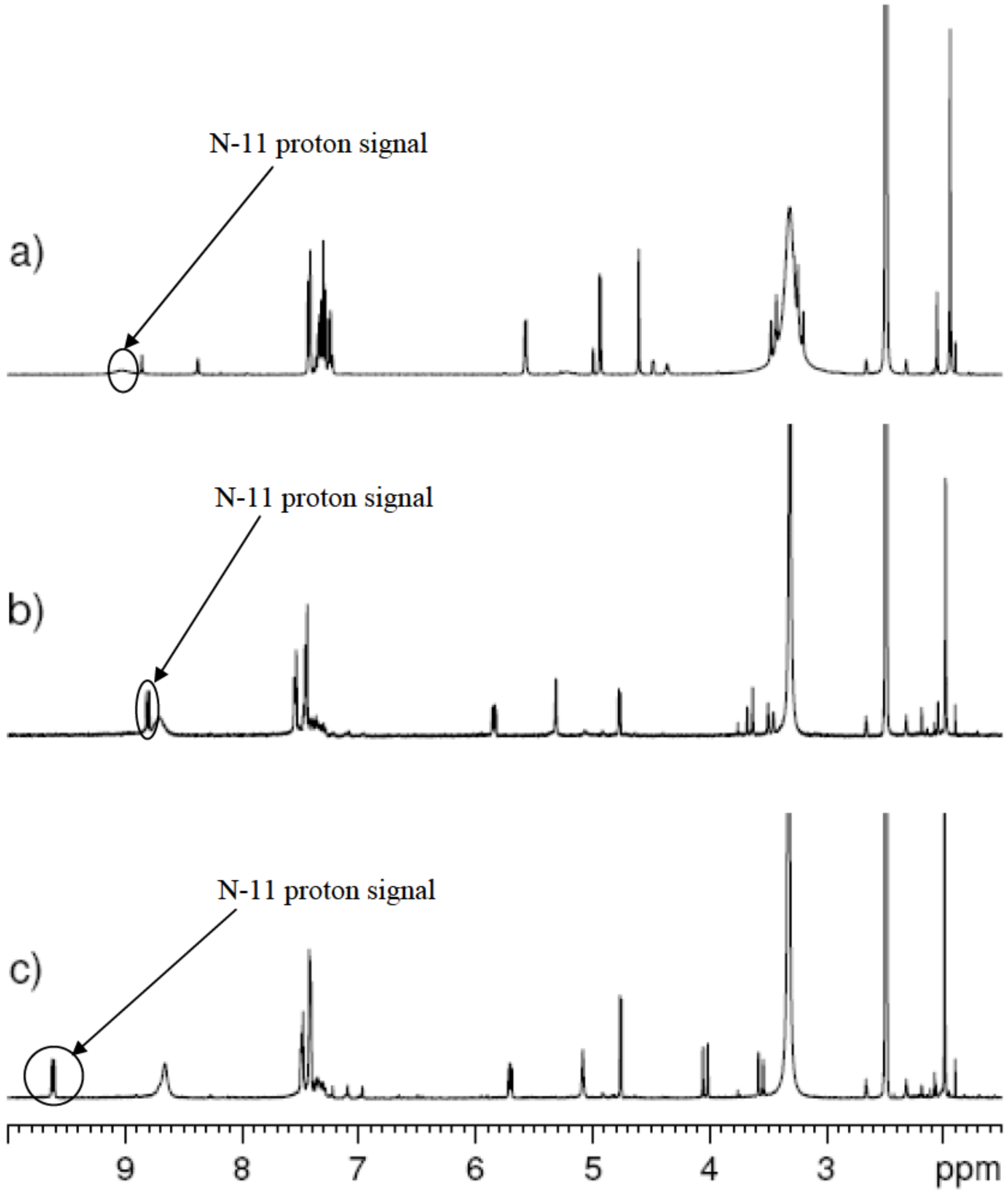

Figure S5.16. **^{1}H NMR spectra acquired for DMSO-d$_6$ solutions (a) CP, (b) CP-(*S*)-sulfoxide, and (c) CP-(*R*)-sulfoxide**

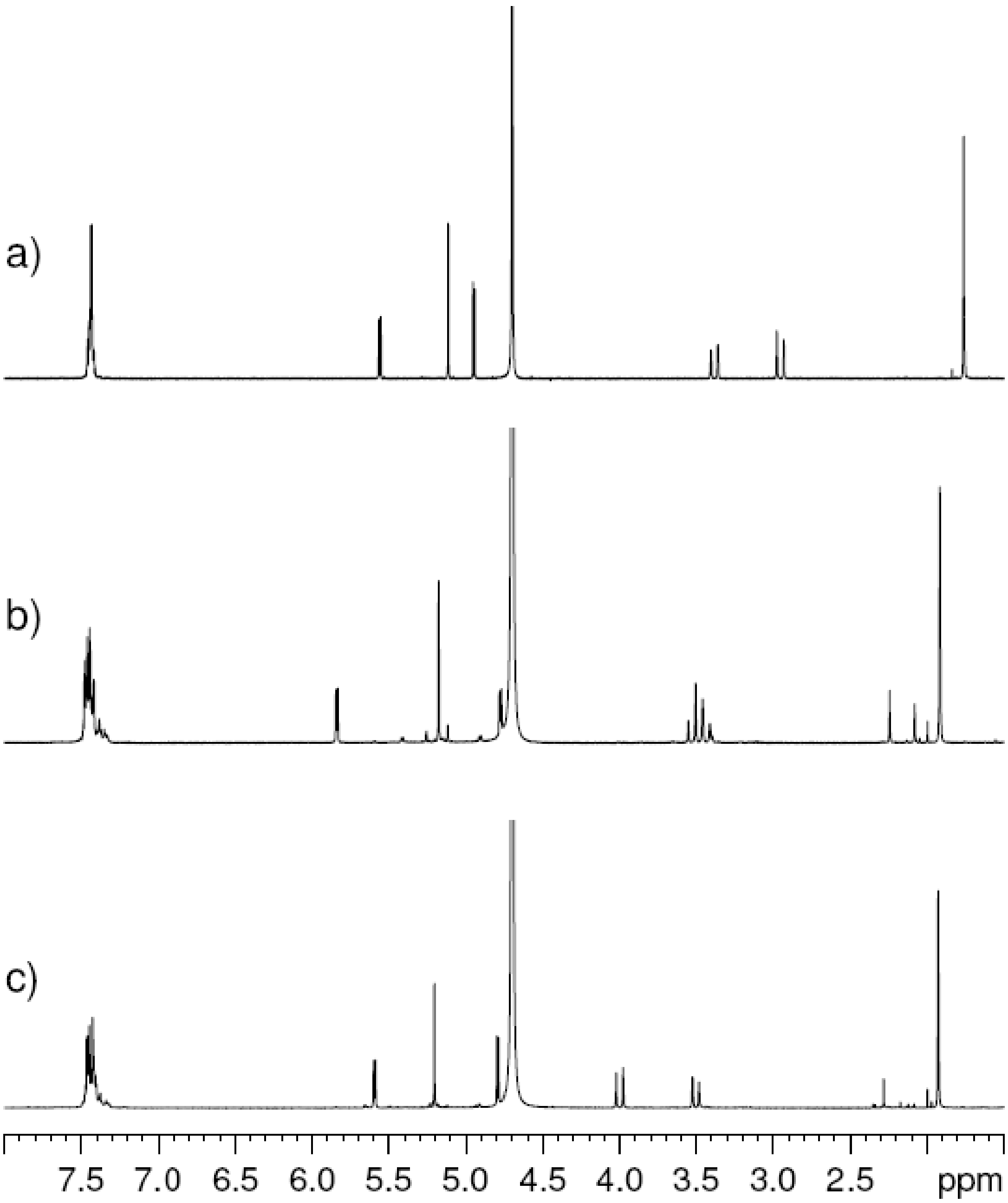

Figure S5.17. **^{1}H NMR spectra acquired for DMSO-d$_6$ solutions of (a) CP-(*S*)-sulfoxide, (b) CP-P24, and (c) CP-P33**

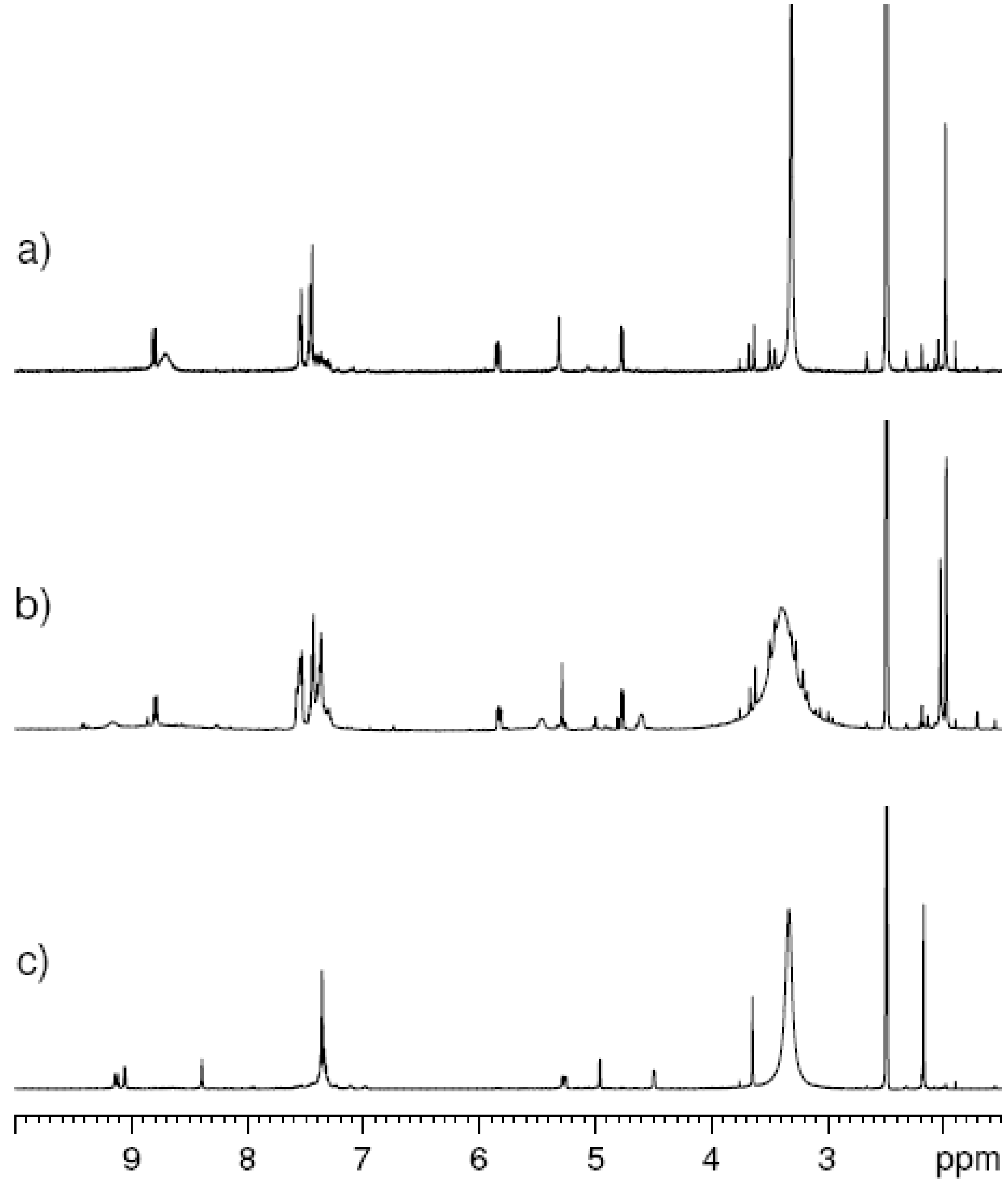

Figure S5.18. ^{1}H NMR spectra acquired for D_2O solutions of (a) CP, (b) CP-(*S*)-sulfoxide, and (c) CP-(*R*)-sulfoxide

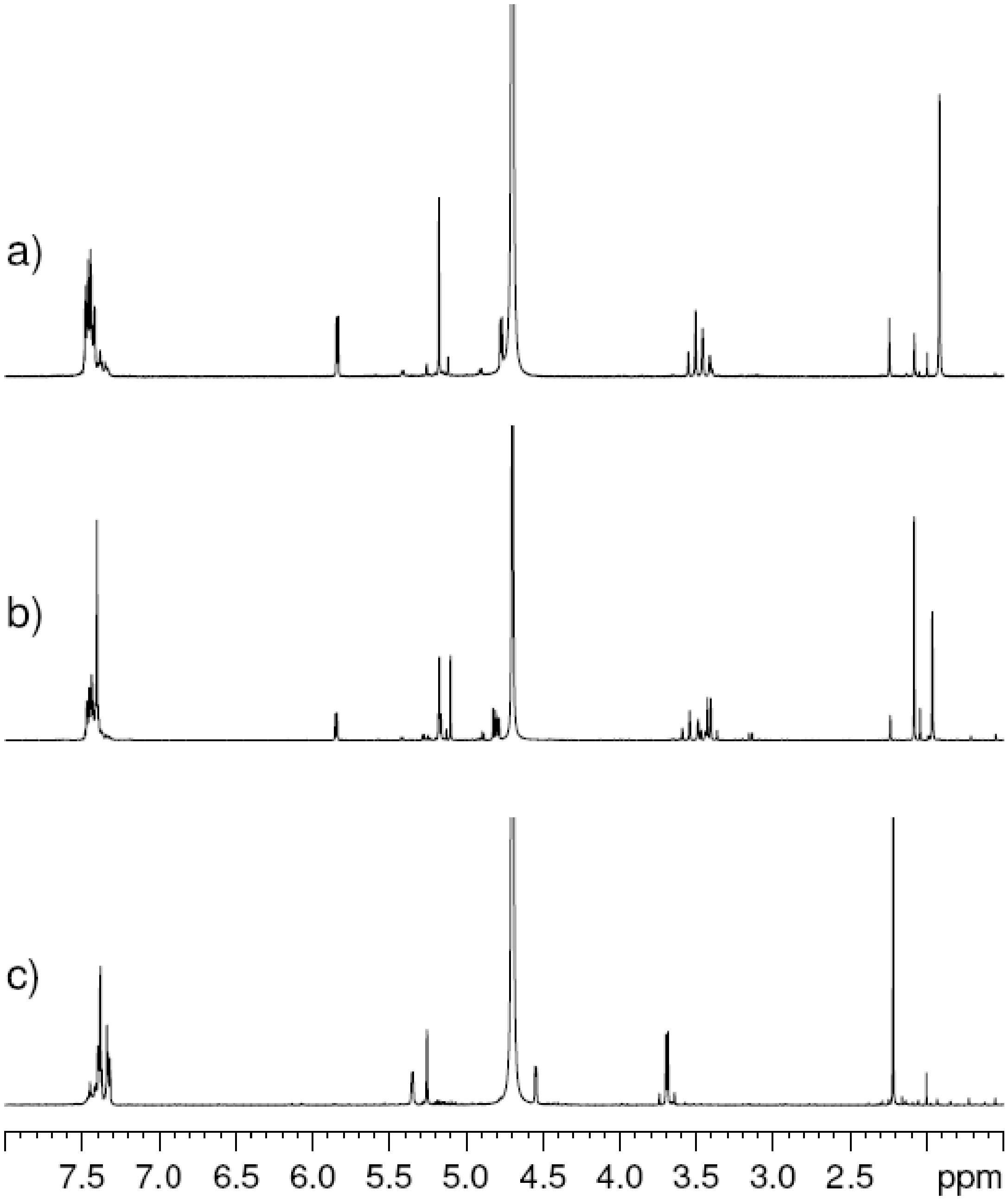

Figure S5.19. ^{1}**H NMR spectra acquired for** D_2O **solutions of (a) CP-(*S*)-sulfoxide, (b) CP-P24, and (c) CP-P33**

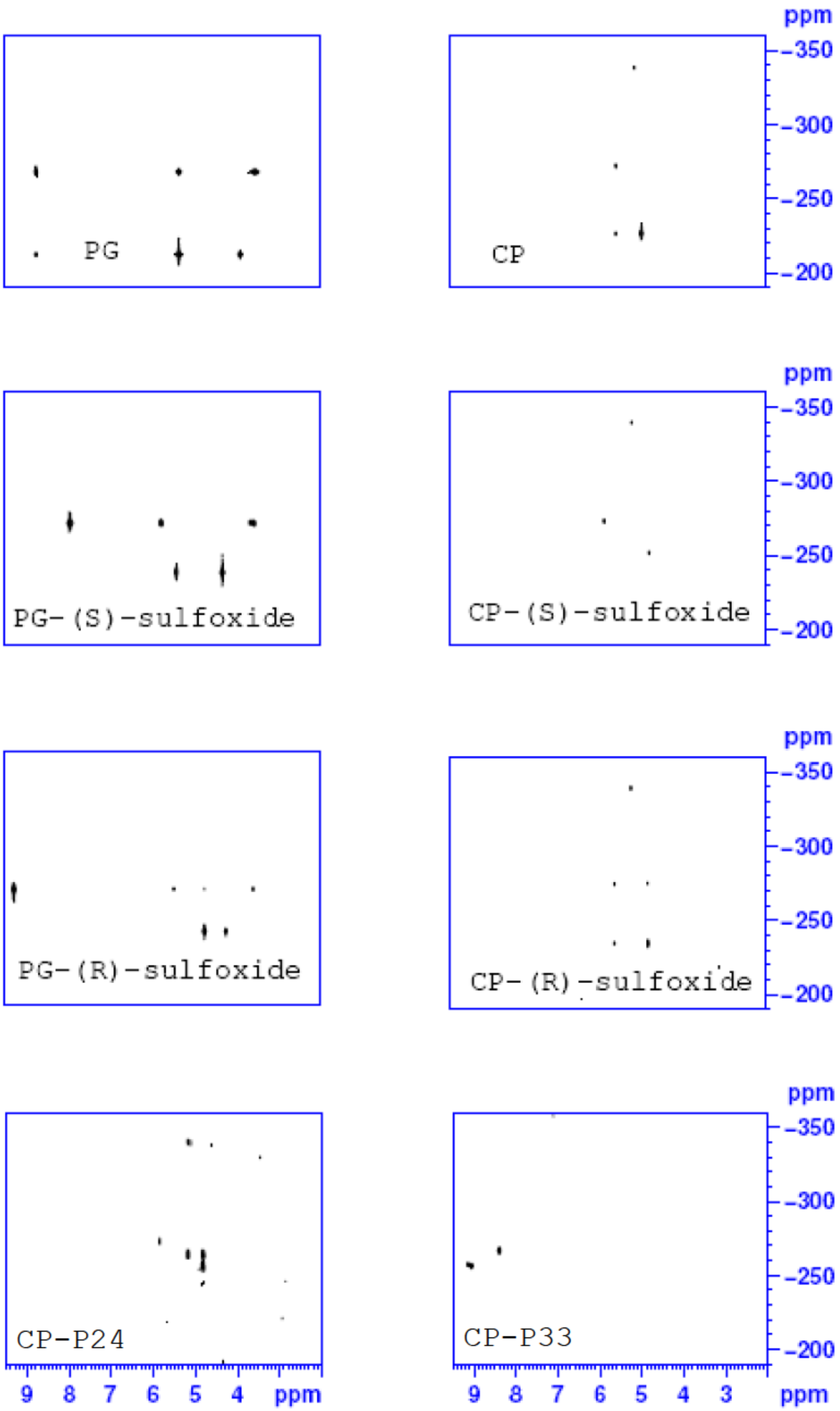

Figure S5.20. Natural abundance ^{1}H,^{15}N HMQC spectra acquired for DMSO-d_6 solutions of PG and PG transformation products and D_2O solutions of CP and CP transformation products, except for CP-P33 which was analyzed in DMSO-d_6

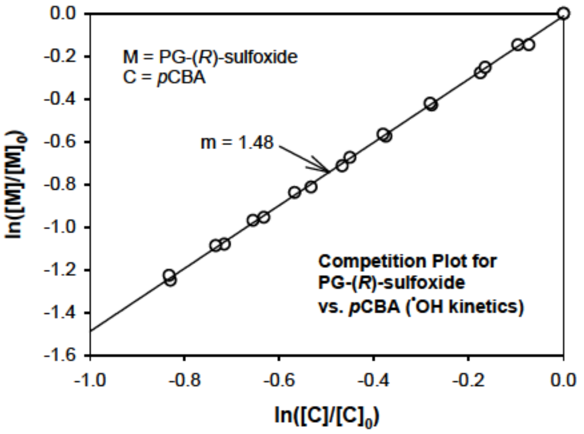

Figure S5.21. Competition kinetics plot for reaction of PG with $^{\bullet}$OH (using *p*CBA as a reference competitor) in 1-mM, pH 7 phosphate buffer

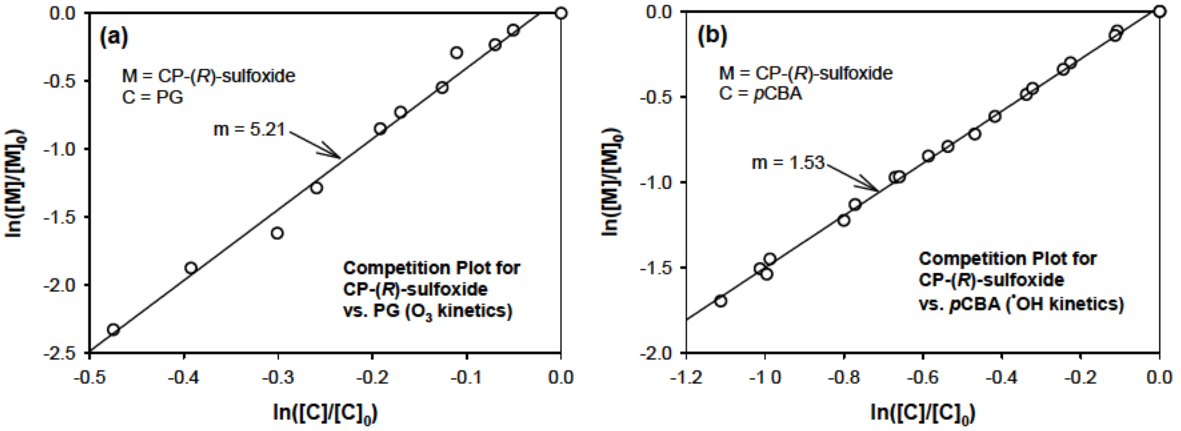

Figure S5.22. Competition kinetics plots for reaction of CP with (a) O_3 (using PG as a reference competitor) and (b) $^{\bullet}$OH (using *p*CBA as a reference competitor) in 1-mM, pH 7 phosphate buffer (which also contained 5-mM *t*-BuOH for the O_3 experiments)

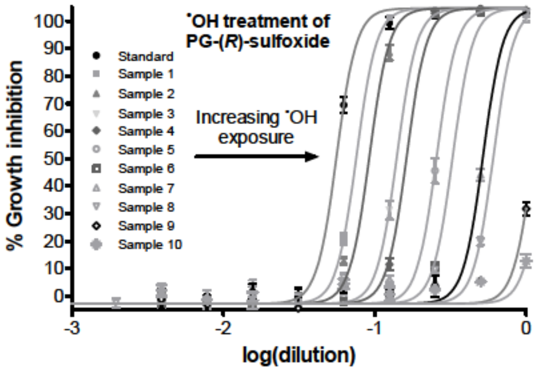

Figure S5.23. Dose-response relationships measured for oxidation of PG-(*R*)-sulfoxide by •OH. %I measurements (symbols) depicted with 95% confidence intervals determined for triplicate data sets. Fits (lines) obtained as described in Materials and Methods section of the main text. The independent variable “dilution” is determined as described in the caption to Figure 5.7 in the main text.

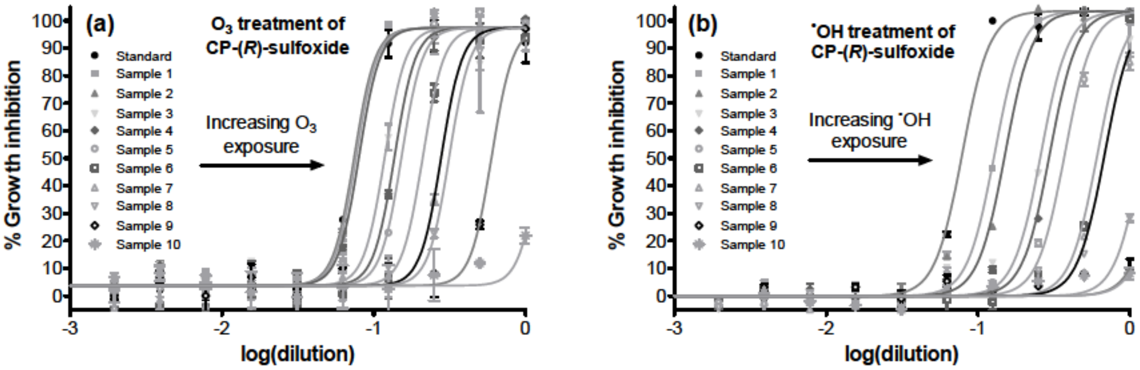

Figure S5.24. Dose-response relationships measured for oxidation of CP-(*R*)-sulfoxide by (a) O_3 and (b) •OH. %I measurements (symbols) depicted with 95% confidence intervals determined for triplicate data sets. Fits (lines) obtained as described in Materials and Methods section of the main text. The independent variable "dilution" is determined as described in the caption to Figure 5.7 in the main text.

Chapter 6. General Conclusions

Wastewater ozonation is rapidly becoming a process of choice for tertiary wastewater treatment applications in which a major objective is micropollutant oxidation prior to discharge or reuse of the treated effluents. Several of the more notable reasons for this resurgence in the popularity of O_3-based treatment have been (a) relatively extensive historical experience in the design and application of gas-liquid ozonation applications in water treatment, (b) the reported effectiveness of ozonation in yielding the apparent elimination of many micropollutant molecules (e.g., pharmaceuticals, natural steroid hormones, biocides, anti-corrosive agents), whether by direct reactions with O_3 or with incidentally-produced $^{\bullet}OH$, and (c) a perception that O_3-based treatment is relatively green (i.e., it leaves no stable residual, and utilizes only O_2 and electricity as inputs).

In regards to the second of these factors, there has been frequent discussion within the literature as to whether the analytically-apparent "disappearance" of various micropollutant classes during ozonation is accompanied by (i) loss of their undesirable properties (in the case of such biologically-active compounds as steroid hormones and antibacterial agents), or (ii) emergence of undesirable properties associated with formation of unidentified transformation products. While each of these two topics is of sufficient importance to merit study in the context of human health and ecotoxicological risks, the first seems to be of substantially greater priority as regards wastewater treatment, primarily due to the fact that certain classes biologically-active wastewater-borne micropollutants that exert target-specific modes of activity - namely the steroid hormones and antibacterial agents - are already sufficiently potent that the concentration levels at which they are present in wastewaters may approach or exceed relevant biological effect levels for various susceptible aquatic organisms. Any deleterious transformation products generated during ozonation would likewise have to be of very high *target-specific* toxicity to exert appreciable effects on a given organism, which is relatively unlikely, considering the restrictive stereochemical and physical-chemical constraints on typical target-specific biological effects.

As of the initiation of this work, appreciable data was available as to the O_3 and $^{\bullet}OH$ reaction kinetics and toxicological outcomes of O_3-based treatment for steroid hormones. However, only limited data was available pertaining to reaction kinetics for oxidation of antibacterial molecules by O_3 and $^{\bullet}OH$, and essentially no information was available as to how the biological activities of antibacterial agents were affected by such reactions during ozonation. Accordingly, the present investigation was undertaken with the primary objectives of (a) measuring the kinetics of O_3 and $^{\bullet}OH$ reactions with representative members of the most prominent antibacterial classes present in municipal wastewaters, (b) determining the resulting changes in biological activities of these model antibacterial compounds, (c) in the case of model compounds not deactivated by reaction with either oxidant – identifying and characterizing the biologically active products, and (d) providing the data necessary to make informed decisions as to the likely benefits of and design requirements for utilizing O_3-based oxidative treatment to achieve elimination of target-specific antibacterial activities. The corresponding outcomes and major conclusions of this work can be summarized as follows:

I. All of the model antibacterial compounds included in this investigation were found to be oxidized by O_3 with apparent second-order rate constants, $k''_{O_3,app} > 1 \times 10^3$ M^{-1}s^{-1}, at pH 7, with the exception of *N*(4)-acetyl-sulfamethoxazole, for which $k''_{O_3,app}$ is 2.5×10^2 M^{-1}s^{-1}. $k''_{O_3,app}$ (pH 7) for macrolides, sulfamethoxazole, trimethoprim, tetracycline, vancomycin, amikacin, and triclosan were found to correspond to oxidation of biochemically essential moieties. Initial reactions of O_3 with N(4)-acetylsulfamethoxazole, fluoroquinolones, lincomycin, and *β*-lactams do not lead to appreciable oxidation of biochemically essential moieties, although O_3 does attack such moieties within the fluoroquinolones and lincomycin via slower secondary reactions. During ozonation of various secondary municipal wastewater effluent samples, measured model compound losses were highly dependent on $k''_{O_3,app}$, but effectively independent of $k''_{\bullet OH,app}$. O_3 doses ≥ 3 mg/L yielded ≥ 99% depletion of fast-reacting substrates ($k''_{O_3,app} > 5 \times 10^4$ M^{-1}s^{-1}). Eleven of the model compounds were oxidized primarily via direct reactions with O_3, whereas only four (amikacin, penicillin G, cephalexin, N(4)-acetylsulfamethoxazole) were oxidized to a substantial degree by $^\bullet$OH. These results provide a strong indication that many antibacterial compounds will be oxidized in wastewater via selective reactions with O_3.

II. Microbiological assays developed to quantify the changes in antibacterial potencies resulting from treatment of each model antibacterial compound with increasing doses of O_3 and $^\bullet$OH show that O_3 and $^\bullet$OH reactions lead in nearly all cases to stoichiometric elimination of antibacterial activity (i.e., loss of one mole equivalent of potency per mole of parent compound consumed). The *β*-lactams penicillin G (PG) and cephalexin (CP) represent the only two exceptions, as bioassay measurements indicate that the direct reaction of these two compounds with O_3 leads to formation of biologically active transformation products. Nevertheless, these data, coupled with knowledge of ozonation process data at the pilot- and full-scale, suggest that wastewater ozonation will generally yield sufficient structural modification of the investigated antibacterial molecules to eliminate their antibacterial activities, whether oxidation results from selective reactions with O_3 or from relatively non-selective reactions with incidentally-produced $^{\bullet}OH$.

III. PG was found to yield two major products in nearly equal yields, together accounting for approximately 100% of the parent compound consumption. These two products were identified unambiguously as the stereoisomeric (*R*)- and (*S*)-sulfoxides of PG. The former of these was determined to retain roughly 15% of the potency of the parent PG molecule, whereas the latter was functionally inactive. Each of the PG sulfoxides was determined to be recalcitrant toward further oxidation by O_3. However, the (*R*)-sulfoxide was readily transformed by $^{\bullet}OH$ (with $k''_{\bullet\mathrm{OH,app}} = 7.4 \times 10^9\ \mathrm{M^{-1}s^{-1}}$, at pH 7), resulting in roughly quantitative elimination of its biological activity. CP was found to yield four major transformation products. These were unambiguously identified as the (*R*)- and (*S*)-sulfoxides of CP (formed in ~34% and ~18% yields) and two C-2/C-3 double bond cleavage products (formed in ~5% and ≥28% yields); one a structural analogue of the penicilloic acid of CP - formed by intermolecular nucleophilic attack of H_2O on the electrophilic C-8 carbon of the CP *β*-lactam ring, and the other a 7-piperazine-8,12-dione containing rearrangement product - formed by intramolecular nucleophilic attack of the N-18 amino nitrogen on the same carbon. As in the case of PG, the (*R*)-sulfoxide of CP was found retain considerable biological activity (~85% that of the parent CP molecule), whereas each of the three other CP transformation products was determined to be functionally inactive. CP-(*R*)-sulfoxide was found to be susceptible to further oxidation by both O_3 and $^{\bullet}OH$ (with $k''_{\mathrm{O_3,app}} = 2.6 \times 10^4\ \mathrm{M^{-1}s^{-1}}$ and $k''_{\bullet\mathrm{OH,app}} = 7.6 \times 10^9\ \mathrm{M^{-1}s^{-1}}$, at pH 7), leading to approximately quantitative elimination of antibacterial activity in each case. These results, when evaluated in the context of the reaction kinetics measured for oxidation of PG, CP, and their O_3-derived transformation products, suggest that the antibacterial activities of these representative *β*-lactams, as well as the activities of many structurally-analogous penicillins and cephalosporins, should be effectively eliminated during ozonation of municipal wastewaters.

In summary, the results obtained from this investigation demonstrate that, not only are most antibacterial molecules rapidly oxidized during ozonation of municipal wastewater by selective reactions with O_3, but that these reactions generally occur at target sites for which structural modification by O_3 results in quantitative loss of the parent antibacterial molecules' mode-specific biological activities. Furthermore, oxidation of every antibacterial molecule included in this investigation by $^{\bullet}OH$ - which will be produced in high yield during any wastewater ozonation process - led to nearly quantitative elimination of the model antibacterials' biological activities. In the only cases for which biological activities were not eliminated via the initial reaction with O_3 – that is, for the two β-lactams PG and CP – the biologically active (*R*)-sulfoxide products formed in these reactions could be further oxidized by either O_3 (CP-(*R*)-sulfoxide only) or $^{\bullet}OH$ (both CP-(*R*)-sulfoxide and PG-(*R*)-sulfoxide) to inactive products. These findings, when taken into consideration with additional operational data obtained here and in other investigations of municipal wastewater ozonation, suggest that effectively complete deactivation of nearly every major antibacterial structural class will be achieved at the 5-10 mg/L O_3 doses typically required to achieve close to 100% depletion of such antibacterial molecules in such matrixes. This in turn leads to the more general conclusion that wastewater ozonation can now be expected to provide a robust, relatively efficient barrier to discharge of biologically-active antibacterial compounds - which are, outside of steroiod hormones, one of the most potent biologically-active sub-classes of micropollutants known to be present in wastewaters.

Appendix A. Ozonation of Source-separated Urine for Resource Recovery and Waste Minimization: Process Modeling, Reaction Chemistry, and Operational Considerations

Dodd, M. C.; Zuleeg, S.; von Gunten, Urs; Pronk W.

Accepted for publication in *Environmental Science and Technology*

Abstract

Bench-scale, semi-batch experiments were performed to examine physical-chemical constraints on ozone (O_3) absorption and micropollutant oxidation during ozonation of source-separated hydrolyzed urine and the concentrate and diluate streams produced via electrodialysis of hydrolyzed urine. O_3 consumption by each matrix was found to occur within a fast pseudo-first-order kinetic regime. Critical constraints on micropollutant oxidation were found through mass transfer modeling to be (i) micropollutant diffusion from the bulk solution into the gas-liquid interfacial film for compounds recalcitrant toward O_3 (e.g., $k''_{O_3,\mathrm{app}} << 10^3\ M^{-1}s^{-1}$), and (ii) aqueous-phase mixing for compounds highly reactive toward O_3 (i.e., $k''_{O_3,\mathrm{app}} >> 10^3\ M^{-1}s^{-1}$). Homogeneous chemical reaction modeling indicated that aqueous reaction chemistry is significantly influenced by the degree to which incidentally-produced hydroxyl radicals are consumed by NH_3 in each matrix, in terms of (a) micropollutant oxidation efficiencies, and (b) potential yields of oxidation by-products. On the basis of the experimental data reported here, per capita energy requirements were estimated for treatment of source-separated urine via (1) ozonation, (2) ozonation with post-electrodialysis, and (3) electrodialysis with post-ozonation. These estimates indicate that scenario (1) would likely be less energy efficient than ozonation of municipal wastewater effluent in achieving equivalent reductions in urine-derived micropollutant loads, whereas scenarios (2) and (3) could be more efficient than equivalent centralized wastewater treatment strategies in achieving equivalent levels of urine-derived nutrient *and* micropollutant attenuation. Furthermore, experimental and model data suggest that urine ozonation efficiency may be substantially improved by optimizing aqueous-phase mixing and specific gas-liquid interfacial area.

A.1 Introduction

The discharge of urine-derived nutrients and micropollutants from municipal sewers has traditionally been attenuated by implementation and augmentation of "end-of-pipe" municipal wastewater treatment processes. However, considering that the per capita volumetric flow of human urine represents < 1 % of the total flow of municipal wastewater (*1*), yet contains a disproportionately large fraction of many biologically-active micropollutants (e.g., pharmaceuticals and natural hormones (*2*)) and nutrients (e.g., 80% of nitrogen, 50% of phosphorous, and 90% of potassium (*1,3*)), treatment of source-separated urine may present an attractive alternative for minimizing the passage of such species into municipal sewers. Urine separation and treatment also enable the recovery of nutrients for potential re-use in agriculture, although for such applications to garner a high degree of public and/or regulatory acceptance, urine-derived micropollutants will likely need to be separated from recoverable nutrient content or deactivated if possible. In principle, various treatment options could be applied to produce an acceptable, minimal-risk agricultural product from urine (e.g., nanofiltration, struvite precipitation, or electrodialysis) (*4*). However, these processes are variably effective in separating inorganic nutrients from organic micropollutants, and none achieves complete separation, necessitating a supplemental treatment process capable of selectively removing or degrading organic micropollutants.

Ozonation presents a particularly attractive option for degrading and deactivating the more potent, biologically-active micropollutants present in urine, such as estrogenic steroid hormones (*5*) and antibiotics (*6*). Prior work has demonstrated that the estrogenic activity of 17-α-ethinylestradiol (EE2)-spiked urine is lowered by greater than two orders of magnitude at an absorbed O_3 dose of 1.1 g/L (*7*). Furthermore, Escher et al. (2006) reported that absorption of ~1-2 g/L of O_3 yields ~70%-90% reductions in the general algal toxicity of a 20:80 tap water:hydrolyzed urine solution and ~60-75% toxicity reductions for a similar solution spiked with a representative suite of pharmaceuticals (*7*).

The As a variety of complementary treatment processes are available for facilitating nutrient recovery and removal from source-separated urine (*4*), ozonation could foreseeably be applied for micropollutant oxidation in a wide range of process configurations. For example, O_3 could be applied with electrodialysis (ED), struvite precipitation, or nanofiltration, or as a stand-alone process if urine is simply collected for pre-treatment prior to discharge into municipal sewers. Several such options were explored here by performing semi-batch ozonation of hydrolyzed urine, ED diluate (the diluted ED membrane reject stream, which is depleted of charged species), and ED concentrate (the concentrated ED membrane permeate, which is enriched in charged species) spiked with a suite of six model micropollutants: *p*-chlorobenzoic acid (*p*CBA), carbamazepine (CM), diclofenac (DC), EE2, ibuprofen (IP), and propranolol (PP) (all shown in Table SA.1). These model compounds, with apparent second-order rate constants for the direct reaction with O_3, $k''_{O_3,\mathrm{app}}$, spanning over nine orders of magnitude under the experimental conditions used here (Table SA.1), were selected to enable characterization of the relative influence of homogeneous reaction kinetics and mass transfer on micropollutant oxidation rates during ozonation of each urine matrix.

Micropollutant losses during ozonation were monitored by HPLC and correlated with absorbed O_3 doses and estimated in situ yields of hydroxyl radical ($^\bullet$OH), which is generated via auto-catalytic O_3 decomposition (*8*) and/or reactions of O_3 with various constituents of dissolved organic matter (*9,10*). Approximate $^\bullet$OH yields were determined by using *p*CBA as a selective $^\bullet$OH probe (*11*). A numerical model accounting for mass transfer constraints on the homogeneous, aqueous-phase kinetics of O_3 and $^\bullet$OH reactions with individual matrix constituents was developed to examine fundamental physical-chemical limitations on the micropollutant oxidation rates observed during heterogeneous ozonation of each urine matrix. Additional homogeneous chemical modeling was utilized to evaluate the importance of secondary reactive species formed via $^\bullet$OH reactions with prominent matrix constituents. Model results were then compared with experimental data to evaluate key operational aspects of urine ozonation, including: (1) energy inputs required to achieve selected effluent quality targets, (2) opportunities for optimization of gas-liquid O_3 transfer and reactor configuration, and (3) potential formation of undesirable oxidation by-products, in order to highlight possible opportunities for enhancing the efficiency and effectiveness of urine ozonation.

A.2 Experimental Section

A.2.1 Chemicals and urine matrixes. All model compounds used in this study were of 95% purity or higher. Chemical sources and stock compound preparations are described in the Supporting Information for Appendix A, Text SA.1. Natural urine (male only), ED diluate, and ED concentrate were collected and/or prepared as described in Text SA.1. Important matrix parameters are listed in Table A.1.

Table A.1. Urine matrix characteristics

Matrix	**pH**	**Alkalinity (M HCO_3^-)**	**$NH_{3,t}$ (g N/L)**	**Phosphate (mg P/L)**	**DOC (g C/L)**
Hydrolyzed urine	9	0.3-0.32	4.1-4.6	200-220	1.8-2.0
ED diluate	8	0.03	0.4	39	1.6[a]
ED concentrate	9	0.99	14.9	630	4.9[a]

[a] Addition of ethanol-based pharmaceutical stocks to the ED feed solution from which ED diluate and ED concentrate solutions were derived resulted in increased DOC levels within the diluate and concentrate (see Text SA.1).

A.2.2 Analytical Methods. All model compounds were measured by HPLC (see Text SA.1 for a method description). Additional water quality parameters were determined as described in Text SA.1.

A.2.3 Experimental conditions and methods. *Ozonation.* Semi-batch experiments were carried out in a stirred, thermostatted glass vessel with a total volume of 1.7 L (see Figure SA.1); typically at 25° C (additional experiments demonstrated that temperature variations from 10° C to 25° C have minimal effect on observed micropollutant oxidation rates, data not shown). O_3 - produced with a Brown Boveri Co. LN103 generator, using pure O_2 (0.8 bar) as a feed gas - was supplied to the urine solutions at a flow rate of 30 L/h, via a 2.5-cm diameter porous glass diffuser disc (Schott Duran P0, with a porosity of ~0.35 and pore-size between 160 and 250 μm) placed 2 cm above a rapidly rotating magnetic stir bar (for continuous mixing of the bulk liquid phase). Gas-phase O_3 concentrations, $C_{O3(g),in}$ and $C_{O3(g),out}$, within the inlet and outlet gas streams of the reactor were measured spectrophotometrically at 258 nm and recorded continuously at 1-s intervals with an on-line data logger to monitor O_3 absorption by each urine matrix. Absorbed O_3 dose was calculated from these concentrations and the gas flow rate.

A.3 Results and Discussion

A.3.1 Oxidation of micropollutants in hydrolyzed urine. Measured losses of *p*CBA, CM, DC, EE2, IP, and PP during ozonation of hydrolyzed urine are presented versus absorbed O_3 dose for four applied gas-phase O_3 concentrations in Figure A.1. The data presented here illustrate that very high doses of O_3 were required to achieve substantial degrees of micropollutant oxidation, on account of the extremely high concentrations of O_3-consuming reactive matrix constituents (RMCs) (e.g., amino acids and activated aromatic compounds) present in hydrolyzed urine (Table A.1) (*12*). The data shown in Figure A.1 also indicate that

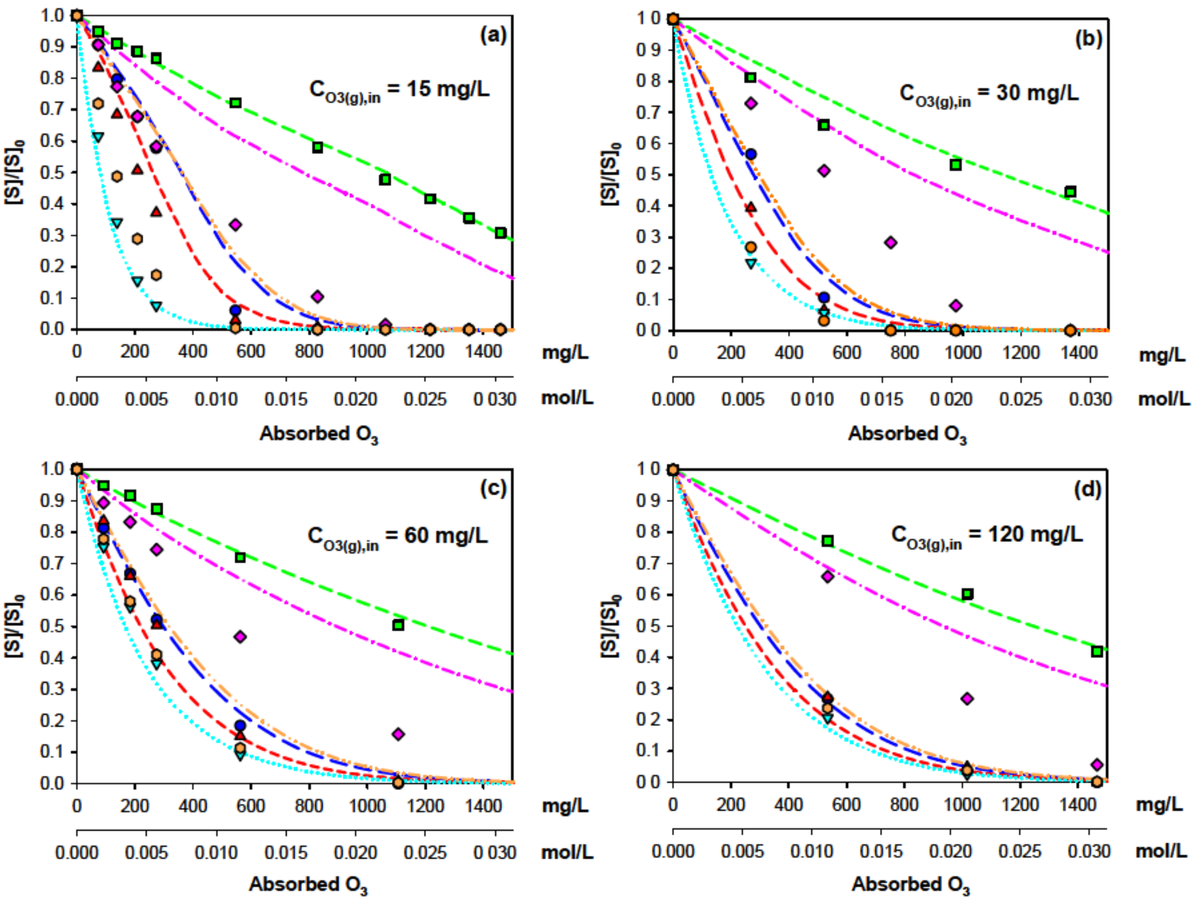

Figure A.1. Observed and modeled losses for each model compound, compared to absorbed O_3 dose, during ozonation of hydrolyzed urine at $C_{O3(g),in}$ = (a) 15 mg/L, (b) 30 mg/L, (c) 60 mg/L, and (d) 120 mg/L. Measured data are represented by symbols (● CM, 🟩 *p*CBA, ▲ DC, ▼ EE2, ◆ IP, ⬢ PP), whereas model results are depicted as lines (— — CM, — — *p*CBA, — — DC, ········EE2, —·—· IP, —··— PP). Solutions treated with $C_{O3(g),in}$ = 15 and 60 mg/L were dosed with 1.0 × 10^{-5} M of CM, DC, IP, EE2, and PP, and 5.0 × 10^{-5} M of *p*CBA, whereas solutions treated with $C_{O3(g),in}$ = 30 and 120 mg/L were dosed with 1.0 × 10^{-5} M of all model compounds.

model compounds with relatively high rate constants for reaction with O_3 (i.e., CM, EE2, DC, and PP - Table SA.1) were generally depleted at lower O_3 doses than compounds with low reactivity toward O_3 (i.e., IP and *p*CBA - Table SA.1), suggesting that direct reactions with O_3 play an important role in governing oxidation rates of the four “fast-reacting” model compounds during urine ozonation.

Furthermore, the absorbed O_3 dose required to reach a given degree of micropollutant oxidation increased with applied O_3 concentrations for fast-reacting model compounds (Figure A.1). For example, approximately 550, 750, 1100, and 1450 mg/L of absorbed O_3 were required to achieve >99% depletion of EE2 at each of the four $C_{O3(g),in}$ values, respectively, indicating that the efficiency with which fast-reacting model micropollutants were oxidized (in terms of mole of micropollutant depleted per mole of O_3 absorbed) decreased significantly as $C_{O3(g),in}$ was increased from 15-120 mg/L. In contrast, the oxidation efficiency for *p*CBA - which does not react directly with O_3 (Table SA.1) - appeared to be much less sensitive to $C_{O3(g),in}$ over the range of applied O_3 concentrations. As shown in Figure A.1, ~50% depletion of *p*CBA was achieved at absorbed O_3 doses of 1050-1200 mg/L in all four cases.

An additional feature of the data shown in Figure A.1 is the decreasing separation in magnitudes of measured depletion rates for the fast-reacting micropollutants EE2, PP, CM, and DC with increasing $C_{O3(g),in}$. That is, the measured loss rates for each compound were widely separated at the lowest applied O_3 concentration, but converged toward a single loss rate as $C_{O3(g),in}$ was raised. This suggests the existence of a physically- or chemically-imposed limit on the rate at which compounds were depleted by direct reaction with O_3 during urine ozonation, which will be discussed in greater detail below.

A.3.2 Oxidation of micropollutants in ED effluents. Measured profiles of micropollutant depletion during ozonation of ED diluate and concentrate at $C_{O3(g),in}$ = 60 mg/L are shown in Figure A.2. Much lower absorbed O_3 doses were required in ED diluate than in hydrolyzed urine to yield equivalent micropollutant losses (Figures A.1c, A.2a). For example, at $C_{O3(g),in}$ = 60 mg/L, >99% EE2 loss was achieved at ~250 mg/L in ED diluate, compared to

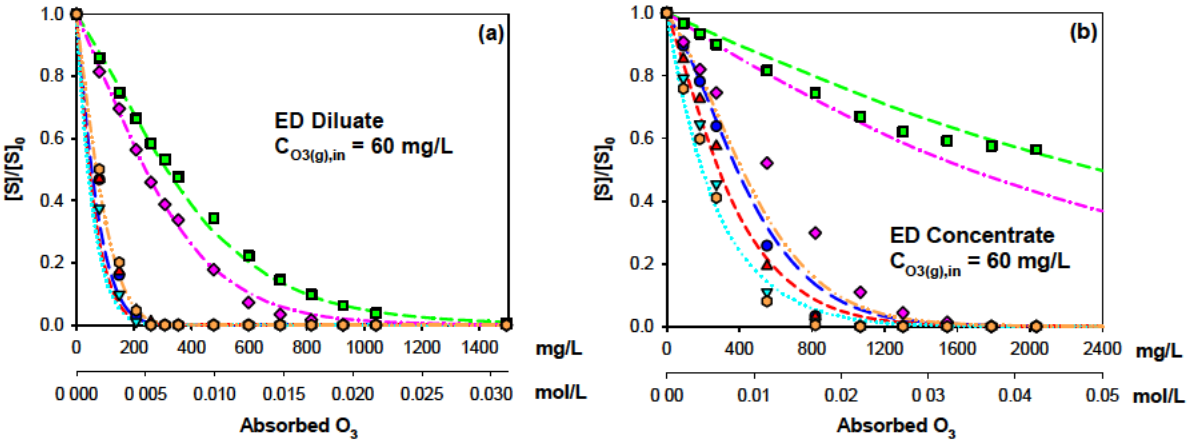

Figure A.2. Observed and modeled losses for each model compound, compared to absorbed O_3 dose, during ozonation of (a) ED diluate and (b) ED concentrate at $C_{O3(g),in}$ = 60 mg/L. Measured data are represented by symbols (● CM, 🟩 *p*CBA, ▲ DC, ▽ EE2, ◆ IP, ⬢ PP), whereas model results are depicted as lines (– – – CM, – – – *p*CBA, – – – DC, ······ EE2, –·–·– IP, –··–·· PP). Solutions were dosed with 1.0 × 10^{-5} M of CM, DC, IP, EE2, and PP, and 5.0 × 10^{-5} M of *p*CBA.

~1100 mg/L in hydrolyzed urine, whereas ~50% *p*CBA loss was achieved at ~350 mg/L in ED diluate, compared to ~1100 mg/L in hydrolyzed urine.

In contrast, the absorbed O_3 doses required to yield equivalent losses of fast-reacting compounds (i.e., CM, DC, EE2, and PP) in ED concentrate were comparable to those for hydrolyzed urine, while oxidation of *p*CBA was much less efficient in ED concentrate (Figures A.1c, A.2b). For example, at $C_{O3(g),in}$ = 60 mg/L, >99% EE2 loss was achieved at ~1050 mg/L in ED concentrate and in hydrolyzed urine, whereas ~50% pCBA loss would have been achieved at ~2400 mg/L (based on extrapolation from measured data) in ED concentrate, compared to ~1100 mg/L in hydrolyzed urine.

The observations pertaining to ED diluate are consistent with expectations, as dilution of charged RMCs (e.g., amino acids) in the ED diluate should result in slower direct consumption of aqueous O_3, relative to the hydrolyzed urine feed solution. This should lead to greater availability of dissolved O_3 for direct reactions with fast-reacting micropollutants in the ED diluate. Furthermore, removal of carbonate, ammonia, and charged dissolved organic matter (DOM) from the diluate stream during electrodialysis would be expected to result in decreased scavenging of $^{\bullet}OH$ by these species during ozonation of this matrix, resulting in enhanced *p*CBA oxidation efficiency.

The observed trends in fast-reacting micropollutant loss during ED concentrate ozonation are also in reasonable agreement with expected changes in ED concentrate composition relative to hydrolyzed urine. Higher levels of charged RMCs in the ED concentrate should yield faster direct consumption of O_3 during ozonation. This should lead to decreased availability of dissolved O_3 for direct reactions with fast-reacting micropollutants. However, the accompanying accumulation of charged $^{\bullet}OH$ scavengers (e.g., HCO_3^-/CO_3^{2-} and NH_4^+) in ED concentrate should result in attenuation of auto-catalytic O_3 decomposition resulting from $^{\bullet}OH$-mediated $O_2^{\bullet-}$ formation (*8*), thereby offsetting the effects of increased direct O_3 consumption by RMCs. As an additional consequence of the higher $^{\bullet}OH$-scavenger levels in ED concentrate relative to hydrolyzed urine, *p*CBA oxidation efficiencies should be decreased during ozonation of the former, in agreement with the trends shown in Figures A.1c and 2b.

Substantial concentrations of ethanol (~87 mM) were present in each of the electrodialysis product streams (as discussed in Text SA.1). Although this should not have had an appreciable effect on oxidation rates of micropollutants with high values of $k''_{O_3,app}$, efficiencies with which O_3-recalcitrant compounds (e.g., IP and *p*CBA) were oxidized by $^{\bullet}OH$

in the ED product solutions were likely lower than would have been observed in the absence of ethanol, due to consequent enhancement of $^{\bullet}$OH scavenging and auto-catalytic O_3 decomposition rates (*8*). This effect is qualitatively illustrated by comparison of micropollutant depletion rates in ethanol-free and ethanol-amended hydrolyzed urine (Figure SA.2).

A.3.3 Quantitative modeling and system characterization. *Modeling Gas-Liquid O_3 Mass Transfer.* Quantitative modeling of the heterogeneous urine ozonation process can aid in elucidating the critical physical and chemical factors influencing the observations discussed above, thereby highlighting potential opportunities for process optimization. Several theoretical approaches are available for development of appropriate chemically-enhanced mass transfer models, including Higbie's and Danckwert's surface renewal theories (*13*), and film theory (*14*). For purposes of conceptual and computational simplification, the latter has been implemented here. Physical-chemical parameters utilized in this modeling are summarized in Table SA.2.

According to film theory, transfer of gas-phase O_3 into solution is governed by its passage through a conceptual "film" separating the surface of each gas bubble from the bulk solution (Figure A.3). In the case of a sparingly soluble gas such as O_3, physical mass transfer is dominated by liquid-phase resistance (*14*). Consequently, dissolved O_3 concentrations can be assumed to be in equilibrium with $C_{O3(g)}$ at the gas-film interface, allowing one to model O_3 mass transfer with a "one-film" approach (*14*).

When gas-phase O_3 is applied to an aqueous matrix containing very high excesses of RMCs, O_3 consumption by RMCs within the film may be so fast as to render rates of gas-phase O_3 absorption into the film insufficient to maintain an appreciable concentration of O_3 in the bulk solution, yielding a "fast pseudo-first-order kinetic regime" of O_3 absorption (Figure A.3), in which reactions between micropollutants and dissolved O_3 are confined to the film. On the initial assumption that such a condition prevailed in each of the systems examined here (on account of the extremely high RMC concentrations present in each matrix - Table A.1), absorption of O_3 was modeled according to eq 1 (*14*),

$$\mathrm{D}_{\mathrm{l,O3}}\frac{\mathrm{d}^2[\mathrm{O}_3]_{\mathrm{l,x}}}{dx^2} - r_{\mathrm{O}_3} = \frac{\mathrm{d}[\mathrm{O}_3]_{\mathrm{l,x}}}{dt} \qquad (1)$$

where $D_{l,O3}$ is the diffusion coefficient for O_3 in water (in m^2 s^{-1}), $[O_3]_{l,x}$ is the aqueous-phase O_3 concentration (in mol L^{-1}) at a given point x within the film, and r_{O3} represents the rate of O_3 depletion within the film (in mol L^{-1} s^{-1}), which is primarily a function of kinetics for the reactions between O_3 and RMCs within the urine matrix. Assuming steady-state and pseudo-

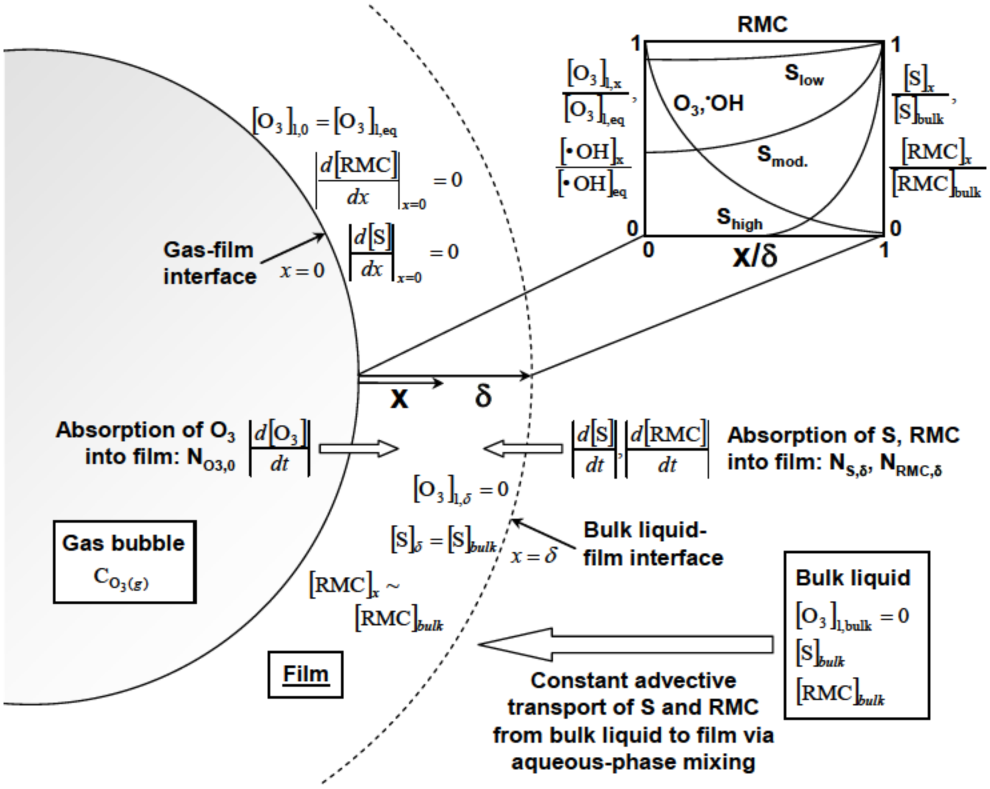
RMC
$\frac{[O_3]_{l,x}}{[O_3]_{l,eq}}$,
$\frac{[\cdot OH]_x}{[\cdot OH]_{eq}}$
$O_3, {}^{\cdot}OH$
S_{low}
$S_{mod.}$
S_{high}
$\frac{[S]_x}{[S]_{bulk}}$,
$\frac{[RMC]_x}{[RMC]_{bulk}}$
1
1
0
0
0
1
x/δ
$[O_3]_{l,0} = [O_3]_{l,eq}$
$\left|\frac{d[RMC]}{dx}\right|_{x=0} = 0$
$\left|\frac{d[S]}{dx}\right|_{x=0} = 0$
Gas-film interface
$x = 0$
x
δ
Absorption of O_3 into film: $N_{O3,0}$
$\left|\frac{d[O_3]}{dt}\right|$
$\left|\frac{d[S]}{dt}\right|$, $\left|\frac{d[RMC]}{dt}\right|$
Absorption of S, RMC into film: $N_{S,\delta}$, $N_{RMC,\delta}$
$[O_3]_{l,\delta} = 0$
$[S]_\delta = [S]_{bulk}$
$x = \delta$
Bulk liquid-film interface
Gas bubble
$C_{O_3(g)}$
$[RMC]_x \sim [RMC]_{bulk}$
Film
Bulk liquid
$[O_3]_{l,bulk} = 0$
$[S]_{bulk}$
$[RMC]_{bulk}$
Constant advective transport of S and RMC from bulk liquid to film via aqueous-phase mixing

Figure A.3. Representation of the interfacial film for a fast pseudo-first-order kinetic regime with respect to O_3 consumption, where $[O_3]_{l,x}$ is governed by $[RMC]_x$ and $[S]_x$ is governed by $[O_3]_{l,x}$ according to the pictured boundary value conditions, and S_{low}, $S_{mod.}$, and S_{high} represent hypothetical model compounds with low, moderate, and high reactivity toward O_3, respectively.

first-order conditions within the film at a given moment (as [RMC] is much larger than $[O_3]_l$), eq 1 could be simplified to eq 2,

$$D_{l,O_3} \frac{d^2[O_3]_{l,x}}{dx^2} - k'_{O_3,RMC}[O_3]_{l,x} = 0 \tag{2}$$

where $k'_{O_3,RMC}$ is the pseudo-first-order rate constant (in s^{-1}) for O_3 consumption by RMCs at a given instant. With knowledge of $D_{l,O3}$ (Table SA.2) and $k'_{O_3,RMC}$, eq 2 could then be modeled as a boundary-value system with the constraints $[O_3]_{l,x} = [O_3]_{l,eq}$ at x = 0 and $[O_3]_{l,x} = 0$ at x = δ, where $[O_3]_{l,eq}$ is the equilibrium O_3 concentration at the gas-film interface, and δ is the film thickness (in m) (Figure A.3).

$[O_3]_{l,eq}$ was determined from the average gas-phase O_3 concentration in the reactor, $[O_3]_{g,avg.}$, at a given time (calculated as described Text SA.2), using the appropriate dimensionless solubility ratio, H_{O3}, for each urine matrix (Table SA.2). The terms δ and $k'_{O_3,RMC}$ were then calculated according to Texts SA.3 and SA.4. Following determination of each of these parameters, the initial assumption of a fast pseudo-first-order kinetic regime was tested and validated for the full extent of modeled reaction times in each matrix, as described in Text SA.4.

Modeling Heterogeneous Oxidation of Individual Micropollutants. Concentration profiles of individual micropollutants, S, within the film were modeled with eq 3,

$$\mathrm{D}_{\mathrm{l,S}}\frac{\mathrm{d}^2[\mathrm{S}]}{dx^2}-\left(k''_{\mathrm{O_3,S}}[\mathrm{O_3}]_{\mathrm{l,x}}[\mathrm{S}]+k''_{\bullet\mathrm{OH,S}}[\bullet\,\mathrm{OH}][\mathrm{S}]\right)=0 \tag{3}$$

where $k''_{\mathrm{O_3,S}}$ and $k''_{\bullet\mathrm{OH,S}}$ are the respective second-order rate constants (in mol $\mathrm{L^{-1}\ s^{-1}}$) for reactions of $\mathrm{O_3}$ and •OH with S, and $[\mathrm{O_3}]_{\mathrm{l,x}}$ was assumed to be governed independently by eq 2, as [S] was negligible compared to [RMC] in the urine matrix (Table A.1). For the same reason, [$^\bullet$OH] was also assumed to be governed by eq 2, as $^\bullet$OH yields are dependent on $[\mathrm{O_3}]_{\mathrm{l,x}}$ (*15*). Accordingly, [$^\bullet$OH] was estimated from the time-dependent term, $R_{\mathrm{ct(t)}} \sim [^\bullet\mathrm{OH}]/[\mathrm{O_3}]_{\mathrm{l}}$ (*15*) - measured using *p*CBA as an $\mathrm{O_3}$-recalcitrant $^\bullet$OH probe, as described in Text SA.5. An empirical function describing $R_{\mathrm{ct(t)}}$ (Table SA.3) was then incorporated into eq 3, to yield eq 4,

$$\mathrm{D}_{\mathrm{l,S}}\frac{\mathrm{d}^2[\mathrm{S}]}{dx^2}-[\mathrm{O_3}]_{\mathrm{l,x}}[\mathrm{S}]\left(k''_{\mathrm{O_3,S}}+k''_{\bullet\mathrm{OH,S}}R_{\mathrm{ct(t)}}\right)=0 \tag{4}$$

where $R_{\mathrm{ct(t)}}$ was assumed to be spatially-invariable at a given time (i.e., a plot of $[^\bullet\mathrm{OH}]_x/[^\bullet\mathrm{OH}]_0$ vs. position, *x*, in the film would have traced that of $[\mathrm{O_3}]_{\mathrm{l,x}}/[\mathrm{O_3}]_{\mathrm{l,0}}$, as shown in Figure A.3).

Equations 2 and 4 in turn constitute a single boundary-value system with the additional constraints $\frac{\mathrm{d}[\mathrm{S}]}{dx}=0$ at x = 0 and [S] = $[\mathrm{S}]_{\mathrm{bulk}}$ at x = δ (Figure A.3). Once the required input parameters (listed in Tables SA.1, SA.2, and SA.3) were available, this system was solved numerically by utilizing the MATLAB ODE system solver "bvp4c" (Mathworks, Inc.), to obtain reactant concentrations at all positions x, across the length, δ, of the film (via Script SA.1), yielding film profiles such as those depicted in Figure SA.4.

Coupling profiles of reactant concentrations in the film to analysis of the bulk solution. When the bulk liquid phase in contact with gas bubbles in such a system as described here is well-mixed, the effects of reactions taking place within the film on micropollutant behavior within the bulk solution can be modeled via the same MATLAB script (Script SA1) by reformulating eq 4 in terms of the flux, $\mathrm{J_{s,x}}$ (in mol $\mathrm{m^{-2}\ s^{-1}}$), according to eq 5.

$$\frac{\mathrm{d}}{dx}\left(\frac{\mathrm{d}[\mathrm{S}]}{dx}\right)=\frac{-1}{\mathrm{D}_{\mathrm{l,S}}}\frac{\mathrm{d}}{dx}\left(J_{\mathrm{s,x}}\right)=\frac{[\mathrm{O_3}]_{\mathrm{l,x}}[\mathrm{S}]}{\mathrm{D}_{\mathrm{l,S}}}\left(k''_{\mathrm{O_3,S}}+k''_{\bullet\mathrm{OH,S}}R_{\mathrm{ct(t)}}\right) \tag{5}$$

The flux of S into the film at x = δ can then be determined at a given time via eq 6 (i.e., Fick's first law, with [S] expressed in units of mol m^{-3}),

$$J_{s,\delta} = -D_{l,S}\left(\frac{d[S]}{dx}\right)_{x=\delta} \tag{6}$$

which can be expressed in terms of the absorption rate, $N_{S,\delta}$, (in mol L^{-1} s^{-1}) of compound S from the bulk solution into the film, according to eq 7,

$$N_{S,\delta} = \frac{J_{s,\delta}A_s}{1000(1-\varepsilon_g)} = -\left(\frac{d[S]}{dt}\right)_{x=\delta} \approx -\left(\frac{d[S]}{dt}\right)_{\text{bulk}} \tag{7}$$

where A_s (Table SA.2) is the specific gas-liquid interfacial area (in m^2/m^3) relative to the bubble-containing volume in the reactor (inclusive of gas and liquid volumes), determined as described in Text SA.6, and 1-ε_g is the liquid holdup in the bubble-containing volume (i.e., $\frac{V_{\text{liquid}}}{V_{\text{liquid}} + V_{\text{gas}}}$) (Text SA.6, Table SA.2).

However, inspection of the ozone reactor (Figure SA.1) reveals that the average diameter of the bubble-containing volume produced by passage of O_3-containing gas through the 2.5-cm glass diffuser used here was significantly smaller than the reactor's full 10-cm inner diameter (Figure SA.1b). Thus, even with mechanical mixing, only a limited portion of the liquid volume in the reactor was in contact with O_3-containing bubbles at any given time. Consequently, because no dissolved O_3 residual was present in the bulk solution during ozonation, the reactor was segregated into two zones (Figure SA.1b): (i) a well-mixed "reactive zone" within the bubble-containing volume, in which micropollutants could interact with O_3 and $^{\bullet}OH$ at the gas-liquid interface (as in Figure A.3), and (ii) a "non-reactive zone" outside of the bubble-containing volume, in which micropollutants were isolated from O_3 or $^{\bullet}OH$.

The reactive zone can be modeled as a typical semi-batch bubble column, within which the liquid phase is completely-mixed, the gas phase in plug flow, and reactant behavior as depicted in Figure A.3. However, modeling the reactive zone in isolation would not account for micropollutant behaviors across the entire reactor, as fluid elements within the non-reactive zone at a given instant would not have been directly affected by processes taking place in the reactive zone (i.e., direct reactions with O_3 and $^{\bullet}OH$ could only have occurred within the reactive zone). Rather, one must consider that fluid elements were continuously exchanged between each zone at a rate governed by aqueous-phase mixing. Thus, the observed rates at which micropollutants in the bulk liquid were depleted (Figures A.1 and

A.2) would have been dependent not only on heterogeneous processes taking place *within* the film, but also on their rate of transport *to* the film (i.e., from the non-reactive zone to the reactive zone).

These considerations suggest that observed micropollutant oxidation rates were actually composites of (1) reactant diffusion rates into the interfacial film adjacent to each gas bubble (as described by eqs 1-7), *and* (2) advective transport rates of micropollutants from the non-reactive zone to the reactive zone. Diffusive limitations likely governed depletion rates of O_3-recalcitrant micropollutants (e.g., *p*CBA), as their diffusion into the film would presumably have been too slow for advective transport to become a limiting factor (as shown for S_{low} in Figure A.3). In contrast, the depletion rates of micropollutants reacting very rapidly with O_3 (e.g., EE2) were likely strongly dependent on mixing limitations, as their rates of diffusion into the film could have been fast enough to exceed their rate of transport from the non-reactive zone to the reactive zone (as illustrated for S_{high} in Figure A.3). Micropollutants with *intermediate* reactivities toward O_3 (e.g., CM, DC, IP, and PP) would have been variably subject to advective *and* diffusive mass transfer limitations (see S_{mod} in Figure A.3).

Depletion of a given compound from the bulk solution was therefore hypothesized to be constrained in series by (a) advective transport and (b) diffusion. Accordingly, micropollutant loss rates were modeled by modifying eq 7 to yield the "resistance-in-series" model represented by eq 8,

$$\left(\frac{\mathrm{d}[\mathrm{S}]}{dt}\right)_{\mathrm{bulk}} = -\left(\frac{1000(1-\varepsilon_{\mathrm{g}})}{\mathrm{J}_{\mathrm{S},\delta}\mathrm{A}_{\mathrm{s}}} + \frac{1}{k'_{\mathrm{mix}}[\mathrm{S}]_{\mathrm{bulk.}}}\right)^{-1} \tag{8}$$

with the first term representing diffusive transport and the second term representing advective transport, where approximate first-order "mixing constants," k'_{mix} (in s^{-1}) - representing the velocity of fluid element transport in the reactor, were extracted from the slopes of plots of $\ln([EE2]/[EE2]_0)$ vs. time (Figure SA.5b) - assuming that EE2 loss rates were governed exclusively by advective transport limitations, according to the rationale discussed in Text SA.7. Next, using Scripts SA.2 and SA.3, eq 8 was stepped by discrete time increments Δt, according to eq 9,

$$[\mathrm{S}]_{\mathrm{bulk},t+\Delta t} \approx [\mathrm{S}]_{\mathrm{bulk},t} - \left(\frac{\mathrm{d}[\mathrm{S}]}{dt}\right)_{\mathrm{bulk},t} \cdot \Delta t \tag{9}$$

to yield concentration profiles of $[S]_{bulk}$ versus time, which were then correlated with measurements of absorbed O_3 dose.

The advective transport term in eq 8 provides a likely physical explanation for the observed decrease in EE2 consumption per mole of O_3 absorbed as $C_{O3(g),in}$ was increased in hydrolyzed urine (Figure A.1). Namely, even though the rate of O_3 diffusion into the film would have increased at higher $C_{O3(g)}$, the EE2 consumption rate could not have exceeded the rate of EE2 transport to the film, resulting in higher apparent O_3 absorption for approximately the same rate of EE2 consumption. Likewise, these phenomena are consistent with the relatively constant *p*CBA oxidation efficiency observed for increasing $C_{O3(g),in}$ (Figure A.1), as *p*CBA loss would have been governed primarily by its rate of diffusion into the film (which is directly proportional to $C_{O3(g)}$), rather than advective transport to the film.

Model results for oxidation of micropollutants in stored, hydrolyzed urine. Model results for hydrolyzed urine are depicted as lines in Figure A.1. As shown here, modeled depletion rates correlated well with corresponding measured depletion rates for CM, *p*CBA, DC, and EE2, whereas IP and PP depletion rates were substantially underpredicted (Figure A.1). On account of the urine matrix's complexity, the reason for these higher than predicted depletion rates is uncertain. However, interactions of IP and PP with secondary reactive species (e.g., $^{\bullet}NH_2$ and $CO_3^{\bullet-}$) formed via reaction of $^{\bullet}OH$ with matrix constituents such as NH_3 and HCO_3^-/CO_3^{2-} could represent one plausible explanation that would be consistent with observed pollutant loss rates, as will be discussed in detail below.

Model results for oxidation of micropollutants in ED effluents. Model results for ED diluate and concentrate are depicted as lines in Figure A.2. Model results for ED concentrate also correlated well with measured rates of CM, *p*CBA, DC, and EE2 depletion, yet substantially underpredicted measured IP and PP depletion rates (Figure A.2b). However, in the case of ED diluate, model predictions correlated very well with observed depletion rates for *all* model compounds (Figure A.2a). This is consistent with the possible role of secondary reactive species derived from NH_3 and HCO_3^-/CO_3^{2-} in mediating IP and PP loss rates in hydrolyzed urine and ED concentrate, as ED diluate contains much lower concentrations of NH_3 and carbonate than the latter two matrixes (Table A.1).

A.3.4 Modeling homogeneous reaction chemistry and formation of secondary radicals. A significant fraction of $^{\bullet}OH$ generated during urine ozonation may react with NH_3 and HCO_3^-/CO_3^{2-} (Table SA.4) to produce the aminyl radical, $^{\bullet}NH_2$, and carbonate radical, $CO_3^{\bullet-}$, respectively (*16*). According to calculations discussed in Text SA.8, resulting levels of $^{\bullet}NH_2$ and $CO_3^{\bullet-}$ should be ~10-50× *higher* than $[^{\bullet}OH]_{ss}$ in hydrolyzed urine and ED concentrate, and ~4-8× *lower* than $[^{\bullet}OH]_{ss}$ in ED diluate (Table SA.7), consistent with the higher IP and PP loss rates in the former two matrixes (Figures A.1 and A.2).

Comparison of the aromatic structures of PP and IP, as well as PP's secondary amine (Table SA.1), with similar structures for which ${}^{\bullet}NH_2$ and $CO_3^{\bullet-}$ rate constants are available (*16*), suggests that PP is likely moderately to highly reactive toward each radical (i.e., $10^4\ M^{-1}s^{-1} < k''_{{}^{\bullet}NH_2,\mathrm{propranolol}} < 10^5\ M^{-1}s^{-1}$ and $10^5\ M^{-1}s^{-1} < k''_{CO_3^{\bullet-},\mathrm{propranolol}} < 10^7\ M^{-1}s^{-1}$), whereas IP is likely only appreciably reactive toward $CO_3^{\bullet-}$ (i.e., $10^4\ M^{-1}s^{-1} < k''_{CO_3^{\bullet-},\mathrm{ibuprofen}} < 10^5\ M^{-1}s^{-1}$). Thus, considering the values of $k''_{{}^{\bullet}OH,\mathrm{ibuprofen}}$ and $k''_{{}^{\bullet}OH,\mathrm{propranolol}}$ (Table SA.1), $[{}^{\bullet}NH_2]_{ss}$ and $[CO_3^{\bullet-}]_{ss}$ would likely have to be ~10^4-10^6× higher than $[{}^{\bullet}OH]_{ss}$ for ${}^{\bullet}NH_2$ and $CO_3^{\bullet-}$ to compete with ${}^{\bullet}OH$ in oxidizing IP and PP. It is therefore unlikely that direct production of ${}^{\bullet}NH_2$ and $CO_3^{\bullet-}$ via reactions of ${}^{\bullet}OH$ with NH_3 and HCO_3^-/CO_3^{2-} alone could account for the discrepancies in modeled and measured IP and PP loss rates.

However, as ${}^{\bullet}NH_2$ would be almost exclusively scavenged by $O_{2(aq)}$ in ozonated urine solutions (Table SA.6), additional $CO_3^{\bullet-}$ could be generated (with an equal yield of nitrogen dioxide, ${}^{\bullet}NO_2$) via formation and decomposition of peroxynitrite, $ONOO^-$, in the presence of $CO_{2(aq)}$, via eqs 10-12 (*17,18*),

$$ {}^{\bullet}NH_2 + O_2 \xrightarrow{k_{10a}} NH_2O_2^{\bullet} \xrightarrow{k_{10b}} {}^{\bullet}NO + H_2O \tag{10} $$

$$ {}^{\bullet}NO + O_2^{\bullet-} \xrightarrow{k_{11}} ONOO^- \tag{11} $$

$$\begin{tikzcd}
ONOO^- + CO_{2(aq)} \arrow[r, shift left, "k_{12a,f}"] & ONOOCO_2^- \arrow[l, shift left, "k_{12a,r}"] \arrow[r, shift left, "k_{12b,f}"] \arrow[dr, "k_{12c}"'] & {}^{\bullet}NO_2 + CO_3^{\bullet-} \arrow[l, shift left, "k_{12b,r}"] \arrow[d, "k_{12d}"] \\
 & & NO_3^- + CO_2
\end{tikzcd} \tag{12}$$

where rate constant magnitudes are as reported in (*16-18*) and $O_2^{\bullet-}$ would be generated via O_2 reduction by carbon-centered radicals produced in reactions of ${}^{\bullet}OH$, $CO_3^{\bullet-}$, or ${}^{\bullet}NH_2$ with DOM (*16*), or by direct reactions of O_3 with certain DOM moieties (*10*). Due to the ~1-mM $CO_{2(aq)}$ concentrations present at equilibrium with $[\mathrm{carbonate}]_t$ in hydrolyzed urine at pH 9, $t_{1/2,ONOO^-}$ in such solutions should have been ~33 ms (*18*), which is of the same order of magnitude as the characteristic time for $ONOO^-$ diffusion through the film to the bulk solution (i.e., $t_{\mathrm{diff..},ONOO^-} = \dfrac{\delta^2}{D_{1,ONOO^-}}$ ~ 72 ms (*14*), assuming $D_{1,ONOO^-} \sim 2 \times 10^{-9}\ m^2/s$ for an inorganic solute such as $ONOO^-$ (*19*)). This suggests that $ONOO^-$ levels within the film would have followed a profile similar to that shown in Figure SA.6, where $ONOO^-$ depletion via eq 12 is offset by its production via eqs 10 and 11 and its diffusion from regions of the film closer to the gas-film interface (where $[O_3]_l$ is higher), thereby sustaining appreciable $^{\bullet}NO_2$ and $CO_3^{\bullet-}$ levels even in the absence of O_3 (Figure SA.6).

The possibility that $^{\bullet}NO_2$ and $CO_3^{\bullet-}$ production via eqs 10-12 might account for the discrepancies in predicted and measured IP and PP loss rates was investigated by using Kintecus (*20*) to model a hypothetical system comprising the reactions expected to be most important in governing homogeneous redox chemistry during ozonation of hydrolyzed urine and ED diluate, at $C_{O3(g),in} = 60$ mg/L (Table SA.8). This system was modeled for each matrix under: (1) steady-state conditions approximating reactant concentrations at the gas-film interface (i.e., $x = 0$), where $[O_3]_{l,x} = [O_3]_{l,eq}$, and (2) dynamic conditions approximating the evolution of reactant concentrations across the film as O_3 is depleted with increasing distance from the gas-film interface (i.e., from $x = 0$ to $x = \delta$). Corresponding model results are included in the Figures SA.7-SA.10.

The Kintecus model output for hydrolyzed urine under condition (1) validates the $[^{\bullet}NH_2]_{ss}/[^{\bullet}OH]_{ss}$ and $[CO_3^{\bullet-}]_{ss}/[^{\bullet}OH]_{ss}$ values discussed above (Figure SA.7). Furthermore, the corresponding results for condition (2) indicate that as O_3 is depleted and $ONOO^-$ diffuses across the film, the levels of $^{\bullet}NO_2$ and $CO_3^{\bullet-}$ generated via $ONOOCO_2^-$ decay within the film may be as much as 10^6-fold higher than $[^{\bullet}OH]_{ss}$ (Figure SA.8). The model output obtained for ED diluate under conditions (1) and (2) also indicates that $^{\bullet}NO_2$ and $CO_3^{\bullet-}$ levels should be ~10-20× lower during ozonation of ED diluate than in hydrolyzed urine (Figures SA.9, SA.10). If the 2- to 10-fold deviations in measured and modeled IP and PP loss rates for hydrolyzed urine were indeed solely attributable to an excess of secondary radical concentrations over $[^{\bullet}OH]$, such a 10-20× decrease in the ratios of $[^{\bullet}NO_2]$ and $[CO_3^{\bullet-}]$ to $[^{\bullet}OH]$ would be expected to yield conditions in which measured loss rates agree with model results, just as observed for ED diluate. Thus, the Kintecus model output is consistent with a positive influence of radicals such as $^{\bullet}NO_2$ and $CO_3^{\bullet-}$ on IP and PP loss rates during ozonation of hydrolyzed urine and ED concentrate.

Oxidation by-products and associated toxicological risks. The Kintecus models described above also indicate that in situ concentrations of $^{\bullet}NO_2$, $^{\bullet}NO$, and carbon-centered radicals may be high enough during urine ozonation to yield appreciable quantities of nitrated and nitrosated by-products via $^{\bullet}NO_2$-$DOC^{\bullet}$ and $^{\bullet}NO$-$DOC^{\bullet}$ addition reactions (Figures SA.7 to SA.10). Such by-products may be important in terms of potential chronic cytotoxic, genotoxic, or carcinogenic effects, as reported for a variety of organic molecules bearing nitro- or nitroso- groups (*21*). Their formation could be circumvented by removing NH_3 prior to ozonation; precluding $^{\bullet}NO_2$ and $^{\bullet}NO$ formation via $^{\bullet}OH$-NH_3 reaction pathways. This could be achieved with optimization of such complementary processes as electrodialysis, ion exchange, or biological nitrification/denitrification (*4,22*).

In a related matter, Br^- levels in urine are quite high (typically ~3-9 mg/L, or ~40-110 μM) (*12*). Although some bromate (BrO_3^-) may form via oxidation pathways mediated by OBr• during urine ozonation (*23*), overall BrO_3^- yields should be suppressed via HOBr/OBr^- scavenging by NH_3 and DOC (*23*). Accordingly, should NH_3 be removed prior to ozonation for the purpose of minimizing nitrated and nitrosated byproduct formation, as discussed above, substantial increases in BrO_3^- yields could result. Thus, any future decisions regarding pre-treatment of urine prior to ozonation must take into account the likely impacts of NH_3 removal on the formation of both nitrogenous oxidation byproducts and BrO_3^-. For this reason, detailed investigations into the potential formation of nitrogenous oxidation by-products and BrO_3^- under various operational conditions are strongly encouraged.

A.3.5 Practical operational implications of experimental observations and model results. *Estimated energy consumption for potential treatment scenarios.* As demonstrated above, ozonation of source-separated urine may provide an effective means of attenuating urine-derived micropollutant loads to municipal sewers. Furthermore, when coupled with additional pre-treatment (e.g., electrodialysis), the relatively high energy costs of ozonation may be offset by the added benefits of nutrient recovery and decreases in nitrogen, phosphorous, and potassium loading to downstream municipal wastewater treatment facilities. However, except for potassium removal, similar effects can be achieved via enhanced "end-of-pipe" wastewater treatment. For ozonation to prove feasible in the context of urine pre-treatment, the costs and benefits of urine treatment strategies in which it is applied must be demonstrated to compare favorably with centralized treatment strategies. Therefore, gross primary energy inputs required to achieve selected treatment criteria related to oxidation of urine-derived micropollutants were estimated - on the basis of the experimental data reported in Figures A.1 and A.2 - for six hypothetical scenarios in which ozonation is utilized alone or with electrodialysis (I-VI), and compared with energy inputs required for four equivalent end-of-pipe treatment scenarios (A-D). Energy needs for pumping and infrastructure fabrication were excluded from these calculations.

In scenarios (I), (III), and (V), energy requirements were calculated for ≥ 99% elimination of estrogenicity derived from steroid hormones (using EE2 as a model) via ozonation of (I) hydrolyzed urine, (III) ED feed (i.e., hydrolyzed urine), and (V) ED effluents (i.e., diluate and concentrate). In scenarios (II), (IV), and (VI), energy requirements were determined for ≥ 50% oxidation of *all* micropollutants (using *p*CBA as a model) in (II) hydrolyzed urine, (IV) ED feed, and (VI) ED effluents. Scenarios (I) and (II) represent stand-alone ozonation processes, whereas scenarios (III)-(VI) represent processes in which ozonation is coupled with continuous electrodialysis. In scenarios (A) and (B), energy needs were calculated for ozonation of the effluent discharged from a typical municipal wastewater treatment facility utilizing conventional secondary activated sludge clarification, with the goal of lowering discharged micropollutant loads to levels otherwise achievable via upstream ozonation of source-separated urine, where absorbed O_3 doses of 2 and 5 mg/L were assumed for (A) >99% elimination of estrogenic activity derived from steroid hormones (*24*) and (B) 50% oxidation of total micropollutant loads (*24,25*), respectively. In scenarios (C) and (D), effluent ozonation (at absorbed O_3 doses of 2 and 5 mg/L, respectively) was assumed to be coupled with full nitrification/denitrification (using methanol as an external carbon source) and enhanced phosphorous removal, so as to evaluate the energy required for end-of-pipe wastewater treatment to produce effluent micropollutant *and* nutrient levels comparable to those otherwise achievable via upstream urine source separation and pre-treatment. Calculated energy requirements (obtained as described in detail within Text SA.9) are summarized for each scenario in Table A.2.

Comparison of scenarios (I) and (II) with scenarios (A) and (B) illustrates that if nutrient recovery/removal steps are omitted (i.e., if only ozonation is implemented), micropollutant oxidation would likely be achieved more efficiently via ozonation of municipal wastewater effluents. In contrast, when costs and benefits of nutrient removal are considered, as shown by comparison of (III) and (IV) with (C) and (D), energy requirements for urine pre-treatment may be significantly lower than those required to achieve similar effluent quality via enhanced downstream wastewater treatment, on account of energy savings derived from upstream resource recovery. Furthermore, if ozonation is applied *after* electrodialysis, additional improvements in energy efficiency may be realized through the overall decrease in O_3 demand achieved via partitioning of RMCs from the higher-volume ED diluate stream into the lower-volume ED concentrate stream during electrodialysis, as demonstrated by comparison of (V) and (VI) with (C) and (D). In addition, as O_3-consumption and $^{\bullet}OH$-scavenging rates for each ED effluent would likely have been appreciably lower if they had not contained ethanol, one may expect that the calculated energy requirements for scenarios (V) and (VI) are relatively conservative, and that electrodialysis with post-ozonation could ultimately yield substantial energy savings over comparable centralized wastewater treatment schemes. However, one benefit of end-of-pipe

Table A.2. Estimated gross primary energy inputs (exclusive of pumping or infrastructure fabrication) for comparable urine and wastewater treatment scenarios (see Text SA.9 for full calculations).[a]

	Gross Primary Energy Consumption (Wh/person/day)					
Urine treatment scenario	**I**	**II**	**III**	**IV**	**V**	**VI**
Treatment Scheme[b]	Urine ⇒ O_3		Urine ⇒ O_3 ⇒ ED		Urine ⇒ ED ⇒ O_3	
Treatment Criterion[c]	*	**	*	**	*	**
Energy Consumed						
Ozonation ($C_{O3(g),in}$ = 60 mg/L)	70	76	70	76	32	64
Electrodialysis	-	-	145	145	145	145
Sum:	70	76	215	221	177	209
Recovered Resources						
N fertilizer	-	-	-81	-81	-81	-81
P fertilizer	-	-	-4	-4	-4	-4
Sum:	-	-	-85	-85	-85	-85
Total:	70	76	130	136	92	124

Wastewater treatment scenario	**A**	**B**	**C**	**D**
Treatment Scheme[d]	WW[e] ⇒ O_3		WW[e] ⇒ N-,P-removal ⇒ O_3	
Treatment Criterion[c]	*	**	*	**
Energy Consumed				
Ozonation	25	63	25	63
Nitr./denitr. w/o ext. carbon	-	-	109	109
Nitr./denitr. w/ MeOH	-	-	55	55
P-precipitation w/ $FeSO_4$	-	-	10	10
Total:	25	63	199	237

[a] Assuming 1.5 L urine/pe/d, 300 L wastewater/pe/d, ~13.1 kWh/g O_3 for a medium-output, air-supplied O_3 generator, and ~31% electricity generation efficiency, as discussed in Text SA.9, which includes details of all calculations. [b] O_3 was assumed to be applied to hydrolyzed urine in scenarios (I) and (II), ED feed (i.e., hydrolyzed urine prior to electrodialysis) in scenarios (III) and (IV), and ED effluents (i.e., ED diluate and concentrate) in scenarios (V) and (VI). [c] Treatment criterion "*" corresponds to >99% elimination of estrogenicity derived from steroid hormones, whereas "**" corresponds to 50% elimination of total urine-derived micropollutant load. Corresponding required absorbed O_3 doses are 1.1, 1.2, 1.1, 1.2, 0.5, and 1.0 g/L for scenarios I, II, III, IV, V, and VI, and 2, 5, 2, and 5 mg/L for scenarios A, B, C, and D, respectively, as discussed in Text SA.9. [d] O_3 was assumed to be applied to a secondary municipal wastewater effluent in scenarios (A) and (B), and nitrified/denitrified, phosphate-depleted secondary effluent in scenarios (C) and (D). [e] WW - wastewater.

ozonation that would not be achievable via urine pre-treatment alone is oxidation of micropollutants from sources other than urine (e.g., industrial discharges, cleaning products).

Physical-chemical process limitations. Further improvements in energy efficiency could likely be achieved by optimizing various physical and chemical aspects of the urine ozonation process. For example, oxidation efficiencies of micropollutants with $k''_{O_3,app}$ lower than ~10^3 $M^{-1}s^{-1}$ (e.g., *p*CBA) are limited in large part by rates of micropollutant diffusion into the film, whereas oxidation efficiencies for compounds with increasing $k''_{O_3,app}$ above ~10^3 $M^{-1}s^{-1}$ (e.g., EE2) are progressively more dependent on mixing efficiency. Thus, higher oxidation efficiencies may be achieved for some micropollutants by increasing specific gas-liquid interfacial area (A_S) (to enhance micropollutant diffusion *into* the film), or in other cases, by enhancing mixing efficiency (to enhance advective transport of micropollutants *to* the film).

For example, doubling A_s could theoretically triple *p*CBA oxidation efficiency (while having negligible effect on EE2 oxidation efficiency) (Figure SA.8). Alternatively, enhancements in mixing may yield up to ~20-fold improvement in EE2 oxidation efficiency (with negligible improvement in *p*CBA oxidation efficiency) (Figure SA.8). In practice, A_s could be increased by decreasing bubble size (e.g., by using Venturi mixers or diffusers with smaller pore sizes (*26*)), or by raising gas flow rate (*26,27*). Mixing efficiencies could be improved for typical bubble contactors by ensuring that the cross-sectional areas of the contactor and gas diffuser are more closely aligned - to improve bubble-driven aqueous-phase mixing and prevent segregation of the contactor into reactive and non-reactive zones, or by physical augmentation of mixing (e.g., via impeller or static mixer).

Acknowledgements

M.C.D. and S.Z. contributed equally to the completion of this work. The research was supported by the Swiss AIB (Amt für Industrielle Betriebe, Baselland) and the Swiss sustainability program Novatlantis. M.C.D. gratefully acknowledges financial support from a United States National Science Foundation Graduate Research Fellowship and the European Commission project RECLAIM WATER (Contract-No. 018309). The authors thank Martin Biebow, Jacqueline Traber, and Elisabeth Salhi for technical assistance. Hansruedi Siegrist is gratefully acknowledged for assistance with energy usage calculations. Special thanks to Marc Huber for providing the foundations of the MATLAB ODE system solution code, and to Yunho Lee and Ioannis Katsoyiannis for helpful discussions.

Supporting Information Available

Tables, figures, texts, MATLAB scripts, Kintecus worksheets, and Kintecus model output addressing experimental methods and modeling approaches, matrix sources and procurement, redox chemistry modeling, and energy input calculations. This information is available free of charge via the Internet at http://pubs.acs.org.

Literature Cited

(1) Larsen, T. A.; Gujer, W. Separate management of anthropogenic nutrient solutions (human urine). *Water Sci. Technol.* **1996**, *34*, 87-94.

(2) Lienert, J.; Gudel, K.; Escher, B. I. Screening method for ecotoxicological hazard assessment of 42 pharmaceuticals considering human metabolism and excretory routes. *Environ. Sci. Technol.* **2007**, *41*, 4471-4478.

(3) Maurer, M.; Muncke, J.; Larsen, T. A. In *Water Recycling and Resource Recovery in Industry*; Lens, P.; Pol, L. H.; Wilderer, P.; Asano, T., Eds.; IWA Publishing: London, 2002, pp 491-510.

(4) Maurer, M.; Pronk, W.; Larsen, T. A. Treatment processes for source-separated urine. *Water Res.* **2006**, *40*, 3151-3166.

(5) Lee, Y.; Escher, B. I.; von Gunten, U. Efficient removal of the estrogenic activity during oxidative treatment of waters containing steroid estrogens. *Environ. Sci. Technol.* **2008**, *42*, 6333-6339

(6) Dodd, M. C.; Kohler, H.-P. E.; Von Gunten, U. Oxidation of antibacterial compounds by ozone and hydroxyl radical: Elimination of biological activity during aqueous ozonation processes. *Submitted for publication in Environ. Sci. Technol.*.

(7) Escher, B. I.; Pronk, W.; Suter, M. J. F.; Maurer, M. Monitoring the removal efficiency of pharmaceuticals and hormones in different treatment processes of source-separated urine with bioassays. *Environ. Sci. Technol.* **2006**, *40*, 5095-5101.

(8) von Gunten, U. Ozonation of drinking water: Part I. Oxidation kinetics and product formation. *Water Res.* **2003**, *37*, 1443-1467.

(9) Mvula, E.; von Sonntag, C. Ozonolysis of phenols in aqueous solution. *Org. Biomol. Chem.* **2003**, *1*, 1749-1756.

(10) Buffle, M. O.; von Gunten, U. Phenols and amine induced HO• generation during the initial phase of natural water ozonation. *Environ. Sci. Technol.* **2006**, *40*, 3057-3063.

(11) Elovitz, M. S.; von Gunten, U. Hydroxyl radical/ozone ratios during ozonation processes. I. The R_{ct} concept. *Ozone: Sci. Eng.* **1999**, *21*, 239-260.

(12) Ciba-Geigy, Ed.^Eds. *Wissenschaftliche Tabellen Geigy, Teilband Körperflüssigkeiten*; 8 ed.: Basel, 1977.

(13) Charpentier, J. C., *Mass-transfer rates in gas-liquid absorbers and reactors*; Academic Press: New York, NY, 1981; Vol. 11.

(14) Beltran, F. J. *Ozone Reaction Kinetics for Water and Wastewater Systems*; Lewis Publishers: Boca Raton, FL, 2004.

(15) Buffle, M. O.; Schumacher, J.; Salhi, E.; Jekel, M.; von Gunten, U. Measurement of the initial phase of ozone decomposition in water and wastewater by means of a continuous quench-flow system: Application to disinfection and pharmaceutical oxidation. *Water Res.* **2006**, *40*, 1884-1894.

(16) Radiation Chemistry Data Center of the Notre Dame Radiation Laboratory. Available at http://allen.rad.nd.edu/. University of Notre Dame Radiation Laboratory

(17) Laszlo, B.; Alfassi, Z. B.; Neta, P.; Huie, R. E. Kinetics and mechanism of the reaction of $^{\bullet}NH_2$ with O_2 in aqueous solutions. *J. Phys. Chem., A* **1998**, *102*, 8498-8504.

(18) Goldstein, S.; Lind, J.; Merenyi, G. Chemistry of peroxynitrites as compared to peroxynitrates. *Chem. Rev.* **2005**, *105*, 2457-2470.

(19) Perry, R. H.; Chilton, C. H. *Chemical Engineers' Handbook*; 5th ed.; McGraw-Hill, Inc.: New York, 1973.
(20) Ianni, J. C., Kintecus, Windows Version 3.95, 2008, Available at www.kintecus.com.
(21) IRIS Database. Available at http://cfpub.epa.gov/ncea/iris/index.cfm. United States Environmental Protection Agency
(22) Pronk, W.; Biebow, M.; Boller, M. Electrodialysis for recovering salts from a urine solution containing micropollutants. *Environ. Sci. Technol.* **2006**, *40*, 2414-2420.
(23) von Gunten, U. Ozonation of drinking water: Part II. Disinfection and by-product formation in presence of bromide, iodide, or chloride. *Water Res.* **2003**, *37*, 1469-1487.
(24) Huber, M. M.; Gobel, A.; Joss, A.; Hermann, N.; Loffler, D.; McArdell, C. S.; Ried, A.; Siegrist, H.; Ternes, T. A.; von Gunten, U. Oxidation of pharmaceuticals during ozonation of municipal wastewater effluents: A pilot study. *Environ. Sci. Technol.* **2005**, *39*, 4290-4299.
(25) Ternes, T. A.; Stuber, J.; Herrmann, N.; McDowell, D.; Ried, A.; Kampmann, M.; Teiser, B. Ozonation: a tool for removal of pharmaceuticals, contrast media and musk fragrances from wastewater? *Water Res.* **2003**, *37*, 1976-1982.
(26) Zhou, H. D.; Smith, D. W. Ozone mass transfer in water and wastewater treatment: Experimental observations using a 2D laser particle dynamics analyzer. *Water Res.* **2000**, *34*, 909-921.
(27) Roustan, M.; Wang, R. Y.; Wolbert, D. Modeling hydrodynamics and mass transfer parameters in a continuous ozone bubble column. *Ozone: Sci. Eng.* **1996**, *18*, 99-115.

Supporting Information for Appendix A.

Ozonation of Source-separated Urine for Resource Recovery and Waste Minimization: Process Modeling, Reaction Chemistry, and Operational Considerations

50 pages, including 9 narratives, 8 tables, 12 figures, and 3 MATLAB scripts

Text SA.1. Materials, methods, and experimental procedures

Chemicals. Diclofenac (DC), propranolol (PP), carbamazepine (CM), ibuprofen (IP) and 17-α-ethinylestradiol (EE2) were purchased from Sigma-Aldrich. *para*-Chlorobenzoic acid (*p*CBA) was obtained from Merck. All model compounds used in this study were of 95% purity or higher. Model compounds were generally added directly to urine solutions to achieve starting concentrations of ~10 μM. *p*CBA was dosed to all solutions at starting concentrations of ~50 μM, with the exceptions of hydrolyzed urine stocks treated with $C_{O3(g),in}$ = 30 and 120 mg/L, to which *p*CBA was added at ~10 μM.

Urine collection and preparation. Natural urine (male only) was obtained from an on-site urine collection system at Eawag (Dübendorf, Switzerland) and stored to ensure complete hydrolysis of urea to ammonia, as described previously (*1*). Prior to ozonation, hydrolyzed urine was passed through a 0.2-μm polypropylene membrane to remove particulate matter. ED effluents were prepared as described previously, using hydrolyzed urine as a feed solution (*2*). ED diluate and concentrate streams were collected during continuous operation at a feed flow rate of 1.03 L/d, a concentration factor of 2.6, and desalination efficiency of 90% (*2*). In the ED experiments, the urine feed solution was initially spiked with micropollutants by adding 5 mL of an ethanol stock containing 2 mM of each model compound to 1 L of feed solution. The resulting ethanol concentration in the feed was ~4 g/L (87 mM). Theoretically, ethanol should then have been distributed equally between the diluate and concentrate during ED, as it is uncharged and quite hydrophilic, though this was not analytically verified. Because a substantial proportion of micropollutants dosed to the feed solution was lost via adsorption to the ED membrane during operation (*2*), micropollutant concentrations in the diluate and concentrate were re-adjusted to 10 μM, and *p*CBA added at 50 μM, by dissolving each compound directly into the appropriate solution.

Analytical Methods. Total ammonia and urea (as N) were determined photometrically (via reaction with bromocresol purple) by flow-injection analysis (Ismatec AG, Glattbrugg, Switzerland). DOC measurements were obtained by acidification followed by oxidation and CO_2 determined by IR spectroscopy. Before each analysis, urea was hydrolyzed to ammonia with urease. Alkalinity was determined by titration with HCl using methyl orange as an indicator.

All model compounds were measured by HPLC, using a Chromcart HPLC column with 125/4 Nucleosil 100-5 C18 packing (125 mmx4mm), and a CC 8/4 Nucleosil 100-5 C18 precolumn. The flow-rate was 1 mL/min and elution was carried out with a linear gradient of acetonitrile and phosphoric acid (10 μM in water) from 5/95 to 40/60 in five minutes and from 40/60 to 60/40 in seven minutes. EE2, PP and IP were measured using a fluorescence detector with excitation at 229 nm and detection at 309 nm. DC, CM, and *p*CBA were measured with a UV detector at 220 and 275 nm respectively.

Measurement of O_2 mass transfer into urine. Pure O_2 was bubbled into hydrolyzed urine under the same experimental conditions utilized for O_3 application. A dissolved O_2 meter (WTW OXI 196, Weilheim, Germany), connected to the same on-line data-logger used in ozonation experiments was used to track changes in dissolved O_2 concentrations during the O_2 mass transfer experiments. Data was obtained from experiments conducted with the same urine on two different dates - spaced three days apart. O_2 mass transfer parameters were calculated from the average of data obtained on these two dates.

Text SA.2. Derivation of the expression for $C_{O3(g),avg.}$ within the reactor during ozonation

In order to accurately model transport of gas-phase O_3 into the aqueous solution within a bubble column reactor, one must account for any evolution in $C_{O3(g)}$ during vertical passage of the bubbles through the reactor. Assuming that the properties of the bulk solution surrounding the gas bubbles remain constant during the time-scale over which an individual bubble passes from the bottom to the top of the reactor, that the bulk solution in contact with the bubbles is well-mixed, and that the gas-phase of the reactor exhibits plug-flow, one can characterize O_3 transport out of the gas-phase (i.e., flux of O_3 through the gas-liquid interface) for differential fluid elements with height *dz* according to eq S1 (*3,4*),

$$Q_g \frac{dC_{O3(g),z}}{dz} = -(1-\varepsilon_g)A_{xs}J_{O_3}A_s = -(1-\varepsilon_g)A_{xs}Ek_{L,O_3}A_sC_{O3(g),z}H_{O_3} \qquad \text{(S1)}$$

where $C_{O3(g),z}$ represents the concentration of O_3 in the gas phase at a given vertical point within the reactor's liquid volume, $Ek_{L,O3}A_s$ is the apparent rate of O_3 absorption by the matrix of interest - determined as described in Text SA.4, Q_g is the gas flow rate through the effective reactive zone of the reactor (i.e., the bubble-containing volume described in the main text, which is shown centered above the glass diffuser disc in Figure SA.1) (Table SA.2), $1\text{-}\varepsilon_g$ is the calculated liquid holdup - determined as described in Text SA.6, A_{xs} is the cross-sectional area of the effective reactive zone (Table SA.2), and H_{O3} is the dimensionless equilibrium solubility ratio ($C_{O3,\text{liquid phase}}/C_{O3,\text{gas phase}}$) for O_3 in the urine matrix of interest (Table SA.2). A solution for $C_{O3(g)}$ at any vertical point in the reactor can be obtained by integrating eq S1 over a given liquid height in the reactor, *z* (Table SA.2), to obtain eq S2.

$$C_{O3(g),z} = C_{O3(g),in} \exp\left(\frac{-(1-\varepsilon_g)}{Q_g} A_{xs} E k_{L,O_3} A_s H_{O_3} z \right) \tag{S2}$$

The average gas-phase concentration in the reactor at a given instant can then be obtained by integrating eq S2 over h_T (= $h_l/(1-\varepsilon_g)$ - the full height of the effective reactive zone (inclusive of gas and liquid volumes), which can be calculated from the values in Table SA.2, and dividing by h_T, to obtain eq S3.

$$C_{O3(g),avg} = C_{O3(g),in} \left(\frac{Q_g}{(1-\varepsilon_g) A_{xs} E k_{L,O_3} A_s H_{O_3}} \right) \left(1 - \exp\left(\frac{-(1-\varepsilon_g) A_{xs} E k_{L,O_3} A_s H_{O_3} h_T}{Q_g} \right) \right) \left(\frac{1}{h_T} \right) \tag{S3}$$

Text SA.3. Estimation of δ

The film thickness, δ, can be estimated from measurements of mass transfer properties for controlled operating conditions, from the definition of the O_3 mass transfer coefficient, $k_{L,O3}$ (eq S4),

$$k_{L,O_3} = D_{l,O_3}/\delta \quad \text{(i.e., } \delta = D_{l,O_3}/k_{L,O_3}\text{)} \tag{S4}$$

where $D_{l,O3}$ is known, and $k_{L,O3}$ can be determined indirectly by measuring *physical absorption* (i.e., exclusive of reactive enhancement) of O_2 as a surrogate for O_3.

The volumetric mass transfer coefficients for each gas are related by eq S5 (*5*) (derived from Danckwert's surface renewal theory (*6*)),

$$\frac{(k_{L,O2} A_{s,f})_{O_2}}{(k_{L,O_3} A_{s,f})_{O_3}} = \left(\frac{D_{l,O_2}}{D_{l,O_3}} \right)^{1/2} \tag{S5}$$

where $A_{s,f}$ is the specific interfacial area (in m^2/m^3) of gas bubbles relative to the full reactor volume (calculated as described in Text SA.6). $A_{s,f}$ was used here rather than A_s - the specific interfacial area relative to the volume of the effective reactive zone during ozonation (i.e., the bubble-containing volume described in the main text, which is shown centered above the glass diffuser disc in Figure SA.1) - because O_2 absorption was purely physical, and was not limited only to the bubble-containing volume.

Variation in the bulk liquid-phase concentration of O_2, $[O_2]_{bulk}$, while continuously bubbling pure O_2 through the reactor can be characterized according to eq S6,

$$J_{O_2} A_{s,f} = \frac{d[O_2]_{bulk}}{dt} = k_{L,O_2} A_{s,f} \left([O_2]_{l,eq} - [O_2]_{bulk} \right) \tag{S6}$$

which applies for purely physical absorption with negligible gas-phase resistance, where $[O_2]_{l,eq}$ is the equilibrium O_2 concentration in solution, which can be calculated from matrix-specific values of H_{O2} - the dimensionless solubility ratio for O_2 (Table SA.2). Integrating eq S6 over time yields eq S7,

$$\ln\left(\frac{[O_2]_{l,eq}-[O_2]_{bulk}}{[O_2]_{l,eq}}\right)=k_{L,O_2}A_{s,f}t \tag{S7}$$

from which the volumetric mass transfer coefficient $(k_{L,O2}A_{s,f})_{O2}$ can be determined by plotting measured values of $\ln\left(\frac{[O_2]_{l,eq}-[O_2]_{bulk}}{[O_2]_{l,eq}}\right)$ vs time. $k_{L,O3}$ can in turn be determined by solving eq S5 for the volumetric mass transfer coefficient $(k_{L,O3}A_{s,f})_{O3}$ and dividing this value by $A_{s,f}$. Assuming only minor variation in physical mass transfer properties amongst the three urine matrixes included in this investigation, the $k_{L,O3}$, A_s, and $A_{s,f}$ values determined for hydrolyzed urine were used as approximations of the corresponding values for ED diluate and ED concentrate.

Text SA.4. Determination of $k'_{O_3,RMC}$.

Analytical solution of eq 2 in the main text for the boundary conditions $[O_3]_{l,x}=[O_3]_{l,eq}$ at $x=0$, and $[O_3]_{l,x}=0$ at $x=\delta$, yields eq S8 (for $[O_3]_{l,x}$ within the film) (*4,7*).

$$[O_3]_{l,x}=\frac{1}{\sinh(Ha)}\left([O_3]_{bulk}\sinh\left((Ha)\left(\frac{x}{\delta}\right)\right)+[O_3]_{l,eq}\sinh\left((Ha)\left(1-\frac{x}{\delta}\right)\right)\right) \tag{S8}$$

where $Ha=\frac{\left(k'_{O_3,RMC}D_{l,O_3}\right)^{1/2}}{k_{L,O_3}}$ is the Hatta number, which represents the ratio of the maximum possible O_3 consumption rate within the film to the maximum rate of physical O_3 mass transfer into the film, and $k_{L,O3}$ represents the liquid-side mass transfer coefficient for O_3 - determined as described in Text SA.3.

By considering the expression for gas flux into a liquid at a gas-liquid interface (eq S9),

$$J_{O3}=-D_{l,O3}\left(\frac{d[O_3]_{l,x}}{dx}\right)_{x=0} \tag{S9}$$

one can obtain from eq S8 the expression, eq S10, for O_3 flux through the film (*4,7*).

$$J_{O_3}=\frac{k_{L,O_3}[O_3]_{l,eq}Ha}{\tanh(Ha)}\left(1-\left(\frac{[O_3]_{bulk}}{[O_3]_{l,eq}}\right)\frac{1}{\cosh(Ha)}\right)=Ek_{L,O_3}[O_3]_{l,eq} \tag{S10}$$

where E (equal to $J_{O_3}/k_{L,O_3}[O_3]_{l,eq}$) represents the enhancement factor for O_3 absorption in the presence of a reaction occurring within the absorbing liquid. By definition, when O_3 is consumed within a "fast" kinetic regime, *Ha* > 3, and tanh(*Ha*) ≈ 1 (*4,7*). In addition, because $[O_3]_{bulk} = 0$ for a fast pseudo-first-order kinetic regime, eq S10 simplifies to eq S11 in this instance.

$$J_{O_3} = Ek_{L,O_3}[O_3]_{l,eq} = Ha\,k_{L,O_3}[O_3]_{l,eq} = [O_3]_{l,eq}\left(k'_{O_3,RMC}D_{l,O_3}\right)^{1/2} \tag{S11}$$

As a result, the enhancement factor, E, is effectively equal to *Ha*. Equation S11 then yields the following generic expression for volumetric O_3 absorption into the film (eq S12)

$$N_{O_3} = Ek_{L,O_3}A_s[O_3]_{l,eq} = A_s[O_3]_{l,eq}\left(k'_{O_3,RMC}D_{l,O_3}\right)^{1/2} \tag{S12}$$

which can be rearranged to eq S13.

$$k'_{O_3,RMC} = \left(\frac{\left(Ek_{L,O_3}A_s\right)}{A_s}\right)^2 \Big/ D_{l,O_3} \tag{S13}$$

The specific interfacial area, A_s (in m^2/m^3), relative to the volume of the effective reactive zone during ozonation (i.e., the bubble-containing volume described in the main text, which is shown centered above the glass diffuser disc in Figure SA.1) can be calculated according to Text SA.6. The apparent rate of O_3 mass transfer into a solution containing large concentrations of RMCs can be determined for a semi-batch process from eq S14 (*4,8*),

$$Ek_{L,O_3}A_s = -\frac{Q_g}{V_l H_{O_3}}\ln\left(\frac{C_{O_3(g),out}}{C_{O_3(g),in}}\right) \tag{S14}$$

where V_l is the liquid volume of the effective reactive zone (in m^3) - calculated from A_{xs} and h_l (Table SA.2), Q_g represents the gas flow rate into the system (m^3/s) (Table SA.2), $C_{O3(g),in}$ is the O_3 concentration in the gas entering the reactor (mg/L), and $C_{O3(g),out}$ (mg/L) is the O_3 concentration in the gas at the reactor outlet. For modeling purposes, the effective reactive zone defined by the bubble-containing volume in the semi-batch reactor (as opposed to the reactor's full liquid volume) was represented as an annular volume with an outer diameter of 2.5 cm (equal to the diameter of the diffuser disc, Figure SA.1b) and an inner diameter of 0.85 cm (equal to the diameter of the glass gas inlet tube connecting the diffuser disc to the O_3 inlet line, Figure SA.1b).

Plots of $Ek_{L,O3}A_s$ vs. time and absorbed O_3 dose are depicted in Figure SA.3 for each of the four O_3 concentrations ($C_{O3(g),in}$ = 15, 30, 60, and 120 mg/L) applied to hydrolyzed urine, as well as for the two pre-treated urine products ($C_{O3(g),in}$ = 60 mg/L). $Ek_{L,O3}A_s$ values for ED diluate and ED concentrate were consistently lower and higher, respectively, than those for hydrolyzed urine, due to the respective dilution and concentration of RMCs in the former two matrixes. Time-dependencies of $Ek_{L,O3}A_s$ could be described by an exponential decay model, $y_0 + ae^{(-bt)}$, where values of the parameters y_0, a, and b (summarized in Table SA.3) were obtained via non-linear regression of the data using SigmaPlot (Systat Software). The corresponding expressions for $Ek_{L,O3}A_s$ as a function of time could be used to determine the pseudo-first-order rate constant, $k'_{O_3,RMC}$, for O_3 consumption by RMCs, according to eq S13.

As a check on the initial assumption of fast pseudo-first-order O_3 consumption kinetics (made on the basis of reasons discussed in the main text), values of *Ha* and E_i, the enhancement factor for instantaneous O_3 consumption by RMCs, were determined for each matrix according to the above expression for *Ha* and the expression $E_i = 1 + D_{l,RMC}[RMC]/D_{l,O3}[O_3]_{l,eq}$, assuming that $D_{l,RMC} \sim 5 \times 10^{-9}$ m^2/s and that RMCs were constituted exclusively of DOC, where DOC concentrations (Table A.1 in the main text) were normalized to $MW_{carbon} = 12$ g/mol. For hydrolyzed urine, values of *Ha* (= E) ranged from ~176 at the commencement of ozonation to ~5 at the highest absorbed O_3 doses and E_i values varied from 6.4×10^3 at $C_{O3(g),in} = 15$ mg/L to 8.0×10^2 at $C_{O3(g),in} = 120$ mg/L, validating the assumption of fast pseudo-first-order O_3 consumption kinetics according to the generally accepted convention that $3 < Ha < E_i/2$ for a fast pseudo-first-order kinetic regime (*4*). For ED diluate, values of *Ha* (= E) ranging from ~15 at the commencement of ozonation to ~3 at the highest absorbed O_3 doses were calculated relative to an E_i value of 1.2×10^3 at $C_{O3(g),in} = 60$ mg/L, also providing sufficient justification for the assumption of fast pseudo-first-order kinetics within the regime of absorbed ozone doses investigated here. For ED concentrate, values of *Ha* (= E) ranged from ~99 at the commencement of ozonation to ~11 at the highest absorbed O_3 doses, while E_i was determined to be 5.6×10^3 at $C_{O3(g),in} = 60$ mg/L; also consistent with the assumption of fast pseudo-first-order kinetics.

Text SA.5. Determination of $R_{ct(t)}$

Prior to attempting to model the ozonation processes described here, one must also be able to account for the [$^\bullet$OH] term within eq 3 in the main text. This value can be indirectly estimated by using an O_3-resistant $^\bullet$OH probe compound to monitor *in situ* $^\bullet$OH yield during ozonation of the urine solution (*9*). *p*-Chlorobenzoic acid, which exhibits second-order rate constants of $k''_{O_3} < 0.15$ M^{-1}s^{-1} (*10*) and $k''_{\bullet OH} = 5.0 \times 10^9$ M^{-1}s^{-1} (*11*), was used as a $^\bullet$OH probe in the present investigation.

As apparent from a plot of ln([*p*CBA]/[*p*CBA]$_0$) vs time (Figure SA.5a), *p*CBA depletion in this system exhibits apparent first-order kinetics. For this to be possible, the steady-state concentration, [$^{\bullet}$OH]$_{ss}$, in the ozonated urine solution must be approximately constant during the course of the ozonation process. This in turn implies that $R_{\mathrm{ct(t)}}$, the time-dependent ratio of [$^{\bullet}$OH]/[O_3]$_l$ within the urine ozonation system, must vary inversely with respect to the evolution of O_3 concentrations in the film over time. Likewise, because the O_3 concentration at a particular point within the film at any given moment is inversely related to $\mathrm{E}k_{\mathrm{L,O3}}\mathrm{A_s}$ over time, one can infer that the temporal variation in $R_{\mathrm{ct(t)}}$ at that point should be proportionally related to $\mathrm{E}k_{\mathrm{L,O3}}\mathrm{A_s}$. On the basis of this assumption, one should be able to model the evolution of $R_{\mathrm{ct(t)}}$ over time according to the same empirical relationship by which $\mathrm{E}k_{\mathrm{L,O3}}\mathrm{A_s}$ can be described, after substitution with the appropriate coefficient. Since in this case, $\mathrm{E}k_{\mathrm{L,O3}}\mathrm{A_s}$ has been modeled by an exponential decay function, $y_0 + a\mathrm{e}^{(-bt)}$, one can simply substitute the y_0 term with a term, $R_{\mathrm{ct(f)}}$, representing the ratio of $^{\bullet}$OH exposure to O_3 exposure at very large times (at which point conditions in the reactor have reached a relatively stable equilibrium, as illustrated by the relatively constant $\mathrm{E}k_{\mathrm{L,O3}}\mathrm{A_s}$ values measured at high ozonation times (Figure SA.3a) (i.e, absorbed O_3 doses, Figure SA.3b), and the term *a* with another time-dependent $R_{\mathrm{ct(t)}}$ term $R_{\mathrm{ct(0)}}$ to adapt the model for the purpose of modeling temporal changes in $R_{\mathrm{ct(t)}}$. The exponent *b* remains the same.

Values of $R_{\mathrm{ct(f)}}$ and $R_{\mathrm{ct(0)}}$ can be determined indirectly by evaluating the film profiles for a given urine matrix (using Script SA.1) first at a very large time (e.g., 8 h) to determine $R_{\mathrm{ct(f)}}$, and then at t = 0 to determine $R_{\mathrm{ct(0)}}$. This is achieved by iteratively varying $R_{\mathrm{ct(f)}}$ and then $R_{\mathrm{ct(0)}}$ until the calculated fluxes, $J_{p\mathrm{CBA},\delta}$, of *p*CBA from the bulk solution into the film equal the fluxes calculated from observed slopes of the ln([*p*CBA]/[*p*CBA]$_0$) plots shown in Figure SA.5a, where the observed pseudo-first-order rate constant for *p*CBA loss, k'_{obs} (in s^{-1}), multiplied by [*p*CBA]$_0$, is equal to the calculated rate of pCBA absorption into the film, $(J_{p\mathrm{CBA},\delta}\mathrm{A_s})/(1000(1-\varepsilon_g))$, defined in eq 7 within the main text, where the factor of 1000 is simply for conversion of the flux from units of mol m^{-3} s^{-1} to units of mol L^{-1} s^{-1}. The resulting values of the $R_{\mathrm{ct(f)}}$ (i.e., "y_0") and $R_{\mathrm{ct(0)}}$ (i.e., "*a*") parameters used to model the exponential time-dependency of $R_{\mathrm{ct(t)}}$ are summarized for each urine matrix in Table SA.3.

Text SA.6. Determination of $\mathrm{A_s}$

The specific interfacial area of the gas-liquid interface relative to the volume of the effective reactive zone in the urine ozonation reactor (i.e., the bubble-containing volume described within the main text, which is shown centered above the glass diffuser disc in Figure SA.1), can be calculated from eq S15 (*12*),

$$A_s = \frac{6\varepsilon_g}{d_{bubble}} \tag{S15}$$

where ε_g is the gas holdup within the effective reactive zone ($\frac{V_{gas}}{V_{liquid} + V_{gas}}$), and d_{bubble} is the system average gas bubble diameter (m). ε_g can be estimated from the empirical relationship in eq S16 (*13*),

$$\varepsilon_g = 1.2 \times 10^{-3} \cdot u \tag{S16}$$

where the superficial gas velocity, u (m/s), can be determined from the cross-sectional area, A_{xs}, of the effective reactive zone, and the gas flow rate, Q_g (Table SA.2). d_{bubble} (Table SA.2) was measured photographically from a sample of 50 bubbles taken during oxygenation of a urine solution at Q_g = 30 L/h (8.3×10^{-6} m^3/s) with the same reactor setup as used for ozonation experiments, according to (*14*). The liquid holdup, $\frac{V_{liquid}}{V_{liquid} + V_{gas}}$, is equal to $1-\varepsilon_g$.

The same value of d_{bubble} was used to model micropollutant losses in each of the three urine matrixes, assuming only minor variation in bubble geometries within each. The specific interfacial area, $A_{s,f}$, of gas bubbles relative to the *full* reactor volume can be calculated by multiplying A_s by the ratio of the full effective reactive zone volume (including gas and liquid volumes) to the full reactor volume (including the effective reactive zone and non-reactive zone), or $\left(\frac{A_{xs}h_l}{(1-\varepsilon_g)}\right) \Big/ \left(A_{xs,f}h_{l,f} + A_{xs}h_l\frac{\varepsilon_g}{(1-\varepsilon_g)}\right)$ = 5.5×10^{-2}, as determined from the dimensions provided in Table SA.2.

Text SA.7. Estimation of k'_{mix}

To provide a quantitative measure of advective transport limitations on micropollutant depletion rates, EE2 was selected as an in situ probe for the approximate rate of fluid element transport from the non-reactive zone into the reactive zone. This decision was based upon the fact that EE2 reacts at extremely high rates with O_3 in homogeneous solution at pH 8-9 (Table SA.1), and should therefore not have been subject to appreciable diffusive limitations on its consumption by O_3 within the reactive zone, on account of its extremely steep concentration gradient across the film to the gas-film interface (as illustrated for S_{high}, in Figure A.3 within the main text). That is, without any appreciable limitation on their diffusion into the film, EE2 molecules should theoretically have been absorbed into the film as soon as they came into contact with the film-bulk liquid interface. Thus, the observed loss rate for EE2 would have been approximately equal to its rate of advective transport to the film within the reactive zone.

The use of EE2 for this purpose is supported by comparing theoretical EE2 absorption rates into the film (i.e., $\frac{J_{S,\delta}A_s}{1000(1-\varepsilon_g)}$, in mol L^{-1} s^{-1}, calculated via Script SA.1) with measured EE2 depletion rates (i.e., $k'_{\mathrm{EE2}}[\mathrm{EE2}]_{\mathrm{bulk.}}$, also in mol L^{-1} s^{-1}, where k'_{EE2} is the observed pseudo-first-order rate constant of EE2 loss, in s^{-1}) for various operating conditions. This comparison showed that the former term (which *excludes* mixing limitations) was consistently ~10-100× higher than the latter (which *includes* mixing limitations) under the investigated conditions (data not shown), confirming that observed EE2 loss rates were constrained primarily by advective transport. Approximate first-order "mixing constants," k'_{mix} (= k'_{EE2}), were therefore extracted from the slopes of plots of ln([EE2]/[EE2]$_0$) vs. time (Figure SA.5b).

Text SA.8. Estimation of $[{}^{\bullet}NH_2]_{ss}/[{}^{\bullet}OH]_{ss}$ and $[CO_3^{\bullet-}]_{ss}/[{}^{\bullet}OH]_{ss}$

Approximate steady-state concentrations of $^{\bullet}NH_2$ and $CO_3^{\bullet-}$ can be estimated by taking into account the relative reactivities of each radical's precursor (i.e., NH_4^+/NH_3 and HCO_3^-/CO_3^{2-}) with $^{\bullet}OH$ at pH 9, in addition to the magnitudes of reactivities of $^{\bullet}NH_2$ and $CO_3^{\bullet-}$ with the predominant RMCs in each matrix.

Assuming steady-state conditions at a particular instant in time, the balance of $^{\bullet}NH_2$, and $CO_3^{\bullet-}$ inputs and outputs within the film can be expressed by eqs S17 and S18,

$$\frac{d[\mathrm{CO_3}^{\bullet-}]}{dt} = r_{\mathrm{in}} - r_{\mathrm{out}} = k'_{{}^{\bullet}\mathrm{OH,carbonate}}[{}^{\bullet}\mathrm{OH}]_{\mathrm{ss}} - k'_{\mathrm{CO_3}^{\bullet-},\mathrm{total}}[\mathrm{CO_3}^{\bullet-}]_{\mathrm{ss}} = 0 \tag{S17}$$

$$\frac{d[{}^{\bullet}\mathrm{NH_2}]}{dt} = r_{\mathrm{in}} - r_{\mathrm{out}} = k'_{{}^{\bullet}\mathrm{OH,ammonia}}[{}^{\bullet}\mathrm{OH}]_{\mathrm{ss}} - k'_{{}^{\bullet}\mathrm{NH_2},\mathrm{total}}[{}^{\bullet}\mathrm{NH_2}]_{\mathrm{ss}} = 0 \tag{S18}$$

where $k'_{{}^{\bullet}\mathrm{OH,ammonia}}$ and $k'_{{}^{\bullet}\mathrm{OH,carbonate}}$ represent the respective pseudo-first-order rate constants for consumption of $^{\bullet}OH$ by excess ammonia (NH_3 only) and excess carbonate (HCO_3^- and CO_3^{2-} only) at a given pH, and $k'_{{}^{\bullet}\mathrm{NH_2},\mathrm{total}}$ and $k'_{\mathrm{CO_3}^{\bullet-},\mathrm{total}}$ are the respective pseudo-first-order rate constants for consumption of $^{\bullet}NH_2$ and $CO_3^{\bullet-}$ by all abundant matrix constituents, as summarized in Tables SA.4-SA.6. By substituting the appropriate values for each of the pseudo-first-order rate constants into eqs S19 and S20 (which follow from the relationships in eqs S17 and S18),

$$\frac{\left[\mathrm{CO_3}^{\bullet-}\right]_{\mathrm{ss}}}{\left[{}^{\bullet}\mathrm{OH}\right]_{\mathrm{ss}}} = \frac{k'_{{}^{\bullet}\mathrm{OH,carbonate}}}{k'_{\mathrm{CO_3}^{\bullet-},\mathrm{total}}} \tag{S19}$$

$$\frac{\left[{}^{\bullet}\mathrm{NH_2}\right]_{\mathrm{ss}}}{\left[{}^{\bullet}\mathrm{OH}\right]_{\mathrm{ss}}} = \frac{k'_{{}^{\bullet}\mathrm{OH,ammonia}}}{k'_{{}^{\bullet}\mathrm{NH_2},\mathrm{total}}} \tag{S20}$$

one can determine that $[{}^{\bullet}NH_2]_{ss}$ and $[CO_3^{\bullet-}]_{ss}$ should each have been approximately 10-50 times higher than $[{}^{\bullet}OH]_{ss}$ in the hydrolyzed urine and ED concentrate, compared to ~4-8 times *lower* in ED diluate (Table SA.7).

Text SA.9. Estimates of energy consumption for urine source separation with pre-treatment and for enhanced treatment measures required in municipal wastewater treatment to reach effluent quality comparable to that achievable by implementing decentralized urine pre-treatment

Urine source separation and pre-treatment. Gross energy requirements were estimated for various hypothetical scenarios in which ozonation (at $C_{O3(g),in}$ = 60 mg/L) was either utilized alone or coupled with electrodialysis to achieve N and P recovery (Table A.2 in the main text). In scenarios (I), (III), and (V), energy requirements were calculated for ≥ 99% elimination of estrogenicity derived from steroid hormones (using EE2 as a model) via ozonation of (I) hydrolyzed urine, (III) ED feed, and (V) ED effluents (i.e., diluate and concentrate). In scenarios (II), (IV), and (VI), energy requirements were determined for ≥ 50% oxidation of *all* micropollutants (using *p*CBA as a model) in (II) hydrolyzed urine, (IV) ED feed, and (VI) ED effluents. Scenarios (I) and (II) represent stand-alone ozonation processes, whereas scenarios (III)-(VI) represent processes in which ozonation is coupled with continuous electrodialysis. Energy needs for each of these scenarios were calculated from the absorbed O_3 doses required to meet each micropollutant oxidation target criterion in the present investigation (Figures A.1 and A.2 in the main text) and available ED process data.

From Figure A.1c in the main text, one can determine that the O_3 doses required for scenarios (I) and (III) amount to ~1100 mg/L, whereas those for scenarios (II) and (IV) amount to ~1200 mg/L, at $C_{O3(g),in}$ = 60 mg/L. In comparison, the required O_3 doses for scenarios (V) and (VI) amount to ~510 mg/L and ~1010 mg/L, as determined from the data in

Figure A.2 by assuming ~68% and ~32% effluent volume contributions (relative to the feed stream) for diluate and concentrate streams, respectively, under the same electrodialysis operating conditions used to produce the diluate and concentrate solutions used in the present investigation (i.e., 506 mg/L = 250 mg/L × 0.68 in ED diluate + 1050 mg/L × 0.32 in ED concentrate for scenario (V) and 1006 mg/L = 350 mg/L × 0.68 in ED diluate + 2400 mg/L × 0.32 in ED concentrate for scenario (VI)). Electricity consumption for O_3 generation was assumed at 13.1 Wh/g O_3 (for a medium-output, air-supplied O_3 generator such as Wedeco model SMA 750 (*15*), excluding peripheral energy consumption via such devices as pumps or compressors), with a 31% electricity generation efficiency (based on a reported average for Europe (*16*)), from which gross energy consumptions of 70, 76, 70, 76, 32, and 64 Wh/pe/d were calculated for scenarios (I), (II), (III), (IV), (V), and (VI), respectively. These calculations incorporate the implicit assumption that applied O_3 is fully utilized (i.e., that each mole of gas-phase O_3 generated and applied to a hypothetical urine ozonation reactor is consumed within the aqueous phase), which should be essentially fulfilled for an optimally-designed reactor (i.e., in which gas-liquid contact time is high enough to ensure nearly 100% transfer of gas-phase O_3 into the surrounding liquid).

As shown in Figure SA.11 (which depicts generic mass flows for decentralized urine treatment and enhanced wastewater treatment), total excreta-derived N and P loads to municipal sewerage can be assumed to be roughly 9 g N/pe/d and 1.5 g P/pe/d (*17*). Of these loads, approximately 7.2 g N/pe/d and 0.76 g P/pe/d are contributed by urine, where daily urine production is assumed to be ~1.5 L/person/d, and fresh urine contains roughly 4.8 g N/L and 0.5 g P/L) (*18*). Following source separation and collection, urine is typically stored for sufficient times to facilitate complete hydrolysis of urea to ammonia. During this storage time, one can assume that roughly 50% of the urine's P content may be precipitated from solution, depending on the degree to which the urine is diluted by water (derived from upstream flushing if practiced) within the tank, and that approximately 50% of this precipitated P load can be recovered as struvite for subsequent use as a slow-release fertilizer (*1*).

Electrodialysis can enable recovery of an additional ~90% of the N and P remaining in stored, hydrolyzed urine (i.e., 6.5 g N/pe/d and 0.34 g P/pe/d), translating to an ultimate reduction in downstream wastewater effluent N and P loads to ~0.27 g N/pe/d and ~0.188 g P/pe/d, respectively, as depicted in Figure SA.11. Assuming that the electrical input required for ED is ~30 Wh per liter of hydrolyzed urine (*19*), and accounting for a 31% electricity generation efficiency, gross energy requirements for electrodialytic pre-treatment can be estimated as approximately 145 Wh/pe/d, though this value is exclusive of pump energy requirements, and may be subject to revision upon availability of data from operational full-scale plants. Using reported average gross energy consumptions for N- and P-based fertilizer production of 45 and 29 MJ per kg N and kg P, respectively (*16*), the gross energy saved by application of electrodialysis with respect to recovered resources can be calculated as 81 and 4 Wh/pe/d.

Conventional and enhanced municipal wastewater treatment without decentralized urine pre-treatment. To provide comparisons of scenarios (I)-(VI) with equivalent end-of-pipe treatment strategies, energy needs were also determined for four hypothetical centralized wastewater treatment scenarios incorporating effluent ozonation (Table A.2 in the main text). Scenarios (A) and (B) were developed to evaluate energy needs for ozonating the effluent discharged from a typical municipal wastewater treatment facility utilizing conventional secondary activated sludge clarification, with the goal of lowering discharged micropollutant loads to levels achievable via upstream ozonation of source-separated urine without actually implementing urine source treatment, where absorbed O_3 doses of 2 and 5 mg/L were assumed for (A) >99% elimination of estrogenic activity derived from steroid hormones (*20*) and (B) 50% oxidation of total micropollutant loads (*20,21*), respectively. In scenarios (C) and (D), effluent ozonation (at absorbed O_3 doses of 2 and 5 mg/L, respectively) was assumed to be coupled with full nitrification/denitrification (using methanol as an external carbon source) and enhanced phosphorous removal, so as to evaluate the energy required for enhanced end-of-pipe wastewater treatment to produce effluent micropollutant *and* nutrient levels comparable to those achievable via upstream urine source separation and pre-treatment (as in scenarios (III)-(VI)). Taking into account a total effluent volume of 300 L/pe/d (*17*) and the energy requirements listed above for ozone generation, O_3-specific gross energy consumptions of 25 Wh/pe/d and 63 Wh/pe/d can be calculated for these two process options at 31% electricity generation efficiency. As above, these calculations include an implicit assumption of ~100% gas-liquid O_3 transfer efficiency, which is consistent with observations for flow-through bubble columns operated continuously at the pilot-scale (*20,21*).

Nitrogen elimination in conventional wastewater treatment plants can be divided into a fixed fraction (incorporation in sludge biomass) and a variable fraction (incidental denitrification). In conventional activated sludge plants practicing secondary clarification, these eliminations are about 1.5 g and 0.75 g/pe/d, respectively (Figure SA.11), taking into account that some incidental denitrification takes place in a typical activated sludge process

(*17*). Conventional biological P elimination removes a fixed amount of phosphorous - typically ~0.6 g P/pe/d (Figure SA.11) (*17*).

Therefore, in order to reach effluent N and P values comparable to those achievable with upstream urine source separation, conventional wastewater plants must be upgraded. For instance, conventional activated sludge treatment can be modified with minimal capital investment by incorporation of a dedicated, oxygen-depleted (i.e., non-aerated), pre-denitrification stage. Such a process can be assumed to yield ~100% nitrification of influent ammonia, at a gross energy cost of approximately 45 MJ/kg N, or 12.5 kWh/kg N (due primarily to energy consumed by aeration of the activated sludge), or 109 Wh/pe/d for nitrification of 8.73 g N/pe/d) (*16*). One can then estimate that, without addition of an external carbon source, approximately 60% of the NO_3^- resulting from nitrification (i.e., ~5.4 of 9 g/pe/d N) can be converted to N_2 via pre-denitrification. As discussed above, an additional ~1.5 g N/pe/d can be assumed to be removed via incorporation into biomass during the aerobic activated sludge clarification (Figure SA.11) (*16*). This leaves ~1.83 g N/pe/d to be removed by process augmentation in order to reach the target effluent N value of 0.27 g/pe/d. This can be achieved within existing physical constraints by implementing full denitrification with methanol addition, at a gross energy cost of ~109 MJ/kg N, or 30.3 kWh/kg N, translating to an additional gross per capita energy consumption of ~55 Wh/pe/d (*16*). Alternatively, full denitrification could be implemented without addition of a supplemental carbon source by upgrading physical facilities to raise solids retention times. However, this would necessitate considerably higher capital investment costs, which are outside the scope of the present operational cost comparison.

Increased phosphorous removal can be achieved in municipal wastewater treatment by precipitation with $FeSO_4$, which requires a gross energy input of ~49 MJ/kg P, or 13.6 kWh/kg P (*16*). As explained above, approximately 0.6 g P/pe/d are removed during conventional nitrification. Thus, an additional 0.712 g P/pe/d must be removed via $FeSO_4$ addition to achieve a target effluent value of 0.188 g P/pe/d, requiring a gross energy consumption of ~10 Wh/pe/d. Furthermore, the resulting precipitate is not suitable for recycling in agriculture (*22*). Consequently, no energetic credits can be derived from this product.

Table SA.1. Model compounds, with important properties and reported apparent second-order rate constants for reactions with O_3[a] (pH 8 and 9) and $^{\bullet}OH$[b], and expected sites of O_3 attack

Compound	Carbamazepine (CM)	*p*-Chlorobenzoic acid (*p*CBA)	Diclofenac (DC)
Structure	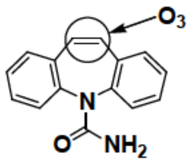	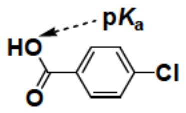	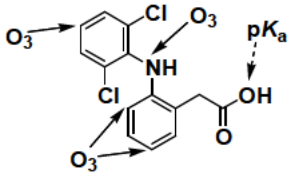
pK_a	NA	4.0 [c]	4.0 [d]
$D_{l,s}$, m^2/s	6.2×10^{-10} [f]	8.2×10^{-10} [f]	5.5×10^{-10} [f]
$k''_{O_3,app}$, M^{-1}s^{-1} (pH 8/9)	$\sim 3 \times 10^5 / \sim 3 \times 10^5$ [g]	$< 0.2 / < 0.2$ [h]	$\sim 1.0 \times 10^6 / \sim 1.0 \times 10^6$ [g]
$k''_{\bullet OH}$, M^{-1}s^{-1}	$8.8\ (\pm 1.2) \times 10^9$ [g]	$5.0\ (\pm 0.8) \times 10^9$ [i]	$7.5\ (\pm 1.5) \times 10^9$ [g]
Compound	17-α-Ethinylestradiol (EE2)	Ibuprofen (IP)	(±)-Propranolol (PP)
Structure	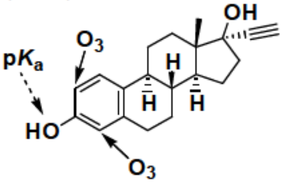	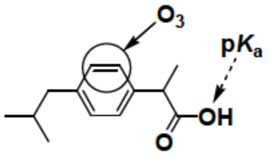	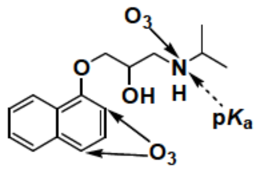
pK_a	10.4 [e]	4.5 [d]	9.5 [d]
$D_{l,s}$, m^2/s	5.0×10^{-10} [f]	5.9×10^{-10} [f]	5.3×10^{-10} [f]
$k''_{O_3,app}$, M^{-1}s^{-1} (pH 8/9)	$2.8 \times 10^7 / 2.7 \times 10^8$ [g,j*]	9.6/9.6 [g]	$\sim 1.1 \times 10^5 / \sim 2.2 \times 10^5$ [k]
$k''_{\bullet OH}$, M^{-1}s^{-1}	$9.8\ (\pm 1.2) \times 10^9$ [g]	$7.4\ (\pm 1.2) \times 10^9$ [g]	$\sim 1.0 \times 10^{10}$ [l]

[a] 20(±0.5) °C. [b] 25(±0.5) °C. [c-e] Values from [c](*23*), [d](*24*), or [e](*25*). [f] Values estimated according to (*26*), using molar volume contributions tabulated in (*27*). [g-j] Values taken from or calculated on the basis of data reported in [g](*28*) (*k_{O3} for anionic EE2 only), [h](*10*), [i](*11*), or [j] (*29*) (*k_{O3} for neutral EE2 only). [k] Calculated from the average of rate constants measured for reaction of O_3 with neutral atenolol, acetbutolol, and metoprolol (i.e., 5.9×10^5 M^{-1}s^{-1} (*30*)) as surrogates for neutral propranolol, in conjunction with the rate constant measured for cationic propranolol (i.e., $\sim 1 \times 10^5$ M^{-1}s^{-1} (*30*)). [l] Value from (*30*).

Table SA.2. Important mass transfer modeling parameters

Symbol(s)	**Dimensions**	**Parameter(s)**	**Value(s)**
$C_{O3(g)}$	g/m^3, mg/L	Gas-phase O_3 concentration	Time-dependent
$[O_3]_{l,x}$	mol/L, mol/m^3	Liquid-phase O_3 concentration at point, x, within the film	Time-dependent
$[O_3]_{l,eq}$	mol/L, mol/m^3	Liquid-phase O_3 equilibrium concentration	Variable
$[O_3]_{bulk}$	mol/L, mol/m^3	O_3 concentration in the bulk solution	0^a
[S]	mol/L	Liquid-phase micropollutant concentration	Time-dependent
H_{O3}, H_{O2}	-	Dimensionless O_3 and O_2 solubility ratios ($C_{liquid\ phase}/C_{gas\ phase}$)	Variable^b
$D_{l,O3}$	m^2/s	O_3 aqueous-phase diffusion coefficient	1.7×10^{-9} (*4*)
$D_{l,S}$	m^2/s	Micropollutant aqueous-phase diffusion coefficients	Table SA.1
$k'_{O_3,RMC}$	s^{-1}	Pseudo-first-order rate constant for O_3 consumption by RMCs	Time-dependent
$R_{ct(t)}$	-	Time-dependent ratio of $^{\bullet}$OH exposure to O_3 exposure	Table SA.3
δ	m	Film thickness	1.0×10^{-5}
$k_{L,O2}$	m/s	O_2 liquid mass transfer coefficient (in hydrolyzed urine)	1.9×10^{-4}
$k_{L,O3}$	m/s	O_3 liquid mass transfer coefficient (in hydrolyzed urine)	1.7×10^{-4}
A_s	m^2/m^3	Specific interfacial area relative to volume of the effective reactive zone (Figure SA.1)	436
$A_{s,f}$	m^2/m^3	Specific interfacial area relative to full reactor volume	24
Ha	-	Hatta number	Time-dependent
E	-	Enhancement factor for O_3 consumption by RMCs	Time-dependent
E_i	-	Enhancement factor for instantaneous O_3 consumption by RMCs	Variable^c
J_{O3}	mol/(m^2·s)	O_3 flux into film	Time-dependent
N_{O3}	mol/(L·s)	O_3 absorption into film	Time-dependent
$J_{S,\delta}$	mol/(m^2·s)	Micropollutant flux into film	Time-dependent
$N_{S,\delta}$	mol/(L·s)	Micropollutant absorption into film	Time-dependent
A_{xs}	m^2	Average cross-sectional area of effective reactive zone	4.3×10^{-4}
$A_{xs,f}$	m^2	Average cross-sectional area of full reactor	7.9×10^{-3}
h_l	m	Height of liquid volume in effective reactive zone	2.0×10^{-1}
$h_{l,f}$	m	Height of full liquid volume in reactor	2.2×10^{-1}
Q_g	m^3/s	Gas flow rate through reactor	8.3×10^{-6}
u	m/s	Superficial gas velocity through the effective reactive zone	1.9×10^{-2}
ε_g	-	Gas holdup fraction within the effective reactive zone	8.3×10^{-2}
$\varepsilon_{g,f}$	-	Gas holdup fraction distributed over full reactor volume	4.6×10^{-3}
d_{bubble}	m	Average gas bubble diameter (Sauter mean (*14*), in urine)	1.1×10^{-3}

^{a}Assumed to be negligible for ozone consumption in the fast pseudo-first-order kinetic regime (*4*), $^b H_{O3}$ = 0.23, 0.27, 0.17, 0.24 and H_{O2} = 0.027, 0.030, and 0.020 for hydrolyzed urine, ED diluate, and ED concentrate, respectively, corrected for ionic composition, according to (*31*), and using H_{O3} = 0.27 (*32*) and H_{O2} = 0.031 (*33*) as benchmark values for pure aqueous solution, $^c E_i$ values of 1.6×10^3, 1.2×10^3, and 5.6×10^3 were calculated for $C_{O3(g),in}$ = 60 mg/L in hydrolyzed urine, ED diluate, and ED concentrate, respectively, according to the equation $E_i = 1 + D_{l,RMC}[RMC]/ D_{l,O3}[O_3]_{l,eq}$, assuming that $D_{l,RMC} \sim 5 \times 10^{-9}$ m^2/s and that RMCs were constituted exclusively of DOC, where DOC concentrations (Table A.1 in the main text) were normalized to MW_{carbon} = 12 g/mol.

Table SA.3. Fitted parameters for exponential decay models of Ek$_L$A$_s$ and $R_{ct(t)}$ (vs. time, in s)

Matrix	$C_{O3(g),in}$ (mg/L)	Ek$_L$A$_s$			$R_{ct(t)}$	
		y_0	a	b[a]	y_0	a
Hydrolyzed Urine	15	0.45	11.8	0.0003	5.3×10^{-4}	1.11×10^{-2}
Hydrolyzed Urine	30	0.43	4.76	0.0005	4.82×10^{-4}	4.16×10^{-3}
Hydrolyzed Urine	60	0.47	3.75	0.0007	5.43×10^{-4}	3.45×10^{-3}
Hydrolyzed Urine	120	0.33	2.61	0.001	4.07×10^{-4}	2.24×10^{-3}
ED Diluate	60	0.21	0.86	0.0018	4.98×10^{-4}	1.14×10^{-3}
ED Concentrate	60	0.74	6.19	0.0012	5.54×10^{-4}	3.87×10^{-3}

[a] The same value of b is used in exponential fits of Ek$_L$A$_s$ and $R_{ct(t)}$ for the same urine matrix

Table SA.4. $^{\bullet}$OH scavenging by key matrix constituents

Matrix	HCO_3^-/CO_3^{2-}		NH_4^+/NH_3		DOC		Total
	$k'_{\mathrm{carbonate}}$ (s^{-1})[a]	$f_{\mathrm{carbonate}}$[a]	k'_{ammonia} (s^{-1})[a]	f_{ammonia}[a]	k'_{DOC} (s^{-1})[a]	f_{DOC}[a]	k'_{total} (s^{-1})[a]
Hydrolyzed urine	8.3×10^{6}	0.12	9.3×10^{6}	0.14	5.1×10^{7}	0.74	6.9×10^{7}
ED diluate	3.0×10^{5}	0.007	1.2×10^{5}	0.003	4.3×10^{7}	0.99	4.4×10^{7}
ED concentrate	2.6×10^{7}	0.14	3.2×10^{7}	0.17	1.3×10^{8}	0.69	1.9×10^{8}

[a] Estimates of the rates at which $^{\bullet}$OH was scavenged by major reactive matrix constituents were calculated from the concentrations of HCO_3^-, NH_3, PO_4^{3-}, and DOC and - after accounting for acid-base speciation at the appropriate pH - the corresponding elementary second-order rate constants for each of these reactions, where $k''_{\bullet OH,HCO_3^-} = 8.5 \times 10^{6}\ M^{-1}s^{-1}$ (*34*), $k''_{\bullet OH,CO_3^{2-}} = 3.9 \times 10^{8}\ M^{-1}s^{-1}$ (*35*), $k''_{\bullet OH,NH_3} = 9 \times 10^{7}\ M^{-1}s^{-1}$ (*36*), $k''_{\bullet OH,DOC} \sim 2.7 \times 10^{4}\ L{\cdot}mg^{-1}s^{-1}$ as estimated from the average of the values determined for three wastewater isolate fractions in (*37*).

Table SA.5. $CO_3^{\bullet-}$ scavenging by key matrix constituents

Matrix	NH_4^+/NH_3		DOC		Total
	k'_{ammonia} $(s^{-1})^a$	$f_{\mathrm{ammonia}}{}^a$	k'_{DOC} $(s^{-1})^a$	$f_{\mathrm{DOC}}{}^a$	k'_{total} $(s^{-1})^a$
Hydrolyzed urine	~1.0×10^4	~0.02	5.3×10^5	0.98	5.4×10^5
ED diluate	~1.4×10^2	<0.001	4.5×10^5	>0.999	4.5×10^5
ED concentrate	~3.6×10^4	~0.03	1.4×10^6	0.97	1.4×10^6

[a] Estimates of the rates at which $CO_3^{\bullet-}$ was scavenged by major reactive matrix constituents were calculated from the concentrations of HCO_3^-, NH_3, PO_4^{3-}, and DOC and - after accounting for acid-base speciation at the appropriate pH - the corresponding elementary second-order rate constants for each of these reactions, where the rate constant for reaction of $CO_3^{\bullet-}$ with NH_3 (which would most likely proceed via H-abstraction, as for •OH, SO_4^-, and PO_4^{2-}(*36*)) was assumed to be no greater than ~1×10^5 $M^{-1}s^{-1}$ on the basis of (a) the range in magnitudes of rate constants tabulated for H-abstraction reactions of $CO_3^{\bullet-}$ with various aliphatic compounds, and (b) the generally close agreement in the tabulated magnitudes of rate constants for H-abstraction of NH_3 by a given inorganic radical with the magnitudes of rate constants for H-abstractions of other aliphatic compounds by the same radical (*38*), whereas $k''_{CO_3^{\bullet-},DOC}$ ranges from 0.4-2.8 × 10^2 $L \cdot mg^{-1}s^{-1}$ as reported in (*39*) (a value of 2.8 × 10^2 $L \cdot mg^{-1}s^{-1}$ was assumed in the present calculations).

Table SA.6. ${}^{\bullet}NH_2$ scavenging by key matrix constituents

Matrix	HCO_3^-/CO_3^{2-}		DOC		O_2		Total
	$k'_{\mathrm{carbonate}}$ $(s^{-1})^a$	$f_{\mathrm{carbonate}}{}^a$	k'_{DOC} $(s^{-1})^a$	$f_{\mathrm{DOC}}{}^a$	k'_{O_2} $(s^{-1})^a$	$f_{O2}{}^a$	k'_{total} $(s^{-1})^a$
Hydrolyzed urine	1.5×10^3	0.002	~1.9×10^3	~0.002	8.8×10^5	0.996	8.8×10^5
ED diluate	1.5×10^2	<0.001	~1.6×10^3	~0.002	9.9×10^5	0.998	9.9×10^5
ED concentrate	4.7×10^3	0.007	~4.9×10^3	~0.007	6.5×10^5	0.986	6.6×10^5

[a] Estimates of the rates at which ${}^{\bullet}NH_2$ was scavenged by major reactive matrix constituents were calculated from the concentrations measured for HCO_3^- and DOC, the calculated values of $O_{2,l,(eq)}$ (8.7 × 10^{-4}, 9.8 × 10^{-4}, and 6.5 × 10^{-4} mol/L, in hydrolyzed urine, ED diluate, and ED concentrate, respectively, for $p_{O2,max}$ = 0.8 bar in the applied O_3 gas streams, using the H_{O2} values shown in Table SA.2), and - after accounting for acid-base speciation at the appropriate pH - the corresponding elementary second-order rate constants for each of these reactions, where $k''_{{}^{\bullet}NH_2,HCO_3^-} < 5.0 \times 10^3$ $M^{-1}s^{-1}$ (*40*), the rate constant for reaction of ${}^{\bullet}NH_2$ with CO_3^{2-} (via e^--transfer) is assumed to be neglible on the basis of estimated reduction potentials for the couples ${}^{\bullet}NH_2/NH_2^-$ (~0.6 V (*41*)) and $CO_3^{\bullet-}/CO_3^{2-}$ (~1.6 V (*42*)) and the reported non-reactivity of ${}^{\bullet}NH_2$ toward the thermodynamically more favorable (relative to CO_3^{2-}) single-electron reductant SO_3^{2-} (*41*), $k''_{{}^{\bullet}NH_2,O_2} = 1.0 \times 10^9$ $M^{-1}s^{-1}$ (*43*), and $k''_{{}^{\bullet}NH_2,DOC}$ ~ 1 $L \cdot mg^{-1}s^{-1}$ as estimated from the general observation that rate constants for reactions of ${}^{\bullet}NH_2$ with organic substrates are typically ~2 orders lower than those of $CO_3^{\bullet-}$ (*38*) - assuming a range of ~40-280 $mg \cdot L^{-1}s^{-1}$ for $k''_{CO_3^{\bullet-},DOC}$ (*39*).

Table SA.7. Estimated ratios of $[CO_3^{\bullet -}]_{ss}$ and $[^{\bullet}NH_2]_{ss}$ to $[^{\bullet}OH]_{ss}$ during ozonation of each urine matrix

Matrix	$[CO_3^{\bullet -}]_{ss}/[^{\bullet}OH]_{ss}$[a]	$[^{\bullet}NH_2]_{ss}/[^{\bullet}OH]_{ss}$[b]
Hydrolyzed urine	1.5×10^{1}	1.1×10^{1}
ED diluate	2.7×10^{-1}	1.2×10^{-1}
ED concentrate	1.9×10^{1}	4.9×10^{1}

[a] Calculated from eq S19, using the rate constant values provided in Tables SA.4 and SA.5. [b] Calculated from eq S20, using the rate constant values provided in Tables SA.4 and SA.6.

Table SA.8. Reactions included in Kintecus models of radical and reactive species yields during urine ozonation

Reactions		**Rate or equilibrium constants: ($M^{-2}s^{-1}$), ($M^{-1}s^{-1}$), (s^{-1}), or dimensionless**	**Refs. and notes**
Ozone, peroxide, and oxide radical reactions			
A1	$O_3 + DOC \rightarrow O_3^{\bullet -} + DOC^{\bullet(+)}$		*a*
A2	$O_3 + DOC \rightarrow O_2^{\bullet -} + DOC_{(oxidized)}$	$\sim 10^5$ in Hydr. Urine,	*a*
A3	$O_3 + DOC \rightarrow O_2(^1\Delta_g) + DOC_{(oxidized)}$	$\sim 10^3$ in ED Diluate	*a*
A4	$O_3 + DOC \rightarrow DOC_{(peroxide)}$		*a*
A5	$O_3 + O_2^{\bullet -} \rightarrow O_3^{\bullet -} + O_2$	1.5×10^9	(*44*)
A6f	$O_3^{\bullet -} \rightarrow O^{\bullet -} + O_2$	2.8×10^3	(*45*)
A6r	$O_2 + O^{\bullet -} \rightarrow O_3^{\bullet -}$	3.6×10^9	(*35*)
A7f	$O_3^{\bullet -} + H^+ \rightarrow HO_3^{\bullet}$	5.2×10^{10}	(*46*)
A7r	$HO_3^{\bullet} \rightarrow O_3^{\bullet -} + H^+$	3.7×10^4	(*46*)
A8	$HO_3^{\bullet} \rightarrow {}^{\bullet}OH + O_2$	1.1×10^5	(*46*)
A9	$DOC^{\bullet} + O_2 \rightarrow DOCOO^{\bullet}$	$\sim 2.5 \times 10^9$	*b*
A10	$DOCOO^{\bullet} \rightarrow DOC_{(oxidized)} + HO_2^{\bullet}$	~ 100	*c*
A11	$DOCOO^{\bullet} + OH^- \rightarrow DOC_{(oxidized)} + O_2^{\bullet -}$	$\sim 5 \times 10^9$	*c*
A12	$O_2^{\bullet -} + DOC_{(oxidized)} \rightarrow O_2 + DOC^{\bullet(-)}$	$\sim 10^5$	*d*
A13	$O_2^{\bullet -} + HO_2^{\bullet} \rightarrow HO_2^- + O_2$	9.6×10^7	(*47*)
A14	$O_3 + HO_2^- \rightarrow {}^{\bullet}OH + O_2 + O_2^{\bullet -}$	2.8×10^6	(*48*)
A15f	$O^{\bullet -} + H_2O \rightarrow {}^{\bullet}OH + OH^-$	1.7×10^6	(*49*)
A15r	${}^{\bullet}OH + OH^- \rightarrow O^{\bullet -} + H_2O$	1.2×10^{10}	(*49*)
Hydroxyl radical reactions			
B1	${}^{\bullet}OH + DOC \rightarrow DOC^{\bullet}$ (+ H_2O, for H-abstr.)	$\sim 3 \times 10^8$	(*37*), *e*
B2	${}^{\bullet}OH + HCO_3^- \rightarrow CO_3^{\bullet -} + H_2O$	8.5×10^6	(*35*)
B3	${}^{\bullet}OH + CO_3^{2-} \rightarrow CO_3^{\bullet -} + OH^-$	3.9×10^8	(*35*)
B4	${}^{\bullet}OH + NH_3 \rightarrow {}^{\bullet}NH_2 + H_2O$	9×10^7	(*36*)
B5	${}^{\bullet}OH + O_3 \rightarrow HO_2^{\bullet} + O_2$	1.1×10^8	(*50*)
B6	${}^{\bullet}OH + H_2O_2 \rightarrow O_2^{\bullet -} + H_2O + H^+$	2.7×10^7	(*51*)
B7	${}^{\bullet}OH + HO_2^- \rightarrow O_2^{\bullet -} + OH^- + H^+$	7.5×10^9	(*51*)
Carbonate radical reactions			
C1	$CO_3^{\bullet -} + DOC \rightarrow DOC^{\bullet(+)} + CO_3^{2-}$	$\sim 3 \times 10^6$	(*39*), *e*
C2	$CO_3^{\bullet -} + NH_3 \rightarrow {}^{\bullet}NH_2 + HCO_3^-$	$\sim 3 \times 10^4$	*f*
C3	$CO_3^{\bullet -} + H_2O_2 \rightarrow HO_2^{\bullet} + HCO_3^-$	8×10^5	(*52*)
C4	$CO_3^{\bullet -} + HO_2^- \rightarrow O_2^{\bullet -} + HCO_3^-$	5.6×10^7	(*52*)
Aminyl radical reactions			
D1	${}^{\bullet}NH_2 + DOC \rightarrow DOC^{\bullet} + NH_3$	$\sim 1.2 \times 10^3$	*g*
D2	${}^{\bullet}NH_2 + O_2 \rightarrow NH_2O_2^{\bullet}$	10^9	(*43*)
Nitrogen redox chains			
E1	$NH_2O_2^{\bullet} \rightarrow {}^{\bullet}NO + H_2O$	$\sim 7 \times 10^5$	(*43*), *h*
E2f	${}^{\bullet}NO + O_2^{\bullet -} \rightarrow ONOO^-$	6.7×10^9	(*53*)
E2r	$ONOO^- \rightarrow {}^{\bullet}NO + O_2^{\bullet -}$	2.0×10^{-2}	(*54*)
E3	$ONOO^- + CO_2 \rightarrow 0.33{}^{\bullet}NO_2 + 0.33CO_3^{\bullet -}$	2.9×10^4	(*54*, *55*)
E4	$ONOO^- \rightarrow NO_3^-$	$\sim 8 \times 10^{-6}$	(*54*)
E5f	$ONOO^- \rightarrow {}^{\bullet}NO_2 + O^{\bullet -}$	$\sim 10^{-6}$	(*54*)

E5r	$^{\bullet}NO_2 + O^{\bullet-} \rightarrow ONOO^-$	3.5×10^9	(*56*)
E6	$ONOO^- + O_3 \rightarrow (^{\bullet}NO_2 + O_2^{\bullet-} + O_2)?$	$\sim 5 \times 10^6$	*i*
E7	$ONOO^- + {}^{\bullet}OH \rightarrow {}^{\bullet}NO + O_2 + OH^-$	4.8×10^9	(*57*)
E8	$ONOO^- + CO_3^{\bullet-} \rightarrow {}^{\bullet}NO + O_2 + CO_3^{2-}$	3.7×10^6	(*57*)
E9f	$^{\bullet}NO_2 + {}^{\bullet}OH \rightarrow ONOOH$	4.5×10^9	(*56*)
E9r	$ONOOH \rightarrow {}^{\bullet}NO_2 + {}^{\bullet}OH$	3.5×10^{-1}	(*54*)
E10	$^{\bullet}NO + HO_2^{\bullet} \rightarrow ONOOH$	3.2×10^9	(*54*)
E11	$ONOOH \rightarrow NO_3^- + H^+$	9.0×10^{-1}	(*54*)
E12	$ONOOH + H^+ \rightarrow NO_3^- + 2H^+$	4.3	(*58*)
E13f	$ONOOH + H_2O + H^+ \rightarrow HNO_2 + H_2O_2 + H^+$	1.1×10^{-1}	(*58*)
E13r	$HNO_2 + H_2O_2 + H^+ \rightarrow ONOOH + H_2O + H^+$	9.6×10^3	(*58*)
E14f	$^{\bullet}NO_2 + O_2^{\bullet-} \rightarrow O_2NOO^-$	4.5×10^9	(*59*)
E14r	$O_2NOO^- \rightarrow {}^{\bullet}NO_2 + O_2^{\bullet-}$	1.0	(*60*)
E15	$O_2NOO^- \rightarrow NO_2^- + O_2$	1.4	(*60*)
E16f	$^{\bullet}NO_2 + HO_2^{\bullet} \rightarrow O_2NOOH$	1.8×10^9	(*59*)
E16r	$O_2NOOH \rightarrow {}^{\bullet}NO_2 + HO_2^{\bullet}$	2.6×10^{-2}	(*54*)
E17	$^{\bullet}NO_2 + DOC \rightarrow DOC^{\bullet(+)} + NO_2^-$	$\sim 3 \times 10^5$	*j*
E18	$^{\bullet}NO_2 + DOC^{\bullet} \rightarrow DOCNO_2$	$\sim 3 \times 10^9$	*k*
E19	$^{\bullet}NO + DOC^{\bullet} \rightarrow DOCNO$	$\sim 3 \times 10^9$	*l*
E20	$NO_2^- + O_3 \rightarrow NO_3^- + O_2$	$6.0 \text{ x} 10^5$	(*61*)
Ammonia acid-base equilibrium			
F1	$NH_4^+ \rightleftharpoons NH_3 + H^+$	5.0×10^{-10} (pK_a = 9.3)	(*62*)
Carbonate acid-base equilibria			
G1	$H_2O + CO_2 \rightleftharpoons HCO_3^- + H^+$	4.0×10^{-7} (pK_a = 6.4)	(*62*)
G2	$HCO_3^- \rightleftharpoons CO_3^{2-} + H^+$	5.0×10^{-11} (pK_a = 10.3)	(*62*)
Superoxide acid-base equilibrium			
H1	$HO_2^{\bullet} \rightleftharpoons O_2^{\bullet-} + H^+$	2.0×10^{-5} (pK_a = 4.7)	(*63*)
Hydrogen peroxide acid-base equilibrium			
I1	$H_2O_2 \rightleftharpoons HO_2^- + H^+$	2.5×10^{-12} (pK_a = 11.6)	(*62*)
Peroxynitrite acid-base equilibrium			
J1	$ONOOH \rightleftharpoons ONOO^- + H^+$	2.5×10^{-7} (pK_a = 6.6)	(*54*)
Peroxynitrate acid-base equilibrium			
K1	$O_2NOOH \rightleftharpoons O_2NOO^- + H^+$	1.3×10^{-6} (pK_a = 5.9)	(*54*)
Nitrite acid-base equilibrium			
L1	$HNO_2 \rightleftharpoons NO_2^- + H^+$	5.0×10^{-4} (pK_a = 3.3)	(*62*)

Initial conditions

Species	Concentrations (mol/L)^m	Notes
H_2O	55.6	
H^+	$10^{-9}/10^{-8}$	
O_2	$8.7 \times 10^{-4}/9.8 \times 10^{-4}$	
O_3	$2.9 \times 10^{-4}/3.3 \times 10^{-4}$	*n*
NH_3	$1.0 \times 10^{-1}/1.4 \times 10^{-3}$	
NH_4^+	$2.1 \times 10^{-1}/2.7 \times 10^{-2}$	
CO_3^{2-}	$1.5 \times 10^{-2}/1.5 \times 10^{-4}$	
HCO_3^-	$2.9 \times 10^{-1}/2.9 \times 10^{-2}$	
CO_2	$7.4 \times 10^{-4}/7.3 \times 10^{-4}$	*o*
DOC	$1.6 \times 10^{-1}/1.3 \times 10^{-1}$	*e*

[a] The total rate of O_3 consumption ($k_{A1} + k_{A2} + k_{A3} + k_{A4}$) was calculated from indirect determination of first-order rate of O_3 consumption by matrix constituents in hydrolyzed urine, using measured DOC concentrations, as described in the main text. The rate constant is normalized to MW_{carbon} = 12 g/mol. O_3 was assumed for the purposes of modeling to be consumed in roughly equal proportion by pathways A1-A4.

[b] Approximation based on range of tabulated values for reactions of $R^{\bullet}$ species with O_2, as listed within (*64*)

[c] Approximation based on range of tabulated values for decay of various $ROO^{\bullet}$ species, as listed within (*65*)

[d] Approximation based on range of tabulated rate constants for $O_2^{\bullet-}$ reactions with oxidized DOC constituents (e.g., carbonyls, carboxylic acids, various quinones), as listed within (*64*)

[e] Normalized to MW_{carbon} = 12 g/mol

[f] Estimated value, based on relative average magnitudes of tabulated rate constants for $^{\bullet}OH$ and $CO_3^{\bullet-}$ H-abstraction reactions, as listed within (*64*)

[g] Estimated value, based on relative average magnitudes of tabulated rate constants for $^{\bullet}OH$, $CO_3^{\bullet-}$-, and $^{\bullet}NH_2$ reactions with organic substrates, as listed within (*64*)

[h] Assuming approximately 1-mM dissolved O_2 concentration

[i] Rate constant estimated from fitting of N_3^-, NO_2^-, and peroxynitrite concentrations during continuous ozonation of N_3^- (*66*); corresponding mechanism proposed here on the basis of analogy with HO_2^--O_3 reaction

[j] Estimated value, based on relative average magnitudes of tabulated rate constants for $NO_2^{\bullet}$, $^{\bullet}OH$, $CO_3^{\bullet-}$, and $^{\bullet}NH_2$ reactions with organic substrates, as listed within (*64*)

[k] Rate constant - used here for exploratory purposes only - based on reported value for nitration of the tyrosyl radical ($TyrO^{\bullet}$) by $^{\bullet}NO_2$ (*67*)

[l] Rate constant - used here for exploratory purposes only - based on reported value for nitrosation of the 1-hydroxyethyl radical $^{\bullet}(CH_3CHOH)$ by $^{\bullet}NO$ (*68*)

[m] Concentration values given for $C_{O3(g),in}$ = 60 mg/L applied to hydrolyzed urine and electrodialysis diluate. In the case of two listed values, the first value corresponds to hydrolyzed urine, second to electrodialysis diluate. Single values indicate no difference between samples.

[n] Values of $[O_3]_{l,eq}$ calculated with the H_{O3} values listed in Table SA.2. Utilized only for analysis of radical concentrations during pulsed or continuous addition of O_3 (i.e., for batch or semi-batch modes, respectively), otherwise turned off during modeling

[o] CO_2 concentration assumed to be constrained by initial carbonate concentration - no input from or loss to gas bubbles containing O_2 and O_3

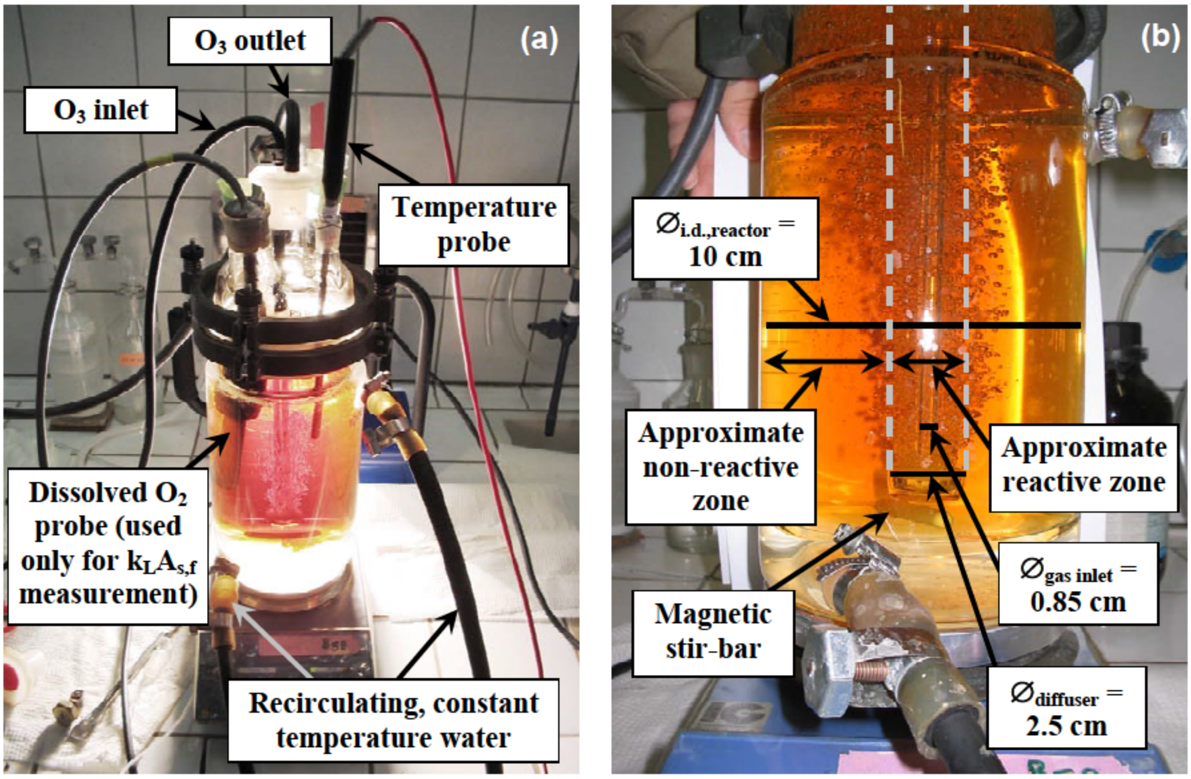
(a)
O3 outlet
O3 inlet
Temperature probe
Dissolved O2 probe (used only for kLAs,f measurement)
Recirculating, constant temperature water
(b)
Ø i.d.,reactor = 10 cm
Approximate non-reactive zone
Approximate reactive zone
Ø gas inlet = 0.85 cm
Magnetic stir-bar
Ø diffuser = 2.5 cm

Figure SA.1. Double-walled, thermal-jacketed, semi-batch reactor used in urine ozonation experiments. (a) Overview of reactor with O_3 inlet and outlet, sensors, and constant temperature water lines. (b) Important internal reactor dimensions.

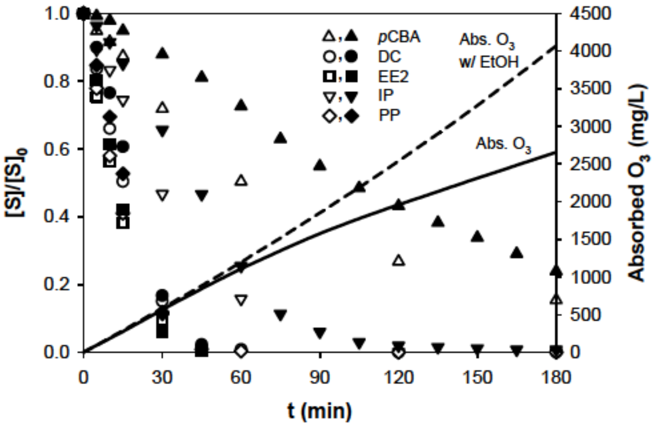

Figure SA.2. Observed depletion rates for each model compound during ozonation of hydrolyzed urine (hollow symbols) and hydrolyzed urine containing 4 g/L (86 mM) of ethanol (solid symbols), compared to measurements of cumulative absorbed O_3 doses at $C_{O3(g),in}$ = 60 mg/L (lines). Solutions were spiked with 1.0×10^{-5} M of each model compound, except *p*CBA, which was spiked at 5.0×10^{-5} M.

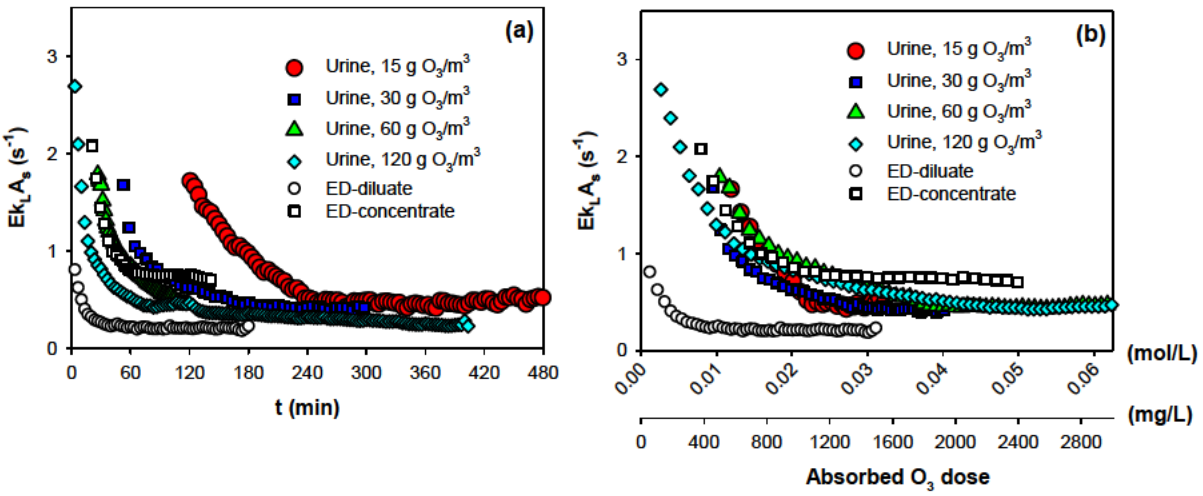

Figure SA.3. Variation in the apparent O$_3$ mass transfer coefficient, Ek$_L$A$_s$, with (a) time and (b) increasing cumulative O$_3$ absorption, during ozonation of hydrolyzed urine (at $C_{O3(g),in}$ = 15, 30, 60, and 120 mg/L) and pre-treated urine solutions (at $C_{O3(g),in}$ = 60 mg/L)

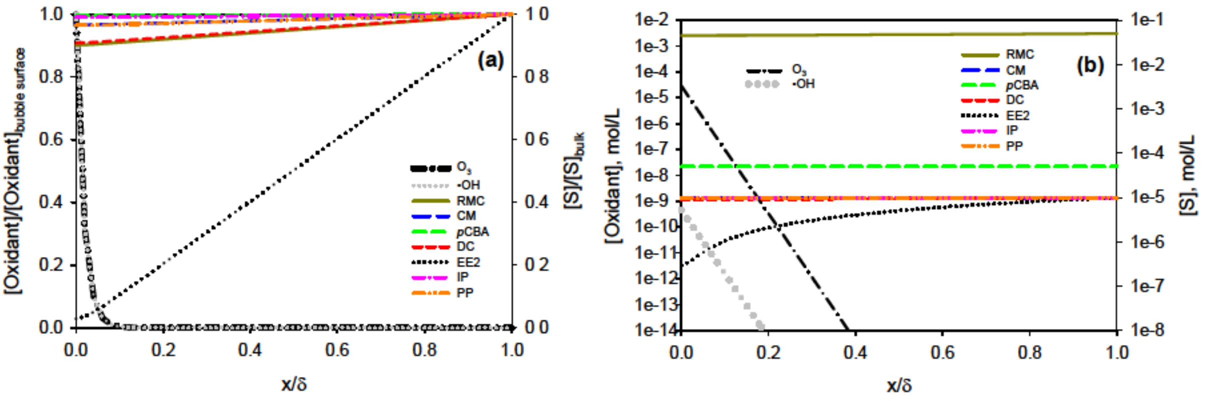

Figure SA.4. Representation of oxidant species and reactive substrate concentration gradients within conceptual film between gas bubble surface and bulk solution, during ozonation of hydrolyzed urine, at t = 0, $C_{O3(g),in}$ = 60 mg/L, and 25 °C. (a) Reactant concentrations (normalized to initial concentrations) on linear scale, (b) Reactant concentrations on log scale

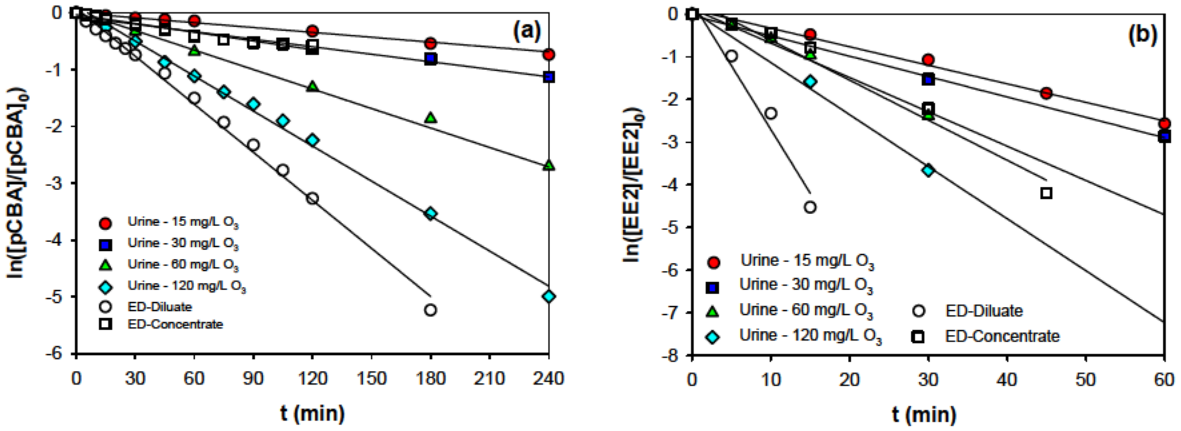

Figure SA.5. Observed depletion rates of (a) *p*CBA and (b) EE2 for various applied, gas-phase O_3 concentrations, during ozonation of unmodified, hydrolyzed urine and pre-treated, hydrolyzed urine products at 25 °C.

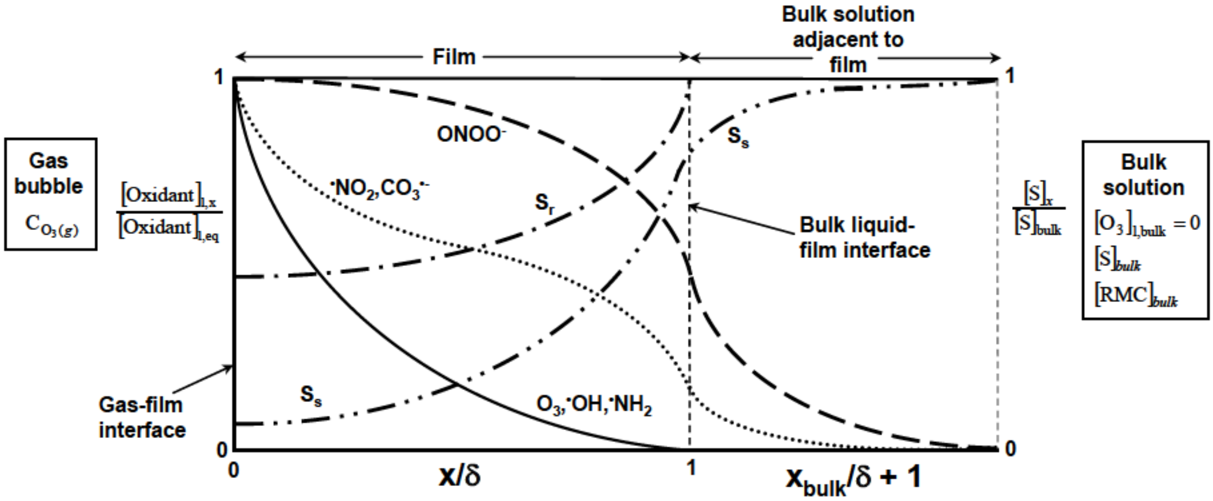
Film
Bulk solution adjacent to film
Gas bubble
$C_{O_3(g)}$
$\frac{[\text{Oxidant}]_{l,x}}{[\text{Oxidant}]_{l,eq}}$
1
0
ONOO$^-$
$^\bullet NO_2, CO_3^{\bullet-}$
S_r
S_s
$O_3, ^\bullet OH, ^\bullet NH_2$
S_s
Gas-film interface
Bulk liquid-film interface
$\frac{[S]_x}{[S]_{bulk}}$
1
0
Bulk solution
$[O_3]_{l,bulk} = 0$
$[S]_{bulk}$
$[RMC]_{bulk}$
0
x/δ
1
$x_{bulk}/\delta + 1$

Figure SA.6. Representation of the film for a fast pseudo-first-order kinetic regime with respect to O_3 consumption, accounting for secondary radical (i.e., $^\bullet NH_2$, $CO_3^{\bullet-}$, and $^\bullet NO_2$) formation and decay within the film and in the adjacent bulk solution, where S_r and S_s represent hypothetical model compounds that are recalcitrant and susceptible to reactions with secondary radicals, respectively.

Figure SA.7. Steady-state conditions at the gas-film interface during ozonation of hydrolyzed urine at $C_{O3(g)}$ = 60 mg/L

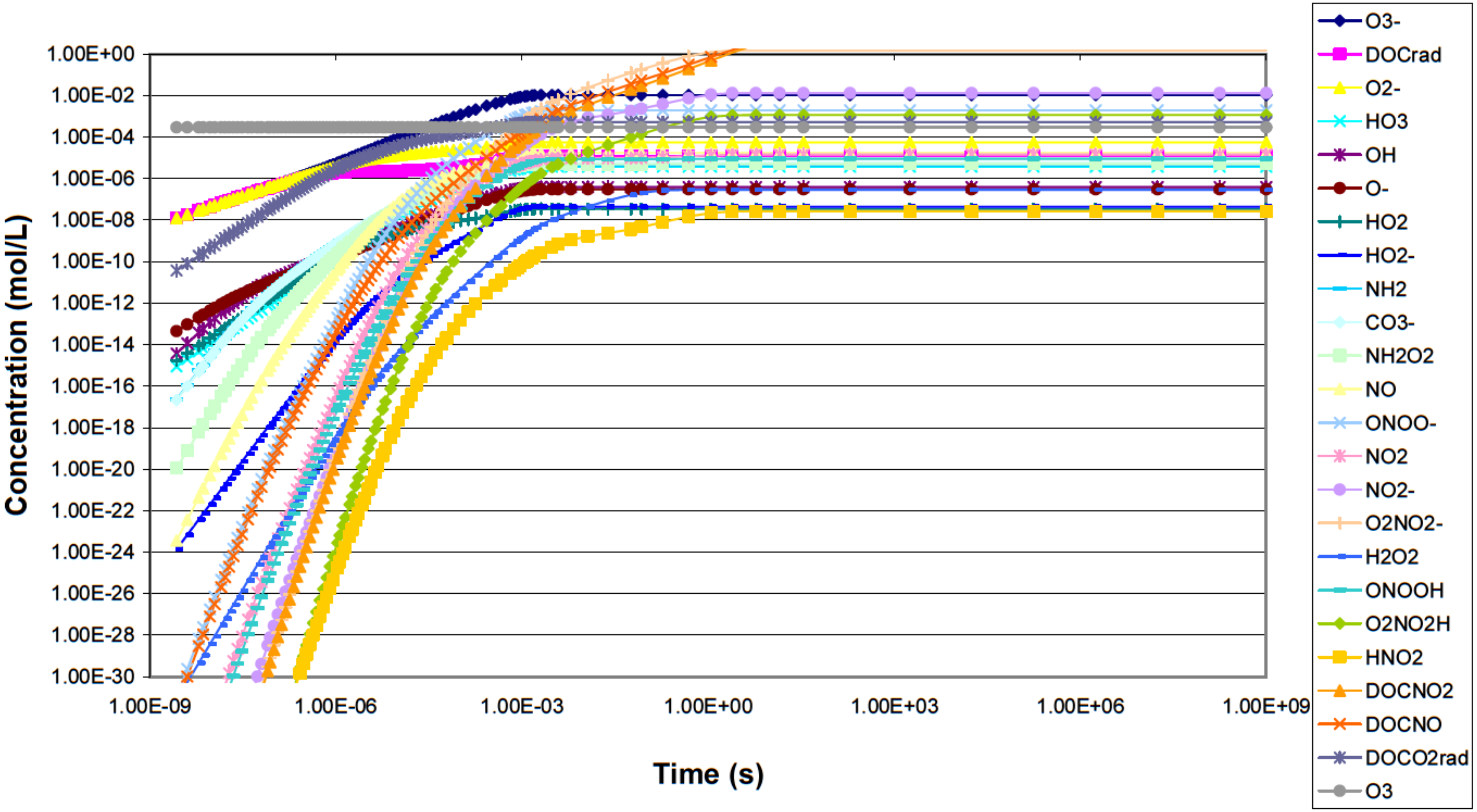

Figure SA.8. Temporal evolution of reactants in hydrolyzed urine in the absence of continuous ozone input (using the steady-state reactant concentrations from Figure SA.7 as initial conditions)

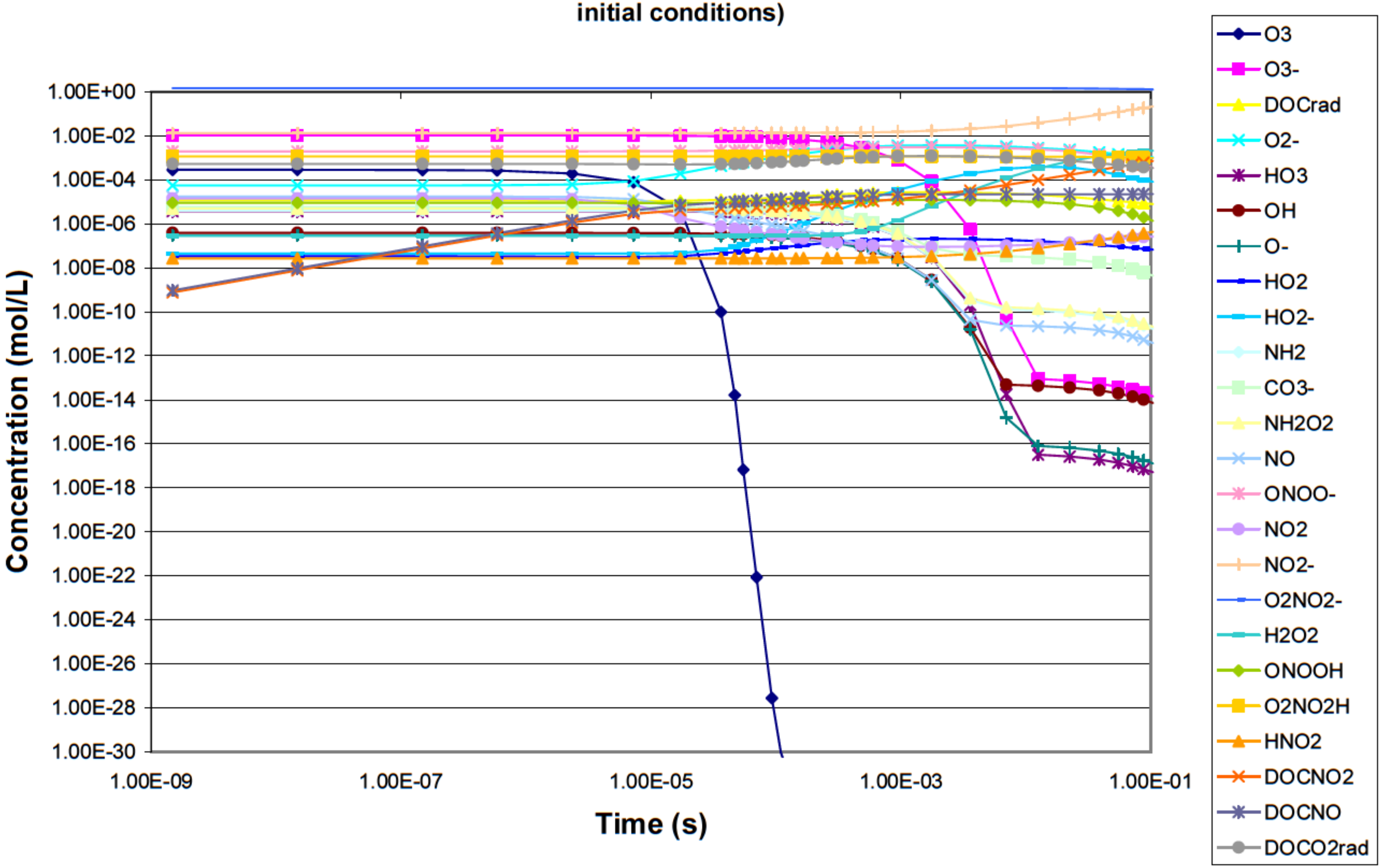

Figure SA.9. Steady-state conditions at the gas-film interface during ozonation of ED diluate at $C_{O3(g)}$ = 60 mg/L

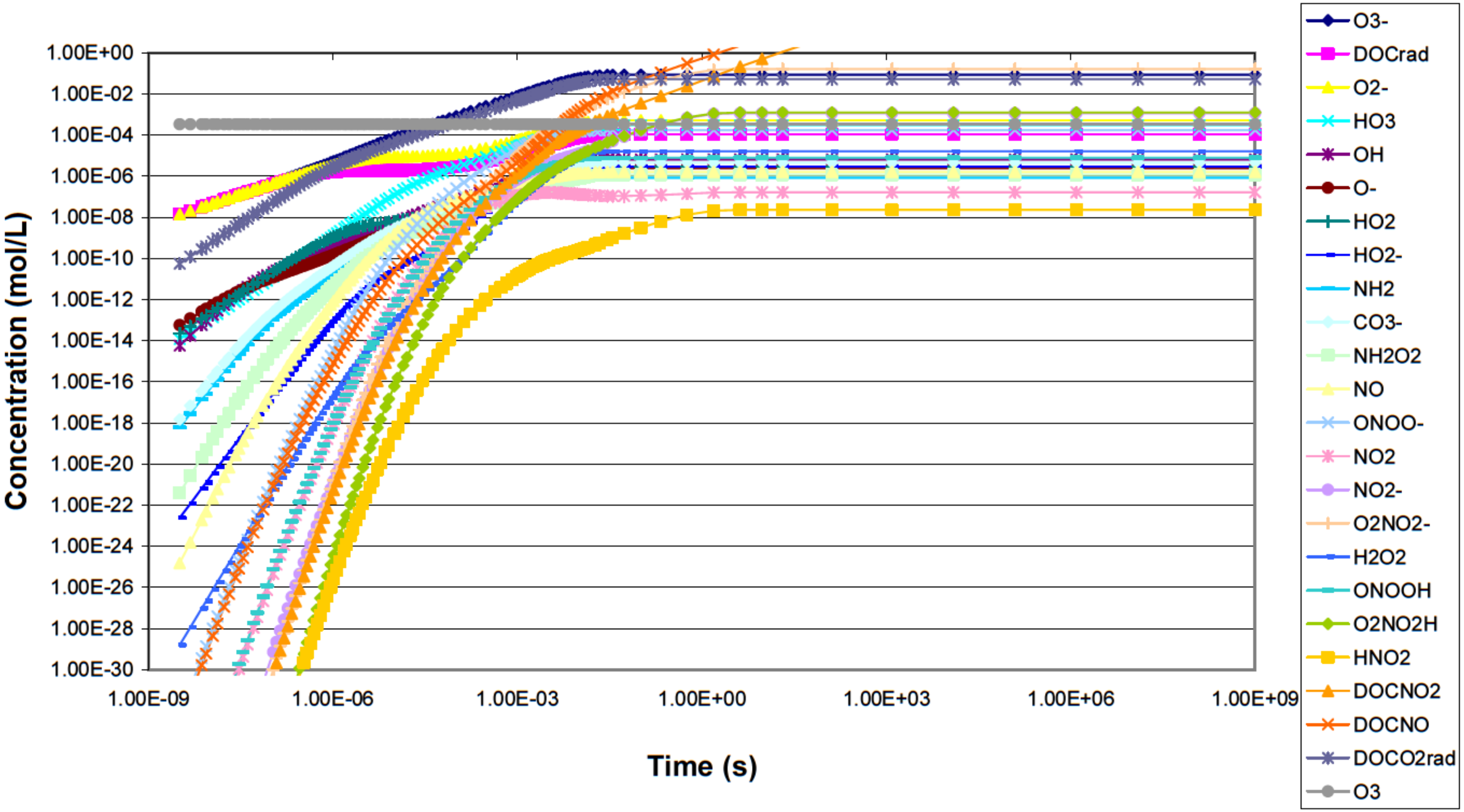

Figure SA.10. Temporal evolution of reactants in ED diluate in the absence of continuous ozone input (using the steady-state reactant concentrations from Figure SA.9 as initial conditions)

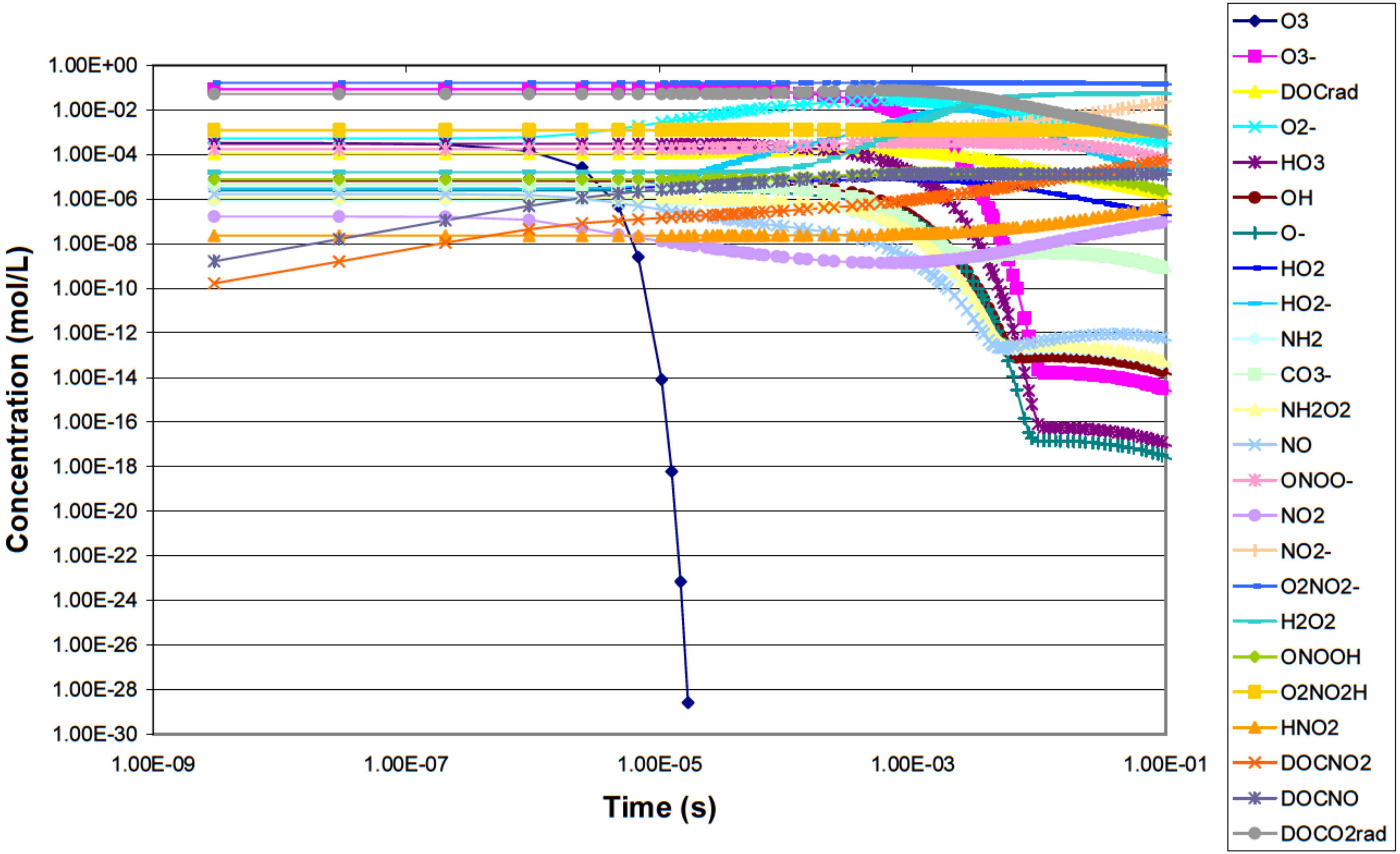

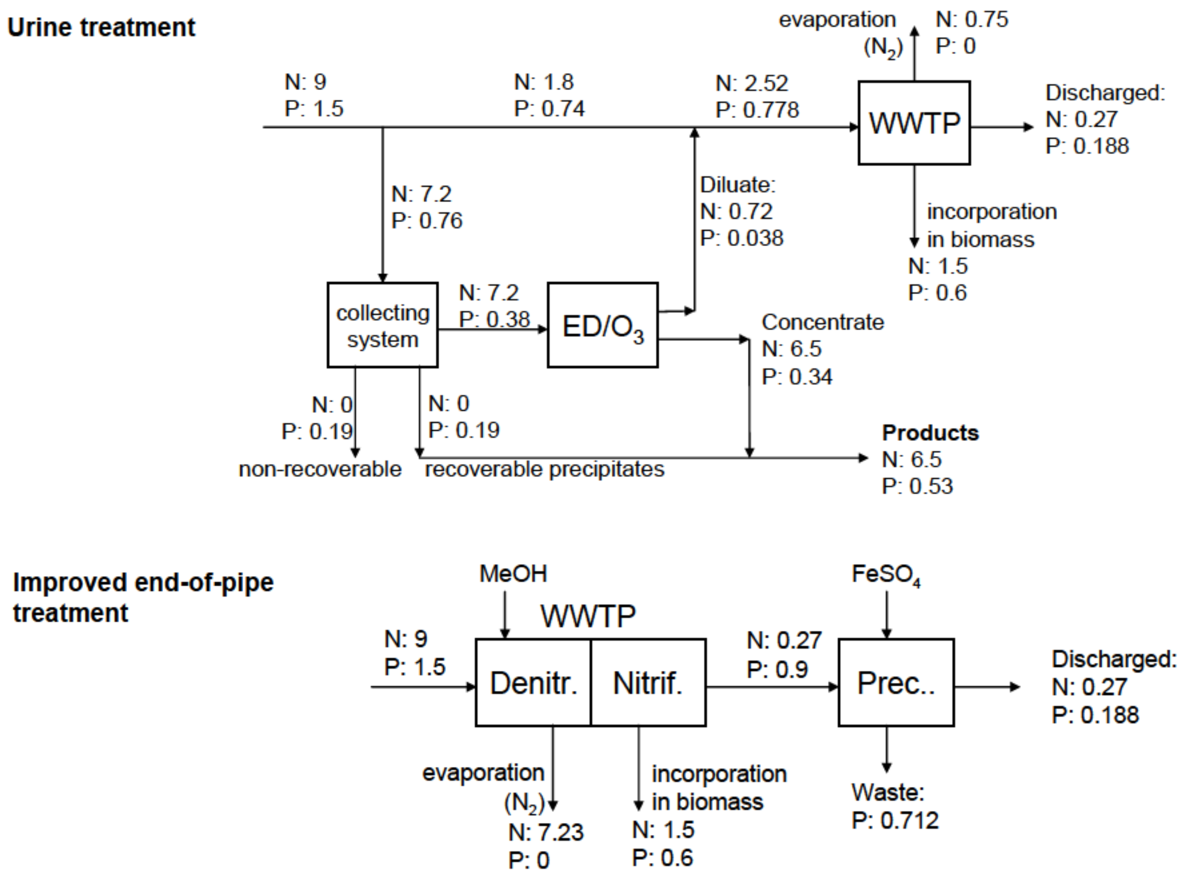
Urine treatment
evaporation
(N_2)
N: 0.75
P: 0
N: 9
P: 1.5
N: 1.8
P: 0.74
N: 2.52
P: 0.778
WWTP
Discharged:
N: 0.27
P: 0.188
N: 7.2
P: 0.76
Diluate:
N: 0.72
P: 0.038
incorporation
in biomass
N: 1.5
P: 0.6
collecting system
N: 7.2
P: 0.38
ED/O_3
Concentrate
N: 6.5
P: 0.34
N: 0
P: 0.19
N: 0
P: 0.19
Products
N: 6.5
P: 0.53
non-recoverable
recoverable precipitates
Improved end-of-pipe treatment
MeOH
WWTP
FeSO$_4$
N: 9
P: 1.5
Denitr.
Nitrif.
N: 0.27
P: 0.9
Prec..
Discharged:
N: 0.27
P: 0.188
evaporation
(N_2)
N: 7.23
P: 0
incorporation
in biomass
N: 1.5
P: 0.6
Waste:
P: 0.712

Figure SA.11. Schematic flow diagram and mass balances of N and P expressed as gram per person per day for a scenario including urine source-separation and pre-treatment (top) and enhanced end-of-pipe wastewater treatment leading to similar effluent values.

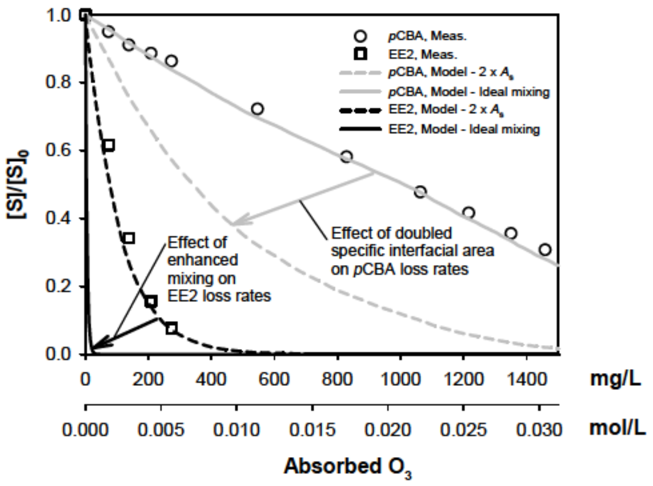

Figure SA.12. Effects of varying A_s and mixing efficiency on *p*CBA and EE2 oxidation efficiencies at $C_{O3(g),in}$ = 15 mg/L. Three scenarios are depicted: (1) the reference scenario, corresponding to the measured data shown in Figure A.1a (discrete points), (2) a model case in which A_s is doubled beyond that of scenario (1) (dashed lines), and (3) a model case in which mixing constraints prevailing in scenario (1) are neglected (solid lines). Model results were obtained using Scripts SA.2 and SA.3.

Script SA.1. “film_profiles_norm.m” used to obtain instantaneous profiles of reactant concentrations within and fluxes into and out of the gas-liquid interface separating ozone bubbles from bulk urine solutions, for the purpose of calibrating the full model (defined by Scripts SA2 and SA3) for •OH exposures determined by measurement of •OH-probe compound (*p*-chlorobenzoic acid) depletion during ozonation

```
% Function "film_profiles_norm" - models reactant concentrations within gas-liquid
% film region for O3 reactions in a semi-batch system (assuming steady-state O3 and
% reactant concentrations throughout the film at a given instant)with consumption of
% O3 by bulk reactive matrix constituents in the fast kinetic regime, and inclusion
% of •OH reactions. Produces a plot of concentration profiles in the film.

function film_profiles_norm

clear all

%  global variables.
global FilmThickness
global O3_Ieqavg
global C0_RMC
global ROHO3
global kO3_CM
global kO3_pCBA
global kO3_DC
global kO3_EE2
global kO3_IP
global kO3_PP
global kOH_CM
global kOH_pCBA
global kOH_DC
global kOH_EE2
global kOH_IP
global kOH_PP
global D_CM
global D_pCBA
global D_DC
global D_EE2
global D_IP
global D_PP
global As
global C0_CM
global C0_pCBA
global C0_DC
global C0_EE2
global C0_IP
global C0_PP
global kO3RMC
global D_O3
global D_RMC

% global variable definitions
HO3 = 0.23; %O3 solubility ratio in Urine (dimensionless)
%HO3 = 0.27; %O3 solubility ratio in Electrodialysis diluate (dimensionless)
%HO3 = 0.17; %O3 solubility ratio in Electrodialysis concentrate (dimensionless)
kO3_CM = 3.0e5; %Apparent, second-order rate constant for CM-O3 reaction, pH 9 (M^-1*s^-1)
kO3_pCBA = 0; %Apparent, second-order rate constant for pCBA-O3 reaction, pH 9 (M^-1*s^-1)
kO3_DC = 1.0e6; %Apparent, second-order rate constant for DC-O3 reaction, pH 9 (M^-1*s^-1)
%kO3_EE2 = 2.8e7; %Apparent, second-order rate constant for EE2-O3 reaction, pH 8 (M^-1*s^-1)
kO3_EE2 = 2.7e8; %Apparent, second-order rate constant for EE2-O3 reaction, pH 9 (M^-1*s^-1)
```

```
kO3_IP = 9.6; %Apparent, second-order rate constant for IP-O3 reaction, pH 9 (M^-1*s^-1)
%kO3_PP = 1.1e5; %Apparent, second-order rate constant for PP-O3 reaction, pH 8 (M^-1*s^-1)
kO3_PP = 2.2e5; %Apparent, second-order rate constant for PP-O3 reaction, pH 9 (M^-1*s^-1)
kOH_CM = 8.8e9; %Apparent, second-order rate constant for CM-•OH reaction, pH 9 (M^-1*s^-1)
kOH_pCBA = 5.0e9; %Apparent, second-order rate constant for pCBA-•OH reaction, pH 9 (M^-1*s^-1)
kOH_DC = 7.5e9; %Apparent, second-order rate constant for DC-•OH reaction, pH 9 (M^-1*s^-1)
kOH_EE2 = 9.8e9; %Apparent, second-order rate constant for EE2-•OH reaction, pH 9 (M^-1*s^-1)
kOH_IP = 7.4e9; %Apparent, second-order rate constant for IP-•OH reaction, pH 9 (M^-1*s^-1)
kOH_PP = 1.1e10; %Apparent, second-order rate constant for PP-•OH reaction, pH 9 (M^-1*s^-1)
D_CM = 6.2e-10; %Diffusion coefficient for CM in H2O (m^2/s)
D_pCBA = 8.2e-10; %Diffusion coefficient for pCBA in H2O (m^2/s)
D_DC = 5.5e-10; %Diffusion coefficient for DC in H2O (m^2/s)
D_EE2 = 5.0e-10; %Diffusion coefficient for EE2 in H2O (m^2/s)
D_IP = 5.9e-10; %Diffusion coefficient for IP in H2O (m^2/s)
D_PP = 5.3e-10; %Diffusion coefficient for PP in H2O (m^2/s)
D_O3 = 1.7e-9; %Diffusion coefficient for O3 in H2O (m^2/s)
D_RMC = 5e-10; %Diffusion coefficient for RMC in H2O (m^2/s)
on_mix = 0; %Switch for inclusion or exclusion of mixing constant, kmix, in model

% local variables
t = 0; %Reaction time (s)
CO3_gin = 15; %Inlet gas-phase O3 concentration (g/m^3)
O3_leq = (CO3_gin/1000/48)*HO3; %Equilibrium aqueous-phase O3 concentration at gas-film
interface (mol/L)
Q_gas = 30/3600/1000; %Inlet gas flow rate (m^3/s)
Axs = 4.3e-4; %Cross-sectional area of effective reactive zone (m^2)
hl = 20/100; %Liquid height in effective reactive zone (m)
GasHoldup = 8.3e-2; %Gas holdup relative to effective reactive zone (dimensionless)
hT = hl/(1-GasHoldup); %Total height (liquid and gas volumes) in effective reactive zone (m)
FilmThickness = 10e-6; %Film thickness (m)
As = 436; %Specific gas-liquid interfacial area relative to effective reactive zone (m^2/m^3)
C0_RMC = 5e-2; %Initial concentration of RMCs in aqueous phase (mol/L)
C0_CM = 1e-5; %Initial concentration of CM in aqueous phase (mol/L)
C0_pCBA = 5e-5; %Initial concentration of pCBA in aqueous phase (mol/L)
C0_DC = 1e-5; %Initial concentration of DC in aqueous phase (mol/L)
C0_EE2 = 1e-5; %Initial concentration of EE2 in aqueous phase (mol/L)
C0_IP = 1e-5; %Initial concentration of IP in aqueous phase (mol/L)
C0_PP = 1e-5; %Initial concentration of PP in aqueous phase (mol/L)

% first-order mixing constant (1/s)
kmix = 7.3e-4; %Hydrolyzed Urine, 15 mg/L O3 dose
%kmix = 8.0e-4; %Hydrolyzed Urine, 30 mg/L O3 dose
%kmix = 1.3e-3; %Hydrolyzed Urine, 60 mg/L O3 dose
%kmix = 2.0e-3; %Hydrolyzed Urine, 120 mg/L O3 dose
%kmix = 5.0e-3; %Electrodialysis diluate, 60 mg/L O3 dose
%kmix = 1.1e-3; %Electrodialysis concentrate, 60 mg/L O3 dose

% time-dependent functions of EkLAs (1/s)
EkLAs = (0.45+11.8*exp(-0.0003*t)); %Hydrolyzed Urine, 15 mg/L O3 dose
%EkLAs = (0.43+4.76*exp(-0.0005*t)); %Hydrolyzed Urine, 30 mg/L O3 dose
%EkLAs = (0.47+3.75*exp(-0.0007*t)); %Hydrolyzed Urine, 60 mg/L O3 dose
%EkLAs = (0.33+2.61*exp(-0.001*t)); %Hydrolyzed Urine, 120 mg/L O3 dose
%EkLAs = (0.21+0.86*exp(-0.0018*t)); %Electrodialysis diluate, 60 mg/L O3 dose
%EkLAs = (0.74+6.19*exp(-0.0012*t)); %Electrodialysis concentrate, 60 mg/L O3 dose

% average dissolved O3 concentration at the film side of the gas-film interface, over the full reactor
height, hT (mol/L)
O3_leqavg = ((O3_leq*(Q_gas/((1-GasHoldup)*Axs*EkLAs*HO3))*(1-exp((-(1-
GasHoldup)*Axs*EkLAs*HO3*hT)/Q_gas)))/hT);
```

```
% first-order rate constant for consumption of O3 by reactive wastewater constituents (RMC) (1/s)
kO3RMC = ((EkLAs/As)^2)/D_O3;

% time-dependent functions of R•OH/O3 (dimensionless)
ROHO3 = (0.53e-3+1.114e-2*exp(-0.0003*t))^2; %Hydrolyzed Urine, 15 mg/L O3 dose
%ROHO3 = (0.482e-3+4.155e-3*exp(-0.0005*t))^2; %Hydrolyzed Urine, 30 mg/L O3 dose
%ROHO3 = (0.543e-3+3.448e-3*exp(-0.0007*t))^2; %Hydrolyzed Urine, 60 mg/L O3 dose
%ROHO3 = (0.407e-3+2.238e-3*exp(-0.001*t))^2; %Hydrolyzed Urine, 120 mg/L O3 dose
%ROHO3 = (0.498e-3+1.14e-3*exp(-0.0018*t))^2; %Electrodialysis diluate, 60 mg/L O3 dose
%ROHO3 = (0.554e-3+3.865e-3*exp(-0.0012*t))^2; %Electrodialysis concentrate, 60 mg/L O3 dose

% helper functions "bvpinit" and "bvpset" prepare ODE BVP system for processing by function "bvp4c"
solinit = bvpinit(linspace(0,FilmThickness,50),@ex1init);
options = bvpset('Stats','on','RelTol',1e-4);

% function "bvp4c" - provides numerical solution of 2nd-order ODE BVP equation system
sol = bvp4c(@ex1ode,@ex1bc,solinit,options);

% solutions of the ODE BVP systemat at mesh points x and y
x = sol.x;
y = sol.y;

% chemical species concentrations at mesh points (mol/L)
O3 = sol.y(1,:)';
OH = O3*ROHO3;
RMC = sol.y(2,:)';
CM = sol.y(5,:)';
pCBA = sol.y(7,:)';
DC = sol.y(9,:)';
EE2 = sol.y(11,:)';
IP = sol.y(13,:)';
PP = sol.y(15,:)';

% concentration gradients at mesh points (mol/(L*m))
Deriv_O3 = sol.y(3,:)';
Deriv_RMC = sol.y(4,:)';
Deriv_CM = sol.y(6,:)';
Deriv_pCBA = sol.y(8,:)';
Deriv_DC = sol.y(10,:)';
Deriv_EE2 = sol.y(12,:)';
Deriv_IP = sol.y(14,:)';
Deriv_PP = sol.y(16,:)';

% x dimensions of concentration gradient arrays
dim_O3 = size(Deriv_O3)
dim_RMC = size(Deriv_RMC);
dim_CM = size(Deriv_CM);
dim_pCBA = size(Deriv_pCBA);
dim_DC = size(Deriv_DC);
dim_EE2 = size(Deriv_EE2);
dim_IP = size(Deriv_IP);
dim_PP = size(Deriv_PP);

% flux of O3 from the gas-phase into the film, and of aqueous-phase reactant species from the bulk
liquid into the film (mol/(m^2*s))
Flux_O3 = Deriv_O3(1,1)*1000*D_O3;
Flux_RMC = Deriv_RMC(dim_RMC(1,1),1)*1000*D_RMC;
Flux_CM = Deriv_CM(dim_CM(1,1),1)*1000*D_CM;
```

```
Flux_pCBA = Deriv_pCBA(dim_pCBA(1,1),1)*1000*D_pCBA
Flux_DC = Deriv_DC(dim_DC(1,1),1)*1000*D_DC;
Flux_EE2 = Deriv_EE2(dim_EE2(1,1),1)*1000*D_EE2
Flux_IP = Deriv_IP(dim_IP(1,1),1)*1000*D_IP;
Flux_PP = Deriv_PP(dim_PP(1,1),1)*1000*D_PP;

% depletion of reactant species from the bulk liquid (mol/(L*s))
Dep_RMC = -1/(1/(Flux_RMC*As/((1-GasHoldup)*1000))+on_mix/(kmix*C0_RMC));
Dep_CM = -1/(1/(Flux_CM*As/((1-GasHoldup)*1000))+on_mix/(kmix*C0_CM));
Dep_pCBA = -1/(1/(Flux_pCBA*As/((1-GasHoldup)*1000))+on_mix/(kmix*C0_pCBA));
Dep_DC = -1/(1/(Flux_DC*As/((1-GasHoldup)*1000))+on_mix/(kmix*C0_DC));
Dep_EE2 = -1/(1/(Flux_EE2*As/((1-GasHoldup)*1000))+on_mix/(kmix*C0_EE2));
Dep_IP = -1/(1/(Flux_IP*As/((1-GasHoldup)*1000))+on_mix/(kmix*C0_IP));
Dep_PP = -1/(1/(Flux_PP*As/((1-GasHoldup)*1000))+on_mix/(kmix*C0_PP));

% data for plot
x1 = x/FilmThickness;
y1(:,1) = O3/O3_leqavg;
y1(:,2) = OH/OH(1);
y2(:,1) = RMC/C0_RMC;
y2(:,2) = CM/C0_CM;
y2(:,3) = pCBA/C0_pCBA;
y2(:,4) = DC/C0_DC;
y2(:,5) = EE2/C0_EE2;
y2(:,6) = IP/C0_IP;
y2(:,7) = PP/C0_PP;

xy = [x1' y1 y2];
xlswrite('film_profiles_norm_out',xy)

% plot of reactant concentrations within the film vs. time
close all

[AX,H1,H2] = plotyy(x1,y1,x1,y2,'plot');

set(H1,'linewidth',2)
set(H2,'linewidth',2)
set(H2(1),'color',[0 1 0])
set(H2(5),'color',[1 0.7 0])
set(H2(6),'color',[0 1 1])
set(AX(1),'YLim', [0 1],'XLim', [0 1],'YTickMode', 'auto','YColor', [0 0 0],'FontSize',14)
set(AX(2),'YLim', [0 1],'XLim', [0 1],'YTickMode', 'auto','YColor', [0 0 0],'FontSize',14)
set(get(AX(1),'Ylabel'),'String','[Oxidant]/[Oxidant]_interface','FontSize',14)
set(get(AX(2),'Ylabel'),'String','C/C_bulk','FontSize',14)
set(get(AX(1),'Xlabel'),'String','x/\delta','FontSize',14)
leg1=legend(AX(1),'•OH','O_3',3);
leg2=legend(AX(2),'RMC','CM','pCBA','DC','EE2','IP','PP',4);
set(leg1,'FontSize',14)
set(leg2,'color',[1 1 1],'FontSize',14)

% -----------------------------------------------------------------------

% helper function - generates reactant concentration gradients at each mesh point for "bvp4c"
function dydx = ex1ode(x,y)

global kO3_CM
global kO3_pCBA
global kO3_DC
global kO3_EE2
global kO3_IP
global kO3_PP
global kOH_CM
global kOH_pCBA
global kOH_DC
global kOH_EE2
global kOH_IP
global kOH_PP
global D_CM
global D_pCBA
global D_DC
global D_EE2
global D_IP
global D_PP
global ROHO3
global kO3RMC
global D_O3
global D_RMC
global C0_RMC

dydx = [ y(3)
        y(4)
        1/D_O3*y(1)*kO3RMC
        1/D_RMC*y(1)*y(2)*(kO3RMC/C0_RMC(1,1))
        y(6)
        1/D_CM*y(5)*y(1)*(kO3_CM+kOH_CM*ROHO3)
        y(8)
        1/D_pCBA*y(7)*y(1)*(kO3_pCBA+kOH_pCBA*ROHO3)
        y(10)
        1/D_DC*y(9)*y(1)*(kO3_DC+kOH_DC*ROHO3)
        y(12)
        1/D_EE2*y(11)*y(1)*(kO3_EE2+kOH_EE2*ROHO3)
        y(14)
        1/D_IP*y(13)*y(1)*(kO3_IP+kOH_IP*ROHO3)
        y(16)
        1/D_PP*y(15)*y(1)*(kO3_PP+kOH_PP*ROHO3)];

%-----------------------------------------------------------------------

% helper function "ex1bc" - compiles boundary conditions for "bvp4c"
function res = ex1bc(ya,yb)

global O3_leqavg
global C0_RMC
global C0_CM
global C0_pCBA
global C0_DC
global C0_EE2
global C0_IP
global C0_PP

res = [ ya(1) - O3_leqavg
       ya(4)
       ya(6)
       ya(8)
       ya(10)
       ya(12)
       ya(14)
       ya(16)
```

```
        yb(1)
        yb(2) - C0_RMC
        yb(5) - C0_CM
        yb(7) - C0_pCBA
        yb(9) - C0_DC
        yb(11) - C0_EE2
        yb(13) - C0_IP
        yb(15) - C0_PP];

%--------------------------------------------------------------------------

% helper function "ex1init" - compiles guesses for initial concentration and concentration gradient
values for "bvp4c"
function v = ex1init(x)

global FilmThickness
global O3_leqavg
global C0_RMC
global C0_CM
global C0_pCBA
global C0_DC
global C0_EE2
global C0_IP
global C0_PP

v = [O3_leqavg-x*O3_leqavg/FilmThickness
     x*C0_RMC/FilmThickness
     -O3_leqavg/FilmThickness
     C0_RMC/FilmThickness
     x*C0_CM/FilmThickness
     C0_CM/FilmThickness
     x*C0_pCBA/FilmThickness
     C0_pCBA/FilmThickness
     x*C0_DC/FilmThickness
     C0_DC/FilmThickness
     x*C0_EE2/FilmThickness
     C0_EE2/FilmThickness
     x*C0_IP/FilmThickness
     C0_IP/FilmThickness
     x*C0_PP/FilmThickness
     C0_PP/FilmThickness];
```

Script SA.2. “film_profiles.m” used to obtain instantaneous profiles of model reactant concentrations within and fluxes into and out of the gas-liquid interface separating ozone bubbles from bulk urine solutions

```
% Helper function "film_profiles" - models reactant concentrations within
% gas-liquid film region for O3 reactions in a semi-batch system (assuming
% steady-state O3 and reactant concentrations throughout the film at a given
% instant) with consumption of O3 by bulk reactive matrix constituents in the fast
% kinetic regime, and inclusion of •OH reactions.

function film_profiles

% global variable definitions
global FilmThickness
global O3_leqavg
global ROHO3
global kO3_CM
global kO3_pCBA
global kO3_DC
global kO3_EE2
global kO3_IP
global kO3_PP
global kOH_CM
global kOH_pCBA
global kOH_DC
global kOH_EE2
global kOH_IP
global kOH_PP
global D_O3
global D_RMC
global D_CM
global D_pCBA
global D_DC
global D_EE2
global D_IP
global D_PP
global C_RMC
global C_CM
global C_pCBA
global C_DC
global C_EE2
global C_IP
global C_PP
global Dep_RMC
global Dep_CM
global Dep_pCBA
global Dep_DC
global Dep_EE2
global Dep_IP
global Dep_PP
global count
global O3
global RMC
global CM
global pCBA
global DC
global EE2
global IP
global PP
global kO3RMC
global Flux_O3
global Flux_CM
global Flux_pCBA
global Flux_DC
global Flux_EE2
global Flux_IP
global Flux_PP
global t
global xpoints

% global variables
HO3 = 0.23; %O3 solubility ratio in Urine (dimensionless)
%HO3 = 0.27; %O3 solubility ratio in Electrodialysis diluate (dimensionless)
%HO3 = 0.17; %O3 solubility ratio in Electrodialysis concentrate (dimensionless)
kO3_CM = 3.0e5; %Apparent, second-order rate constant for CM-O3 reaction, pH 9 (M^-1*s^-1)
kO3_pCBA = 0; %Apparent, second-order rate constant for pCBA-O3 reaction, pH 9 (M^-1*s^-1)
kO3_DC = 1.0e6; %Apparent, second-order rate constant for DC-O3 reaction, pH 9 (M^-1*s^-1)
%kO3_EE2 = 2.8e7; %Apparent, second-order rate constant for EE2-O3 reaction, pH 8 (M^-1*s^-1)
kO3_EE2 = 2.7e8; %Apparent, second-order rate constant for EE2-O3 reaction, pH 9 (M^-1*s^-1)
kO3_IP = 9.6; %Apparent, second-order rate constant for IP-O3 reaction, pH 9 (M^-1*s^-1)
%kO3_PP = 1.1e5; %Apparent, second-order rate constant for PP-O3 reaction, pH 8 (M^-1*s^-1)
kO3_PP = 2.2e5; %Apparent, second-order rate constant for PP-O3 reaction, pH 9 (M^-1*s^-1)
kOH_CM = 8.8e9; %Apparent, second-order rate constant for CM-•OH reaction, pH 9 (M^-1*s^-1)
kOH_pCBA = 5.0e9; %Apparent, second-order rate constant for pCBA-•OH reaction, pH 9 (M^-1*s^-1)
kOH_DC = 7.5e9; %Apparent, second-order rate constant for DC-•OH reaction, pH 9 (M^-1*s^-1)
kOH_EE2 = 9.8e9; %Apparent, second-order rate constant for EE2-•OH reaction, pH 9 (M^-1*s^-1)
kOH_IP = 7.4e9; %Apparent, second-order rate constant for IP-•OH reaction, pH 9 (M^-1*s^-1)
kOH_PP = 1.1e10; %Apparent, second-order rate constant for PP-•OH reaction, pH 9 (M^-1*s^-1)
D_CM = 6.2e-10; %Diffusion coefficient for CM in H2O (m^2/s)
D_pCBA = 8.2e-10; %Diffusion coefficient for pCBA in H2O (m^2/s)
D_DC = 5.5e-10; %Diffusion coefficient for DC in H2O (m^2/s)
D_EE2 = 5.0e-10; %Diffusion coefficient for EE2 in H2O (m^2/s)
D_IP = 5.9e-10; %Diffusion coefficient for IP in H2O (m^2/s)
D_PP = 5.3e-10; %Diffusion coefficient for PP in H2O (m^2/s)
D_O3 = 1.7e-9; %Diffusion coefficient for O3 in H2O (m^2/s)
D_RMC = 5e-10; %Diffusion coefficient for RMC in H2O (m^2/s)
on_mix = 1; %Switch for inclusion or exclusion of mixing constant, kmix, in model

% local variables
CO3_gin = 15; %Inlet gas-phase O3 concentration (g/m^3)
O3_leq = (CO3_gin/1000/48)*HO3; %Equilibrium aqueous-phase O3 concentration at gas-film interface (mol/L)
Q_gas = 30/3600/1000; %Inlet gas flow rate (m^3/s)
Axs = 4.3e-4; %Cross-sectional area of effective reactive zone (m^2)
hl = 20/100; %Liquid height in effective reactive zone (m)
GasHoldup = 8.3e-2; %Gas holdup relative to effective reactive zone (dimensionless)
hT = hl/(1-GasHoldup); %Total height (liquid and gas volumes) in effective reactive zone (m)
FilmThickness = 10e-6; %Film thickness (m)
As = 436; %Specific gas-liquid interfacial area relative to effective reactive zone (m^2/m^3)

% first-order mixing constant (1/s)
kmix = 7.3e-4; %Hydrolyzed Urine, 15 mg/L O3 dose
%kmix = 8.0e-4; %Hydrolyzed Urine, 30 mg/L O3 dose
%kmix = 1.3e-3; %Hydrolyzed Urine, 60 mg/L O3 dose
%kmix = 2.0e-3; %Hydrolyzed Urine, 120 mg/L O3 dose
%kmix = 5.0e-3; %Electrodialysis permeate, 60 mg/L O3 dose
%kmix = 1.1e-3; %Electrodialysis concentrate, 60 mg/L O3 dose

% time-dependent functions of EkLAs (1/s)
EkLAs = (0.45+11.8*exp(-0.0003*t(1,count))); %Hydrolyzed Urine, 15 mg/L O3 dose
```

```
%EkLAs = (0.43+4.76*exp(-0.0005*t(1,count))); %Hydrolyzed Urine, 30 mg/L O3 dose
%EkLAs = (0.47+3.75*exp(-0.0007*t(1,count))); %Hydrolyzed Urine, 60 mg/L O3 dose
%EkLAs = (0.33+2.61*exp(-0.001*t(1,count))); %Hydrolyzed Urine, 120 mg/L O3 dose
%EkLAs = (0.21+0.86*exp(-0.0018*t(1,count))); %Electrodialysis permeate, 60 mg/L O3 dose
%EkLAs = (0.74+6.19*exp(-0.0012*t(1,count))); %Electrodialysis concentrate, 60 mg/L O3 dose

% average dissolved O3 concentration at the film side of the gas-film interface, over the full reactor
height, hT (mol/L)
O3_leqavg = ((O3_leq*(Q_gas/((1-GasHoldup)*Axs*EkLAs*HO3))*(1-exp((-(1-
GasHoldup)*Axs*EkLAs*HO3*hT)/Q_gas)))/hT);

% first-order rate constant for consumption of O3 by reactive wastewater constituents (RMC) (1/s)
kO3RMC = ((EkLAs/As)^2)/D_O3

% time-dependent functions of R•OH/O3 (dimensionless)
ROHO3 = (0.53e-3+1.114e-2*exp(-0.0003*t(1,count)))^2; %Hydrolyzed Urine, 15 mg/L O3 dose
%ROHO3 = (0.482e-3+4.155e-3*exp(-0.0005*t(1,count)))^2; %Hydrolyzed Urine, 30 mg/L O3 dose
%ROHO3 = (0.543e-3+3.448e-3*exp(-0.0007*t(1,count)))^2; %Hydrolyzed Urine, 60 mg/L O3 dose
%ROHO3 = (0.407e-3+2.238e-3*exp(-0.001*t(1,count)))^2; %Hydrolyzed Urine, 120 mg/L O3 dose
%ROHO3 = (0.498e-3+1.14e-3*exp(-0.0018*t(1,count)))^2; %Electrodialysis permeate, 60 mg/L O3
dose
%ROHO3 = (0.554e-3+3.865e-3*exp(-0.0012*t(1,count)))^2; %Electrodialysis concentrate, 60 mg/L
O3 dose

% desired number of meshpoints on which the ODE BVP system is to be solved
meshpoints=50;

% helper functions "bvpinit" and "bvpset" prepare ODE BVP system for processing by function "bvp4c"
solinit = bvpinit(linspace(0,FilmThickness,meshpoints),@ex1init);
options = bvpset('Stats','on','RelTol',1e-4);

% function "bvp4c" - provides numerical solution of 2nd-order ODE BVP equation system
sol = bvp4c(@ex1ode,@ex1bc,solinit,options);

% solutions of the ODE BVP systemat at mesh points x and y
x = sol.x;
y = sol.y;

% creation of null matrix to receive data generated by ODE BVP system solution functions
dim = size(sol.y);
rows(1,count) = dim(1,2);
zerorows(1,count) = 4*meshpoints-rows(1,count);
zerospace = zeros(zerorows(1,count),1);
xspacing = FilmThickness/rows(1,count);

% chemical species concentrations at mesh points (mol/L)
O3 = cat(1,sol.y(1,:)',zerospace);
RMC = cat(1,sol.y(2,:)',zerospace);
CM = cat(1,sol.y(5,:)',zerospace);
pCBA = cat(1,sol.y(7,:)',zerospace);
DC = cat(1,sol.y(9,:)',zerospace);
EE2 = cat(1,sol.y(11,:)',zerospace);
IP = cat(1,sol.y(13,:)',zerospace);
PP = cat(1,sol.y(15,:)',zerospace);

% array containing the horizontal coordinates of mesh points within the film
xpoints = cat(1,xspacing.*linspace(0,FilmThickness,rows(1,count))',zerospace);
```

```
% concentration gradients at mesh points (mol/(L*m))
Deriv_O3 = sol.y(3,:)';
Deriv_RMC = sol.y(4,:)';
Deriv_CM = sol.y(6,:)';
Deriv_pCBA = sol.y(8,:)';
Deriv_DC = sol.y(10,:)';
Deriv_EE2 = sol.y(12,:)';
Deriv_IP = sol.y(14,:)';
Deriv_PP = sol.y(16,:)';

% flux of O3 from the gas-phase into the film, and of aqueous-phase reactant species from the bulk
liquid into the film (mol/(m^2*s))
Flux_O3(1,count) = Deriv_O3(1,1)*1000*D_O3;
Flux_RMC(1,count) = Deriv_RMC(dim(1,2),1)*1000*D_RMC;
Flux_CM(1,count) = Deriv_CM(dim(1,2),1)*1000*D_CM;
Flux_pCBA(1,count) = Deriv_pCBA(dim(1,2),1)*1000*D_pCBA;
Flux_DC(1,count) = Deriv_DC(dim(1,2),1)*1000*D_DC;
Flux_EE2(1,count) = Deriv_EE2(dim(1,2),1)*1000*D_EE2;
Flux_IP(1,count) = Deriv_IP(dim(1,2),1)*1000*D_IP;
Flux_PP(1,count) = Deriv_PP(dim(1,2),1)*1000*D_PP;

% depletion of reactant species from the bulk liquid (mol/(L*s))
Dep_RMC(1,count) = -1/(1/(Flux_RMC(1,count)*As/((1-
GasHoldup)*1000))+on_mix/(kmix*C_RMC(1,count)));
Dep_CM(1,count) = -1/(1/(Flux_CM(1,count)*As/((1-
GasHoldup)*1000))+on_mix/(kmix*C_CM(1,count)));
Dep_pCBA(1,count) = -1/(1/(Flux_pCBA(1,count)*As/((1-
GasHoldup)*1000))+on_mix/(kmix*C_pCBA(1,count)));
Dep_DC(1,count) = -1/(1/(Flux_DC(1,count)*As/((1-
GasHoldup)*1000))+on_mix/(kmix*C_DC(1,count)));
Dep_EE2(1,count) = -1/(1/(Flux_EE2(1,count)*As/((1-
GasHoldup)*1000))+on_mix/(kmix*C_EE2(1,count)));
Dep_IP(1,count) = -1/(1/(Flux_IP(1,count)*As/((1-GasHoldup)*1000))+on_mix/(kmix*C_IP(1,count)));
Dep_PP(1,count) = -1/(1/(Flux_PP(1,count)*As/((1-GasHoldup)*1000))+on_mix/(kmix*C_PP(1,count)));

% -----------------------------------------------------------------------

% helper function "ex1ode" - generates reactant concentration gradients at each mesh point
function dydx = ex1ode(x,y)

global kO3_CM
global kO3_pCBA
global kO3_DC
global kO3_EE2
global kO3_IP
global kO3_PP
global kOH_CM
global kOH_pCBA
global kOH_DC
global kOH_EE2
global kOH_IP
global kOH_PP
global D_O3
global D_RMC
global D_CM
global D_pCBA
global D_DC
global D_EE2
global D_IP
global D_PP
global ROHO3
global kO3RMC
global C_RMC
global on_prim

dydx = [ y(3)
         y(4)
         1/D_O3*y(1)*kO3RMC
         1/D_RMC*y(1)*y(2)*(kO3RMC/C_RMC(1,1))
         y(6)
         1/D_CM*y(5)*y(1)*(kO3_CM+kOH_CM*ROHO3)
         y(8)
         1/D_pCBA*y(7)*y(1)*(kO3_pCBA+kOH_pCBA*ROHO3)
         y(10)
         1/D_DC*y(9)*y(1)*(kO3_DC+kOH_DC*ROHO3)
         y(12)
         1/D_EE2*y(11)*y(1)*(kO3_EE2+kOH_EE2*ROHO3)
         y(14)
         1/D_IP*y(13)*y(1)*(kO3_IP+kOH_IP*ROHO3)
         y(16)
         1/D_PP*y(15)*y(1)*(kO3_PP+kOH_PP*ROHO3)];

%-------------------------------------------------------------------------

% helper function "ex1bc" - compiles boundary conditions
function res = ex1bc(ya,yb)

global O3_leqavg
global C_RMC
global C_CM
global C_pCBA
global C_DC
global C_EE2
global C_IP
global C_PP
global count

res = [ ya(1) - O3_leqavg
        ya(4)
        ya(6)
        ya(8)
        ya(10)
        ya(12)
        ya(14)
        ya(16)
        yb(1)
        yb(2) - C_RMC(1,count)
        yb(5) - C_CM(1,count)
        yb(7) - C_pCBA(1,count)
        yb(9) - C_DC(1,count)
        yb(11) - C_EE2(1,count)
        yb(13) - C_IP(1,count)
        yb(15) - C_PP(1,count)];

%-------------------------------------------------------------------------

% helper function "ex1init" - compiles guesses for initial concentration and concentration gradient values
```

```
function v = ex1init(x)

global FilmThickness
global O3_leqavg
global C_RMC
global C_CM
global C_pCBA
global C_DC
global C_EE2
global C_IP
global C_PP
global count

v = [O3_leqavg-x*O3_leqavg/FilmThickness
    x*C_RMC(1,count)/FilmThickness
    -O3_leqavg/FilmThickness
    C_RMC(1,count)/FilmThickness
    x*C_CM(1,count)/FilmThickness
    C_CM(1,count)/FilmThickness
    x*C_pCBA(1,count)/FilmThickness
    C_pCBA(1,count)/FilmThickness
    x*C_DC(1,count)/FilmThickness
    C_DC(1,count)/FilmThickness
    x*C_EE2(1,count)/FilmThickness
    C_EE2(1,count)/FilmThickness
    x*C_IP(1,count)/FilmThickness
    C_IP(1,count)/FilmThickness
    x*C_PP(1,count)/FilmThickness
    C_PP(1,count)/FilmThickness];
```

Script SA.3. "bulk_profiles.m" used for implementing iterations of "film_profiles.m" to model changes in model reactant concentrations within bulk urine solutions during ozonation

```
% Function "bulk_profiles" - models depletion of pharmaceuticals from bulk liquid
% in a semi-batch system according to film theory (assuming steady-state O3 and
% reactant concentrations throughout the film at a given instant) with consumption
% of O3 by bulk reactive matrix constituents in the fast pseudo-first-order kinetic regime,
% and inclusion of •OH reactions. Models time-evolution of reactant concentrations in the
% bulk liquid, by looping the instantaneous solutions of reactant depletion rates at the
% film-bulk liquid interface - generated by the "film_profiles" helper function - over
% differential changes in time.

clear all

%  global variable definitions
global C_O3
global C_RMC
global C_CM
global C_pCBA
global C_DC
global C_EE2
global C_IP
global C_PP
global O3_leqavg
global Dep_RMC
global Dep_CM
global Dep_pCBA
global Dep_DC
global Dep_EE2
global Dep_IP
global Dep_PP
global Depf_RMC
global Depf_CM
global Depf_pCBA
global Depf_DC
global Depf_EE2
global Depf_IP
global Depf_PP
global Depk_RMC
global Depk_CM
global Depk_pCBA
global Depk_DC
global Depk_EE2
global Depk_IP
global Depk_PP
global dt
global count
global O3
global RMC
global CM
global pCBA
global DC
global EE2
global IP
global PP
global Flux_O3
global Flux_CM
global Flux_pCBA
global Flux_DC
global Flux_EE2
global Flux_IP
global Flux_PP
global t
global xpoints

% local variables
C_RMC(1,1) = 5e-2; %Initial concentration of RMCs in aqueous phase (mol/L)
C_CM(1,1) = 1e-5; %Initial concentration of CM in aqueous phase (mol/L)
C_pCBA(1,1) = 5e-5; %Initial concentration of pCBA in aqueous phase (mol/L)
C_DC(1,1) = 1e-5; %Initial concentration of DC in aqueous phase (mol/L)
C_EE2(1,1) = 1e-5; %Initial concentration of EE2 in aqueous phase (mol/L)
C_IP(1,1) = 1e-5; %Initial concentration of IP in aqueous phase (mol/L)
C_PP(1,1) = 1e-5; %Initial concentration of PP in aqueous phase (mol/L)
dt = 50; %differential time interval (s)
count = 1; %initial value for counter
t(1,1) = 0; %initial time for time matrix



% loop to perform numerical integration of reactant concentration profiles in film over time
while t(1,count) < 14400

    % Helper function "film_profiles" - models reactant concentrations within
    % gas-liquid film region for O3 reactions in a semi-batch system (steady-state
    % O3 and reactant concentrations throughout system at a given instant) with
    % consumption of O3 by bulk matrix consituents in the fast kinetic regime,
    % and inclusion of •OH reactions.
    film_profiles

    C_O3(1,count) = O3_leqavg; %matrix of C_O3 at times, t(1,t), in (mol/L)
    C_RMC(1,count+1) = C_RMC(1,count)+Dep_RMC(1,count)*dt; %matrix of C_RMC at times, t(1,t),
in mol/L
    C_CM(1,count+1) = C_CM(1,count)+Dep_CM(1,count)*dt; %matrix of C_CM at times, t(1,t), in
mol/L
    C_pCBA(1,count+1) = C_pCBA(1,count)+Dep_pCBA(1,count)*dt; %matrix of C_pCBA at times,
t(1,t), in mol/L
    C_DC(1,count+1) = C_DC(1,count)+Dep_DC(1,count)*dt; %matrix of C_DC at times, t(1,t), in mol/L
    C_EE2(1,count+1) = C_EE2(1,count)+Dep_EE2(1,count)*dt; %matrix of C_EE2 at times, t(1,t), in
mol/L
    C_IP(1,count+1) = C_IP(1,count)+Dep_IP(1,count)*dt; %matrix of C_IP at times, t(1,t), in mol/L
    C_PP(1,count+1) = C_PP(1,count)+Dep_PP(1,count)*dt; %matrix of C_PP at times, t(1,t), in mol/L

    t(1,count+1) = t(1,count)+dt; %matrix of times, t(1,t), in (s)
    count = count+1 %counter
end

% reactant concentrations at film-bulk liquid interface (for further analysis), in mol/L
C_bulk(:,1) = C_CM/C_CM(1,1);
C_bulk(:,2) = C_pCBA/C_pCBA(1,1);
C_bulk(:,3) = C_DC/C_DC(1,1);
C_bulk(:,4) = C_EE2/C_EE2(1,1);
C_bulk(:,5) = C_IP/C_IP(1,1);
C_bulk(:,6) = C_PP/C_PP(1,1);

% reactant concentrations at film-bulk liquid interface (for plot), in mol/L
y(:,1) = C_RMC/C_RMC(1,1);
y(:,2) = C_CM/C_CM(1,1);
y(:,3) = C_pCBA/C_pCBA(1,1);
```

```
y(:,4) = C_DC/C_DC(1,1);
y(:,5) = C_EE2/C_EE2(1,1);
y(:,6) = C_IP/C_IP(1,1);
y(:,7) = C_PP/C_PP(1,1);

% flux of O3 from the gas-phase into the film, and of aqueous-phase reactant species from the bulk liquid into the film, in mol/(m^2*s)
fl(:,1) = Flux_O3;
fl(:,2) = Flux_CM;
fl(:,3) = Flux_pCBA;
fl(:,4) = Flux_DC;
fl(:,5) = Flux_EE2;
fl(:,6) = Flux_IP;
fl(:,7) = Flux_PP;

% volumetric rates of reactant depletion at film-bulk liquid interface (for plot), in mol/(L*s)
d(:,1) = Dep_CM;
d(:,2) = Dep_pCBA;
d(:,3) = Dep_DC;
d(:,4) = Dep_EE2;
d(:,5) = Dep_IP;
d(:,6) = Dep_PP;

% plot of reactant concentrations at film_bulk liquid interface (i.e., in bulk solution) vs. time, in mol/L
close all
H=plot(t,y);
set(gca,'YLim', [0 1])
set(gca,'XLim', [0 t(length(t))])
set(gca,'XTickMode', 'auto')
set(gca,'YTickMode', 'auto')
set(get(gca,'Ylabel'),'String','C/C_0')
set(get(gca,'Xlabel'),'String','time [s]')

title('Depletion of model compounds in bulk solution during ozonation')
legend(gca,'RMC','CM','pCBA','DC','EE2','IP','PP',4)
```

Literature Cited

(1) Udert, K. M.; Larsen, T. A.; Gujer, W. Estimating the precipitation potential in urine-collecting systems. *Water Res.* **2003**, *37*, 2667-2677.
(2) Pronk, W.; Biebow, M.; Boller, M. Electrodialysis for recovering salts from a urine solution containing micropollutants. *Environ. Sci. Technol.* **2006**, *40*, 2414-2420.
(3) Qiu, Y. Q.; Kuo, C. H.; Zappi, M. E. Performance and simulation of ozone absorption and reactions in a stirred-tank reactor. *Environ. Sci. Technol.* **2001**, *35*, 209-215.
(4) Beltran, F. J. *Ozone Reaction Kinetics for Water and Wastewater Systems*; Lewis Publishers: Boca Raton, FL, 2004.
(5) Zhou, H. D.; Smith, D. W. Ozone mass transfer in water and wastewater treatment: Experimental observations using a 2D laser particle dynamics analyzer. *Water Res.* **2000**, *34*, 909-921.
(6) Danckwerts, P. V. *Gas-Liquid Reactions*; McGraw-Hill Book Company: New York, 1970.
(7) Charpentier, J. C., *Mass-transfer rates in gas-liquid absorbers and reactors*; Academic Press: New York, NY, 1981; Vol. 11.
(8) Zhou, H. D.; Smith, D. W. Process parameter development for ozonation of kraft pulp mill effluents. *Water Sci. Technol.* **1997**, *35*, 251-259.
(9) Elovitz, M. S.; von Gunten, U. Hydroxyl radical/ozone ratios during ozonation processes. I. The R_{ct} concept. *Ozone: Sci. Eng.* **1999**, *21*, 239-260.
(10) Yao, C. C. D.; Haag, W. R. Rate constants for direct reactions of ozone with several drinking water contaminants. *Water Res.* **1991**, *25*, 761-773.
(11) Neta, P.; Dorfman, L. M. Pulse radiolysis studies. XIII. Rate constants for the reaction of hydroxyl radicals with aromatic compounds in aqueous solutions. *Adv. in Chem.* **1968**, *81*, 222-230.
(12) Gurol, M. D.; Nekouinaini, S. Effect of organic substances on mass transfer in bubble aeration. *J. Water Poll. Control Fed.* **1985**, *57*, 235-240.
(13) Roustan, M.; Wang, R. Y.; Wolbert, D. Modeling hydrodynamics and mass transfer parameters in a continuous ozone bubble column. *Ozone: Sci. Eng.* **1996**, *18*, 99-115.
(14) Zieminski, S. A.; Caron, M. M.; Blackmore, R. B. Behavior of air bubbles in dilute aqueous solutions. *Industrial and Engineering Chemistry. Fundamentals* **1967**, *6*, 233-&.
(15) Electricity consumption of a medium scale ozone generator (8.3 kg/h), using air as a feed. Available at http://www.wedecoag.com. Wedeco AG. 2006
(16) Maurer, M.; Schwegler, P.; Larsen, T. A. Nutrients in urine: energetic aspects of removal and recovery. *Water Sci. Technol.* **2003**, *48*, 37-46.
(17) Siegrist, H., Personal communication.
(18) Ciba-Geigy, Ed.^Eds. *Wissenschaftliche Tabellen Geigy, Teilband Körperflüssigkeiten*; 8 ed.: Basel, 1977.
(19) Maurer, M.; Pronk, W.; Larsen, T. A. Treatment processes for source-separated urine. *Water Res.* **2006**, *40*, 3151-3166.
(20) Huber, M. M.; Gobel, A.; Joss, A.; Hermann, N.; Loffler, D.; McArdell, C. S.; Ried, A.; Siegrist, H.; Ternes, T. A.; von Gunten, U. Oxidation of pharmaceuticals during ozonation of municipal wastewater effluents: A pilot study. *Environ. Sci. Technol.* **2005**, *39*, 4290-4299.
(21) Ternes, T. A.; Stuber, J.; Herrmann, N.; McDowell, D.; Ried, A.; Kampmann, M.; Teiser, B. Ozonation: a tool for removal of pharmaceuticals, contrast media and musk fragrances from wastewater? *Water Res.* **2003**, *37*, 1976-1982.

(22) Römer, W. Vergleichende Untersuchung der Phosphatverfügbarkeit von Produkten des P-Recyclings und bekannter Phosphatdünger. *Abwasser Abfall* **2006**, *53*, 483-489.

(23) PhysProp Database. Available at http://www.syrres.com/esc/physdemo.htm. Syracuse Research Corporation

(24) Avdeef, A.; Box, K. J.; Comer, J. E. A.; Hibbert, C.; Tam, K. Y. pH-metric logP 10. Determination of liposomal membrane-water partition coefficients of ionizable drugs. *Pharm. Res.* **1998**, *15*, 209-215.

(25) Weber, E. J.; Kenneke, J. F., SPARC. Available at http://www.epa.gov/athens/research/projects/sparc. US EPA, National Exposure Research Laboratory: Athens, GA.

(26) Wilke, C. R.; Chang, P. Correlation of diffusion coefficients in dilute solutions. *AIChE J.* **1955**, *1*, 264-270.

(27) Perry, R. H.; Chilton, C. H. *Chemical Engineers' Handbook*; 5th ed.; McGraw-Hill, Inc.: New York, 1973.

(28) Huber, M. M.; Canonica, S.; Park, G. Y.; Von Gunten, U. Oxidation of pharmaceuticals during ozonation and advanced oxidation processes. *Environ. Sci. Technol.* **2003**, *37*, 1016-1024.

(29) Deborde, M.; Rabouan, S.; Duguet, J. P.; Legube, B. Kinetics of aqueous ozone-induced oxidation of some endocrine disruptors. *Environ. Sci. Technol.* **2005**, *39*, 6086-6092.

(30) Benner, J.; Salhi, E.; Ternes, T. A.; von Gunten, U. Ozonation of reverse osmosis concentrate: Kinetics and efficiency of beta blocker oxidation. *Water Res.* **2008**, *42*, 3003-3012.

(31) Weisenberger, S.; Schumpe, A. Estimation of gas solubilities in salt solutions at temperatures from 273 K to 363 K. *AIChE J.* **1996**, *42*, 298-300.

(32) Rischbieter, E.; Stein, H.; Schumpe, A. Ozone solubilities in water and aqueous salt solutions. *J. Chem. Eng. Data* **2000**, *45*, 338-340.

(33) Stumm, W.; Morgan, J. J. *Aquatic Chemistry*; 3rd ed.; John Wiley and Sons, Inc.: New York, NY, 1996.

(34) Buxton, G. V.; Elliot, A. J. Rate constant for reaction of hydroxyl radicals with bicarbonate ions. *Radiat. Phys. Chem.* **1986**, *27*, 241-243.

(35) Buxton, G. V.; Greenstock, W. P.; Helman, W. P.; Ross, A. B. Critical review of rate constants for reactions of hydrated electrons, hydrogen atoms, and hydroxyl radicals ($^{\bullet}OH/O^{\bullet-}$) in aqueous solution. *J. Phys. Chem. Ref. Data* **1988**, *17*, 513-886.

(36) Neta, P.; Maruthamuthu, P.; Carton, P. M.; Fessenden, R. W. Formation and reactivity of the amino radical. *J. Phys. Chem.* **1978**, *82*, 1875-1878.

(37) Westerhoff, P.; Mezyk, S. P.; Cooper, W. J.; Minakata, D. Electron pulse radiolysis determination of hydroxyl radical rate constants with Suwannee river fulvic acid and other dissolved organic matter isolates. *Environ. Sci. Technol.* **2007**, *41*, 4640-4646.

(38) Neta, P.; Huie, R. E.; Ross, A. B. Rate constants for reactions of inorganic radicals in aqueous solution. *J. Phys. Chem. Ref. Data* **1988**, *17*, 1027-1284.

(39) Canonica, S.; Kohn, T.; Mac, M.; Real, F. J.; Wirz, J.; Von Gunten, U. Photosensitizer method to determine rate constants for the reaction of carbonate radical with organic compounds. *Environ. Sci. Technol.* **2005**, *39*, 9182-9188.

(40) Poskrebyshev, G. A.; Huie, R. E.; Neta, P. Radiolytic reactions of monochloramine in aqueous solutions. *J. Phys. Chem., A* **2003**, *107*, 7423-7428.

(41) Neta, P.; Huie, R. E. One-electron redox reactions involving sulfite ions and aromatic amines. *J. Phys. Chem.* **1985**, *89*, 1783-1787.

(42) Huie, R. E.; Clifton, C. L.; Neta, P. Electron transfer reaction rates and equilibria of the carbonate and sulfate radical anions. *Radiat. Phys. Chem.* **1991**, *38*, 477-481.

(43) Laszlo, B.; Alfassi, Z. B.; Neta, P.; Huie, R. E. Kinetics and mechanism of the reaction of $^{\bullet}NH_2$ with O_2 in aqueous solutions. *J. Phys. Chem., A* **1998**, *102*, 8498-8504.

(44) Sehested, K.; Holcman, J.; Hart, E. J. Rate constants and products of the reactions of e_{aq}^-, $O_2^{\bullet -}$, and H with ozone in aqueous solutions. *J. Phys. Chem.* **1983**, *87*, 1951-1954.

(45) Elliot, A. J.; McCracken, D. R. Effect of temperature on $O^{\bullet -}$ reactions and equilibria: A pulse radiolysis study. *Radiat. Phys. Chem.* **1989**, *33*, 69-74.

(46) Bühler, R. E.; Staehelin, J.; Hoigné, J. Ozone decomposition in water studied by pulse radiolysis.1. $HO_2^{\bullet}/O_2^{\bullet -}$ and $HO_3^{\bullet}/O_3^{\bullet -}$ as intermediates. *J. Phys. Chem.* **1984**, *88*, 2560-2564.

(47) Christensen, H.; Sehested, K. $HO_2^{\bullet}$ and $O_2^{\bullet -}$ radicals at elevated temperatures. *J. Phys. Chem.* **1988**, *92*, 3007-3011.

(48) Staehelin, J.; Hoigné, J. Decomposition of ozone in water: Rate of initiation by hydroxide ions and hydrogen peroxide. *Environ. Sci. Technol.* **1982**, *16*, 676-681.

(49) Buxton, G. V. Pulse radiolysis of aqueous solutions: Rate of reaction of $^{\bullet}OH$ with OH^-. *Trans. Faraday Soc.* **1970**, *66*, 1656-&.

(50) Sehested, K.; Holcman, J.; Bjergbakke, E.; Hart, E. J. A pulse radiolytic study of the reaction $^{\bullet}OH + O_3$ in aqueous medium. *J. Phys. Chem.* **1984**, *88*, 4144-4147.

(51) Christensen, H.; Sehested, K.; Corfitzen, H. Reactions of hydroxyl radicals with hydrogen peroxide at ambient and elevated temperatures. *J. Phys. Chem.* **1982**, *86*, 1588-1590.

(52) Behar, D.; Czapski, G.; Duchovny, I. Carbonate radical in flash photolysis and pulse radiolysis of aqueous carbonate solutions. *J. Phys. Chem.* **1970**, *74*, 2206-&.

(53) Huie, R. E.; Padmaja, S. The reaction of $NO^{\bullet}$ with superoxide. *Free Radical Res. Commun.* **1993**, *18*, 195-199.

(54) Goldstein, S.; Lind, J.; Merenyi, G. Chemistry of peroxynitrites as compared to peroxynitrates. *Chem. Rev.* **2005**, *105*, 2457-2470.

(55) Lymar, S. V.; Hurst, J. K. Rapid reaction between peroxonitrite ion and carbon dioxide: Implications for biological activity. *J. Am. Chem. Soc.* **1995**, *117*, 8867-8868.

(56) Merenyi, G.; Lind, J.; Goldstein, S.; Czapski, G. Mechanism and thermochemistry of peroxynitrite decomposition in water. *J. Phys. Chem., A* **1999**, *103*, 5685-5691.

(57) Goldstein, S.; Saha, A.; Lymar, S. V.; Czapski, G. Oxidation of peroxynitrite by inorganic radicals: A pulse radiolysis study. *J. Am. Chem. Soc.* **1998**, *120*, 5549-5554.

(58) Merenyi, G.; Lind, J.; Czapski, G.; Goldstein, S. Direct determination of the Gibbs' energy of formation of peroxynitrous acid. *Inorg. Chem.* **2003**, *42*, 3796-3800.

(59) Løgager, T.; Sehested, K. Formation and decay of peroxynitric acid: A pulse radiolysis study. *J. Phys. Chem.* **1993**, *97*, 10047-10052.

(60) Goldstein, S.; Czapski, G.; Lind, J.; Merenyi, G. Mechanism of decomposition of peroxynitric ion (O_2NOO^-): Evidence for the formation of $O_2^{\bullet -}$ and $^{\bullet}NO_2$ radicals. *Inorg. Chem.* **1998**, *37*, 3943-3947.

(61) Liu, Q.; Schurter, L. M.; Muller, C. E.; Aloisio, S.; Francisco, J. S.; Margerum, D. W. Kinetics and mechanisms of aqueous ozone reactions with bromide, sulfite, hydrogen sulfite, iodide, and nitrite ions. *Inorg. Chem.* **2001**, *40*, 4436-4442.

(62) Lide, D. R., Ed.^Eds. *CRC Handbook of Chemistry and Physics*; 82 ed.; CRC Press: Boca Raton, FL, 2001.

(63) Bielski, B. H. J. Reevaluation of spectral and kinetic properties of $HO_2^{\bullet}$ and $O_2^{\bullet -}$ free radicals. *Photochem. Photobiol.* **1978**, *28*, 645-649.

(64) Radiation Chemistry Data Center of the Notre Dame Radiation Laboratory. Available at http://allen.rad.nd.edu/. University of Notre Dame Radiation Laboratory

(65) von Sonntag, C.; Schuchmann, H.-P. In *The Chemistry of Free Radicals: Peroxyl Radicals*; Alfassi, Z. B., Ed.; John Wiley & Sons Ltd.: Hoboken, NJ, 1997, pp 173-234.

(66) Pryor, W. A.; Cueto, R.; Jin, X.; Koppenol, W. H.; Nguschwemlein, M.; Squadrito, G. L.; Uppu, P. L.; Uppu, R. M. A practical method for preparing peroxynitrite solutions of low ionic strength and free of hydrogen peroxide. *Free Radical Biol. Med.* **1995**, *18*, 75-83.
(67) Prutz, W. A.; Monig, H.; Butler, J.; Land, E. J. Reactions of nitrogen dioxide in aqueous model systems: Oxidation of tyrosine units in peptides and proteins. *Arch. Biochem. Biophys.* **1985**, *243*, 125-134.
(68) Czapski, G.; Holcman, J.; Bielski, B. H. J. Reactivity of nitric oxide with simple short-lived radicals in aqueous solutions. *J. Am. Chem. Soc.* **1994**, *116*, 11465-11469.

Appendix B. Kinetics and Mechanistic Aspects of As(III) Oxidation by Aqueous Chlorine, Chloramines, and Ozone: Relevance to Drinking Water Treatment

Dodd, M. C.,* Vu, N. D.;* Ammann, A.; Le, V. C.; Kiessner, R.; Berg, M.; Pham, H. V.; Cao, T. H.; von Gunten, U. *Environmental Science and Technology* **2006**, 40(10), 3285-3292.
*Co-primary authors contributed equally to this work

Abstract

Kinetics and mechanisms of As(III) oxidation by free available chlorine (FAC - the sum of HOCl and OCl^-), ozone (O_3), and monochloramine (NH_2Cl) were investigated in buffered reagent solutions. Each reaction was found to be first order in oxidant and in As(III), with 1:1 stoichiometry. FAC-As(III) and O_3-As(III) reactions were extremely fast, with pH-dependent, apparent second-order rate constants, k''_{app}, of 2.6 (±0.1) × 10^5 $M^{-1}s^{-1}$ and 1.5 (±0.1) × 10^6 $M^{-1}s^{-1}$ at pH 7, whereas the NH_2Cl-As(III) reaction was relatively slow (k''_{app} = 4.3 (±1.7) × 10^{-1} $M^{-1}s^{-1}$ at pH 7). Experiments conducted in real water samples spiked with 50 µg/L As(III) (6.7 × 10^{-7} M) showed that a 0.1 mg/L Cl_2 (1.4 × 10^{-6} M) FAC dose was sufficient to achieve depletion of As(III) to <1 µg/L As(III) within 10 s of oxidant addition to waters containing negligible NH_3 concentrations and DOC concentrations <2 mg-C/L. Even in a water containing 1 mg-N/L (7.1 × 10^{-5} M) of NH_3, >75% As(III) oxidation could be achieved within 10 s of dosing 1-2 mg/L Cl_2 (1.4-2.8 × 10^{-5} M) of FAC. As(III) residuals remaining in NH_3-containing waters 10 s after dosing FAC were slowly oxidized ($t_{1/2} \geq 4$ h) in the presence of NH_2Cl formed by the FAC-NH_3 reaction. Ozonation was sufficient to yield >99% depletion of 50 µg/L As(III) within 10 s of dosing 0.25 mg/L O_3 (5.2 × 10^{-6} M) to real waters containing <2 mg-C/L of DOC, while 0.8 mg/L O_3 (1.7 × 10^{-5} M) was sufficient for a water containing 5.4 mg-C/L of DOC. NH_3 had negligible effect on the efficiency of As(III) oxidation by O_3, due to the slow kinetics of the O_3-NH_3 reaction at circumneutral pH. Time-resolved measurements of As(III) loss during chlorination and ozonation of real waters were accurately modeled using the rate constants determined in this investigation.

B.1 Introduction

Arsenic is a common contaminant of groundwater resources around the world (*1-4*). Soluble inorganic arsenic occurs in surface waters and groundwaters primarily as a combination of arsenous acid (As(III)) and arsenic acid (As(V)) *(1)*. The former state predominates under anoxic conditions (e.g., in oxygen-limited groundwaters), and the latter under oxic conditions *(1)*, although As(III) can exist as a meta-stable species even in oxygen-rich environments, due to the slow kinetics of its oxidation by oxygen *(1)*. Generally, dissolved arsenic occurs in groundwaters at concentrations <5 μg/L (*1,2,5*). However, in certain regions, including the Western United States (*2,6*) and southern Asia (*3,4*), groundwaters utilized for drinking water often contain arsenic concentrations in substantial excess of the 10 μg/L guideline value recommended by the WHO (*5*) and adopted as a regulatory limit by the EU (*7*) and USEPA (*8*).

When sufficient infrastructure is available, aqueous arsenic concentrations can be lowered to ≤10 μg/L by a variety of conventional drinking water treatment methods, though many of these methods remove As(III) substantially less efficiently than As(V) (*9*). In cases for which As(total) is constituted in large part by As(III), arsenic removal can be improved by pre-oxidizing As(III) to As(V) (*9-11*). However, oxidant-scavenging matrix constituents such as dissolved organic matter (DOM) and NH_3 - which can be present at high concentrations within reduced, As(III)-laden groundwaters (*3,12,13*) - may impair As(III) oxidation efficiency by competing with As(III) for available oxidant (*10*). Quantitative knowledge of the rate constants and mechanisms governing oxidation of As(III) by common drinking water oxidants would greatly facilitate modeling and optimization of As(III) oxidation processes for treatment of such waters.

Apparent second-order rate constants, k''_{app}, were measured for oxidation of As(III) by FAC, NH_2Cl, and O_3 within the pH range 2 to 11, to permit evaluation of pH-dependencies for each reaction. Stoichiometries and reaction orders were also measured, to facilitate identification of probable oxidation mechanisms. Additional experiments were conducted in water samples collected from Lake Zurich, in Switzerland, and from two groundwater treatment facilities in Hanoi, Vietnam, to quantify the effects of matrix composition on As(III) oxidation efficiency, and to test the suitability of measured rate constants for modeling As(III) oxidation in real water systems.

B.2 Materials and Methods

B.2.1 Chemical Reagents. As(III) and As(V) stock solutions were prepared from $NaAsO_2$ (purity ≥ 99%) and $Na_2HAsO_4 \cdot 7H_2O$ (purity ≥ 98.5%) obtained from Fluka. FAC stock solutions were prepared from NaOCl (~7% available chlorine) obtained from Riedel-de Haën, and standardized by iodometric titration (*14*). Chloramine and O_3 stocks were prepared according to published procedures (*15,16*). Additional reagents were commercially-available and of at least reagent grade purity. All stock solutions were prepared in deionized water ($\Omega \geq$ 18.2 m /cm) obtained from a Millipore Milli-Q® or Barnstead NANOpure® water purifier. Fifty-mM As(III) stocks were prepared approximately bi-monthly, during which time they were stable to within 5% of their initial concentration. Working As(III) solutions were prepared from these stocks before each experiment. Aluminosilicate adsorbent - for the separation of As(III) and As(V) - was purchased from Dr. Xiaoguang Meng, Stevens Institute of Technology, Hoboken, NJ..

B.2.2 Analytical Methods. As(III) and As(V) concentrations were measured by ion-chromatography/ICP-MS (see Supporting Information for Appendix B, Text SB.1 for details). *p*-Chlorobenzoic acid (*p*CBA) and benzaldehyde analyses were performed by HPLC-UV (Text SB.1).

B.2.3 Determination of Rate Constants. Rate constants for the reactions of As(III) with FAC, NH_2Cl, $NHCl_2$, and O_3, were measured by various techniques selected according to reactant characteristics and reaction rates. In each case, oxidant consumption was measured in the presence of a large excess of As(III), to maintain pseudo-first-order conditions. Individual experimental procedures are summarized in Table B.1 and described in detail within Text SB.2.

B.2.4 Stoichiometric Measurements. Stoichiometries of the reactions between As(III) and each oxidant (excluding $NHCl_2$) were measured with either As(III) or the oxidant in excess. In each case, increasing concentrations of the limiting reactant were dosed under constant, rapid stirring to buffered solutions of the reactant-in-excess. Reactions were allowed to proceed for time intervals sufficient to ensure complete consumption of the limiting reactant, prior to sampling and analysis for the reactant-in-excess. When As(III) was dosed to solutions containing excess O_3, experiments were conducted under gas-tight conditions to minimize evaporative O_3 losses (details in Text SB.3).

B.2.5 Real Water Experiments. Water samples used for real water experiments are listed with corresponding water quality parameters in Table B.2. These waters, which contained native As(III) concentrations <2 μg/L As(III), were spiked with 50 μg/L As(III) for

Table B.1. Experimental approaches used for rate constant measurements and real water experiments

Experiment (Method)[a]	**T (°C)**	**Measurement Endpoint**[e]	**Experimental Matrix(es)**[f,g]	**Quenching Agent(s)**[g]
NH_2Cl kinetics (Batch[b])	25 (±0.5)	NH_2Cl loss (measured at λ = 243 nm)	Buffered As(III) stock	NA
$NHCl_2$ kinetics (Batch[b])	25 (±0.5)	$NHCl_2$ loss (measured at λ = 310 nm)	Buffered As(III) stock	NA
FAC kinetics (CFL[b])	23 (±2)[d]	FAC loss (measured via DPD method)	Buffered As(III) stock (C1), Buffered FAC stock (C2)	DPD (C3)
O_3 kinetics (CFL[b])	23 (±2)[d]	O_3 loss (measured via indigo method)	Buffered As(III) stock (C1), pH 4 O_3 stock (C2)	Indigo (C3)
O_3 kinetics (SFL[b])	20 (±0.5)	O_3 loss (measured at λ = 258 nm)	Buffered As(III) stock (C1), Buffered O_3 stock (C2)	NA
Real water chlorination (Batch[c])	25 (±0.5)	Measurement of As(III) loss for various FAC doses	As(III)-spiked real water	Ascorbic acid or DPD[i]
Real water chlorination (Batch[c])	25 (±0.5)	Measurement of As(III) loss in the presence of various NH_2Cl concentrations	As(III)-spiked real water	Ascorbic acid or DPD[i]
Real water ozonation (Batch[c])	20 (±0.5)	Measurement of As(III) loss for various O_3 doses	As(III)-spiked real water	None
Real water chlorination (CFL[c])	23 (±2)[d]	Time-resolved monitoring of As(III) loss for an applied excess of FAC	As(III)-spiked real water (C1), Buffered FAC stock (C2)	Ascorbic acid or DPD (C3)[i]
Real water ozonation (CFL[c])	23 (±2)[d]	Time-resolved monitoring of As(III) loss for an applied excess of O_3	As(III)-spiked real water (C1), pH 4 O_3 stock (C2a), Buffer (C2b)[h]	Cinnamic acid (C3)[j]

[a]CFL-continuous-flow, SFL-Stopped-flow, [b]Experimental details included in Text SB.2, [c]Experimental details included in Text SB.5. [d]Room temperature, [e]Reaction kinetics experiments conducted with As(III) in large excess of each oxidant. Real water experiments conducted at starting concentrations of 50 µg/L As(III) (6.7×10^{-7} M), [f]Phosphate, acetate, and borate buffers adjusted to desired pH values in reaction kinetics experiments, or - in real water experiments - to the appropriate real water's native pH. O_3 stocks acidified to pH 4 by dropwise addition of 150 mM sulfuric acid, [g]As(III)-containing solutions introduced on channel 1 (C1) of the CFL system, oxidant solutions on channel 2 (C2), and quenching reagent solutions on channel 3 (C3), [h]O_3 stock (C2a) and buffer (C2b) pre-mixed to yield a buffered O_3 stock (C2) at the real water pH immediately prior to further mixing with As(III)-spiked real water (C1), [i]Ascorbic acid used to quench samples intended for As(III) analyses and DPD used to monitor FAC residuals, [j]The O_3-cinnamic acid reaction yields benzaldehyde in 1:1 stoichiometry (*17*). Residual O_3 concentrations were calculated from benzaldehyde concentrations in quenched samples.

Table B.2. Water sources and important parametric measurements[a]

Water	**pH**	**DOC, mg-C/L**	**Alkalinity, mM HCO_3^-**	**NH_3, mg-N/L (mol-N/L)**
Lake Zurich (LZ)	8.0	1.5-1.6	2.6-2.7	<0.01 ($<7.1 \times 10^{-7}$)
Lake Zurich (LZ1)[b]	8.0	1.5-1.6	2.6-2.7	1 (7.1×10^{-5})
Lake Zurich (LZ20)[b]	8.0	1.5-1.6	2.6-2.7	20 (1.4×10^{-3})
Phap Van (PV)	7.3	5.3-5.4	5.1-5.2	20-25 ($1.4\text{-}1.8 \times 10^{-3}$)
Yen Phu (YP)	7.2	1.1	2.1-2.9	<0.01 ($<7.1 \times 10^{-7}$)

[a]Multiple samples of each water - collected on different dates over a four-month time-span - were utilized to conduct the real water experiments described herein; thus, ranges of measurements are provided for each water quality parameter. Single values indicate that measurements were the same for each sample. [b]Separate aliquots of native LZ water were amended with NH_4Cl (LZ1 with 1 mg-N/L (7.1×10^{-5} M), and LZ20 with 20 mg-N/L (1.4×10^{-3} M)) for use in batch and time-resolved chlorination experiments.

experiments. Separate aliquots of Lake Zurich water were spiked with 1 or 20 mg-N/L (7.1×10^{-5} or 1.4×10^{-3} M) of NH_3 to simulate waters containing high NH_3 and low DOC concentrations. Sample procurement details and source water descriptions are provided in Text SB.4. Methods utilized for real water experiments are summarized in Table B.1, and described in detail within Text SB.5.

B.3 Results and Discussion

B.3.1 As(III) Oxidation Kinetics. Pseudo-first-order rate constants, k'_{obs}, were obtained for reactions of As(III) with each oxidant by linear regression of plots of ln([Oxidant]) versus time, or by exponential regression of plots of [Oxidant] versus time, where appropriate. As(III) reaction orders were determined by evaluating the dependence of k'_{obs} on [As(III)] for each reaction. Plots of log(k'_{obs}) v. log([As(III)]) for FAC, NH_2Cl, and O_3 reactions yielded slopes of 1.0 (±0.08) (Figure SB.1), indicating that each reaction is first-order with respect to As(III). The reactions of As(III) with FAC, NH_2Cl, and O_3 could thus be described by a second-order kinetic model (eq 1),

$$\frac{d([\mathrm{As(III)}])}{dt} = \frac{d([\mathrm{Ox}])}{dt} = -k''_{app}[\mathrm{As(III)}][\mathrm{Ox}] = -k'_{obs}[\mathrm{Ox}] \qquad (1)$$

where k''_{app} (calculated by dividing k'_{obs} by [As(III)]) represents the pH-dependent, apparent second-order rate constant at a particular pH. In contrast to its reactions with the other oxidants, As(III) was found to react with $NHCl_2$ with an order of 0.7 (Figure SB.1).

Free available chlorine. Figure B.1a - which shows the magnitude of $k''_{app,\mathrm{FAC}}$ at various pH values - illustrates that As(III) reacts very rapidly with FAC. $k''_{app,\mathrm{FAC}}$ is 2.6 (±0.1) × 10^5 $M^{-1}s^{-1}$ at pH 7, corresponding to a $t_{1/2,\mathrm{As(III)}}$ of 95 ms in the presence of 2 mg/L Cl_2 (2.8 × 10^{-5} M) of FAC. The pH-dependency of $k''_{app,\mathrm{FAC}}$ can be attributed to the varying contributions of each reactant's acid-base species to apparent FAC-As(III) reactivity.

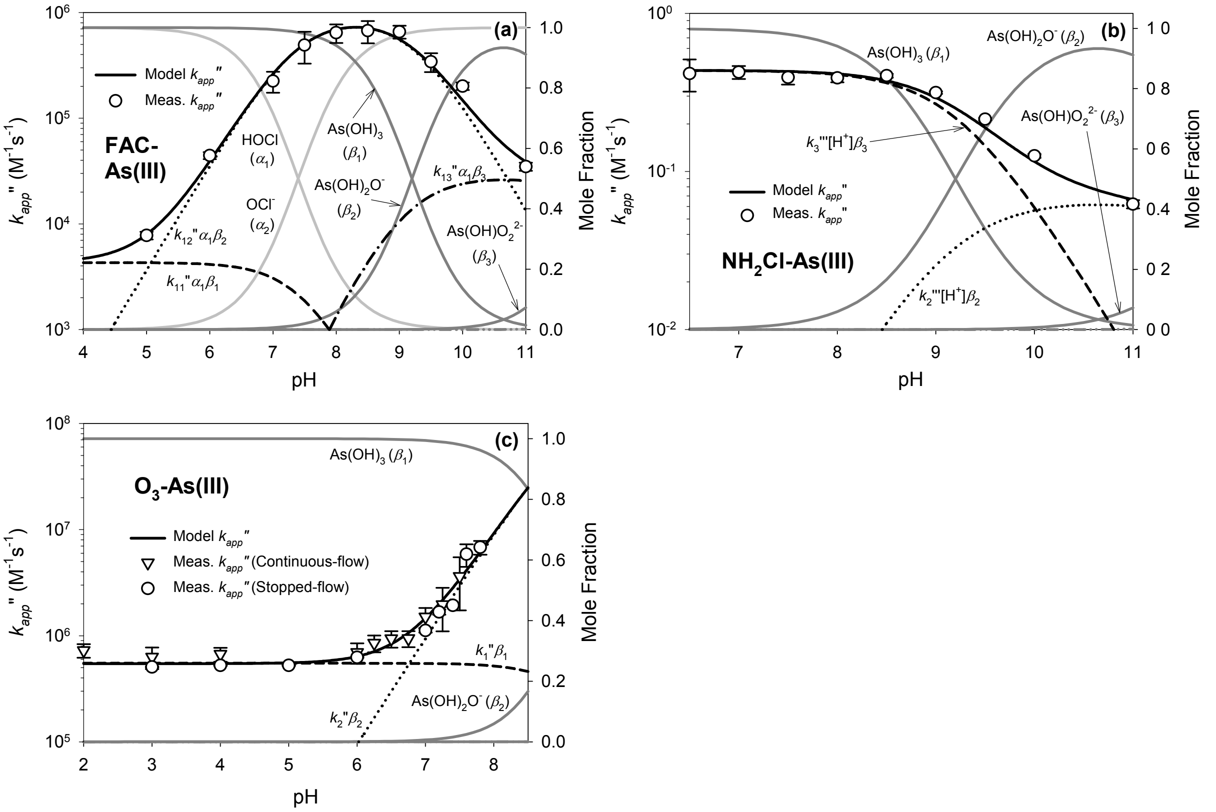

Figure B.1. Apparent second-order rate constants for As(III) oxidation by (a) FAC, (b) NH_2Cl, and (c) O_3. FAC experiments conducted at [As(III)] = 15-50 × 10^{-6} M, $[\mathrm{FAC}]_0$ = 1.5-5 × 10^{-6} M, and 23 (±2) °C, NH_2Cl experiments at [As(III)] = 5 x 10^{-3} M, $[NH_2Cl]_0$ = 2 × 10^{-4} M, and 25 (±0.5) °C, and O_3 experiments at [As(III)] = 10-200 × 10^{-6} M, $[O_3]_0$ = 1-10 × 10^{-6} M, and 23 (±2) °C.

$As(OH)_3$ dissociates in aqueous solution according to eqs 2-4 (*18*).

$$As(OH)_3 \xrightleftharpoons{K_{a1}} As(OH)_2O^- + H^+ \qquad pK_{a1} = 9.2 \tag{2}$$

$$As(OH)_2O^- \xrightleftharpoons{K_{a2}} As(OH)O_2^{2-} + H^+ \qquad pK_{a2} = 12.1 \tag{3}$$

$$As(OH)O_2^{2-} \xrightleftharpoons{K_{a3}} AsO_3^{3-} + H^+ \qquad pK_{a3} = 12.7 \tag{4}$$

At circumneutral pH, $As(OH)_3$ represents the most abundant As(III) species. A small fraction (up to ~0.1) of As(III) is present as $As(OH)_2O^-$ under these conditions, and very small fractions ($< 5 \times 10^{-6}$) are present as $As(OH)(O)_2^{2-}$ and $As(O)_3^{3-}$ (Figure B.1a). FAC speciation can be described by eq 5 (*19*).

$$\mathrm{HOCl} \overset{K_a}{\rightleftharpoons} \mathrm{OCl^-} + \mathrm{H^+} \qquad \mathrm{p}K_\mathrm{a} = 7.4 \tag{5}$$

FAC-As(III) reaction kinetics can be characterized according to eight possible reactions between the four As(III) species (eqs 2-4) and two FAC species (eq 5), by incorporating species distribution terms into eq 1 and rearranging to yield eq 6,

$$k''_{app,\mathrm{FAC}} = \sum_{\substack{i=1,2\\ j=1,2,3,4}} \frac{k''_{ij}\alpha_i[\mathrm{FAC}]\beta_j[\mathrm{As(III)}]}{[\mathrm{FAC}][\mathrm{As(III)}]} = \sum_{\substack{i=1,2\\ j=1,2,3,4}} k''_{ij}\alpha_i\beta_j \tag{6}$$

where α_i and β_j represent the respective fractions of oxidant and substrate present as the species *i* and *j* at a given pH (*20*), and k''_{ij} represents the specific second-order rate constant for each *i* and *j* pair.

The increase in magnitude of $k''_{app,\mathrm{FAC}}$ up to pH 8.3 can be attributed primarily to an increase in the fraction of As(III) present as $As(OH)_2O^-$, which is expected to be a stronger nucleophile than $As(OH)_3$. The decrease in magnitude of $k''_{app,\mathrm{FAC}}$ above pH 8.3 can be attributed to an accompanying decrease in proportion of HOCl relative to OCl^-, which is a much weaker oxidant than HOCl (*15,21-23*). Consequently, the magnitude of $k''_{app,\mathrm{FAC}}$ is highest near pH 8.3 (the average of $\mathrm{p}K_{\mathrm{a1,As(III)}}$ and $\mathrm{p}K_{\mathrm{a,HOCl}}$), where the product $\alpha_{\mathrm{HOCl}}\beta_{\mathrm{As(OH)_2O^-}}$ ($\alpha_1\beta_2$) reaches a maximum (Figure B.1a). These observations indicate that OCl^- reactions are unimportant relative to HOCl reactions within the pH range studied. The magnitude of $k''_{app,\mathrm{FAC}}$ is therefore governed primarily by the reactions of each acid-base species of $As(OH)_3$ with HOCl. $k''_{app,\mathrm{FAC}}$ can thus be modeled by neglecting OCl^- reactions.

Specific rate constants, k''_{1j} - calculated by non-linear regression of measured $k''_{app,\mathrm{FAC}}$ values according to eq 6 (via SigmaPlot 2002, SPSS Software) - are summarized in Table B.3. The model fit shown in Figure B.1a, which was obtained by using these k''_{1j} values, demonstrates the accuracy of eq 6 in describing measured magnitudes of $k''_{app,\mathrm{FAC}}$. k''_{14} could not be accurately determined from available data. However, this term is unimportant within

Table B.3. Specific rate constants determined for reactions of As(III) with HOCl, NH_2Cl, and O_3

Oxidant	**Substrate**	**Specific Rate Constant**	k''_{app} **($M^{-1}s^{-1}$), pH 7** **($t_{1/2}$ at 2 mg/L oxidant concentration)**[b]
HOCl	$As(OH)_3$	$k''_{11} = 4.3\ (\pm 0.8) \times 10^{3}\ M^{-1}s^{-1}$	$2.6\ (\pm 0.1) \times 10^{5}$ ($t_{1/2}$ = 95 ms)
	$As(OH)_2O^-$	$k''_{12} = 5.8\ (\pm 0.1) \times 10^{7}\ M^{-1}s^{-1}$	
	$As(OH)(O)_2^{2-}$	$k''_{13} = 1.4\ (\pm 0.1) \times 10^{9}\ M^{-1}s^{-1}$	
NH_2Cl	$As(OH)_2O^-$	k'''_{2}[a] $= 6.9\ (\pm 2.7) \times 10^{8}\ M^{-2}s^{-1}$	$4.3\ (\pm 1.7) \times 10^{-1}$ ($t_{1/2}$ = 16 h)
	$As(OH)(O)_2^{2-}$	k'''_{3}[a] $= 8.3\ (\pm 7.8) \times 10^{10}\ M^{-2}s^{-1}$	
O_3	$As(OH)_3$	$k''_{1} = 5.5\ (\pm 0.1) \times 10^{5}\ M^{-1}s^{-1}$	$1.5\ (\pm 0.1) \times 10^{6}$ ($t_{1/2}$ = 11 ms)
	$As(OH)_2O^-$	$k''_{2} = 1.5\ (\pm 0.1) \times 10^{8}\ M^{-1}s^{-1}$	

[a] Third-order, H^+-catalysis rate constant, [b] calculated for pseudo-first-order conditions of excess oxidant, assuming 2 mg/L concentrations of FAC (28 μM), NH_2Cl (28 μM), and O_3 (42 μM).

the pH range studied, as HOCl-As(III) reactivity is governed almost exclusively by k''_{11}, k''_{12}, and k''_{13} under these conditions (Figure B.1a).

Chloramines. The magnitude of k''_{app,NH_2Cl} is shown at various pH values in Figure B.1b. These data illustrate that As(III) reacts relatively slowly with NH_2Cl. k''_{app,NH_2Cl} is 4.3 (±1.7) × 10^{-1} $M^{-1}s^{-1}$ at pH 7, corresponding to a $t_{1/2,As(III)}$ of 16 h in the presence of 2 mg/L Cl_2 (2.8 × 10^{-5} M) of NH_2Cl. The inverse relationship between pH and magnitude of k''_{app,NH_2Cl} from pH 8 to 11 (Figure B.1b) is suggestive of acid-catalysis, in analogy to the reactions of NH_2Cl with SO_3^{2-} (*24*), NO_2^- (*25*), and I^- (*15*). This catalysis appears to be H^+-specific, as k''_{app,NH_2Cl} exhibited no measurable dependence on phosphate (50-182 mM) or borate (10-80 mM) concentrations.

The plateau in magnitude of k''_{app,NH_2Cl} below pH 8 indicates that NH_2Cl-As(III) reaction kinetics are not significantly influenced by neutral $As(OH)_3$ within the pH range studied, because H^+-catalyzed oxidation of $As(OH)_3$ would require that the magnitude of k''_{app,NH_2Cl} increase continuously with increasing acidity. The trends in Figure B.1b can therefore be attributed to H^+-catalyzed reactions of NH_2Cl with one or more anionic As(III) species, according to eq 7,

$$k''_{app,\mathrm{NH_2Cl}} = \left[\mathrm{H^+}\right]\left(\sum_{j=2,3,4} k'''_j \beta_j\right) \tag{7}$$

where k'''_j represents respective third-order H^+-catalysis rate constants for each of the three anionic As(III) species, *j*. In the context of eq 7, the data in Figure B.1b also suggest that the magnitude of $k''_{app,\mathrm{NH_2Cl}}$ is governed primarily by $As(OH)_2O^-$ below pH 8. Under these conditions, each successive unit decrease in pH is offset by an order of magnitude decrease in the mole fraction of $As(OH)_2O^-$, resulting in a constant value for the product of the $[H^+]$ and β_j terms in eq 7. This should in turn lead to a constant value of $k''_{app,\mathrm{NH_2Cl}}$, assuming that $As(OH)O_2^{2-}$ and AsO_3^{3} have minimal influence on reaction kinetics below pH 8.

These inferences were tested by non-linear regression of measured $k''_{app,\mathrm{NH_2Cl}}$ values according to eq 7. The resulting model fit - obtained with the $k'''_{\mathrm{As(OH)_2O^-}}$ and $k'''_{\mathrm{As(OH)O_2^{2-}}}$ values listed in Table B.3 - is shown in Figure B.1b. $k'''_{\mathrm{AsO_3^{3-}}}$ could not be accurately determined, due to lack of data above pH 11. However, this term is unimportant within the pH range studied, because the magnitude of $k''_{app,\mathrm{NH_2Cl}}$ is influenced primarily by $k'''_{\mathrm{As(OH)_2O^-}}$ and $k'''_{\mathrm{As(OH)O_2^{2-}}}$ between pH 6.5 and 11 (Figure B.1b).

An Arrhenius plot of $k''_{app,\mathrm{NH_2Cl}}$ from 10-30 °C showed that E_a for the As(III)-NH_2Cl reaction is 27 (±2) kJ/mol (Figure SB.2). A temperature change of 10 °C will therefore result in variation of $k''_{app,\mathrm{NH_2Cl}}$ by a factor of 1.4-1.5 within temperature ranges relevant to drinking water treatment.

$NHCl_2$-As(III) reaction kinetics were found to be far slower than NH_2Cl-As(III) kinetics. $k'_{obs,\mathrm{NHCl_2}}$ increased from 0.4×10^{-5} to 2.4×10^{-5} s^{-1} (i.e., $t_{1/2}$ = 8-48 h) in the presence of 13.2 mM of As(III), as pH decreased from 4 to 5 (Figure SB.3). These data indicate that the reaction of As(III) with $NHCl_2$ can be neglected under typical drinking water disinfection conditions.

Ozone. The magnitude of $k''_{app,\mathrm{O_3}}$ - measured by CFL and SFL methods - is shown at various values of pH in Figure B.1c. As illustrated by these data, As(III) reacts extremely rapidly with O_3. k''_{app,O_3} is 1.5 (±0.1) × 10^6 $M^{-1}s^{-1}$ at pH 7, corresponding to a $t_{1/2,\text{As(III)}}$ of 11 ms in the presence of 2 mg/L O_3 (4.2 × 10^{-5} M). The magnitude of k''_{app,O_3} is also strongly pH-dependent. However, oxidant speciation does not need to be considered for O_3 reactions, so k''_{app,O_3} can be characterized according to As(III) speciation alone. The constancy of k''_{app,O_3} below pH 6 can be attributed to the O_3-As(OH)_3 reaction, whereas the increase in k''_{app,O_3} above pH 6 can be attributed primarily to the O_3-$\text{As(OH)}_2\text{O}^-$ reaction. As(OH)O^{2-} and AsO_3^{3-} exert negligible influence on the magnitude of k''_{app,O_3} below pH 8.5, since molar fractions of these two species are very small under such conditions (<5 × 10^{-6}).

k''_j values were determined for the O_3-As(III) reaction by fitting eq 6 to k''_{app,O_3} in the same manner as for the As(III)-FAC reaction (with O_3 terms substituted for FAC terms). The resulting model fit - obtained with the $k''_{\text{As(OH)}_3}$ and $k''_{\text{As(OH)}_2\text{O}^-}$ values listed in Table B.3 - is shown in Figure B.1c. $k''_{\text{As(OH)O}_2^{2-}}$ and $k''_{\text{AsO}_3^{3-}}$ could not be accurately determined from available data. However, the importance of these terms is negligible within the pH range studied, as apparent from the nearly exclusive dependence of k''_{app,O_3} on $k''_{\text{As(OH)}_3}$ and $k''_{\text{As(OH)}_2\text{O}^-}$ under these conditions (Figure B.1c).

B.3.2 Mechanistic Considerations. As mentioned above, each reaction was found to be first-order with respect to As(III) and oxidant (Figure SB.1). In addition, stoichiometries of As(III) oxidation by FAC, NH_2Cl, and O_3 were found to be 1:1 for all three reactions; that is, one mole of As(III) was consumed for each mole of oxidant consumed, whether experiments were conducted with As(III) or oxidant in excess (Figure SB.4). Experiments conducted with As(III) in excess also verified that one mole of As(V) is produced for every mole of As(III) consumed (Figure SB.4).

Free available chlorine. On the basis of reaction order and stoichiometry, the oxidation of As(OH)_3 by HOCl - yielding AsO(OH)_3 - superficially resembles a direct oxygen transfer reaction. O-transfer would involve direct nucleophilic substitution by As(III) at the oxygen atom in HOCl, with HCl as a leaving group. However, comparison with FAC reaction systems involving other inorganic nucleophiles (e.g., SO_3^{2-}, NO_2^-, I^-, CN^- (*22*)) suggests that As(III) oxidation more likely proceeds via initial Cl^+-transfer from HOCl to the As atom, with concomitant loss of OH^- (a much more favorable leaving group than HCl), to yield a transient

$As(III)Cl^+$ intermediate that hydrolyzes to Cl^- and As(V) (eqs 8 and 9). This pathway is expected to apply to HOCl reactions with all four As(III) species.

$$HOCl + As(OH)_3 \xrightarrow{k''_{HOCl,As(OH)_3}} Cl^+As(OH)_3 + OH^- \tag{8}$$

$$Cl^+As(OH)_3 + H_2O \xrightarrow{k'_{Cl^+As(OH)_3}} AsO(OH)_3 + 2H^+ + Cl^- \tag{9}$$

Monochloramine. NH_2Cl is known to react with a number of inorganic nucleophiles (e.g., SO_3^{2-}, NO_2^-, I^-) by acid-catalyzed Cl^+-transfer, to yield the same chloro-intermediates produced in corresponding FAC reactions (*15,24,25*). The order and 1:1 stoichiometry of the NH_2Cl-As(III) reaction, together with the pH-dependence of k''_{app,NH_2Cl}, are consistent with a similar mechanism (eq 10), which should apply to oxidation of all three anionic As(III) species. The chloro-intermediate formed in eq 10 would hydrolyze in analogy to eq 9.

$$H^+ + NH_2Cl + As(OH)_2O^- \xrightarrow{k'''_{H^+,NH_2Cl,As(OH)_2O^-}} Cl^+As(OH)_2O^- + NH_3 \tag{10}$$

Ozone. O_3 generally reacts with inorganic nucleophiles by two-electron processes involving O-transfer from O_3 to the nucleophile via a primary ozonide adduct, which decomposes to yield the oxidized substrate and O_2 (*26,27*). The order and 1:1 stoichiometry of the As(III)-O_3 reaction indicate that As(III) is similarly oxidized to As(V) by O-transfer from O_3 to the As atom (eqs 11 and 12). The same pathway is expected to apply to reactions of O_3 with all four As(III) species.

$$O_3 + As(OH)_3 \xrightarrow{k''_{O_3,As(OH)_3}} OOOAs(OH)_3 \tag{11}$$

$$OOOAs(OH)_3 \xrightarrow{k'_{OOOAs(OH)_3}} AsO(OH)_3 + O_2 \tag{12}$$

B.3.3 Oxidation of As(III) in Real Waters. *Chlorination - free available chlorine reactions.* Figure B.2a depicts measured As(III) losses at various FAC doses in each of the real waters listed in Table B.2. Fifty µg/L As(III) (6.7×10^{-7} M) was depleted to <1 µg/L As(III) by as little as 0.1 mg/L Cl_2 (1.4×10^{-6} M) of FAC during batch experiments conducted with LZ and YP waters (Figure B.2a). Such high As(III) oxidation efficiency is consistent with the low DOC concentrations and lack of NH_3 in these two waters (Table B.2). In contrast, As(III) oxidation efficiency was markedly suppressed in LZ1, LZ20, and PV waters (Figure B.2a), due to rapid scavenging of FAC by the NH_3 present in the latter three waters ($k''_{app,FAC,NH_3} > 1 \times 10^4$ $M^{-1}s^{-1}$ between pH 7 and 8 (*23*)).

Time-resolved As(III) losses during chlorination of LZ, LZ1, and YP waters were monitored by the CFL system mentioned in Table B.1. Results obtained from these experiments are summarized in Figure B.2b. FAC residuals were present during the monitored reaction periods in all three waters, ensuring rapid As(III) oxidation in each case. The higher rate of As(III) oxidation in LZ water, compared to YP water, can be attributed to

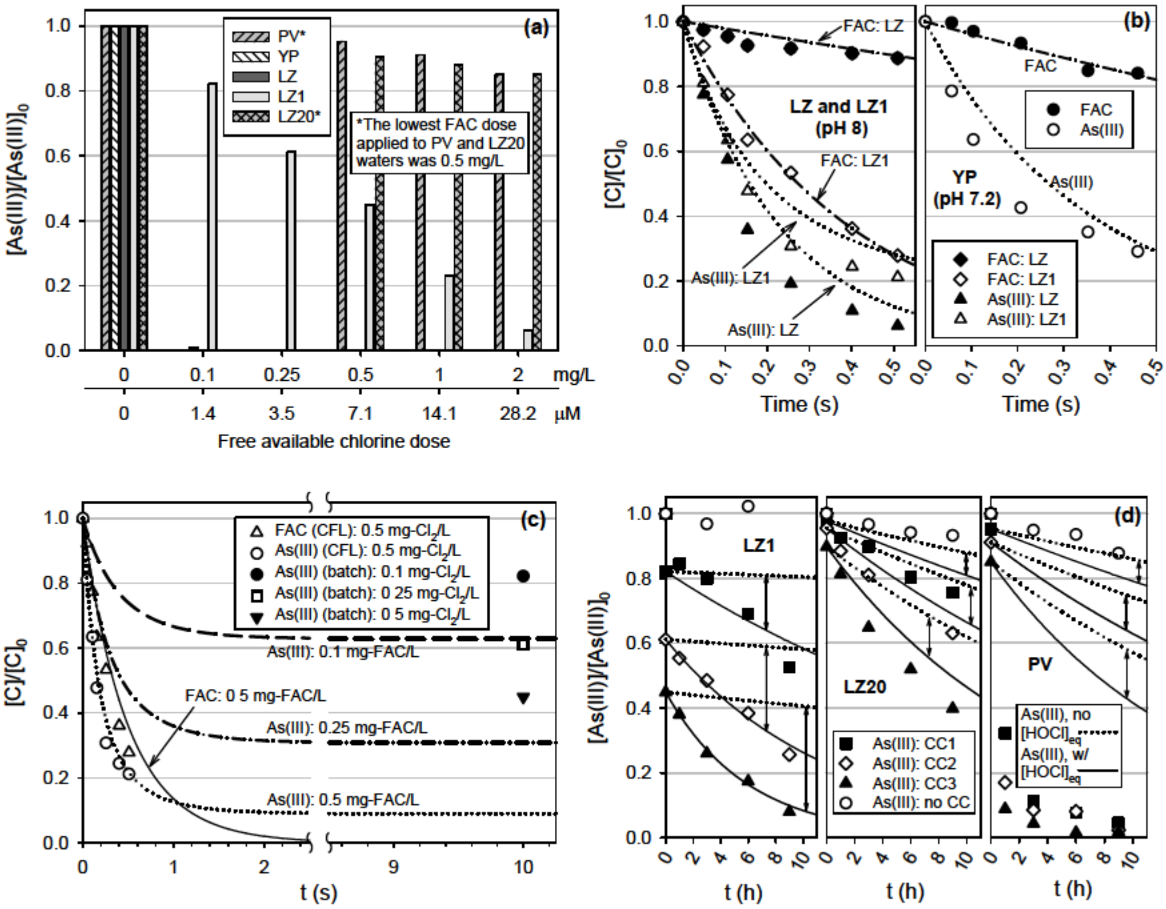

Figure B.2. As(III) oxidation during chlorination of real waters spiked with 50 µg/L As(III) (6.7×10^{-7} M) (water quality data in Table B.2). (a) As(III) loss 10 s after FAC addition to each real water at 25 (±0.5) °C, (b) time-resolved As(III) loss within LZ, LZ1, and YP waters for an applied FAC dose of 0.5 mg/L Cl_2 (7.1×10^{-5} M) at 23 (±2) °C, (c) comparison of As(III) losses measured within LZ1 water - in batch (25 (±0.5) °C) and by CFL (23 (±2) °C), with As(III) losses predicted for the same water by modeling FAC losses according to the second-order reaction between FAC and NH_3. The CFL system achieves much more efficient mixing than the batch setup, as discussed in the main text. (d) As(III) losses in LZ1, LZ20, and PV waters, in the presence of NH_2Cl formed from various FAC doses at 25 (±0.5) °C. CC1, CC2, and CC3 represent “combined chlorine” (i.e., NH_2Cl) concentrations of 0.1, 0.25, and 0.5 mg/L Cl_2 (1.4×10^{-6}, 3.5×10^{-6}, and 7.1×10^{-6} M) for LZ1 water, and 0.5, 1.0, and 1.8 mg/L Cl_2 (7.1×10^{-6}, 1.4×10^{-5}, and 2.5×10^{-5} M) for LZ20 and PV waters. DPD measurements verified that [NH_2Cl] did not decrease more than 10% during the total reaction times in any of these reaction solutions. Symbols in (b)-(d) refer to measurements, lines to model predictions.

the difference in pH of the two waters; with $k''_{app,\mathrm{FAC}}$ = 6.9 × 10^5 $\mathrm{M}^{-1}\mathrm{s}^{-1}$ at pH 8 (LZ water), and 3.6 × 10^5 $\mathrm{M}^{-1}\mathrm{s}^{-1}$ at pH 7.2 (YP water). Comparison of the results for LZ and LZ1 waters shows that As(III) oxidation efficiency was appreciably impaired in the latter, due to rapid consumption of FAC by $\mathrm{NH_3}$ (Figure B.2b). These findings are consistent with the results obtained for batch experiments with the same waters (Figure B.2a).

The As(III) losses shown in Figure B.2b can be modeled with the rate constants reported in Table B.3, by compensating for contemporaneous FAC loss to side-reactions with matrix constituents in each water. FAC losses were modeled according to pseudo-first-order rate "constants," $k'_{\mathrm{FAC,matrix}}$, obtained from plots of ln([FAC]) vs time in each water. As(III) oxidation was in turn modeled by inserting the pseudo-first-order expression for FAC decay (eq 13) into a separate expression for As(III) oxidation (eq 14), and integrating to yield eq 15.

$$[\mathrm{FAC}] = [\mathrm{FAC}]_0 e^{(-k'_{\mathrm{FAC,matrix}}\, t)} \tag{13}$$

$$[\mathrm{As(III)}] = [\mathrm{As(III)}]_0 e^{(-k''_{app,\mathrm{FAC}} \int_0^t [\mathrm{FAC}] dt)} \tag{14}$$

$$[\mathrm{As(III)}] = [\mathrm{As(III)}]_0 e^{\left(\frac{k''_{app,\mathrm{FAC}} [\mathrm{FAC}]_0}{k'_{\mathrm{FAC},matrix}} \left(e^{(-k'_{\mathrm{FAC,matrix}}\, t)} - 1 \right)\right)} \tag{15}$$

The resulting model fits are shown as dotted lines in Figure B.2b. The close agreement between model predictions and measured data for each real water demonstrates that one can accurately predict oxidation of As(III) by FAC in various real waters if the rate of FAC loss for a given water is known. However, in certain cases, one can make predictions of expected As(III) oxidation efficiencies even without directly measuring FAC loss rates. For example, FAC reacts with $\mathrm{NH_3}$ far more rapidly than with DOM and most other matrix constituents; thus, in systems containing substantial $\mathrm{NH_3}$ concentrations (e.g., >0.5 mg-N/L), FAC loss will likely be dominated by FAC-$\mathrm{NH_3}$ reaction kinetics. In such cases, FAC loss can be predicted by modeling FAC consumption according to the second-order reaction between $\mathrm{NH_3}$ and FAC. As(III) loss can in turn be modeled by substituting a second-order expression for FAC loss (eq 16) into eq 14 and integrating with respect to *t,* as described in Text SB.6, to yield eq 17.

$$[\mathrm{FAC}] = \frac{[\mathrm{FAC}]_0 \left(1 - \frac{[\mathrm{NH_3}]_0}{[\mathrm{FAC}]_0}\right)}{\left(1 - \frac{[\mathrm{NH_3}]_0}{[\mathrm{FAC}]_0}\right) e^{(([\mathrm{NH_3}]_0 - [\mathrm{FAC}]_0) k''_{app,\mathrm{FAC,NH_3}}\, t)}} \tag{16}$$

$$[\mathrm{As(III)}]=[\mathrm{As(III)}]_0\, e^{\left(\frac{-k''_{app,\mathrm{FAC,As(III)}}[\mathrm{FAC}]_0\left(1-\frac{[\mathrm{NH_3}]_0}{[\mathrm{FAC}]_0}\right)}{\left([\mathrm{NH_3}]_0-[\mathrm{FAC}]_0\right)k''_{app,\mathrm{FAC,NH_3}}}\left(\ln\left(\frac{e^{\left(\left([\mathrm{NH_3}]_0-[\mathrm{FAC}]_0\right)k''_{app,\mathrm{FAC,NH_3}}\,t\right)}}{\frac{[\mathrm{NH_3}]_0}{[\mathrm{FAC}]_0}e^{\left(\left([\mathrm{NH_3}]_0-[\mathrm{FAC}]_0\right)k''_{app,\mathrm{FAC,NH_3}}\,t\right)}-1}\right)-\ln\left(\frac{1}{\frac{[\mathrm{NH_3}]_0}{[\mathrm{FAC}]_0}-1}\right)\right)\right)} \tag{17}$$

Model predictions obtained by eq 17 are compared with measurements from LZ1 water in Figure B.2c. The model substantially over-predicted As(III) losses with respect to batch measurements. This was presumably a consequence of suboptimal mixing in the batch systems, which would have resulted in disproportionately large consumption of FAC by NH_3 during FAC dosage, in turn leading to lower As(III) loss than predicted for an ideally-mixed system. However, model predictions correlated very well with CFL measurements (Figure B.2c), consistent with the superior mixing efficiency achieved by the CFL system (i.e., FAC and real water solutions are mixed through a tee in 1:1 proportion during CFL experiments, as described in Text SB.2).

Chlorination - NH_2Cl reactions. As(III) loss is expected to occur within two phases during chlorination of a water containing significant NH_3 concentrations: (i) initial, rapid oxidation of As(III) by FAC, and (ii) secondary, slow oxidation of As(III) in the presence of NH_2Cl generated by the FAC-NH_3 reaction, if insufficient FAC is added to completely oxidize As(III) during the first phase. As(III) losses measured within the latter phase, during chlorination of LZ1, LZ20, and PV waters, are shown in Figure B.2d.

With the exception of LZ1 water dosed with 0.1 mg/L Cl_2 (1.4×10^{-6} M) of FAC, NH_2Cl concentrations in each water were in substantial excess of [As(III)], and remained essentially constant during monitored reaction periods in these waters (i.e., <10% change from $[NH_2Cl]_0$, data not shown). As(III) losses were therefore modeled initially by eq 18.

$$[\mathrm{As(III)}]=[\mathrm{As(III)}]_0\, e^{\left(-k''_{app,\mathrm{NH_2Cl}}[\mathrm{NH_2Cl}]t\right)} \tag{18}$$

However, this model substantially under-predicted the rate of As(III) loss observed within LZ1, LZ20, and PV waters (dotted lines in Figure B.2d), presumably because it does not account for effects of the equilibrium between NH_2Cl and HOCl (eq 19) on As(III) oxidation.

$$\mathrm{NH_3 + HOCl} \xrightleftharpoons{K_{\mathrm{hyd}}} \mathrm{NH_2Cl + H_2O} \tag{19}$$

The importance of eq 19 can be investigated by using the equilibrium constant, $K_{\mathrm{Hyd}} = 1.5 \times 10^{11}\ \mathrm{M}^{-1}$ (*28*) to determine the equilibrium concentration, $[\mathrm{HOCl}]_{\mathrm{eq}}$, from known concentrations of NH_3 (Table B.2) and NH_2Cl. $[\mathrm{FAC}]_{\mathrm{eq}}$ (including both HOCl and OCl^-) can then be calculated from $[\mathrm{HOCl}]_{\mathrm{eq}}$ and incorporated with $k''_{\mathrm{FAC},app}$ into eq 18, to yield eq 20, by which contributions of NH_2Cl and HOCl to As(III) loss can be modeled together.

$$[\mathrm{As(III)}] = [\mathrm{As(III)}]_0 e^{\left(-\left(k''_{app,\mathrm{NH_2Cl}}[\mathrm{NH_2Cl}] + k''_{app,\mathrm{FAC}}[\mathrm{FAC}]_{eq}\right)t\right)} \tag{20}$$

As shown by the solid lines in Figure B.2d, eq 20 yielded predictions that are in very good accord with measured As(III) loss in LZ1 and LZ20 waters, illustrating that the NH_2Cl-HOCl equilibrium plays a significant role in governing As(III) loss in the presence of excess NH_2Cl. However, predictions obtained for PV water by eq 20 still deviated substantially from measured As(III) losses (Figure B.2d). The reason for these discrepancies is presently unknown.

Ozonation. Figure B.3a depicts measured As(III) losses for various O_3 doses in LZ, YP, and PV waters. A dose of only 0.25 mg/L O_3 (5.2×10^{-6} M) was sufficient to achieve >99% loss of 50 μg/L As(III) (6.7×10^{-7} M) in LZ and YP waters. Comparable oxidation of 50 μg/L As(III) was also achieved in PV water at a relatively low O_3 dose (0.8 mg/L O_3, or 1.7×10^{-5} M) (Figure B.3a), because O_3 - in contrast to FAC - reacts very slowly with NH_3 (k''_{app} = 0.2 $M^{-1}s^{-1}$ at pH 7.3 (*29*)). The observation that more O_3 than FAC (on a molar basis) is required to achieve comparable oxidation of As(III) in LZ and YP waters (Figures B.2a and B.3a) can be attributed to the higher reactivity of O_3 toward DOM, which results in comparably more rapid O_3 loss to side-reactions with water matrix constituents.

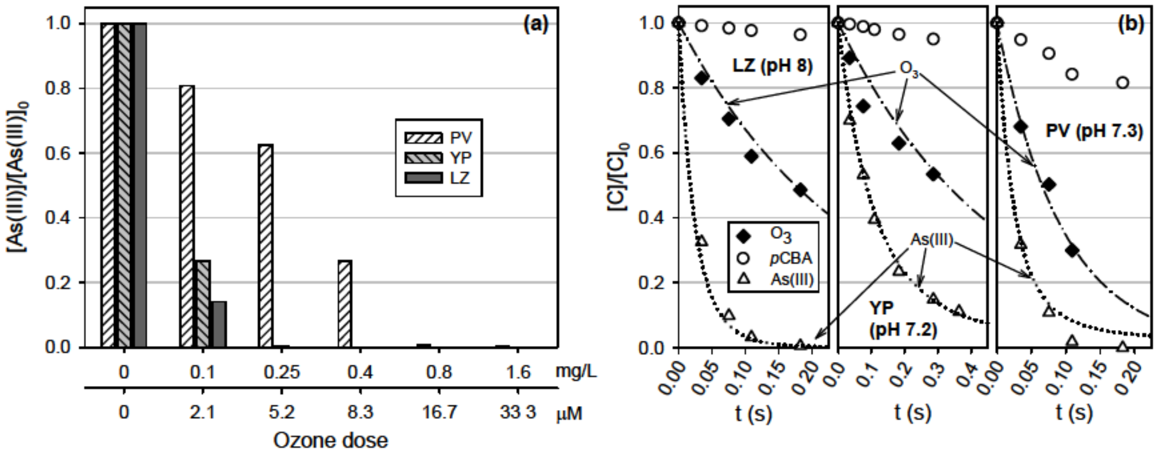

Figure B.3. As(III) oxidation during ozonation of real waters spiked with 50 μg/L As(III) (6.7×10^{-7} M) (water quality data in Table B.2). (a) As(III) loss for various O_3 doses within real waters included in this study, at 25 (±0.5) °C, (b) time-resolved As(III) loss within LZ water ($[O_3]_0$ = 0.25 mg/L (5.2×10^{-6} M), 23 (±2) °C), YP water ($[O_3]_0$ = 0.25 mg/L (5.2×10^{-6} M), 23 (±2) °C), and PV water ($[O_3]_0$ = 1 mg/L (2.1×10^{-5} M), 23 (±2) °C). Symbols refer to measurements, lines to model predictions.

Figure B.3b - depicting time-resolved measurements of O_3 and As(III) losses in LZ, YP, and PV waters - illustrates that $t_{1/2,\mathrm{O}_3}$ is less than 0.33 s in LZ and YP waters, whereas $t_{1/2,\mathrm{FAC}}$ exceeds 1.8 s for the same waters (Figure B.2b). Molar-equivalent doses of FAC and O_3 therefore resulted in similar rates of As(III) oxidation within these waters, even though the magnitude of k''_{app,O_3} exceeds that of $k''_{app,\mathrm{FAC}}$ by a factor of 5 to 15 at circumneutral pH. Figure B.3b also shows that O_3 loss is more rapid in PV water than in LZ or YP waters, due to the higher DOC concentration in PV water. This is consistent with the comparably lower efficiency of As(III) oxidation by O_3 in PV water (Figure B.3a). Furthermore, Figure B.3b shows that the rate of As(III) loss is significantly faster in LZ water than in YP water, and approximately equivalent to the rate of As(III) loss in PV water, even though the latter was dosed with four times as much O_3. This can be attributed in part to the higher pH of LZ water; that is, k''_{app,O_3} is 9.4×10^6 $M^{-1}s^{-1}$ at pH 8 (LZ water), compared to 2.0×10^6 $M^{-1}s^{-1}$ at pH 7.2 (YP water) and 2.4×10^6 $M^{-1}s^{-1}$ at pH 7.3 (PV water).

Hydroxyl radicals (•OH) - generated by autocatalytic O_3 decomposition or by direct reactions of O_3 with water matrix constituents (*30,31*) - also react rapidly with As(III) ($k''_{\bullet\mathrm{OH,As(OH)}_3}$ = 8.5 (±0.9) × 10^9 $M^{-1}s^{-1}$ (*32*)). *p*-Chlorobenzoic acid (*p*CBA) - which reacts rapidly with •OH, but is effectively nonreactive toward O_3 - was used as an *in situ* probe (*33*) to evaluate the importance of •OH-As(III) reactions during ozonation of each real water. The *p*CBA losses depicted in Figure B.3b show that •OH was generated in measurable yield within each system. However, calculated contributions of •OH to observed As(III) losses were very low (i.e., <5% of total observed loss for LZ and YP waters, and <10% for PV water - see Text SB.7 for a detailed discussion). Time-resolved measurements of As(III) losses in these waters were therefore modeled by considering only O_3-As(III) reaction kinetics (via eq 15, with O_3 terms substituted for FAC terms). The close agreement of model predictions with experimental data confirms that As(III) loss was dominated by direct reactions with O_3 (Figure B.3b).

B.3.4 Implications for As(III) Oxidation during Full-Scale Drinking Water Treatment. As demonstrated here and in prior work (*10*), oxidant-scavenging matrix constituents such as NH_3 and DOM can lower the efficiency of As(III) pre-oxidation processes. Fe(II) - which reacts very rapidly with FAC and O_3 at pH ≤ 2 (*34,35*) - may represent another important oxidant scavenger in such waters, though FAC-Fe(II) and O_3-

Fe(II) reaction kinetics must be measured at circumneutral pH to permit quantitative evaluation of its potential influence on chlorination or ozonation processes.

When oxidant-scavenger concentrations are relatively low, their influence on As(III) oxidation efficiency during chlorination or ozonation processes will likely be offset by the extremely fast kinetics of FAC-As(III) and O_3-As(III) reactions. However, high scavenger concentrations may substantially impair As(III) oxidation efficiency (Figures B.2a and B.3a). Proper selection of oxidants can minimize matrix effects in the latter case. For example, ozonation will generally be preferable to chlorination for oxidation of As(III) in waters containing high NH_3 concentrations (e.g., PV water), because O_3 reacts slowly with NH_3. In comparison, chlorination is likely to prove more efficient than ozonation for As(III) oxidation in waters lacking NH_3, because FAC typically reacts more slowly than O_3 with DOM over time-scales relevant to FAC-As(III) reactions (Figures B.2b and B.3b).

In waters with high oxidant scavenging rates, As(III) oxidation efficiencies will also be highly sensitive to mixing efficiency during oxidant application (Figure B.2c). The high sensitivity of FAC-As(III) and O_3-As(III) reaction kinetics to pH (Figure B.1) indicates that pH control may also play an important role in As(III) oxidation efficiency. Careful attention to these considerations will facilitate optimization of oxidant dose when As(III) oxidation must be balanced with constraints such as disinfection by-product formation.

In an optimized chlorination or ozonation process, complete pre-oxidation of As(III) should generally be achievable at oxidant doses for which disinfection by-product formation will be minimal. For example, THM and NDMA formation potentials in YP and PV waters are known to be far below WHO, EU, and USEPA limits at FAC doses required to achieve full As(III) oxidation within these waters during the present investigation (*13*). Bromate formation during ozonation of these waters is also expected to be low, because YP water contains low Br^- concentrations (i.e., <30 μg/L), and PV water contains high NH_3 concentrations, which will substantially suppress bromate formation by scavenging HOBr generated by reaction of O_3 with Br^- (*36*).

NH_2Cl formed during chlorination of ammoniacal waters will likely only have appreciable effect on As(III) fate in special cases; for example, if source waters undergo limited or no treatment prior to chlorination, and insufficient FAC is added to directly oxidize As(III) during chlorination. Although the direct NH_2Cl-As(III) reaction may result in minimal As(III) oxidation subsequent to chlorination, indirect NH_2Cl-mediated oxidation reactions can yield substantial As(III) oxidation within such systems over reaction times of several hours (e.g., within disinfection contact chambers or distribution networks), as illustrated in Figure B.2d.

Acknowledgements

M.C.D. and N.D.V. contributed equally to this work. Travel scholarships and financial support for N.D.V. and V.C.L. were obtained from the Swiss Agency for Development and Cooperation (SDC), in the framework of the Swiss-Vietnamese project ESTNV (Environmental Science and Technology in Northern Vietnam). M.C.D. acknowledges financial support from a U.S. National Science Foundation Graduate Research Fellowship. The authors thank Elisabeth Salhi, Caroline Stengel, and Sebastien Meylan for their technical assistance. Willem Koppenol is acknowledged for support in obtaining stopped-flow measurements of As(III)-O_3 reaction kinetics. The authors also thank Stephan Hug, Linda Roberts, Olivier Leupin, Marc-Olivier Buffle, and Gretchen Onstad for many helpful discussions. The Hanoi Water Works Company is acknowledged for assistance in obtaining water samples from Hanoi.

Literature Cited

(1) Cullen, W. R.; Reimer, K. J. Arsenic Speciation in the Environment. *Chem. Rev.* **1989**, *89*, 713-764.

(2) Frey, M. M.; Edwards, M. A. Surveying arsenic occurrence. *J. Am. Water Works Ass.* **1997**, *89*, 105-117.

(3) Berg, M.; Tran, H. C.; Nguyen, T. C.; Pham, H. V.; Schertenleib, R.; Giger, W. Arsenic contamination of groundwater and drinking water in Vietnam: A human health threat. *Environ. Sci. Technol.* **2001**, *35*, 2621-2626.

(4) Smith, A. H.; Lingas, E. O.; Rahman, M. Contamination of drinking-water by arsenic in Bangladesh: a public health emergency. *Bulletin of the World Health Organization* **2000**, *78*, 1093-1103.

(5) *Guidelines for Drinking-water Quality*; 3 ed.; World Health Organization: Geneva, Switzerland, 2004; Vol. 1.

(6) Hering, J. G.; Chiu, V. Q. Arsenic occurrence and speciation in municipal ground-water-based supply system. *Journal of Environmental Engineering - ASCE* **2000**, *126*, 471-474.

(7) Council Directive 98/83/EC of 3 November 1998 on the quality of water intended for human consumption. *Official Journal of the European Communities* **1998**, *41*, 32-54.

(8) United States Environmental Protection Agency. 40 CFR, Part 141, National Primary Drinking Water Regulations. 2001 Available at http://www.epa.gov/epahome/cfr40.htm.

(9) United States Environmental Protection Agency - Office of Water. *Technologies and Costs for Removal of Arsenic from Drinking Water*; Publisher, 2000 Available at http://www.epa.gov/safewater/ars/treatments_and_costs.pdf.

(10) Ghurye, G.; Clifford, D. As(III) oxidation using chemical and solid-phase oxidants. *Journal American Water Works Association* **2004**, *96*, 84-96.

(11) Leupin, O. X.; Hug, S. J.; Badruzzaman, A. B. M. Arsenic removal from Bangladesh tube well water with filter columns containing zerovalent iron filings and sand. *Environ. Sci. Technol.* **2005**, *39*, 8032-8037.

(12) McArthur, J. M.; Ravenscroft, P.; Safiulla, S.; Thirlwall, M. F. Arsenic in groundwater: Testing pollution mechanisms for sedimentary aquifers in Bangladesh. *Water Resour. Res.* **2001**, *37*, 109-117.

(13) Duong, H. A.; Berg, M.; Hoang, M. H.; Pham, H. V.; Gallard, H.; Giger, W.; von Gunten, U. Trihalomethane formation by chlorination of ammonium- and bromide-containing groundwater in water supplies of Hanoi, Vietnam. *Water Res.* **2003**, *37*, 3242-3252.

(14) APHA *Standard Methods for the Examination of Water and Wastewater*; 20 ed.; APHA, AWWA, WPCF: Washington, 1998.

(15) Kumar, K.; Day, R. A.; Margerum, D. W. Atom-transfer redox kinetics: General-acid-assisted oxidation of iodide by chloramines and hypochlorite. *Inorg. Chem.* **1986**, *25*, 4344-4350.

(16) Bader, H.; Hoigné, J. Determination of ozone in water by the indigo method. *Water Res.* **1981**, *15*, 449-456.

(17) Leitzke, A.; Reisz, E.; Flyunt, R.; von Sonntag, C. The reactions of ozone with cinnamic acids: formation and decay of 2-hydroperoxy-2-hydroxyacetic acid. *J. Chem. Soc., Perkin Trans. 2* **2001**, 793-797.

(18) Sadiq, M.; Zaidi, T. H.; Mian, A. A. Environmental behavior of arsenic in soils - theoretical. *Water Air and Soil Pollution* **1983**, *20*, 369-377.

(19) Lide, D. R., Ed.^Eds. *CRC Handbook of Chemistry and Physics*; 82 ed.; CRC Press: Boca Raton, FL, 2001.

(20) Stumm, W.; Morgan, J. J. *Aquatic Chemistry*; 3rd ed.; John Wiley and Sons, Inc.: New York, NY, 1996.

(21) Fogelman, K. D.; Walker, D. M.; Margerum, D. W. Non-metal redox kinetics: hypochlorite and hypochlorous acid reactions with sulfite. *Inorg. Chem.* **1989**, *28*, 986-993.

(22) Gerritsen, C. M.; Margerum, D. W. Non-metal redox kinetics: hypochlorite and hypochlorous acid reactions with cyanide. *Inorg. Chem.* **1990**, *29*, 2757-2762.

(23) Qiang, Z.; Adams, C. D. Determination of monochloramine formation rate constants with stopped-flow spectrophotometry. *Environ. Sci. Technol.* **2004**, *38*, 1435-1444.

(24) Yiin, B. S.; Walker, D. M.; Margerum, D. W. Non-metal redox kinetics: general-acid-assisted reactions of chloramine with sulfite and hydrogen sulfite. *Inorg. Chem.* **1987**, *26*, 3435-3441.

(25) Margerum, D. W.; Schurter, L. M.; Hobson, J.; Moore, E. E. Water Chlorination Chemistry: Nonmetal Redox Kinetics of Chloramine and Nitrite Ion. *Environ. Sci. Technol.* **1994**, *28*, 331-337.

(26) Hoigné, J. In *The Handbook of Environmental Chemistry*; Hrubec, J., Ed.; Springer Verlag: Berlin, Germany, 1998, pp 83-141.

(27) Liu, Q.; Schurter, L. M.; Muller, C. E.; Aloisio, S.; Francisco, J. S.; Margerum, D. W. Kinetics and mechanisms of aqueous ozone reactions with bromide, sulfite, hydrogen sulfite, iodide, and nitrite ions. *Inorg. Chem.* **2001**, *40*, 4436-4442.

(28) Gray, E. T., Jr.; Margerum, D. W.; Huffman, R. P. In *Organometals and Organometalloids, Occurence and Fate in the Environment*; Brinkman, F. E.; Bellama, J. M., Eds.; American Chemical Society: Washington, D.C., 1978, pp 264-277.

(29) Hoigné, J.; Bader, H. Ozonation of water: Kinetics of oxidation of ammonia by ozone and hydroxyl radicals. *Environ. Sci. Technol.* **1978**, *12*, 79-84.

(30) Buffle, M.-O.; Schumacher, J.; Salhi, E.; von Gunten, U. Measurement of the initial phase of ozone decomposition in water and wastewater by means of a continuous quench flow system: Application to disinfection and pharmaceutical oxidation. *Water Research* **2005**, *Accepted for publication*.
(31) von Gunten, U. Ozonation of drinking water: Part I. Oxidation kinetics and product formation. *Water Res.* **2003**, *37*, 1443-1467.
(32) Klaening, U. K.; Bielski, B. H. J.; Sehested, K. Arsenic(IV) - a Pulse-Radiolysis Study. *Inorg. Chem.* **1989**, *28*, 2717-2724.
(33) Elovitz, M. S.; von Gunten, U. Hydroxyl radical/ozone ratios during ozonation processes. I. The R_{ct} concept. *Ozone Science and Engineering* **1999**, *21*, 239-260.
(34) Conocchioli, T. J.; Hamilton, E. J.; Sutin, N. Formation of Iron(IV) in Oxidation of Iron(II). *J. Am. Chem. Soc.* **1965**, *87*, 926-927.
(35) Løgager, T.; Holcman, J.; Sehested, K.; Pedersen, T. Oxidation of Ferrous-Ions by Ozone in Acidic Solutions. *Inorg. Chem.* **1992**, *31*, 3523-3529.
(36) Pinkernell, U.; von Gunten, U. Bromate minimization during ozonation: Mechanistic considerations. *Environ. Sci. Technol.* **2001**, *35*, 2525-2531.

Supporting Information for Appendix B.

Kinetics and Mechanistic Aspects of As(III) Oxidation by Aqueous Chlorine, Chloramines, and Ozone: Relevance to Drinking Water Treatment

14 pages, including 7 narratives and 4 figures

Text SB.1. Analytical methods

Ion Chromatography/ICP-MS method. Samples were diluted (generally 10-20 times) in 2 μM phosphate solution prior to injection, and introduced to the column by automated injection-loop filling (20 μL) via an auto-sampler module (ASX-510, CETAC). A micro-bore gradient pump 40 (Dionex) was used to deliver samples through the anion-exchange column (AG11/AS11, 250 × 2 mm, Dionex). Arsenic species were eluted (0.3 mL/min) by a NH_4NO_3-gradient (5 mM at 0 min to 72 mM at 4 min, 72 mM from 4-7 min and equilibration at 5 mM from 7-10.5 min) at pH = 7.0-7.3. The effluent of the anion-exchange column was connected to a micro-flow PFA nebulizer (ESI, Elemental Scientific Instrumentation) mounted on a cooled (5 °C) Scott-type quartz spray chamber of an Element2 (Thermo Electron) high-resolution, double-focusing, sector-field ICP-MS. Arsenic in the ion-exchange column effluent was tracked in low resolution at m/z 75. Plasma conditions were: power forward 1150 W (3 W reflected), argon gas flows 15.5 L/min cooling, 0.9 L/min plasma and 0.9 L/min sample. MS chromatograms were exported from MS software in ASCII format and peak areas were integrated in Excel. Method detection and quantification limits were 0.4 μg/L As (5.3×10^{-9} M) and 1.4 μg/L As (1.9×10^{-8} M), respectively. Relative standard deviations for each measurement ranged from ±2-3%.

Preservation of As(III)-As(V) speciation. Samples intended for measurement of As(III) and As(V) content within one day of preparation were stored at 4 °C, without additional preservation, until analysis by IC/ICP-MS. Stability of arsenic speciation in the Phap Van water (described below) - spiked with equal concentrations of As(III) and As(V) ranging from 0.5-50 μg/L (6.7×10^{-9}-6.7×10^{-7} M) - was found to be stable for up to 7 days of storage under such conditions. Additional controls indicated that As(III) was stable for at least two days in all other samples kept under such storage conditions.

In cases for which prolonged sample storage was necessary, an aluminosilicate adsorbent (0.1-0.3 mm particle diameter) was used to selectively remove As(V) from samples. Additional details of the adsorbent characteristics are available in ref. (*1*). One-mL cartridges packed with ~ 0.8 g of the adsorbent were used for As(V) removal. 2.5-mL water samples collected with a 10 mL-syringe were filtered through these cartridges at a flow rate of ~ 10 mL/min. Total arsenic content in the filtrate was taken to represent As(III) content in a given sample. Individual filter cartridges were only used for a single As(V) removal.

Recoveries of As(III) and breakthrough of As(V) during aluminosilicate filtration were evaluated in Milli-Q water and in the Phap Van groundwater described below. To evaluate As(III) recovery, these waters were each spiked with an As(III) concentration of 100 μg/L

(1.3×10^{-6} M). The difference in measured As(III) concentrations between filtered and non-filtered samples was less than 5 %. To evaluate As(V) breakthrough under typical sampling conditions, a sample of Milli-Q water was spiked with 300 μg/L As(V) (4.0×10^{-6} M) and a sample of Phap Van water spiked with 100 μg/L As(V) (1.3×10^{-6} M). Less than 1 % of the starting As(V) concentrations passed through a 1-mL filter cartridge during filtration of a 5-mL sample. Adsorbent capacity was evaluated by repeatedly passing 5-mL volumes of Milli-Q water containing 250 μg/L As(V) (3.3×10^{-6} M) through a single 1-mL filter cartridge. Negligible As(V) breakthrough was observed even after filtration of 110 mL. All samples were filtered at pH values within the range recommended by the aluminosilicate provider (i.e., between pH 4 and 9)

HPLC analyses. All *p*-chlorobenzoic acid (*p*CBA) and benzaldehyde analyses were performed on a Hewlett-Packard 1050 HPLC system equipped with a Supelco Discovery RP Amide C16 column (3 mm × 250 mm, 5 μm), and a single-wavelength UV detector ($\lambda = 250$ nm). Isocratic separations were performed with 35% acetonitrile and 65% 0.05 M H_3PO_4 (adjusted to pH 2.2 with NaOH). Limits of quantification by this method were approximately 0.05 μM for each analyte. Standard deviations for each measurement varied from ±1-3%.

Text SB.2. Rate constant measurements

Free available chlorine. FAC decay ($[FAC]_0 = 1.5\text{-}5 \times 10^{-6}$ M) was monitored in the presence of 15-20× molar excesses of As(III) ($[As(III)] = 15\text{-}50 \times 10^{-6}$ M) via a continuous-flow, quenched-reaction (CFL) apparatus described in detail previously (*2*). Solutions of As(III) and FAC were mixed through a tee at constant flow-rate, $Q_{reaction} = Q_{FAC} + Q_{As(III)}$, in 1:1 proportion with a multi-position Harvard Apparatus 22 syringe pump. The effluent of this tee was directed through one of seven PTFE loops with volumes, V_{loop}, ranging from 16.1-199.3 μL (inclusive of dead volume). The effluent end of each PTFE loop was directed into a second tee receiving a stream of quenching reagent (DPD sulfate) to stop the reaction between As(III) and FAC after reaction times corresponding to $V_{loop}/Q_{reaction}$. Residual FAC concentrations were measured by monitoring DPD cation radical absorbance at 515 nm (*3*). Desired reaction pH was achieved by buffering FAC and As(III) solutions with 10 mM acetate (pH 5), 10 mM phosphate (pH 6-8.5), or 40 mM borate (pH 9-11). FAC and As(III) solutions containing twice the desired reaction concentrations were mixed in 1:1 proportion to initiate the reaction, which was quenched after various reaction times (ranging from ~ 30-1400 ms) with a deoxygenated solution containing 3 mM of DPD sulfate (buffered at pH 6.5 with 0.1 M phosphate). Experiments were performed in triplicate, at room-temperature

(23(±2) °C). Pseudo-first-order rate constants, k'_{obs}, were obtained from plots of ln([FAC]) versus time. As(III) reaction order was determined at pH 6, by varying [As(III)] from 25-100 µM. Additional details of FAC-As(III) rate constant determinations and the raw data from which these rate constants were calculated are included in additional Supporting Information files accompanying the manuscript from which this chapter is derived (*4*), at http://pubs.acs.org.

Calibrations of FAC measurement were performed by measuring the absorbance of the DPD cation radical generated from various known concentrations of FAC, and were found to be linear over the full range of FAC concentrations employed in these studies. DPD solutions (3 mM) were prepared as described previously (*2*). Calibration of the CFL apparatus – by means of the reaction between NH_3 and HOCl – yielded a calculated value of $k''_{\mathrm{HOCl,NH_3}} = 2.4 \times 10^6\ M^{-1}s^{-1}$, compared to the most precisely-determined literature value of $3.1 \times 10^6\ M^{-1}s^{-1}$ (*5*).

Chloramines. Rate constants for reactions of As(III) with NH_2Cl and $NHCl_2$ were measured in batch, by monitoring NH_2Cl or $NHCl_2$ decay (via spectrophotometric analysis at 243 nm and 310 nm, respectively) in the presence of [As(III)] >> $[\text{chloramine}]_0$ at 25(±0.5) °C. In NH_2Cl experiments, 25-ml volumes of 5 mM As(III), buffered with 50 mM phosphate (pH 6.5 to 8.5) or borate (pH 9 to 11), were dosed under constant, rapid stirring with 0.2 mM of NH_2Cl, to initiate the reaction. Samples were then taken every 3 min for NH_2Cl analysis. Experiments were performed in triplicate at each pH. Controls verified that NH_2Cl losses in the absence of As(III) were negligible during each experiment.

In $NHCl_2$ experiments, 6-mL volumes of 13 mM As(III), buffered with 60 mM acetate (pH 4-5) were pipetted into each of two 2-cm spectrophotometer cells. These As(III) solutions were then dosed with 60 mM acetate solutions containing 350-550 µM of $NHCl_2$, stoppered to prevent evaporative loss of $NHCl_2$, and agitated by rotating the stoppered cell several times. Decay of $NHCl_2$ in these duplicate cells was followed for 2 to 5 h, depending on the pH, by measurement at 310 nm. Controls verified that $NHCl_2$ was stable in the absence of As(III) during experiments conducted at pH 4-4.3. Non-negligible losses of $NHCl_2$ were observed in As(III) controls at pH 4.5 and 5. Measured rates of $NHCl_2$ loss in the presence of As(III) at pH 4.5 and 5 were corrected for NH_2Cl loss rates observed in the corresponding As(III) controls.

k'_{obs} values were obtained from plots of ln([NH_2Cl]) and ln([$NHCl_2$]) versus time, respectively. As(III) reaction orders were determined in the case of NH_2Cl by varying

[As(III)] from 2-15 mM, at pH 8.5, and in the case of $NHCl_2$ by varying [As(III)] from 5-40 mM, at pH 4. Additional details of rate constant determinations for the NH_2Cl-As(III) and $NHCl_2$-As(III) reactions, in addition to the raw data from which these rate constants were calculated, are included in additional Supporting Information files accompanying the manuscript from which this chapter is derived (*4*), at http://pubs.acs.org.

Ozone (continuous-Flow). Rate constants for the reaction between O_3 and As(III) were measured using the same apparatus and procedures as for the FAC-As(III) reaction. O_3 loss ($[O_3]_0 = 1\ \mu M$) was monitored in the presence of 10 μM of As(III). The reaction between As(III) and O_3 was quenched with a 4 μM solution of indigo trisulfonate (which was adjusted to pH 2 with H_3PO_4 to ensure 1:1 stoichiometry of the indigo-O_3 reaction (*6*)), and O_3 residual was followed by monitoring the quenched solution's absorbance at 600 nm (*6*).

Working O_3 stocks were prepared in Milli-Q water adjusted to pH 4 with sulfuric acid to stabilize O_3 (*7*). These O_3 stocks were stored in a stoppered 1-L flask connected to a Metrohm Dosimat dispensing system, prior to transfer from the Dosimat to a 25-mL, Hamilton gas-tight syringe for use in kinetics experiments. Working O_3 stock concentrations were checked before each experiment by mixing a syringe-full of the O_3 stock solution in 1:1 proportion with Milli-Q water (in place of As(III)). Constant solution pH was maintained by buffering As(III) solutions in phosphate buffers of approximately 10 mM concentration. Separate experiments conducted by manually mixing equal volumes of pH 4 water and each buffered solution indicated that pH of the mixed solutions did not change by more than 0.1 unit from that of the buffered As(III) stock. 10 mM *t*-BuOH was added as a hydroxyl radical (•OH) scavenger to each As(III) solution. However, this was later found to be unnecessary, because stoichiometric data and mechanistic findings obtained subsequent to CFL experiments indicated that the reaction of As(III) with O_3 does not generate •OH (see the Mechanistic Considerations section in the main text), and As(III)-O_3 reaction kinetics are fast enough to ensure that •OH formation via autocatalytic O_3 decomposition is negligible at the pH values used for these experiments. All experiments were performed at room-temperature (i.e., 23(±2) °C). k'_{obs} values were obtained from plots of ln([O_3]) versus time. Each [O_3] value used in these plots was obtained by averaging the [O_3] values measured for at least three individual samples collected at the corresponding reaction time during a single CFL experiment. Detailed examples of these calculations are provided with the corresponding raw experimental data in in additional Supporting Information files accompanying the manuscript from which this chapter is derived (*4*), at http://pubs.acs.org. As(III) reaction order was determined by varying [As(III)] from 10-30 μM, at pH 2.

Ozone (stopped-flow). Stopped-flow measurements of O_3 decay in the presence of excess As(III) were performed using an Applied PhotoPhysics SX-17MV system, with temperature controlled at 20(±0.5) °C. As(III) and O_3 solutions, at concentrations ranging from [As(III)] = 40-200 μM, and $[O_3]$ = 2-10 μM, were buffered with either 10 mM phosphate (pH 3, and 6-7.8) or acetate (pH 4 and 5). O_3 solutions were prepared by transferring appropriate volumes of undiluted O_3 stock (via gas-tight syringe) from a Dosimat to 10 mM buffer solutions immediately prior to each experiment. Buffered O_3 and As(III) solutions were then mixed at 1:1 proportion to initiate the reaction between As(III) and O_3, and O_3 loss was monitored directly at λ = 258 nm. $k_{obs}^{'}$ values were calculated by exponential regression (SigmaPlot 2002, SPSS Software) of the average O_3 decay curves calculated from at least nine replicate curves for each pH. Details of these calculations are included with the corresponding raw experimental data in additional Supporting Information files accompanying the manuscript from which this chapter is derived (*4*), at http://pubs.acs.org. *t*-BuOH was not added to solutions used in stopped-flow experiments, for reasons mentioned above. As(III) reaction order was investigated at at pH 3 and 7, by varying [As(III)] from 100-500 μM.

Text SB.3. Measurements of O_3-As(III) stoichiometry with O_3 in excess

Solutions of As(III) were prepared at 8-120 μM concentration in either pH 2 water acidified with sulfuric acid or in 10 mM, pH 7 phosphate buffers. O_3 was prepared at 200 μM in Milli-Q water adjusted to pH 2 (for experiments with pH 2 As(III) solutions) or pH 4 (for experiments with pH 7 As(III) solutions) with sulfuric acid. Working O_3 stocks were stored and transferred as in the reaction kinetics experiments conducted using the continuous-flow apparatus. After transfer of a working O_3 stock into a Hamilton gas-tight syringe, initial O_3 concentration in the syringe was checked by mixing in 1:1 proportion with As(III)-free water (for pH 2 experiments) or 10 mM, pH 7 phosphate buffer (for pH 7 experiments) contained within an identical 25-mL syringe. The two solutions were driven by a multi-position syringe pump (at a flow rate of 10 mL/min) through the inlet channels of a mixing tee whose outlet was directed through a 1-cm flow-through spectrophotometer cell. O_3 concentrations were directly measured at λ = 258 nm. The standardized O_3 solution contained within the first syringe was then similarly mixed in 1:1 proportion with a solution of As(III) contained within a third syringe, and the residual O_3 concentration was recorded after 5 s of reaction time ($t_{0.999,\mathrm{As(III)}}$, or *t* for 99.9% depletion of As(III), was ~ 13 and 5 ms under these conditions at pH 2 and 7, respectively). This procedure was repeated in duplicate for each As(III) dose. Control experiments showed that O_3 losses between each standardization step and As(III)-O_3 mixing step were negligible.

Text SB.4. Real water sample procurement and composition

Real water samples were collected from Lake Zurich, Switzerland, and from two partially-treated drinking waters derived from reduced groundwater sources in Hanoi, Vietnam to validate the applicability of reaction kinetics reported here to modeling reactions in real water systems. Lake Zurich samples were taken from a depth of 30 m below the surface of the lake, which represents the raw water for Zurich's drinking water supply. The Vietnamese water samples were taken from Hanoi's Phap Van and Yen Phu drinking water treatment facilities. Each water sample was filtered through a 0.45-μm membrane immediately after collection, protected from light, and transported to the laboratory (EAWAG) as rapidly as possible (typically 2-3 days transport time), whereupon it was refrigerated at ~ 4 °C prior to usage.

The Phap Van and Yen Phu plants draw raw water from two separate groundwater supplies that contain relatively high total arsenic concentrations comprised predominantly of As(III), in addition to high Fe(II) concentrations, and - in the case of PV water - high NH_3 concentrations (*8*). At each plant, the respective raw groundwater sources first undergo aeration to oxidize dissolved Fe(II), followed by a settling step to allow precipitation of Fe(III)-(hydr)oxides formed during oxidation of Fe(II). The aerated waters are then passed through a gravity-filter bed containing quartz-sand filter media, before chlorination and final passage into the city's distribution network. The Phap Van and Yen Phu samples were taken from locations in each plant between their filtration and final chlorination steps, at which point As(III) concentrations are very low. IC/ICP-MS analyses showed that native As(III) concentrations were < 2 μg/L in the Yen Phu and Phap Van water samples. Because these water samples were saturated with dissolved oxygen by the time they passed through the filter beds in the plants, and were subsequently filtered through 0.45-μm membranes, Fe(total) concentrations in each were also negligible. Other important water quality parameters are provided in the main text (Table B.2).

Separate volumes of Lake Zurich water were amended with a NH_4Cl dose of either 1 mg-N/L (7.1×10^{-5} M) to yield LZ1 water, or 20 mg-N/L (1.4×10^{-3} M) to yield LZ20 water, to provide synthetic waters for quantitatively assessing the affect of various NH_3 concentrations on As(III) oxidation rates in a real water dosed with FAC. Native As(III) concentration is < 1 μg/L in Lake Zurich water.

Text SB.5. Monitoring reactions in real waters.

Batch chlorination experiments. Each real water was spiked with 50 μg/L As(III) (6.7×10^{-7} M) and added in various volumes to either 30-mL amber, borosilicate glass vials, or 100-mL glass bottles wrapped in aluminum foil to exclude light, depending on the number of samples desired from each experiment. These solutions were thermostatted at 25(±0.5) °C and, under constant, rapid stirring (via magnetic stir-bars), dosed with various concentrations of FAC. Samples were taken from all waters after 10 s of reaction time, quenched with 1 mM ascorbic acid, filtered through aluminosilicate media to remove As(V), and subsequently analyzed by IC/ICP-MS for residual As(III). Additional samples were taken from LZ1, LZ20, and PV waters at 1- or 3-h intervals, up to 9 h reaction time, and analyzed in the same manner. In the latter two cases, reaction vials were capped after taking the 10-s samples to prevent unnecessary exposure to light. Samples collected at 10 s of reaction time were used to assess oxidation of As(III) by FAC. Subsequent samples were collected to monitor oxidation of residual As(III) in the presence of the excess NH_2Cl formed by reaction of FAC with NH_3 in the LZ1, LZ20, and PV waters. NH_2Cl concentrations were monitored during each reaction by DPD-colorimetry (*3*).

Continuous-flow chlorination experiments. Oxidation of As(III) by FAC was directly monitored in real waters by means of the CFL apparatus described above, at room temperature (i.e., 23(±2) °C). The contents of two 25-mL syringes – one containing the real water spiked with 100 μg/L (1.3×10^{-6} M) of As(III); the other containing 10 mM phosphate buffer adjusted to the pH of the real water and spiked with the appropriate FAC concentration – were mixed in 1:1 proportion to initiate the reaction. FAC consumption by each real-water matrix was monitored by quenching FAC residuals with DPD. As(III) oxidation was monitored separately by quenching residual chlorine in the reaction solution with a 10-mM ascorbic acid solution, to eliminate the possibility of side-reactions between the DPD cation radical and residual As(III) after sampling. As(III) samples were taken from the effluent leaving the CFL mixing valve, filtered through the aluminosilicate media to remove As(V), and analyzed by IC/ICP-MS.

Batch ozonation experiments. 20-mL volumes of each real water, spiked with 50 μg/L of As(III) (6.7×10^{-7} M), were added to 30-mL, amber, borosilicate glass vials, and thermostatted at 20(±0.5) °C. Under constant, rapid stirring, these solutions were dosed with various concentrations of O_3. Samples were taken from each water after 10-s reaction intervals, dosed with 1-mM 3-buten-2-ol to ensure quenching of any residual O_3, filtered through aluminosilicate media to remove As(V), and subsequently analyzed by IC/ICP-MS.

Continuous-flow ozonation experiments. Oxidation of As(III) by aqueous O_3 was monitored via CFL reaction monitoring (*2*), at room temperature (i.e., 23(±2) °C). Each real water solution was dosed with 100 μg/L As(III) (1.3×10^{-6} M) and 2 μM of *p*CBA (used as a hydroxyl radical probe (*9*)), to yield reaction conditions of 50 μg/L As(III) (6.7×10^{-7} M) and 1 μM of *p*CBA. Working O_3 stocks were prepared in Milli-Q water adjusted to pH 4 with sulfuric acid, and handled as in As(III)-O_3 reaction kinetics measurement experiments. Online pH-adjustment of the O_3 working stocks was required to permit execution of experiments at each real water's native pH, because O_3 is quite unstable in aqueous solution at circumneutral and higher pH values (*7*). This was achieved by pumping the O_3 working stock and a 10 mM phosphate buffer of the same pH as the corresponding real water through a mixing tee in 1:1 proportion, and routing the effluent directly into one channel of a second mixing tee receiving a parallel stream of real water at a flow rate equal to that of the pre-mixed O_3 stream. The effluent of the second mixing tee was directed through one of the CFL reaction loops described above. After passage of the reaction solution through a given reaction loop, residual O_3 was quenched with a 1-mM solution of cinnamic acid, which reacts with O_3 to yield benzaldehyde in 1:1 stoichiometry (with $k''_{app,\mathrm{O_3}} \sim 3.8 \times 10^{5}\ \mathrm{M^{-1}s^{-1}}$ at circumneutral pH (*10*)). Quenched samples were collected for analysis of As(III), benzaldehyde, and *p*CBA. Residual ozone concentrations and •OH exposures were calculated from benzaldehyde and *p*CBA measurements, respectively (see Text SB.7 for additional discussion of •OH exposure calculations). Initial O_3 concentrations were measured by the same procedure, with Milli-Q water substituted for As(III)-amended real water.

Text SB.6. Modeling As(III) loss by second-order kinetics in NH_3-dominated systems

In waters containing NH_3 concentrations (in mg-N/L) at least 0.5 times greater than the concentration of DOC (in mg-C/L), FAC loss will most likely dominated by the NH_3-FAC reaction. FAC loss can be modeled in such cases according to the second-order model represented by eq S1.

$$[\mathrm{FAC}] = \frac{[\mathrm{FAC}]_0\left(1 - \dfrac{[\mathrm{NH_3}]_0}{[\mathrm{FAC}]_0}\right)}{1 - \dfrac{[\mathrm{NH_3}]_0}{[\mathrm{FAC}]_0} e^{\left(\left([\mathrm{NH_3}]_0 - [\mathrm{FAC}]_0\right) k''_{app,\mathrm{FAC,NH_3}}\, t\right)}} \qquad \text{(S1)}$$

This can be incorporated into a rate expression for As(III) loss (eq S2),

$$[\mathrm{As(III)}] = [\mathrm{As(III)}]_0 e^{\left(-k''_{app,\mathrm{FAC}}\int_0^t [\mathrm{FAC}]dt\right)} \tag{S2}$$

to yield eq S3.

$$[\mathrm{As(III)}] = [\mathrm{As(III)}]_0 e^{\left(-k''_{app,\mathrm{FAC}}\int_0^t \frac{[\mathrm{FAC}]_0\left(1-\frac{[\mathrm{NH_3}]_0}{[\mathrm{FAC}]_0}\right)}{1-\frac{[\mathrm{NH_3}]_0}{[\mathrm{FAC}]_0}e^{\left(([\mathrm{NH_3}]_0-[\mathrm{FAC}]_0)k''_{app,\mathrm{FAC,NH_3}}t\right)}}dt\right)} \tag{S3}$$

The integral in eq S3 can be represented by the general form shown in eq S4,

$$\int_0^t \frac{a}{1-be^{(ct)}}dt = \int_0^t \frac{-a}{be^{(ct)}-1}dt = \int_0^t\left(\frac{a\left(be^{(ct)}-1\right)}{be^{(ct)}-1} - \frac{abe^{(ct)}}{be^{(ct)}-1}\right)dt = \int_0^t a\left(1-\frac{be^{(ct)}}{be^{(ct)}-1}\right)dt \tag{S4}$$

where $a = [\mathrm{FAC}]_0\left(1-\frac{[\mathrm{NH_3}]_0}{[\mathrm{FAC}]_0}\right)$, $b = \frac{[\mathrm{NH_3}]_0}{[\mathrm{FAC}]_0}$, and $c = \left([\mathrm{NH_3}]_0 - [\mathrm{FAC}]_0\right)k''_{app,\mathrm{FAC,NH_3}}$. Eq S4 can be integrated with respect to t, to yield eq S5.

$$\left|at - \ln\left(be^{(ct)}-1\right)\right|_0^t = \left|\frac{a}{c}\ln\left(e^{(ct)}\right) - \ln\left(be^{(ct)}-1\right)\right|_0^t = \left|\frac{a}{c}\ln\left(\frac{e^{(ct)}}{be^{(ct)}-1}\right)\right|_0^t = \frac{a}{c}\left(\ln\left(\frac{e^{(ct)}}{be^{(ct)}-1}\right) - \ln\left(\frac{1}{b-1}\right)\right) \tag{S5}$$

Eq S5 can then be substituted with appropriate variables and incorporated into eq S3 to yield eq S6.

$$[\mathrm{As(III)}] = [\mathrm{As(III)}]_0 e^{\left(\frac{-k''_{app,\mathrm{FAC,As(III)}}[\mathrm{FAC}]_0\left(1-\frac{[\mathrm{NH_3}]_0}{[\mathrm{FAC}]_0}\right)}{\left([\mathrm{NH_3}]_0-[\mathrm{FAC}]_0\right)k''_{app,\mathrm{FAC,NH_3}}}\left(\ln\left(\frac{e^{\left(([\mathrm{NH_3}]_0-[\mathrm{FAC}]_0)k''_{app,\mathrm{FAC,NH_3}}t\right)}}{\frac{[\mathrm{NH_3}]_0}{[\mathrm{FAC}]_0}e^{\left(([\mathrm{NH_3}]_0-[\mathrm{FAC}]_0)k''_{app,\mathrm{FAC,NH_3}}t\right)}-1}\right)-\ln\left(\frac{1}{\frac{[\mathrm{NH_3}]_0}{[\mathrm{FAC}]_0}-1}\right)\right)\right)} \tag{S6}$$

Text SB.7. Contributions of •OH to observed As(III) losses during real water ozonation experiments

Hydroxyl radicals (•OH) are generated continuously during real water ozonation processes, as a consequence of autocatalytic ozone decay or direct reactions between O_3 and various functional moieties within dissolved organic matter (*11,12*). Oxidation of As(III) will therefore be governed by contributions from O_3 and •OH in such systems, according to eq S7,

$$\ln\left(\frac{[\mathrm{As(III)}]_t}{[\mathrm{As(III)}]_0}\right) = -k''_{app,\mathrm{O_3,As(III)}}\int_0^t [\mathrm{O_3}]dt - k''_{app,\bullet\mathrm{OH,As(III)}}\int_0^t [\bullet\mathrm{OH}]dt \tag{S7}$$

where $k''_{app,\bullet\mathrm{OH,As(III)}}$ (for reaction between •OH and $\mathrm{As(OH)_3}$), is $8.5(\pm 0.9) \times 10^9\ \mathrm{M^{-1}s^{-1}}$. $\int_0^t [\mathrm{O_3}]dt$ can be determined by direct measurement of O_3 (*9*). $\int_0^t [\bullet\mathrm{OH}]dt$ can be calculated with eq S8 (*9*),

$$\int_0^t [\bullet\,\mathrm{OH}]dt = \frac{-1}{k''_{app,\bullet\mathrm{OH,P}}}\ln\left(\frac{[\mathrm{P}]_t}{[\mathrm{P}]_0}\right) \tag{S8}$$

where P represents a probe compound that reacts selectively with •OH. *p*-Chlorobenzoic acid (*p*CBA) was used as a •OH probe in this case, because it reacts rapidly with •OH ($k''_{app,\bullet\mathrm{OH},p\mathrm{CBA}} = 5.0 \times 10^9\ \mathrm{M^{-1}s^{-1}}$ (*13*)), and very slowly with O_3 ($k''_{app,\mathrm{O_3},p\mathrm{CBA}} < 0.15\ \mathrm{M^{-1}s^{-1}}$ (*14*)). The relative importance of •OH radical reactions in oxidation of As(III) during real water ozonation ex

$$\mathrm{f}_{\bullet\mathrm{OH,M}(t)} = \frac{k''_{app,\bullet\mathrm{OH,As(III)}}\int_0^t [\bullet\,\mathrm{OH}]dt}{k''_{app,\mathrm{O_3,As(III)}}\int_0^t [\mathrm{O_3}]dt + k''_{app,\bullet\mathrm{OH,As(III)}}\int_0^t [\bullet\,\mathrm{OH}]dt} \tag{S9}$$

which represents the ratio of observed oxidation due to •OH, relative to that due to direct reactions with O_3. Eq S9 was substituted with eqs S7 and S8 to yield eq S10, which was used to calculate $\mathrm{f}_{\bullet\mathrm{OH,M}(t)}$.

$$\mathrm{f}_{\bullet\mathrm{OH,M}(t)} = \frac{-\left(\frac{k''_{app,\bullet\mathrm{OH,As(III)}}}{k''_{app,\bullet\mathrm{OH},p\mathrm{CBA}}}\ln\left(\frac{[p\mathrm{CBA}]_t}{[p\mathrm{CBA}]_0}\right)\right)}{k''_{app,\mathrm{O_3,As(III)}}\int_0^t [\mathrm{O_3}]dt - \left(\frac{k''_{app,\bullet\mathrm{OH,As(III)}}}{k''_{app,\bullet\mathrm{OH},p\mathrm{CBA}}}\ln\left(\frac{[p\mathrm{CBA}]_t}{[p\mathrm{CBA}]_0}\right)\right)} \tag{S10}$$

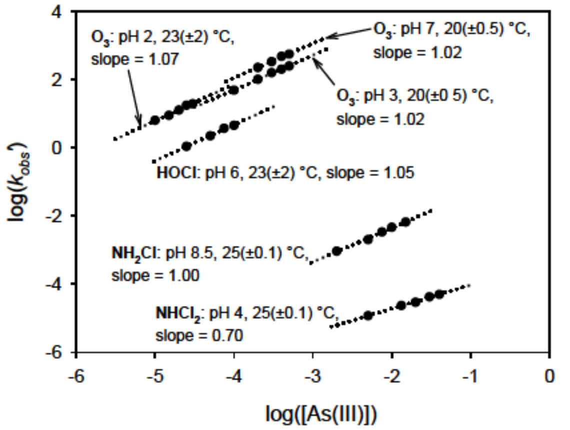

Figure SB.1. Reaction orders with respect to As(III) in the reactions of As(III) with FAC, NH_2Cl, $NHCl_2$, and O_3. pH 2 O_3 experiments were conducted by continuous-flow, quenched reaction monitoring. pH 3 and 7 O_3 data were obtained by stopped-flow spectrophotometry.

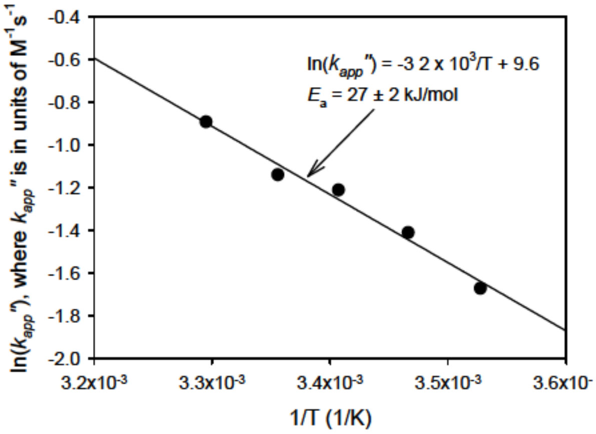

Figure SB.2. Temperature-dependence of apparent, second-order rate constant for decay of NH_2Cl in the presence of excess As(III). Experiments conducted at [As(III)] = 5 x 10^{-3} M, and $[NH_2Cl]_0$ = 2 x 10^{-4} M, in pH 9, 10 mM borate buffer, except for the 25° C experiment, which was performed under the same conditions in 50 mM borate buffer.

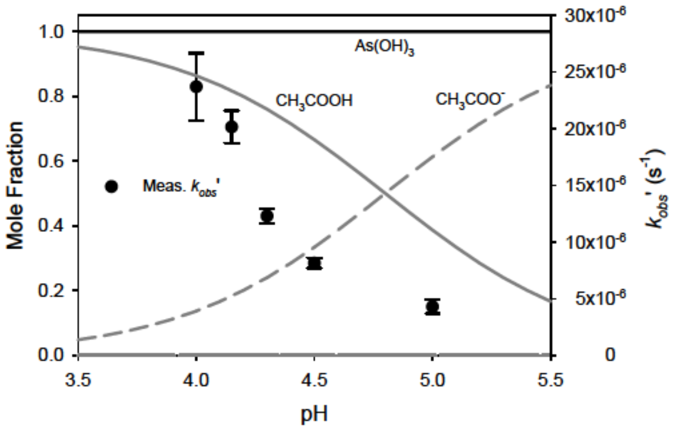

Figure SB.3. pH-dependence of observed pseudo-first order rate constants for decay of $NHCl_2$ in the presence of excess As(III). Experiments conducted in 60 mM acetate buffer, at $[As(III)] = 1.3 \times 10^{-2}$ M, $[NHCl_2]_0 = 3.5\text{-}5.5 \times 10^{-4}$ M, and 25(±0.5) °C. Values measured at pH 4.5 and 5 corrected for observed losses of $NHCl_2$ in corresponding As(III) controls.

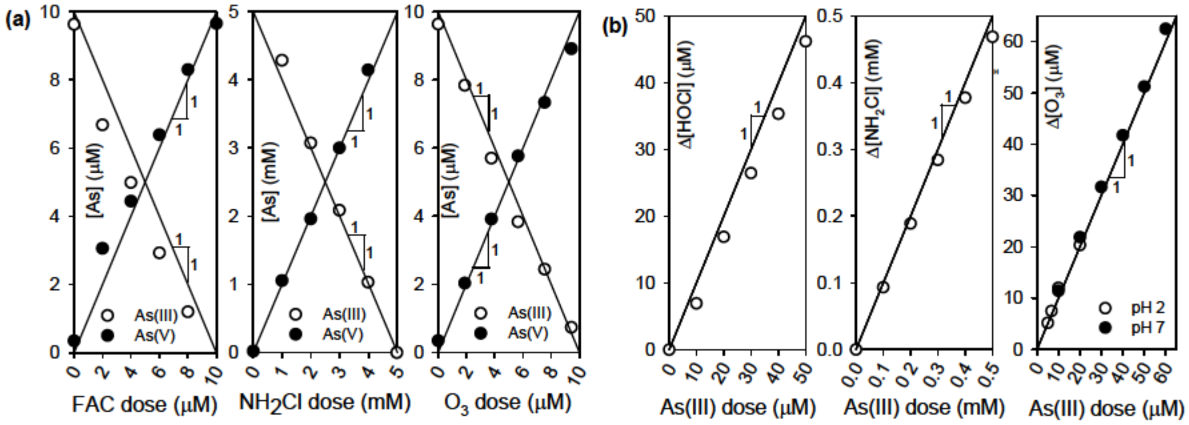

Figure SB.4. Observed stoichiometries for the reactions of As(III) with FAC, NH_2Cl, and O_3: (a) As(III) in molar excess, and (b) oxidants in molar excess. FAC experiments conducted at pH 7, NH_2Cl experiments conducted at pH 9, and O_3 experiments conducted at pH 7. All experiments were conducted at room temperature (23(±2) °C).

Literature Cited

(1) Meng, X. G.; Wang, W. Speciation of Arsenic by Disposable Cartridges. Extended abstracts of the *Book of Posters of the Third International Conference on Arsenic Exposure and Health Effects*, San Diego, CA, July 12-15, 1998; Society of Environmental Geochemistry and Health: University of Colorado at Denver.

(2) Dodd, M.; Shah, A. D.; von Gunten, U.; Huang, C.-H. Interactions of fluoroquinolone antibacterial agents with aqueous chlorine: Reaction kinetics, mechanisms, and transformation pathways. *Environ. Sci. Technol.* **2005**, *39*, 7065-7076.

(3) APHA *Standard Methods for the Examination of Water and Wastewater*; 20 ed.; APHA, AWWA, WPCF: Washington, 1998.

(4) Dodd, M. C.; Vu, N. V.; Le, V. C.; Kissner, R.; Pham, H. V.; Cao, T. H.; Berg, M.; von Gunten, U. Kinetics and mechanistic aspects of As(III) oxidation by aqueous chlorine, chloramines, and ozone: Relevance to drinking water treatment. *Environ. Sci. Technol.* **2006**, *40*, 3285-3292.

(5) Qiang, Z.; Adams, C. D. Determination of monochloramine formation rate constants with stopped-flow spectrophotometry. *Environ. Sci. Technol.* **2004**, *38*, 1435-1444.

(6) Bader, H.; Hoigné, J. Determination of ozone in water by the indigo method. *Water Res.* **1981**, *15*, 449-456.

(7) Staehelin, J.; Hoigné, J. Decomposition of ozone in water: Rate of initiation by hydroxide ions and hydrogen peroxide. *Environ. Sci. Technol.* **1982**, *16*, 676-681.

(8) Berg, M.; Tran, H. C.; Nguyen, T. C.; Pham, H. V.; Schertenleib, R.; Giger, W. Arsenic contamination of groundwater and drinking water in Vietnam: A human health threat. *Environ. Sci. Technol.* **2001**, *35*, 2621-2626.

(9) Elovitz, M. S.; von Gunten, U. Hydroxyl radical/ozone ratios during ozonation processes. I. The R_{ct} concept. *Ozone Science and Engineering* **1999**, *21*, 239-260.

(10) Leitzke, A.; Reisz, E.; Flyunt, R.; von Sonntag, C. The reactions of ozone with cinnamic acids: formation and decay of 2-hydroperoxy-2-hydroxyacetic acid. *J. Chem. Soc., Perkin Trans. 2* **2001**, 793-797.

(11) Buffle, M.-O.; Schumacher, J.; Salhi, E.; von Gunten, U. Measurement of the initial phase of ozone decomposition in water and wastewater by means of a continuous quench flow system: Application to disinfection and pharmaceutical oxidation. *Water Research* **2005**, *Accepted for publication*.

(12) von Gunten, U. Ozonation of drinking water: Part I. Oxidation kinetics and product formation. *Water Res.* **2003**, *37*, 1443-1467.

(13) Neta, P.; Dorfman, L. M. Pulse radiolysis studies. XIII. Rate constants for the reaction of hydroxyl radicals with aromatic compounds in aqueous solutions. *Adv. in Chem.* **1968**, *81*, 222-230.

(14) Yao, C. C. D.; Haag, W. R. Rate constants for direct reactions of ozone with several drinking water contaminants. *Water Res.* **1991**, *25*, 761-773.

Curriculum Vitae

Michael Cameron Dodd

Born on 14. May, 1978 in Atlanta, GA (U.S.A.)
Citizen of the United States of America

1983 to 1984 – Elementary School (Kindergarten to Grade 1) – Morris Brandon Elementary School, Atlanta, GA (U.S.A.)

1984 to 1989 – Elementary School (Grades 1 to 5) – Sarah Smith Elementary School, Atlanta, GA (U.S.A.)

1989 to 1992 – Middle School – Sutton Middle School, Atlanta, GA (U.S.A.)

1992 to 1996 – High School – North Atlanta High School, Atlanta, GA (U.S.A.)

1996 – High School Diploma

1996 to 2001 – Undergraduate Studies at the Georgia Institute of Technology, Atlanta, GA (U.S.A.)

1997 to 1998 – Undergraduate Research Assistant – Georgia Institute of Technology, School of Earth and Atmospheric Sciences, with Dr. Philippe Van Cappellen

1998 to 1999 – Undergraduate Research Assistant – Georgia Institute of Technology, School of Civil and Environmental Engineering, with Dr. Dennis Grubb

1997 to 2000 – Environmental Engineer – Blue Circle Aggregates, Inc. (now Lafarge, N.A.)

2000 to 2001 – Engineering Technician – Camp Dresser and McKee Inc.

2001 – Undergraduate Research Assistant – Georgia Institute of Technology, School of Civil and Environmental Engineering, with Dr. Ching-Hua Huang

2001 – B .S., Civil Engineering, Georgia Institute of Technology Cooperative Education Program, Highest Honors

2001 to 2003 – Graduate Studies at the Georgia Institute of Technology, Atlanta, GA (U.S.A.)

2001 to 2003 – Graduate Research Assistant – Georgia Institute of Technology, School of Civil and Environmental Engineering, with Dr. Ching-Hua Huang

2003 – M.S., Environmental Engineering, Georgia Institute of Technology

2003 to 2008 – Doctoral Thesis in Environmental Chemistry at the Swiss Federal Institute of Technology-Zurich (ETH-Zurich)